PROVENANCE OF ORDOVICIAN TO SILURIAN CLASTIC ROCKS OF THE ARGENTINEAN PRECORDILLERA AND ITS GEOTECTONIC IMPLICATIONS.

by

Paulina Abre

THESIS

presented in fulfilment of the requirements for the degree of

PHILOSOPHIAE DOCTOR

in

GEOLOGY

in the

FACULTY OF SCIENCE

of the

UNIVERSITY OF JOHANNESBURG

(former RAND AFRIKAANS UNIVERSITY)

Supervisor

Dr. U. Zimmermann

Co-supervisors

Professor B. Cairncross

Professor C. Cingolani

November 2007

DECLARATION

I declare that this thesis is my own original work, conducted under the supervision of Dr. Udo Zimmermann, and co-supervision of Prof. Bruce Cairncross and Prof. Carlos Cingolani. It is submitted for the degree Philosophiae Doctor in Geology in the Faculty of Sciences at the University of Johannesburg (former Rand Afrikaans University), Johannesburg, South Africa. No part of this research has been submitted in the past, or is being submitted, for a degree or examination at any other University.

Paulina Abre.
Date: 11-07
Signed:

ABSTRACT

A Mesoproterozoic basement and a Cambrian-Ordovician carbonate platform characterize the Precordillera terrane. These characteristics and its distinct geologic history mark a difference between this suspected exotic-to-Gondwana terrane and the Gondwanan autochthonous, leading to speculation that the Precordillera was derived from Laurentia. The surprising similarities of the carbonate sequences between the Precordillera and certain parts of southeast Laurentia suggest a common geological history. However, other models interpret the origin of the Precordillera terrane as being para-autochthonous with respect to Gondwana. All these models are still controversial.

A combination of several methodologies including petrography and heavy minerals analysis, geochemistry, Sm-Nd and Pb-Pb isotopes and zircon dating were applied to several Ordovician and Ordovician to Silurian units of the Precordillera terrane.

Geochemistry and petrography indicates that all the Formations studied have similar characteristics, with at least two sources providing detritus to the basin. The dominant source has an unrecycled upper continental crust composition whereas the other component is more depleted. The study of detrital chromian spinels suggests that mid-ocean ridge basalts, continental intraplate flood basalts and ocean island basalt-related rocks were among the sources for the detrital record of the Precordillera terrane. Nevertheless, the mafic sources and their ages remain unknown.

Nd isotopes account for negative ε_{Nd} values and T_{DM} ages in a range of variation found elsewhere within Gondwana and basement rocks of the Precordillera. The Sm/Nd ratios of certain samples indicate fractionation of LREE. Pb isotopes indicate that a source with high $^{207}Pb/^{204}Pb$ was important, and point to Gondwanan sources.

Detrital zircon dating constrain the sources as being dominantly of Mesoproterozoic age (but with a main peak in the range 1.0 to 1.3 Ga), with less abundant populations of Neoproterozoic (with a main peak in the range 0.9 to 1.0 Ga), Palaeoproterozoic, Cambrian and Ordovician ages in order of abundance.

The uniformity shown by the provenance proxies indicate that there were no important changes in the provenance from the Lower Ordovician until the Early Silurian. Several areas are evaluated as sources for the Precordillera terrane. The rocks that fit best all the provenance constraints are found within the basement of the Precordillera terrane and the Western Pampeanas Ranges. Basement rocks from the Arequipa-Antofalla area (Central Andes) also match the isotopic characteristics, but a northern source is less probable, except for the Western tectofacies. On the other hand, areas such as Antarctica, Falklands/Malvinas Microplate, the Natal-Namaqua Metamorphic belt and the Grenville Province of Laurentia can be neglected as sources.

The proposal of these areas as sources is in agreement with palaeocurrents and facies analyses and suggests proximity between them and the Precordillera since at least the Late Arenig to Early Llanvirn. This has important implications for the proposed models regarding the geotectonic evolution of the Precordillera terrane. The models would need to be adjusted to the here proposed youngest timing of collision.

Keywords: Precordillera terrane, provenance, geochemistry, Sm-Nd and Pb-Pb isotopes, detrital zircon dating, Proto-Andean Gondwana margin, Laurentia.

ACKNOWLEDGEMENTS

I would like to express my sincere and deep acknowledgements to:

my supervisor Dr. Udo Zimmermann for the great opportunity he gave, through which I had the chance to learn not only about geology, but also about South Africa and its people.

my co-supervisor Prof. Bruce Cairncross for his kind battle against my ‘almost King-style’ English. His honesty would always be an example to me.

my co-supervisor Prof. Carlos Cingolani for all his support. The decades he has dedicated to study the Precordillera, allowed him to guide me up and down mountains and valleys without hesitation, directly to outcrops we needed to study. He knows the terrain like the palm of his hand. From his expertise, I learnt how to be a researcher. I am honoured for the time and effort he has dedicated to me and to this work.

the Faculty of Sciences of the University of Johannesburg (South Africa) for the bursary awarded to me as a post-graduate student. I also thank the Faculty for all other financial support received that allowed me to visit laboratories overseas and to analyze samples. I appreciate particularly the dedication to sort out all formal issues of Mrs. Strydom.

external reviewers Prof. Víctor Ramos (UBA) and Prof. Suzanne Kay, (Cornell University) are deeply acknowledge for the revision of the thesis. Their contribution helped to enhance the manuscript and would be absolutely useful for the near come publications. I consider a great luck to have the opinion of researchers with historical experience in the Precordillera.

the National Research Foundation (NRF), South Africa for the grant awarded for detrital zircon dating.

the International Association of Sedimentologists (IAS) and it’s students awards programs 2004 and 2005, through which funding for geochemical and isotope geochemical analyses was provided.

the Consejo Nacional de Investigaciones Científicas y Tecnológicas (CONICET), and the Agencia Nacional de Promoción Científica y Tecnológica

(ANPCYT), both from Argentina, which via Prof. Cingolani had financially supported most of the fieldwork done.

the International Geological Correlation Program (IGCP) project 436 “Pacific Gondwana margin” for provided funding for one fieldwork.

SPECTRAU, the Central Analytical Facilities of the University of Johannesburg, permitted the use of their equipment. Special thanks to the staff: Dr. Willie Oldewage, Dr. Herman van Niekerk and Mr L.L. Coetzee.

the Department of Geology of the University of Johannesburg (South Africa) and all the staff, that hosted me during my three-year stay. I would like particularly acknowledge the advice received from Prof. Jens Gutzmer.

the Centro de Investigaciones Geológicas, La Plata, Argentina, that allowed the use of their facilities.

the Laboratorio de Geología Isotópica, Universidade Federal do Rio Grande do Sul, Porto Alegre (Brazil) is gratefully acknowledge for hosting me in several times. I am very grateful to the Head of the laboratory Prof. Dr. Farid Chemale Jr, but also to Prof. Dr. Koji Kawashita and Prof. Dr. Dussin, I.

the Departamento Científico de Geología del Museo de Ciencias Naturales de la Universidad Nacional de La Plata and all its staff.

various people that helped me during fieldworks: Lic. Norberto Uriz; Lic. Maximiliano Naipauer; Lic. Paula Frigerio; Dr. Marcelo Manassero; Lic. Diego Licitra. To all those that helped me during different types of laboratory work, either teaching me techniques or processing material for me: Claudia Pereyra (CONICET, Argentina); Mario Campaña (CONICET, Argentina); MSc. Marcia (LGI-UFRGS, Porto Alegre, Brazil); MSc. Anelise Bertotti (LGI-UFRGS, Porto Alegre, Brazil); Dr. Ana Maria Sato (CIG, Argentina); Dr. Ricardo Varela (CIG, Argentina); Lic. Jorge Maggi (CIG, Argentina).

to the staff of the Centro de Investigaciones Geológicas (La Plata, Argentina) and the Laboratório de Geologia Isotópica da Universidade Federal do Rio Grande do Sul (Porto Alegre, Brazil).

to my family, that always fully supported me often not understanding the decisions and all that travelling.

to all my friends, who tolerated my very long e-mails. You know that no matter the distance, you would always be with me.

to all the post-graduate mates from the University of Johannesburg that shared a couple of beers on Thursday afternoons.

finally, To Gonzalo Blanco, my beloved partner, the best gift this thesis ever gave me.

To you all, I will treasure the memory.

TABLE OF CONTENTS

CHAPTER 5

PROVENANCE ANALYSIS OF ORDOVICAN CLASTIC UNITS OF THE WESTERN TECTOFACIES OF THE PRECORDILLERA TERRANE, ARGENTINA

APPENDIX B

APPENDIX C

CHAPTER 1

INTRODUCTION

1.1 PREAMBLE

Several different processes cause cratonic growth and change, either by addition of crustal material through mantle plumes or along active continental margins or by simple terrane accretion or separation (e.g. McLennan *et al.*, 2006). The latter process is regarded as frequent in the history of cratonic blocks since the establishment of global tectonics in geology.

Several cases of long-distance terrane transport have been identified during the Earth's history. The so-called Precordillera could be one of those. This continental fragment is today located in western-central Argentina, and it is interpreted as being derived from Laurentia and collided with Gondwana either during the Upper Ordovician (e.g. Astini *et al.*, 1995) or during the Silurian - Devonian (e.g. Keller, 1999). The tectonic evolution of the Precordillera terrane is a substantial part of the understanding of the evolution of the western border of southwest Gondwana.

Although the debate of the origin of the Precordillera has been ongoing for decades, comprehensive provenance studies on clastic rocks were rarely done (e.g. Spalletti *et al.*, 1989; Loske, 1994). The origin of this terrane is explained based on palaeogeographical, palaeontological, sedimentological and isotope data. Only in recent times, some provenance studies involving advanced techniques such as detrital zircon dating were initiated (Cingolani *et al.*, 2003a; Abre *et al.*, 2005; Finney *et al.*, 2005; Naipauer *et al.*, 2005a; Gleason *et al.*, 2006).

This study presents the first comprehensive provenance analyses of clastic sedimentary rocks from Ordovician and Silurian strata of the Precordillera terrane. The objective is to gain insights into the crustal evolution of the Precordillera terrane in order to decipher its origin. A combination of several methodologies including sedimentology, petrography, geochemistry and isotope geochemistry data and detrital zircon age dating was applied to constrain the sources of detritus, as well as to test the different models proposed to explain the origin of the Precordillera terrane.

1.2 THE GENERAL PROBLEM

The origin and evolution during the Lower Palaeozoic of the Argentine Precordillera terrane has been debated for years. Although there is a consensus about its geological different character compared with Gondwanan successions of the same age, it has not been proved whether the Precordillera is a crustal block derived from Laurentia or a block located in the south (present coordinates) of Western Gondwana for the Lower Palaeozoic, and later displaced by strike-slip movements along the Gondwana margin. Several lines of research (sedimentology, biostratigraphy, sequence stratigraphy, geochronology, palaeomagnetism, isotope geochemistry) support the palaeogeographic proximity of this terrane to Laurentia and allow the development of different models to explain the transference from Laurentia to its present position. Although most of these models assume a collision between the two continents, the models differ primarily in the time and type of collision. Detrital zircon ages were recently used to prove a Gondwana affinity for the Early Palaeozoic of the Precordillera terrane (e.g. Finney *et al.*, 2005). However, it is important to evaluate, control and understand detrital zircon ages with other provenance techniques to avoid controversial palaeotectonic interpretations.

The proposal of several models to explain the palaeogeographic evolution of the Lower Palaeozoic record of the Argentinean Precordillera terrane demonstrate the outstanding uncertainties regarding the tectonic evolution of this continental fragment. The general objective of this thesis is to add new provenance data and evidence in order to contribute to the understanding of its tectonic evolution. Due to the thick and widely distributed Lower Palaeozoic sedimentary record in the Precordillera and considering the Ordovician to Early Silurian as the clue time according to the different geotectonic models proposed, the study was concentrated on the Ordovician to Silurian clastic record. The geotectonic evolution during the Lower Palaeozoic of the western border of

Gondwana in adjacent regions seems to be understood and data from those areas can be used for comparisons (e.g. Bahlburg, 1998; Bock *et al.*, 2000; Lucassen *et al.*, 2000; Zimmermann and Bahlburg, 2003).

1.3 LOCATION

The Precordillera *sensu stricto* (*s.s.*) was initially defined (Furque and Cuerda, 1979 and references therein) as a north-south elongated geological province of western Argentina (500 km long by 80 km to 110 km wide; Fig. 1.1). Since it was considered as a probable exotic landmass, it was called “Precordillera terrane” (Ramos *et al.*, 1986). Several regions were consequently added to the “Greater Precordillera” (Astini *et al.*, 1995), which in turn was named Cuyania composite terrane (Ramos *et al.*, 1996) or Occidentalia terrane (Dalla Salda *et al.*, 1992a) to differentiate it from the Precordillera *s.s.* as originally described.

The main characteristics of the Precordillera terrane that allows its consideration as a separate entity are its difference in the lithostratigraphic record during the Cambrian and Ordovician, as thick carbonate deposits are unknown from southwest Gondwana. The fossil record, especially for the Cambrian and Lower Ordovician is as well fundamentally different from a typical Gondwana assemblage (Benedetto, 1993; Benedetto *et al.*, 1999). The Grenvillian-age[1] (0.95 to 1.3 Ga) basement of the Precordillera terrane is characterized by Nd, Sr and Pb depleted isotopic signatures and Mesoproterozoic T_{DM} ages, which resemble rocks of the same age of Laurentia (Sato *et al.*, 2004 and references therein; Ramos, 2004). Although

[1] The term ‘‘Grenville’’ was used as equivalent of a region (The Grenville Province within USA and Canada, with internal variations in composition, a distinctive isotopic signature, style and a time span from 0.98 to 1.36 Ga; Rivers *et al.*, 1989; Dickin and McNutt, 1989; Mosher, 1998; Eriksson *et al.*, 2003), of a style of orogenic events (the worldwide recorded Grenville Orogenic Cycle, with differences in age and composition within different continents and even within the same continents, and that received different names and not necessarily involved a collision with Laurentia; Fail, 1997; Wareham *et al.*, 1998; Aceñolaza *et al.*, 2002), or as a time concept (1.0 to 1.2 Ga; Rogers *et al.*, 1995; Fail, 1997). Several authors that studied basement rocks of the Precordillera and surrounding areas sometimes used the term “Grenvillian” or ‘Grenville-age’ or ‘Grenville’ to refer to rocks contemporaneous (~0.95 to ~1.3 Ga) with the basement rocks of the Grenville Province of North America (e.g. Kay *et al.*, 1996; Sato *et al.*, 2004).

Middle Proterozoic ages can be found within Gondwana, they are associated with Late Proterozoic ages (Brasiliano) and they have a distinctive Pb isotopic signature (Ramos, 2004).

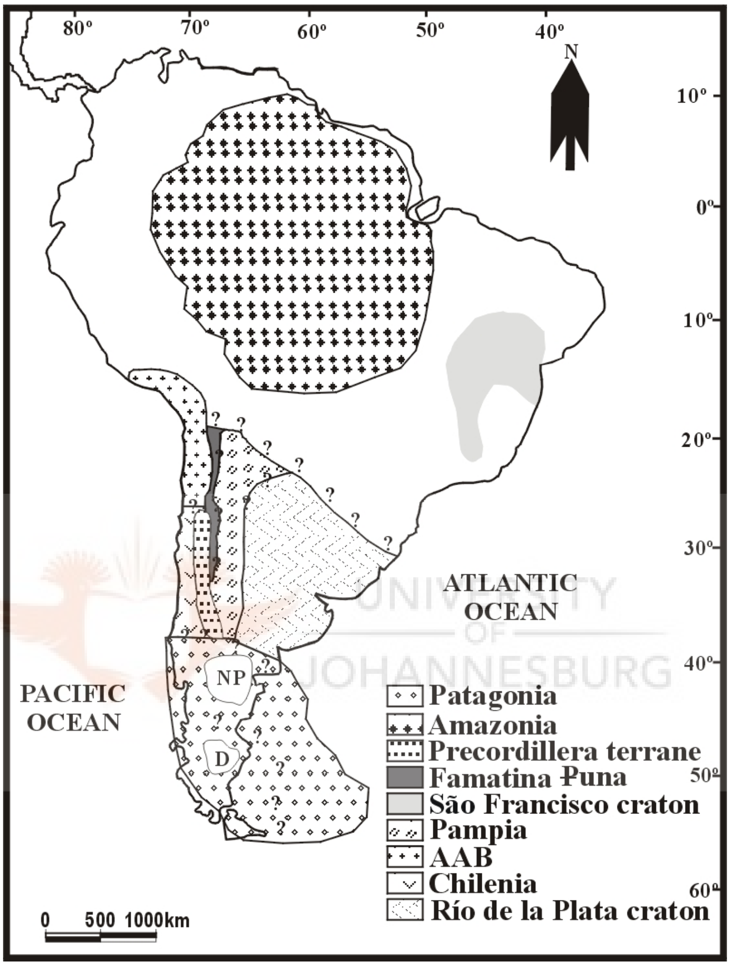

Figure 1.1: The Precordillera terrane and neighbouring main tectonostratigraphic units of South America (modified from Rapalini, 2005). NP: North Patagonian Massif; D: Deseado Massif; AAB: Arequipa-Antofalla Basement.

The mentioned distinct geological characteristics point out the difference between this suspected exotic-to-Gondwana terrane and the neighbouring areas like the Pampia terrane, the Puna and the Famatina areas (located towards east), the Chilenia terrane (located towards west; Fig. 1.1) and Patagonia.

1.4 OBJECTIVES

The present study attempts to describe and interpret new data obtained by petrographical and geochemical analyses, Sm-Nd and Pb-Pb isotopes studies and detrital zircon age dating from Ordovician to Silurian clastic rocks in order to understand the provenance and in turn the tectonic evolution of the Precordillera terrane. Both the Precordillera *s.s.* and the San Rafael block were sampled with this objective. The Las Matras block is the southernmost continuation of the Precordillera, but Ordovician clastic rocks are not exposed. Although the San Rafael block is considered the continuation towards the south of the Precordillera *s.s.* (Ramos *et al.*, 1996), it is shortly described separately (see Chapter 2).

The supracrustal record of the Precordillera *s.s.* is marked by drastic facies changes, therefore sampling was carried out in transversal and longitudinal sections (Appendix B). Fourteen different successions from the Precordillera *s.s.* were studied, namely: Gualcamayo, Los Azules, La Cantera, Las Vacas, Las Plantas, Trapiche, Don Braulio, La Chilca, Los Sombreros, Empozada, Portezuelo del Tontal, Sierra de la Invernada, Alcaparrosa and Yerba Loca Formations. Two of these successions record the transition Ordovician-Silurian: Don Braulio and La Chilca Formations. The Ordovician clastic record in the San Rafael block is less developed in time and space, being represented by only two units, the Ponón Trehué and Pavón Formations.

A brief introduction about the geological setting of the Argentine Precordillera terrane is given, as well as a summary of the evidence that were interpreted by several authors as indicative of an exotic origin for the landmass (Chapter 2). An extensive description of the geotectonic models proposed by several authors is also presented, with particular emphasis on those models that fit best all the existing evidence (Chapter 2).

All the techniques used (petrography, geochemistry, geochronology) may become more relevant and give stronger arguments when the results given by each technique is compared with and constrained by the conclusions reached using other techniques. The use of integrate provenance analyses allow the separation of the whole dataset according to the stratigraphic framework and facies, avoiding mixing the results of sequences that belong to different sub-basins or even more, linked to different tectonic settings. The Precordillera terrane had been subdivided into three morphostructural regions (known as Eastern, Central and Western Precordillera) which are linked to the Andean fold-and-thrust belt. However, the stratigraphic framework and facies distribution of the Early Palaeozoic Precordilleran successions are not in correspondence with the morphostructural regions. Therefore, it seems better to analyze the Ordovician to Silurian sedimentary sequences in terms of facies distribution because they are directly link to the tectonic setting and evolution of the basin morphology. In this regard, in several previous studies the Precordillera had been subdivided into the Eastern and Western basins, with a continent-ocean transition zone (so called slope-type deposits). The Eastern Precordillera was interpreted as a strike and slip basin (Finney, *et al.*, 2005) or as synorogenic clastic wedge deposits (Thomas and Astini, 2003). The sequences related to the slope were interpreted as linked to a pull-apart basin (Peralta, 2005; Peralta and Heredia, 2005), westward thrusting of basement faults (discussion in Thomas *et al.*, 2001) or to passive margin slope deposits (Thomas and Astini, 2003). The Western tectofacies (Astini, 1993a) was deposited as deep-marine sediments with interlayered mafic subvolcanic rocks. Despite the uncertainties regarding basin type and evolution, the differences in facies, depositional environments and tectonic setting between the Eastern and the Western basin are undoubted and allowed their separate study (Chapters 3 and 5 respectively). The slope-type deposits are bounded by faults or unconformities and are developed as a transition zone in between the Eastern and Western settings. More recently, the slope deposits were interpreted as extensional pull-apart basin along strike-slip faults, with subaerial exposures and fluvial transport to the basin or as passive margin sequences deposited as sliding-down unconsolidated sediments which suffered extensional deformation during submarine sliding (and not due to sedimentary processes such as debris flows; Alonso *et al.*, 2007). In spite of the uncertainties related to the so called ‘slope-type’ deposits, the existence of faults denoting the presence of a Lower Palaeozoic slope allowed to study the Los Sombreros and Empozada Formations in a separate chapter (Chapter 4), to determine a probable different provenance component and to identify a tectonic setting regarding the geotectonic evolution of the Precordillera.

A southern continuation of the Precordillera terrane in the San Rafael block comprises two Ordovician units. The provenance of one of these units, the Ponón Trehué Formation, was studied in detail (Chapter 6). The provenance of the other Ordovician clastic sequence (Pavón Formation) is known (Cingolani *et al.*, 2003a), and therefore insights were gained through the chemical analyses of the detrital chromian spinels (Chapter 7). However, these data are presented as a separate chapter since it was accepted for publication (Journal of South American Earth Sciences, Special Issue on Mafic and Ultramafic complexes in South America and the Caribbean), following the regulations from the Faculty of Sciences. In the last chapter (Chapter 8), a general review of the provenance of the different areas is presented. The geotectonic models are evaluated according to the source areas detected as the more probable contributors of detritus for each Ordovician sequence, and conclusions obtained through the studies carried out for this project are outlined.

1.5 METHODOLOGY

Provenance studies on sedimentary rocks aim at deciphering the composition and geological evolution of their source areas as well as to characterize the tectonic setting of the depositional basin. A meaningful provenance analysis necessarily concentrates on the evaluation of indicators, which mirror the original composition of source rocks and areas. However, the data need to be tested for the effects of secondary factors that have the potential to obscure this information, i.e. sorting, weathering and metamorphism. Accordingly, the combination of several independent analytical approaches is required. In view of the general relatively complex history of rocks, only the combination of fieldwork, petrographical, geochemical and isotope data (especially Nd and Pb isotopes and detrital zircon dating) seems appropriate to achieve the objectives of a comprehensive study. These dataset can ideally be used to relate the composition and evolution of the source regions to the plate tectonic setting of the depositional basins under examination, and to evaluate the potential role of exotic terranes in the development of a particular crustal block.

Data from the sixteen different successions from the Precordillera terrane were obtained using techniques such as: i) light microscopy to define the clastic rocks based on their mineralogy. ii) Whole rock X-ray diffraction analyses to aid in the identification of certain phases not discernable by petrography (cement and matrix compositions) as well as illite crystallinity data to determine the grade of diagenesis to very low-grade metamorphism. iii) Identification of heavy minerals by the means of light microscopy and SEM-EDS-BSE (scanning and backscattered electronic microscope, along with energy dispersive system). iv) Chemical analyses of clue phases using microprobe techniques to determine source rock types or settings. v) Geochemical analyses of major and trace elements to characterize the detrital record, to understand sedimentary processes as weathering, reworking and sorting and to evaluate relationships between source and depositional areas. vi) Further characterisation of the detrital material regarding its crustal histories by determining their Sm-Nd and Pb-Pb isotope signatures. vii) Detrital zircon dating and cathodoluminiscence imaging help to determine the ages and types of probable source rocks. The use of all the abovementioned techniques results in a massive database regarding the provenance of the Ordovician to Silurian clastic record of the Precordillera terrane, to understand its origin and tectonic evolution. Tables compiling the data obtained are presented in the Appendix A, whereas details on the methods and analytical techniques are given in the Appendix B, and detailed petrographic and geochemical descriptions as well as additional data are presented in Appendix C.

CHAPTER 2

THE PRECORDILLERA TERRANE: A COMPILATION

2.1 INTRODUCTION

Several arguments including isotope geochemical data from the basement rocks support the allochthonous models of the Precordillera terrane as derived from Laurentia (e.g. Ramos *et al.*, 1986; Dalla Salda *et al.*, 1992a; Astini *et al.*, 1995). Less certain are the time and type of the collision with Gondwana. However, some authors have proposed a para-autochthonous evolution based on biostratigraphical and structural data as well as on detrital zircon age dating, where the Precordillera terrane was displaced during Ordovician-Devonian times from southern regions of Gondwana (e.g. Aceñolaza *et al.*, 2002; Finney *et al.*, 2005). To contribute to the discussion about tectonic models for the Precordillera, a comprehensive provenance study on the Ordovician record is achieved for the present thesis.

Several morphostructural units (Fig. 2.1) form the Cuyania composite terrane (Ramos *et al.*, 1996) or Precordillera terrane (Astini *et al.*, 1995): The Precordillera *s.s.* (*sensu stricto*), parts of the Western Pampeanas Ranges and the San Rafael and Las Matras blocks (Criado Roqué and Ibañez, 1979; Sato *et al.*, 2000). However, boundaries are still not well constrained (e.g. Porcher *et al.*, 2004). Nevertheless, it is accepted that the Precordillera *s.s.* and the two southern blocks shared a common history during at least the Lower Palaeozoic.

2.2 BOUNDARIES

2.2.1 Precordillera *s.s.*

The Precordillera *s.s.* (Furque and Cuerda, 1979; Baldis *et al.*, 1984 and references therein) is situated in western Argentina between 28º and 33º south latitude (Fig. 2.1). To the south, it is in tectonic contact with Mesozoic and Cenozoic rocks (Keller, 1999). To the east, it is separated from the Pampeanas Ranges by the Bermejo-

Tulúm valley (BTV). In the northern part, the Frontal Cordillera (FC) overthrusts the Precordillera *s.s.*, forming a wedge against the Famatina Range (FR; see Fig. 2.1b). To the west, it is separated from the Frontal Cordillera by the Iglesias-Calingasta-Uspallata valley (ICUV).

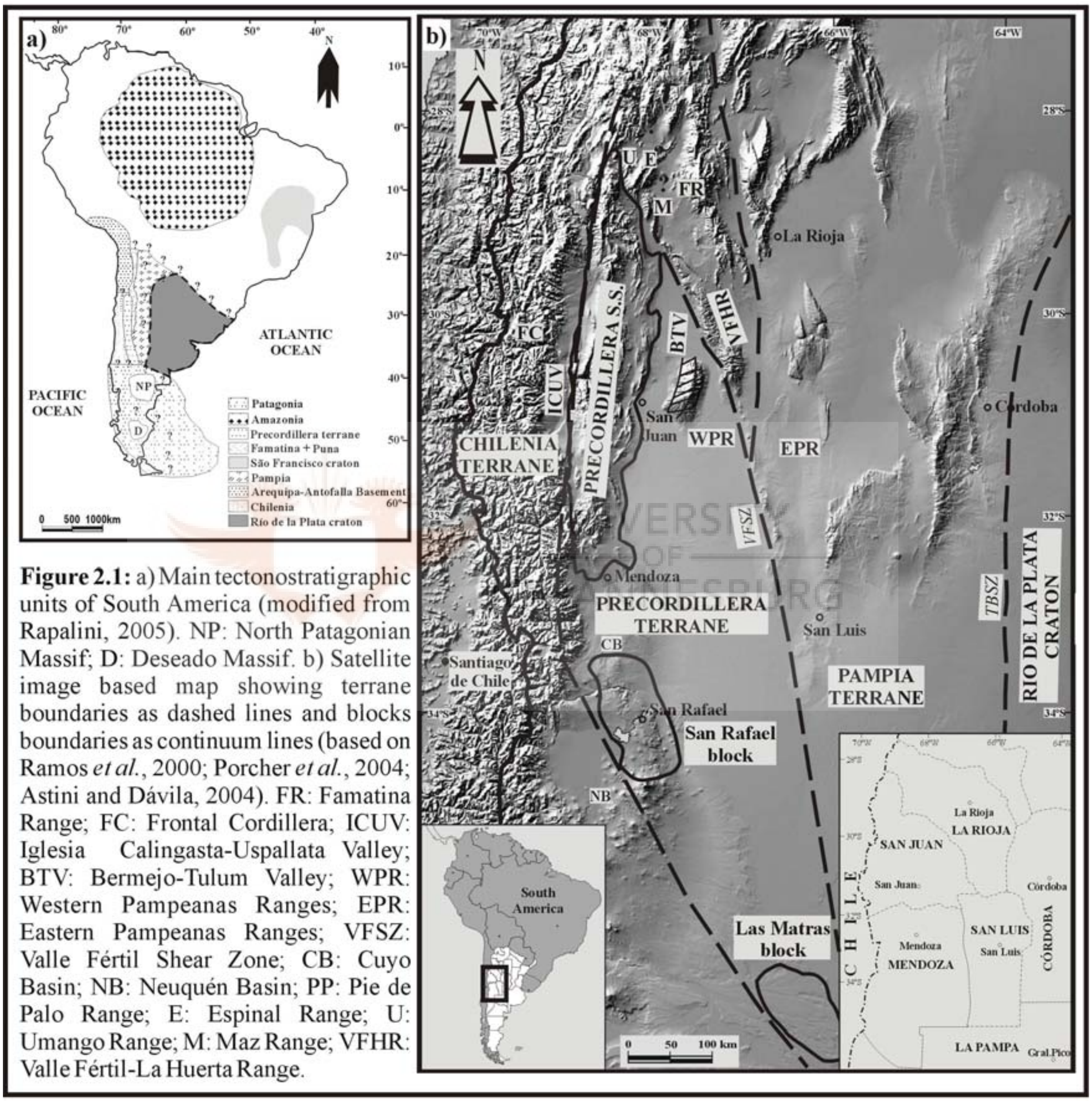

Figure 2.1: a) Main tectonostratigraphic units of South America (modified from Rapalini, 2005). NP: North Patagonian Massif; D: Deseado Massif. b) Satellite image based map showing terrane boundaries as dashed lines and blocks boundaries as continuum lines (based on Ramos *et al.*, 2000; Porcher *et al.*, 2004; Astini and Dávila, 2004). FR: Famatina Range; FC: Frontal Cordillera; ICUV: Iglesia Calingasta-Uspallata Valley; BTV: Bermejo-Tulum Valley; WPR: Western Pampeanas Ranges; EPR: Eastern Pampeanas Ranges; VFSZ: Valle Fértil Shear Zone; CB: Cuyo Basin; NB: Neuquén Basin; PP: Pie de Palo Range; E: Espinal Range; U: Umango Range; M: Maz Range; VFHR: Valle Fértil-La Huerta Range.

2.2.2 San Rafael block

The San Rafael block lies in the central-western region of the Mendoza province, Argentina (Fig. 2.1b inlet). To the north and south, it is bounded by the

Mesozoic Cuyo (CB) and Neuquén (NB) oil basins respectively. Towards the east, the San Rafael block grades to the Pampean Plains vanishing under Quaternary cover. The Frontal Cordillera defines the western boundary and to the southeast, the block disappears under modern retro-arc basin volcanic rocks (Fig. 2.1b).

2.2.3 Precordillera (Cuyania) terrane

The Precordillera or Cuyania terrane includes the Precordillera *s.s.*, the San Rafael and Las Matras blocks, and the Pie de Palo Range (Ramos *et al.*, 1996). Several authors have recently debated whether probably minor ranges from the Western Pampeanas Ranges form part of this crustal block as well (e.g. Umango Range and Cerro Salinas; Porcher *et al.*, 2004; Naipauer *et al.*, 2005b). The western boundary of the terrane coincides with the western boundaries of the Precordillera *s.s.* and the San Rafael and Las Matras blocks, and is delimited by the Chilenia terrane. However, the recognition of Chilenia as an independent terrane (Ramos *et al.*, 1986) is nowadays controversial (Ramos and Basei, 1997; Rapela *et al.*, 1998; Bahlburg *et al.*, 2001; López and Gregori, 2004).

The Cuyania terrane extends southwards to the Las Matras block in the northwestern part of the La Pampa province (e.g. Tickyj *et al.*, 2003; Fig. 2.1b). The northernmost limit is somewhere within the wedge formed by the Famatina Range and Frontal Cordillera, but it is still under investigation (Astini and Dávila, 2004; Vujovich *et al.*, 2005; Frigerio *et al.*, 2005). The eastern boundary lies along mylonitic belts affecting the eastern part of Western Pampeanas Ranges (WPR; Fig. 2.1), forming the contact between the Precordillera and the Pampia terranes (Fig. 2.1). The Pampia terrane therefore develops to the east of the Pie de Palo, Umango, Maz and Espinal Ranges (Ramos *et al.*, 1996). Based on Nd-isotopes, Porcher *et al.* (2004) interpreted the Maz and Espinal (including Las Ramaditas) Ranges as representing the active Gondwana margin during the Lower Palaeozoic, while the Umango Range could have been derived from Laurentia and therefore, part of the Cuyania terrane. In contrast, geophysical data locates the suture zone to the east of the Espinal and Maz Ranges (Fig. 2.1b; Porcher *et al.*, 2004). Moreover, the eastern boundary of the Precordillera

(Pie de Palo Range; Fig. 2.1b), has been recently questioned and interpreted as autochthonous to Gondwana prior to the Lower Palaeozoic (Casquet *et al.*, 2006). To the south, Cuyania is structurally truncated against the northern Patagonia outcrops (Chernicoff and Zappettini 2004; Fig. 2.1a). Cuyania is considered as a composite terrane, as it is formed by the amalgamation of previous sub-terranes like the Precordillera sub-terrane (equivalent to the Precordillera *s.s.*) and the Pie de Palo sub-terrane, which were accreted as an island arc collision during the Grenvillian Orogeny (Ramos *et al.*, 1996).

All the entities forming the Cuyania terrane develop a Grenvillian-age (0.95 to 1.3 Ga) basement. Grenvillian-aged rocks are present within closely related areas (such as the Northern Patagonia; Dalla Salda, 1992b). Although Middle Proterozoic ages can be found within Gondwana, they are associated with Late Proterozoic ages (Brasiliano) and they have a distinctive Pb isotopic signature (Ramos, 2004). However, the Mesoproterozoic basement of the Cuyania (Precordillera) terrane is characterized by Nd, Sr and Pb depleted isotopic signatures and Mesoproterozoic T_{DM} ages, which resemble rocks of the same age of Laurentia (Ramos, 2004; Sato *et al.*, 2004 and references therein).

2.3 LITHOSTRATIGRAPHY

2.3.1 Precordillera *s.s.*

The basement of the Precordillera *s.s.* is only known from xenoliths associated with two andesitic to dacitic Miocene volcanic centres: Ullúm and Cerro Blanco (Leveratto, 1968; Abruzzi *et al.*, 1993). The xenoliths are highly deformed, greenschist to granulite facies mafic and silicic rocks (gneiss, granulite, amphibolite and greenschist facies mafic schists, and acidic gneisses), with chemical affinities suggesting a juvenile Grenville arc-back-arc protolith (Abruzzi *et al.*, 1993). Conventional zircon dating indicates an age between 1.1 and 1.2 Ga (Abruzzi *et al.*, 1993; Kay *et al.*, 1996). The xenoliths are similar although not identical to the basement of the Pie de Palo Range (Fig. 2.1b). The Pb and Nd isotopic characteristics of the xenoliths resemble the signature of the Mesoproterozoic (Grenville) basement of the Appalachians, East and West Antarctica, Natal-Namaqua Metamorphic belt and Falkland/Malvinas Islands, while they differ from other Mesoproterozoic basement rocks of neighbouring areas as the Arequipa-Antofalla Massif and southern Central Andes (Kay *et al.*, 1996; Wareham *et al.*, 1998; Bock *et al.*, 2000).

The thick Lower Palaeozoic sedimentary sequence starts with very thin Lower Cambrian rift-type deposits followed by a thick Cambrian-Ordovician carbonate platform (Astini *et al.*, 1996). Lehnert *et al.* (1997), suggest a tropical to subtropical position for the carbonate platform of the Precordillera based on sedimentological features (e.g. Cañas, 1995), trilobites (Vaccari, 1994) and conodonts (Lehnert *et al.*, 1997). The Cambrian-Ordovician carbonate platform (2000m in thickness) received some siliciclastic input most likely from the east or southeast (Keller, 1996). However, this input decreased stratigraphically upwards and no siliciclastic material within the Lower Ordovician carbonate deposits was found (Keller, 1996). The estimated size of the carbonate platform is 1000 km long and 600 km to 800 km wide (Keller, 1996).

Mainly clastic sedimentary rocks were deposited from the Lower Ordovician until the end of the Palaeozoic. The transition from carbonates to black shales marks the diachronic drowning of the platform, which occurred during the Late Arenig in the southern parts of the Precordillera *s.s.* (Gualcamayo Formation) but at the Early Llanvirn in the central and northern region (Gualcamayo and Los Azules Formations; Fig. 2.2). Locally, the carbonate sedimentation persisted even until the Late Llanvirn to Caradoc. The transition from carbonates to black shales was controlled by a rising sea level and ash fall-out, now preserved as K-bentonites (Huff *et al.*, 1998; 2003; Carrera and Astini, 1998).

Based on Astini (1991), the sedimentary deposits of the Precordillera *s.s.* can be subdivided into two synchronic tectofacies (Figs. 2.2 and 2.3) due to differences in deposition, deformation and metamorphism during the Lower Palaeozoic. The Eastern tectofacies was deposited in a shallow basin. It is characterized by a carbonate platform

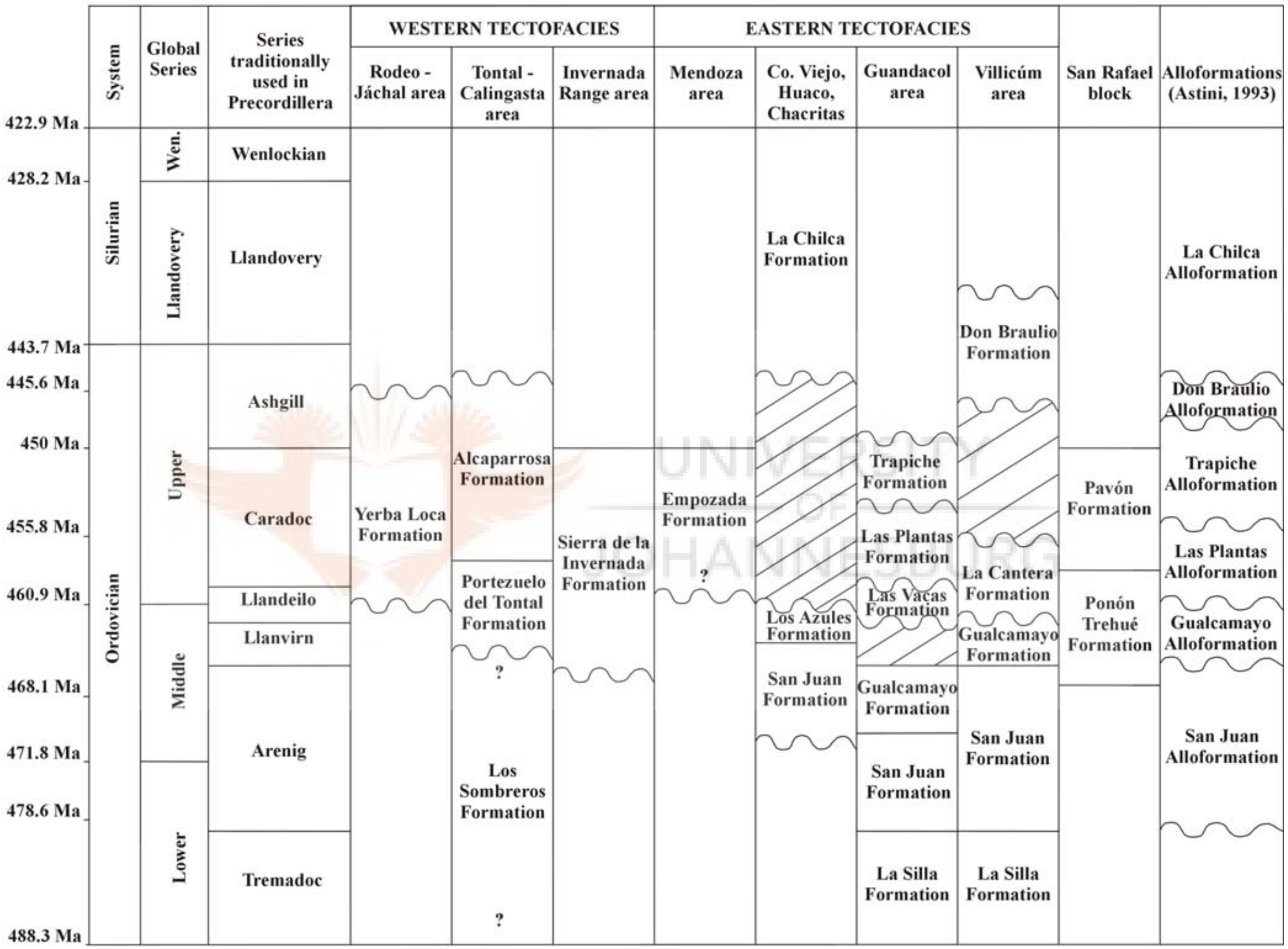

Figure 2.2: Stratigraphy of the Ordovician of the Precordillera terrane based on Keller (1999). The distribution of alloformations is according to Astini (1993a). Absolute ages are as recommended by Gradstein *et al.* (2004). Except for the La Silla and San Juan Formations, all these units were studied. Diagonal lines indicate hiatuses.

(San Juan Formation) and black shales (Gualcamayo and Los Azules Formations), that are followed by conglomerates and turbidite-type sequences deposited within a clastic-wedge (Las Vacas, La Cantera, Las Plantas and Trapiche Formations). Two units record the Ordovician – Silurian transition and are composed of diamictites from the Hirnantian ice age (Don Braulio Formation) and platform clastic deposits (La Chilca Formation). Based on sequence stratigraphy, the Eastern tectofacies can be simplified into six stratigraphic units separated by discontinuities (alloformations; Astini, 1993a). These units are named: San Juan, Gualcamayo, Las Plantas, Trapiche, Don Braulio and La Chilca Alloformations, and their time spans are showed in Figure 2.2.

Towards the west, two structurally complex olistostromic units represent the slope-type deposits: the Empozada (Eastern tectofacies) and the Los Sombreros Formations (Western tectofacies; Figs. 2.2 and 2.3). Peralta (2005) and Peralta and Heredia (2005), reinterpreted the Los Sombreros Formation as a Devonian sedimentary mélange formed in response to an extensional regime (rift–type basin). They include all the deposits exposed from north of the Río Jáchal to the San Isidro area in Mendoza (Fig. 2.3). The Devonian age is determined based on the composition of certain olistoliths that resemble Devonian units (Peralta, 2005; Peralta and Heredia, 2005). Nevertheless, according to their graptolite contents, the matrix-layers of the olistostrome sampled for the present study are undoubtedly of Ordovician age, and therefore only the outcrops sampled are draw in the map as the slope-type deposits (diagonal dark-grey lines of Fig. 2.3).

The Western tectofacies (Astini, 1991) was deposited in a deep-sea basin with high subsidence and sedimentation rates and is characterized by turbidite successions overprinted by regional low-grade metamorphism. The Western tectofacies cannot be analyzed in terms of sequence stratigraphy because it is folded and affected by low-grade metamorphism (Astini, 1993a). However, a simplified stratigraphy in ascending order involves the Los Sombreros, Yerba Loca (and its southern continuations, the Sierra de la Invernada and Portezuelo del Tontal Formations), and Alcaparrosa Formations. This Western basin was parallel to and mainly coeval to the Eastern tectofacies (Figs. 2.2 and

Figure 2.3: Exposures of the Eastern and Western tectofacies within the Precordillera *s.s.* Diagonal dark grey lines denote the slope-type outcrops sampled, whereas the slope-type deposits as defined by Peralta (2005) are comprised within the dashed line. IR: Invernada Range; dTR: del Tigre Range; dlTR: de la Tranca Range; YLR: Yerba Loca Range; TR: Talacasto Range; TtR: Tontal Range; CZR: Chica de Zonda Range; VR: Villicúm Range. Modified after Astini (1991).

2.3), and it is characterized by the presence of mafic to ultramafic rocks interlayered and intruded within the clastic record.

The Ordovician sequences (Fig. 2.2) can be subdivided in terms of eustatic sea level changes into three cycles separated by discontinuities (Beresi, 1990; 1992). Cycle I is characterized by a carbonate platform deposition and its corresponding carbonate - clastic slope existing from Cambrian to Llanvirn times and formed by a relative rise in sea level. The unconformity that separates Cycles I and II is assigned to the Guandacol Phase and it is related to a sea level lowstand during the Llanvirn - Caradoc. The *Nemagraptus gracilis* Biozone (Caradoc) marks the end of the Cycle II clastic deposition. Cycle III (Ashgill – Llandovery) represents a rising sea level that lead to the deposition of clastic sediments containing the typical Hirnantia fauna. The massive global extinction during the Ashgill is also recorded at the Precordillera *s.s.* by the extinction of the Hirnantia fauna (Sánchez *et al.*, 1993). However, Astini and Thomas (1999) suggested that deposition during the Middle and Upper Ordovician was mainly controlled by tectonism (horst and graben structures) rather than by eustatic sea level changes.

The series of discontinuous outcrops of mafic and ultramafic rocks (here named as Western Precordillera Belt) were initially assigned to the 'Famatinian Ophiolite' sequence (Haller and Ramos, 1984), and were interpreted as the suture between the Chilenia and the Cuyania composite terranes (Ramos *et al.*, 1986). However, detailed studies carried out by Davis *et al.* (1999) showed the presence of a number of ophiolite-like units with ages ranging from Middle Proterozoic to Early Palaeozoic and juxtaposed in the Early to Middle Devonian.

Although the rocks of the Western Precordillera Belt were formed in different extensional settings and at different times (Davis *et al.*, 1999; 2000), most of them have initial ε_{Nd} values ranging from +6 to +9 (Kay *et al.*, 2005) and were interpreted as E-MORB related based on chemical grounds (e.g. Kay *et al.*, 1984). The northern part of the Western Precordillera Belt was interpreted as a segment of a transitional to plume-type mid-ocean ridge or unevolved back-arc basalts whereas the southern part has a within plate origin or a plume or plateau setting (Ramos *et al.*, 2000 and references therein).

The Silurian of the Precordillera is generally characterized by clastic sedimentary rocks (upper part of the La Chilca Formation, Los Espejos, Tambolar, Calingasta, Mogotes Negros and Rinconada Formations), deposited on a continental platform and at an abyssal plain (Baldis *et al.*, 1982). The Devonian was also deposited in a marine environment but the successions correspond to two different sedimentary cycles. The first cycle shows characteristics of a stable platform, while submarine fans represent the second one (Punta Negra, Cerro Lojote and Villavicencio Formations; Baldis *et al.*, 1984).

The Upper Palaeozoic is separated from the previous rocks by a regional unconformity. The Paganzo Group comprise Carboniferous to Permian continental, glacial-marine and marine deposits, while continental sedimentary and volcanic rocks characterize the Permo-Triassic (compilation in Baldis *et al.*, 1982). During a long period during the Mesozoic, the Precordillera acted as a positive area providing sediment to marginal basins. Two main sedimentary basins (Bermejo and Uspallata) were developed during the Triassic (compilation in Baldis *et al.*, 1982). The Tertiary sequences are mainly composed of alluvial sediments (Peralta, 2003a) with minor extrusive and subvolcanic rocks (Baldis *et al.*, 1984).

2.3.2 San Rafael block

The basement of the San Rafael block (Fig. 2.4) is known as the Cerro La Ventana Formation and consists of mafic to intermediate gneisses, quartz-diorites, diorites, tonalites, amphibolites and migmatites (Cingolani and Varela, 1999). Rb-Sr as well as U-Pb geochronological methods indicate a Mesoproterozoic crystallization age (Cingolani and Varela, 1999; Thomas and Astini, 1999; Cingolani *et al.*, 2005a). The basement is partially covered by carbonate-siliciclastic sedimentary rocks bearing Ordovician fossils (Nuñez, 1979; Bordonaro, 1999) defined as the Ponón Trehué and Pavón Formations. The former is biostratigraphically equivalent to the carbonate platform of the Precordillera *s.s.*, while the latter is correlated to Caradoc clastic units of the Precordillera *s.s.* such as the

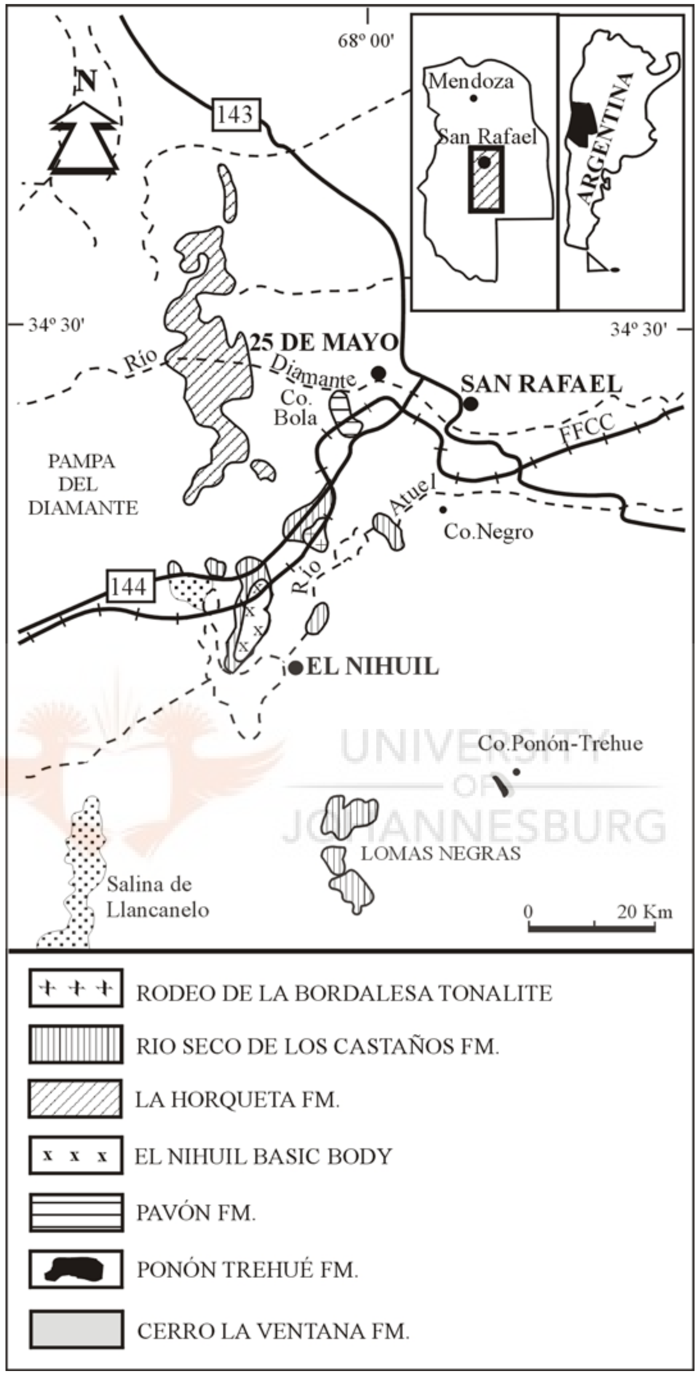

Figure 2.4: Pre-Carboniferous geology of the San Rafael block, Precordillera terrane. Modified from Cingolani *et al.* (2003a).

Empozada, Portezuelo del Tontal, Sierra de la Invernada, Las Plantas and La Cantera Formations (Cingolani *et al.*, 2003a). The El Nihuil Basic body (Fig. 2.4) consists of deformed gabbros and tonalites intruded by dolerite dykes, and contains ultramafic differentiates associated with tholeiitic diabases (Cingolani *et al.*, 2000). This intrusive body is Pre- to Upper-Ordovician in age and displays MORB-geochemical characteristics (Cingolani *et al.*, 2000). As the San Rafael block is interpreted as a southern continuation of the Precordillera *s.s.*, hence this basic body is inferred to be the southernmost part of the Western Precordillera Belt (Cingolani *et al.*, 2000).

The Ordovician deposits are followed by siliciclastic Silurian turbidites (La Horqueta Formation) intruded by an Early Devonian tonalitic to granodioritic body (Rodeo de la Bordalesa; Cingolani *et al.*, 2003b). The Río Seco de los Castaños Formation is a Late Silurian to Early Devonian (González Díaz, 1981; Poiré *et al.*, 2002) shallow water sequence. From the Carboniferous to the Permian the geological record is characterized by sedimentary and volcaniclastic deposits (e.g. the El Imperial, Agua Escondida and Carapacha Formations), which occur above a regional unconformity. The Permian to Triassic time is represented by a felsic magmatic event, generally known as Choiyoi or Cochicó Groups, which includes intrusive rocks (e.g. Agua de la Chilena Stock; Cingolani *et al.*, 2005b) as well as volcaniclastics deposits.

The San Rafael block is a key area for the western margin of Gondwana, and in particular regarding the origin and tectonic evolution of the Precordillera terrane, as it is the only place where the Ordovician sedimentation (Ponón Trehué Formation) was directly deposited over Precordilleran basement rocks of the Cerro La Ventana Formation (Criado Roqué, 1972; Heredia, 2002; 2006).

2.3.3 Other regions belonging to the Precordillera terrane

As new data (e.g. Casquet *et al.*, 2001) allow the link between some other Grenvillian-type basement rocks (for instance a part of the Western Pampeanas Ranges and the Las Matras block) and the Precordillera to be considered as forming the same exotic-to-Gondwana terrane, their geological records are briefly described here. These areas, in particular their pre-Ordovician rocks, are important as potential source areas for the Ordovician to Silurian clastic record of the Precordillera terrane.

The Pie de Palo Range (Fig. 2.1b), is a top-to-the-west imbricate ductile thrust system composed of Grenvillian-age medium to high grade metamorphic rocks of the Pie de Palo Complex (Ramos and Vujovich, 2000; Vujovich *et al.*, 2004), the Neoproterozoic metasedimentary Difunta Correa unit (Baldo *et al.*, 1998; Galindo *et al.*, 2004) and the Caucete Group (Borrello, 1969). The metamorphic Caucete Group is composed of the El Quemado Quartzite, La Paz Formation, El Desecho Formation and the Angaco Limestone (marbles and carbonate-schists) in stratigraphic order (Vujovich, 2003). The Caucete Group is considered to be the metamorphosed (greenschist facies) equivalent of the Palaeozoic cover of the Precordillera terrane (Vujovich and Kay, 1998; Naipauer *et al.*, 2005a).

U-Pb SHRIMP data on nine detrital zircon cores from schists belonging to the Difunta Correa metasedimentary sequence indicate a crystallization age for the zircons of 1.03 to 1.22 Ga and a metamorphic overprint (probably associated with the ductile thrusting) at 460 Ma (Casquet *et al.*, 2001). Therefore, the schists were eroded from a Grenvillian-age basement and probably represent the oldest (Neoproterozoic) sedimentary cover to the basement of the Precordillera terrane (Casquet *et al.*, 2001). Zircon age dating using LA-ICP-MS of 163 concordant grains from El Quemado Quartzite of the Caucete Group comprise two main zircon populations with ages of 1040 to 1228 Ma and 1289 to 1492 Ma respectively, while any Ordovician zircons are absent and only few Cambrian-Neoproterozoic grains (dominant peak between 532 and 697 Ma) were found (Naipauer *et al.*, 2005a).

Conventional U-Pb and SHRIMP zircon analyses from intrusive and metasedimentary rocks of the Pie de Palo Complex indicate a Mesoproterozoic age with a peak around 1.2 Ga (Vujovich *et al.*, 2004). A thermal event during the Middle Ordovician (455-470 Ma) was recognized in dated zircon rims, and interpreted as due to the collision of Cuyania against Gondwana (Vujovich *et al.*, 2004).

Early Ordovician (Famatinian) magmatic activity is described from the Pie de Palo Range. El Indio and Difunta Correa plutons with U-Pb SHRIMP crystallization ages of 481±6 Ma and 470±10 Ma respectively are interpreted as emplaced in an upper plate setting, therefore in contradiction to the interpretation of the Pie de Palo Range as the Precordilleran basement (Baldo *et al.*, 2005). A better knowledge of magma genesis and tectonic setting of emplacement are still needed.

Other areas, which are debated as part of the Precordillera terrane are, the Umango, Maz and Espinal Ranges that probably constitute the northernmost basement outcrops of the Precordillera terrane (Fig. 2.1b). These rocks underwent medium to high amphibolite facies metamorphism. At the Maz and Espinal Ranges, the basement is represented by: i) El Taco Complex, composed of marbles, calc-silicate rocks and quartz-mica schists, associated with amphibolites and ultramafic rocks (Porcher *et al.*, 2004). The ultramafic rocks have a typical magmatic arc signature (Vujovich *et al.*, 2005). ii) Maz Complex, composed by metapelites and metasandstones (muscovite-biotite schists, graphite schists, quartz-rich gneisses and quartzites) associated with amphibolites, metagabbros and metatonalites (Porcher *et al.*, 2004). All these rocks were interpreted as formed in different tectonic environments ranging from intraplate to magmatic arc settings (Vujovich *et al.*, 2005). iii) El Zaino Complex, composed of metasandstones, metapelites and metacalc-silicate rocks (schists), amphibolites and marbles (Porcher *et al.*, 2004).

The Umango Range comprises tonalitic to granitic orthogneisses associated with metamorphosed mafic rocks (Porcher *et al.*, 2004), that represent the root of a magmatic arc (Vujovich *et al.*, 2001), and a metasedimentary sequence associated to amphibolites and few gneisses and pegmatites (Porcher *et al.*, 2004). The last mentioned sequence was interpreted as shelf sediments deposited on a cratonic basement of Middle Proterozoic age (Varela *et al.*, 2001). The geochemical signature of the amphibolites indicates intraplate alkaline magmatism (Vujovich *et al.*, 2005). The El Peñón Granite intruded the metamorphic basement at 473 Ma (Varela *et al.*, 2003). There are also Devonian granitic intrusions (e.g. Guandacolinos and Veladeros; Cingolani *et al.*, 1993; Varela *et al.*, 1996).

The Las Matras pluton (Las Matras block), belongs to the basement of the Precordillera terrane (Sato *et al.*, 2004). It represents a TTG (trondhjemite-tonalite-granodiorite) association with a continental and island arc signature, with crystallization ages of about 1.2 Ga (zircon conventional method), T_{DM} model ages of 1.6 Ga and ε_{Nd} (t) = +1.6 to +2.1. The Las Matras block is the southernmost extension of the Precordilleran terrane (Sato *et al.*, 2004).

2.4 STRUCTURAL GEOLOGY

2.4.1 Precordillera *s.s.*

Ordovician tectonic movements were responsible for the deposition of two well-developed conglomerates within the Eastern tectofacies of the Precordillera terrane. The oldest one corresponds to the Middle Ordovician Las Vacas Formation (Fig. 2.2), which resulted from the Guandacol Orogenic Phase (Furque and Cuerda, 1979). The Villicúm Orogenic Phase (Baldis *et al.*, 1982) produced the conglomerate developed in between the La Cantera and Don Braulio Formations during the Late Ordovician.

During Late Silurian to Early Devonian, compressive tectonism resulted in very low-grade metamorphism and deformation (folding and penetrative cleavage) that affected the Western tectofacies, while the Eastern tectofacies suffered distension (von Gosen and Buggisch, 1992; Astini *et al.*, 1996). During Middle Devonian to Early Carboniferous, block faulting occurred due to the Chanic Orogenic Phase (Astini *et al.*, 1996).

The Precordillera *s.s.* was affected by the compressive Andean Orogenic Phase, developing a thrusted and folded structure during the Late Tertiary with an estimated shortening of 50% (von Gosen, 1992).

2.4.2 San Rafael block

A major compressional deformation event affected this block, although the timing spans from Silurian to Carboniferous times and was preliminary assigned to the Chanic Phase (Cingolani *et al.*, 1999). The San Rafaelic tectonic phase affected the block during the Lower Permian. During the Cenozoic, it acquired its south southeast-north northwest structural trend related to faulting that uplifted the San Rafael block.

2.5 METAMORPHISM

2.5.1 Precordillera *s.s.*

The metamorphism that affected Early Palaeozoic units from the Precordillera *s.s.* was studied by several authors (Keller *et al.*, 1993; Buggisch *et al.*, 1993; Voldman and Albanesi, 2005; Robinson *et al.*, 2005). Voldman and Albanesi (2005), based on Conodonts Alteration Index (CAI) established that the CAI values increase westwards and southwards from diagenesis to very low-grade metamorphism. Accompanying this distribution, the development of slaty cleavage and quartz recrystallization can be seen. The metamorphism was dated by K-Ar method on micas and shows a pre-Carboniferous, probably Silurian to Early Devonian age (Varela, 1973; Buggisch *et al.*, 1993). Using the same tool, Keller *et al.* (1993) established low-grade metamorphic conditions for the western part of the Precordillera *s.s.* in agreement with illite crystallinity data (Buggisch *et al.*, 1993). The low-grade metamorphism is difficult to interpret in the context of collisional events, particularly in the eastern part of the Precordillera terrane.

Using microprobe techniques on metamorphic minerals, Robinson *et al.* (2005) determined a low-grade metamorphism in metabasites from the Yerba Loca and Alcaparrosa Formations (pillow lavas and mafic lavas of the Western Precordillera Belt). This coincides with results from Rubinstein *et al.* (1995), who deciphered lower greenschist facies conditions for the Alcaparrosa Formation of the Western tectofacies. The metamorphism in the metabasites is related to the collision of Chilenia with the Precordillera during early Devonian times and not to ocean floor processes (Robinson *et al.*, 2005).

2.5.2 San Rafael block

The Ordovician clastic record (Pavón Formation) shows very low-grade metamorphic conditions determined using the illite crystallinity index (Cingolani *et al.*, 2003a). The rocks developed cleavage, deformation and siliceous recrystallization (Cingolani *et al.*, 2003a). In contrast, the Silurian strata (La Horqueta Formation) were affected by biotite grade greenschist facies regional metamorphism during the Devonian according to whole rock Rb-Sr method (Tickyj *et al.*, 2001). The Río Seco de los Castaños Formation was overprinted by very low-grade metamorphism (Cingolani *et al.*, unpublished). The Grenville-aged basement reached amphibolite facies although the age of the superimposed metamorphism is unknown (Cingolani and Varela, 1999).

2.6 PREVIOUS PROVENANCE STUDIES

2.6.1 Precordillera *s.s.*

According to Loske (1993; 1994), the modal analyses as well as the geochemistry of Cambrian to Carboniferous rocks of the Precordillera showed a retro-arc tectonic setting with a variable influence from continental or arc sources. The heavy mineral content is characterized by zircon, tourmaline and rutile for the Cambrian to Silurian rocks, while it is more variable for the Devonian to Carboniferous interval (e.g. apatite, epidote, garnet, titanite and zoisite; Loske, 1994). Detrital mode analyses of several Ordovician and Devonian sandstones indicate a continental passive margin setting, while some Devonian rocks indicate a dissected arc provenance (Loske, 1994).

A provenance from a recycled-orogen source was deduced for the synorogenic Ordovician clastic wedge from the Eastern Precordillera (Las Vacas, Las Plantas, Trapiche and La Cantera Formations) and for the Western tectofacies (Astini, 1991) based on petrography. The only palinspastically-restored palaeocurrents mentioned in the literature are those for the La Cantera Formation, which indicates north to south and northwest to southeast directions (Peralta, 1993 in Gleason *et al.*, 2006). Other measurements indicate palaeocurrents mainly towards the west and northwest for the Las Vacas, Trapiche, Don Braulio, Empozada, Los Sombreros, Portezuelo del Tontal, Alcaparrosa and Sierra de la Invernada Formations (Cingolani *et al.*, 1986; Spalletti *et al.*, 1989; Banchig *et al.*, 1993; Astini and Buggisch, 1993; Astini, 1994a; Astini *et al.*, 1996; Heredia and Gallardo, 1996; Astini, 1998a; Astini *et al.*, 2000). However, some units show a 120º dispersion (e.g. Las Vacas and Portezuelo del Tontal Formations; Spalletti *et al.*, 1989; Astini, 1998b), and others show directions towards the south (La Chilca Formation; Astini and Maretto, 1993). In the case of the Portezuelo del Tontal Formation the dispersion in palaeocurrents is due to the deposition as a deep-sea fan system (Spalletti *et al.*, 1989). However, the latter mentioned unit along with the Yerba Loca and Sierra de la Invernada Formations are also interpreted as storm dominated shallow marine shelf deposits with palaeocurrents from north to south according to Basilici *et al.* (2005).

Detrital zircon dating on the La Cantera, Las Vacas and Empozada Formations shows a large Mesoproterozoic population (Finney *et al.*, 2003a; Gleason *et al.*, 2006). Zircons of Neoproterozoic and Early Palaeozoic age are rare, whereas no zircon ages contemporaneous with the magmatic rocks of the Famatina System were found (Finney *et al.*, 2003b; Gleason *et al.*, 2006). A para-autochthonous model propose that the Lower Palaeozoic sequences of the Precordillera were deposited within a pull-apart extensional basin developed along the transcurrent fault that transported the Precordillera to its present position adjacent to the Famatina Range (Finney *et al.*, 2003c).

Gleason *et al.* (2006) presented Nd and Pb isotope data from Precordilleran graptolite-rich shales of Middle to Upper Ordovician ages. The T_{DM} ages and the Pb-Pb isotopes on whole-rocks are similar to those found in the basement and the overlying Palaeozoic sedimentary rocks of northwest Argentina (Bock *et al.*, 2000; Lucassen *et al.*, 2000; Zimmermann and Bahlburg, 2003). Furthermore, Pb isotopes are substantially different from values obtained in the xenoliths from the basement of the Precordillera as well as those from the Pie de Palo Range (Kay *et al.*, 1996).

The provenance for the Silurian to Devonian rocks came from a basement located to the northeast and east, but some source from the west could also have been active particularly during Devonian times (Astini *et al.*, 1995). The Ordovician to Silurian Don Braulio Formation and the Silurian Los Espejos Formation were linked to a continental magmatic arc source (Abre *et al.*, 2005).

2.6.2 San Rafael block

Petrographic provenance analysis on the Upper Ordovician record (Pavón Formation) indicates a recycled orogen and a continental block as the main source areas (Manassero *et al.*, 1999). Geochemical data demonstrated that the Pavón Formation displays detrital components of an upper continental crust composition mixed with a less fractionated component (Cingolani *et al.*, 2003a). The general character of the less fractionated source was interpreted as related to ocean floor and continental flood basalts (Abre *et al.*, 2005; submitted). T_{DM} ages are in the range 1.4 and 1.5 Ga (Cingolani *et al.*, 2003a), coincidently to the underlying basement rocks of the Cerro La Ventana Formation (Cingolani *et al.*, 2005a). Palaeocurrents indicate source areas located towards east (Manassero *et al.*, 1999).

Modal analyses on arenites from Devonian rocks (Río Seco de los Castaños Formation) also indicate recycled orogen and/or continental block as a source (Manassero *et al.*, 2005).

2.7 ORDOVICIAN NOMENCLATURE

Scientists that have been studying the Precordillera for decades have mainly followed the Traditional British Series for the Ordovician. These Series were redefined by Fortey *et al.* (1995; see Fig. 2.5). However, the British Series cannot be used worldwide and the Subcommission on Ordovician Stratigraphy of the International Commission on Stratigraphy (ICS) is developing a standard set of Global Series and Stages for the Ordovician System (Finney, 2005). Figure 2.5 shows the Traditional, and the Regional

British Series and their correlation to the developing and newly defined Series and Stages according to the ICS. In the present thesis, the ages of the units were kept as defined by the correspondent authors and Figure 2.5 can be used to compare them with the new but still unapproved Global proposal.

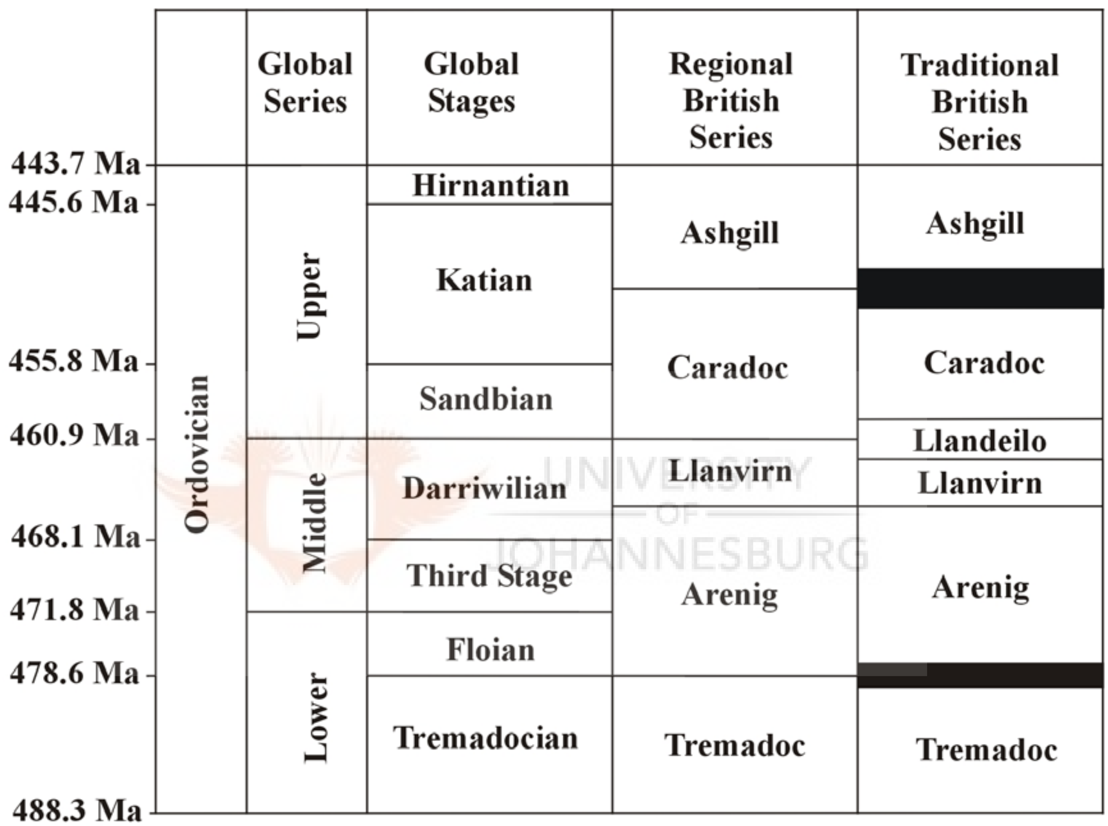

Figure 2.5: Ordovician stratigraphic nomenclature traditionally used in the Precordillera terrane (Traditional British Series) and its equivalents according to Fortey *et al.* (1995), Finney (2005) and the International Commission on Stratigraphy, Subcommision on Ordovician (2006).

2.8 EVIDENCE OF ALLOCHTHONY

The starting-point to consider the Precordillera an allochthonous terrane is the fact that there is no lithostratigraphic continuity between the Precordillera and neighbouring areas (e.g. Famatina System and Pampeanas Ranges) at least until the Upper Palaeozoic (Carboniferous) when continental sediments (e.g. the Paganzo basin) covered the Precordillera and surrounding areas, indicating that this part of Gondwana was already assembled. Several arguments (basement characteristics, stratigraphy, palaeontological record, K-bentonites and palaeomagnetism) were used to determine a Laurentian or Gondwanan origin for the Precordillera terrane. The analyses and interpretation of all these evidence allowed several authors to model the tectonic evolution of the Precordillera terrane. A summary of the different models proposed follow after a compilation of the more remarkable evidence used to base them.

2.8.1 Basement

As briefly described above, Grenvillian ages and a lead isotope signature typical of the Laurentian Grenville belt (Abruzzi *et al.*, 1993; McDonough *et al.*, 1993; Kay *et al.*, 1996) characterize the basement of the Precordillera known from xenoliths. This basement is geochemically similar to the basement of the Llano uplift at the Texas promontory of Laurentia (Fig. 2.6; Thomas and Astini, 1996). Although Middle Proterozoic ages can be found within Gondwana, they are associated with Late Proterozoic ages (Brasiliano) and they have a distinctive Pb isotopic signature (Ramos, 2004). However, most of the outcrops assigned to the basement of the Precordillera are debated, as discussed above. The strongest evidence is therefore given by the xenoliths (Abruzzi *et al.*, 1993; Kay *et al.*, 1996). The Cerro La Ventana Formation has been recently accepted as the basement of the Precordillera terrane within the San Rafael block. It is similar to the Laurentian Grenville basement regarding crystallization ages and Sm-Nd juvenile signatures (Cingolani *et al.*, 2005a).

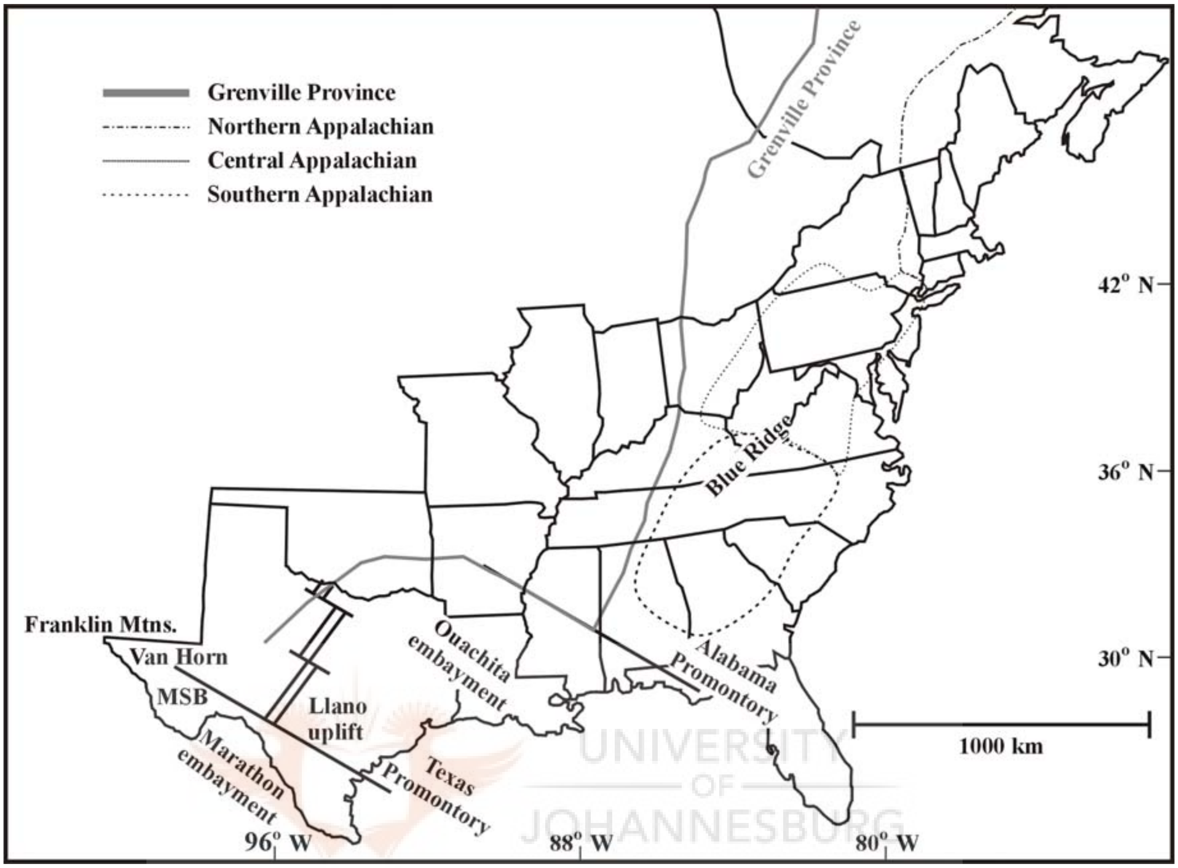

Figure 2.6: Main features from North America mentioned in the text. Compiled from Thomas (1991); Fail (1998); Keller (1999) and Bickford *et al.* (2000). The Early Palaeozoic rifted margin is represented by the Ouachita and Marathon embayments and by the Texas and Alabama Promontories.

2.8.2 Stratigraphy

Bond *et al.* (1984) compared the tectonic subsidence histories of both Precordillera and Appalachia and concluded, based on their similarities, that both could have had the same origin. Thomas (1976; 1991) noted that a crustal fragment is missing from the Ouachita Embayment (Fig. 2.6) and that can coincide with the proposed Precordillera terrane, which could be separated from the embayment after the Arenig, according to the dissimilarity in age-distribution of the K-bentonites layers in both areas (Kolata *et al.*, 1994; Huff *et al.*, 1995).

The stratigraphy of the Precordillera *s.s.* and Appalachia are similar, in particular regarding to lithostratigraphy, thickness and faunal assemblages (Astini *et al.*, 1995). The similarities match better with the southern Appalachians (Fig. 2.6; Tennessee-Alabama), from which the Precordillera was separated due to the effect of the Oklahoma-Alabama transcurrent fault (Fig. 2.6; Thomas, 1991).

Keller and Dickerson (1996) compared the Cambrian-Ordovician Precordillera *s.s.* basin with the Marathon Solitario Basin (MSB; West Texas; see Fig. 2.6) and found that the Precordillera could represent the missing continent of Llanoria that has shed detritus into the MSB, supporting the hypotheses of proximity between Precordillera and Laurentia during Early-Middle Ordovician. The presence of felsic volcaniclastic detritus and bimodal palaeocurrents support the idea of a missing landmass located to the east and southeast of the MSB and named Llanoria. The western margin of the Precordillera documents activity of extensional faults from Late Cambrian onwards, while the MSB underwent synsedimentary extension and block faulting of its platform succession.

Benedetto (1993) compared the Precordillera *s.s.* with the central and south Appalachia (West Terranova) and concluded that stratigraphically and biogeographically these two areas are similar for the period Cambrian-Early Ordovician (Arenig). The carbonate platform represents the conjugate margin of Eastern Laurentia. Palaeontological affinities between the Precordillera and Gondwana (e.g. Suri Formation of the Famatina System; Fig. 2.1a) suggest proximity of these two areas since Middle to Late Arenig.

The model of an allochthonous Precordillera terrane that collided with Gondwana implies the development of a foreland basin during the Middle to Upper Ordovician (Thomas and Astini, 1996). However, Finney *et al.* (2005) interpreted the Middle-Upper Ordovician stratigraphy of the Precordillera terrane and its basin asymmetry, subsidence rate, facies changes and unconformities as controlled by a set of strike-slip (pull apart) basins developed along a transform fault. Nevertheless, in this scenario, it is difficult to explain the geological differences between the Precordillera terrane and the subsequent adjacent areas that would had been in contact with it. This subject was intensely discussed by several authors (Ramos, 1988; Aceñolaza and Toselli, 1988; Baldis *et al.*, 1989, Aceñolaza *et al.*, 2002; Ramos, 2004; Finney, 2007 among others).

2.8.3 Palaeontology

The faunal content of the Precordillera terrane varies from completely typical Laurentian forms in the Cambrian to typically Gondwanan in the Late Ordovician to Early Silurian (Benedetto *et al.*, 1999). Regarding trilobites, the ollenelid Cambrian forms are endemic to Laurentia and more similar to equivalent forms from Southern Appalachia (Vaccari, 1994). During the Lower and Middle Ordovician the trilobites show a mixture of Laurentian, Baltic and pandemic genera, but from the Llanvirn on, the genera are more likely cosmopolitan. The same pattern of changes in faunal provenance is shown by conodonts. Brachiopods show mixed assemblages during the Lower Ordovician (Toquima – Table Head, Celtic and Baltic provinces). They are Hirnantian-like for the Ashgill but are undoubtedly related to Gondwana from the Silurian onwards, when the *Clarkeia* fauna was developed (Benedetto, 2004). The Celtic fauna has never been found in Laurentian sequences with the exception of the intra-Iapetus island arcs of Newfoundland, Maine and New Brunswick.

A previously unknown fossil from Gondwana (*Salterella*) was described from a Cambrian olistolith within the Los Sombreros Formation, reinforcing the idea of a Cambrian link between the Precordillera and Laurentia (Astini *et al.*, 2004). However, larvae transported via ‘favourable’ oceanic currents could explain the presence of Laurentian faunas within Gondwana, particularly in those models that postulate a para-autochthonous origin of the Precordillera. Moreover, the interpretation of the faunal content in terms of percentages instead of numbers of genera can mislead interpretations (Finney, 2007).

2.8.4 K-bentonites

The presence of Arenig-Llanvirn K-bentonites (altered volcanic ash) in both, Appalachia (Marathon/Solitario basin at the Ouachita embayment) and Precordillera *s.s.* initially supported the connection for the Early Palaeozoic between Precordillera and Laurentia (Keller and Dickerson, 1996). However, the K-bentonites from the Precordillera terrane (interlayered within the upper part of the San Juan Formation and lower part of the Gualcamayo Formation; Huff *et al.*, 1995; 1998; 2003) are contemporaneous with the volcanism from the Famatinian belt, active at about 470 Ma (Baldo *et al.*, 2003). If the Famatinian arc were the source of this ash, it would imply that the Precordillera was close enough to it by the Early Arenig (Fanning *et al.*, 2004) or Middle Arenig (Astini *et al.*, 2006), although ash can be transport thousands of kilometres as modern examples demonstrate. Furthermore, Huff *et al.* (2003) had demonstrated that Precordilleran K-bentonites differ substantially from those from Laurentia (North America), implying different tectonomagmatic histories for both. The presence of Early Arenig K-bentonites within the Famatinian deposits that have no correlation within the Precordillera terrane deposits imply that the volcanism within the Famatina arc started before the arrival of the Precordillera terrane in the Middle Ordovician (Pankhurst *et al.*, 1998; Astini *et al.*, 2006).

A K-bentonite level was also reported from limestones (San Jorge Formation) within the Las Matras block (Tickyj *et al.*, 2003).

2.8.5 Palaeomagnetism

The effects of at least two remagnetization events (a Recent one and a more regional event associated to the Permian Sanrafaelic Tectonic Phase) did not allow the determination of a palaeomagnetic pole or original magnetization of several units within the Precordillera terrane (Rapalini and Tarling, 1993; Rapalini, 1996).

However, two palaeopoles were obtained from the Precordillera terrane. The Cambrian one obtained from the Cerro Totora Formation at the Precordillera *s.s.* coincides with the Laurentian palaeopole and wander-path for that age if the Precordillera terrane was situated within the Ouachita embayment (Rapalini and Astini, 1998). Palaeomagnetic data do not rule out the possibility that during the Early Cambrian, the Precordillera was at its present location with respect to South America, although geological differences are against a side-by-side relation as explained above. The Upper Ordovician palaeopole (obtained from the Pavón Formation, San Rafael block) is also consistent with the Laurentian one for the same period of time (Rapalini and Cingolani, 2004). This palaeopole could be interpreted as either the Precordillera remained attached to Laurentia (probably the Texas plateau) until the Caradoc, as recording the last stages of approximation of Precordillera to Gondwana or as already accreted to Gondwana by the Caradoc if a local block rotation is considered (Rapalini and Cingolani, 2004).

2.9 GEOTECTONIC MODELS

Although there is a general agreement on the allochthonous nature of the Precordillera terrane (Penrose Conference 1995), the timing and processes involved in the transfer from Laurentia to Gondwana are still controversial. Thus, some authors still argue against these models and favour an autochthonous or para-autochthonous origin. Aceñolaza *et al.* (2002) pointed out that biogeographical relationships could neither support nor reject any continental reconstruction. Magmatism (K-bentonites), basement geochronology and isotope composition (particularly Pb data) and palaeomagnetic evidence are all still debatable.

2.9.1 Autochthonous models

González Bonorino and González Bonorino (1991) using mainly stratigraphic and sedimentological data, explained the development of the Lower Palaeozoic of the Precordillera as a continental passive margin. These authors also suggest that there is no evidence of a suture zone between the Frontal Cordillera (Fig. 2.1b) and the Precordillera. The tectonic model that explains the sedimentation at the Precordillera from the Cambrian to the Devonian, involves the development of a continental slope during Cambrian times and the deposition of platform and deepwater sediments during the Cambrian and Lower

Ordovician. During the Middle Ordovician, the magmatism at the Pampeanas Ranges heated the crust and produced a distensive pattern at the Precordillera, which in turn provoked the sliding of large carbonate blocks into the internal platform. The extensional thinning (within the passive margin) is the cause for mafic to ultramafic magmatism of the Western Precordillera Belt. During the Silurian, the crust suffered shortening and thickening with a concomitant obduction of ocean floor, magmatism and slight metamorphism of the sedimentary wedge (particularly within the western sequences). However, an autochthonous origin is considered improbable according to current knowledge.

2.9.2 Para-autochthonous models

Baldis *et al.* (1989) suggested that the Precordillera was always part of Gondwana and was transported from the south (present coordinates) by large-scale strike-slip movements (several hundreds to thousands of km) to its later position, implying though a para-autochthonous origin. The evolution of different facies has been controlled by deeply seated megafaults. This movement did not begin before Middle Ordovician and ended during the Devonian.

Aceñolaza and Toselli (1988; 1998) also assumed that the Precordillera was originally located southwards of its present position and was transferred along the palaeopacific margin of Gondwana (together with the Western Pampeanas Ranges) by right-lateral shear movements (500 km displacement) until its present position. It differs from the previous model mainly on considering the Late Silurian to Early Devonian as the more probable time of displacement.

Aceñolaza and Toselli (2000) and Aceñolaza *et al.* (2002), proposed a modification on the Baldis *et al.* (1989) model, where during the Neoproterozoic the Precordillera terrane originated as a platform between South America, Africa and Antarctica (SAFRAN). This is similar to the model of Dalziel (1997), although the latter proposed that the Precordillera was a Laurentian promontory instead of a part of Gondwana

(SAFRAN). As the platform was stable, the development during the Cambrian of thick limestone sequences was possible. The Mozambique belt reopened during the Cambrian generating the rotation of East Gondwana and strike-slip movements along the border of the Precordillera. These displacements ended during Devonian times. This model is in agreement with geological and palaeontological data and explains the allochthonous character of the terrane in the simplest way compared with the rest of the models (Aceñolaza *et al.*, 2002). However, the model neither accounts for the palaeomagnetic data (Astini and Rapalini, 2003) nor explains the faunal similarities between the Precordillera and Laurentia or the faunal differences between the Precordillera and Gondwana (Benedetto, 2004). The strike-slip model cannot explain the deep burial metamorphism undergone by the Pie de Palo Complex during the Middle Ordovician (Vujovich *et al.*, 2004). This model also ignores the different lithostratigraphy between the Precordillera and the Kalahari craton.

Loske (1992; 1993; 1994) interpreted the Precordillera as the southern continuation of the Famatinian retro-arc basin. As in the model of Baldis *et al.* (1989), strike-slip movements were assumed. However, there is no evidence for those movements (von Gosen *et al.*, 1995) and faunas between Famatina and Precordillera are clearly different (i.e. Albanesi and Vaccari, 1994). Later, Loske in collaboration with other authors (Buggisch *et al.*, 2000) agreed that the Precordillera was part of Laurentia. Furthermore, using palaeontology, stratigraphy and heavy mineral analyses, they demonstrated that the Precordillera was attached to Laurentia until the Early Ordovician, then rifted away during Middle Ordovician (extensional tectonic regime), and was close to Gondwana by the Silurian and finally accreted between the Late Silurian and the Middle Carboniferous.

Detrital zircon dating on several Cambrian-Ordovician units from the Precordillera *s.s.* (Cerro Totora, Las Vacas, Empozada and La Cantera Formations), allowed Finney and co-workers Gleason *et al.*, 2001; Peralta *et al.*, 2003a; Finney *et al.*, 2003a; 2003c; 2004; 2005; Gleason *et al.*, 2006) to assign an Early Palaeozoic Gondwanan affinity to the Precordillera terrane. According to their model, the Precordillera terrane was not close to the Famatina System until after the Late Ordovician. Furthermore, they have not linked the subduction-related Famatina magmatic arc to the docking of the Precordillera due to the lack of zircons of that age within the detrital record, proposing instead a Late Ordovician to Devonian age as the time of arrival to its present location. However, the uncertainties regarding palaeomorphology make it difficult to interpret isotopic data in terms of palaeogeography. They explain the similarities in stratigraphy and palaeontological content between Laurentia and Precordillera during the Cambrian and the Ordovician assuming that the Precordillera occupied a northern position in Gondwana as an isolated microcontinent separated by a narrow ocean from Laurentia.

2.9.3 Allochthonous models

Ramos *et al.* (1986; 1993) and Ramos (1988) interpreted the Precordillera as an allochthonous terrane (Cuyania composite terrane). A subduction zone was active towards the west of the Precordillera since the Cambrian, while a passive margin was developed at the eastern margin. During the uppermost Ordovician to Lower Silurian, the ocean ridge (located to the west) subducted, leading to interlayered mafic igneous rocks within clastic sediments. The subduction controlled the sedimentation and deformation until the accretion of Chilenia (Devonian). After the implementation of this new margin, the subduction zone was reinstalled and continued at least until the Triassic. In this model, the limit of the Pampia terrane (Gondwanaland) was located to the west of the Pie de Palo Range during Proterozoic times. The Precordillera was approaching Gondwana due to an eastward subduction (Cambrian to uppermost Ordovician - Lower Silurian) of an oceanic slab beneath the Pampia terrane (Rapela *et al.*, 1990; 1992; Ramos *et al.*, 1993).

Dalla Salda *et al.* (1992a; 1992b; 1993; Dalla Salda, 2005) proposed the existence of the Occidentalia terrane, which includes the Arequipa-Belén-Antofalla Massif, the Mejillones, Chilenia, and Precordillera terranes and the Western Pampeanas Ranges (the Toro Negro, Umango, Maz, Pie de Palo, Valle Fértil and El Gigante Ranges). The Occidentalia terrane is characterized by a Precambrian metamorphic basement (Dalla

Salda *et al.*, 1993) and was originated within eastern Laurentia. The transference of the Occidentalia terrane from Laurentia to its present location involved an extension which opened the Iapetus ocean (Latest Precambrian), a subduction stage along the Gondwana margin (Cambrian) which closed the Iapetus ocean, while at least one island arc (within the Pie de Palo Range) was accreted to the active Gondwana margin (Vujovich and Kay, 1998). A continent collision took place between Laurentia and Gondwana with a climax at c. 460-480 Ma. At the final stage, Laurentia rifted and drifted away during Late Ordovician times leaving attached to Gondwana the Occidentalia terrane (Dalla Salda *et al.* 1992a; 1992b; 1993; Dalziel, 1993; Dalziel *et al.*, 1994). The presence of glacigenic deposits at the end of the Ordovician (Ashgill) indicate that the Precordillera was attached to or at least close to Gondwana (Dalziel *et al.*, 1994). Although Ramos *et al.* (1986) support the idea of an open ocean basin towards west of the terrane, this model assumed an open ocean basin towards the eastern margin of the Occidentalia terrane.

The suture that resulted from that continental collision (Dalla Salda *et al.*, 1992a) is represented by the Ocloyic event of the Famatinian Orogeny (540-330 Ma; Aceñolaza and Toselli, 1976), which includes pre-, syn- and post-tectonic granitoids, high-grade metamorphism and deformation. However, the continent-continent collision is not supported by palaeontological data (e.g. Herrera and Benedetto, 1991). Detailed comparison of sedimentological features (including K-bentonites among others) also support that the Taconic and Ocloyic Orogens were not in continuity (Thomas *et al.,* 2002 and references therein). Furthermore, Tosdal *et al.* (1994) and Tosdal (1996) demonstrated based on Pb isotopes, that at least not all the basement of the Occidentalia terrane was part of Laurentia, because only the Pb signatures from the xenoliths of the Precordillera and a part of the Western Pampeanas Ranges are similar to the Laurentian signature. Bahlburg and Hervé (1997) had also challenged this model because of the lack of Late Ordovician glacial deposits within the Ocloyic Orogen (similar to those found in the Precordillera), and because tectonism within northwestern Argentina was during the Late Ordovician.

Dalziel (1997) proposed that Laurentia was attached to Gondwana, but through the

Laurentian Texas plateau (Precordillera terrane) and formed a supercontinent named Artexia. This supercontinent had a brief history from the Middle Ordovician to Caradoc. The pillow-lavas interlayered with sedimentary rocks of Llandeilo to Caradoc age (Alcaparrosa and Yerba Loca Formations) are interpreted as the evidence for the detachment of Laurentia from Gondwana. The Texas plateau was bounded by transform faults and had been formed during the break-up of Pannotia (latest Neoproterozoic), as a result of the opening of the Iapetus (Dalziel, 1997). This model therefore involved arc-continent collision and ophiolite obduction, followed by Caradoc rifting that separated the two continents leaving a part of the plateau attached to Gondwana. The slope facies of the Western Precordillera are interpreted as due to a rifting process instead of due to the presence of an ocean basin towards west (as in the model presented by Astini *et al.*, 1995 and Thomas and Astini, 1996). Furthermore, it was suggested that this plateau was not derived from within the Ouachita embayment, but originated as a horst block within an extended continental plateau outboard of the Texas margin of the Ouachita embayment (Dalziel, 1997). This model explains the increasing affinities between Precordilleran and Gondwanan faunas but does not account for the increase in the faunal differences between Precordillera and Laurentia (Benedetto, 1998). Moreover, the uses of faunal percentages instead of number of genera can lead to misinterpretations (Finney, 2007). The existence of a marginal plateau seems to be incongruent with clastic deposition interlayered with the Cambrian carbonate platform and furthermore, Caradoc rift-related deposits are not found.

Another model was proposed by Benedetto (1993) and Astini *et al.* (1995) and refined by Thomas and Astini (1996; 1999; 2003), Astini (1998a), Benedetto (1998), Benedetto *et al.* (1999) and Thomas *et al.* (2002). It suggests that before rifting, the Precordillera was placed at the Ouachita embayment and was bounded by the Blue Ridge Rift and the Alabama – Oklahoma transform fault to the north and by the Texas transform fault and Marathon rift to the south (Fig. 2.6; Thomas and Astini, 1996). To the west, it was in continuity with the Texas promontory (Llano uplift) while to the east it was facing an ocean. The action of both the Alabama – Oklahoma transform fault and the Ouachita rift during the opening of the Iapetus ocean (ca. 550 – 570 Ma) had lead to the separation of the Precordillera from Laurentia during the Middle Cambrian. As an independent microcontinent (separated from both, Laurentia and Gondwana for more than 1000 km as indicated by fossil fauna), it drifted across the Iapetus ocean until the Middle Ordovician (ca. 470 Ma) were the fauna content indicates at least less than a 1000 km proximity to Gondwana. During Llanvirn-Llandeilo, an eastward subduction was active leading to the collision (Guandacol Orogenic event) of the Precordillera with Gondwana. At Caradoc-Ashgill times a forebulge was developed, a new foreland basin was formed and glacial sediments were deposited which clearly link the Precordillera to Gondwana. However, assumptions made using faunal content in terms of percentages instead of numbers of genera can mislead interpretations (Finney 2007). Moreover, larvae transported via 'favourable' oceanic currents could explain the presence of Laurentian faunas within Gondwana (Finney, 2007).

The faunal mixing with several associations typical from Avalonia an other intra-Iapetus crustal blocks is clearly explained because the Iapetus ocean also contained these crustal fragments (Thomas and Astini, 1996). The collision of the Precordillera terrane occurred due to the evolution of a subduction zone of the eastern Iapetus crust underneath the western margin of Gondwana (Thomas and Astini, 1996). It was suggested that this was an oblique collision between the Cuyania terrane and the Gondwanan autochthonous (Rapela *et al.*, 1998; Benedetto, 2004). A consequence of an oblique collision could be the transformation of the subduction margin into a strike-slip margin, which displaced the terrane towards the south (Benedetto, 2004). This can explain the diachronous character of the carbonate-platform drowning deposits (Gualcamayo and Los Azules Formations), the northward deepening of the basin and also explains the restriction of a clastic wedge to the northern area of the Precordillera terrane (Guandacol area; Benedetto, 2004).

Keller (1999) also agreed that the Precordillera is an exotic bock separated from Laurentia during Middle to Late Ordovician but accreted to Gondwana during the Silurian-Devonian. Rapela *et al.* (1998) also proposed such age for the collision. The extensional regime during Cambrian times was interpreted as a stretching of the crust that leaved the Precordillera as a marginal-to-Laurentia plateau (Keller, 1999).

In summary, although the Laurentian microcontinent model (Thomas and Astini (1996; 1999; 2003) seems to be the more widely accepted, strong arguments against this model can also be found (e.g. Finney, 2007). A critical evaluation of all evidence is needed as well as an increase of the databases particularly regarding isotopic signatures of probable source areas of the sedimentary Precordilleran successions, to further reconsider, update and/or adapt all the models proposed. The explanation of the tectonic evolution of the Precordillera terrane has to take into account all evidence recorded up today such as the geological record of all probable adjacent areas during the Lower Palaeozoic, metamorphism and deformation style, to mention some.

CHAPTER 3

PROVENANCE ANALYSIS OF ORDOVICIAN AND ORDOVICIAN-SILURIAN CLASTIC UNITS FROM THE EASTERN TECTOFACIES OF THE PRECORDILLERA TERRANE, ARGENTINA.

3.1 INTRODUCTION

Several arguments support the allochthonous models of the Precordillera terrane (Fig. 3.1) as derived from Laurentia (e.g. Ramos *et al.*, 1986; Dalla Salda *et al.*, 1992a; Astini *et al.*, 1995; Keller, 1999), although no agreement regarding the time and type of collision with Gondwana has been reached. Other authors have proposed a para-autochthonous evolution based on biostratigraphical and structural data and on detrital zircon dating, where the Precordillera terrane was displaced along the Pacific margin of Gondwana during Ordovician-Devonian times (e.g. Aceñolaza *et al.*, 2002; Finney *et al.*, 2005). To contribute to the discussion about the tectonic evolution of the Precordillera, a comprehensive provenance study on clastic Ordovician to Silurian units of the Eastern tectofacies of the Precordillera is here presented. The Eastern tectofacies is characterized by a carbonate platform, black shales, conglomerates and turbidite-type sequences, which along with deformation style and absence of metamorphism allowed its separation from the Western tectofacies (Astini, 1991).

The Eastern tectofacies (Astini, 1993a; Fig. 3.2) can be subdivided into six alloformations (which are stratigraphic units separated by discontinuities; Fig. 3.3), known as San Juan, Gualcamayo (Gualcamayo Formation and the lower and middle members of the Los Azules Formation), Las Plantas (Las Plantas, La Cantera and Las Vacas Formations, and the upper member of the Los Azules Formation), Trapiche, Don Braulio (only the lower member of the unit) and La Chilca (La Chilca Formation and the upper member of the Don Braulio Formation) Alloformations. All these units are exposed on the eastern side of the Precordillera *s.s.* (Figs. 3.2 and 3.3), mainly at the Guandacol area (Gualcamayo, Las Vacas, Las Plantas and Trapiche Formations), at the

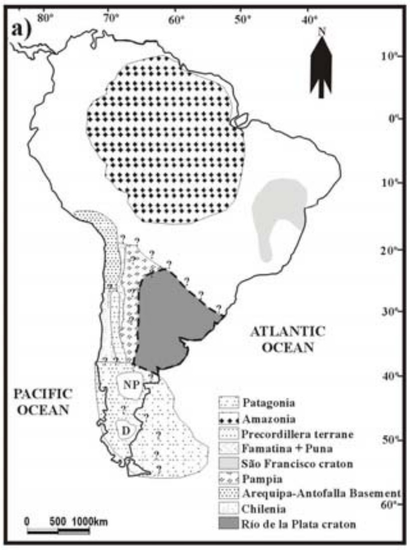

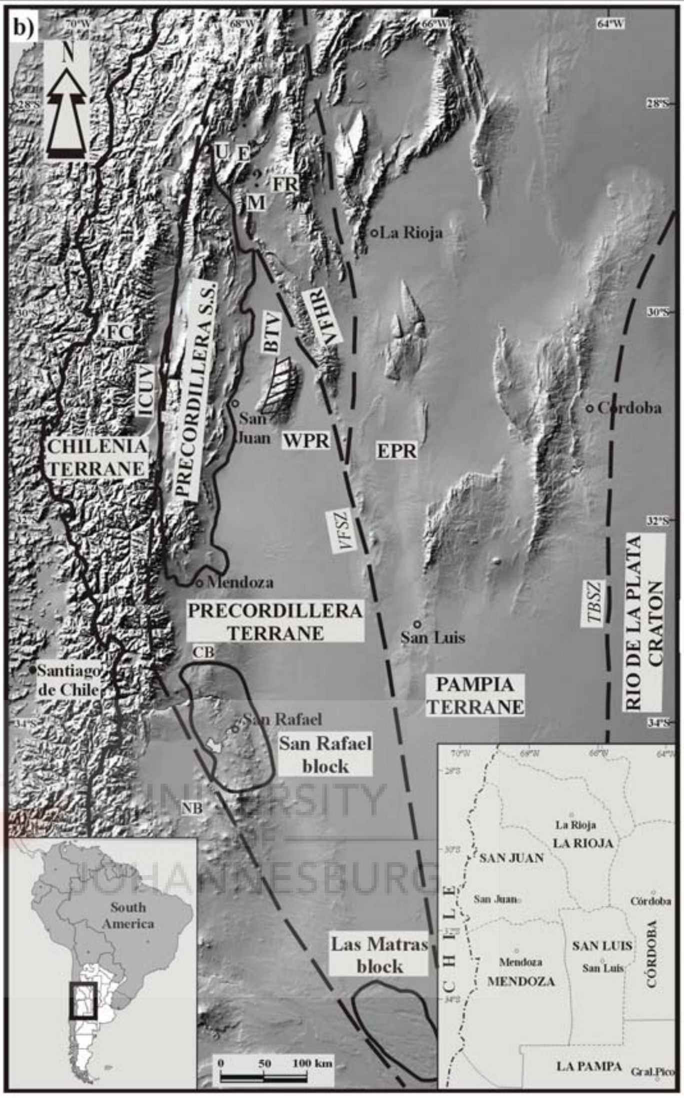

Figure 3.1: a) Main tectonostratigraphic units of South America (modified from Rapalini, 2005). NP: North Patagonian Massif; D: Deseado Massif. b) Satellite image based map showing terrane boundaries as dashed lines and blocks boundaries as continuum lines (based on Ramos *et al.*, 2000; Porcher *et al.*, 2004; Astini and Dávila, 2004). FR: Famatina Range; FC: Frontal Cordillera; ICUV: Iglesia Calingasta-Uspallata Valley; BTV: Bermejo-Tulum Valley; WPR: Western Pampeanas Ranges; EPR: Eastern Pampeanas Ranges; VFSZ: Valle Fértil Shear Zone; CB: Cuyo Basin; NB: Neuquén Basin; PP: Pie de Palo Range; E: Espinal Range; U: Umango Range; M: Maz Range; VFHR: Valle Fértil-La Huerta Range.

Villicúm Range (Gualcamayo, La Cantera and Don Braulio Formations) and at Cerro Viejo de Huaco (Los Azules and La Chilca Formations). The Empozada Formation also belongs to the Eastern tectofacies. However, this unit differs because it is an olistostromic sequence and it is therefore analyzed in the following chapter as part of the slope-type deposits and along with the other olistostromic succession (the Los Sombreros Formation). The Gualcamayo Formation and the equivalent part of the Los Azules Formation represent the drowning of the Cambrian-Ordovician carbonate

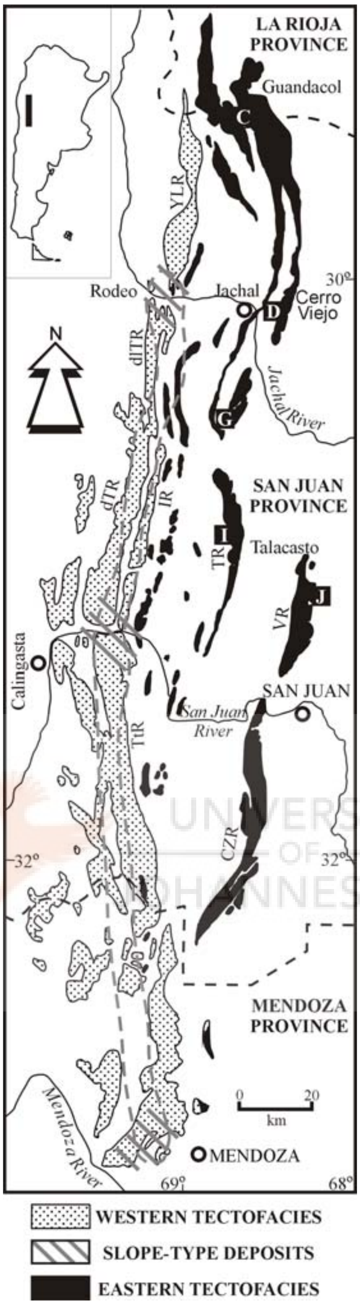

Figure 3.2: Sampling locations of the Eastern tectofacies of the Precordillera terrane (white letters C, D, G, I and J correspond to locations showed on Table 2 in Appendix B). Dashed line represent the slope-type deposits as defined by Peralta (2005) whereas dark grey diagonal lines represent the slope-type deposits in the areas sampled for studies presented in Chapter 4. IR: Invernada Range; dTR: del Tigre Range; dlTR: de la Tranca Range; YLR: Yerba Loca Range; TR: Talacasto Range; TtR: Tontal Range; CZR: Chica de Zonda Range; VR: Villicúm Range. Modified from Astini (1991).

platform. They also record evidence of contemporaneous explosive volcanism in the form of ash beds nowadays altered into K-bentonites (Kolata *et al.*, 1994; Huff *et al.*, 1998). The Las Vacas, Las Plantas, Trapiche and the La Cantera Formations are part of a clastic-wedge also called Guandacol basin (Thomas and Astini, 2003). The clastic-wedge was formed within faulted blocks in an extensional tectonic environment that occurred as a result of the accretion of the Precordillera terrane onto the Gondwana margin during the Ordovician (ca. 460 Ma; Astini *et al.*, 1996). The Don Braulio and La Chilca Formations record the transition Ordovician – Silurian within the Precordillera terrane. The glacial deposits of the Don Braulio Formation along with faunal contents of the La Chilca Formation are interpreted as evidence of the final accretion of the terrane to Gondwana (e.g. Astini, 1993b).

A combination of petrography and heavy minerals analyses, geochemistry, Sm-Nd and Pb-Pb isotopes and detrital zircon age dating was applied to constrain the sources that provided detritus to the Eastern tectofacies. The samples from the Los Azules and Don Braulio Formations were analyzed in different groups according to the alloformation to which they belong. In the same way, samples from the La Chilca Formation were split into two groups according to age (one group of samples is Ordovician and the other is Silurian in age). However, when analysing the different groups for each unit, no changes in provenance-proxies values were observed, and therefore the data of each unit is presented as a single group.

3.2 GEOLOGICAL BACKGROUND

The Gualcamayo Formation (Harrington and Leanza, 1957; Furque, 1963), uncomformably overlies the San Juan Formation and it is separated from the subsequent units (Las Vacas or La Cantera Formations) by an erosive contact (Astini, 1994b; 1994c; Fig. 3.3). The Gualcamayo Formation has a thickness of 700m (Furque, 1963), and it is folded. Graptolites provide an Upper Arenig to Lower Llandeilo age for the Gualcamayo Formation (Ortega *et al.*, 1993; Cuerda *et al.*, 1994). It is subdivided into three members (Astini, 1986): the lowermost is composed by an alternation of limestones and black shales, where several K-bentonites are present (Huff *et al.*, 1998). The middle member is composed of black shales and represents a restricted basin (Astini, 1994b). The upper member is made up by laminated mudstones with interlayered blocks of limestones (Astini, 1994b). The lower and middle members were deposited during a transgressive event, while the upper member represents less stable conditions and a rising sea level associated with the Guandacolic Tectonic Phase (Astini, 1994c).

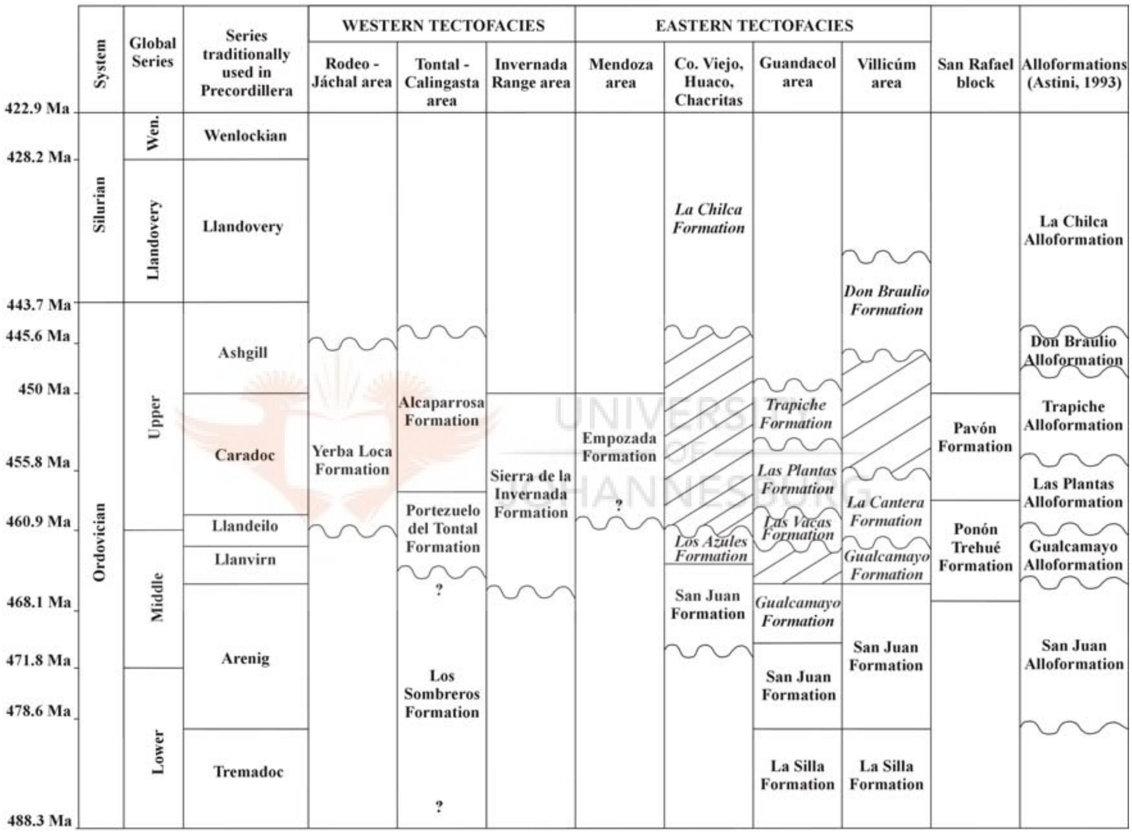

Figure 3.3: Stratigraphy of the Ordovician to Silurian of the Precordillera terrane based on Keller (1999). The distribution of alloformations is according to Astini (1993a). Absolute ages are as recommended by Gradstein *et al.* (2004). The units studied from the Eastern tectofacies for the present chapter are those in italics. Crossed lines indicate hiatus.

The Gualcamayo Formation is correlated with the Los Azules Formation (Fig. 3.3) based on the occurrence in both units of *Loganograptus logani* (Cuerda and

Ortega, 1982). In a regional context, the Gualcamayo Formation and its equivalents represent the flood deposits that covered the carbonate platform in the Precordillera (Astini, 1986; Astini *et al.*, 1988; Beresi, 1990; 1991; González Bonorino, 1991).

The Los Azules Formation (Cuerda and Furque, 1975; Fig. 3.3) is composed of black shales and interbedded limestones. The age is Llanvirn-Caradoc based on graptolites (Cuerda and Ortega, 1982). It uncomformably overlies the San Juan Formation (Astini, 1994c) and it is in turn uncomformably overlain by the La Chilca or by the Guandacol (Carboniferous) Formations (Ottone *et al.*, 1999). The Los Azules Formation contains an abundant fauna composed of graptolites, trilobites, phyllocarids, nautiloids, articulate brachiopods, conodonts, ostracods, sponge spicules, gastropods, bryozoans, crinoids and palynomorphs (Ottone *et al.*, 1999 and references therein). It is subdivided into three members: the lower and middle members are composed of mudstones, carbonate-mudstones and siltstones, while the upper member comprises black shales (Ottone *et al.*, 1999). This member contains graptolites from the *Nemagraptus gracilis* Biozone (Cuerda, 1986) and it is separated from the underlying members by a discontinuity (Astini, 1993a). This unit contains K-bentonites dated by conventional U-Pb method at 464 to 461 Ma (Huff *et al.*, 1998).

The La Cantera Formation (Furque and Cuerda, 1979; *emended* Baldis *et al.*, 1982) is a 2000m thick unit composed of conglomerates, wackes and mudstones. The base and top are bounded by erosive unconformities that separate this unit from the underlying Gualcamayo Formation and the overlying Don Braulio Formation (Peralta, 1993). The La Cantera Formation is subdivided into three members (Peralta, 1993): the lowermost is composed of pebble-arenites and conglomerates with sedimentary and igneous clasts. The middle member is composed of arenites and mudstones and the uppermost member is composed of turbidite wackes and mudstones. The age of the La Cantera Formation is Late Llanvirn-Lower Caradoc (Peralta, 1986; Albanesi *et al.*, 2005). Flute casts indicate from north to south and from northwest to southeast palinspastically restored palaeocurrents (Peralta, 1993 in Gleason *et al.*, 2006).

The Las Vacas Formation (Furque, 1963) is a 300m thick sequence composed of coarse conglomerates with rounded clasts, which includes olistoliths (Astini, 1998b).

It unconformably overlies the San Juan or the Gualcamayo Formations, and it is separated from the overlying Las Plantas Formation by an erosive boundary (Astini, 1998b). The unconformity at the base of the Las Vacas Formation is interpreted as due to the Guandacolic Tectonic Phase (Furque, 1965). The age of the Las Vacas Formation was initially considered Upper Llanvirn to Lower Llandeilo (Hünicken and Pensa, 1989), but was reassigned to the Lower Caradoc (Astini and Brussa, 1996). Conglomerate Clasts of the Las Vacas Formation are composed of basement rocks from the Pampean Ranges, carbonate clasts from the San Juan Formation, shales from the Gualcamayo Formation as well as olistoliths (Hunicken and Pensa, 1989). Palaeocurrents are directed mainly towards west and northwest, however directions show 120º dispersion (Astini *et al.*, 1996; Astini, 1998b).

The Las Plantas Formation (Furque, 1963) is a 300m thick sequence composed of dark grey shales, with interbedded siltstones in the upper levels (Aceñolaza and Baldis, 1986). The Las Plantas Formation is in erosive contact with the Las Vacas Formation, and it is uncomformably overlain by the Trapiche Formation (Astini, 1993a; 1998b). Apart from graptolites, this unit contains brachiopods and trilobites (Benedetto *et al.*, 1991) as well as pelecypodes (Sánchez, 1990), bryozoans, gastropods and nautiloids (Astini *et al.*, 1986). The age for the complete succession based on palaeontological data is Late Llandeilo–Early Caradoc (Sánchez, 1990). It represents a sedimentary event related vertically and laterally with the Las Vacas Formation, and coincides with an increment in the carbonate content of the deposits (Benedetto *et al.*, 1991).

The Trapiche Formation (Furque, 1963), is a 1150m thick sequence of mudstones, quartz-arenites, conglomerates, carbonate megabreccias and chaotic deposits with carbonate olistoliths (Astini, 1994a). It uncomformably overlies the Las Plantas or the Las Vacas Formations (Astini, 1993a). It contains a diverse fauna characterized by brachiopods, bryozoans, gastropods, trilobites and bivalves (Astini, 1986). The Trapiche Formation is Upper Caradoc-Lower Ashgill in age (Benedetto and Herrera, 1987; Benedetto, 1999). Palaeocurrents are south-north within the megabreccias and directed from east to west for the quartz-sandstones (Astini, 1994a).

Clasts from the matrix-supported conglomerates are predominantly well rounded and composed of quartz (Benedetto, 1999).

The Don Braulio Formation (Uliarte, 1977; defined by Baldis *et al.*, 1982; reviewed by Peralta and Baldis, 1990) is separated from the underlying La Cantera Formation by an erosive unconformity and the Rinconada Formation overlies it with another erosive unconformity. The Don Braulio Formation is 50m thick (Astini, 1993b), and records the Ordovician-Silurian transition. This transition is coincident with the presence of glacial deposits with Hirnantia fauna in other parts of Gondwana for this age (Astini, 1993b and references therein). It is subdivided into two members: the lower member is composed of a glacial diamictite sequence of matrix-supported, massive diamictites, clast-supported channelized-conglomerates and sand-diamictites, and varved shale deposits with drop-stones and interlayered conglomerates (Astini, 1993b). The massive diamictites have angular intraclast pebbles and cobbles, derived mainly from the underlying La Cantera Formation; they also contain rounded lithoclasts from igneous and metasedimentary rocks. The clasts are generally oriented east southeast–west northwest. The matrix of the diamictite shows synsedimentary deformation structures, and it is composed of quartz, feldspar, rock fragments and very fine (clayey) material (Astini and Buggisch, 1993). The rhythmic deposits of sandstones and mudstones were interpreted as deposited in a restricted glacial lake. The upper member is composed of laminated mudstones with Hirnantia fauna near the base, and arenites and iron-rich ooids with interlayered mudstones towards the top (Peralta, 1993). It is a muddy extra-glacial transgressive-regressive platform (Astini, 1991; Astini and Buggisch, 1993). A conglomerate separates both members. The ferruginous deposits of the Don Braulio Formation were interpreted as related to humid tropical climate accompanied by chemical strong weathering (Beresi, 1978). The mild weather is confirmed by the presence of microflora that lived in these conditions (Pöthe de Baldis, 2001). The age for the succession is Late Ashgill-Early Llandovery (Astini, 1993b). Palaeocurrents indicate a main provenance from the actual east and southeast (Astini and Buggisch, 1993). Keller *et al.* (1998) interpreted the diamictite as formed as ice-rafted deposits, not related to the final accretion of the Precordillera to Gondwana.

The La Chilca Formation (Cuerda, 1966) unconformably overlies the Don Braulio, Los Azules or San Juan Formations. It is in turn paraconformably overlain by the Los Espejos Formation. These collectively constitute the Tucunuco Group (Cuerda, 1969). The La Chilca Formation is composed of a 128m thick sequence of interbedded fine sandstones and siltstones. Wenlockian fauna (*Monograptus priodon* and the *Deunffia-Domasia* Association) were found 11m after the discontinuity between the San Juan and La Chilca Formations (Cuerda *et al.*, 1982; Kerlleñevich, 1985a; Pöthe de Baldis, 1987). However, the first 0.6m are Upper Ordovician and dominated by the *Persculptus* Biozone (Cuerda *et al.*, 1988a). Brachiopods, bivalves, trilobites and graptolites provide an Ashgill to Lower Wenlockian age for the entire unit (Benedetto *et al.*, 1985; Aceñolaza and Peralta, 1985; Kerlleñevich and Cuerda, 1986; Cuerda *et al.*, 1988a). It also contains trace fossils, palynomorphs and acritarchs. The sequence has a basal cherty-pebble conglomerate overlain by a thin ironstone bed. Sandstones and siltstones are phosphate-rich. At the upper part, carbonate layers are interbedded. A ferriferous-phosphate bed appears to the top indicating slow sedimentation but high bioturbation rates (Peralta, 2003b). The lower part of the unit was interpreted as a shallow marine platform while the upper part indicates a higher energy shoreface environment (Astini and Benedetto, 1992). Palaeocurrents data indicate bimodal currents mainly directed south, but also towards the north (Astini and Maretto, 1993).

Voldman and Albanesi (2005), based on Conodonts Alteration Index establish that several units from the Eastern tectofacies (Gualcamayo, Los Azules, La Cantera Formations) were affected by diagenesis. However, illite crystallinity index suggests anchimetamorphic (very low-grade metamorphism) conditions for the Gualcamayo Formation (Astini, 1991). Colour alteration index measured on conodonts indicate a maximum temperature of 140ºC for the diagenetic conditions reached by the Upper member of the Los Azules Formation (Ottone *et al.*, 1999). The diagenetic conditions were probably reached during a tectonothermal event of probable Late Silurian-Early Devonian age (Keller *et al.,* 1993). During the Ordovician, two tectonic movements were recognized within the Eastern tectofacies. The oldest one corresponds with the Guandacol Orogenic Phase (Furque and Cuerda, 1979) and is related to the deposition of the Middle Ordovician Las Vacas Formation (conglomerates). The Villicúm Orogenic Phase (Baldis *et al.*, 1982) produced the conglomerate developed in between the La Cantera and Don Braulio Formations during the Late Ordovician. During Late Silurian to Early Devonian, the Eastern tectofacies suffered distension (von Gosen and Buggisch, 1992; Astini *et al.*, 1996). During Middle Devonian to Early Carboniferous, block faulting occurred due to the Chanic Orogenic Phase (Astini *et al.*, 1996).

3.3 PETROGRAPHY

As the Gualcamayo and Los Azules Formations are claystone-dominated sequences, their main mineralogical components were determined by X-ray diffraction (XRD) and SEM (scanning electron microscope) techniques. Rocks from both units are composed of quartz, plagioclase, muscovite, illite, scarce microcline and very scarce dolomite, calcite, kaolinite, chlorite and biotite. More details regarding the petrographic techniques applied are given in Appendix B while additional XRD data is shown in Appendix C.

La Cantera, Las Vacas, Las Plantas, Trapiche and Don Braulio Formations are composed of arenites with low matrix content (5% to 10%), and carbonate-cemented arenites (10% to 20% cement contents). The detrital components of the arenites are moderately to poorly sorted, subrounded to subangular and range in size from silt to coarse sand. Main minerals are monocrystalline quartz with normal extinction. Pressure solution effects could be observed on quartz boundaries as well as quartz-overgrowths. Graphic quartz is present as a coarse detrital grain. Polycrystalline undulose quartz is less frequent than monocrystalline quartz, although it is normally present in higher quantities compared with all the lithoclast-types, except for the Las Plantas, Trapiche and Don Braulio Formations. Plagioclase is unaltered and often calcite-replaced. K-feldspar is either partially altered to clay minerals or totally replaced by chlorite. Plagioclase is more abundant than K-feldspar within the Las Vacas and Don Braulio Formations, but the opposite is true for the La Cantera, Las Plantas and Trapiche Formations. The matrix is composed of white mica and quartz. The cement is composed predominantly of calcite. Sedimentary lithoclasts were derived from mudstones, siltstones, chert, very fine-grained sandstones and carbonates, in order of abundance. The volcanic lithoclasts were mainly derived from very fine volcanic rocks. Within the metamorphic lithoclasts, the commonest were derived from low-grade rocks such as phyllites, followed by quartz-mica schists and very rarely, gneisses. The lithoclast population for all the abovementioned units is dominated by sedimentary lithoclasts. For the La Cantera, Las Plantas and Trapiche Formations the sedimentary lithoclasts are followed by volcanic lithoclasts and metamorphic lithoclasts in order of abundance, while for the Las Vacas and Don Braulio Formations the sedimentary lithoclasts are followed by metamorphic lithoclasts and volcanic lithoclasts in order of abundance.

The Las Plantas and Trapiche Formations also contain quartz-arenites with neither cement nor matrix. The grains of these arenites are fine to medium in size, well sorted and subangular to well rounded. Monocrystalline undulose quartz is the main constituent. Wrapped grains and overgrowths are common, as well as sutured contact between grains. Polycrystalline quartz is very scarce. K-feldspar is more abundant than plagioclase. Lithoclasts are represented almost exclusively by chert, although siltstone fragments were observed as well. The La Chilca Formation is composed of coarse siltstones and minor very fine arenites, moderately well sorted and with subrounded grains. Certain samples are partially carbonate-cemented. They are characterized by monocrystalline quartz that predominates over the polycrystalline one and normally has low sphericity. Chert is very scarce. Plagioclase is unaltered whereas K-feldspar is partially altered to clay minerals.

Accessory minerals for all the arenites within the different units are tourmaline, zircon, chlorite, epidote, muscovite, biotite, titanite, apatite, hematite and other opaque minerals. These minerals range in size from very fine to coarse and they range from subangular to rounded. Considering a general overview, the arenites are composed mainly of quartz, feldspars and lithic fragments in order of abundance. A detailed petrographic description for each formation is given in Appendix C.

3.4 GEOCHEMISTRY

The objective of provenance studies is to reconstruct and interpret the history of sediment supply, from initial erosion of a parent rock to the final burial of its detritus and so eventually deduce the geographic location and characteristics of the source area. It has been established that the average composition of sedimentary rocks on a global scale changes through time reflecting changes in the average composition of the crystalline source rocks (Taylor and McLennan, 1985). However, several other factors such as weathering, diagenesis and sorting, also control the composition of sedimentary rocks, and therefore the evaluation of these factors is crucial to constrain the provenance of a sedimentary succession (e.g. Nesbitt and Young, 1982; Cullers *et al.*, 1987; McLennan *et al.*, 1990; 1993; Cox and Lowe, 1995; Cox *et al.*, 1995; Andersson *et al.*, 2004).

3.4.1 Major elements and alteration

The major elements abundances and mineralogy of clastic rocks depend strongly on chemical weathering and diagenetic processes (e.g. Nesbitt and Young, 1982; McLennan, 1993; Fedo *et al.*, 1995; 1997). The chemical index of alteration (CIA = $\{Al_2O_3 / (Al_2O_3 + CaO^* + Na_2O + K_2O)\} \times 100$; Nesbitt and Young, 1982) potentially reflects the intensity of weathering, although the possible effects of potassium-metasomatism during diagenesis may seriously affect CIA values. This metasomatism is responsible for the change of kaolin (derived from plagioclase alteration) to illite, and this effect can be quantitatively evaluated, and CIA values corrected, by using the A-CN-K (Al_2O_3 - CaO^* + Na_2O - K_2O) diagram. The weathering trends are parallel to the A-CN join, and hence deviations towards the K apex suggest K-metasomatism (Fedo *et al.*, 1995) or mixing of different sources (McLennan *et al*., 1993). CIA values calculated for all the Formations are listed on Table 1 in Appendix A, along with their chemical analyses.

Mudstones from the Gualcamayo and Los Azules Formations have a distribution of major elements similar to post-Archaean Australian Shales (PAAS; Taylor and McLennan, 1985), except for some samples that show CaO enrichment with values of up to 33% and consequently SiO_2 concentrations as low as 25.8%. The high MgO concentration (about 8%) of these samples from the Gualcamayo Formation is also in agreement with XRD data, which indicate dolomite, probably as cement. However, the rest of the samples from the Gualcamayo Formation have low MgO concentrations (between 0.8% and 1.8%) and XRD data indicate very scarce dolomite. The low MgO concentration of the Los Azules Formation indicates that the cement is most probably calcite. The major elements composition of the arenites and carbonate-cemented arenites of the La Cantera, Las Vacas, Las Plantas and Trapiche Formations is characterized by low to intermediate SiO_2 concentrations and low to high CaO concentration. The samples petrographically described as quartz-arenites of the Las Plantas and Trapiche Formations are SiO_2-rich, with values of up to 95%. Al_2O_3 concentrations of all the samples from these four mentioned units vary strongly from trace amounts to 18.8%, whereas Fe_2O_3 concentrations range from 0.32% to 8.5%. Samples from the Don Braulio Formation are CaO rich, with one exception. The latter is associated with the carbonate cement of sandstones. The La Chilca Formation is a SiO_2-rich (average 82.6%) and poor in Al_2O_3 and Fe_2O_3 sequence. Only one sample has a slight enrichment in CaO concentration (of about 2.9%) compared with the rest of the samples within this unit. No enrichments in P_2O_5 were detected.

Some samples of the several units studied could not be used to calculate the CIA due to their high SiO_2 (>than 89%) and/or high CaO concentrations (see Table 1 in Appendix A). The CIA values for the samples used range from 57 to 75, indicating intermediate to strong chemical alteration (Fedo *et al.*, 1995). The sandstones from the La Cantera and La Chilca Formations with high SiO_2 concentrations (>73% but less than 89% SiO_2) plot in the A-CN-K diagram (Fig. 3.4a and b) towards the A-CN boundary. Their CIA values are probably reflecting the effects of other processes superimposed to the chemical alteration and that resulted in the loss of K_2O (which for these samples ranges from 0.2% to 1.27%) with respect to Na_2O (0.96% to 2.14%). Discarding these sandstones with SiO_2 concentrations between 73% and 89%, the rest of the samples of all the units studied follow a general weathering trend (i.e. Fedo *et al.*, 1995; Nesbitt, 2003). However, certain deviations towards the A-K boundary are observed (Fig. 3.4a and b) and could be a result of postdepositional metasomatic potassium enrichment (Nesbitt and Young, 1989), since some of the samples that show the deviation are enriched in their K_2O concentration compared with the upper continental crustal (UCC) average value of 3.4% (McLennan *et al.*, 2006). Nevertheless, most of the samples of all the units presented in this work are slightly depleted in the K_2O concentration compared with the UCC, and therefore the deviation towards the A-K tie line are more probably related to other processes that resulted in Na_2O and CaO depletion rather than in potassium metasomatism (e.g. mixing of sources that undergone different stages of alteration; McLennan *et al*., 1993).

The K/Cs ratio is also an indicator of weathering, because Cs tends to be fixed in weathering profiles whereas K tends to be lost in solution (McLennan *et al.*, 1990). The low K/Cs ratio shown by the Gualcamayo, Los Azules, Las Plantas, Trapiche and Don Braulio Formations (Table 1 in Appendix A), along with the enrichment in their

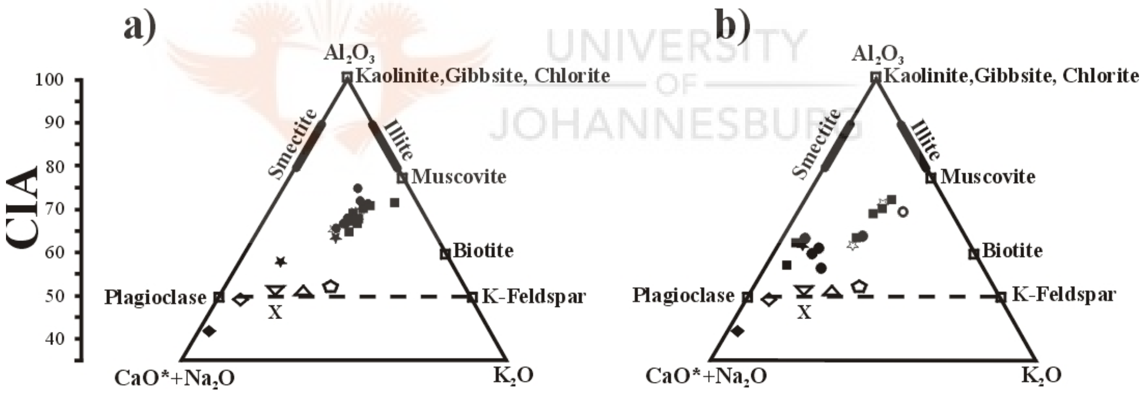

Figure 3.4: A-CN-K diagram constructed using molecular proportions of the oxides and with the CIA scale shown on the left. The average upper continental crust is plotted (X; Taylor and McLennan, 1985), as well as idealized mineral compositions (empty squares). Empty pentagon: average granite; empty triangle: average adamellite; empty inverted triangle: average granodiorite; empty diamond: average tonalite; solid diamond: average gabbro (Nesbitt and Young, 1984). a) Squares: Gualcamayo Fm.; circles: Los Azules Fm.; stars: La Cantera Fm. b) Squares: Las Plantas and Trapiche Fms.; stars: Don Braulio Fm.; circles: La Chilca Fm. Empty symbols represent mudstones whereas solid symbols are for sandstones.

Cs concentration compared with the UCC value of 4.6ppm (McLennan *et al.*, 2006) indicates significant chemical weathering. The same can be deduced for the mudstones of the La Cantera and Las Vacas Formations and is in accordance with petrographic results. Sandstones from the latter mentioned units are depleted in Cs, with values between 1ppm and 2ppm, with one exception. Although these sandstones are also depleted in K compared with the UCC, the very low Cs concentration resulted in K/Cs ratios above the UCC value of 6136 (McLennan *et al.*, 2006). On the other hand, the La Chilca Formation also shows Cs (average 3±1.23ppm) and K (1.09±0.87%) values below the UCC concentration. However, the K/Cs ratios for the La Chilca Formation are lower than the UCC, indicating strong chemical weathering, although the low Cs values could probably be related to dilution effects due to the high SiO_2 concentrations of this unit.

The Th/U ratio in average UCC is 3.8, and for most sedimentary rocks derived from average crust the Th/U ratio is around 3.5-4.0, indicating that they have not undergone weathering and/or recycling (McLennan *et al.*, 1993). Under oxidizing conditions, the Th/U ratio increases because U^{4+} oxidizes to the more soluble U^{6+} and is therefore easily removed from the sediments during weathering and/or recycling (McLennan *et al.*, 1993). A low Th/U ratio can also be due to U enrichment (McLennan, *et al.*, 1993). In this study, a poorly understood correlation between low Th and high CaO concentrations is observed (see below). Samples from the Gualcamayo and Los Azules Formations cluster well below the 3.8 Th/U limit (Fig. 3.5). Compared with UCC averages of Th (10.7ppm) and U (2.8ppm) according to McLennan *et al.* (2006), most of the samples are enriched in U (with values of up to 8.6ppm) and have similar to enriched Th concentrations (between 10ppm and 13ppm; see Table 1 in Appendix A). However, certain samples of the Los Azules Formation have lower Th concentrations compared with the UCC, and these depletions are related to high CaO (more than 11%) or SiO_2 (more than 73%) concentrations.

Mudstones from the La Cantera Formation show Th/U values between 3.5 and 4 (Fig. 3.5), and Th and U concentrations similar to the UCC (McLennan *et al.*, 2006). The low Th concentration of the sandstones instead seems to be affected by the high

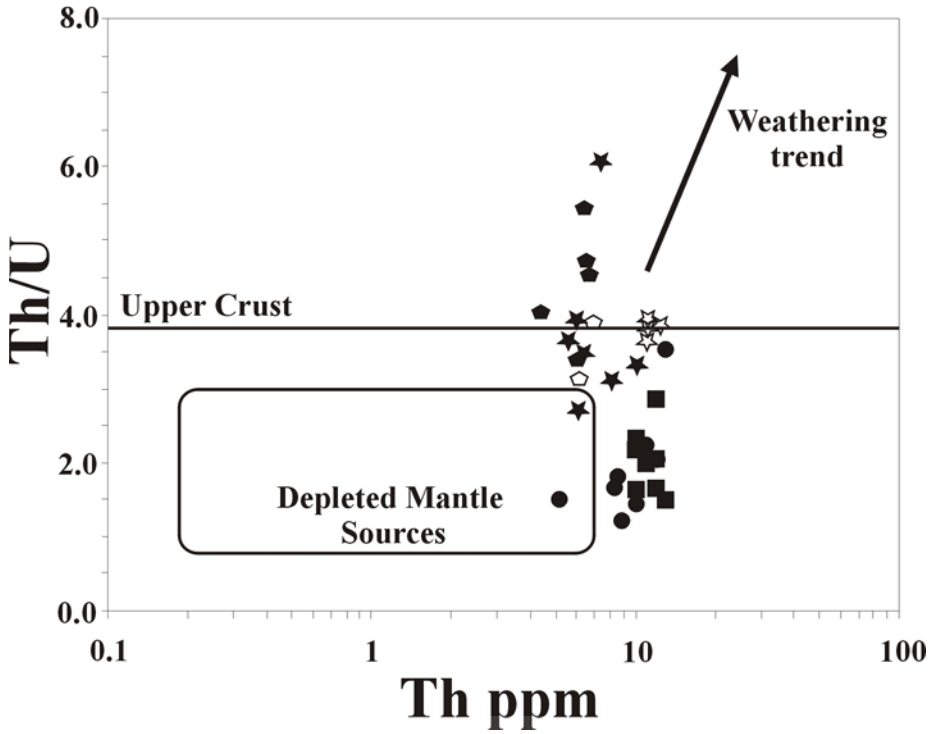

Figure 3.5: Plot of Th/U versus Th (McLennan *et al.*, 1993). Solid squares: Gualcamayo Formation; circles: Los Azules Formation; stars: La Cantera Formation; pentagons: Las Vacas Formation. For the last two units: empty symbols are mudstones whereas solid symbols are sandstones.

CaO concentration. Furthermore, the sandstones are depleted in U (with some exceptions) compared with the UCC. The Th/U ratios for the sandstones of the La Cantera Formation vary strongly and include values similar to the Th/U ratio of the UCC, but also lower and higher values. The Zr concentration and the Zr/Sc ratios are indicators of recycling. Sandstones of this unit are enriched in Zr and have Zr/Sc ratios higher than the UCC (14), indicating recycling. Therefore, if recycling (and weathering) would had been the sole factor controlling the Th/U ratio, higher values of this ratio would be expected for these sandstones (which is the case for only one sandstone). The other sandstones have high Zr/Sc ratios (indicating recycling) and have therefore low U concentrations, but also low Th concentrations and low Th/U ratios. The low Th/U ratio could be explained either by the negative correlation between Th and CaO or by the influence of a source with low Th concentrations (inheritance).

Similar to the sandstones of the previously described unit, samples from the Las Vacas Formation have lower Th and U concentrations than the UCC values (Fig. 3.5). Their Th/U ratios are similar to higher than the UCC ratio, indicating that recycling and/or weathering could have depleted the U concentration or that the Th/U ratio could also be affected by the negative correlation between CaO and Th.

In general, samples from the Las Plantas and the Trapiche Formations show Th/U ratios typical of the UCC (Fig. 3.6), notwithstanding their variation in Th and U concentrations. However, some samples have very low Th/U ratios (as low as 0.6) along with low Th and U concentrations, but with Zr concentrations and Zr/Sc ratios suggesting recycling (Table 1 in Appendix A). This means that recycling and/or weathering were not the only processes controlling the Th/U ratio. Dilution provoked by high SiO_2 and CaO concentrations might have sometimes influenced the trace elements absolute concentrations. The mudstones from the Don Braulio Formation are enriched in Th, and slightly enriched in U and in the Th/U ratio compared with the UCC (Fig. 3.6). On the other hand, sandstones are depleted in Th and U, but their Th/U ratios are similar to slightly lower than the UCC (Fig. 3.6). Samples from the La Chilca Formation can be subdivided into two groups. The one group comprises sandstones showing very low Th/U ratios and correspondingly having low Th and U concentrations (Table 1 on Appendix A). These samples also exhibit recycling effects (see Fig. 3.9) with concomitant enrichment in zircon and therefore implying that zircon is not the main host of Th. Coincidently, petrographic data indicate rather textural and mineralogical mature subfeldspathic to quartz-arenites. Although the second group of samples from the La Chilca Formation has Th and U concentrations lower than the UCC, it has high Th/U ratios (4.7 to 5.8) along with the highest CIA (64 to 70), and therefore some weathering effects that had extracted the U could be assessed. However, the loss of U could have occurred during recycling, since samples from the second group are also characterized by high Si_2O concentrations (75.1% to 76.8%)

Conclusively, the samples seem to be intermediate to strongly altered and comprise mainly recycled detrital material. However, it is not clear if the detritus were affected by weathering and/or reworking during transport or if the concentration of certain elements were inherited from the sources. Besides some quartz-arenites, petrographic data point to rather short transport. The Gualcamayo and Los Azules Formations display low Th/U ratios caused by high U concentrations compared with the UCC. The enrichment in the U content commonly occurred in black shales and it is related to the reducing (anoxic) environmental conditions that prevent U to oxidize (Calvert and Pedersen, 1993).

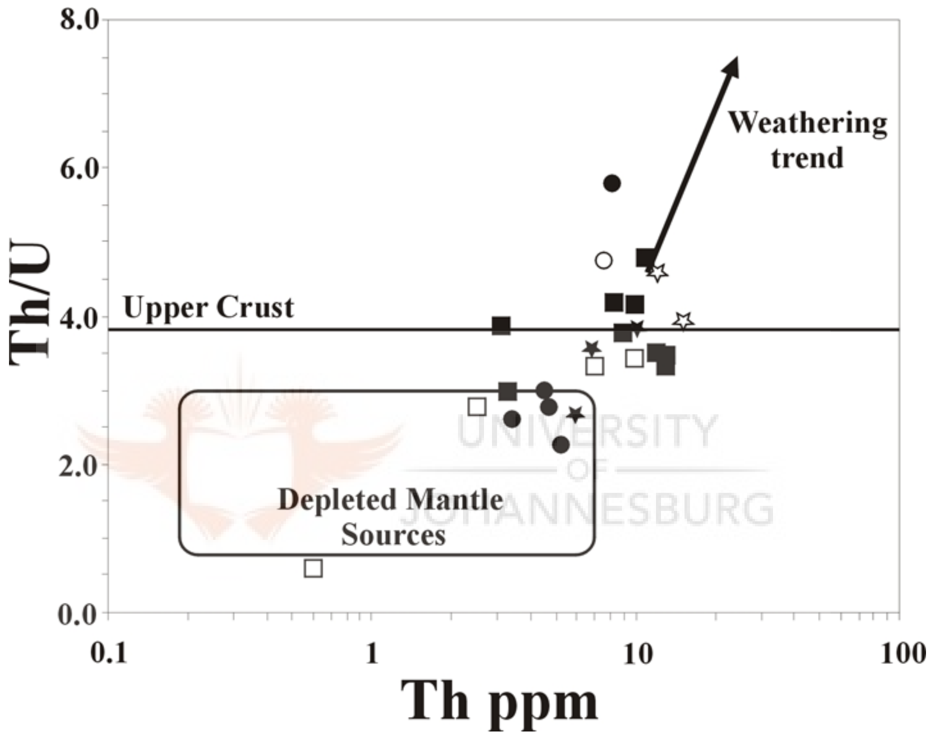

Figure 3.6: Plot of Th/U versus Th (McLennan *et al.*, 1993). Squares: Las Plantas and Trapiche Formations (empty squares are sandstones while solid squares are mudstones); stars: Don Braulio Formation and circles represent La Chilca Formation (empty symbols are mudstones and solid symbols are sandstones).

3.4.2 Trace elements

The trace elements are considered useful for provenance determination, because they tend to reflect provenance compositions (Taylor and McLennan, 1985). In particular, the concentrations of HFSE (high field strength elements) such as Zr, Nb, Hf, Y, Th and U are enriched in felsic rather than mafic sources and they reflect provenance compositions because of their immobile behaviour (Taylor and McLennan, 1985). On the other hand, compatible elements such as Sc, Cr, V, Ni are preferable concentrated in mafic rocks (Taylor and McLennan, 1985). However, their absolute abundances are affected by Ca or Si dilution. Therefore, the use of ratios between trace elements is more reliable, since ratios are not supposed to change even in cases of dilution. In the present study case, however, it is observed that low Th abundances are related to high Ca concentrations. Although it is known that these two elements can substitute for each other in mineral structures (Hole *et al.*, 1992), it is not clear if the amounts of substitution would be enough to provoke such diminution of the Th concentrations. Consequently, certain important ratios for provenance analysis (e.g. Th/Sc) are not constant and their interpretations that regard to provenance could be molested. A low Th concentration might also be a result of a low concentration of this element within the source rocks.

The input of a mafic source could be discriminated using the Cr/V and Y/Ni ratios. The Cr/V ratio indicates the enrichment of Cr over other ferromagnesian trace elements. The main minerals that concentrate Cr over other ferromagnesian are chromites. The Y/Ni ratio indicates the concentration of ferromagnesian trace elements (such as Ni) compared with Y that represents a proxy for heavy rare earth elements. The Cr/V and Y/Ni ratios for PAAS is about 0.73 and 0.49 respectively (Taylor and McLennan, 1985), while for the UCC are 0.78 and 0.5 respectively (McLennan *et al.*, 2006). However, ophiolitic components would have Cr/V ratios higher than 10 (discussion in McLennan *et al.*, 1993).

The Cr/V ratio for the Gualcamayo and Los Azules Formations is between 0.31 and 0.93, whereas the Y/Ni ratio varies between 0.37 and 3.1. The Cr/V and Y/Ni ratios for the La Cantera Formation vary between 0.99 and 1.59 and between 0.38 and 2.04 respectively. The Las Vacas Formation have Cr/V ratio of 0.83±0.08 on average whereas the Y/Ni ratio is 0.72±0.26 on average. The Cr/V ratio for the Las Plantas and Trapiche Formations varies from 0.79 and 5.8, while the Y/Ni ratio varies from 0.03 and 2.68. The Don Braulio Formation shows Cr/V ratios varying between 0.56 and 5.9, and Y/Ni ratios varying between 0.65 and 1.72. The Cr/V ratio for the La Chilca is between 0.90 and 1.62, and the Y/Ni ratio is between 0.27 and 0.81. Certain relatively high Cr/V ratios (e.g. 5.9 for sample DB1; see Table 1 in Appendix A), low Y/Ni ratios (e.g. 0.03 for sample LPT13; see Table 1 in Appendix A), along with high Sc, Cr, V and Ni abundances (e.g. samples G7 and 020446; Table 1 in Appendix A) might indicate a subordinate depleted input. However, the distribution of Cr, V and Ni could be affected during sedimentary processes like diagenesis (Feng and Kerrich, 1990), weathering or other sedimentary processes (McLennan *et al.*, 2006). Furthermore, Cr is concentrated in the heavy mineral chromite that can be recycled.

Interestingly, chromian-spinels of the Don Braulio Formation (see section 3.5) where obtained from a sandstone (020438; Table 1 in Appendix A) with Cr, V and Ni concentrations lower than the UCC (59, 75 and 34ppm respectively) and showing Cr/V and Y/Ni ratios slightly higher than the UCC (0.79 and 0.65 respectively). The sandstone with the highest Cr/V ratio (5.9 for sample DB1) shows a Y/Ni ratio higher than the UCC (0.93), and Cr, V and Ni concentrations considerably lower than the UCC (59, 10 and 16ppm respectively). For sample 020438, processes of reworking of chromian spinels could be invoked to explain its behaviour, since it shows Si_2O concentrations of 70.2% and the Zr content (242ppm) is enriched compared with the UCC (although Zr/Sc ratios of 26.9 does not indicate important recycling). Sample DB1 instead show Zr/Sc ratios of 96.2 indicated recycling.

Mechanical processes are responsible for the transport of rare earth elements (REE) into a sedimentary basin and they therefore represent reliable provenance indicators (Cullers *et al.*, 1979; Taylor and McLennan, 1985; McLennan, 1989). However, mobility of REE (plus Y) had been widely reported (i.e. Awwiller, 1994; Bock *et al.*, 1994; McDaniel *et al.*, 1994; Bau, 1999). The shape of the REE pattern (including the presence or not of an Eu-anomaly) can provide information about both bulk composition of the provenance and the nature of the dominant igneous process affecting the provenance (McLennan *et al.*, 1990; McLennan and Taylor, 1991).

The chondrite normalized rare earth elements patterns for mudstones and sandstones of all the units studied for this chapter show a moderately enriched light REE pattern (LREE), a negative Eu-anomaly and a rather flat heavy REE (HREE) distribution. Absolute abundances of REE are higher for mudstones than for sandstones, as is expected (Fig. 3.7 and Table 1 in Appendix A). All these features match with the PAAS pattern, which is considered in turn to reflect the average composition of the upper continental crust. However, certain samples tend to be depleted in LREE and enriched in HREE compared with the PAAS. Of course, dilution effects due to high SiO_2 or CaO concentrations are observed within some samples from the Las Plantas, Trapiche and Don Braulio Formations. The effects of dilution are notable in those samples with low ΣREE. Figure 3.7 shows the average REE pattern for mudstones and sandstones of each unit and the PAAS pattern for comparison.

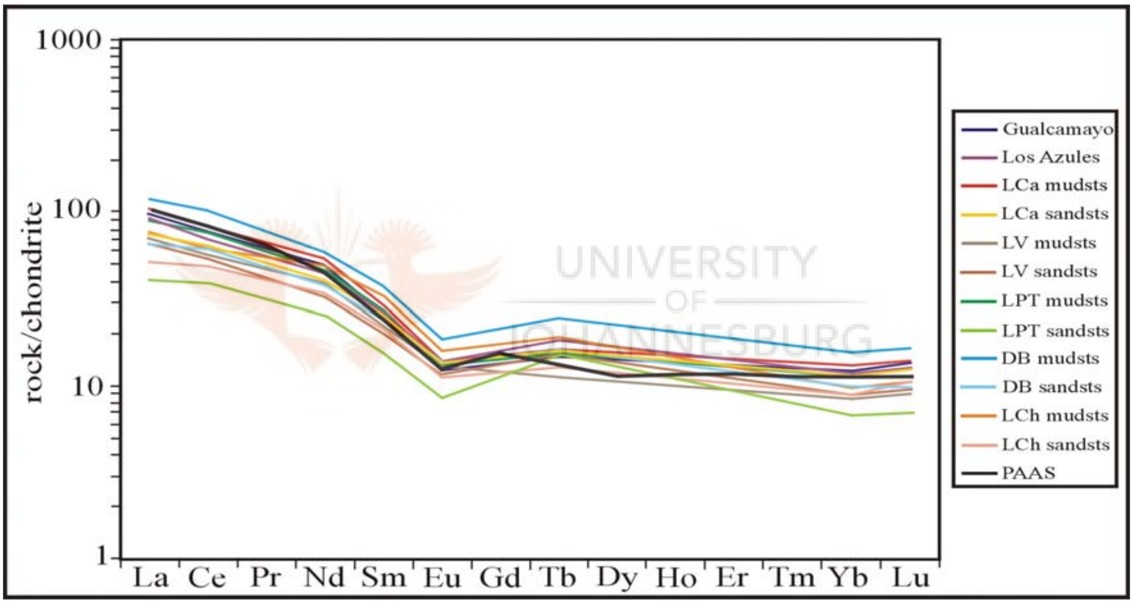

Figure 3.7: Chondrite normalized rare earth elements patterns for mudstones (mudsts) and sandstones (sandsts) of the Eastern tectofacies. PAAS= post-Archaean Australian shales pattern (Nance and Taylor, 1976) is draw for comparison. REE patterns are drawn as a continuous line although certain elements were not measured (see Table 1 in Appendix A). Subscript N denotes chondrite normalized values. Chondrite normalization factors are those listed by Taylor and McLennan (1985). LCa: La Cantera Formation; LV: Las Vacas Formation; LPT: Las Plantas and Trapiche Formations; DB: Don Braulio Formation; LCh: La Chilca Formation. The Eu anomaly is calculated as follows: $Eu_N/Eu^* = Eu_N / (0.67 Sm_N + 0.33 Tb_N)$. See text for discussion and Appendix C for REE patterns of individual samples.

The La_N/Yb_N ratios are between 6.1 and 8.1 whereas the Tb_N/Yb_N ratios vary from 1.22 to 1.63 for all the units studied from the Eastern tectofacies. The Ce-anomaly is very slightly negative to slightly positive (ranges between 0.98 and 1.06) for all the units with the exception of the Gualcamayo and Los Azules Formations which have Ce/Ce* values of 0.94 and 0.93 in average respectively.

The negative Eu-anomaly is more pronounced for the Gualcamayo, Los Azules and Las Plantas and Trapiche Formations (0.53, 0.57 and 0.53 respectively), whereas it is less negative for the other units. Particularly noteworthy is the less negative Eu-anomaly for the Las Vacas Formation, which has values as high as 0.70. The same can be deduced for the Don Braulio Formation, which has individual Eu_N/Eu^* values of 0.88. These less pronounced negative Eu-anomalies are typical for differentiated arcs, whereas recycled sedimentary rocks and those derived from old upper continental crust would have Eu-anomalies between 0.6 and 0.7 and those derived from young undifferentiated arcs world have values of about 1 (McLennan *et al.*, 1993). Th interference on Tb had not been taken into account and therefore, the Eu-anomalies should be analyzed with caution (see Appendix B).

3.4.3 Provenance and tectonic setting

The Zr/Sc ratio reflects reworking because Zr is strongly enriched in zircon and zircon can be easily recycled, whereas Sc is present in labile phases (McLennan *et al.*, 1993). On the other hand, Th/Sc ratio indicates the degree of igneous differentiation processes of the source rocks since Th is an incompatible element whereas Sc is compatible in igneous systems (McLennan *et al.*, 1990; 1993).

Although samples from the Gualcamayo and Los Azules Formations have depleted to enriched Th (3.5 to 13ppm) and Sc (7.4 to 18.7) concentrations compared with the UCC values of 10.7ppm and 13.6ppm respectively (McLennan *et al.*, 2006), their Th/Sc ratios are lower than the UCC value of 0.79 (McLennan *et al.*, 2006), indicating an input from a source more depleted than the UCC (Fig. 3.8 and Table 1 in Appendix A). Nevertheless, some samples have Th/Sc values indicating a provenance from an average upper continental crustal component. The Zr concentration is below the average for the UCC (190ppm; McLennan *et al.*, 2006), and the Zr/Sc ratios are in general below the UCC value of 14, indicating that recycling was not a dominant sedimentary process.

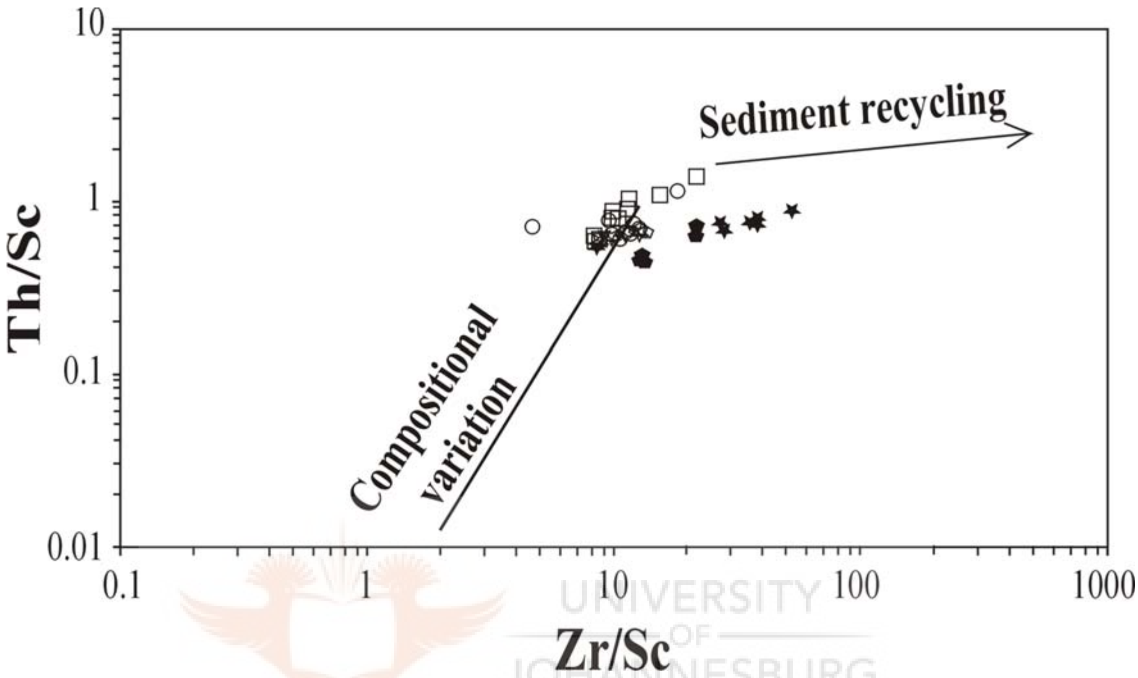

Figure 3.8: Th/Sc vs. Zr/Sc diagram adapted from McLennan *et al.* (1990). Squares: Gualcamayo Formation; circles: Los Azules Formation; solid stars: La Cantera sandstones; empty stars La Cantera mudstones; empty pentagons: Las Vacas mudstones while solid pentagons represent Las Vacas sandstones.

Mudstones from the La Cantera Formation display Th and Sc concentrations enriched compared with the UCC values, and Zr concentrations lower to slightly enriched compared with the UCC. Their Zr/Sc and Th/Sc ratios, both below UCC values indicate no recycling and a depleted component as a source. Sandstones instead have Zr concentrations of up to 390ppm, but lower than the UCC Th and Sc concentrations. These samples show recycling effects and an input from a slightly less evolved to typical upper continental crust component (Fig. 3.8). The one exception to this is the sandstone with very low Th/Sc (0.52) and Zr/Sc ratios (8.6).

The Las Vacas Formation instead shows a cluster of data indicating no recycling and a provenance from a source slightly less evolved than the typical UCC composition (Fig. 3.8). Th/Sc ratios of three sandstones are very low (0.4), and might indicate the presence of a mafic source component. Although Sc abundances are slightly enriched compared with the UCC, the Zr/Sc ratios for these samples are not typical for a mafic source (McLennan *et al.*, 1990; 1993). It is probable that the Th/Sc ratios are not only controlled by the composition of the source, but rather affected by the CaO concentrations. However, as stated above, it seems not probable that important amounts of Th-Ca replacement might occurred. Furthermore, samples from the Las Vacas Formation with higher Ca concentrations (up to 22.4%) display higher Th/Sc ratios (0.64), making difficult to fully support the influence of Ca for all samples.

Samples from the Las Plantas and Trapiche Formations could be subdivided into two groups: one does not show any recycling and reflects an input from a source with upper continental crust composition while the second group displays an important process of recycling also reflected in its high SiO_2 concentration (Table 1 in Appendix A and Fig. 3.9). Samples from this second group do not follow a normal recycling trend, since the more recycled samples show lower Th/Sc ratios than the less recycled ones, but the Ca concentrations are low (for example, the sandstone with the highest Zr/Sc ratio of 235.4 shows Ca content of 0.37%). It is noteworthy the high Zr concentration of sandstones and mudstones of the unit, with values of up to 573ppm. It could be argued that these samples were derived from Zr-rich and Th-depleted rocks.

As can be seen in Figure 3.9, samples from the Don Braulio Formation could be subdivided into two groups: one does not show any recycling while the second group shows processes of recycling. All the samples show a provenance from an UCC composition and a subordinate less fractionated component. Similarly to what is observed for the Las Plantas and Trapiche samples, the more recycled ones have the lower Th/Sc ratios.

The La Chilca Formation shows the effect of recycling, in accordance to their high SiO_2 and Zr concentrations, and a source from an upper continental crust composition (Fig. 3.9). In this case, and differently to what happened in Las Plantas, Trapiche and Don Braulio Formations, the more recycled samples show the higher Th/Sc ratios, which represents a difference with respect to the other units analyzed.

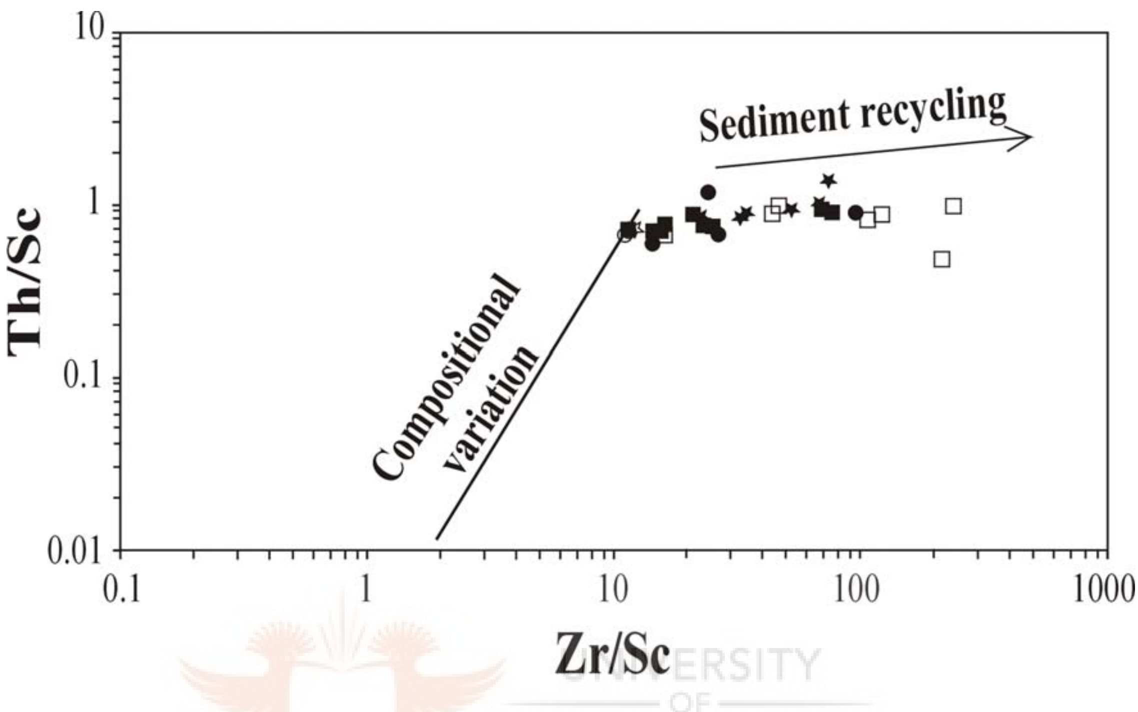

Figure 3.9: Th/Sc vs. Zr/Sc diagram adapted from McLennan *et al.* (1990). Solid squares: Las Plantas and Trapiche mudstones; empty squares: Las Plantas and Trapiche sandstones; empty circles: Don Braulio mudstones; solid circles: Don Braulio sandstones; empty stars: La Chilca mudstones; solid stars: La Chilca sandstones.

According to McLennan (1989), continental margins should be subdivided into active and passive, but the discrimination of them using geochemistry is controversial (McLennan *et al.*, 2003). It is important to consider that the sediments can be transported across tectonic boundaries and thus may not necessarily be indicative of the tectonic setting of the site of deposition (McLennan, 1989). However, using Bhatia and Crook (1986) diagrams broad trends can be deduced and interpret, and to a certain extent controlled with petrographic observations. According to the tectonic classification from Bhatia and Crook (1986), the oceanic island arc (A in Figs. 3.10 and 3.11) and continental arc settings (B in Figs. 3.10 and 3.11) represent convergent plate margins. The active continental margin setting (C in Figs. 3.10 and 3.11) comprises the

Andean-type margins and strike-slip continental margins. The passive margin setting (D in Figs. 3.10 and 3.11) comprises rifted continental margins of the Atlantic-type.

In Figures 3.10 and 3.11 mudstones and sandstones from all the units studied are shown. The depositional setting of the Eastern tectofacies was most probably within a continental arc or active continental margin settings. Some samples of the La Cantera and Don Braulio Formations, display a trend towards the Zr apex but this is related to depletion of absolute concentrations of Sc and Th rather than an important enrichment in Zr for the samples considered. These two formations along with Las Vacas, Gualcamayo and Los Azules Formations plot in Figure 3.11 in the active continental margin field or towards higher Ti/Zr ratios (indicating the influence of a depleted component). Some samples from the Las Plantas, Trapiche and La Chilca Formations instead, plot towards either the La or Zr apexes or towards the passive margin field (Figs. 3.10 and 3.11).

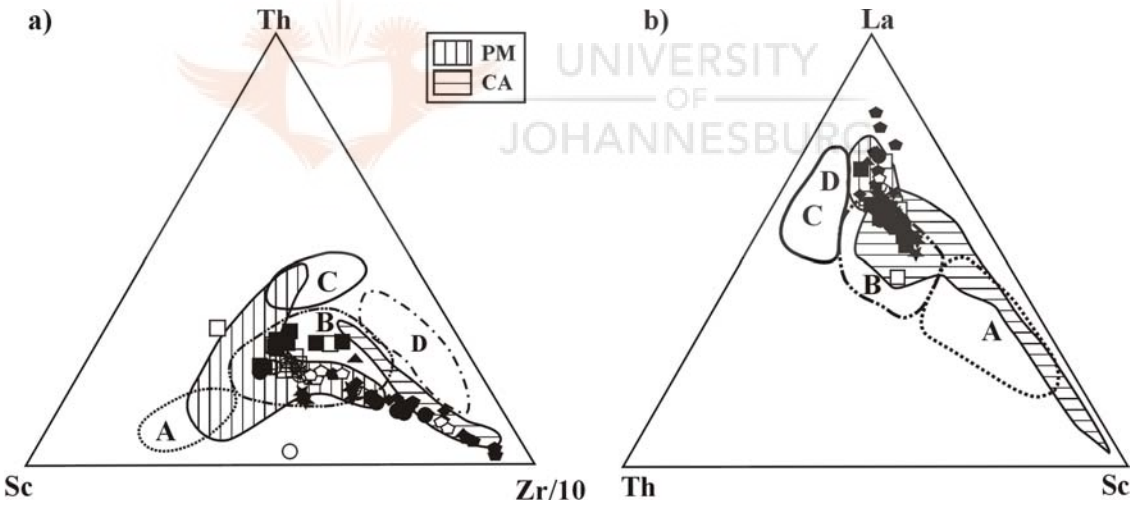

Figure 3.10: a) Th-Sc-Zr/10 and b) La -Th-Sc discriminatory plots after Bhatia and Crook (1986). A: Oceanic island arc; B: Continental island arc; C: Active continental margin; D: Passive margin. PM: recent deep-sea turbidites derived from and deposited at a passive margin. CA: recent deep-sea turbidites derived from and deposited at a continental arc margin (data from McLennan *et al.*, 1990). Sandstones are represented by solid symbols whereas mudstones are represented by empty symbols, except for the Gualcamayo Formation (solid squares) and the Los Azules Formation (empty squares). Circles: La Cantera Formation; stars: Las Vacas Formation; pentagons: Las Plantas and Trapiche Formations; triangles: Don Braulio Formation; diamonds: La Chilca Formation.

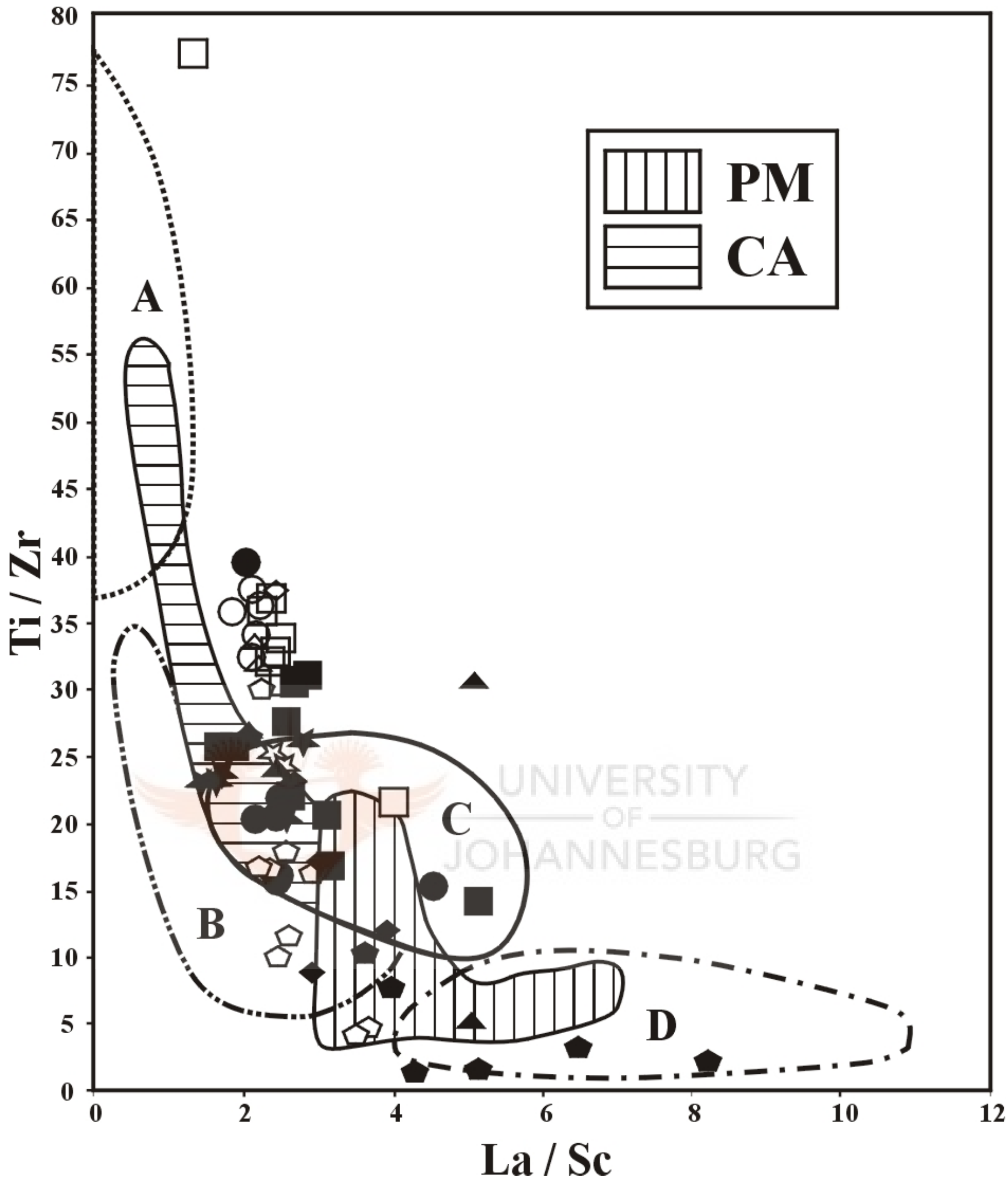

Figure 3.11: Ti/Zr versus La/Sc discriminatory plot from Bhatia and Crook (1986). A: Oceanic island arc; B: Continental island arc; C: Active continental margin; D: Passive margin. PM: recent deep-sea turbidites derived from and deposited at a passive margin. CA: recent deep-sea turbidites derived from and deposited at a continental arc margin (data from McLennan *et al.*, 1990). Sandstones are represented by solid symbols whereas mudstones are represented by empty symbols, except for Gualcamayo Formation (solid squares) and Los Azules Formation (empty squares). Circles: La Cantera Formation; stars: Las Vacas Formation; pentagons: Las Plantas and Trapiche Formations; triangles: Don Braulio Formation; diamonds: La Chilca Formation.

When analyzing the absolute values of samples plotting towards the La or Zr apexes (see Table 1 in Appendix A; Las Plantas, Trapiche and La Chilca Formations), no enrichment in La is observed, but instead an important depletion of Sc and Th compared with the UCC values (McLennan *et al.*, 2006). The same samples show instead high Zr absolute values. The same behaviour is shown by these samples in the Ti/Zr – La/Sc diagram (Fig. 3.11), because due to their low Sc concentration the La/Sc ratios are higher than the UCC and the Ti/Zr ratio is low.

The influence of an arc-provenance component might be deciphered using trace elements ratios such as Th/Sc and Eu_N/Eu^* and element concentrations of Ti and Nb. Low Th/Sc ratios, Eu_N/Eu^* of about 1 and strong negative Nb and Ti anomalies characterize continental arc components, although differentiated arcs would have variable Th/Sc ratios and Eu_N/Eu^* between 0.6 and 0.9 (Hofmann, 1988; McLennan *et al.*, 1993; Zimmermann, 2005). Th/Sc ratios for the Eastern tectofacies range from below to above UCC values. Eu_N/Eu^* are generally below 0.66 (with some exceptions already discussed). The Nb and Ti negative anomalies are not present (Table 1 in Appendix A). Therefore, an arc component seems unlikely.

3.5 HEAVY MINERALS

The heavy minerals fraction of the La Cantera, Las Plantas and Trapiche Formations is composed of zircon, tourmaline, epidote and hematite, but titanite is also present in the Las Plantas and Trapiche Formations. All the abovementioned minerals plus chlorite and apatite compose the heavy minerals fraction of the La Chilca Formation. The heavy minerals fraction of the Las Vacas Formation is composed of zircon, tourmaline, epidote and pyrite. The latter is partially altered to iron oxides and iron oxy-hydroxides (goethite or lepidocrocite). Ti-bearing oxides inclusions were also observed in other minerals. Detrital and authigenic apatites were observed.

The heavy mineral fraction of the Don Braulio Formation is composed of zircon, chromian-spinel, pyrite, apatite, tourmaline and barite, in order of abundance. Chlorite is a very common phase containing Ti-bearing oxides as inclusions, but this phenomenon was also observed in K-feldspar and quartz. As spinel is the more important heavy mineral phase from this unit regarding provenance, it is described below.

3.5.1 Spinels

Detrital spinel grains can provide important information regarding source areas closely related to the depositional site (Arai, 1992; Oberhänsli *et al.*, 1999; Asiedu *et al.*, 2000; Garzanti *et al.* 2000; 2002; Zhu *et al.*, 2004). The main tool to decipher the nature of the source is geochemical analysis of individual grains, as melting and crystallization processes depend on the tectonic setting, and can be recorded in the chemistry of a single grain (Dick and Bullen, 1984; Kamenetsky *et al.*, 2001; Barnes and Roeder, 2001).

Chromian spinels were separated following standard methods outlined in Appendix B, from a sandstone of the Don Braulio Formation which has a Cr concentration of 59ppm. As only total iron is measured with the electron microprobe, the stoichiometric compositions of the spinels were calculated using Visual Basic macro in Microsoft Excel based on the stoichiometric formula of spinels, in order to discriminate Fe^{2+} and Fe^{3+}. Each grain was measured several times (two to four spots) depending on grain size and then an average composition was computed (Table 6 in Appendix A), as differences due to fractionation could not be observed in any one grain.

The Cr# = Cr/ (Cr+Al) atomic ratios of the separated chromian spinels range from 0.58 to 0.80 and the Mg# = Mg/ (Mg+Fe^{2+}) atomic ratios range from 0.02 to 0.62. The chromium concentration has an average of 46.3%, the ratio Fe^{2+}/Fe^{3+} ranges between 1.8 and 4.2. Fe^{3+}# ratio (Fe^{3+}# = Fe^{3+}/ (Cr+Al+Fe^{3+})) range from 0.05 to 0.17. MnO, V_2O_5 and ZnO concentrations are very low (0.40%, 0.27% and 0.63% on average respectively). The spinels are on average 50µm per 60µm in size and are anhedral to subhedral. Under the binocular microscope, the chromian spinels are black.

Chemical zoning due to changes in the composition of both melt and solid phases during crystallization might be recorded by the chromian spinels. However, no compositional variations were determined, as there is no difference between core and rim, neither intergrowths nor exsolution of other mineral species. This homogeneous pattern indicates that there was no sub-solidus re-equilibration between spinels and other minerals (Scowen *et al.*, 1991).

The TiO_2 versus Cr# relationships (Arai, 1992) gives a first approximation to the original magma type from where the spinels had crystallised. Samples from the Don Braulio Formation are related to tholeiitic intra-plate basalts, although two samples plot in the area where the tholeiitic intra-plate basalts field overlaps the MORB field and one plots within the arc field (Fig. 3.12).

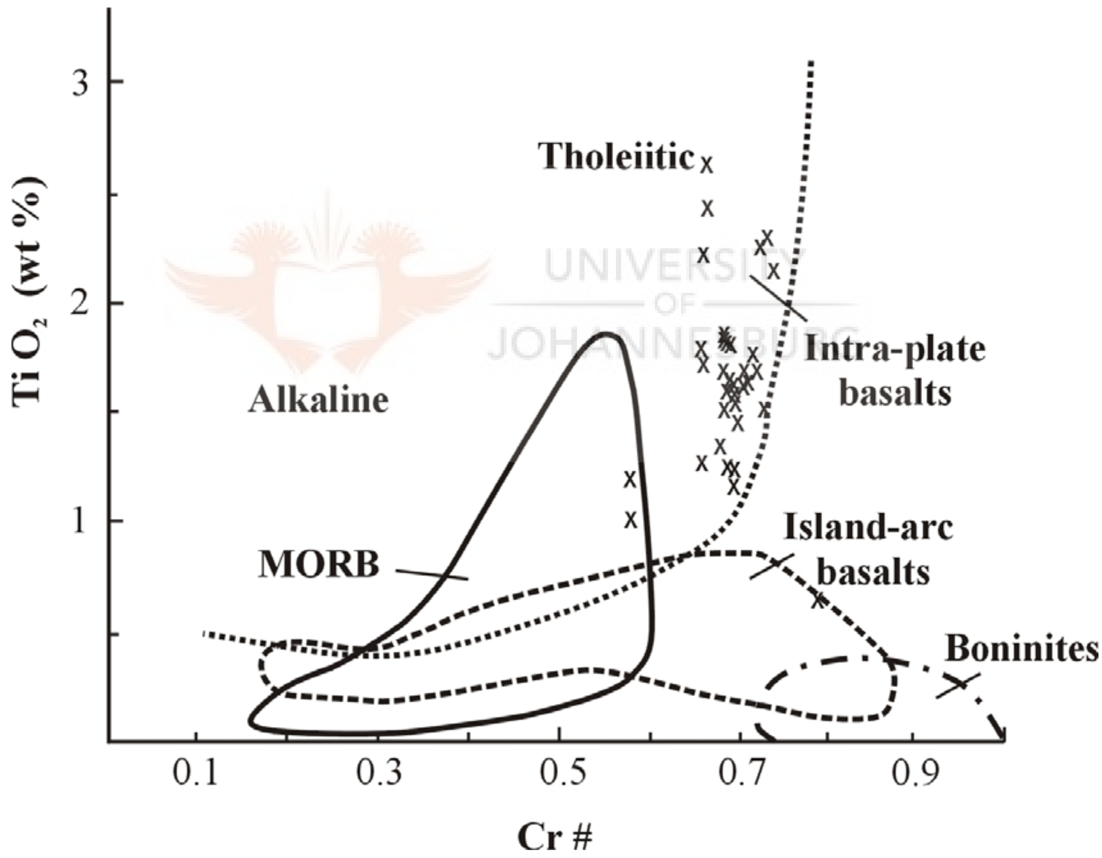

Figure 3.12: TiO_2 versus Cr# relationships for the spinels of the Don Braulio Formation according to Arai (1992). Samples plot within the tholeiitic intra-plate basalts field. MORB: mid-ocean ridge basalt.

Spinel Al_2O_3 and TiO_2 concentrations depend on the parental melt composition and therefore, their relationship allows the discrimination between different tectonic settings (Kamenetsky *et al.*, 2001). In Figure 3.13, it is evident that the chromian spinels from the Don Braulio Formation are derived from rocks related to ocean island basalts, although again some samples show certain spreading as mentioned above. The spinels have the same composition as the 'tholeiitic basalts and boninites' group from Barnes and Roeder (2001); they are in particular, especially comparable to spinels from ocean islands (OIB in the sense of Kamenetsky *et al.*, 2001), while they differ significantly from ophiolitic basalts, boninites, MORB, Hawaiian lava lakes and island arcs.

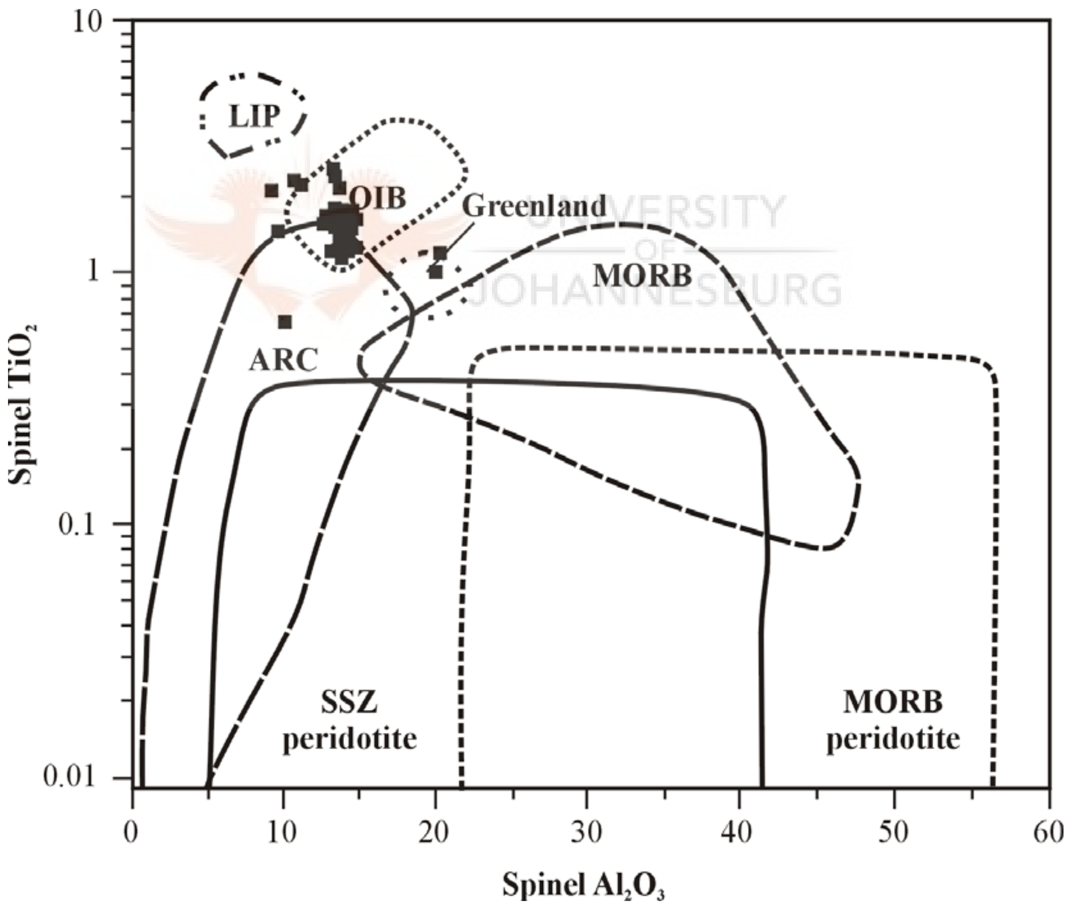

Figure 3.13: Spinel TiO_2 vs. Spinel Al_2O_3 after Kamenetsky *et al.* (2001). The spinels from the Don Braulio Formation plot mostly within the OIB field. SSZ: supra-subduction zone; OIB: ocean island basalts; LIP: large igneous provinces; MORB: mid-ocean ridge basalt.

In the Fe^{3+}# - Fe^{2+}# diagram (Fig. 3.14a) the spinels plot between the 50th and 90th percentile lines, but most of the samples do not plot inside the ocean island basalts field. Nevertheless, In the TiO_2-Fe^{3+}# diagram (Fig. 3.14b), most of the spinel grains plot within the 50th percentile of the ocean island field or between the 50th and 90th percentile. In the Cr-Fe^{2+}# diagram (Fig. 3.14c), most of the spinels plot within the 50th percentile line of the ocean island field, although some grains plot between the 50th and 90th percentiles and even a few grains plot outside any field. In the triangular diagram Fe^{3+}-Cr-Al (Fig. 3.14d) the spinels plot between the 90th and 50th percentile of the ocean island field.

Taking into account that the detrital chromian spinels of the Don Braulio Formation were formed related to an oceanic island setting and regarding the tectonic history of the Precordillera terrane, it is relevant to decipher the location of the source rocks, to understand their role in the geotectonic scenario. However, a chemical and textural comparison of these spinels with those hosted in probable source rocks is limited by the scarcity of spinels chemical analyses and descriptions within the surrounding ocean-island derived rocks. Nevertheless, rock assemblages with oceanic island (intraplate) affinities have been described on the Western Pampeanas Ranges (Vujovich and Kay, 1996). No spinel chemistry is currently available for any of the lithologies, and it is not possible to either accept or reject these rocks as the source area.

3.6 ISOTOPE GEOCHEMISTRY

3.6.1 Sm-Nd

The Sm/Nd ratio is primarily modified during processes of mantle-crust differentiation (although secondary processes may alter this ratio); this allows the estimation of the model age or the time at which the initial magma was separated from the upper mantle (Nelson and DePaolo, 1988). In the case of sediments, it can only approximate the average crustal residence age of the protoliths. The Sm-Nd model age method, as applied to whole-rock systems, provides the opportunity to see back through

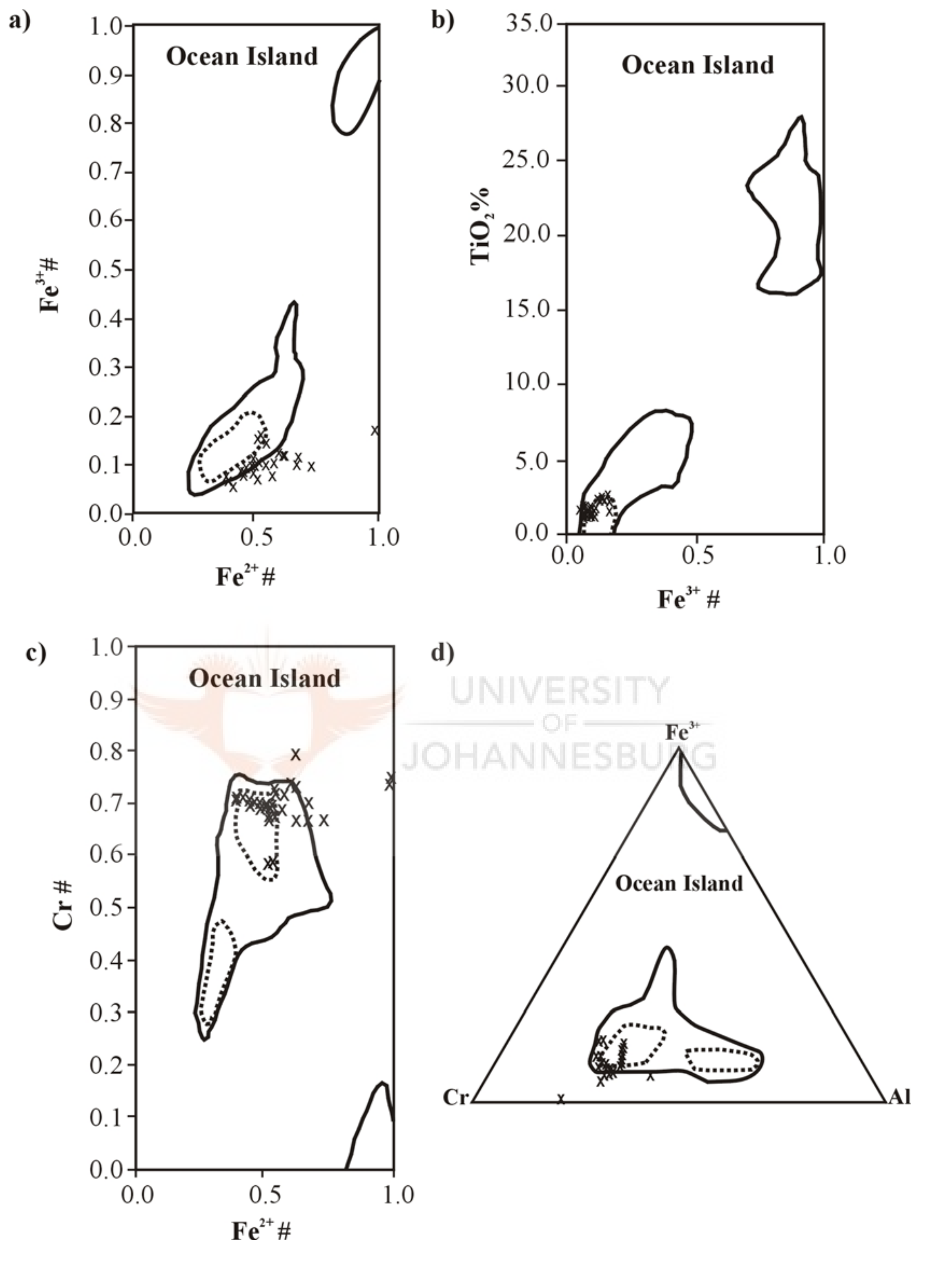

Figure 3.14: a) Fe^{3+}# - Fe^{2+}#, b) TiO_2% – Fe^{3+}#, c) Cr# - Fe^{2+}#, and d) Fe^{3+} - Cr – Al diagrams from Barnes and Roeder (2001). The solid line represents the 90th percentile while the dotted line enclosed the 50th percentile. Crosses represent spinels and the ocean-island basalt field is drawn for comparison.

erosion, sedimentation, high-grade metamorphism and even crustal melting events (McLennan et *al.*, 1989).

The ε_{Nd} (t) indicates the deviation of the $^{143}Nd/^{144}Nd$ value of the sample from that of CHUR (Chondritic Uniform Reservoir; DePaolo and Wasserburg 1976). Various studies have addressed processes that might alter the Sm-Nd isotopic signatures in detrital sediments. These include the alteration of Sm/Nd ratios and Nd isotopic signatures during weathering, diagenesis or sorting (McLennan *et al.*, 1989; McDaniel *et al.*, 1994; Bock *et al.*, 1994).

Fifteen selected samples from the Gualcamayo (n=5), Los Azules (n=5), and La Chilca (n=5) Formations were analyzed. Results are shown on Table 3 (Appendix A) and data was calculated according to DePaolo (1981), although T_{DM} according to DePaolo *et al.* (1991) are also shown and were used to compare with data from the literature that was expressed according to the three-stage model (DePaolo *et al.,* 1991). For more details about methods and analytical techniques, see Appendix B. Depositional ages (t) values are based on average ages according to the palaeontological record for each unit. ε_{Nd} (t) values (where t = 467 Ma) range from -3.50 to -5.70 (average -4.95 ± 0.88), $f_{Sm/Nd}$ (the fractional deviation of the sample $^{147}Sm/^{144}Nd$ from a chondritic reference) ranges from -0.39 to -0.45 (average -0.42 ± 0.03) whereas the T_{DM} ages range from 1.32 to 1.42 Ga (average 1.33 ± 0.033 Ga) for the Gualcamayo Formation. Los Azules Formation have ε_{Nd} (t= 462 Ma) values ranging from -4.24 to -6.42 (average -5.39 ± 0.86), $f_{Sm/Nd}$ ranging from -0.26 to -0.42 (average -0.36 ± 0.06) and T_{DM} ages ranging from 1.35 to 1.98 Ga (average 1.58 ± 0.249 Ga). ε_{Nd} (t= 436 Ma) values for samples of the La Chilca Formation range from -3.44 to -5.19 (average -4.55 ± 0.60), $f_{Sm/Nd}$ ranges from -0.28 to -0.36 (average -0.33 ± 0.03) whereas the T_{DM} ages range from 1.41 to 1.72 Ga (average 1.54 ± 0.129 Ga).

Nd-isotope systematic shows intermediate values between those typical for the UCC or older continental crust (average values from McLennan *et al.,* 1990) and those typical for source rocks derived from a magma with a Sm/Nd ratio higher than CHUR (e.g. depleted mantle), which is evident in Figure 3.15. As shown in Figure 3.16, different crustal areas would have different ε_{Nd} values calculated for the same time. The relationship between ε_{Nd} (t) and Th/Sc ratio (Fig. 3.15a) of samples from the three units analyzed show a narrow range of variation of the ε_{Nd} (t) with respect to a more significant variation in the Th/Sc ratio.

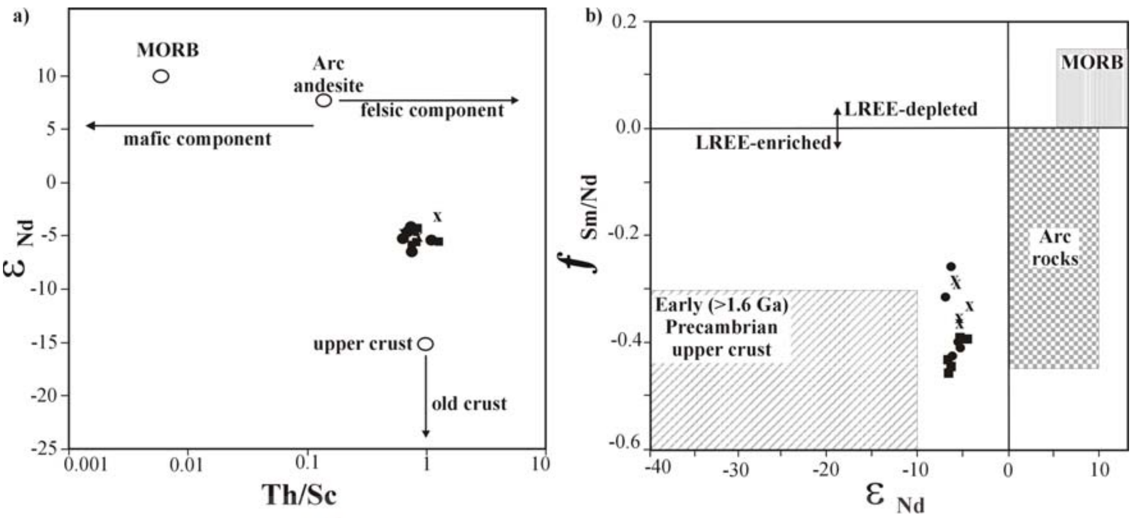

Figure 3.15: a) ε_{Nd} (t) versus Th/Sc ratio and b) Plot of $f_{Sm/Nd}$ vs. ε_{Nd} (t) for samples of the Gualcamayo (squares), Los Azules (circles), and La Chilca (crosses) Formations. $f_{Sm/Nd}$ = $(^{147}Sm/^{144}Nd)_{sample}$ $/(^{147}Sm/^{144}Nd)_{CHUR}$ - 1. ε_{Nd} (t) = $\{[(^{143}Nd/^{144}Nd)_{sample\ (t)}\ /(^{143}Nd/^{144}Nd)_{CHUR\ (t)}] - 1\}$ *10000. $(^{147}Sm/^{144}Nd)_{CHUR}$ = 0.1967. $(^{143}Nd/^{144}Nd)_{CHUR}$ = 0.512638. Data were calculated based on the depleted mantle model (DePaolo, 1981).

Figure 3.15b plots $f_{Sm/Nd}$ (the fractional deviation of the sample $^{147}Sm/^{144}Nd$ from a chondritic reference) of the Gualcamayo, Los Azules and La Chilca Formations versus ε_{Nd} (t), where ε_{Nd} (t) is ε_{Nd} at the age of sedimentation. Except for two, samples of the Los Azules Formation have $f_{Sm/Nd}$ values similar to those from the Gualcamayo Formation. However, two samples from the Los Azules Formation (020405 and 020407) show clearly less negative $f_{Sm/Nd}$ values (-0.26 and -0.31 respectively) forming a vertical array (Fig. 3.15b). The Sm/Nd ratio of these two samples is higher than the ratio of the rest of the samples. Fractionation of LREE can occur during diagenesis or even during weathering (Bock *et al.*, 1994; McDaniel *et al.*, 1994). This behaviour could be explained by the loss of a mineral phase crystallized at the time of deposition (Bock *et al.*, 1994). Similarly, two samples from the La Chilca Formation (020401 and 020402) also show lower $f_{Sm/Nd}$ values (-0.29 and -0.28 respectively) comparing to the rest of the samples of this unit, but nor CIA neither Ce/Ce* anomalies indicating weathering. On the other hand, these two samples are the less silica-rich rocks of the La Chilca Formation and they show the highest ΣREE. Instead, they show enrichment in Nd (35ppm for both), that could be assigned to selective sorting (of monazite for example; Burt, 1989; Taylor and McLennan, 1985; McDaniel *et al.*, 1994) or the formation of authigenic mineral phases LREE- (and particularly Nd-) enriched such as florencite (McDaniel *et al.*, 1994).

Nd-isotope analyses carried out by Gleason *et al.* (2006) on thirteen samples from the Gualcamayo (n= 9) and Los Azules (n= 4) Formations yield average values of ε_{Nd} (t) of -6.83 ± 0.35 and -5.08 ± 0.32 respectively and average T_{DM} ages (calculated according to DePaolo, 1981) of 1.57 ± 0.12 Ga and of 1.47 ± 0.17 Ga respectively. Their dataset is therefore similar to the here presented data and differences between samples from the Villicúm and the Guandacol areas (Fig. 3.2) are not detected by them so as not in the presented data (for both studies the two areas were sampled; Gleason *et al.*, 2006; this study). Data for the La Cantera ($\varepsilon_{Nd\ t=450\ Ma}$ values are -6.0 and -6.4), Don Braulio ($\varepsilon_{Nd\ t=450\ Ma}$ values are -6.5), and for the Las Vacas Formations ($\varepsilon_{Nd\ t=450\ Ma}$ values are -6.5) are also comparable to Nd-data for other units from the Eastern tectofacies (this study; Gleason *et al.*, 2006).

The similarity between the ε_{Nd} (t) values of the older (Gualcamayo and Los Azules Formations) and younger (La Chilca Formation) units indicate that the isotopic signature of the source mix seems to be constant through time, which do not exclude changes in the source area or in the tectonic setting of the basins, despite subtle changes observed by a few geochemical indicators (Th/Sc; see above). The T_{DM} ages are comparable to T_{DM} ages for Mesoproterozoic and Palaeozoic supracrustal rocks of the Precordillera terrane (Kay *et al.*, 1996; Cingolani *et al.*, 2003a; Cingolani *et al.*, 2005a; Gleason *et al.*, 2006). They are also comparable to Neoproterozoic to Palaeozoic sequences from northwestern Argentina (Rapela *et al.*, 1998; Bock *et al.*, 2000; Lucassen *et al.*, 2000; Zimmermann and Bahlburg, 2003; Table 3.1. Table 3 in Appendix A compile data calculated according to DePaolo *et al.,* 1991 as well in order to compared with data found in the literature). Similar data is known from the basement of Chilenia (Fig. 3.1a; Bahlburg *et al.*, 2001) and from Mesoproterozoic rocks from Antarctica, Falklands/Malvinas plateau and Natal-Namaqua Metamorphic belt (Wareham *et al.,* 1998).

Location	**Age (Ga)**	ε_{Nd}	T_{DM} **(Ga)**
Pampeanas Ranges[1]	0. 52	-3.1 to -7.7	1.48 to 1.82
Patagonia, Argentina[1]	0. 46 to 0.58	-0.7 to -6.1	1.13 to 1.66
Puna, Northern Argentina[1]	0.47 to 0.49	-1.4 to -11.6	1.32 to 2.05
Pampeanas Range, Velasco area[2]	Lower Palaeozoic	-5.5 to -10	1.23 to 1.56
Pampeanas Range, Paimán area[2]	Lower Palaeozoic	-6.1 to -6.3	1.32 to 1.34
Pampeanas Range, Copacabana area[2]	Lower Palaeozoic	-8.4 to -10	1.4 to 1.54
xenoliths Precordillera basement[3]	1.1	+2 to +7	0.8 to1.68
granite within Pie de Palo[4]	0.47 to 0.48	-3.6 to -2.6	1.41 to 1.48
Angaco, Pie de Palo Range[5]		-4.7 to -7.5	1.4 to 1.7
Cerro Salinas carbonates[5]		-11 to -30.5	1.7 to 1.8
La Laja Fm., Precordillera terrane[5]	Cambrian	-8.3 to -10.9	1.3 to 1.7
Las Matras block[6]	1.2	+1.6 to +2.1	1.55 to 1.6
Cerro La Ventana Fm.[7]	1.1 to 1.2	+1.4 to +3.3	1.2 to 1.3
Southern Africa, Natal (Mzumbe gneiss and Equeefa)[8]	1.1 to 1.23		1.21 to 1.47
East Antarctica, Dronning Maud Land gneisses[8]	1.13 to 1.15		1.4 to 2.46
Falkland/Malvinas Islands (Cape Meredith gneiss)[8]	1.1		1.3
Falkland/Malvinas plateau (Maurice Ewing gneiss)[8]	1.1		1.6
Chilenia basement[9]		-6 to -10	1.3 to 1.6
Chilenia basement (juvenile input)[9]		4.5	0.8

Table 3.1: Nd-isotope data from considered probable source areas of the Eastern tectofacies. See text for discussion. [1]Compiled in Adams *et al.* (2005); [2]López *et al.* (2006); [3]Kay *et al.* (1996); [4]Baldo *et al.* (2005); [5]Naipauer *et al.* (2005b); [6]Sato *et al.* (2004); [7]Cingolani *et al.* (2005a); [8]Wareham *et al.* (1998); [9]Bahlburg *et al.* (2001); [1,2,8] ε_{Nd} initial and T_{DM} according to DePaolo *et al.*, 1991; for the rest of the data, ε_{Nd} is (t) and T_{DM} according to DePaolo, 1981. See also Table 3 in Appendix A.

ε_{Nd} (t) values for the Eastern tectofacies are similar to those from the Pavón Formation, San Rafael block of the Precordillera terrane (Cingolani *et al.*, 2003a). Figure 3.16 shows that ε_{Nd} values for the Eastern tectofacies are similar to those from Famatina (Pankhurst *et al.*, 1998), but a main provenance from the arc itself is not supported neither by geochemistry nor by detrital zircon dating (see section 3.7). ε_{Nd} values are within the range of variation of Laurentian Grenville crust (Patchett and Ruiz, 1989), Central and Southern domains of the Arequipa-Antofalla Basement (Loewy *et al.*, 2004), and the basement of the Precordillera known as the Cerro La Ventana Formation (Cingolani, unpublished data). ε_{Nd} values from the Western Pampeanas Ranges are scarce, but a broad similarity with data here presented is evident

(Fig. 3.16). The abovementioned imply that the source cannot be defined based solely on Sm-Nd signature and geochemistry, particularly when data are widespread such as the case of the Central and Southern domains of the Arequipa-Antofalla Basement (light grey area on Fig. 3.16).

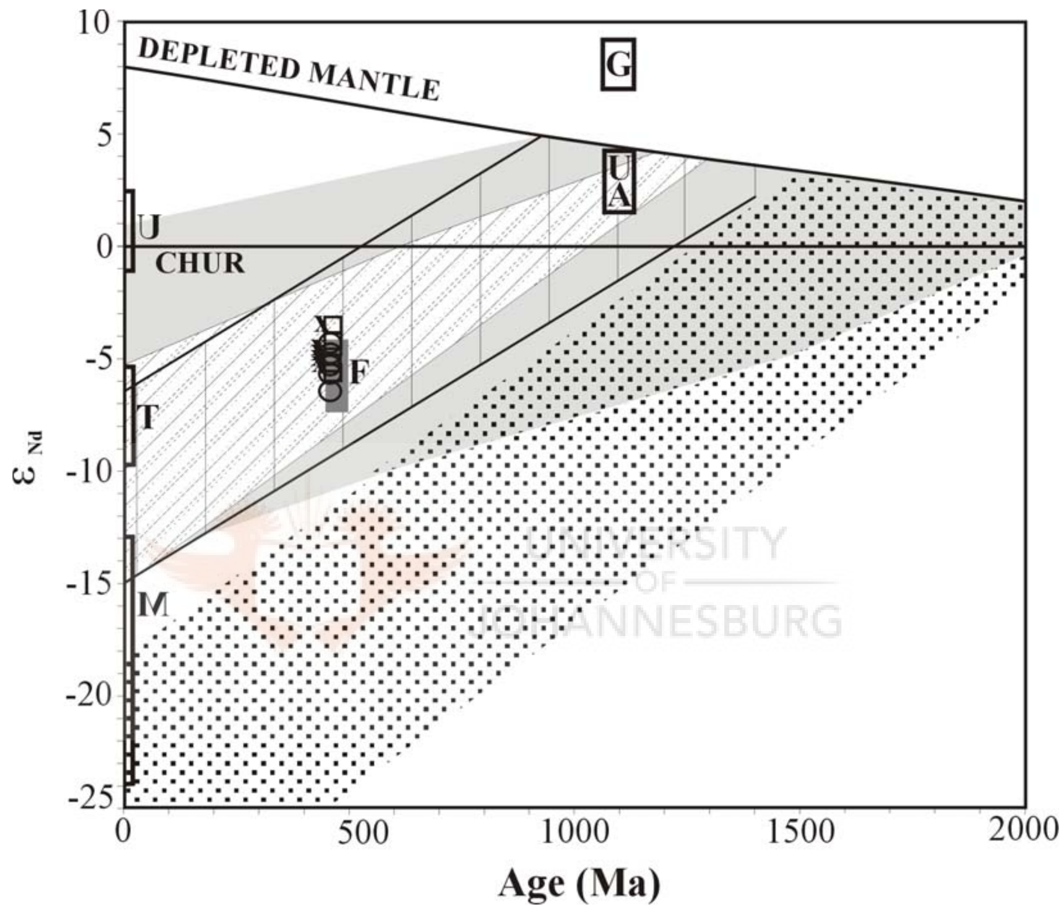

Figure 3.16: ε_{Nd} versus age of the units studied (Empty circles: Los Azules Formation; empty squares: Gualcamayo Formation; crosses: La Chilca Formation) and of areas evaluated as probable sources. Dotted area: range of ε_{Nd} for the Northern domain of the Arequipa-Antofalla Basement and light grey area: Central and Southern domains of the Arequipa-Antofalla Basement (Loewy *et al.*, 2004). Field of vertical lines: Laurentian Grenville crust (Patchett and Ruiz, 1989). A: granulitic and amphibolitic, and G: acidic-gneissic, xenoliths from the inferred basement of the Precordillera (Kay *et al.*, 1996). F denoting dark grey rectangle: Famatinian magmatic rocks (Pankhurst *et al.*, 1998). U: Umango Range, T: El Taco Complex, and M: Maz Complex from the Western Pampeanas Ranges (Vujovich *et al.*, 2005). White field with diagonal lines: Cerro La Ventana Fm. (Cingolani *et al.*, 2005a).

3.6.2 Pb-Pb

Pb isotopes provide a different view of sediment provenance compared with other isotope systems. The relationship between Pb isotopic composition and tectonic setting is not straightforward, but it is possible to discriminate between ancient upper continental crust and younger terrains (especially in terms of $^{207}Pb/^{204}Pb$). Studying Pb-isotopes on whole-sedimentary rocks might be complex due to the effect that several processes like U enrichment and selective sorting can have on the Pb system (McLennan *et al.*, 2000; Hemming and McLennan, 2001).

The black shales from the Gualcamayo and Los Azules Formations have uranogenic lead compositions similar to the upper continental crust value (Fig. 3.17), whereas the thorogenic-Pb is more similar to that from globally subducted sedimentary rocks (GLOSS; Fig. 3.18). $^{206}Pb/^{204}Pb$, $^{207}Pb/^{204}Pb$ and $^{208}Pb/^{204}Pb$ range from 19.2 to 19.60, 15.68 to 15.77, and 38.7 to 39.22 respectively for the Gualcamayo Formation and from 19.1 to 19.76, 15.7 to 15.83, and 38.83 to 39.01 respectively for the Los Azules Formation (Table 4 in Appendix A). In the various present-day Pb-ratios diagrams, the samples from the La Chilca Formation plot along a trend from values similar to the upper continental crust and towards higher values for all the Pb-ratios (Figs. 3.17 and 3.18). $^{206}Pb/^{204}Pb$, $^{207}Pb/^{204}Pb$ and $^{208}Pb/^{204}Pb$ range from 19.04 to 21.2, 15.7 to 17.3, and 39.11 to 42.93 respectively for the La Chilca Formation (Table 4 in Appendix A). Pb data provided by Gleason *et al.* (2006) indicate for the Gualcamayo, La Cantera and Los Azules Formations $^{206}Pb/^{204}Pb$, $^{207}Pb/^{204}Pb$ and $^{208}Pb/^{204}Pb$ ratios ranging from 18.89 to 19.81, from 15.65 to 15.72, and from 38.51 to 39.46 respectively.

On an uranogenic-Pb diagram, the samples from the Eastern tectofacies plot slightly above the Stacey and Kramers (1975) second stage Pb evolution curve for the average crust. The comparison between the here presented Pb dataset with those available from the literature is important to decipher the probable source. The probable rock sources used for comparison are dependent on both, palaegeographical possibilities of acted as a source (and this linked to the different models proposed for the geotectonic evolution of the Precordillera terrane), and availability of Pb data.

Comparing the lead isotopic system of the Eastern tectofacies with probable source areas (Figs. 3.17 and 3.18), it is evident the similarity with Middle Proterozoic rocks of the Arequipa–Antofalla Basement (Aitcheson *et al.*, 1995; Tosdal, 1996 and references therein; Loewy *et al.*, 2004).

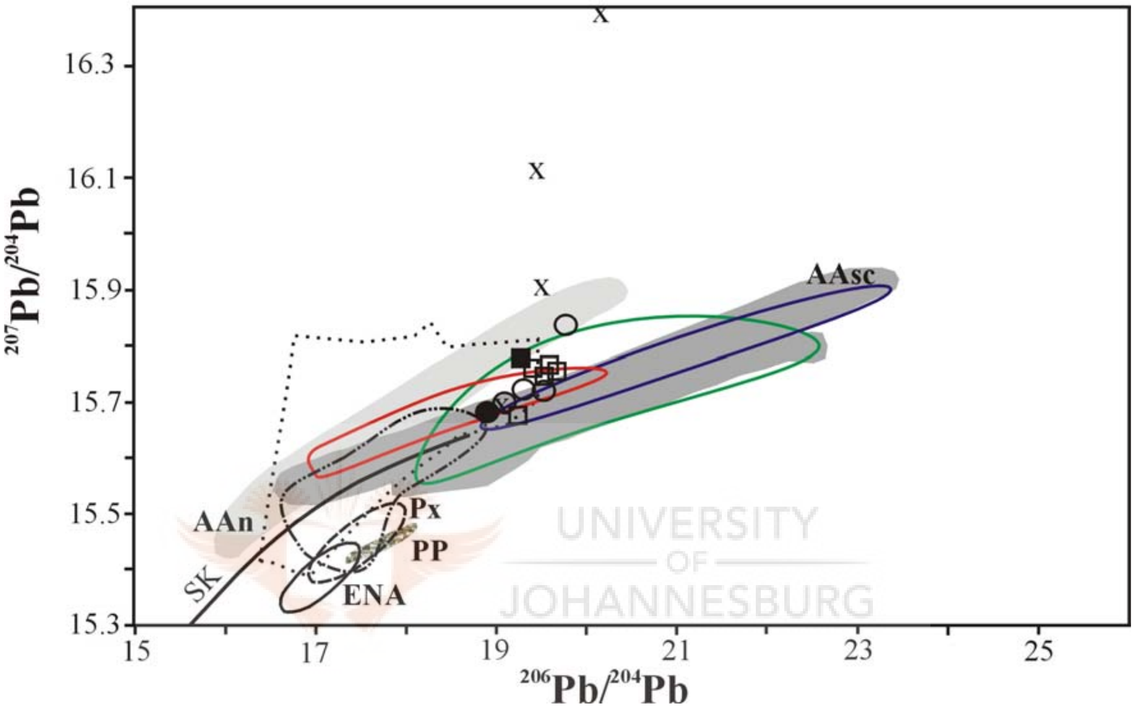

Figure 3.17: $^{207}Pb/^{204}Pb$ versus $^{206}Pb/^{204}Pb$ present-day ratios. Empty circles: Los Azules Formation; empty squares: Gualcamayo Formation; crosses: La Chilca Formation; solid square is the average value for the upper crust and solid circle the average value for GLOSS, both from Hemming and McLennan (2001). Fields obtained from several sources as indicated in the text. ENA denoting solid line: Eastern North America; Px denoting dashed line: xenoliths from the Precordillera terrane; AAsc and AAn: Arequipa-Antofalla Basement Southern and Central domains, and Northern domain respectively; PP: Pie de Palo Range; SK: Stacey and Kramers reference line; blue line: supracrustal Ordovician rocks from the Precordillera terrane (Gleason *et al.*, 2006); dotted line: Palaeozoic rocks from the Central Andes (Lucassen *et al.*, 2002); green line: Palaeozoic rocks from southern Central Andes (Bock *et al.*, 2000); red line: Ordovician rocks from south Bolivia (Egenhoff and Lucassen, 2003); double dotted-dashed line: data from Wareham *et al.* (1998; see text).

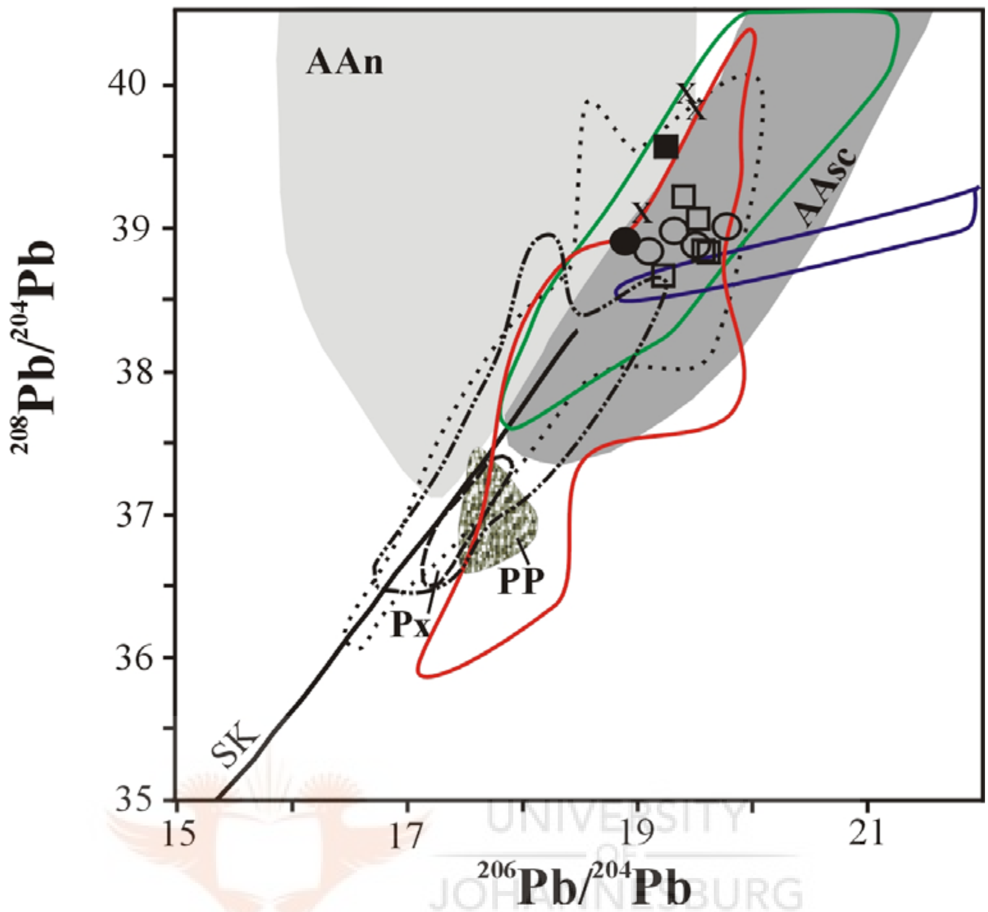

Figure 3.18: $^{208}Pb/^{204}Pb$ versus $^{206}Pb/^{204}Pb$ present-day ratios. Empty circles: Los Azules Formation; empty squares: Gualcamayo Formation; crosses: La Chilca Formation; solid square is the average value for the upper crust and solid circle the average value for GLOSS, both from Hemming and McLennan (2001). Fields obtained from several sources as indicated in the text. Px denoting dashed line: xenoliths from the Precordillera terrane; AAsc and AAn: Arequipa-Antofalla Basement Southern and Central domains, and Northern domain respectively; PP: Pie de Palo Range; SK: Stacey and Kramers reference line; blue line: supracrustal Ordovician rocks from the Precordillera terrane (Gleason *et al.*, 2006); dotted line: Palaeozoic rocks from the Central Andes (Lucassen *et al.*, 2002); green line: Palaeozoic rocks from southern Central Andes (Bock *et al.*, 2000); red line: Ordovician rocks from south Bolivia (Egenhoff and Lucassen, 2003); double dotted-dashed line: data from Wareham *et al.* (1998; see text).

The Arequipa-Antofalla Basement comprises three domains (Loewy *et al.*, 2004): the Northern domain exists in southern Peru and western Bolivia. The Central domain extends from the Peru-Chile border to the northernmost part of Chile, while the

Southern domain is extended from 23º S to the northernmost part of Argentina. The area comprised in the so-called Central and Southern domains in the sense of Loewy *et al.* (2004) is almost equivalent to the ca. 500 Ma Mobile Belt of the Pampean Cycle according to Lucassen *et al.* (2000). However, the terminology of Loewy *et al.* (2004) is followed for this discussion, notwithstanding the relevance that the inclusion of the mentioned area in the Pampean Orogeny might have.

The Pb data from the Eastern tectofacies differ consistently from the xenoliths interpreted as the basement of the Precordillera terrane (Kay *et al.*, 1996), from Proterozoic rocks from Eastern North America, from Early Proterozoic rocks from the Arequipa Massif (metamorphosed terrane located in southern Perú; Tosdal, 1996 and references therein). Mesoproterozoic granitoids and orthogneisses from the Natal-Namaqua Metamorphic belt (Mzumbe gneiss), Falkland/Malvinas Microplate (Cape Meredith Complex), West Antarctica (Haag Nunataks block) and East Antarctica (Kirwanveggan and Sverdrupfjella ranges, Maud Province) have different Pb isotopic signatures (Wareham *et al.*, 1998). The Pb signature is similar to supracrustal Palaeozoic rocks from the Central Andes (Bock *et al.*, 2000; Lucassen *et al.*, 2002), as well as Ordovician sedimentary rocks of south Bolivia (Egenhoff and Lucassen, 2003). Compared with Pb data from Ordovician sedimentary rocks of the Precordillera terrane (Gleason *et al.*, 2006), these samples have higher $^{207}Pb/^{204}Pb$ and $^{208}Pb/^{204}Pb$ ratios and a narrower range of $^{206}Pb/^{204}Pb$ variation.

In summary, the Pb data from the Eastern tectofacies are comparable to source rocks from the Southern and Central domains of the Arequipa-Antofalla Basement, while the 'Laurentian' (e.g. Eastern North America and Pie de Palo Range) signature is not observed.

3.7 ZIRCON DATING

U–Pb dating of single detrital zircons is an important tool that allows the identification of mainly felsic to intermediate provenance components in clastic sedimentary rocks. Although the reasons are not well understood yet, it has been demonstrated that the Th/U ratio of metamorphic zircons is of about 0.1 or lower, whereas the Th/U ratio of igneous zircons is >0.2 or >0.5 (Vavra *et al.*, 1999; Hoskin and Schaltegger, 2003). The detrital zircon populations of the Don Braulio and La Cantera Formations, are composed of grains most probably magmatic in origin, because their Th/U ratio is >0.2. The exception is the one zircon with a Th/U ratio of 0.09 in the Don Braulio sample and one with a Th/U ratio of 0.16 within the La Cantera sample (Table 5 in Appendix A). This is confirmed by internal textures observable on cathodoluminescence (CL) photographs of the zircons dated (Figs. 3.19 and 3.20).

Detrital zircon ages main populations for the Don Braulio Formation (Fig. 3.19) cluster at 1000 – 1300 Ma, at 542 – 1000 Ma and at 1300 – 1600 Ma. Only three grains are Palaeoproterozoic in age and one grain has a Cambrian age. The youngest detrital zircon age is 524 Ma, whereas the oldest has an age of 1964 Ma for the Don Braulio Formation (n= 42). Figure 3.20 shows main peaks of detrital zircon ages for the La Cantera Formation (n= 38) at 1000 – 1300 Ma, at 1300 – 1600 Ma and at 542 – 774 Ma. Only two zircons are older than 1600 (Palaeoproterozoic), one is 440 Ma old and two data which correspond to two areas of the same grain are Ordovician in age (463 and 477 Ma). The youngest detrital zircon age is 440 Ma, whereas the older is 1978 Ma for the La Cantera Formation. The age distribution shown by the detrital zircons is highly consistent with data from Gleason *et al.* (2006), although they found one concordant Archaean grain (2.6 Ga). Both datasets together cover a wide range of grain sizes and totalized 204 grains for the same unit. Therefore, the probability of excluding certain populations is highly unlikely.

The zircon spectrum of the Las Vacas Formation (Gleason *et al.*, 2006) also shows a main contribution from a 900 to 1300 Ma (Grenvillian-age) source (about 60% of the total zircons) and from a Late Mesoproterozoic (1300 to 1600 Ma) source (about 30% of the data). The rest of the zircon population is composed of two Pampean/Brazilian in age grains (656 and 691 Ma), six Palaeoproterozoic grains (1624 to 2191 Ma) and two Neoarchaean grains (2619 and 2717 Ma). Zircon dating done on selected clasts from the conglomerates of the clastic-wedge of the Eastern tectofacies

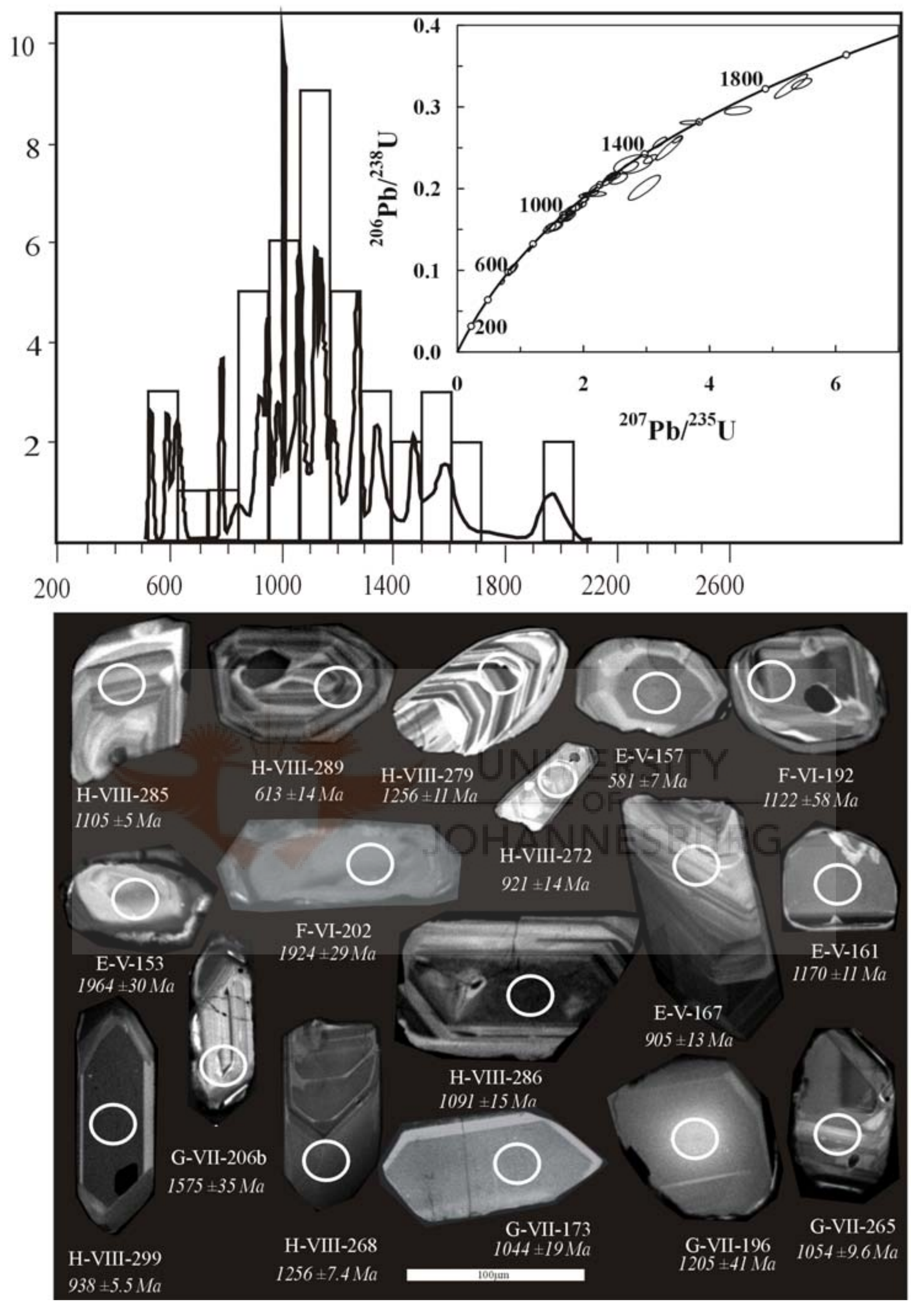

Figure 3.19: U-Pb distribution of analyzed detrital zircons with probability curves for the Don Braulio Formation (above). Concordia plot diagram in the inset area. Isoplot/Ex (Ludwig, 2001) was used for age calculations. Representative CL microphotographs of selected zircon grains used for detrital dating showing the predominance of magmatic internal textures (below). White circles denoting area of dating. Bar length is 100µm.

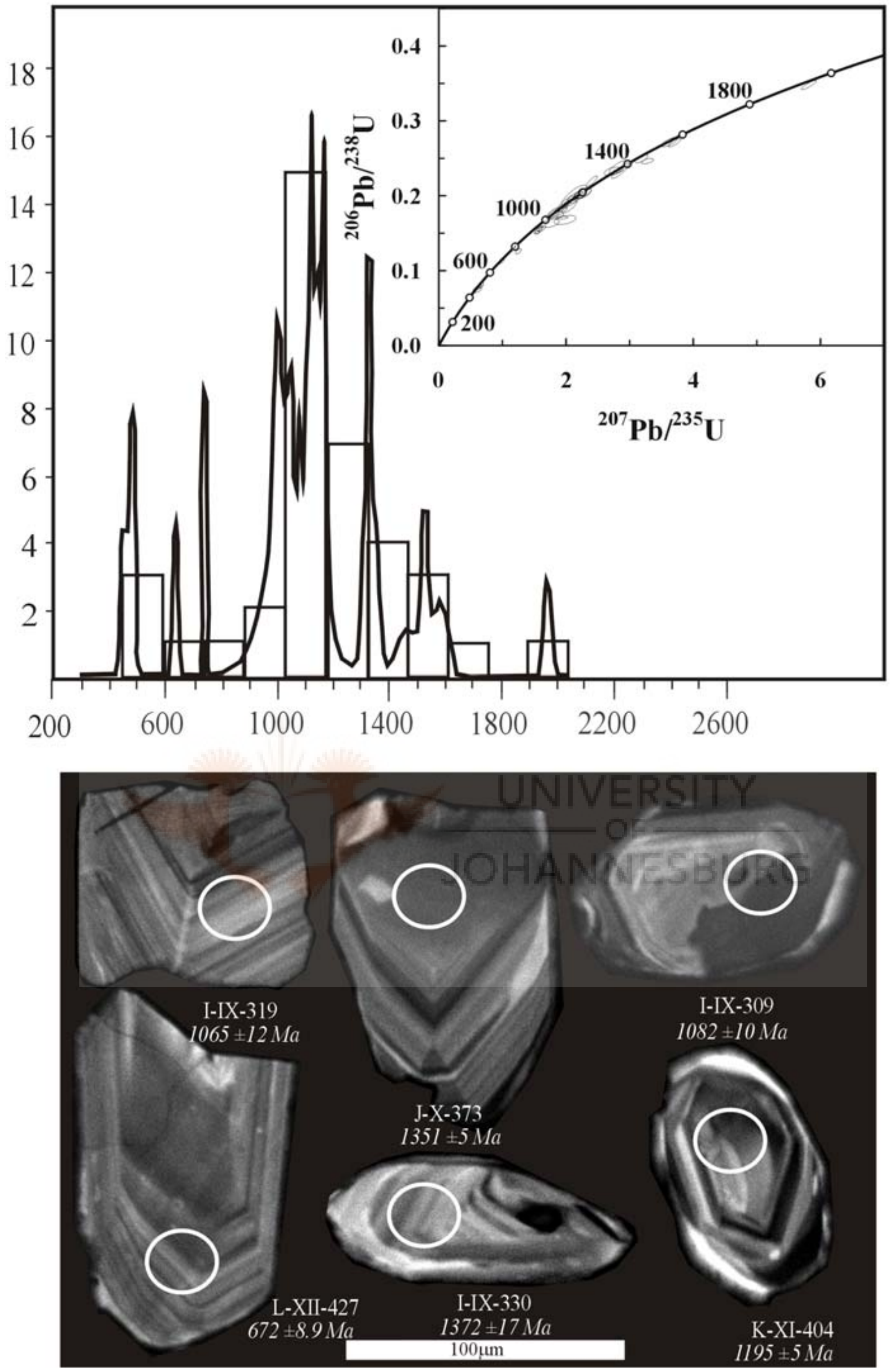

Figure 3.20: U-Pb distribution of analyzed detrital zircons with probability curves for the La Cantera Formation (above). Concordia plot diagram in the inset area. Isoplot/Ex (Ludwig, 2001) was used for age calculations. Representative CL microphotographs of selected zircon grains used for detrital dating showing the predominance of magmatic internal textures (below). White circles denoting area of dating. Bar length is 100µm.

showed that the intra and extrabasinal clasts yielded mainly Grenvillian and Neoproterozoic ages with minor older than Grenvillian peaks (Astini *et al.*, 2005).

The Neoproterozoic to Lower Palaeozoic zircons are considered most likely derived from the Pampean/Brazilian Orogen and the Famatinian arc respectively. Ages between 0.9 and 1.0 Ga (Neoproterozoic) had been found intruded within the Western Pampeanas Ranges and the Arequipa-Antofalla Basement. Rocks that match this age range are also present in the Amazon craton (Sunsas belt), although a source located further afield is improbable according to sedimentological features. Mesoproterozoic rocks that could have contributed to the more important cluster of detrital zircons of the Don Braulio and the La Cantera Formations are present in several neighbouring areas. For example, in the basement of the Precordillera terrane (Cerro La Ventana Formation, San Rafael block; Cingolani and Varela, 1999; Cingolani *et al.*, 2005a), in Western Pampeanas Ranges (Pie de Palo, Umango, Maz and Espinal Ranges; Varela and Dalla Salda, 1992; McDonough *et al.*, 1993; Varela *et al.*, 1996; Casquet *et al.*, 2006), in the Arequipa-Antofalla Basement (Bahlburg and Hervé, 1997 and references therein), in the Amazon craton (Loewy *et al.*, 2004, and Schwartz and Gromet 2004 and references therein), in the Grenville Province of Laurentia (summary from Carrigan *et al.*, 2003) and in the basement rocks of the Chilenia terrane (Ramos and Basei, 1997).

Palaeoproterozoic rocks are also found in the Arequipa-Antofalla Basement (Bahlburg and Hervé, 1997 and references therein), the Amazon craton (see Loewy *et al.*, 2004, and Schwartz and Gromet 2004 and references therein), within Laurentia (summary from Carrigan *et al.*, 2003) but also at certain areas of the Western Pampeanas Ranges (Maz Range; Casquet *et al.*, 2006). Palaeoproterozoic ages had been reported from the Río de la Plata Craton as well, but they are older than those found in the present study within the detrital record of the Eastern tectofacies (Rapela *et al.*, 2007).

Detrital zircon dating (U-Pb SHRIMP) from sedimentary and metasedimentary rocks presented by Rapela *et al.* (2007) shows that a conspicuous Mesoproterozoic population similar to the one observed in this study for the Eastern tectofacies, is present in the El Gigante Complex, Morteritos schists (n= 54), from the Western Pampeanas Ranges. However, samples from Balcarce Formation (Tandilia Belt; n=48) and Ancasti Formation (Pampean Belt; n= 73) also display an important Mesoproterozoic population, but in either cases it is accompanied by equally or more important Neoproterozoic to Lower Palaeozoic populations and also by older than 1.6 Ga zircons, being therefore different to the detrital zircon ages pattern of the Eastern tectofacies. The zircon age distribution from the El Gigante Complex is interpreted as derived from Western Pampeanas Ranges (Rapela *et al.,* 2007). Detrital zircon age dating of Famatinian Ordovician sedimentary rocks indicate that the Río de la Plata Craton was a source in Early Ordovician times, and that the Famatinian basin received detritus from Western Pampeanas Ranges (Rapela *et al.*, 2007). Therefore, zircons from the Río de la Plata should have not easily reached the Precordilleran basin (as demonstrated by detrital zircon ages).

3.8 DISCUSSION

Petrographic analyses indicate a main provenance from an igneous-metamorphic complex including an input from reworked sedimentary successions. Geochemical data indicate a variable major element composition influenced by highly variable CaO and SiO_2 concentrations. Geochemical indicators of alteration (CIA, K/Cs and Th/U) suggest moderately to advanced weathering and the effects of potassium metasomatism. Certain Th/U ratios suggest a U gain, particularly for the Gualcamayo and Los Azules Formations, which can be related to environmental constraints. Low Th concentrations of certain samples are influenced by high CaO concentrations, although a low concentration of Th in the main source rocks can be an explanation as well.

Combining trace elements geochemistry and petrography it is shown that most of the samples studied have similar characteristics, with a mixed provenance of an upper continental crust component and a less fractionated component. However, the influence of the latter is difficult to determine. Th concentrations of certain samples are disturbed in CaO-rich rocks. For the Gualcamayo and Los Azules Formations the mafic input is evident through the concentration of compatible elements, in spite of the processes of sedimentary fractionation of V from Cr observable in several samples, whereas for other samples such an input is denoted by Th/Sc ratio less than 0.78, Eu-anomalies of 0.77 and low La_N/Yb_N ratios (6.53). On the other hand, the UCC component is demonstrated by the REE pattern, La_N/Yb_N ratios of about 9 (similar to the PAAS) and Eu-anomalies of 0.53 and 0.57 for other samples. The geochemical differences observable between the Gualcamayo and Los Azules Formations and the La Cantera, Las Vacas, Las Plantas and Trapiche Formations are better related to the effects of high CaO and SiO_2 concentrations and selective sorting within sandstones of the latter group of units. The La Cantera, Las Vacas and Las Plantas and Trapiche Formations also show a provenance from a dominant UCC component and a subordinated more depleted input. The less evolved component is represented by the volcanic lithoclasts, and it is geochemically represented by high concentrations of compatible elements, Th/Sc ratios of 0.64, 0.55 and 0.75 respectively and Eu-anomalies of up to 0.77. Geochemical data indicate that there were no important changes in the composition of the source area not only between the units located below (Gualcamayo and Los Azules Formations) and above the main unconformity (Guandacol Tectonic Phase) but neither between the La Cantera, Las Vacas, Las Plantas and Trapiche Formations. However, sedimentary lithoclasts had been observed within the latter group of units which are absent in the other formations.

The determination of this sedimentary component is important, because a part of the Las Plantas and Trapiche Formations samples along with the Don Braulio and La Chilca samples do not indicate such a component. It is clear that towards younger depositional ages the detrital grains tend to be more rounded, better sorted, and finer grained, and sandstones are more quartz-rich, with less matrix and cement, with less polycrystalline quartz and a more restricted lithoclast composition (mainly chert). The changes can be related to more recycling, which produced more rounded and better-sorted framework minerals with concomitant loss of matrix and labile elements (feldspars and volcanic and sedimentary lithoclasts). These mineralogical changes caused geochemical changes such as SiO_2 and Zr enrichment, depletion in the abundances of Al_2O_3, Sc, Cr, V and ΣREE. However, some silica-rich samples are not concomitantly enriched in Zr, probably due to selective sorting. Even so, the younger units still show the dominant provenance from an upper continental crustal component and a subordinate input from a more depleted source. The less evolved input is demonstrated for the Don Braulio and La Chilca Formations by Th/Sc and La_N/Yb_N ratios as low as 0.66 and 4.9 in average respectively. The recycling could have triggered the concentration of ocean island basalt-related chromian-spinels within the Don Braulio Formation. Probable source rocks linked to ocean island settings that could have provided the detrital spinels are found within the Western Pampeanas Ranges, although this is still highly speculative.

The Sm-Nd isotope compositions of the Eastern tectofacies are characterized by ε_{Nd} (t) values between -3.4 and -6.4. A wide range of T_{DM} and $f_{Sm/Nd}$ variations (1.3 to 1.98 Ga and -0.26 to -0.45 respectively) indicate some disturbance of the Sm-Nd isotopes on certain samples of the Los Azules and La Chilca Formations. The homogeneous Nd isotopes can be caused either by complete recycling of older basement material or by the mixing of different components of different model ages. The comparison of the Sm-Nd signature with probable sources indicate similarities with the Laurentian Grenville crust, Central and Southern domains of the Arequipa-Antofalla Basement, the Cerro La Ventana Formation, the Western Pampeanas Ranges, the Famatinian arc and the Chilenian basement. Sedimentological characteristics such as palaeocurrents and the lack of important recycling tend to indicate that areas located far away of the Eastern Precordilleran basin or those located to the west can be ruled out as sources (the Amazon craton and the Chilenia terrane).

Further constraints are indicated by Pb-isotopes of the Gualcamayo, Los Azules and La Chilca Formations, since they record an influence of a source with a “Gondwanan Pb-signature”, excluding a provenance from the Laurentian Grenville crust, the Natal-Namaqua Metamorphic belt, Falkland/Malvinas Microplate and Antarctica (despite certain similarities in $^{207}Pb/^{204}Pb$ ratios for a few samples). They also exclude the xenoliths interpreted as the basement of the Precordillera terrane, which were linked to Laurentia (Kay *et al.*, 1996). Pb data from the only basement outcrop known from the San Rafael block (the Cerro La Ventana Formation) are unknown. Regarding the Western Pampeanas Ranges, the only data available from the Pie de Palo Range are dissimilar as well.

Detrital zircon dating from the Don Braulio and La Cantera Formations constrain the sources as being dominantly of Mesoproterozoic age, with a Neoproterozoic population mainly concentrated between 0.9 and 1.0 Ga. Less common are the inputs of both, older (1.6 to 2.0 Ga) and younger (Cambrian and Ordovician) sources. The same was deduced for the Las Vacas Formation (Gleason *et al.*, 2006). The scarcity of Famatinian-aged zircons indicates the absence of an important arc source. However, the presence of scarce Cambrian and Ordovician detrital zircons might suggest a vicinity of the Precordillera terrane to the western border of Gondwana as early as Middle Ordovician.

Conclusively, the sources for the eastern tectofacies might have had the following characteristics: igneous-metamorphic rocks (but also sedimentary successions), a geochemical signature similar to unrecycled UCC but including also material more depleted compared with the UCC, as well as rocks bearing chromian spinels. Constraints given by Sm-Nd, Pb-Pb, detrital zircon age dating along with sedimentological features indicate a main Mesoproterozoic source, which excludes the Laurentian Grenville crust, the Natal-Namaqua Metamorphic belt, Falkland/Malvinas Microplate, Antarctica, the Chilenia terrane, the Amazon craton and any other source located further aside.

On the other hand, the best fit to the constraints obtained according to the different approaches used to understand the provenance of the Eastern tectofacies of the Precordillera terrane, is given by the Western Pampeanas Ranges, the Arequipa-Antofalla Basement (in the sense of Loewy *et al.*, 2004; Central Andes), and the Cerro La Ventana Formation. Inputs by reworking of the underlying sedimentary successions (e.g. San Juan and Gualcamayo Formations eroded into the Las Vacas conglomerate; Hünicken and Pensa, 1989) are also clear.

The Cerro La Ventana Formation consists of mafic to intermediate gneisses, foliated quartz-diorites and tonalites that partially graded to amphibolites and migmatites, as well as acidic to intermediate granitoids and pegmatitic and aplitic veins

(Cingolani *et al.*, 2005a). Only some of all the basement rock types had been studied until today (diorites and tonalites). Sm-Nd, Rb-Sr and U-Pb on zircons indicate Mesoproterozoic ages (1.1 to 1.2 Ga; Cingolani and Varela, 1999; Cingolani *et al.*, 2005a). Samples analyzed showed geochemical and isotopic characteristics of primitive (depleted) rocks (e.g. positive ε_{Nd} values; Cingolani *et al.*, 2005a). Nd data presented by Cingolani *et al.* (2005a) of the Cerro La Ventana Formation show ε_{Nd} values in the range of variation of data calculated to the time of deposition of the Eastern tectofacies (Fig. 3.16). The consideration of the Cerro La Ventana Formation as a source, agree well with Sm-Nd data. However, Pb data from this unit are not available and only a few palaeocurrents would match a southern (present coordinates) location for an important source. Furthermore, not a complete matching for the detrital ages is found according to the current knowledge of these basement rocks. Therefore, the Cerro La Ventana Formation could have been a source, but a better knowledge is needed to further support this.

The Western Pampeanas Ranges comprise a wide range of igneous and metamorphic rocks including biotitic and dioritic-granodioritic gneisses, metamorphic rhyolites and amphibolites of Mesoproterozoic age (McDonough *et al.,* 1993). Greenschists facies metamorphic rocks such as carbonate marbles and schists, metaquartz-arenites and talc-, tremolite- and chlorite-serpentine schists are also present (Ramos *et al.*, 1993). The northernmost outcrops of the Western Pampeanas Ranges comprise marbles, calc-silicated rocks and quartz-mica schists, associated with amphibolites and ultramafic rocks, metapelites, metasandstones, metagabbros, metatonalites and tonalitic to granitic orthogneisses (Porcher *et al.*, 2004). The rocks age range includes Mesoproterozoic, Neoproterozoic (e.g. Baldo *et al.*, 2006), Palaeoproterozoic (Maz Range; Casquet *et al.*, 2006), and intrusions of Famatinian-aged granites (Casquet *et al.*, 2001). Apart from the well matching of ages, the scarce Sm-Nd isotope data available from the Western Pampeanas Ranges seems to correlate with the Sm-Nd signature of the Eastern tectofacies. Nevertheless, the few Pb data available from the Pie de Palo Range are different. However, and eastern source is very likely according to palaeocurrents. The contribution from the Western Pampeanas

Ranges is also implied by the detrital chromian-spinels of the Don Braulio Formation, although this origin for the spinels is still highly speculative due to the lack of spinel chemical analyses from the probable source.

The lack of a significant Sm-Nd and Pb-Pb dataset from the Western Pampeanas Ranges make it difficult to fully support this area as a source. However, if these Ranges along with the Arequipa-Antofalla Basement constitute a para-autochthonous single continental crustal block since the Mesoproterozoic (Casquet *et al.*, 2006), then similar isotopic signatures could be expected within both areas. Therefore, the isotopic signatures of the Eastern tectofacies are compared with those from the Arequipa-Antofalla Basement (Central Andes), which are well known. Its characteristics fit the constraints provided by the provenance proxies applied to the Eastern tectofacies. However, the northern termination of the Precordillera terrane (Jagüé area) is still under investigation and therefore the tectonic relationship with the Arequipa-Antofalla Basement rocks is currently not well determined (e.g. Astini and Dávila, 2004). Several tectonic frameworks presented had located the Precordillera terrane immediately south of the Arequipa-Antofalla Basement for the Precambrian to Early Palaeozoic (Lucassen *et al.*, 2000; Rapela *et al.*, 2007), and current outcrops are located about 300kms north of the northernmost outcrops of the Eastern tectofacies. Furthermore, a northern provenance (present coordinates) is not supported by the bulk of palaeocurrent data available.

In summary, the rocks that fit best the constraints are found within the Western Pampeanas Ranges and the Arequipa-Antofalla Basement (Fig. 3.1a), despite age and Nd signature agreements with the Cerro La Ventana Formation. However, Pb data from the latter are not available and it does not account for the complete detrital zircon dataset of the Eastern tectofacies. Furthermore, a northern provenance (from the Arequipa-Antofalla Basement) is not supported by palaeocurrents. Intensive studies regarding the isotopic signatures of the Western Pampeanas Ranges are needed to further support it as a source. Notwithstanding the uncertainties, a provenance from the Western Pampeanas Ranges was deduced for Cambrian units based on detrital zircon dating, invoking an allochthonous model (Naipauer, 2007). The subduction of the

Iapetus Ocean crust towards east started during the Cambrian (530-500 Ma; Fig. 3.21), and a Famatinian magmatic arc was accordingly developed towards west (climax at 480 to 460 Ma). As a response to the accretion, the Western Pampeanas Ranges (and its probable continuation towards north) were uplifted at 460 Ma (Casquet *et al.*, 2001; Fig. 3.21), providing thus detritus to the basin. The uplifting of such positive source also prevented the arrival to the Eastern tectofacies of the detrital material from the Famatinian arc (Figs. 3.21 and 3.22). If the Western Pampeanas Ranges was autochthonous to Gondwana and considering these Ranges as the more probable and significant sources, then a Late Arenig to Llanvirn time for the final accretion is implied.

3.9 CONCLUSIONS

From the oldest Gualcamayo Formation (Upper Arenig to Lower Llandeilo) to the youngest La Chilca Formation (Ashgill to Lower Wenlockian) the provenance of the Eastern tectofacies is mainly derived from an upper continental crustal component and a subordinated more depleted component. The absence of important changes in provenance from the Arenig to the Wenlockian has important implications on the geotectonic evolution of the Precordillera terrane. Geochemical indicators of alteration suggest moderately to advanced weathering and the effects of potassium metasomatism. The less evolved input is demonstrated for the Don Braulio Formation by the presence of detrital spinels linked to ocean island settings.

The Sm-Nd and Pb isotope compositions of the Eastern tectofacies tend to link it to typical Gondwanan areas. Detrital zircon dating for the Don Braulio and La Cantera Formations constrain the sources as dominantly of Mesoproterozoic age, but also with a peak in the range 0.9 to 1.0 Ga, and with subordinate inputs of both older (1.6 to 2.0 Ga) and younger (Cambrian and Ordovician) sources.

The Western Pampeanas Ranges and less probably the Arequipa-Antofalla Basement give the best fit to all the provenance constraints, including the chemistry of

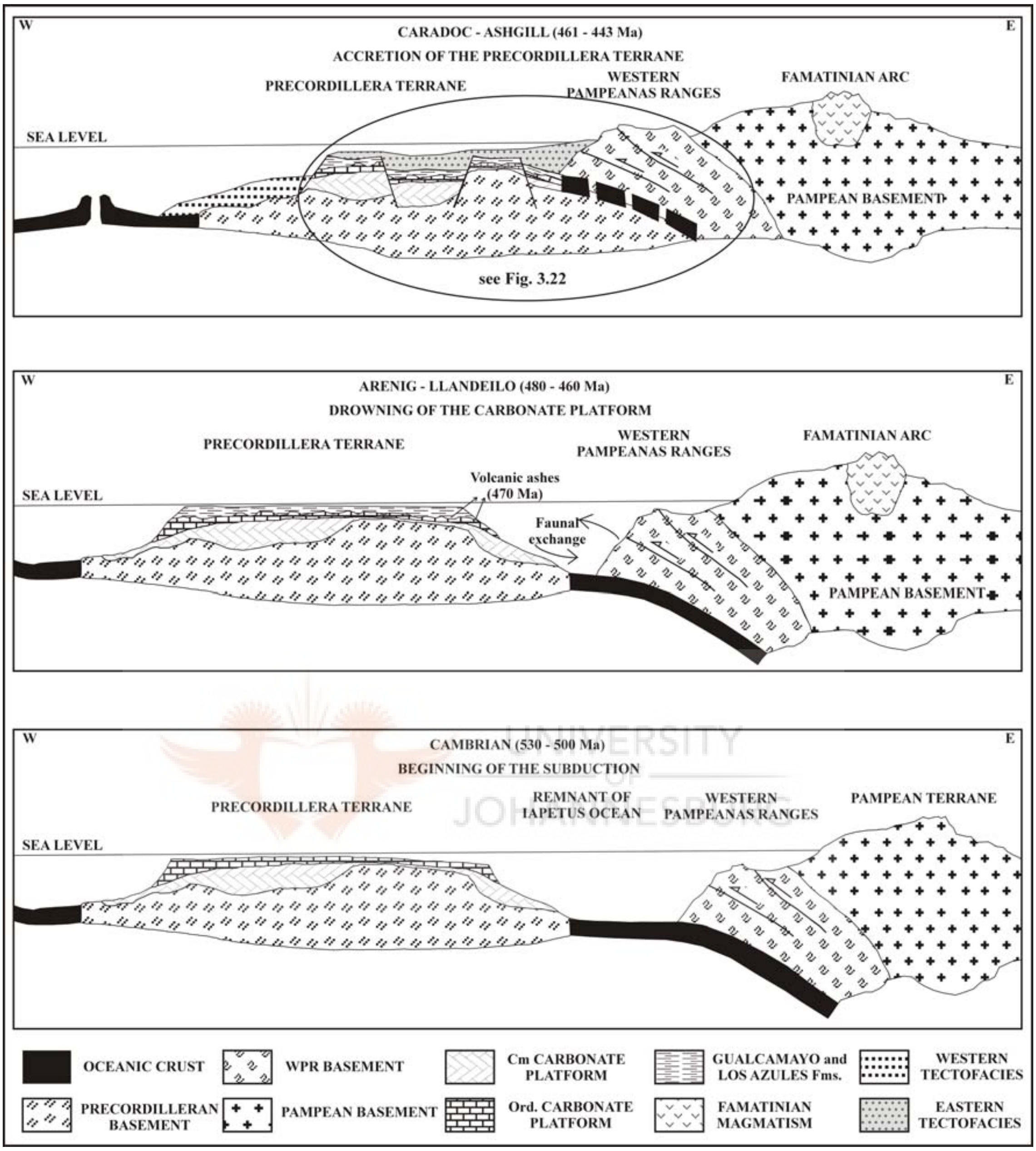

Figure 3.21: Geotectonic evolution of the Precordillera terrane. The subduction was active since the Cambrian as documented by the magmatic arc (Famatina). The volcanic ashes (nowadays K-bentonites) found within the uppermost San Juan Formation and the lowermost Gualcamayo Formation record the activity of such magmatism in the context of the Precordillera terrane. A Late Arenig to Llanvirn final accretion age is estimated for the Precordillera terrane based on data presented in this chapter, which indicate that the Cerro La Ventana Formation, the Western Pampeanas Ranges and the Arequipa-Antofalla Basement (Central Andes) are the more probable sources. (see text for discussion).

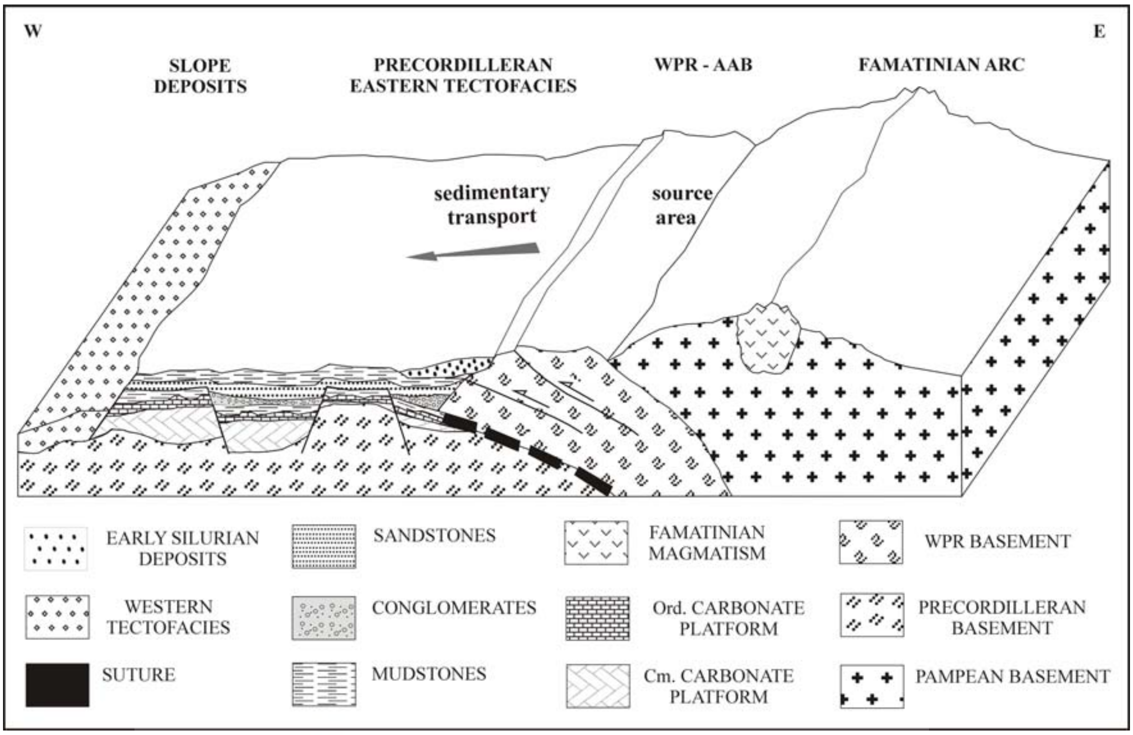

Figure 3.22: Schematic cross section showing the depositional setting (peripheral foreland) of the Eastern tectofacies. The Western Pampeanas Ranges (WPR) and its northern continuation known as the Arequipa – Antofalla Basement (AAB) are the most probable source areas and acted as the geographic obstacle for the magmatic-arc (Famatinian) detritus to reach the Precordilleran basin.

detrital chromian-spinels. The scarcity of a contribution from a contemporaneous magmatic arc (Famatina) might simply indicate that the erosional products of such area did not find their way towards the basin of the Eastern tectofacies. Because the Western Pampeanas Ranges and the Arequipa-Antofalla Basement were autochthonous to Gondwana by the time of deposition of the Eastern tectofacies, then the Precordillera terrane would have reached its present position with respect to them by the Late Arenig - Llanvirn. Palaeotectonic models that propose a later emplacement for the Precordillera terrane cannot be brought in harmony with these data.

CHAPTER 4

PROVENANCE ANALYSIS OF THE LOS SOMBREROS AND EMPOZADA FORMATIONS (SLOPE-TYPE DEPOSITS) OF THE PRECORDILLERA TERRANE, CENTRAL ARGENTINA.

4.1 INTRODUCTION

The Precordillera terrane differs from the surrounding geological provinces because a thick Cambrian-Ordovician carbonate platform succession is exposed. The presence of this carbonate platform together with sedimentological, palaeontological, palaeomagnetic and isotope data from the basement, led to speculation that the Precordillera was a terrane exotic to Gondwana, and furthermore, derived from Laurentia (Ramos *et al.*, 1986; Dalla Salda *et al.*, 1992a; Dalziel *et al.*, 1994; Astini *et al.*, 1995; Keller, 1999). However, there are models that attempt to interpret the origin of the Precordillera terrane as being para-autochthonous (Baldis *et al.*, 1989; Loske, 1992; Aceñolaza *et al.*, 2002; Finney *et al.*, 2005). All these models are still controversial and recent detrital zircon dating and Nd-isotopes data tend to indicate that the origin of the Precordillera terrane would be unresolved at least until more useful provenance data from both the Precordilleran successions and the source rocks is provided (Gleason *et al.*, 2006).

Within the Precordillera *sensu stricto* (*s.s.*) two different tectono-sedimentary environments are recognized (Fig. 4.1; Keller *et al.*, 1998). The easternmost is composed of a carbonate platform overlain by predominately clastic deposits (see Chapter 3), and a western clastic basin developed and is supposed to be a response to rifting during Middle to Late Ordovician. The western basin could in turn be divided into "slope-type" deposits adjacent to the continental rise (namely Empozada and Los Sombreros Formations) and deep-basin deposits developed "towards west" (see Chapter 5). Although the Empozada Formation is part of the San Juan, Las Plantas and Trapiche Alloformations of the Eastern tectofacies (Chapter 3) and the Los Sombreros Formation belongs to the Western tectofacies in the sense of Astini (1993a), they are

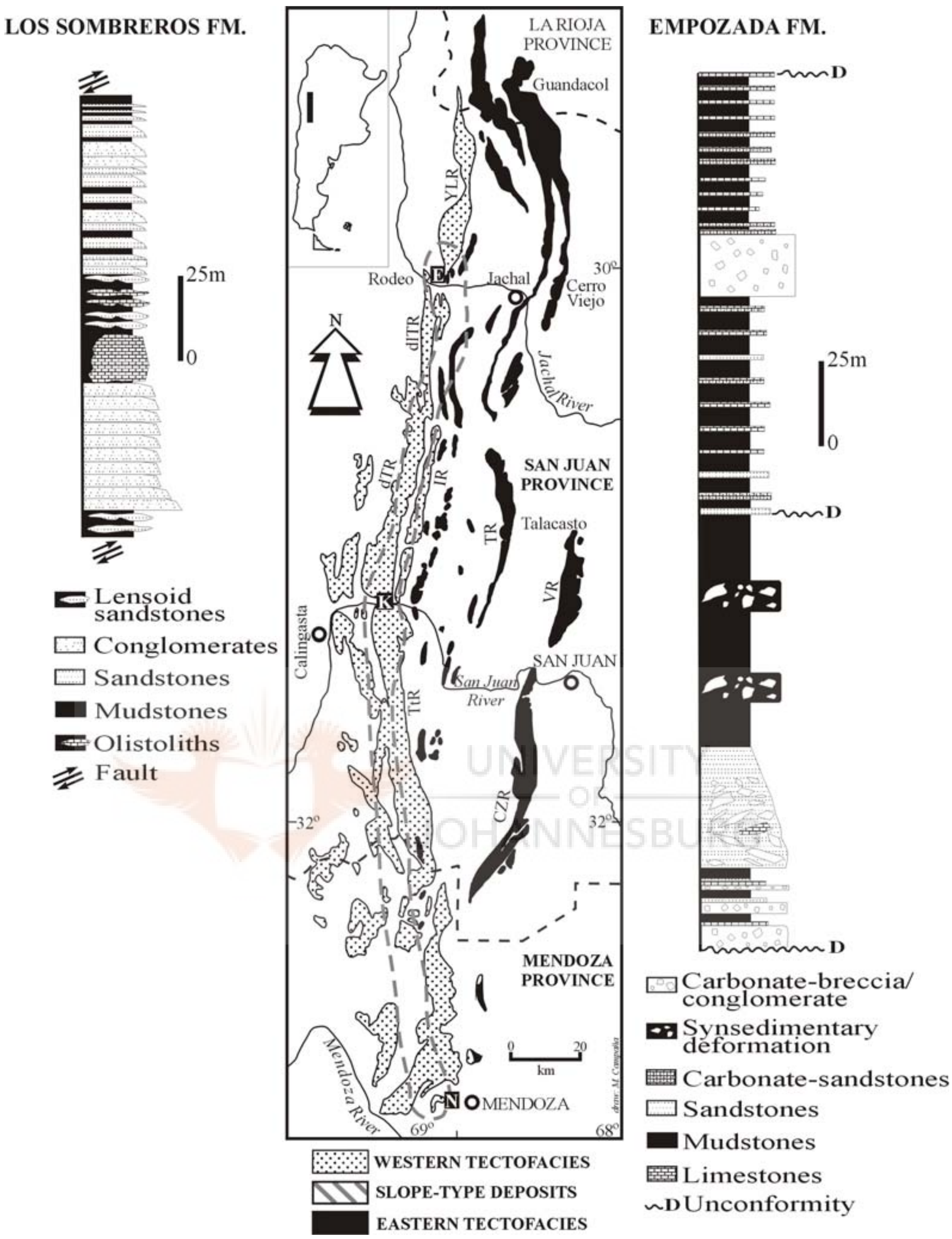

Figure 4.1: Sampling locations within the Precordillera terrane (white letters correspond to samples in Table 2 in Appendix B). Dashes line represents the Los Sombreros Formation defined by Peralta (2005). IR: Invernada Range; dTR: del Tigre Range; dlTR: de la Tranca Range; YLR: Yerba Loca Range; TR: Talacasto Range; TtR: Tontal Range; CZR: Chica de Zonda Range; VR: Villicúm Range. Modified from Astini (1991). Stratigraphic sections of the Los Sombreros Formation modified from Banchig *et al.* (1993) and of the Empozada Formation modified from Heredia and Gallardo (1996).

considered together here as part of the slope-type deposits, as they were previously by other authors (e.g. Dalla Salda *et al.*, 1992b; von Gosen *et al.*, 1995). The slope-type deposits are bounded by faults or unconformities and are developed as a transition zone in between the Eastern and Western settings. However, some faults are interpreted as reactivation of ancient faults indicating the existence of a Lower Palaeozoic slope. The presence of faults allowed studying the Los Sombreros and Empozada Formations in a separate chapter, to determine a probable different provenance component or otherwise, to support the existence of such Lower Palaeozoic slope. Furthermore, uncertainties were more recently introduced regarding their age by Peralta (2005) and Peralta and Heredia (2005), since they reinterpreted the Los Sombreros Formation as a Devonian sedimentary mélange formed in response to an extensional regime (rift–type basin). They include all the deposits exposed from north of the Río Jáchal to the San Isidro area in Mendoza (Fig. 4.1; dashed line). The Devonian age is determined based on the composition of certain olistoliths that resemble Devonian units (Peralta, 2005; Peralta and Heredia, 2005). Nevertheless, according to their graptolite contents, the matrix-layers of the olistostrome sampled for the present study are undoubtedly of Ordovician age, and therefore the outcrops sampled are denoted in the map with white letters (Fig. 4.1).

Allochthonous terranes are fundamental to the growth of continents. They mainly comprise two components to their tectonic history, one relating to their original tectonic setting and the other reflecting their subsequent histories of dispersal and accretion (McLennan *et al.*, 2006). Since the latter component tends to mask the former, considerable uncertainty might exist. The main aim of this chapter is to add new provenance-indicators data for both the Empozada and Los Sombreros Formations, with special emphasis in sedimentary geochemistry, and Sm-Nd and Pb-Pb isotopes, supported by detailed petrography including heavy minerals and clay minerals identification. The combination of these different approaches can give accurate information regarding the probable sources of the clastic detritus of the Precordillera terrane during the Ordovician, thereby constraining the existing models about its origin.

4.2 GEOLOGICAL BACKGROUND

The Empozada Formation (Harrington and Leanza, 1957) crops out in the proximity of Mendoza, Mendoza province, Argentina (Fig. 4.1). It is a 430m thick sequence of Llandeilo to Caradoc in age. The Villavicencio Formation (Devonian) overlies it through an erosive unconformity and it is in tectonic contact with the Middle Triassic Uspallata Group (Heredia and Gallardo, 1996).

The Empozada Formation is subdivided into two members (Heredia and Gallardo, 1996): the lower one is composed of breccias, conglomerates, shales, laminated mudstones, arenites and matrix-supported conglomerates deposited as gravity flows and represent olistostromic deposits with mainly Cambrian but also Lower Ordovician olistoliths from the eastern carbonate platform. Towards the top of the lower member, black shales bearing graptolites and inarticulate brachiopods are related to a sea level rise (Heredia and Gallardo, 1996). The upper member of the Empozada Formation is composed of a coarsening-up sequence of mudstones and calcarenites (carbonate-arenites), deposited in an open marine platform influenced by storms (Heredia, 1990). Based on palaeontological content the Empozada Formation can be correlated to the La Cantera (Gallardo and Heredia, 1995), Los Sombreros (Cuerda *et al.*, 1983), Portezuelo del Tontal (Spalletti *et al.*, 1989), Yerba Loca (Pereyra, 1989), Pavón (Cingolani *et al.*, 2003a), and Ponón Trehué (Heredia, 2006) Formations (Fig. 2.2).

The Los Sombreros Formation (Cuerda *et al.*, 1983) is a 1000m thick olistostromic sequence composed of Cambrian olistoliths within an Ordovician siliciclastic matrix. It crops out in the Tontal Range (Ortiz and Zambrano, 1981; Fig. 4.1). The top and bottom have inverse-fault contacts (Lehnert, 1994). The Los Sombreros Formation comprises concordantly interlayered intrusive mafic rocks (Cuerda *et al.*, 1986a) as well as conglomerate beds associated with sandstones. These conglomerates were interpreted as upper-fan channel-fills, and are composed mainly of metamorphic clasts (quartz-feldspar-mica schists, quartz-schists, quartzites, marbles, biotite gneisses and migmatites), that resemble those from the Pie de Palo Complex, in particular the Caucete Group (Mendoza *et al.*, 1997). In contrast, the olistoliths are composed of quartzites, conglomerates, granitoids and carbonate blocks. The first three rock-types are presumably derived from the basement (e.g. Pie de Palo Range), whereas the carbonates are derived from the Eastern tectofacies of the Precordillera (Astini *et al.*, 2000). Palaeocurrents indicate an east-west to southeast-northwest transport direction coincident with the slope dip-direction (Banchig *et al.*, 1993).

Graptolites provide ages from Tremadoc to Llandeilo for the matrix of the olistostrome (Cuerda *et al.*, 1983; 1986a), while the conodont ages of the carbonate olistoliths is uppermost Cambrian to lowermost Ordovician (Lehnert, 1994). The Los Sombreros Formation correlates to the Las Plantas, Los Azules and Empozada Formations (Cuerda *et al.*, 1986a). The Los Sombreros Formation is not in contact with the Empozada Formation. However, according to the reinterpretation of the Los Sombreros Formation as a Devonian sedimentary mélange formed in response to an extensional regime (rift–type basin), it overlies the Empozada Formation through an erosive discontinuity (Peralta, 2005; Peralta and Heredia, 2005). The latter interpretation includes all the deposits exposed from north of the Río Jáchal to the San Isidro area in Mendoza (Fig. 4.1). The Devonian age is determined based on the composition of certain olistoliths that resemble Devonian units (Peralta, 2005; Peralta and Heredia, 2005).

The slope deposits (Los Sombreros and Empozada Formations) were interpreted as related to a passive continental margin (González Bonorino and González Bonorino, 1991), or as an intracontinental rift basin (Dalla Salda *et al.*, 1992b), and related to crustal extension during Middle to Late Ordovician (von Gosen *et al.*, 1995). More recently, a deposition within an extensional pull-apart basin along strike-slip faults was deduced (Alonso *et al.*, 2007). Within the matrix, the penetrative cleavage planes are accompanied by the parallel growth of sericite and chlorite. Microfabrics suggest a greenschist facies metamorphism within the chlorite zone (von Gosen, 1997). Conodont Colour Alteration Index also supports this grade of metamorphism (Keller *et al.*, 1993). Deformation and metamorphism had tentatively been assigned to a Late Silurian-Early Devonian age (von Gosen, 1997).

4.3 PETROGRAPHY OF FRAMEWORK AND HEAVY MINERALS

Samples of the Empozada Formation range from limestones/silicate-sandstones (carbonate-cemented arenites where cement is almost 50%) to carbonate-cemented sandstones with 10% carbonate cement. The carbonate cement in all lithotypes has sparitic and micritic sizes and is mainly composed of calcite, although ankerite was also found. However, chlorite is present also as cement in a few samples. The siliciclastic framework components are in general subangular to subrounded, with low sphericity and are moderately to well sorted. Poorly sorted samples are also present. Grain sizes are very fine and medium, but the poorly sorted samples have granule size grains. Monocrystalline non-undulose quartz is the most abundant framework mineral and frequently presents fluid and mineral inclusions (booklets of kaolinite, muscovite and monazite). Some grains show undulose extinction. Polycrystalline quartz is also common. Rounded quartz grains with high sphericity were also observed, and in most cases, they do not show any overgrowth. However, overgrowths of quartz are present in a few cases. K-feldspar is normally more abundant than plagioclase. The latter varies from unaltered to partial replaced by calcite, and shows the typical polysynthetic twinning. K-feldspar (microcline and anorthoclase) is either altered to clay minerals or calcite replaced, or does not show any alteration; they show the typical tartar twin-type and perthites are present as well. Both feldspars present overgrowths. Lithoclasts are predominantly sedimentary and mainly derived from chert and siltstones, but volcanic lithoclasts with a very fine crystalline matrix are present as well. Calcite and quartz veins, as well as hematite and other opaque minerals occur frequently.

In order of abundance, the heavy mineral fraction of the Empozada Formation is composed of apatite, zircon, brown spinel, rutile, tourmaline and detrital muscovite, epidote, chlorite and biotite. Apatite is subhedral and ranges in size from 50µm to 250µm. Zircon is subhedral and ranges in size from 50µm to 100µm. Apatite is more abundant than zircon. The chromian spinels do not show any rim or visible zonation; they are subhedral and from 80µm to 200µm in size. Ti-oxides included in quartz, calcite and feldspar were observed, as well as barite included in carbonate lithoclasts.

The Los Sombreros Formation is composed of olistoliths embedded in a very fine siliciclastic matrix. Most of the rocks composing the matrix of the olistoliths are mudstones and their compositions were determined mainly by X-ray diffraction (XRD) techniques (see Table 3 in Appendix C): quartz, plagioclase, muscovite, illite, and chlorite are present as the main constituent while hematite and carbonate phases (ankerite, calcite and dolomite) are minor components. Petrographic analyses of siltstones and fine sandstones confirm the presence of the abovementioned minerals. Detrital grains are subangular to subrounded with low sphericity. Quartz is mainly monocrystalline, although polycrystalline grains are also present. Within the feldspar group, plagioclase is more abundant than K-feldspar and is unaltered. Microcline is partially altered to clay minerals. Muscovite and chlorite as well as biotite are detrital phases, although chlorite has been identified as an alteration product on biotite as well. Lithoclasts are derived from low-grade metamorphic rocks (phyllite) and less commonly from fine-grained volcanic rocks. Accessory minerals are zircon, apatite, tourmaline, detrital epidote and opaque minerals.

Illite crystallinity index (ICI) measured on mudstones from the Empozada Formation revealed that the unit was affected by late diagenesis to very low-grade metamorphism, although the results varied from the air-dried to the ethylene-glycol attacked specimens and the low quantity of samples analyzed may not be statistically meaningful (see Table 2 in Appendix A). The ICI analyzed from only one sample for the Los Sombreros Formation indicates a very low-grade metamorphism, in agreement with the greenschist facies metamorphism determined by Keller *et al.* (1993) and von Gosen (1997).

4.4 GEOCHEMISTRY

The chemical composition of sedimentary rocks reflects the average composition of the continental crust that shed detritus to a certain basin (Taylor and McLennan, 1985), and therefore, the geographic location and characteristics of the source area can be recognized in the ultimate composition of the sedimentary succession (McLennan and Taylor, 1991; Cox *et al.*, 1995; Andersson *et al.*, 2004). However, the signatures of the source rock may be modified by several factors such as weathering, hydraulic sorting and diagenesis, and therefore the evaluation of these factors is crucial to constrain the provenance of a sedimentary succession (Nesbitt and Young, 1982; Cullers *et al.*, 1987; Nesbitt *et al.*, 1996). Elements derived from mafic (Sc, Cr, Co) and silicic (La, Th, REE) rocks, along with REE patterns and the Eu-anomaly has been used for provenance and tectonic determinations (e.g. McLennan *et al.*, 1993). Whole-rock geochemistry also aid in the evaluation and interpretation of isotope geochemistry (e.g. McDaniel *et al.*, 1994; Bock *et al.*, 1994; McLennan *et al.*, 2000; Hemming and McLennan, 2001). In Table 1 (Appendix A), the chemistry of all samples analyzed is shown.

4.4.1 Major elements and alteration

Certain major elements can be easily mobilized during processes of diagenesis and very low-grade metamorphism (Cox *et al.*, 1995). The effects of weathering on sedimentary rocks can be quantitatively assessed using the Chemical Index of Alteration (CIA; Nesbitt and Young, 1982). This index uses molecular proportions as follows: CIA = $\{Al_2O_3 / (Al_2O_3 + CaO^* + Na_2O + K_2O)\} \times 100$. CaO* refers to the calcium associated with silicate minerals. Therefore, corrections for the measured CaO concentration regarding the presence of Ca in carbonates (calcite and dolomite) and phosphates (apatite) are needed. For this study, CaO was corrected for phosphate assuming that the P_2O_5 is entirely present in apatite. However, CO_2 data needed to calculate the CaO concentration in carbonates were unavailable. Thus, if the remaining number of CaO moles obtained after deducing those moles associated with apatite are less that the number of Na_2O moles, then this CaO value was adopted to calculate the CIA (McLennan, 1993). If the number of moles is greater than Na_2O, then those samples were not used to calculate the CIA.

Samples from the Empozada Formation have a variable major element distribution, with SiO_2 concentrations ranging from 30% to 76.4%, Al_2O_3 varies from 1.3% to 15.3%, Fe_2O_3 ranges from 1.01% to 8.5%, CaO from 2.3% to 34.7%, K_2O is between 0.26% and 3.85% and Na_2O is between 0.8% and 3.68%. Although the Los Sombreros Formation also shows variable major element composition, the range of variation is smaller than for the Empozada Formation. The SiO_2 concentration ranges from 56.5% to 70.7%, Al_2O_3 varies from 3% to 21%, Fe_2O_3 ranges from 5.4% to 9%, CaO from 0.16% to 10.4%, K_2O is between 0.45% and 4.5% and Na_2O is between 0.5% and 2.8%.

Most of the samples from the Empozada Formation have high CaO concentrations, thus only one sample could be used to calculate the CIA value (Fig. 4.2). Although it is not statistically valid, it is worth noting that this mudstone has a CIA value of about 70, indicating a strong degree of weathering. However, the close proximity of this sample to the A-K boundary is probably due to the very low CaO and Na_2O concentrations of the sample rather than a consequence of enrichment in K_2O, since a concentration of 4.1 % does not represent an enrichment compared with the UCC. The CIA value for the Los Sombreros Formation is between 64 and 77 (see Table 1 in Appendix A and Fig. 4.2), indicating intermediate to strong weathering. Some mudstones plot towards the A-K boundary and they are enriched in K_2O (up to 4.5%) compared with the upper continental crust (UCC) average of 3.4% (McLennan *et al.*, 2006). Potassic metasomatism probably influenced the A-CN-K composition, meaning that a higher CIA value (of about five CIA values assuming a UCC source) should be expected in the pre-metasomatized rocks (Fedo *et al.*, 1995). Although samples follow a trend, it seems not to correspond to a general weathering trend since it is oblique with respect to the A-CN line, supporting the idea of potassic metasomatism (i.e. Fedo *et al.*, 1995).

The K/Cs ratio is also an indicator of weathering, because Cs tends to be fixed in weathering profiles whereas K tends to be lost in solution (McLennan *et al.*, 1990). Samples from the Empozada and Los Sombreros Formations show variable Cs concentrations, varying from depleted to enriched compared with the UCC value of 4.6ppm (McLennan *et al.*, 2006). However, the K/Cs ratios are low compared with the UCC (3384 and 3671 in average for the Empozada and Los Sombreros Formations respectively) and therefore indicate moderate to advance weathering. However, if potassium had been added to the Los Sombreros Formation, then the pre-metasomatized K/Cs ratio should be lower.

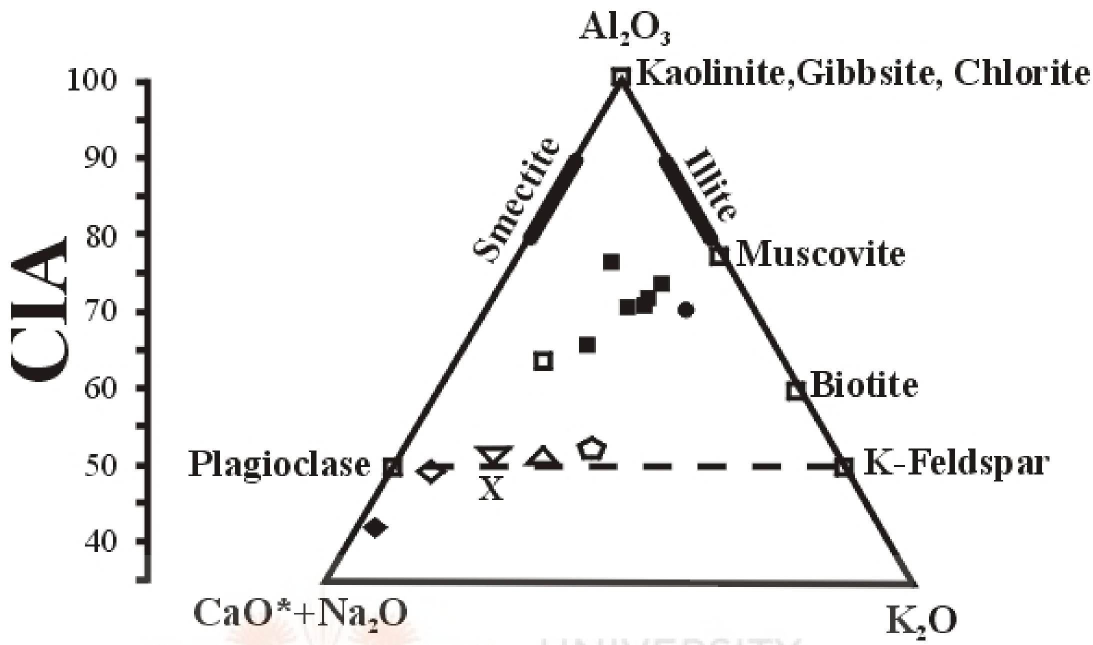

Figure 4.2: A-CN-K diagram based on molecular proportions of the oxides and with the CIA scale shown on the left. The average upper continental crust is plotted (X; Taylor and McLennan, 1985), as well as idealized mineral compositions (empty squares). Empty pentagon: average granite; empty triangle: average adamellite; empty inverted triangle: average granodiorite; empty diamond: average tonalite; solid diamond: average gabbro (Nesbitt and Young, 1984). For the Los Sombreros Formation, mudstones are represented by solid squares whereas sandstones are represented by empty squares. The circle represents the sample used from the Empozada Formation.

During weathering and/or recycling, there is a tendency for an elevation of the ratio between Th and U above upper crustal igneous values of 3.8 to 4.0, because under oxidizing conditions U^{4+} oxidizes to the more soluble U^{6+} and is therefore more easily removed from the sediments than Th (McLennan *et al.*, 1993). A low Th/U ratio can also be due to U enrichment (McLennan *et al.*, 1993).

Compared with UCC averages of Th (10.7ppm) and U (2.8ppm) according to McLennan *et al.* (2006), most of the samples from the Empozada Formation are depleted in U and have depleted to similar Th concentrations (Table 1 in Appendix A).

However, certain samples have higher U concentrations compared with UCC, with one exceptional sample (E8) that shows values of up to 10ppm. Low Th concentrations seem to be link to high CaO and SiO_2 concentrations (Table 1 in Appendix A). The Th/U ratios are highly variable, with lower, similar and higher values compared with the UCC (Fig. 4.3). The group of samples showing low Th/U ratios has also low Th and U concentrations, except for the mentioned sample E8 that has very low Th/U ratio (0.31) due to its U enrichment compared with the UCC. The group of samples with normal Th/U ratios and normal Th and U abundances for the UCC (McLennan *et al.*, 2006) is made up entirely by mudstones. Sample E7 reflects the effects of weathering and/or recycling under oxidizing conditions, with the concomitant loss of U but maintaining a normal Th value for the UCC.

Samples from the Los Sombreros Formation can be subdivided into two groups. One group displays enriched Th concentrations and U concentrations similar to slightly depleted, both compared with the upper continental crust. Their Th/U ratios are higher than the UCC and seem to indicate weathering and/or recycling, but the ratios are affected by the Th concentrations since no U loss is observed. The other group of samples instead displays a depletion in Th concentrations probable link to dilution caused by high CaO or SiO_2 concentrations (Table 1 in Appendix A), whereas their U concentrations are strongly depleted compared with the UCC (with values as low as 0.8ppm). Their Th/U ratios are higher than the UCC values, and although the Th concentrations are depleted the loss of U due to weathering and/or recycling under oxidising conditions is evident for these samples.

4.4.2 Trace elements

Several trace elements are known as immobile elements and therefore they are considered useful for provenance determination, because they reflect provenance compositions (Taylor and McLennan, 1985). The concentrations of high field strength elements (Zr, Nb, Hf, Y, Th and U) occurred in silicic rocks, whereas trace elements such as Sc, Cr, V and Ni are concentrated in mafic rocks. Therefore, ratios between incompatible and compatible elements such as Zr/Sc and Th/Sc may be the most useful (Taylor and McLennan, 1985).

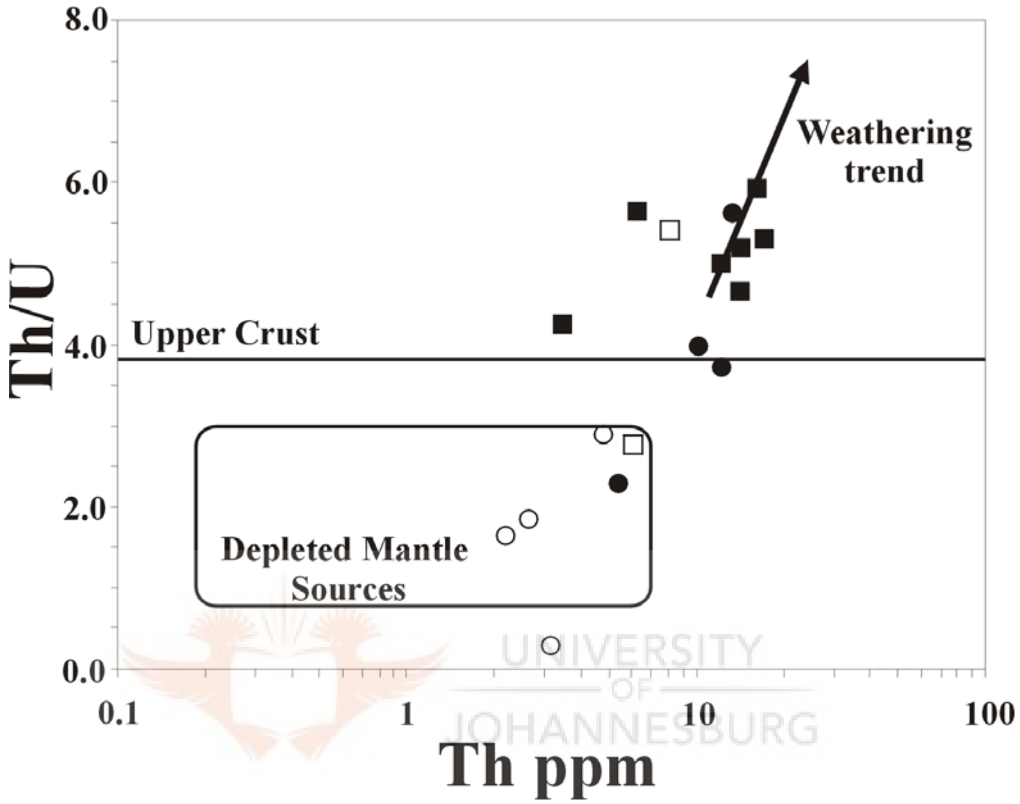

Figure 4.3: Plot of Th/U versus Th (McLennan, *et al.*, 1993). Sandstones are represented by empty symbols whereas mudstones are represented by solid symbols. Circles: Empozada Formation; squares: Los Sombreros Formation.

Compared with UCC values (listed on Table 1 in Appendix C) the mudstones of the Empozada Formation are enriched in the compatible elements Sc (except one sample with 6.4ppm). These samples are depleted in other compatible elements such as Cr and V (except for one sample that is enriched in Cr and V). Sandstones are depleted in Sc, Cr and V, except for one sample, which is enriched in compatible elements (see below). This depletion can be linked to the SiO_2 concentration for sandstone E6 that is enriched in silica compared with the UCC. However, such depletion seems not to be related to SiO_2 concentration for the other samples. The Los Sombreros mudstones are depleted to enriched in Sc, Cr and V, whereas the sandstones are depleted in these compatible elements. The depletion in compatible elements can be linked to high SiO_2 concentration for sandstones of the Los Sombreros Formation, since those samples with the lowest SiO_2 concentration have the higher Cr, Sc and V concentrations and the opposite occurs for samples with the highest SiO_2 concentrations.

Regarding incompatible elements such as Y and Zr, the mudstones of the Empozada Formation are depleted (except for one sample that is enriched in Zr and another mudstone that is enriched in Y). Sandstones are depleted in Y and Zr. The Los Sombreros mudstones are depleted to enriched in Zr but enriched in Y (except for one sample), whereas the sandstones are depleted in Y and they are depleted to enriched in Zr.

The Y/Ni ratio indicates the concentration of ferromagnesian trace elements (such as Ni) compared with Y that represents a proxy for heavy rare earth elements. The Cr/V ratio indicates the enrichment of Cr over other ferromagnesian trace elements. The main minerals that concentrate Cr over other ferromagnesian are chromites. Then, the input of a mafic source could be discriminated using the Cr/V and Y/Ni ratios. The Cr/V and Y/Ni ratios for PAAS (post-Archaean Australian Shales) is about 0.73 and 0.49 respectively (Taylor and McLennan, 1985), while for the UCC are 0.78 and 0.5 respectively (McLennan *et al.*, 2006). However, ophiolitic components would have Cr/V ratios higher than 10 (discussion in McLennan *et al.*, 1993).

The Cr/V ratio for these units is between 0.61 to 1.08 for mudstones and 0.72 to 3.59 for sandstones, and the Y/Ni ratio varies between 0.11 and 1.03 for mudstones and between 0.12 and 2.19 for sandstones, indicating an input from less fractionated material (although not ophiolitic) into the detrital mix. The greater concentrations of the Empozada Formation are probably related to sorting and the difference in grain size with the Los Sombreros Formation. The enrichment in compatible elements (Sc, Cr and V) of the Los Sombreros Formation have maximum abundances of 19.7ppm, 110ppm and 115ppm respectively, and the sample with the highest Cr/V ratio shows the lowest Y/Ni ratio for this unit. The Empozada Formation has individual values within sandstones as high as 17.8ppm of Sc, 220ppm of Cr and 130ppm of V, and the sample with the highest Cr/V ratio (3.59) shows the lowest Y/Ni ratio (0.12) for sandstones of this unit (sample E3; Table 1 in Appendix A).

Rare earth elements (REE) are mainly transported with the detrital phases into a sedimentary basin (Taylor and McLennan, 1985). The redistribution of the REE abundances within weathering profiles would not have a significant effect on the REE patterns in well mixed sedimentary rocks and would therefore represent reliable provenance indicators (Taylor and McLennan, 1985), as they would reflect the average REE composition of the source material (Cullers *et al.*, 1979; McLennan, 1989; McLennan *et al.*, 1990). However, mobility of REE has been widely reported (i.e. McDaniel *et al.*, 1994; Bock *et al.*, 1994). The shape of the REE pattern can provide information about both the bulk composition of the provenance and the nature of the dominant igneous process that affected the source and therefore the composition of the detrital material (Taylor and McLennan, 1985; McLennan and Taylor, 1991). Deviations in the REE patterns compared with the PAAS are significant since they may allow identification of different source rocks or sedimentary processes that fractionated REE such as weathering, sorting of selective mineral phases or diagenesis.

The chondrite normalized rare earth elements patterns for mudstones and sandstones of the Empozada Formation (Fig. 4.4) show a moderately enriched light REE pattern (LREE; La_N/Yb_N of about 6.48 in average), and a rather flat heavy REE (HREE; Tb_N/Yb_N of 1.46 in average). The Eu-anomaly ($Eu_N/Eu^*= Eu_N/(0.67Sm_N+0.33Tb_N)$) is negative, with Eu_N/Eu^* of about 0.61 on average. Although REE patterns of the samples are almost parallel to the PAAS pattern (except for E10), they tend to be depleted in LREE and enriched in HREE compared with the PAAS pattern (Fig. 4.4). Sample E10 (Fig. 4.4) has Eu_N/Eu^* about 1 (no Eu-anomaly), a low ΣREE (98ppm; UCC= 128.54ppm after McLennan *et al.*, 2006), is enriched in Cr, Sc and V compared with the UCC (McLennan *et al.*, 2006) implying therefore the influence of a less evolved source.

The chondrite normalized rare earth elements patterns for mudstones and sandstones of the Los Sombreros Formation (Fig. 4.5) show a moderately enriched LREE pattern (La_N/Yb_N of about 6.9 in average), a negative Eu-anomaly (Eu_N/Eu^* of about 0.63 on average) and a rather flat HREE (Tb_N/Yb_N of 1.65 in average). REE patterns of the samples tend to be enriched in rare earth elements compared with the PAAS (Fig. 4.5). Three samples have a different REE pattern and are therefore described below.

It is noteworthy the behaviour of samples 020419, SOM7 and SOM9 in the REE diagram (Fig. 4.5). Sample 020419 shows a clear enrichment of MREE (medium rare earth elements) compared with the PAAS and a disturbance of the REE composition is evident. This sample is discarded when evaluating the REE composition of the unit because the rare earth elements were fractionated and therefore, their concentrations are not reflecting the provenance composition.

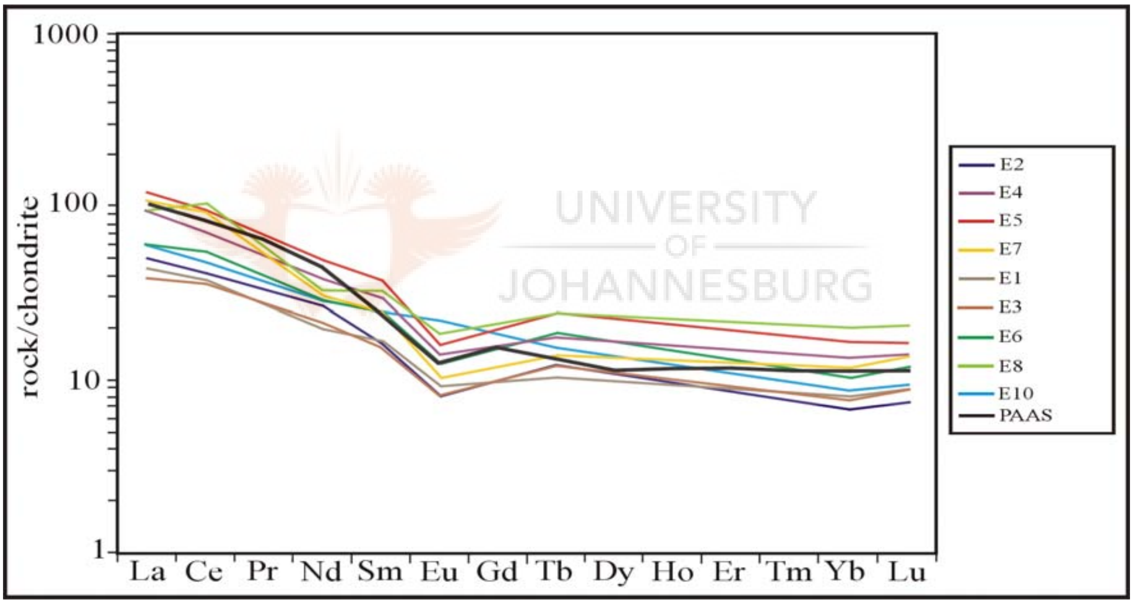

Figure 4.4: Chondrite normalized REE patterns for the Empozada Formation. PAAS= post-Archaean Australian shales pattern (Nance and Taylor, 1976) is draw for comparison. REE patterns are drawn as a continuous line although certain elements were not measured (see Table 1 in Appendix A). Chondrite normalization factors are those listed by Taylor and McLennan (1985).

Sample SOM7 shows a relatively low sum of REE (118ppm), high concentrations of Y (60ppm), low Zr and Th concentrations (91ppm and 6ppm respectively), high P_2O_5 concentrations (1.38%) but very low TiO_2 concentrations

(0.27%). The normalization of the REE to PAAS values shows that La, Ce and Nd concentrations of sample SOM7 are moderately depleted with respect to PAAS, Sm, Eu and Tb are two to three times enriched, whereas Yb and Lu have almost the same concentrations compared with the PAAS (Taylor and McLennan, 1985). Based on these

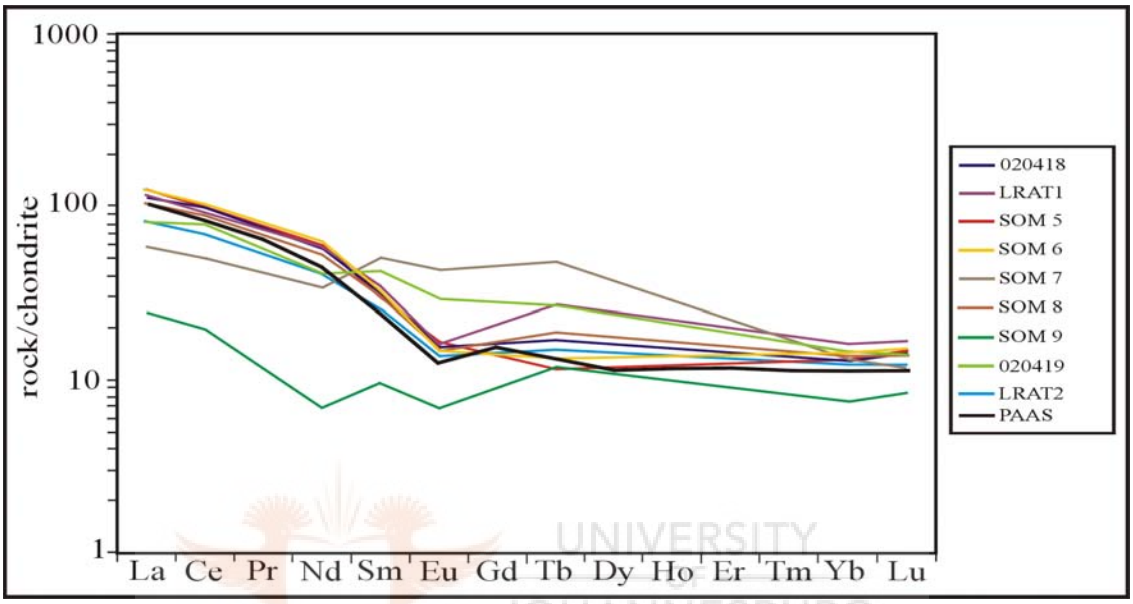

Figure 4.5: Chondrite normalized REE patterns for the Los Sombreros Formation. PAAS= post-Archaean Australian shales pattern (Nance and Taylor, 1976) is draw for comparison. REE patterns are drawn as a continuous line although certain elements were not measured (see Table 1 in Appendix A). Chondrite normalization factors are those listed by Taylor and McLennan (1985). The remobilization of REE on samples 020419, SOM7 and SOM9 can clearly be observed in this diagram. For more details see discussion in the text.

geochemical considerations, the distribution of the REE is better explained by the sorting of heavy minerals rich in MREE (Bock *et al.*, 1994). Apatite and titanite are both MREE-rich, but according to high P_2O_5 and low TiO_2 concentrations, the heavy mineral enriched in this sample is most probably apatite. On the other hand, the moderately depletion in LREE and Th might be due to the loss of phases that concentrate these elements such as monazite and allanite, whereas Zr and HREE concentrations are in accordance with PAAS values, indicating no important concentrations of zircon. A Sm/Nd ratio of 0.47 for sample SOM7 indicates that there is a fractionation of REE (Sm/Nd for PAAS is of about 0.2), that could be either related to selective sorting (Bock *et al.*, 1994) or to the very low-grade metamorphism that affected these rocks. If the metamorphism would affected the distribution of the rare earth elements it should be expected to be a wider spread feature within the Los Sombreros Formation. Because sample SOM7 is a mudstone, no petrographic control can be made to understand the chemical differences shown by this sample (Table 1 in Appendix A). XRD data indicate the presence of ankerite and the absence of albite as the main differences (Table 3 in Appendix C).

The sample SOM9 has a very low sum of REE (39ppm), high CaO (10.5%) and Fe_2O_3 concentrations (related to the presence of ankerite), and very low TiO_2, P_2O_5 and Th concentrations (0.24%, 0.05% and 3.4ppm respectively). The normalization of the REE to the PAAS shows that La, Ce, Nd, Sm, and Eu concentrations of sample SOM9 are highly depleted with respect to the PAAS, whereas Tb, Yb and Lu are slightly depleted. Because not all elements are depleted in similar proportions, it seems more likely to assume fractionation than dilution. The distribution of the REE might be affected by the presence of zircon, responsible for the Zr and HREE concentrations that approximate their abundances to PAAS values (Taylor and McLennan, 1985), and the loss of heavy minerals characterized by high concentrations of LREE, MREE, P_2O_5, TiO_2 and Th, e.g., monazite, allanite, apatite and titanite.

A Sm/Nd ratio of 0.46 for sample SOM9 indicates that the rare earth elements were fractionated. This fractionation can result from different processes such as the very low-grade metamorphism that affected this unit. However, if this would be the case, fractionation of the rare earth elements should be a conspicuous feature for the Los Sombreros Formation. The absence of a Ce-anomaly for samples SOM7 and SOM9 (Ce/Ce* of 0.99 and 1.04 respectively) also shows that redistribution did not occur during weathering but either diagenesis or very low-grade metamorphism (McDaniel *et al.*, 1994; Bock *et al.*, 1994). The remobilization of the REE of these two samples has important implications on the interpretations of their Sm-Nd isotopes (see section 4.7).

4.4.3 Provenance and tectonic setting

The Zr/Sc ratio reflects reworking because Zr is strongly enriched in zircon whereas Sc is not, and zircon can easily be recycled (McLennan *et al.*, 1993). On the other hand, Th/Sc ratio indicates the degree of igneous differentiation processes since Th is an incompatible element whereas Sc is compatible in igneous systems (McLennan *et al.*, 1990; 1993).

Samples from the Empozada Formation can be subdivided into two groups (Fig. 4.6): one does not show any recycling and reflects an input from the upper continental crust while the second group shows an important element of recycling. The Zr concentration is lower than the upper continental crust value of 190ppm (McLennan *et al.*, 2006) for the first group except for one sample (E5). The Zr concentration of the recycled samples ranges from enriched (with values of up to 323ppm) to depleted compared with the upper continental crust. The high Zr/Sc ratio of those samples with low Zr concentration is affected by the very low Sc concentrations (less than 3ppm) compared with the upper continental crust, rather than by an enrichment of Zr. The sandstone E10 has a Th/Sc ratio of 0.19, indicating that a less evolved rock (probably basaltic or andesitic in composition) was a source (Table 1 in Appendix A and Fig. 4.6). Petrographically, E10 is a coarse subfeldspathic arenite similar to E9 (Table 2 in Appendix B), depleted in Th and slightly enriched in Sc compared with the upper continental crust (Table 1 in Appendix A).

Definitely, sandstones are enriched in Zr/Sc but display nearly similar Th/Sc ratios. The mudstones have a composition similar to upper continental crust, whereas recycling controls the sandstone composition. One sample is strongly depleted regarding Th/Sc ratios and displays similar Zr/Sc ratios caused by mixing of unrecycled upper continental crust with a less fractionated source. The Los Sombreros Formation instead shows a cluster of data indicating no recycling (confirmed by a low Zr concentration except for two samples; Table 1 in Appendix A) and a provenance from a upper continental crust composition (Fig. 4.6). One sample (a mudstone) has a Th/Sc ratio of 0.34 probably related to a depleted source.

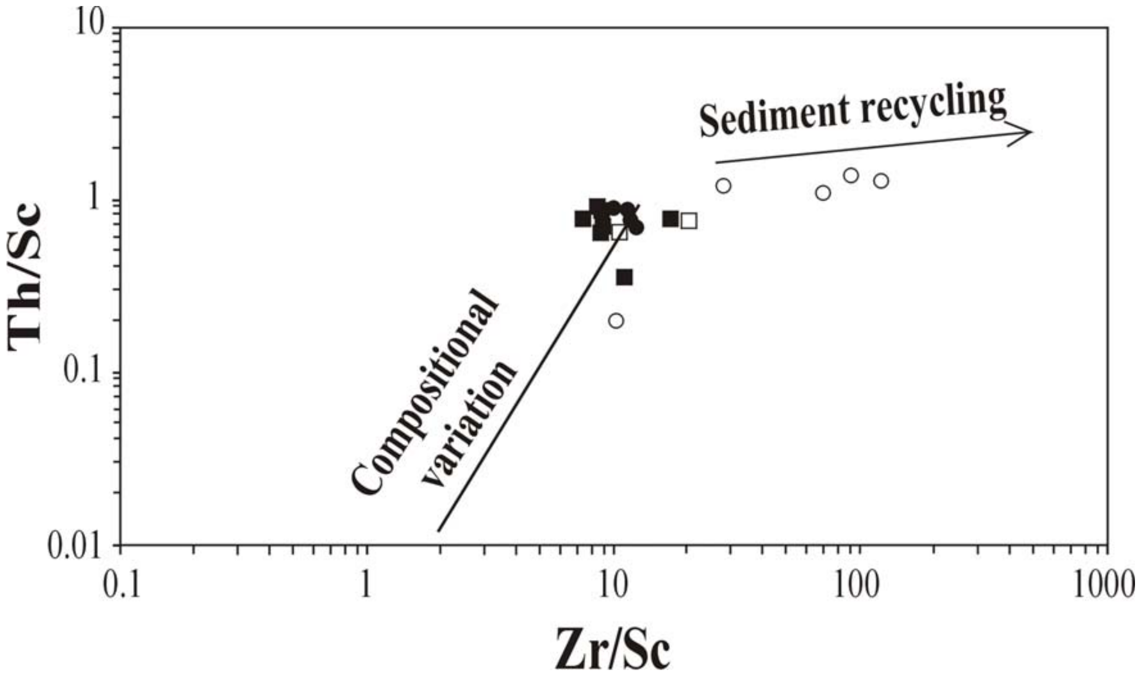

Figure 4.6: Th/Sc versus Zr/Sc adapted from McLennan *et al.* (1990). Sandstones are represented by empty symbols whereas mudstones are represented by solid symbols. Circles: Empozada Formation; squares: Los Sombreros Formation.

When identifying tectonic settings (e.g. using Bhatia and Crook diagrams) it is important to take into account that the sediments can be transported across tectonic boundaries and thus their chemical signatures may not necessarily be indicative of the tectonic setting of the depositional basin (McLennan, 1989). However, using Bhatia and Crook (1986) diagrams broad trends regarding the basins geotectonic settings can be deduced and interpret using also the knowledge of other features (such as sedimentological characteristics and petrography). According to the tectonic classification from Bhatia and Crook (1986), the oceanic island arc (A in Figs. 4.7 and 4.8) and continental arc (B in Figs. 4.7 and 4.8) settings represent convergent plate margins involving orogenic volcanic rocks (related to thin or thick continental crust). The active continental margin setting (C in Figs. 4.7 and 4.8) comprises the Andean-type margins and strike-slip continental margins (involving a thick continental crust). The passive margin setting (D in Figs. 4.7 and 4.8) comprises rifted continental margins of the Atlantic-type.

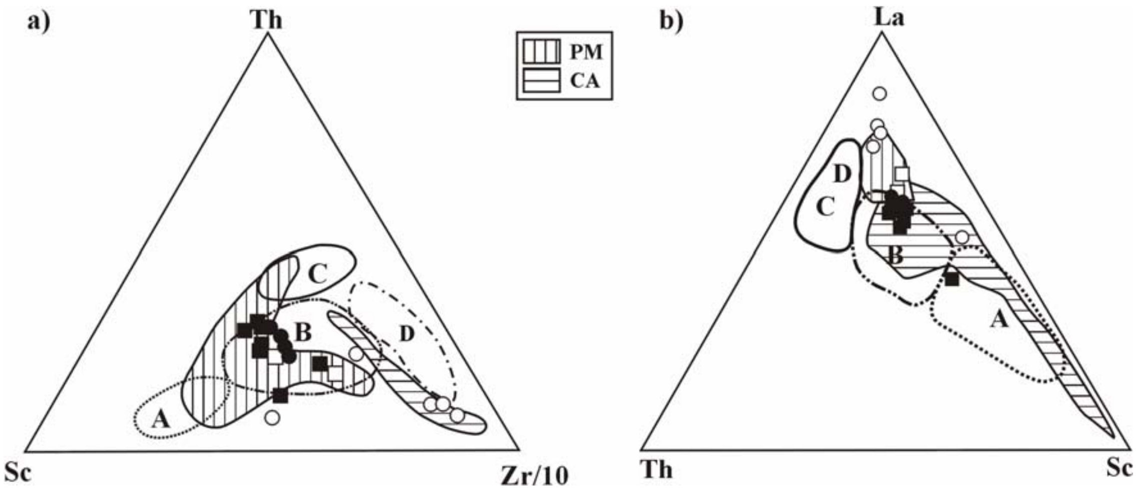

Figure 4.7: a) Th-Sc-Zr/10 and b) La-Th-Sc tectonic setting discriminatory plots after Bhatia and Crook (1986). For both diagrams: A: Oceanic island arc setting; B: Continental island arc setting; C: Active continental margin setting; D: Passive margin setting. PM: recent deep-sea turbidites derived from and deposited at a passive margin. CA: recent deep-sea turbidites derived from and deposited at a continental arc margin (data from McLennan *et al.*, 1990). Sandstones are represented by empty symbols whereas mudstones are represented by solid symbols. Circles: Empozada Formation; squares: Los Sombreros Formation.

In Figure 4.7, mudstones from the Empozada Formation plot within the field of continental island arc setting. Only one sandstone sample shows the influence of a less evolved source plotting towards the field of oceanic island arc. Other sandstone samples plot either towards the La or Zr apexes. However, when analyzing the absolute values (Table 1 in Appendix A), no enrichments in La and Zr for those samples are observed, but instead an important depletion of Sc and Th (with absolute values of about 2ppm and 3ppm respectively). The factor that could be addressed to explain these deviations is sorting, with the correspondent enrichment on certain heavy minerals, particularly apatite. In Figure 4.8, the same samples show the same tendencies mainly indicating an active continental margin setting, as well as the influence of a less evolved source (deviations towards higher Ti/Zr ratios). The La/Sc ratios are rather constant for both units pointing to unrecycled UCC. The samples that plot in the passive margin field are also the more recycled ones (Zr/Sc between 69.6 and 118.3; Table 1 in Appendix A). The deposition in a basin linked to active continental margin settings is evident in the same diagrams (Figs. 4.7 and 4.8) for the Los Sombreros Formation.

Low Th/Sc ratios, Eu_N/Eu^* of about 1 and strong negative Nb and Ti anomalies characterize continental arc components, although differentiated arcs would have variable Th/Sc ratios and Eu_N/Eu^* between 0.6 and 0.9 (Hofmann, 1988; McLennan *et*

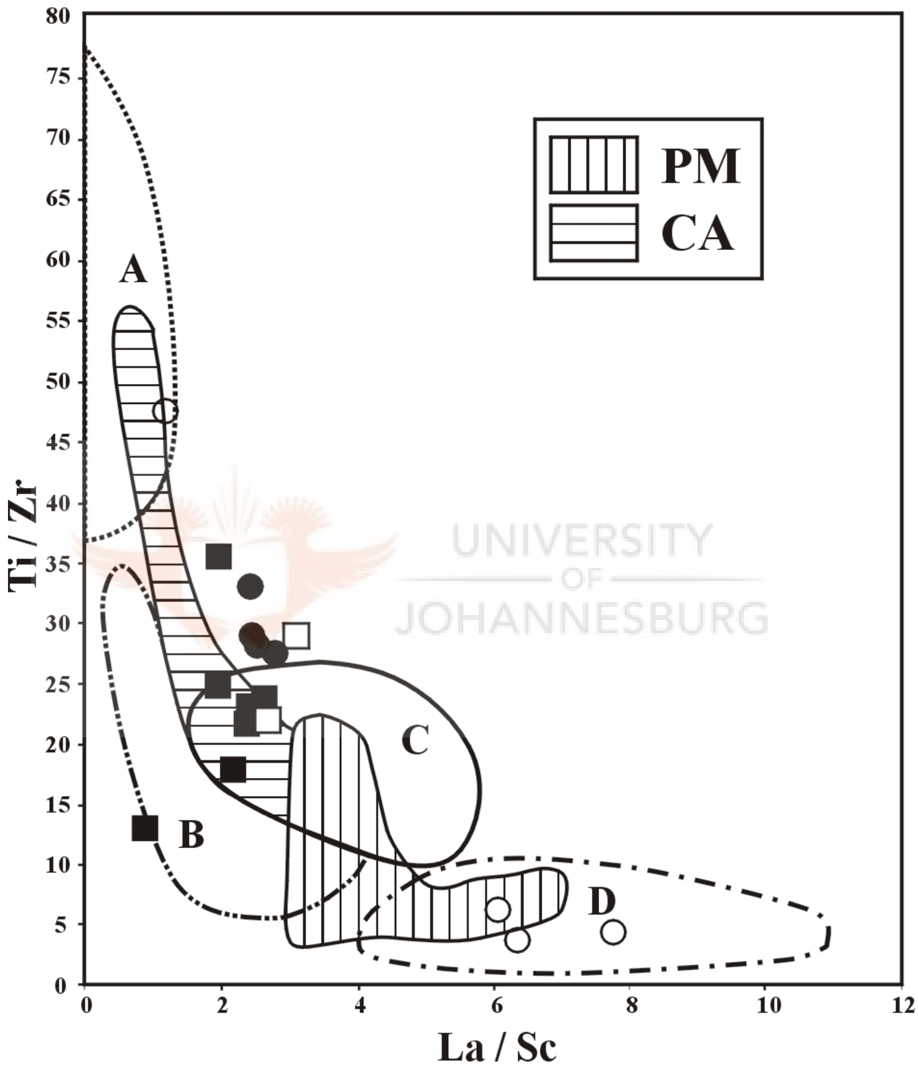

Figure 4.8: Ti/Zr versus La/Sc discriminatory plot from Bhatia and Crook (1986). A: Oceanic island arc; B: Continental island arc; C: Active continental margin; D: Passive margin. PM: recent deep-sea turbidites derived from and deposited at a passive margin. CA: recent deep-sea turbidites derived from and deposited at a continental arc margin (data from McLennan *et al.*, 1990). Sandstones are represented by empty symbols whereas mudstones are represented by solid symbols. Circles: Empozada Formation; squares: Los Sombreros Formation.

al., 1993; Zimmermann, 2005). Four samples from the Empozada Formation show the negative Nb and Ti anomalies typical of arc (Table 1 in Appendix A), but their Th/Sc ratios are above the UCC value and their Eu_N/Eu^* are below 0.62. Nb and Ti are present in heavy minerals such as ilmenite and rutile and since their occurrence might be affected by sorting (McLennan *et al.*, 2006), the concentrations of Nb and Ti may not be indicative of the source. Furthermore, the CaO enrichment might be provoking dilution on concentrations of certain elements. The rest of the samples from this unit are also indicating that a provenance from an arc is not likely. The three samples from the Los Sombreros Formation showing REE disturbances display negative Nb and Ti anomalies. These samples also show very low Th/Sc ratios (between 0.34 and 0.62) and Eu_N/Eu^* ranging from 0.65 and 0.87. Therefore, they seem to indicate a provenance from a differentiated arc, but since it has been demonstrated that immobile elements are disturbed it is expected that Ti would be affected as well. The rest of the samples from this unit do not indicate a provenance from an arc component.

4.5 ISOTOPE GEOCHEMISTRY

4.5.1 Sm-Nd

The model ages based on Nd isotopes depend on assumptions about the fractionation of Sm-Nd ratios in major crustal processes (DePaolo, 1981). However, other processes might sometimes fractionate the ratios, as metamorphism, anatexis and weathering. Sm-Nd model ages in general contain two components of information: the average crustal residence age of the detrital mix, and a component of Sm/Nd fractionation. The model ages of sedimentary rocks might be disturbed by small amounts of diagenetic alteration and therefore, the ε_{Nd} value is a better indicator of provenance compared with the model ages (i.e. McLennan *et al.*, 1989; 1993).

Five samples from the Los Sombreros Formation were analyzed. Results are shown on Table 3 (Appendix A); data was calculated according to DePaolo (1981), although T_{DM} according to DePaolo *et al.* (1991) are also shown and were used to compared with data from the literature that was expressed according to the three-stage model (DePaolo *et al.,* 1991). For more details about methods and analytical techniques, see Appendix B. Two samples showed REE fractionation as described in section 4.6.2. Accordingly, T_{DM} ages of these samples are aberrant (see Table 3 in Appendix A), although their ε_{Nd} (t) are consistent with values of unaffected samples.

ε_{Nd} (t) values where t = 465 Ma (t being the depositional age) ranges from -5.37 to -7.58 (average -6.33 ± 0.92), $f_{Sm/Nd}$ ranges from -0.39 to -0.47 (average -0.42 ± 0.03) whereas the T_{DM} ages range from 1.48 to 1.49 Ga (average 1.48 ± 0.007 Ga) discarding the two samples that show evident remobilization of the Sm and Nd isotopes. Figure 4.9a shows the relationship between ε_{Nd} (t) and Th/Sc ratio of samples from the Los Sombreros Formation. It is evident that ε_{Nd} (t) values are neither typical of the UCC average nor of an arc (values from McLennan *et al.,* 1990), and that the Th/Sc ratios are variable from values close to the UCC composition to low values pointing to an input from a depleted source, most likely andesitic. The narrow range in ε_{Nd} (t) values compared with the variation range of the Th/Sc ratio might be interpreted as reflecting

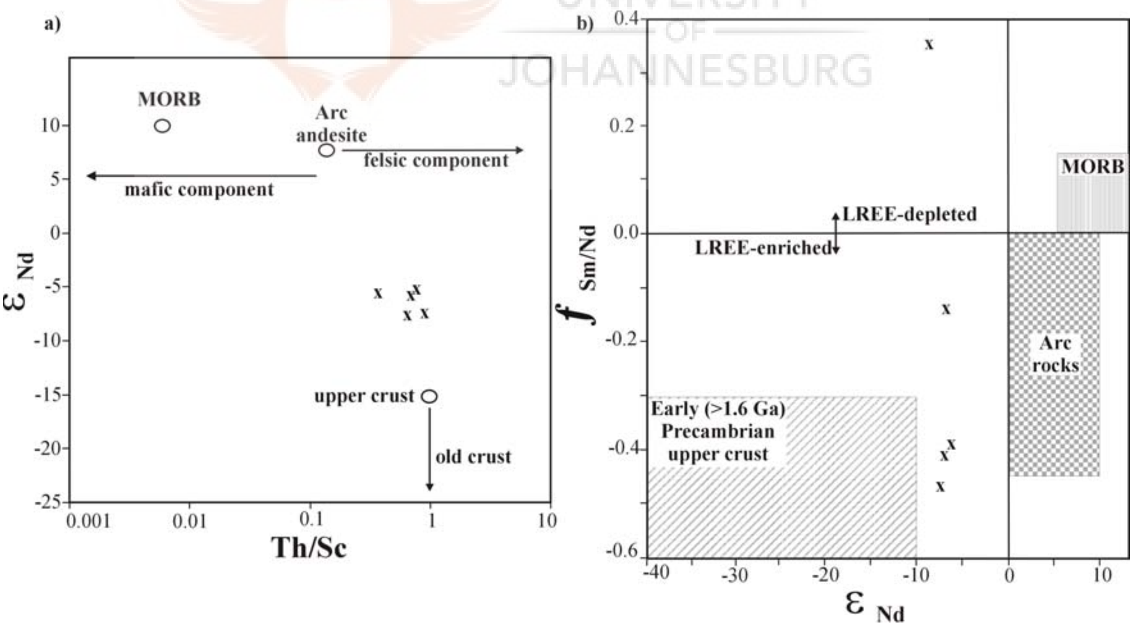

Figure 4.9: a) ε_{Nd} (t) versus Th/Sc ratio and b) $f_{Sm/Nd}$ (the fractional deviation of the sample $^{147}Sm/^{144}Nd$ from a chondritic reference) of the Los Sombreros Formation versus ε_{Nd} (t), where ε_{Nd} (t) is ε_{Nd} at the age of sedimentation. $f_{Sm/Nd} = (^{147}Sm/^{144}Nd)_{sample} / (^{147}Sm/^{144}Nd)_{CHUR} - 1$. $\varepsilon_{Nd}(t) = \{[(^{143}Nd/^{144}Nd)_{sample\ (t)} / (^{143}Nd/^{144}Nd)_{CHUR\ (t)}] - 1\} * 10000$. $(^{147}Sm/^{144}Nd)_{CHUR} = 0.1967$. $(^{143}Nd/^{144}Nd)_{CHUR} = 0.512638$.

chemically different rocks but from the same basement. Using the plot of $f_{Sm/Nd}$ versus ε_{Nd} (Fig. 4.9b), two samples from the Los Sombreros Formation (SOM9 and SOM7) clearly show less negative to positive $f_{Sm/Nd}$ values (-0.14 and 0.34 respectively) forming a vertical array (Fig. 4.9b). The Sm/Nd ratio of these two samples is higher than the ratio of the rest of the samples, indicating fractionation (Bock *et al.*, 1994; see section 4.6.2).

T_{DM} ages for the Los Sombreros are within the range of variation of several typical Palaeozoic Gondwanan areas, for example northwestern Argentina including the igneous rocks of the Pampia terrane (Rapela *et al.*, 1998; Bock *et al.*, 2000; Lucassen *et al.*, 2000; Zimmermann and Bahlburg, 2003; see Table 4.1). They are also comparable to Nd-isotopes from other Ordovician sedimentary rocks from the Precordillera terrane (Cingolani *et al.*, 2003a; Gleason *et al.*, 2006).

Location	Age (Ga)	ε_{Nd}	T_{DM} (Ga)
Pampeanas Ranges[1]	0. 52	-3.1 to -7.7	1.48 to 1.82
Patagonia, Argentina[1]	0. 46 to 0.58	-0.7 to -6.1	1.13 to 1.66
Puna, Northern Argentina[1]	0.47 to 0.49	-1.4 to -11.6	1.32 to 2.05
Pampeanas Range, Velasco area[2]	Lower Palaeozoic	-5.5 to -10	1.23 to 1.56
Pampeanas Range, Paimán area[2]	Lower Palaeozoic	-6.1 to -6.3	1.32 to 1.34
Pampeanas Range, Copacabana area[2]	Lower Palaeozoic	-8.4 to -10	1.4 to 1.54
xenoliths Precordillera basement[3]	1.1	+2 to +7	0.8 to1.68
granite within Pie de Palo[4]	0.47 to 0.48	-3.6 to -2.6	1.41 to 1.48
Angaco, Pie de Palo Range[5]		-4.7 to -7.5	1.4 to 1.7
Cerro Salinas carbonates[5]		-11 to -30.5	1.7 to 1.8
La Laja Fm. Precordillera[5]	Cambrian	-8.3 to -10.9	1.3 to 1.7
Las Matras block[6]	1.2	+1.6 to +2.1	1.55 to 1.6
Cerro La Ventana Fm.[7]	1.1 to 1.2	+1.4 to +7.9	1.2 to 1.3
Southern Africa, Natal (Mzumbe gneiss and Equeefa)[8]	1.1 to 1.23		1.21 to 1.47
East Antarctica, Dronning Maud Land gneisses [8]	1.13 to 1.15		1.4 to 2.46
Falkland/Malvinas Islands (Cape Meredith gneiss)[8]	1.1		1.3
Falkland/Malvinas plateau (Maurice Ewing gneiss)[8]	1.1		1.6
Chilenia basement[9]		-6 to -10	1.3 to 1.6
Chilenia basement (juvenile input)[9]		4.5	0.8

Table 4.1: ε_{Nd} and T_{DM} ages of selected probable source areas to compare with values from the Los Sombreros Formation. [1]Compiled in Adams *et al.* (2005); [2]López *et al.* (2006); [3]Kay *et al.* (1996); [4]Baldo *et al.* (2005); [5]Naipauer *et al.* (2005b); [6]Sato *et al.* (2004); [7]Cingolani *et al.* (2005a); [8]Wareham *et al.* (1998); [9]Bahlburg *et al.* (2001); [1,2,8] ε_{Nd} initial and T_{DM} according to DePaolo *et al.*, 1991; for the rest of the data, ε_{Nd} is (t) and T_{DM} according to DePaolo, 1981. See also Table 3 in Appendix A.

Similar T_{DM} ages were also found within the Chilenia terrane (Bahlburg *et al.*, 2001), the Natal-Namaqua Metamorphic belt, Falkland/Malvinas Microplate and Antarctica (Mesoproterozoic granitoids and orthogneisses; Wareham *et al.*, 1998), the Western Pampeanas Ranges (Vujovich *et al.*, 2005) and the basement rocks of the Precordillera terrane located within the southern extension (Sato *et al.*, 2004; Cingolani *et al.*, 2005a), but also present as xenoliths (Kay *et al.*, 1996). Figure 4.10 shows the similarity of the ε_{Nd} (t) values from the Los Sombreros Formation (this study) and those from the Empozada Formation (Gleason *et al.*, 2006). According to Gleason *et al.* (2006), the Empozada Formation has ε_{Nd} (t= 450) values ranging from -5.4 to -6.4 and T_{DM} ages between 1.34 and 1.48 Ga (calculated according to DePaolo, 1981). ε_{Nd} (t) values for the slope-type deposits are similar to those from other Ordovician sedimentary rocks from the Precordillera terrane (Cingolani *et al.*, 2003a).

They are also comparable to those from the Famatina (Pankhurst *et al.*, 1998). ε_{Nd} values are within the range of variation of the Laurentian Grenville crust (Patchett and Ruiz, 1989), Central and Southern domains of the Arequipa-Antofalla Basement (Loewy *et al.*, 2004), and the basement of the Precordillera known as the Cerro La Ventana Formation (Cingolani, unpublished data). ε_{Nd} values from the Western Pampeanas Ranges are scarce, but a broad similarity with data here presented is evident (Fig. 4.10). The abovementioned imply that the source cannot be defined based solely on the Sm-Nd signature, particularly when data are widespread such as the case of the Central and Southern domains of the Arequipa-Antofalla Basement (light grey area on Fig. 4.10.

4.5.2 Pb-Pb

The relationship between Pb isotopic composition and tectonic setting is not straightforward, but it is possible to discriminate between ancient upper continental crust and younger terranes (especially in terms of $^{207}Pb/^{204}Pb$). Studying Pb-isotopes on whole-sedimentary rocks might be complex due to the effect that several processes taking place during erosion and deposition or even during post-depositional stages can have on the Pb system (e.g. McLennan *et al.*, 2000; Hemming and McLennan, 2001).

The same five samples used for Sm-Nd isotopes were analyzed for their Pb isotopic composition. Results are presented on Table 4 in Appendix A and details regarding methodology and analytical techniques are given in Appendix B.

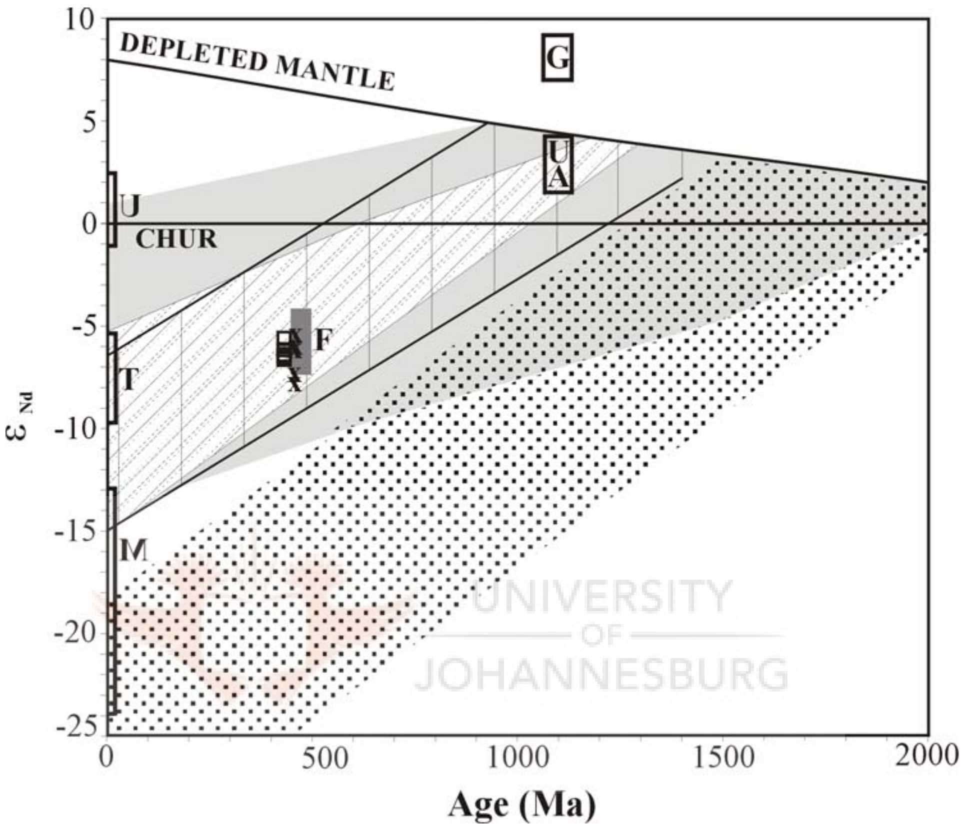

Figure 4.10: ε_{Nd} versus age of the Los Sombreros (crosses) and Empozada (squares; data from Gleason *et al.*, 2006) Formations and of areas evaluated as probable sources. Dotted area: range of ε_{Nd} for the Northern domain and light grey area: Central and Southern domains of the Arequipa-Antofalla Basement (Loewy *et al.*, 2004). Field of vertical lines: Laurentian Grenville crust (Patchett and Ruiz, 1989). A: granulitic and amphibolitic, and G: acidic-gneissic, xenoliths from the inferred basement of the Precordillera (Kay *et al.*, 1996). F denoting dark grey rectangle: Famatinian magmatic rocks (Pankhurst *et al.*, 1998). U: Umango Range, T: El Taco Complex, and M: Maz Complex from the Western Pampeanas Ranges (Vujovich *et al.*, 2005; note that most data are ε_{Nd} (0)). White field with diagonal lines: Cerro La Ventana Fm. (Cingolani *et al.*, 2005a).

The $^{206}Pb/^{204}Pb$, $^{207}Pb/^{204}Pb$ and $^{208}Pb/^{204}Pb$ ratios range from 18.82 to 19.5, 15.7 to 15.92, and 39.12 to 39.94 respectively for the Los Sombreros Formation (see Table 4 in Appendix A). The widest scatter is observable for the $^{207}Pb/^{204}Pb$ ratio. Two samples (SOM7 and SOM9) have been detected as having an important mobilization of trace elements, and therefore incongruent Pb values are also expected. On both, an uranogenic-and thorogenic-Pb diagrams, samples from the Los Sombreros Formation plot above the Stacey and Kramers (1975) second stage Pb evolution curve for average crust (Figs. 4.11 and 4.12).

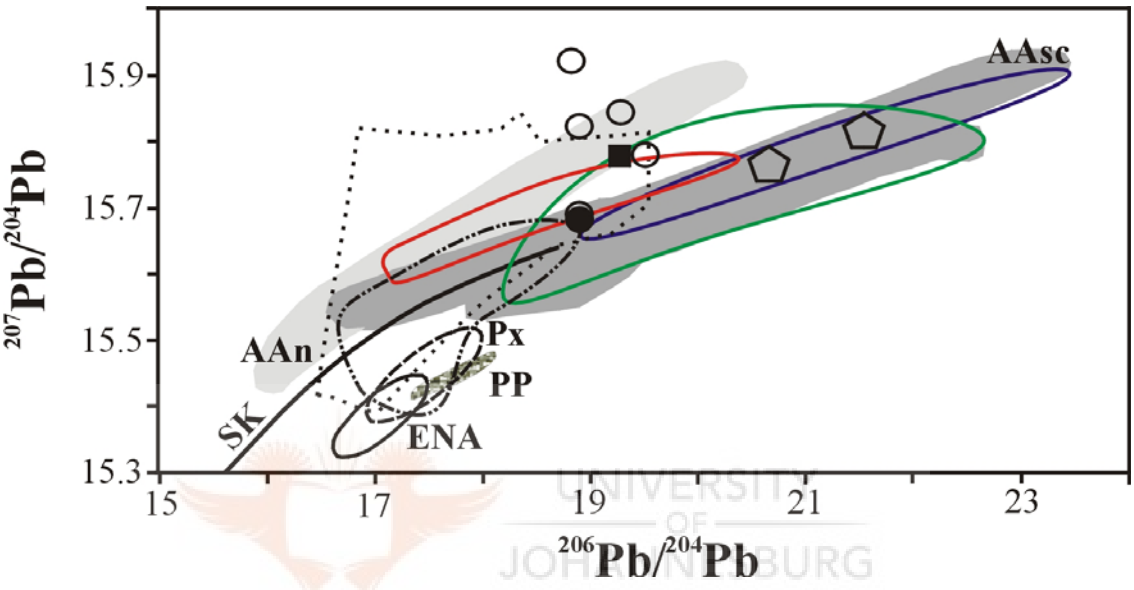

Figure 4.11: $^{207}Pb/^{204}Pb$ versus $^{206}Pb/^{204}Pb$ present-day ratios. Empty circles represent samples from the Los Sombreros Formation; solid square is the average value for the upper crust and solid circle the average value for GLOSS, both from Hemming and McLennan (2001). Fields obtained from several sources as indicated in the text. ENA denoting solid line: Eastern North America; Px denoting dashed line: xenoliths from the Precordillera terrane; AAsc and AAn: Arequipa-Antofalla Basement Southern and Central domains, and Northern domain respectively; PP: Pie de Palo Range; SK: Stacey and Kramers reference line; blue line: supracrustal Ordovician rocks from the Precordillera terrane and data from the Empozada Formation is denoted by the pentagons (Gleason *et al.*, 2006); dotted line: Palaeozoic rocks from the Central Andes (Lucassen *et al.*, 2002); green line: Palaeozoic rocks from southern Central Andes (Bock *et al.*, 2000); red line: Ordovician rocks from south Bolivia (Egenhoff and Lucassen, 2003); double dotted-dashed line: data from Wareham *et al.* (1998; see text).

Pb data provided by Gleason *et al.* (2006) indicate for the Empozada Formation $^{206}Pb/^{204}Pb$, $^{207}Pb/^{204}Pb$ and $^{208}Pb/^{204}Pb$ ratios ranging from 20.39 to 21.57, 15.76 to 15.82, and 38.54 to 38.85 respectively. These results indicate for the Empozada

Formation higher $^{206}Pb/^{204}Pb$ and lower $^{208}Pb/^{204}Pb$ compared with the Los Sombreros Formations for the same range of variation of the $^{207}Pb/^{204}Pb$ ratio. The Pb composition of the Los Sombreros Formation is similar to rocks from the Arequipa-Antofalla Basement (Aitcheson *et al.*, 1995; Tosdal, 1996 and references therein; Figs. 4.11 and 4.12).

The Arequipa-Antofalla Basement comprises three domains (Loewy *et al.*, 2004): the Northern domain exists in southern Peru and western Bolivia. The Central extends from the Peru-Chile border to the northernmost part of Chile, while the Southern is extended from 23º S to the northernmost Argentina. The area comprised in the so-called Central and Southern domains in the sense of Loewy *et al.* (2004) is almost equivalent to the ca. 500 Ma Mobile Belt of the Pampean Cycle according to Lucassen *et al.* (2000). Notwithstanding the relevance of the inclusion of the mentioned area in the Pampean Orogeny, the terminology of Loewy *et al.* (2004) is followed.

On the other hand, they differ consistently from the Grenvillian xenoliths from the inferred basement of the Precordillera terrane and the Pie de Palo Range (Kay *et al.*, 1996; Figs. 4.11 and 4.12) and Proterozoic rocks from Eastern North America. Mesoproterozoic granitoids and orthogneisses from the Natal-Namaqua Metamorphic belt (Mzumbe gneiss), Falkland/Malvinas Microplate (Cape Meredith Complex), West Antarctica (Haag Nunataks block) and East Antarctica (Kirwanveggan and Sverdrupfjella ranges, Maud Province) have different Pb isotopic signatures (Wareham *et al.*, 1998).

Compared with Pb data from supracrustal Ordovician rocks of the Precordillera terrane, except for the Empozada Formation already discussed (Gleason *et al.*, 2006), samples from the Los Sombreros Formation have higher $^{207}Pb/^{204}Pb$ and $^{208}Pb/^{204}Pb$ ratios and a narrower range of $^{206}Pb/^{204}Pb$ variation. They are quite similar to Pb data from Palaeozoic rocks from the Central Andes (Bock *et al.*, 2000; Lucassen *et al.*, 2002), and similar to Ordovician sedimentary rocks of south Bolivia (Egenhoff and Lucassen, 2003), although some samples from the Los Sombreros Formation have higher $^{207}Pb/^{204}Pb$ (Fig. 4.11).

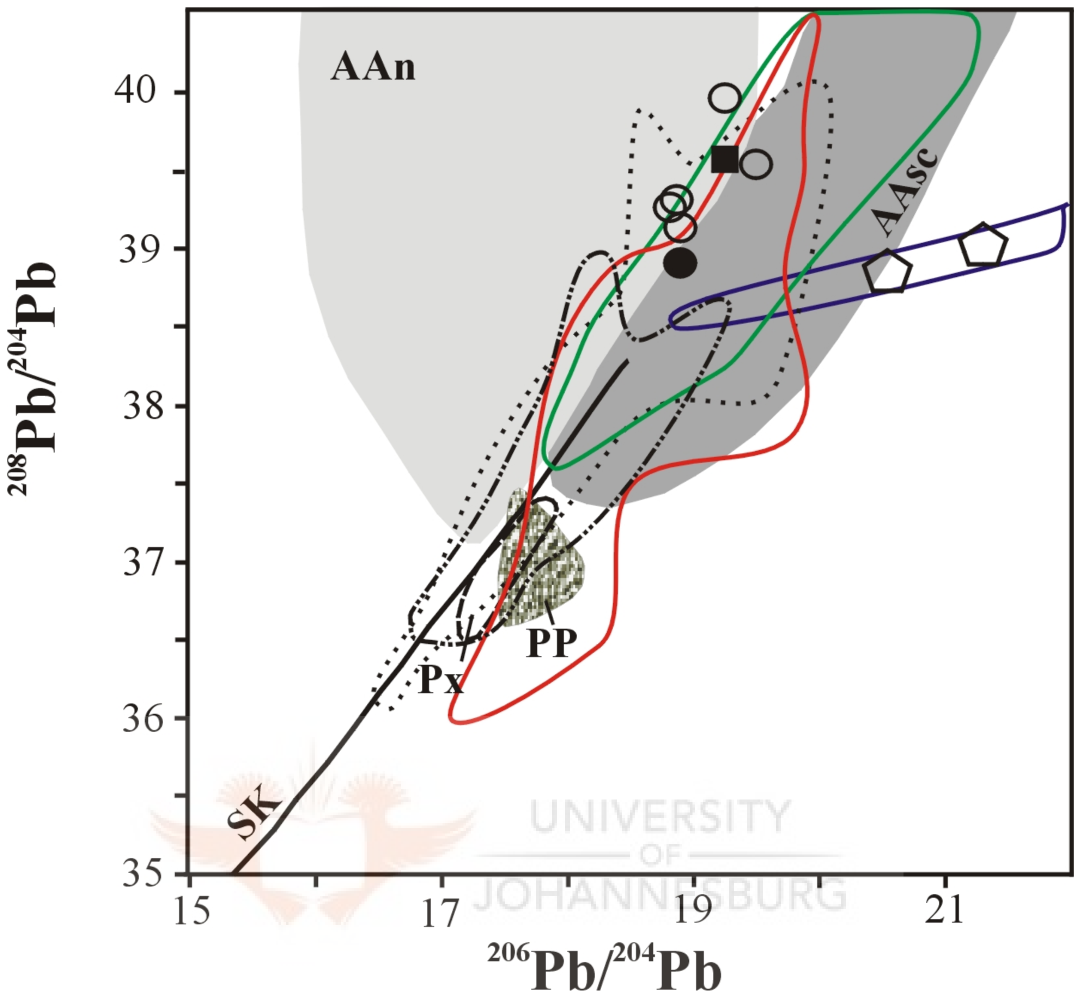

Figure 4.12: $^{208}Pb/^{204}Pb$ versus $^{206}Pb/^{204}Pb$ present-day ratios. Empty circles represent samples from the Los Sombreros Formation; solid square is the average value for the upper crust and solid circle the average value for GLOSS, both from Hemming and McLennan (2001). Fields obtained from several sources as indicated in the text. References are as in Fig. 4.11.

4.6 DISCUSSION

Petrographic analyses indicate for the slope-type deposits a main provenance from an igneous-metamorphic complex including an input from sedimentary successions. The presence of brown spinels within the heavy minerals fraction supports an input from a mafic source. It is clear that at least two compositionally different sources were involved in providing detritus to the basin slope. The main source has an unrecycled upper continental crustal signature whereas the subordinate component is more depleted in its composition. The high proportion of apatite and the fractionation during the very low-grade metamorphism are probably governing the behaviour of trace elements in certain samples.

Geochemical data display variable major element compositions, influenced by highly variable CaO concentrations. Geochemical indicators of alteration suggest rather intense weathering and a potassium metasomatism is deduced on samples with high K_2O concentrations compared with the UCC value. K/Cs ratios lower than the upper continental crust also supports strong weathering for the Empozada and Los Sombreros Formations. The high Cr/V and low Y/Ni ratios observed in sandstones and mudstones support the influence of a source more depleted than the UCC (although not ophiolitic), which is more notable for the Empozada Formation. Further assumptions regarding this depleted component are provided by the absence of Eu-anomaly (Eu_N/Eu^* of about 1) and by Th/Sc ratios as low as expected for andesite-like rocks. The depleted component is represented by the chromian spinels found within the heavy mineral suite. Conversely, negative Eu-anomalies reflect the upper continental crustal component. REE patterns are LREE depleted and HREE enriched compared with the PAAS for certain samples. Three samples from the Los Sombreros Formation are enriched in MREE and have high Sm/Nd ratios indicative of disturbances of the rare earth elements. The wide scatter of the $f_{Sm/Nd}$ (Fig. 4.9b) also indicates this fractionation of rare earth elements for the Los Sombreros Formation. The Zr/Sc ratios demonstrate that recycling was not an important process for both units, although some Zr/Sc ratios for the Empozada Formation are higher than the Zr/Sc ratios from the Los Sombreros Formation. Relationships between La, Th, Sc, Ti and Zr suggest that the Empozada and Los Sombreros Formations were deposited on an active continental margin or a continental island arc setting, although input from an arc component seems to be ruled out based on Eu_N/Eu^*, Nb, Ti and the Th/Sc ratios. However, typical arc signatures are often not recorded in other than basins spatially closely related to the arc itself, and rocks derived from dissected arc terranes would show variable Eu_N/Eu^* values (McLennan *et al.*, 1990; Zimmermann, 2005). The active continental margin setting used by Bathia and Crook (1986) involves retro-arc foreland as well as pull-apart basins. Passive margin and foreland basin deposits cannot be easily discriminated using Th-Sc-Zr-La relationships (Zimmermann, 2005).

Similar Nd compositions for the Los Sombreros (this study) and Empozada Formations (Gleason *et al.*, 2006) support a common provenance for both units. The narrow range in ε_{Nd} (t) values compared with the range in variation of the Th/Sc ratio might be interpreted as reflecting chemically different rocks that belong to the same basement. The models proposed to explain the tectonic evolution of the Precordillera terrane imply the evaluation of sources such as the Famatinian arc, the Grenville Province of Laurentia and Western Pampeanas Ranges (which probably continued within the Arequipa-Antofalla Basement; Casquet *et al.*, 2006). On the other hand, the para-autochthonous models (Aceñolaza *et al*. 2002; Finney *et al.*, 2005) placed the Precordillera surrounded by Antarctica, Falklands/Malvinas Microplate and the Natal-Namaqua Metamorphic belt (SAFRAN), being therefore important to evaluate these areas as probable sources as well. ε_{Nd} values are within the range of variation of the Laurentian Grenville crust (Patchett and Ruiz, 1989), Central and Southern domains of the Arequipa-Antofalla Basement (Loewy *et al.*, 2004), the basement of the Precordillera known as the Cerro La Ventana Formation (Cingolani, unpublished data), the Western Pampeanas Ranges and the Famatinian arc (Pankhurst *et al.*, 1998).

Pb isotopes from the Los Sombreros Formation provide evidence that at least some of the source components have a "Gondwanan Pb-signature", characterized by high $^{207}Pb/^{204}Pb$ ratios. Data presented by Gleason *et al.* (2006) from the Empozada Formation are dissimilar to those from the Los Sombreros Formation. Nevertheless, the Pb signature for the Los Sombreros Formation rules out the Eastern North American crust as a source, emphasizing the similarity to other probable sources such as the Arequipa-Antofalla Basement. Although Nd isotopes showed similarities with the Central and Southern domains of the Arequipa-Antofalla Basement (Loewy *et al.*, 2004), Pb data indicate similarities with all domains, but $^{207}Pb/^{204}Pb$ ratios values are as high as those showed by the Northern domain and even higher. The Pb isotopic composition from the Cerro La Ventana Formation and the Famatinian arc are unknown. Scarce data available from the Pie de Palo Range (Western Pampeanas Ranges) and from xenoliths interpreted as the basement of the Precordillera (Kay *et al.*, 1996) are however different to those from the Los Sombreros Formation, in contraposition to the similarities found regarding the Sm-Nd signature.

The zircon spectra reported for the Empozada Formation by Gleason *et al.* (2006) shows a main contribution from a 900 to 1300 Ma ("Grenvillian-age") source (about 64% of the total zircons) and from a Late Mesoproterozoic (1300 to 1600 Ma) source (about 30% of the data). The rest of the zircon population is composed of four grains in the 647 to 892 Ma range, and two Palaeoproterozoic grains. The detrital zircon dating therefore constrains the provenance of the slope-type deposits to a dominant Mesoproterozoic crust. Detrital zircon dating therefore seems to indicate that the Famatinian arc was not a source. Ages that match the detrital zircon spectra are found within the Western Pampeanas Ranges, the Arequipa - Antofalla Basement (Figs. 4.13 and 4.14) and basement rocks from a southern continuation of the Precordillera known as the San Rafael block (Cerro La Ventana Formation). However, the latter account only for Mesoproterozoic ages.

Several features such as the lack of important recycling and petrographic characteristics indicate that sources located far away should be neglected. Palaeocurrents indicate transport directions from east-southeast towards west-northwest (Banchig *et al.*, 1993). Several areas (Laurentian Grenville crust, the Arequipa-Antofalla Basement, the Cerro La Ventana Formation, the Western Pampeanas Ranges, the Famatinian arc, Antarctica, Falklands/Malvinas Microplate and the Natal-Namaqua Metamorphic belt) match the Sm-Nd signature found within the slope-type deposits. From these, the Laurentian Grenville crust, Antarctica, Falklands/Malvinas Microplate and the Natal-Namaqua Metamorphic belt can be ruled out based on Pb differences. The Famatinian arc cannot be considered as an important source based on detrital zircon dating.

Regarding the remaining areas, Pb data from the Cerro La Ventana Formation is missing and furthermore, this unit does not fulfil the complete detrital ages range not the transport directions indicated by palaeocurrents. The scarce Pb data available from

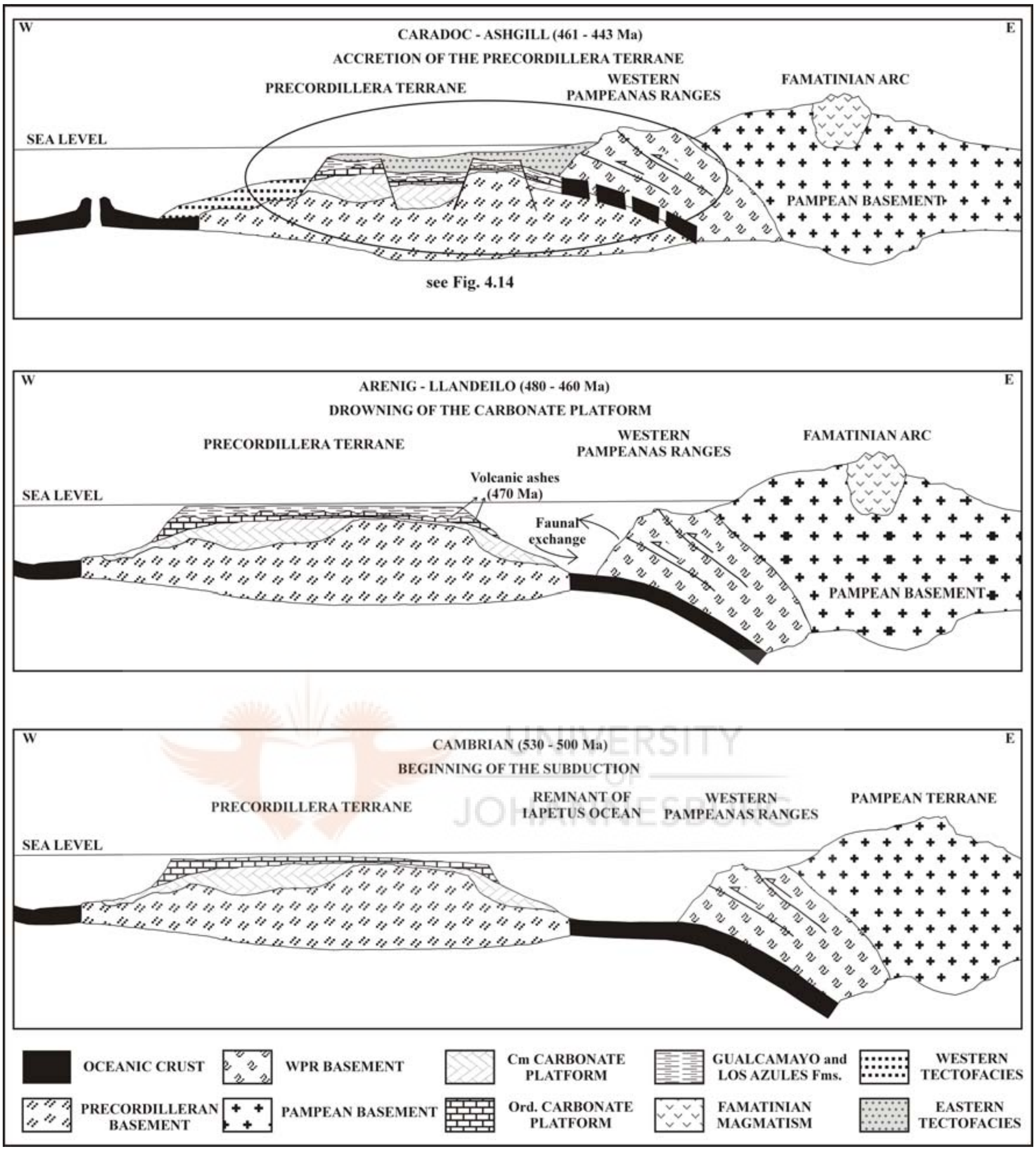

Figure 4.13: Geotectonic evolution of the Precordillera terrane. An eastern subduction was active since the Cambrian as documented by the continental magmatic arc (Famatina). The volcanic ashes (nowadays K-bentonites) found within the uppermost San Juan Formation and the lowermost Gualcamayo Formation record the activity of such magmatism in the context of the Precordillera terrane. A Late Arenig to Llanvirn final accretion age is estimated for the Precordillera terrane based on petrographical, geochemical and isotope geochemical data presented in this and previous chapters, which indicate that the Western Pampeanas Ranges and the Arequipa-Antofalla Basement are the more probable sources for the Ordovician sedimentary sequences of the Precordillera terrane.

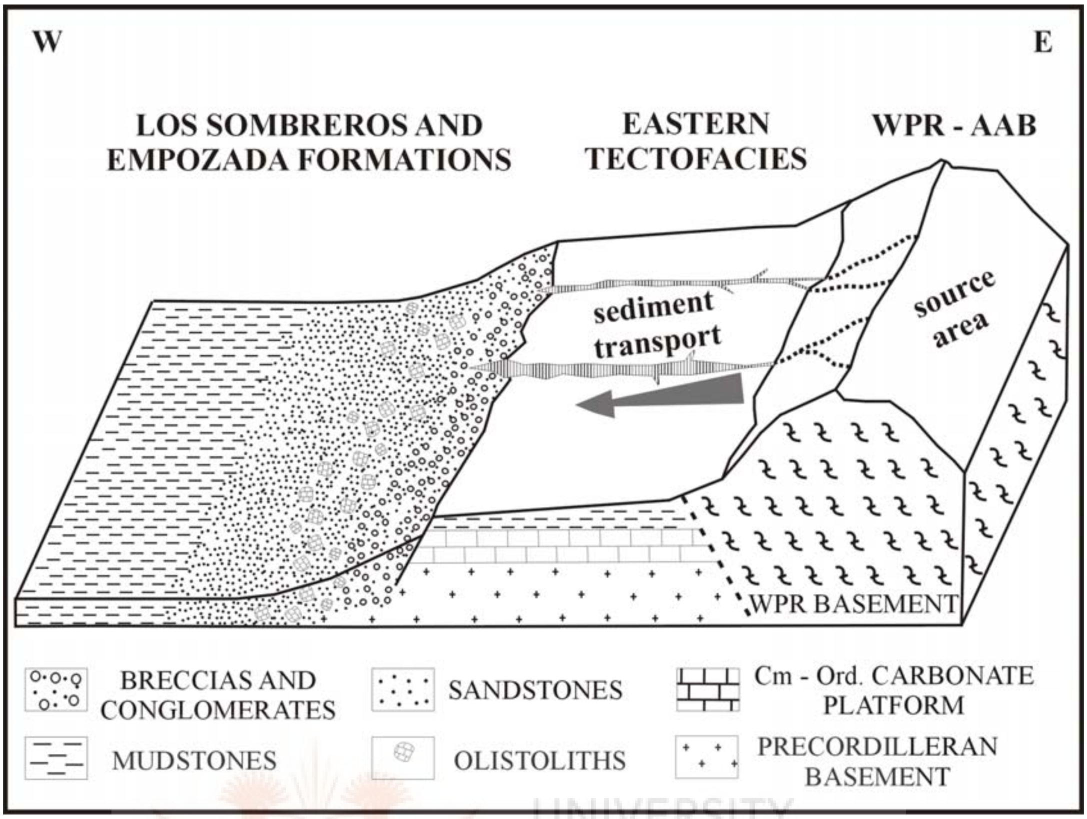

Figure 4.14: Schematic cross section showing the depositional setting of the Los Sombreros and Empozada Formations at the slope base. The Western Pampeanas Ranges (WPR) and its northern continuation known as the Arequipa – Antofalla Basement (AAB) are the most probable source areas. Olistoliths as well as sedimentary lithoclasts are derived from the Eastern tectofacies of the Precordillera terrane (located at the platform).

the Western Pampeanas Ranges (Pie de Palo Range) are different to the Pb composition of the slope deposits. The Sm-Nd signature is not well known but certain similarities were found. The crystallization ages found within the context of the Western Pampeanas Ranges match the detrital zircon spectra. Furthermore, palaeocurrent directions support a provenance from eastern sources (Banchig *et al.*, 1993). However, a better knowledge of the isotopic characteristics is needed to further support this area as a source. The Arequipa-Antofalla Basement gives the best matching to almost all the provenance proxies determined in this study. However, the northern termination of the Precordillera terrane (Jagüé area) is still under investigation and therefore the tectonic relationship with the Arequipa - Antofalla rocks is currently not well determined (e.g. Astini and Dávila, 2004), but a northern provenance is not supported by palaeocurrents. Nevertheless, if the Arequipa – Antofalla Basement constitute a single continental crustal block along with the Western Pampeanas Ranges (Casquet *et al.*, 2006), then it could be speculated that similar isotopic characteristics would be found within the Western Pampeanas Ranges.

Naipauer (2007) deduced a Laurentian derivation for the Neoproterozoic to Cambrian successions of the Precordillera terrane, invoking an allochthonous model to understand such a provenance for the detrital record. The Mesoproterozoic basement of the Precordillera (Cuyania) terrane was at least partially exposed and provided detritus to a clastic level interlayered with the Angacos Formation (based on detrital zircon dating; Naipauer, 2007). Therefore, an allochthonous origin for the Precordillera terrane is here preferred. In this scenario, the eastwards subduction would have been active during the Cambrian (Fig. 4.13), when the Precordillera terrane comprised a carbonate platform. At Arenig-Llandeilo times (480-460 Ma) the Famatinian arc was developed as a response to the subduction (Fig. 4.13) and volcanic ashes reached the upper part of the carbonate platform as well as the following black shales (Gualcamayo Formation). The Western Pampeanas Ranges were uplifted (Casquet *et al.*, 2001) and provided detritus to the basin, and also acted as a positive area preventing that detrital material from the Famatinian arc reached the basin (Figs. 4.13 and 4.14). The Western Pampeanas Ranges and the Arequipa-Antofalla Basement were source areas of the units here studied. Considering that these areas might composed a block autochthonous or para-autochthonous with respect to the pre-Famatinian margin of Gondwana (Casquet *et al.*, 2006), then the Precordillera terrane might have reached its present position for the time of the beginning of the sedimentation of the Empozada and Los Sombreros Formations (Figs. 4.13 and 4.14).

4.7 CONCLUSIONS

According to petrography and geochemistry of the slope-type deposits, the main provenance component has an unrecycled upper continental crustal signature whereas the subordinate component is more depleted in its composition. An igneous-metamorphic complex including an input from reworked sedimentary successions represents the upper continental crustal composition. The presence of brown spinels within the heavy minerals fraction supports an input from a mafic source. Mudstones and sandstones were affected by weathering, potassium metasomatism and selective sorting of certain heavy mineral phases such as apatite. Based on geochemistry, the basin where these units were deposited can be related to an active margin setting, although the influence of an arc source component is not clear. The similarities in Nd-isotopic compositions between the two units tend to indicate a common provenance for both sequences. Certain samples from the Los Sombreros Formation show REE (including Sm and Nd) fractionation. Pb isotope compositions of the Los Sombreros Formation tend to link it to typical Gondwanan areas.

Constraints given by Sm-Nd, Pb-Pb and detrital zircon dating along with sedimentological features allowed excluding the Laurentian Grenville crust, the Natal-Namaqua Metamorphic belt, Falkland/Malvinas Microplate, Antarctica and the Famatinian arc as sources. The constraints of ages of the sources provided by detrital zircon dating, and the constraints provided by the other provenance proxies (petrography, geochemistry, palaeocurrents and isotope geochemistry) suggest that the more probable source areas are the Western Pampeanas Ranges and less probably the Arequipa-Antofalla Basement. In these regard, an allochthonous origin for the Precordillera terrane is preferred, although extensive studies of the basement rocks are needed to further support this. If these two areas were autochthonous to Gondwana, then the Precordillera terrane must have reached its present position with respect to them prior to the deposition of the slope-type deposits.

CHAPTER 5

PROVENANCE ANALYSIS OF ORDOVICIAN CLASTIC UNITS OF THE WESTERN TECTOFACIES OF THE PRECORDILLERA TERRANE, ARGENTINA.

5.1 INTRODUCTION

The tectonic evolution of the Precordillera terrane (Fig. 5.1) is a subject for debate,since the different approaches used to determine its origin (e.g. sedimentology, palaeontology, palaeomagnetism, etc.) suggest either a Laurentian (i.e. Ramos *et al.*, 1986; Dalla Salda *et al.*, 1992a; Cingolani *et al.*, 1992; Dalziel *et al.*, 1994; Astini *et al.*, 1995; Thomas and Astini, 1996; Keller, 1999) or a Gondwanan origin (i.e. Baldis *et al.*, 1982; Aceñolaza *et al.*, 2002; Finney *et al.*, 2005). Furthermore, the different models proposed to explain the tectonic evolution of the Precordillera terrane differ regarding timing and mode of collision. Nevertheless, integrated provenance analyses, which have been useful in deciphering the nature of crustal blocks, are scarce within the context of the Precordillera (Loske, 1992; Cingolani *et al.*, 2003a).

The Western tectofacies (Astini, 1993a) of the Lower Palaeozoic of the Precordillera terrane (Fig. 5.2a) is composed of deep-sea clastic rocks, affected by intense deformation and Early Devonian low-grade metamorphism (Robinson *et al.*, 2005). This tectofacies comprises the Yerba Loca, Alcaparrosa, Portezuelo del Tontal and Sierra de la Invernada Formations (Fig. 5.2b) which host mafic to ultramafic rocks. These mafic to ultramafic rocks outcrop as a discontinuous belt along the western margin of the terrane. Several studies demonstrated that these rocks range in age from Late Proterozoic to Late Ordovician and do not represent a single ophiolite (Davis *et al.*, 1999; 2000). Although the Los Sombreros Formation belongs to the Western tectofacies in the sense of Astini (1993a), it is excluded here as it was considered together with the Empozada Formation since both represent the slope-type deposits (see Chapter 4). This slope is located to the east of the Western tectofacies, whereas further east the contemporaneous Eastern tectofacies (see Chapter 3) was developed. Contrary to the Western tectofacies, the Eastern tectofacies was not affected by metamorphism, but only by diagenesis. Furthermore, the mafic rocks are not present either.

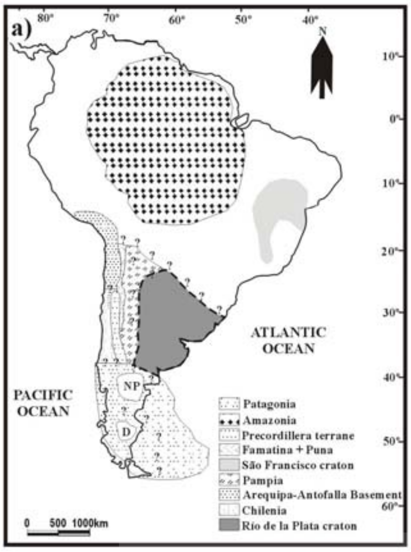

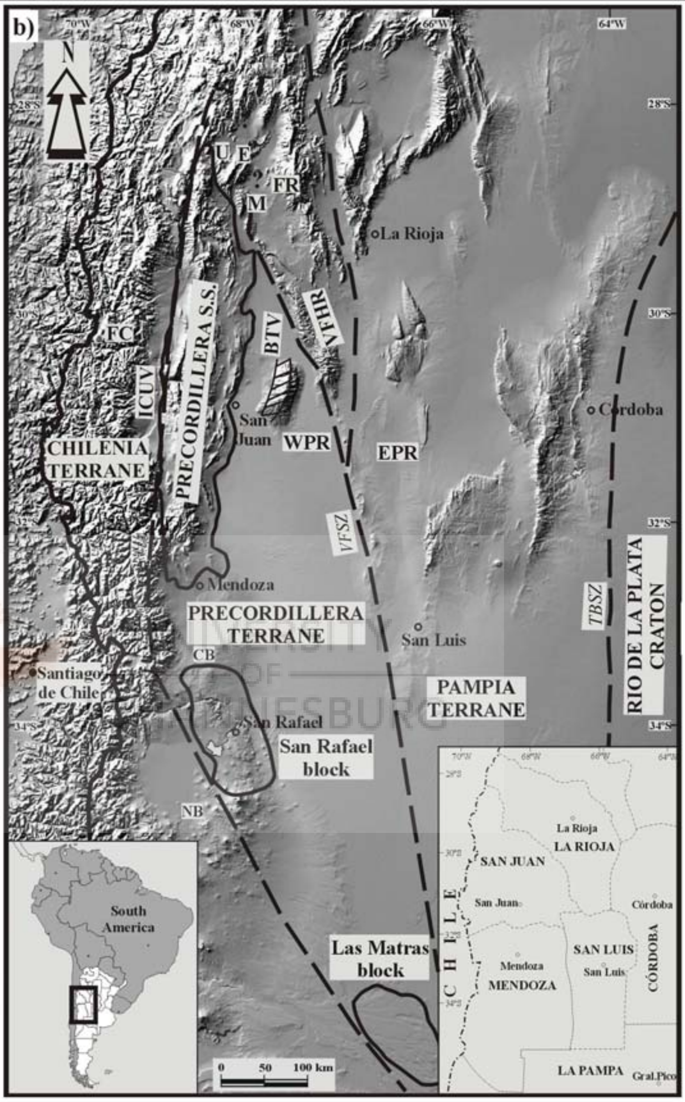

Figure 5.1: a) Main tectonostratigraphic units of South America (modified from Rapalini, 2005). NP: North Patagonian Massif; D: Deseado Massif. b) Satellite image based map showing terrane boundaries as dashed lines and blocks boundaries as continuum lines (based on Ramos *et al.*, 2000; Porcher *et al.*, 2004; Astini and Dávila, 2004). FR: Famatina Range; FC: Frontal Cordillera; ICUV: Iglesia Calingasta-Uspallata Valley; BTV: Bermejo-Tulum Valley; WPR: Western Pampeanas Ranges; EPR: Eastern Pampeanas Ranges; VFSZ: Valle Fértil Shear Zone; CB: Cuyo Basin; NB: Neuquén Basin; PP: Pie de Palo Range; E: Espinal Range; U: Umango Range; M: Maz Range; VFHR: Valle Fértil-La Huerta Range.

Provenance data obtained from sedimentary rocks of the Yerba Loca, Alcaparrosa, Sierra de la Invernada and Portezuelo del Tontal Formations are presented here (Fig.5.2). A combination of different methodologies including petrography and heavy minerals, geochemistry, Sm-Nd and Pb-Pb isotopes and zircon dating was applied to constrain the sources. The volcanic rocks interlayered with the Yerba Loca

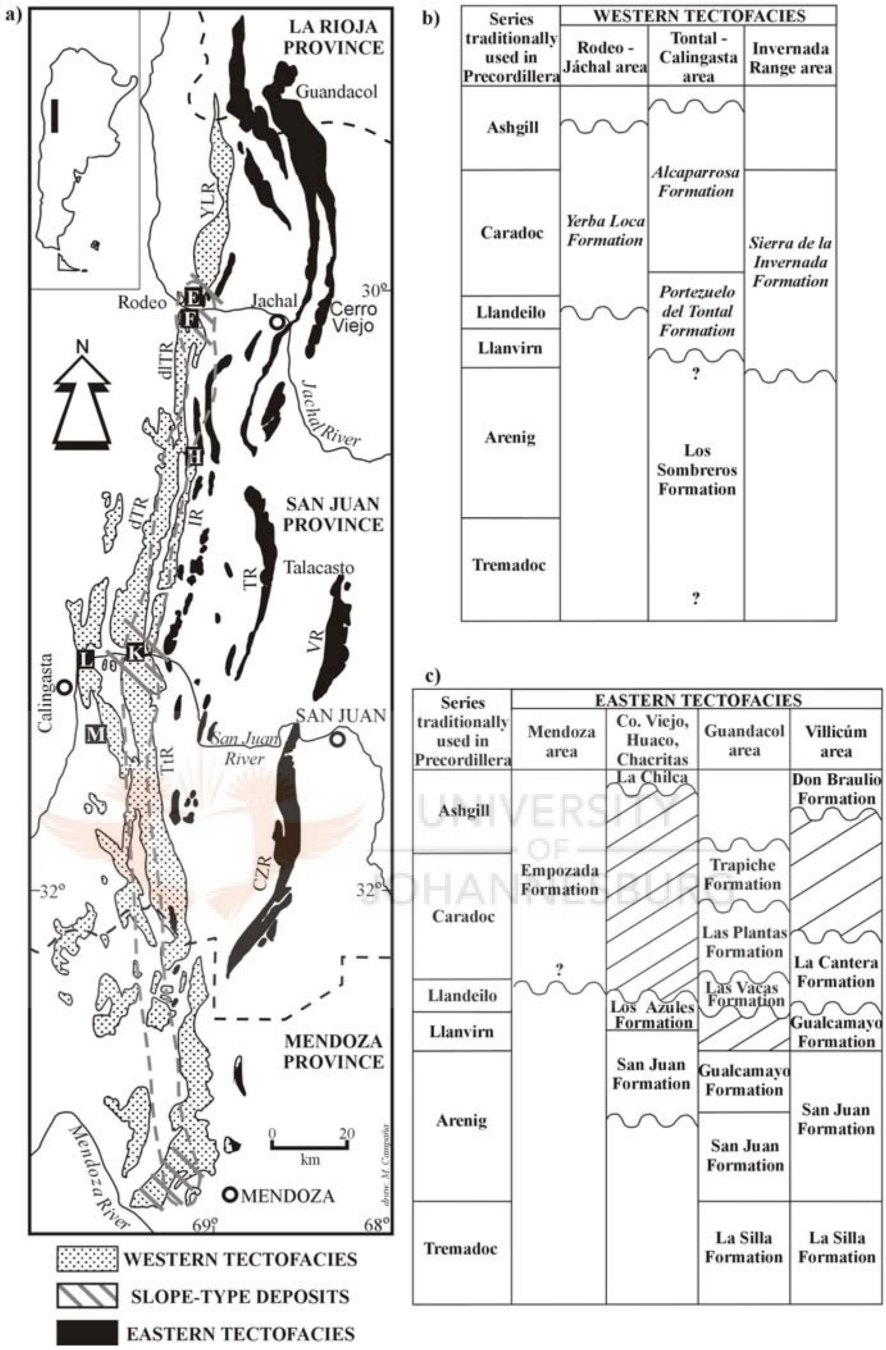

Figure 5.2: a) Sampling locations from the Western tectofacies of the Precordillera terrane (white letters correspond to samples in Table 2 in Appendix B). IR: Invernada Range; dTR: del Tigre Range; dlTR: de la Tranca Range; YLR: Yerba Loca Range; TR: Talacasto Range; TtR: Tontal Range; CZR: Chica de Zonda Range; VR: Villicúm Range. Modified from Astini (1991). b) and c) Stratigraphy of the Ordovician of the Precordillera terrane based on Keller (1999). Diagonal lines indicate hiatus. Units studied are in italics.

Formation were analyzed petrographically and geochemically. The different components that provided detritus to the Western basin of the Precordillera *s.s.* are distinguished and characterized and tentative source areas are determined.

5.2 GEOLOGICAL BACKGROUND

The Yerba Loca Formation (Furque, 1963), crops out in the Yerba Loca, La Tranca and del Tigre Ranges (Fig. 5.2), northern and central parts of the Western Precordillera. It is one of the most representative units of the Western tectofacies (Astini, 1994d). This Formation is characterized by mudstones, carbonate-hemipelagites, arenites, hybrid arenites (arenites comprising high proportions of carbonates) and greywackes (frequently carbonate cemented), subordinated conglomerates and concordant to sub-concordant mafic to ultramafic magmatic rocks (Fernández Noia *et al.*, 1990; Astini, 1991). The hybrid arenites and greywackes contain intrabasinal carbonate clasts, which were provided by the uppermost sequences of the San Juan Formation (Astini, 1991; Ortega *et al.*, 1991). The thickness of the sequence is unknown due to the presence of faulted basal and top contacts, but was estimated to be more than 1000m (Furque and Cuerda, 1979). The clastic rocks were affected by greenschist metamorphism within the chlorite zone and by at least two major deformational events. Deformation and metamorphism were tentatively assigned to the Late Silurian to Early Devonian (Keller *et al.*, 1993; von Gosen, 1997). The westernmost outcrops of the Yerba Loca Formation were deposited as fine-grained turbidites interlayered and intruded by mafic magmatic rocks (e.g. Ramos *et al.*, 1986; Astini *et al.*, 1996), while the eastern section lack such an igneous record and is interpreted as arenite-turbidites and mixed clastic-carbonate turbidites (Astini, 1994d).

The interlayered magmatic rocks are present as pillow lavas, columnar-jointed basalts, dykes and sills. They were interpreted as evolved oceanic tholeiites formed at an early stage of a transitional-type or plume-type oceanic ridge segment, or in a retro-arc basin (Kay *et al.*, 1984). The presence of graptolites (*Nemagraptus gracilis* and *Paraglossograptus tentaculatus* Zones) provides a Lower Llanvirn to Caradoc age. The

Yerba Loca Formation can be correlated to the upper part of the San Juan Formation, to the Los Azules and Gualcamayo Formations, as well as to the Las Plantas, La Cantera, Los Sombreros and Empozada Formations (Blasco and Ramos, 1976; Ortega *et al.*, 1991; Fig. 5.2b and c).

The Alcaparrosa Formation (Harrington, 1957) crops out on the western side of the del Tontal Range (Fig. 5.2). It is composed of feldspathic-wackes and arenites with interlayered shales, with occasionally interlayered basalts, dolerites and pillow lavas (Kerlleñevich, 1985b). The top of the unit contains interbedded quartz-rich sandstones with flute marks pointing to sediment transport from east to west (Astini *et al.*, 2000) and were interpreted as resedimented deposits from channel-complexes, within a relatively proximal marine environment (Astini, 1991). The interlayered shales contain graptolites (*Climacograptus* cf. antiquus, *Dicranograptus* sp. and *N. extraordinarius* Biozone) which suggest a Llanvirn-Llandeilo to Ashgill (Hirnantia) age (Aceñolaza and Baldis, 1986; Brussa *et al.*, 1999). The Alcaparrosa Formation is folded and faulted due to a Late Ordovician to Silurian tectonic event. A maximum thickness of 1300m was calculated, although top and bottom contacts are tectonic (Kerlleñevich, 1985b). The mafic rocks were dated by K-Ar giving an age of 416 ±19 Ma (Vilas and Valencio, 1970). The effects of the remagnetization associated to the Sanrafaelic phase (Permo-Triassic) did not allow the determination of a palaeomagnetic pole or original magnetization of the rocks (Rapalini, 1996).

Mafic volcanic rocks from both the Yerba Loca and Alcaparrosa Formations show the effects of metamorphism from a sub-greenschist (prehnite-pumpellyite) facies and constrained to low temperature (250º-350º C) and low pressure (2-3 kbars) conditions (Robinson *et al.*, 2005). These metamorphic characteristics are due to the collision between the Chilenia and Precordillera terranes during Early Devonian times, particularly if the subduction of the slab of Chilenia was towards the east (Robinson *et al.*, 2005). Therefore, the metamorphism is not related to the accretion of the Precordillera terrane to Gondwana.

The Portezuelo del Tontal Formation (Cuerda *et al.*, 1985) crops out at the central part of the Sierra del Tontal Range (Fig. 5.2). It is a 1500m to 2000m thick turbidite sequence, although the base and top are faulted bounded. The unit is folded and faulted (Spalletti *et al.*, 1989). It has a rich graptolite assemblage of Llanvirn to Late Llandeilo-Caradoc age (Cuerda *et al.*, 1986b; Cuerda *et al.*, 1988b). Based on its fauna content, it is correlated with the Gualcamayo, Los Azules and Las Plantas Formations (Cuerda *et al.*, 1986b; Fig. 5.2b and c). The Portezuelo del Tontal Formation consists of fining-upwards cycles composed of subordinated massive conglomerates or coarse sandstones at the base, predominant sandstones or siltstones with wavy-lamination, cross-lamination and convolute lamination, and followed by laminated siltstones with interbedded siltstones and shales towards the top (Cingolani *et al.*, 1986; Cuerda *et al.*, 1986b). Mafic and ultramafic sills intruded the succession during the Silurian (Gerbi *et al.*, 2002; dating tool not specified). The conglomerate clasts comprise limestones (most probably from the San Juan Formation), mafic volcanic rocks, sandstones and resedimented conglomerates (Peralta *et al.*, 2003a).

Spalletti *et al.* (1989) identified several facies and interpreted them as high- and low-density turbidites, debrites and contourites-hemipelagites from a deep-sea fan system on a passive continental margin. Palaeocurrents (measured on flute casts, cross-bedding and imbricated pebbles) show a radial pattern, coherent with the depositional fan model (Spalletti *et al.*, 1989). However, the regional trend is mainly to the west, in agreement with the inferred position of the basin slope (Cingolani *et al.*, 1986).

The Sierra de la Invernada Formation (Furque, 1983; *emend*. Furque and Caballé, 1985), crops out in the de la Invernada Range, within the central part of the Western Precordillera (Fig. 5.2). The maximum thickness recorded is 1100m although basal and top contacts are covered or tectonized (Furque and Caballé, 1985). The sequence is folded and faulted and metamorphosed to very low-grade (Brussa, 1997). It has an Upper Arenig to Caradoc age based on graptolites (*Paraglossograptus tentaculatus* and *Nemagraptus gracilis* Biozones (Caballé *et al.*, 1992; Brussa, 1997). The Sierra de la Invernada Formation can be correlated with the Empozada, Las Plantas, Los Azules, Alcaparrosa, Los Sombreros and Portezuelo del Tontal Formations (Caballé *et al.*, 1992; Fig. 5.2b and c). The Sierra de la Invernada Formation is mainly composed of fine to medium arenites, wackes and mudstones with interlayered carbonate-arenites (Brussa, 1997) and interpreted as a turbidite sequence (Furque and Caballé, 1985). It comprises interlayered mafic magmatic rocks in the form of sills and pillow lavas (Caballé *et al.*, 1992), which are contemporaneous with the sedimentary rocks (Banchig *et al.*, 2004). Palaeocurrents indicate an east-west direction coincident with the slope dip-direction. The composition of lithoclasts indicates a provenance from the metamorphic basement of the Pampean Ranges (Banchig *et al.*, 1993).

Basilici *et al.* (2005) established that the Portezuelo del Tontal, Yerba Loca and Sierra de la Invernada Formations were deposited above the storm wave-base, with palaeocurrents dominantly from north to south and as storm dominated shallow marine shelf rather than deep-water fan systems as they were previously interpreted (Spalleti *et al.*, 1989), although an extensive discussion regarding these differences is not presented. According to Basilici *et al.* (2005), the western Gondwana margin was deepening towards south. The units are characterized by sole marks, buoyant muddy clasts, traction carpet structures and anisotropic hummocky cross-stratification and they were deposited within the same depositional basin by gravitational flows combined with storm activity (Basilici *et al.*, 2005).

5.3 PETROGRAPHY OF FRAMEWORK AND HEAVY MINERALS

5.3.1 Sedimentary rocks

A total of fifty-three mudstones and sandstones from the four units studied were analyzed under the microscope, X-ray diffraction (XRD) and SEM-BSE-EDS (scanning and backscattered electronic microscope, and energy dispersive system). For more details about sampling, methodologies and analytical techniques see Appendix B. Samples are mostly arenites and greywackes, moderately well to very poorly sorted. Their grain size ranges from silt to coarse sand. Some samples contain low amounts of matrix, while greywackes with matrix content between 31% and 37% are also present. The matrix is composed predominantly of white mica (sericite and illite) and quartz, but chlorite is also present. A group of sandstones are calcite-cemented and less commonly dolomite-cemented. Framework minerals are subrounded to subangular and with low sphericity, but rounded and highly spherical grains (most commonly of quartz) are present.

The main mineralogical component is monocrystalline quartz, with normal extinction; grains with undulose extinction are rare. Fluid inclusions are present and in some cases, they even form strained quartz. Booklets of kaolinite as well as muscovite are frequently included in quartz whereas rare mineral inclusions are zircon, apatite and biotite. Occasionally, grains with embayments were observed as well as polycrystalline quartz with sutured edges and undulose extinction. Graphic quartz had been observed in several thin sections.

K-feldspar is more abundant than plagioclase for the Yerba Loca, Portezuelo del Tontal and Sierra de la Invernada Formations but the contrary is true for the Alcaparrosa Formation. K-feldspar (microcline is dominant and less common is anorthoclase) is altered to clay minerals and less frequently to calcite, while plagioclase is smaller and range from unaltered to partial or totally replaced by calcite and clay minerals. Inclusions in plagioclase are not frequent, but when present they are composed of apatite and Ti-oxides. Some quartz and K-feldspar grains are several times larger than the medium grain size of the rocks.

Muscovite, chlorite and epidote are present as large crystals, and are the result of the greenschist facies metamorphism. Intergrowths of muscovite and chlorite are frequent. Muscovite and biotite are also present as detrital lamellae, and chlorite is frequently replacing biotite. The lithoclasts are sedimentary (siltstones, mudstones, carbonates and cherts), volcanic (with typical textures of fine-grained rocks such as basalts and andesites), and metamorphic (fine flat-grained from phyllitic rocks and rarely from coarse-grained schist-type rocks or even gneisses).

Zircon, tourmaline, epidote, staurolite, rutile, apatite, monazite, titanite, hematite and other opaque minerals represent the detrital accessory assemblage. Sometimes, these heavy minerals are as large as the main light framework minerals. Ti-oxides are a frequent component of greywackes, but are also common within the mudstones. They are present as small (between 10μm and 20μm) anhedral to subhedral grains within the matrix or as lamellae included within other minerals such as chlorite, muscovite, quartz and plagioclase. In several cases, the lamellae are conspicuous and cover almost the entire grain. Fe-oxyhydroxides such as goethite or lepidocrocite were also observed.

Illite crystallinity index (ICI) measured on claystones from the Alcaparrosa Formation showed that this unit underwent late diagenesis to very low-grade metamorphism, whereas ICI results of the Portezuelo del Tontal Formation indicate a very low-grade metamorphism (see Table 2 in Appendix A). However, previous works indicate up to greenschist facies metamorphic grades for the Alcaparrosa Formation (Rubinstein *et al.,* 1995) and greenschist metamorphism within the chlorite zone for the Yerba Loca Formation (Keller *et al.*, 1993; von Gosen, 1997).

5.3.2 Volcanic rocks

The igneous rocks associated with the Yerba Loca sequence show the effects of metamorphism. They are dominantly mafic. The phenocrysts of olivine, pyroxene and plagioclase are embedded within a plagioclase-rich groundmass forming a pilotaxitic (felty) texture. A greenschist facies assemblage can be assumed due to the intergrowth of chlorite, calcite and epidote (not ICI data are available neither from the volcanic rocks nor from the clastic rocks of the Yerba Loca Formation). This is in agreement with the results of Robinson *et al.* (2005).

5.4 GEOCHEMISTRY

Geochemical analysis is a valuable tool for provenance studies of sedimentary rocks as long as the bulk composition is not strongly affected by weathering, diagenesis and metamorphism (McLennan *et al.*, 1993). Representative samples (n=53) from the sedimentary record of the four units and from the volcanic rocks (n=10) interlayered with the Yerba Loca Formation were analyzed. Table 1 (Appendix A) contains the chemistry of all samples analyzed.

5.4.1 Sedimentary rocks

5.4.1.1 Major elements and alteration

The Yerba Loca Formation is characterized by SiO_2 concentrations ranging from 56% to 75%, Al_2O_3 ranging from 8.5% to 19.7%, Fe_2O_3 is between 4.7% and 9.3%, MgO ranges from 1.5% to 3%. CaO from 0.2% to 4.3% and the Na_2O concentration is of 2.21±0.65 on average. Sandstones have a low K_2O concentration (between 1.4% and 2.1%) whereas mudstones are enriched (between 3.4% and 4.9%) compared with the sandstones and with the upper continental crust (UCC) value of 3.4% (McLennan *et al.*, 2006). Two sandstones have a distinctive chemical composition and are therefore separately described and discussed. Samples YL411 and YL454 (see Table 1 in Appendix A) have lower SiO_2 and higher Fe_2O_3, MgO and CaO abundances compared with the rest of the samples of the Yerba Loca Formation. Notwithstanding, these two samples have similar Al_2O_3 and Na_2O concentrations. Samples YL411 and YL454 are depleted in K_2O (0.25% and 1.25% respectively) compared with the UCC (McLennan *et al.*, 2006), but with a concentration similar to the rest of the sandstones from this unit.

Sandstones and mudstones from the Alcaparrosa, Portezuelo del Tontal and Sierra de la Invernada Formations have similar chemical characteristics, with SiO_2 concentrations ranging from 56.5% to 77.5%, Al_2O_3 ranging from 8.5% to 18.5%, Fe_2O_3 is between 3.3% and 8.3%, MgO ranges from 0.74% to 2.9% and the Na_2O is between 1.45% and 2.64%. The CaO of the Portezuelo del Tontal and Sierra de la Invernada Formations is approximately 1%, and therefore duplicates the CaO concentration of the Alcaparrosa Formation (0.5% in average). The K_2O abundances for the three units range from 1.3% to 4.74%. Mudstones of the Alcaparrosa and Sierra de la Invernada Formations are enriched in K_2O compared both with the sandstones within the same units and with the UCC (McLennan *et al.*, 2006). Even though one mudstone of the Portezuelo del Tontal Formation has higher K_2O concentration compared with the sandstones of the same unit, it is not enriched compared with the UCC (McLennan *et al.*, 2006). However, the mudstone named PDT3 from the Portezuelo del Tontal Formation has a major elements composition substantially different to the above described. This sample has lower SiO_2 (51%) and higher Al_2O_3

(20%), Fe_2O_3 (10%) and MgO (3.6%) concentrations compared with the rest of the samples of the Portezuelo del Tontal Formation. On the other hand, the CaO and Na_2O abundances of sample PDT3 (0.89% and 1.6% respectively), are similar to the average values of the unit. K_2O is of about 5% for this sample and therefore it is enriched compared with the other samples of the Portezuelo del Tontal Formation and with the UCC (McLennan *et al.*, 2006). Petrographic analysis of sample PDT3 indicates coarse intergrowths of chlorite and muscovite probably due to metamorphism. Chlorite is related to the high Fe_2O_3 and MgO whereas the K_2O abundance is related to muscovite.

Weathering effects on sedimentary rocks can be quantitatively assessed using the Chemical Index of Alteration (CIA; Nesbitt and Young, 1982), where CIA = $\{Al_2O_3 / (Al_2O_3 + CaO^* + Na_2O + K_2O)\} \times 100$, and CaO* refers to the calcium associated with silicate minerals and oxides are expressed as molecular proportions. Corrections to the measured CaO concentration for the presence of Ca in carbonates and phosphates are needed. For this study, CaO was corrected for phosphate assuming that the P_2O_5 is entirely associated with apatite. However, CO_2 data were unavailable. Thus, if the remaining number of CaO moles obtained after deducing those moles associated with apatite are less that the number of Na_2O moles, then this CaO value was adopted to calculate the CIA (McLennan, 1993). If the number of moles is greater than Na_2O, then those samples were not used to calculate the CIA. Although these approximations seems to be useful (e.g. Bock *et al.*, 2000), in the present case study a correlation between low CIA values (between 52 and 58) and CaO concentrations above 1.1% is evident. Therefore, these low CIA values need to be taken with caution.

The CIA values for the sandstones of all the units studied range from 52 to 70, whereas the CIA values of the mudstones range from 64 to 73. According to Fedo *et al.* (1995), these values correspond to intermediate to strong weathering. In a broad sense, the samples tend to follow a normal weathering path (Fig. 5.3), which is parallel to the A-CN line (Fedo *et al.*, 1995). However, the enrichment of potassium of some samples causes the deviations towards the A-K boundary in the A-CN-K space (i.e. Fedo *et al.*, 1995; Nesbitt, 2003). This metasomatic process results in a CIA value lower than the pre-metasomatized one (Fedo *et al.*, 1995). However, the CIA value prior to the K-enrichment can be determined. In Figure 5.3, the field of vertical lines represents the assumed weathering trend for the UCC. Dashed lines represent metasomatic trends of the minimum and maximum CIA values to indicate the range of variation. Dotted lines end on the CIA scale indicating the corresponding pre-metasomatized CIA value for that interval. Some samples show an important K-enrichment and consequently their recalculated CIA values change drastically. For instance, the sample with a metasomatized CIA value of about 73 change to a pre-metasomatized CIA value of about 78, indicating an advanced stage of chemical weathering.

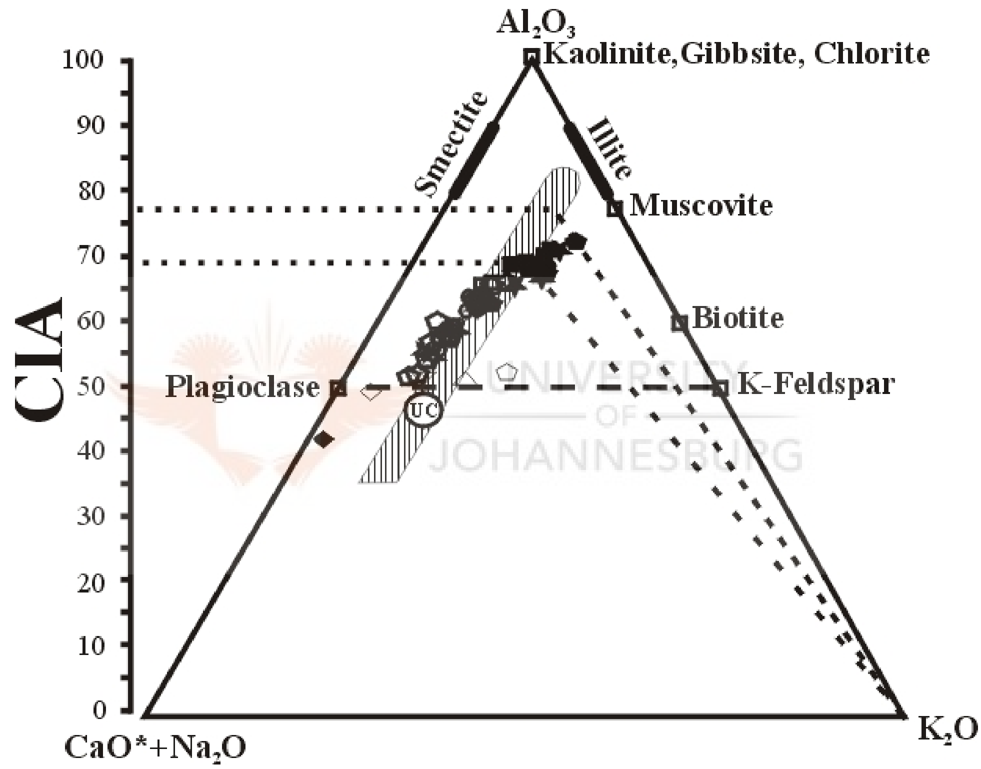

Figure 5.3: A-CN-K diagram and the CIA scale is shown on the left. The average upper continental crust is plotted (X; Taylor and McLennan, 1985), as well as idealized mineral compositions (empty squares). Data showing the CIA values for unweathered primary rocks are represented by cross: average granite; empty triangle: average adamellite; empty inverted triangle: average granodiorite; empty diamond: average tonalite; solid diamond: average gabbro (Nesbitt and Young, 1984). Solid symbols represent mudstones whereas empty symbols are for sandstones. Pentagons: Yerba Loca Formation; squares: Alcaparrosa Fm.; stars: Sierra de la Invernada Fm.; circles: Portezuelo del Tontal Fm. Field of vertical lines indicates the predicted weathering trend for the average upper crustal composition and it was used to recalculate the CIA. See text for discussion.

The K/Cs ratio is also an indicator of weathering, because Cs tends to be fixed in weathering profiles whereas the smaller cation of K tends to be lost in solution (McLennan *et al.*, 1990). Mudstones from the Yerba Loca, Alcaparrosa, Sierra de la Invernada and Portezuelo del Tontal Formations are enriched in Cs compared with the UCC value of 4.6ppm (McLennan *et al.*, 2006) and show K/Cs ratios below the value for the UCC (6136; McLennan *et al.*, 2006), indicating weathering (McLennan *et al.*, 1990). Sandstones instead show Cs values between 2ppm and 4ppm (values between 5ppm and 6ppm are scarce), which are below the UCC average (McLennan *et al.*, 2006). The K/Cs ratios of the sandstones vary strongly, from lower to higher values compared with the upper continental crust average. However, those samples showing potassium addition would have K/Cs ratios influenced towards lower values.

U and Th have similar properties and they both occur in rock-forming minerals. During weathering and sedimentary recycling, there is a tendency for an elevation of the ratio Th/U above upper crustal igneous values (3.8 to 4.0), due to the oxidation of U^{+4} to U^{+6} and the loss of the more mobile U^{+6} (McLennan, *et al.*, 1993).

For all the units studied, mudstones in general have Th and U abundances similar to enriched compared with the upper continental crust averages (10.7ppm and 2.8ppm for Th and U respectively; McLennan *et al.*, 2006). Their Th/U ratios are either between 3.5 and 4 (which is typical for derivation from upper crustal rocks), or higher than this range (Fig. 5.4; Table 1 in Appendix A). On the other hand, sandstones have Th and U concentrations lower than the UCC, although some samples have U concentrations similar to higher than the UCC. The Th/U ratios of the sandstones are variable (Fig. 5.4). Some samples have Th/U ratios between 3.5 and 4, whereas a few samples have less than 3.5 values. Samples with high Th/U ratios probably caused by loss of U due to weathering and/or recycling are also present mainly within the Portezuelo del Tontal and the Yerba Loca Formations.

5.4.1.2 Trace elements

The use of trace elements for provenance determinations is based on the immobile character and low residence time in seawater of certain elements, particularly high field strength elements (HFSE). It is also based on the fact that compatible elements (e.g. Sc, Cr, V and Ni) concentrate in mafic rocks whereas incompatible elements (such as Th, Zr, Y, U and Hf) concentrate in felsic rocks (Taylor and McLennan, 1985). Ratios such as Th/Sc, Th/U, Zr/Sc, and Cr/V are the most useful for provenance determination (Taylor and McLennan, 1985).

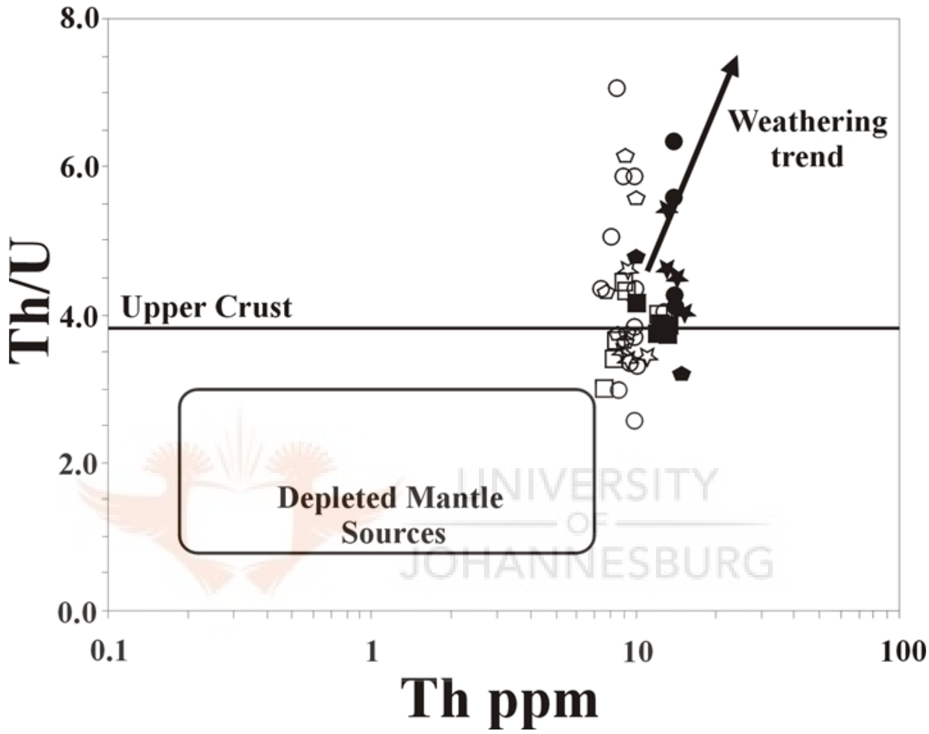

Figure 5.4: Plot of Th/U versus Th (McLennan *et al.*, 1993). Sandstones are represented by empty symbols whereas mudstones are represented by solid symbols. Circles: Yerba Loca Formation; squares: Alcaparrosa Formation; stars: Sierra de la Invernada Formation; pentagons: Portezuelo del Tontal Formation.

The input of a mafic source could be discriminated using the Cr/V and Y/Ni ratios. The Cr/V ratio indicates the enrichment of Cr over other ferromagnesian trace elements. The main minerals that concentrate Cr over other ferromagnesian are chromites. The Y/Ni ratio indicates the concentration of ferromagnesian trace elements (such as Ni) compared with Y that represents a proxy for heavy rare earth elements. The Cr/V and Y/Ni ratios for the PAAS (post-Archaean Australian Shales) is about

0.73 and 0.49 respectively (Taylor and McLennan, 1985), while for the UCC are 0.78 and 0.5 respectively (McLennan *et al.*, 2006). However, ophiolitic components have Cr/V ratios higher than 10 (discussion in McLennan *et al.*, 1993).

The Cr/V ratio for the Yerba Loca Formation is between 0.66 and 0.73 for mudstones and between 0.43 and 2.37 for sandstones. The Y/Ni ratio is between 0.31 and 0.96 for mudstones and sandstones. Although not clearly, these ratios along with enrichment in Sc (values up to 35.6ppm), Cr (up to 220ppm) and V (enrichments up to 230ppm) compared with the UCC averages of 13.6ppm, 83ppm and 107ppm respectively (McLennan *et al.*, 2006) may show the influence of a depleted source. The highest V concentrations are found within sandstones. The Cr/V ratio for the Alcaparrosa, Portezuelo del Tontal and Sierra de la Invernada Formations ranges from 0.80 to 0.96 for mudstones and from 0.70 to 1.12 for sandstones, whereas the Y/Ni ratio ranges from 0.41 to 0.9. These ratios along with the high Sc (25ppm), Cr (120ppm) and V (150ppm) concentrations of certain samples indicate the contribution from a depleted source.

The rare earth elements (REE) are reliable provenance indicators in well-mixed sedimentary rocks, as they reflect the average REE composition of the source material (Cullers *et al.*, 1979; Taylor and McLennan, 1985; McLennan, 1989). However, some mobility of REE may occur during weathering and diagenesis (i.e. Bock *et al.*, 1994; McDaniel *et al.*, 1994). The shape of the REE pattern can provide information about both bulk composition of the provenance and the nature of the dominant igneous process affecting the provenance (Taylor and McLennan, 1985; McLennan and Taylor, 1991).

The average chondrite normalized REE patterns for mudstones and sandstones of the Yerba Loca, Alcaparrosa, Portezuelo del Tontal and the Sierra de la Invernada Formations (Fig. 5.5) show a moderately enriched light REE pattern (LREE; La_N/Yb_N of about 6.95, 6.8, 7.25 and 5.69 on average respectively), a negative Eu-anomaly (Eu_N/Eu^* about 0.55, 0.54, 0.65 and 0.53 on average respectively) and a flat heavy REE pattern (HREE; Tb_N/Yb_N of 1.4, 1.29, 1.26 and 1.38 on average respectively). In general, REE patterns of the samples tend to be depleted in LREE and enriched in

HREE compared with the PAAS pattern (Fig. 5.5), which is considered in turn to reflect the average composition of the UCC (Taylor and McLennan, 1985).

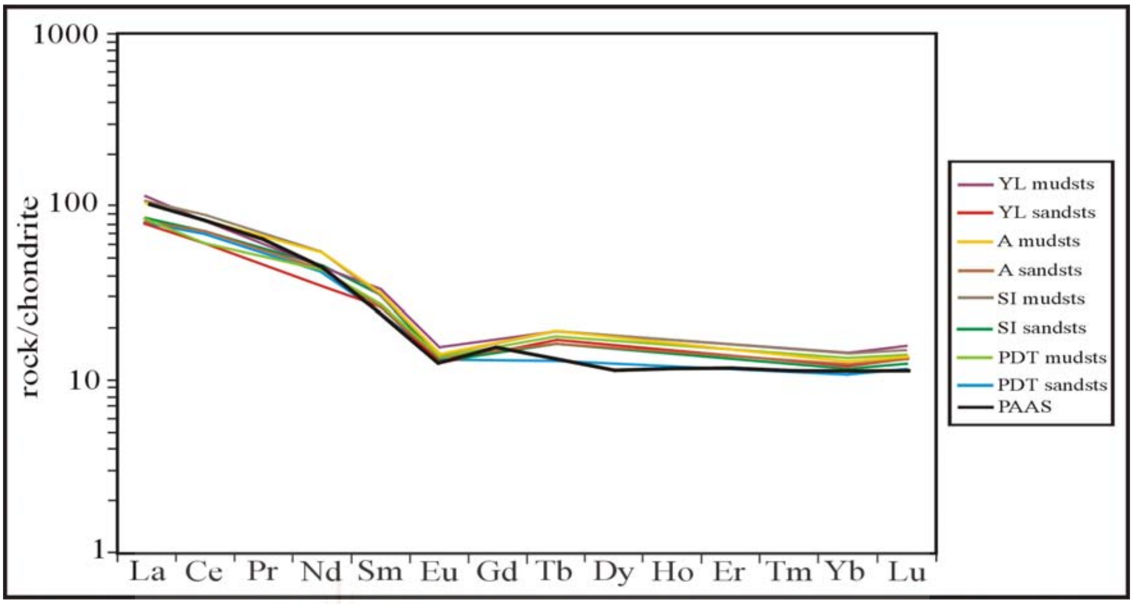

Figure 5.5: Average chondrite normalized rare earth elements patterns for mudstones (mudsts) and sandstones (sandsts) of the Ordovician to Silurian clastic sequences of the Western tectofacies. PAAS= post-Archaean Australian Shales pattern (Nance and Taylor, 1976) is draw for comparison. REE patterns are drawn as a continuous line although certain elements were not measured (see Table 1 in Appendix A). Chondrite normalization factors are those listed by Taylor and McLennan (1985). YL: Yerba Loca Formation; A: Alcaparrosa Formation; SI: Sierra de la Invernada Formation; PDT: Portezuelo del Tontal Formation. The Eu anomaly is calculated as $Eu_N/Eu^{*}= Eu_N/ (0.67Sm_N + 0.33Tb_N)$, where subscript N denotes chondrite normalized values (Taylor and McLennan, 1985). See Appendix C for REE patterns of individual samples.

Sample PDT3 (mudstone) from the Portezuelo del Tontal Formation shows the less negative Eu-anomaly (Eu_N/Eu^* of 0.8) and also a very low La_N/Yb_N (5.69) and La/Sc (1.3) ratios compared with the average value for the unit. Accordingly, this sample shows a slight enrichment of compatible elements indicating an input from a less fractionated source. However, remobilization and fractionation of certain elements due to metamorphism cannot be ruled out. The two samples of the Yerba Loca Formation with less fractionated compositions also show low La_N/Yb_N and La/Sc ratios

(Table 1 in Appendix A) but their negative Eu-anomaly is more pronounced than that for the sample of the Portezuelo del Tontal Formation. Because a less depleted component was detected, the REE patterns nearly parallel to PAAS reflect mixing of such a component with a component more recycled than the average PAAS.

5.4.1.3 Provenance and tectonic setting

The ultrastable heavy mineral zircon can be recycled and consequently the Zr concentration would be enriched in a sedimentary rock. On the other hand, Th is an incompatible element whereas Sc is compatible in igneous systems (McLennan *et al.*, 1993). Furthermore, Sc is present in labile phases. Therefore, the Zr/Sc and Th/Sc ratios are very useful for provenance analysis, since the first ratio reflects reworking and the latter indicates the degree of igneous differentiation processes (McLennan *et al.*, 1993).

As it can be seen in Figure 5.6, Th/Sc ratios for the units studied in the present chapter do not show great variations indicating that the input for the four formations was mostly from rocks with an average unrecycled upper continental crust composition. However, low Th/Sc ratios indicating the influence of a source with a composition less fractionated than the UCC are also present, particularly within the Portezuelo del Tontal and Yerba Loca Formations, which have Th/Sc ratios of 0.53 and 0.72 on average respectively.

Two samples from the Yerba Loca Formation have very low Th/Sc ratios (0.02 and 0.27). One of these samples has an important provenance component with a composition close to average andesite (empty diamond in Fig. 5.6) while the other one have an important provenance component with a composition close to average basalt (solid diamond in Fig. 5.6). The Portezuelo del Tontal Formation shows a cluster of data indicating no recycling of the source mix. The Sierra de la Invernada Formation shows an incipient recycling. The Zr/Sc values increase for the Alcaparrosa and Yerba Loca Formations with a consequent increase in Zr concentrations (with values of up to 366ppm and 570ppm respectively), and therefore indicating a greater influence of recycling processes than the other two units.

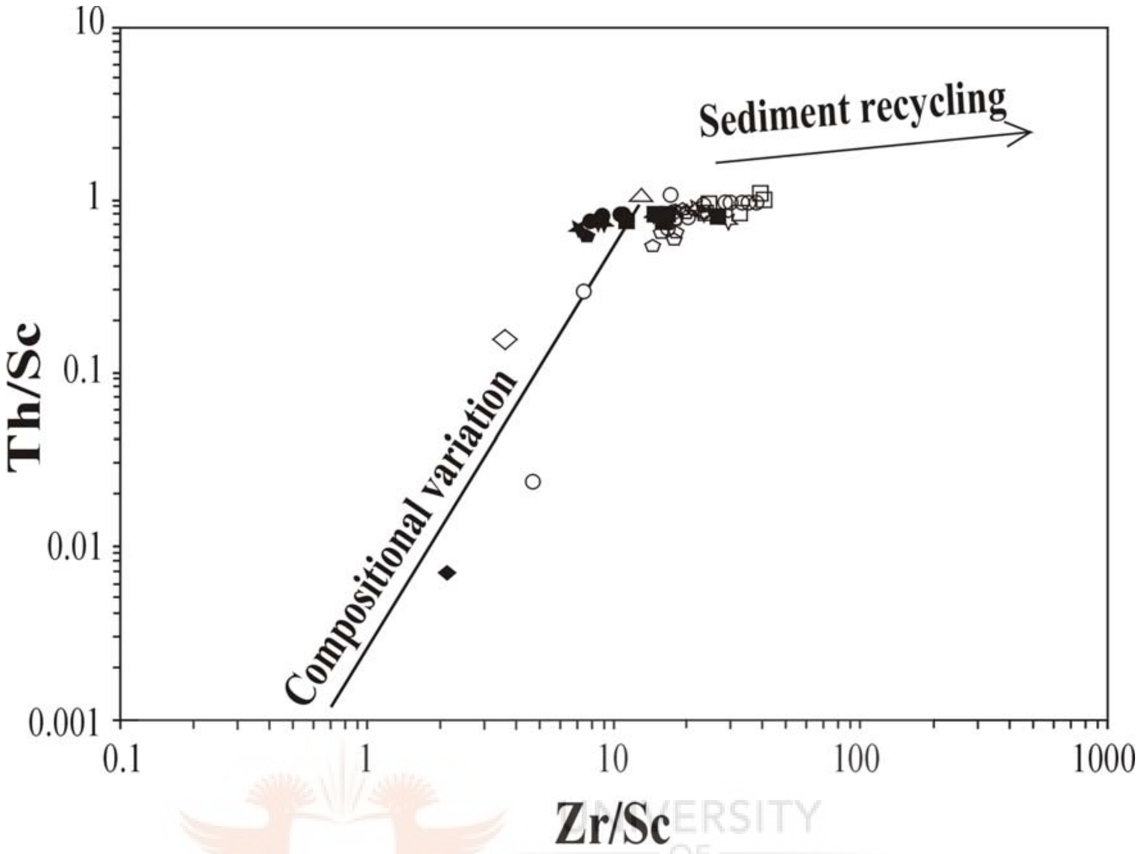

Figure 5.6: Th/Sc versus Zr/Sc diagram adapted from McLennan *et al.* (1990). Empty triangle: granodiorite (average upper continental crust); empty diamond: average andesite; solid diamond: mid-ocean ridge basalts. Sandstones are represented by empty symbols whereas mudstones are represented by solid symbols. Circles: Yerba Loca Formation; squares: Alcaparrosa Formation; stars: Sierra de la Invernada Formation; pentagons: Portezuelo del Tontal Formation. Two samples from the Yerba Loca Formation plot closer to the andesite and basalt averages than the rest of the samples.

According to Bhatia and Crook (1986), the oceanic island arc setting (A in Figs. 5.7 and 5.8) and the continental arc setting (B in Figs. 5.7 and 5.8), represent convergent plate margins. The active continental margin setting (C in Figs. 5.7 and 5.8) comprises the Andean-type margins and strike-slip continental margins. The passive margin setting (D in Figs. 5.7 and 5.8) comprises rifted continental margins of the Atlantic-type. Nevertheless, caution in the interpretation of tectonic setting based solely on geochemistry is needed, since sediments can be transported across tectonic boundaries and thus their geochemical signature may not necessarily be indicative of the tectonic setting of the deposition (McLennan, 1989). However, using Bhatia and Crook (1986) diagrams broad trends regarding the tectonic setting can be deduced, particularly when used along with other characteristics provided by sedimentology and petrography.

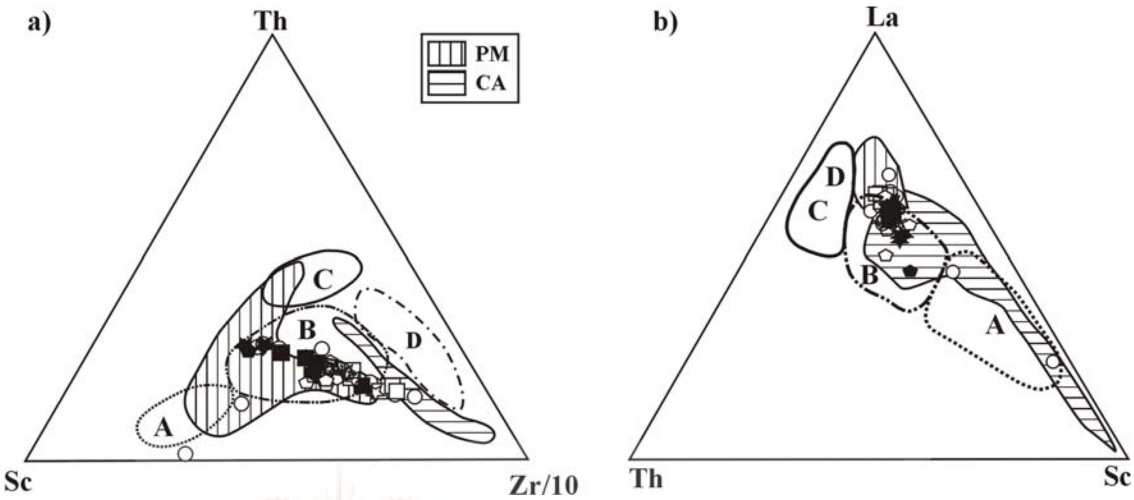

Figure 5.7: a) Th-Sc-Zr/10 and b) La-Th-Sc tectonic discriminatory plots, both after Bhatia and Crook (1986). A: Oceanic island arc; B: Continental island arc; C: Active continental margin; D: Passive margin. PM: recent deep-sea turbidites derived from and deposited at a passive margin. CA: recent deep-sea turbidites derived from and deposited at a continental arc margin (data from McLennan *et al.*, 1990). Sandstones are represented by empty symbols whereas mudstones are represented by solid symbols. Circles: Yerba Loca Formation; squares: Alcaparrosa Formation; stars: Sierra de la Invernada Formation; pentagons: Portezuelo del Tontal Formation.

In Figures 5.7 and 5.8 sandstones and mudstones from the Yerba Loca Formation, indicate the deposition of this unit within a basin related to a continental island arc or an active continental margin setting. Sandstones and mudstones from the Alcaparrosa and Portezuelo del Tontal Formations indicate the deposition within a basin linked to an active margin (continental island arc or an active continental margin setting) rather than within a passive one (Merodio and Spalletti, 1990). The deposition in a basin related to the same tectonic settings is also evident for the Sierra de la Invernada Formation (Figs. 5.7 and 5.8).

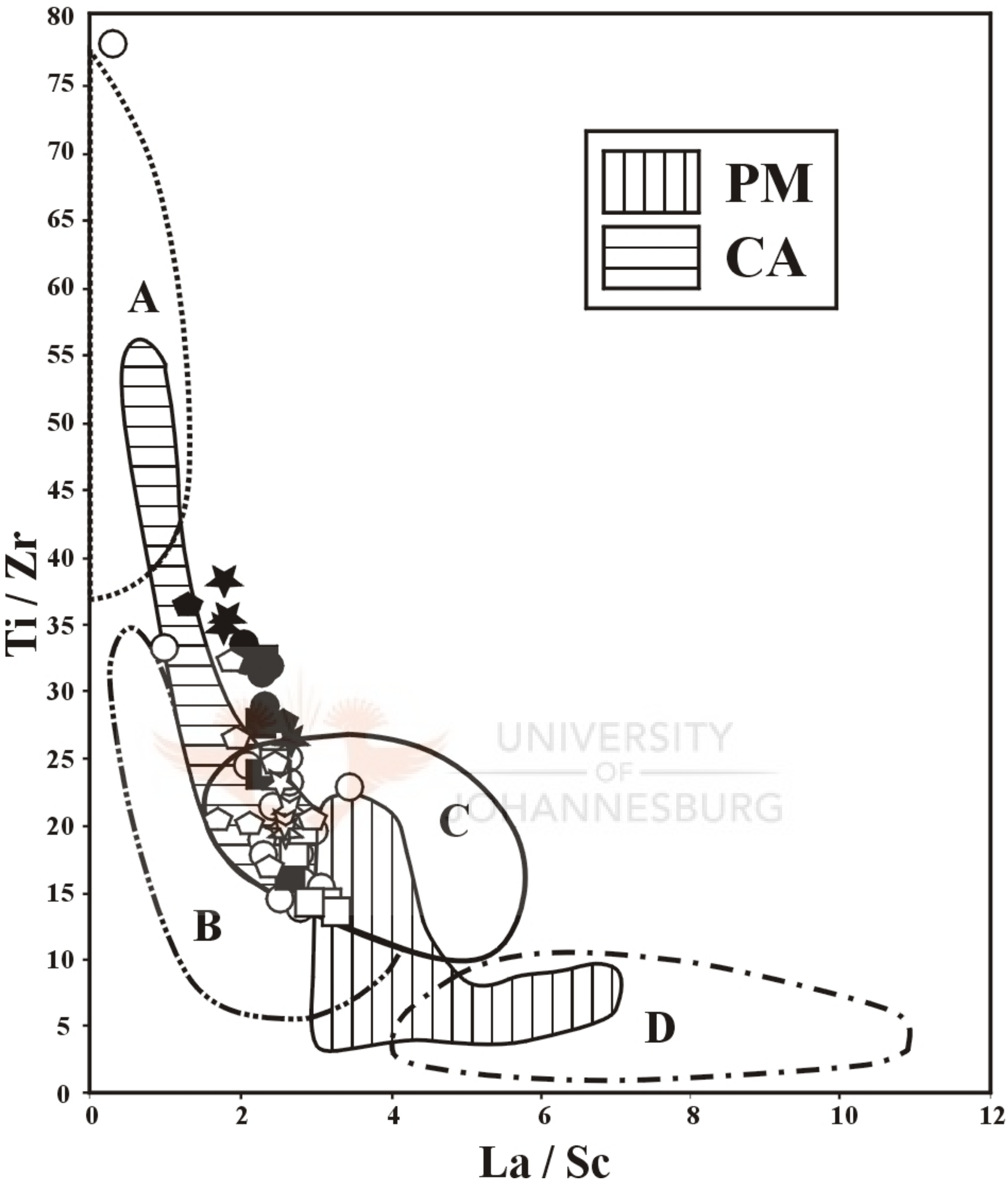

Figure 5.8: Ti/Zr versus La/Sc discriminatory plot from Bhatia and Crook (1986). A: Oceanic island arc; B: Continental island arc; C: Active continental margin; D: Passive margin. PM: recent deep-sea turbidites derived from and deposited at a passive margin. CA: recent deep-sea turbidites derived from and deposited at a continental arc margin (data from McLennan *et al.*, 1990). Sandstones are represented by empty symbols whereas mudstones are represented by solid symbols. Circles: Yerba Loca Formation; squares: Alcaparrosa Formation; stars: Sierra de la Invernada Formation; pentagons: Portezuelo del Tontal Formation.

An arc-provenance component might be deciphered using Th/Sc, Eu_N/Eu^* and Ti and Nb concentrations. Low Th/Sc ratios, Eu_N/Eu^* of about 1 and strong negative Nb and Ti anomalies characterize continental arc components, although differentiated arcs would have variable Th/Sc ratios and Eu_N/Eu^* between 0.6 and 0.9 (Hofmann, 1988; McLennan *et al.*, 1993; Zimmermann, 2005). Samples from the Yerba Loca, Alcaparrosa, Portezuelo del Tontal and Sierra de la Invernada Formation do not display the negative Nb and Ti anomalies.

5.4.2 Volcanic rocks

5.4.2.1 Major elements

The volcanic rocks interlayered within the Yerba Loca clastic rocks show SiO_2 ranging from 37.6% to 49% (ultramafic to mafic), Al_2O_3 concentrations ranges from 9.9% to 16.5% and TiO_2 concentrations are between 1.35% and 2.1%. MgO varies from 4.59% to 12.4%. The Na_2O (ranging between 1.1% and 4.4%), K_2O (varying from 0.14% to 0.81%) and CaO (ranges from 7.64% to 13.23%) concentrations are variable. Fe_2O_3 ranges from 11.13% to 17.06%. These rocks were affected by greenschist facies metamorphism (Robinson *et al.*, 2005).

5.4.2.2 Trace elements

An initial segregation of magmatic suites is revealed by a Zr/TiO_2 – Nb/Y diagram (Winchester and Floyd, 1977), which shows that only a sub-alkaline suite is present (Fig. 5.9), although dominated by a basaltic composition but with subordinate more evolved andesitic-basaltic rocks.

The volcanic rocks interlayered within the Yerba Loca Formation show sloping chondrite-normalized rare earth elements patterns characterized by no Eu-anomaly (Fig. 5.10) and low REE sum.

The mantle-normalized diagram (Fig. 5.11) shows that the volcanic rocks have geochemical characteristics intermediate between the enriched mid-ocean ridge basalts (E- MORB) and ocean island basalts (OIB). Mantle normalization values were taken from Sun and McDonough (1989). The sample YL455 displays anomalously high Pb

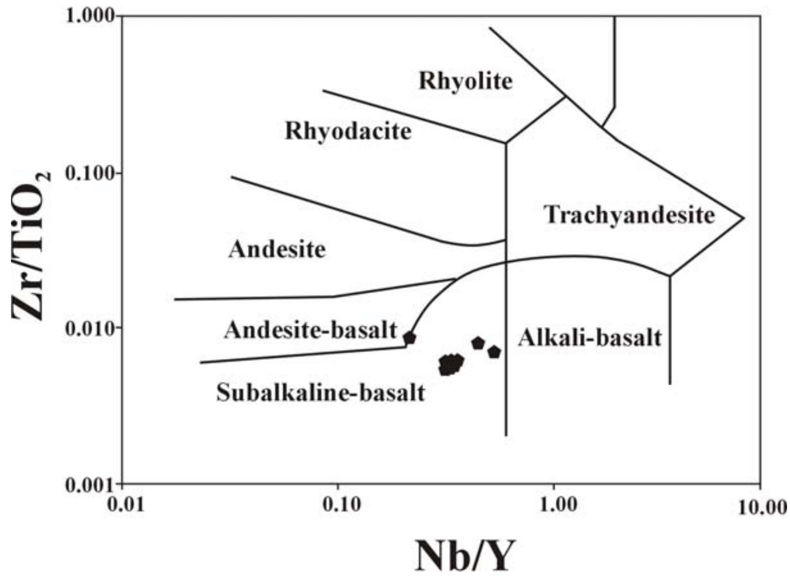

Figure 5.9: Zr/TiO_2 – Nb/Y diagram from Winchester and Floyd (1977), showing the predominance of a sub-alkaline basaltic composition of the volcanic rocks of the Yerba Loca Formation.

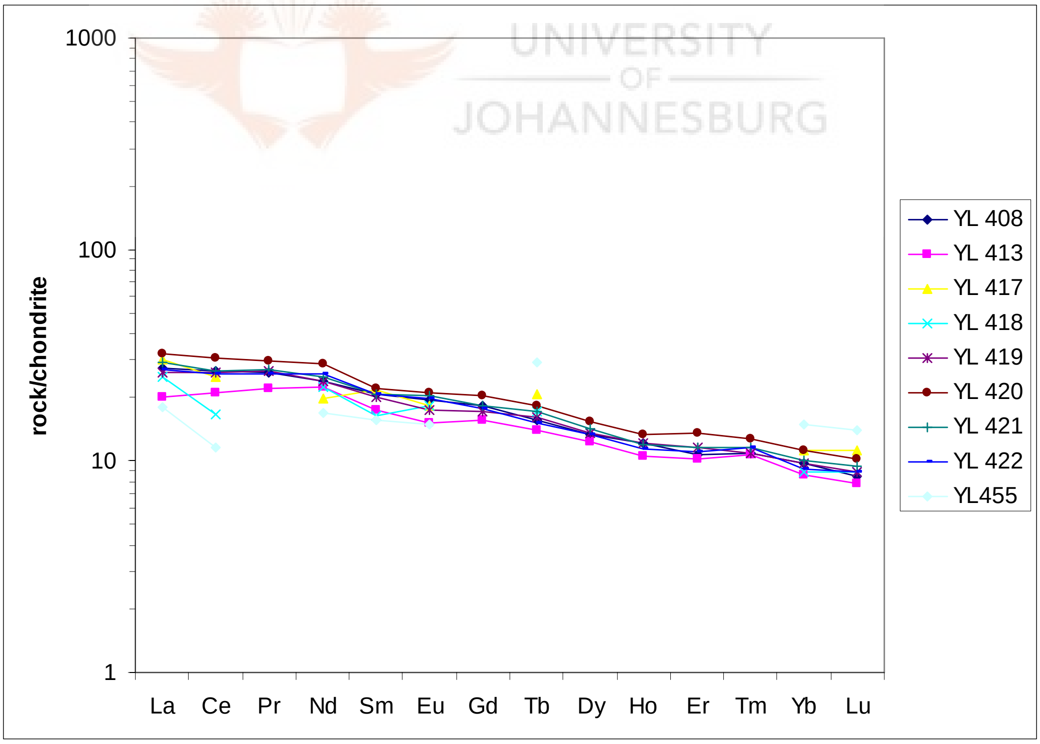

Figure 5.10: Chondrite normalized REE patterns for volcanic rocks interlayered with the Yerba Loca sandstones. Chondrite normalization factors are those listed by Taylor and McLennan (1985).

concentrations of up to 8.9ppm (Table 1 in Appendix A). Nb concentrations are similar to slightly enriched compared with enriched mid-ocean ridge basalts, whereas Ti concentrations are slightly higher than E-MORB, but lower than average values for ocean island basalts.

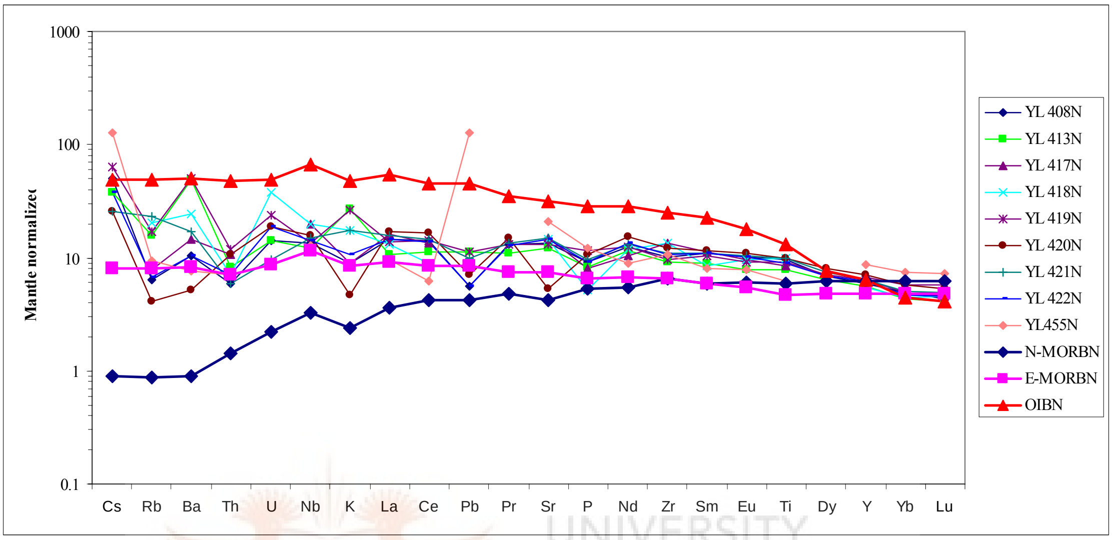

Figure 5.11: Mantle normalized elements for each sampled volcanic rock interlayered within the Yerba Loca clastic sequence. N-MORB: normal mid-ocean ridge basalts; E-MORB: enriched mid-ocean ridge basalts; OIB: ocean island basalts. Subscript N denotes normalized to mantle values. This diagram and the normalization factors are after Sun and McDonough (1989).

5.4.2.3 Tectonic setting

In Figure 5.12a (following Wood *et al.*, 1979), volcanic rock samples interlayered within the Yerba Loca Formation plot in the plume-type mid-ocean ridge basalts (P-MORB) field, according to the relationship between a third part of Hafnium, Thorium and Thallium. The exception is one sample that plots outside any field. In Figure 5.12b, the relation between two times the Niobium concentration, Zr/4 and Yttrium indicate that the volcanic rocks samples scatter along the within-plate tholeiitic (WPT) and plume-type mid-ocean ridge basalts fields, with deviations to the normal mid-ocean ridge basalts field (N-MORB). Therefore, the volcanic rocks are related to a mid-ocean ridge setting.

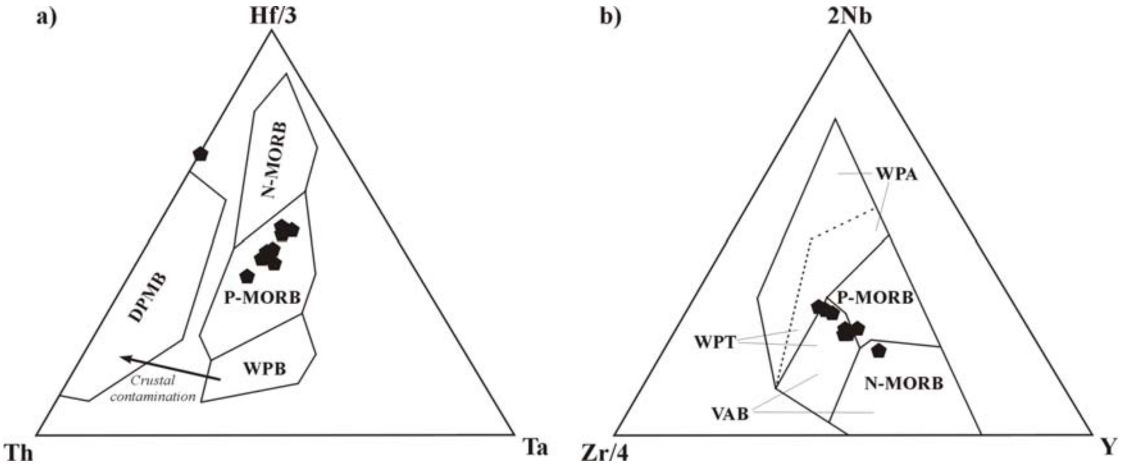

Figure 5.12: a) Hf/3-Th-Ta tectonomagmatic discrimination diagram for basalts and more differentiated rocks (after Wood *et al.*, 1979). b) 2Nb-Zr/4-Y tectonomagmatic discrimination diagram for basalts (after Meschede, 1986). P-MORB: plume-type mid-ocean ridge basalts; N-MORB: normal mid-ocean ridge basalts; WPB: within-plate basalts; DPMB: destructive plate margin basalts. WPT: within-plate tholeiitic; WPA: within-plate alkalic; VAB: volcanic arc basalts.

5.5 ZIRCON DATING

Although the reasons are not well understood yet, it has been demonstrated that the Th/U ratio of metamorphic zircons is of about 0.1 or lower, whereas the Th/U ratio of igneous zircons is >0.2 or >0.5 (Vavra *et al.*, 1999; Hoskin and Schaltegger, 2003). The detrital zircon population of the Alcaparrosa Formation is composed of zircon grains with a Th/U ratio >0.25, and are therefore more probably magmatic in origin (Table 5 in Appendix A; e.g. Vavra *et al.*, 1999).

Detrital zircon dates (n=49) cluster at 440-520, 560-610, 940-1370 and 1780-1900 Ma and are scattered sparsely at 805 (n=1) and 1600 (n=1) Ma (Fig. 5.13). Grains older than 1901 Ma are absent. Five zircons are in the range of 1778 and 1901 Ma. The biggest population is of Mesoproterozoic age (51% of the total grains measured); in particular the 1000-1300 Ma population (n=20) is more abundant than the 1300-1600 Ma group (n=5). The Neoproterozoic population is the second most common comprising 12 grains. Three grains are Cambrian in age while three other have an age

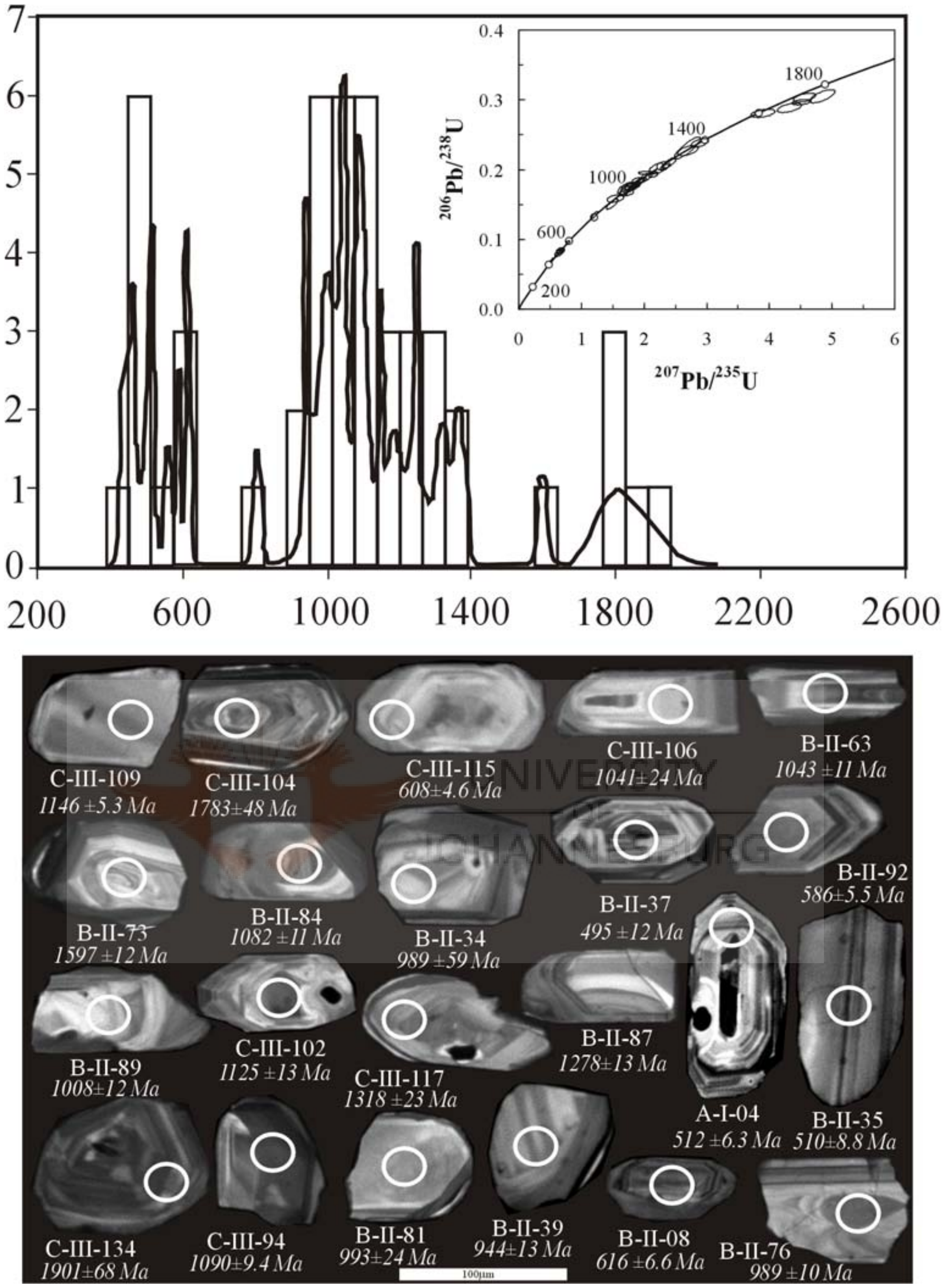

Figure 5.13: U-Pb distribution of analyzed detrital zircons with probability curves (above). Histogram bars represent time intervals of 80 Ma. Concordia plot diagram in the inset area. Isoplot/Ex (Ludwig, 2001) was used for age calculations. Representative cathodoluminescence (CL) images of zircons used for detrital dating of the Alcaparrosa Formation, showing the predominance of magmatic internal textures. White circles denote dating areas. Bar length 100μm.

in between 460 and 495 Ma. The zircon dated at 451 Ma is in the range of the depositional age of the Alcaparrosa Formation. Another 432 Ma zircon is younger than the sedimentary sequence, as its isotopic Pb system is fractionated due to very high ^{204}Pb concentrations.

The group of zircons with ages between 460 Ma and 495 Ma may have an origin related to the Famatinian magmatic arc (Pankhurst *et al.*, 1998; Fanning *et al.*, 2004), whereas the cluster of detrital zircon ages between 510 Ma and 616 Ma can be linked to the Pampean/Brazilian Orogeny. Mesoproterozoic rocks that most likely contributed to the more important cluster of detrital zircons are present in several neighbouring areas (Fig. 5.1a) as in the southern basement of the Precordillera (Cerro La Ventana Formation, San Rafael block; Cingolani and Varela, 1999; Cingolani *et al.*, 2005a). They are also present in the Western Pampeanas Ranges (Pie de Palo, Umango, Maz and Espinal; Varela and Dalla Salda, 1992; McDonough *et al.*, 1993; Varela *et al.*, 1996; Casquet *et al.*, 2006) and in the Arequipa-Antofalla Basement (Central Andes; Bahlburg and Hervé, 1997 and references therein).

According to the different models proposed to explain the tectonic evolution of the Precordillera terrane, and considering the uncertainties regarding terrane boundaries and palaeogeography, other areas need to be evaluated as sources. Probable source areas that comprise Mesoproterozoic rocks are the Grenville Province of Laurentia (summary from Carrigan *et al.*, 2003), Antarctica, Natal-Namaqua Metamorphic belt and Falkland/Malvinas Microplate (Wareham *et al.*, 1998). Other areas located further aside as the Amazon craton (see Loewy *et al.*, 2004, and Schwartz and Gromet 2004 and references therein) can be neglected, because such an input is not consistent with sedimentological features (see section 5.7).

Palaeoproterozoic rocks are found also in the Arequipa-Antofalla Basement (Bahlburg and Hervé, 1997 and references therein), within Laurentia (summary from Carrigan *et al.*, 2003), The Río de la Plata Craton (Rapela *et al.,* 2007), but also at certain areas of the Western Pampeanas Ranges (Maz Range; Casquet *et al.*, 2006).

5.6 ISOTOPE GEOCHEMISTRY

5.6.1 Sm-Nd

Nd isotopes have been widely used as provenance indicators (e.g. McLennan *et al.*, 1989; 1993) and their utility for provenance studies stems from the coherent behaviour of the rare earth elements during the sedimentary processes. Nd isotopic signatures of terrigenous sedimentary rocks average those of the various sources from which the sediments were derived. Various studies have addressed processes that might alter the Sm-Nd isotopic signatures in detrital sediments. These include the alteration of Sm/Nd ratios and Nd isotopic signatures during weathering, diagenesis or sorting (McLennan *et al.*, 1989; McDaniel *et al.*, 1994; Bock *et al.*, 1994).

Nd-isotopes of five samples from the Yerba Loca clastic record were analyzed. Results are shown in Table 3 (Appendix A); data was calculated according to DePaolo (1981), although T_{DM} according to DePaolo *et al.* (1991) are also shown in Appendix A and were used to compare with data from the literature that was expressed according to the three-stage model (DePaolo *et al.,* 1991). For more details regarding methods and analytical techniques, see Appendix B.

ε_{Nd} (t= 455 Ma) values where (t) values were calculated based on average depositional age according to the palaeontological record range from -4.81 to -7.28 for the Yerba Loca Formation (average -5.92 ± 0.81). The $f_{Sm/Nd}$ ranges from -0.37 to -0.41 (average -0.40 ± 0.02), whereas the T_{DM} ages range from 1.45 to 1.57 Ga (average 1.5 ± 0.045 Ga). Nd-isotope analyses carried out by Gleason *et al.* (2006) on samples from the Alcaparrosa Formation yield ε_{Nd} (t=450) values of -6.84 ± 0.32 in average and average T_{DM} ages of 1.59 ± 0.16 Ga (calculated according to the model from DePaolo, 1981), similar to the here presented and Gleason *et al.* (2006) data for the Yerba Loca Formation.

The relationship between ε_{Nd} (t) and Th/Sc ratio for the Yerba Loca Formation indicate that the ε_{Nd} (t) values are neither typical of UCC nor of an arc (values from McLennan *et al.,* 1990), and the Th/Sc ratio is indicative of a source less fractionated than the upper continental crust (Fig. 5.14a). The same can be deduced using the plot of

$f_{Sm/Nd}$ versus ε_{Nd} (Fig. 5.14b), where the $f_{Sm/Nd}$ values could be assigned to an old upper crust or an arc component but the ε_{Nd} (t) values are between the two fields.

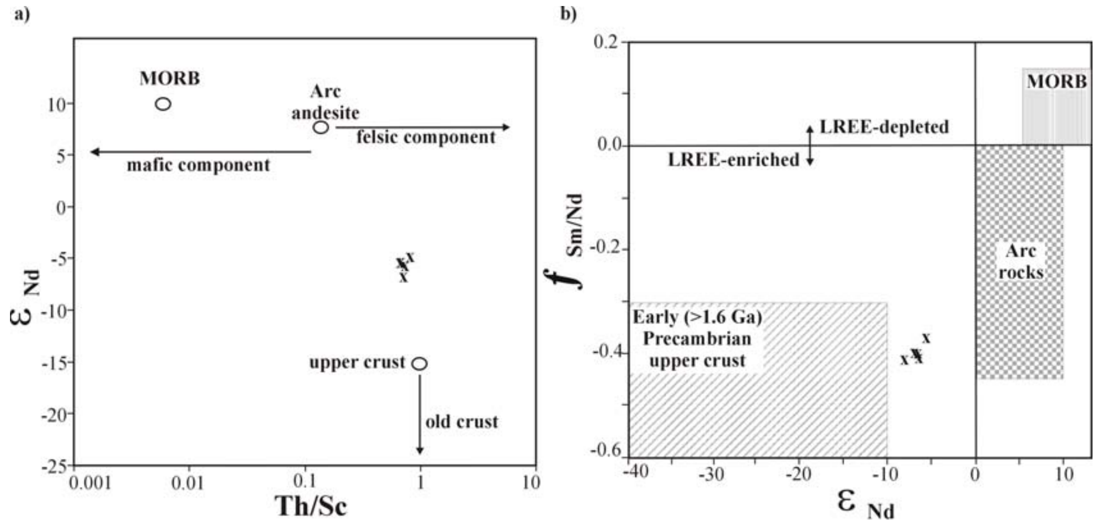

Figure 5.14: a) ε_{Nd} (t) versus Th/Sc ratio and b) Plot of $f_{Sm/Nd}$ against ε_{Nd} (t) for samples of the Yerba Loca Formation, where $f_{Sm/Nd}$ is the fractional deviation of the sample $^{147}Sm/^{144}Nd$ from a chondritic reference and ε_{Nd} (t) is ε_{Nd} at the age of sedimentation (455 Ma). MORB: mid-ocean ridge basalts; LREE: light rare earth elements. $f_{Sm/Nd} = (^{147}Sm/^{144}Nd)_{sample} / (^{147}Sm/^{144}Nd)_{CHUR} - 1$. ε_{Nd} (t) = $\{[(^{143}Nd/^{144}Nd)_{sample\ (t)} / (^{143}Nd/^{144}Nd)_{CHUR\ (t)}] - 1\} * 10000$. $(^{147}Sm/^{144}Nd)_{CHUR} = 0.1967$. $(^{143}Nd/^{144}Nd)_{CHUR} = 0.512638$. T_{DM} (model ages) were calculated based on the depleted mantle model (DePaolo, 1981).

Comparing the Nd-system of the Yerba Loca Formation with the probable sources discussed using detrital zircon dating, it is evident that T_{DM} ages are comparable to those from the Mesoproterozoic xenoliths interpreted as the basement of the Precordillera terrane. They are also comparable to the Mesoproterozoic Cerro La Ventana Formation (Table 5.1). T_{DM} ages are also similar to values known from other supracrustal rocks of the Precordillera terrane (Kay *et al.*, 1996; Cingolani *et al.*, 2003a; Gleason *et al.*, 2006). They are also within the range of variation of the T_{DM} ages of Neoproterozoic to Palaeozoic sequence in northwestern Argentina (Rapela *et al.*, 1998; Bock *et al.*, 2000; Lucassen *et al.*, 2000; Zimmermann and Bahlburg, 2003; Table 5.1; Fig. 5.1b). Mesoproterozoic granitoids and orthogneisses from Antarctica, Natal-

Namaqua Metamorphic belt and Falkland/Malvinas Microplate studied by Wareham *et al.* (1998) have also comparable T_{DM} ages.

Location	Age (Ga)	ε_{Nd}	T_{DM} (Ga)
Pampeanas Ranges[1]	0. 525	-3.1 to -7.7	1.48 to 1.82
Patagonia, Argentina[1]	0. 46 to 0.58	-0.7 to -6.1	1.13 to 1.66
Puna, Northern Argentina[1]	0.47 to 0.49	-1.4 to -11.6	1.32 to 2.05
Pampeanas Range, Velasco area[2]	Lower Palaeozoic	-5.5 to -10	1.23 to 1.56
Pampeanas Range, Paimán area[2]	Lower Palaeozoic	-6.1 to -6.3	1.32 to 1.34
Pampeanas Range, Copacabana area[2]	Lower Palaeozoic	-8.4 to -10	1.4 to 1.54
xenoliths Precordillera basement[3]	1.1	+2 to +7	0.8 to1.68
granite within Pie de Palo[4]	0.47 to 0.48	-3.6 to -2.6	1.41 to 1.48
Angaco, Pie de Palo Range[5]		-4.7 to -7.5	1.4 to 1.7
Cerro Salinas carbonates[5]		-11 to -30.5	1.7 to 1.8
La Laja Fm., Precordillera [5]	Cambrian	-8.3 to -10.9	1.3 to 1.7
Las Matras block[6]	1.2	+1.6 to +2.1	1.55 to 1.6
Cerro La Ventana Fm.[7]	1.1 to 1.2	+1.4 to +7.9	1.2 to 1.3
Southern Africa, Natal (Mzumbe gneiss and Equeefa)[8]	1.1 to 1.23		1.21 to 1.47
East Antarctica, Dronning Maud Land gneisses [8]	1.13 to 1.15		1.4 to 2.46
Falkland/Malvinas Islands (Cape Meredith gneiss)[8]	1.1		1.3
Falkland/Malvinas plateau (Maurice Ewing gneiss)[8]	1.1		1.6
Chilenia basement[9]		-6 to -10	1.3 to 1.6
Chilenia basement (juvenile input)[9]		4.5	0.8

Table 5.1: ε_{Nd} and T_{DM} ages of selected probable source areas used to compare with values from the Western tectofacies (Yerba Loca Formation). [1]Compiled in Adams *et al.* (2005); [2]López *et al.* (2006); [3]Kay *et al.* (1996); [4]Baldo *et al.* (2005); [5]Naipauer *et al.* (2005a); [6]Sato *et al.* (2004); [7]Cingolani *et al.* (2005a); [8]Wareham *et al.* (1998); [9]Bahlburg *et al.* (2001); [1,2,8] ε_{Nd} is initial and T_{DM} ages were calculated according to DePaolo *et al.* (1991). For the rest of the data, ε_{Nd} is (t) and T_{DM} according to DePaolo, 1981. See also Table 3 in Appendix A.

Figure 5.15 shows that ε_{Nd} values for the Yerba Loca Formation are similar to those from the Famatinian magmatic arc (Pankhurst *et al.*, 1998), but a main provenance from the arc itself is not supported neither by geochemistry nor by detrital zircon dating (see section 5.5). ε_{Nd} (t) values for the Yerba Loca Formation are similar to those from other Ordovician sedimentary rocks from the Precordillera terrane (Cingolani *et al.*, 2003a; Gleason *et al.*, 2006). ε_{Nd} values are within the range of variation of the Laurentian Grenville crust (Patchett and Ruiz, 1989), the Central and Southern domains of the Arequipa - Antofalla Basement (Central Andes; Loewy *et al.*, 2004), and the basement of the Precordillera terrane within the San Rafael block known as the Cerro La Ventana Formation (Cingolani, unpublished data). ε_{Nd} values from the Western Pampeanas Ranges are scarce, but a broad similarity with data here presented is evident (Fig. 3.16). Therefore, none of the mentioned sources can be ruled out based on Sm-Nd signatures alone.

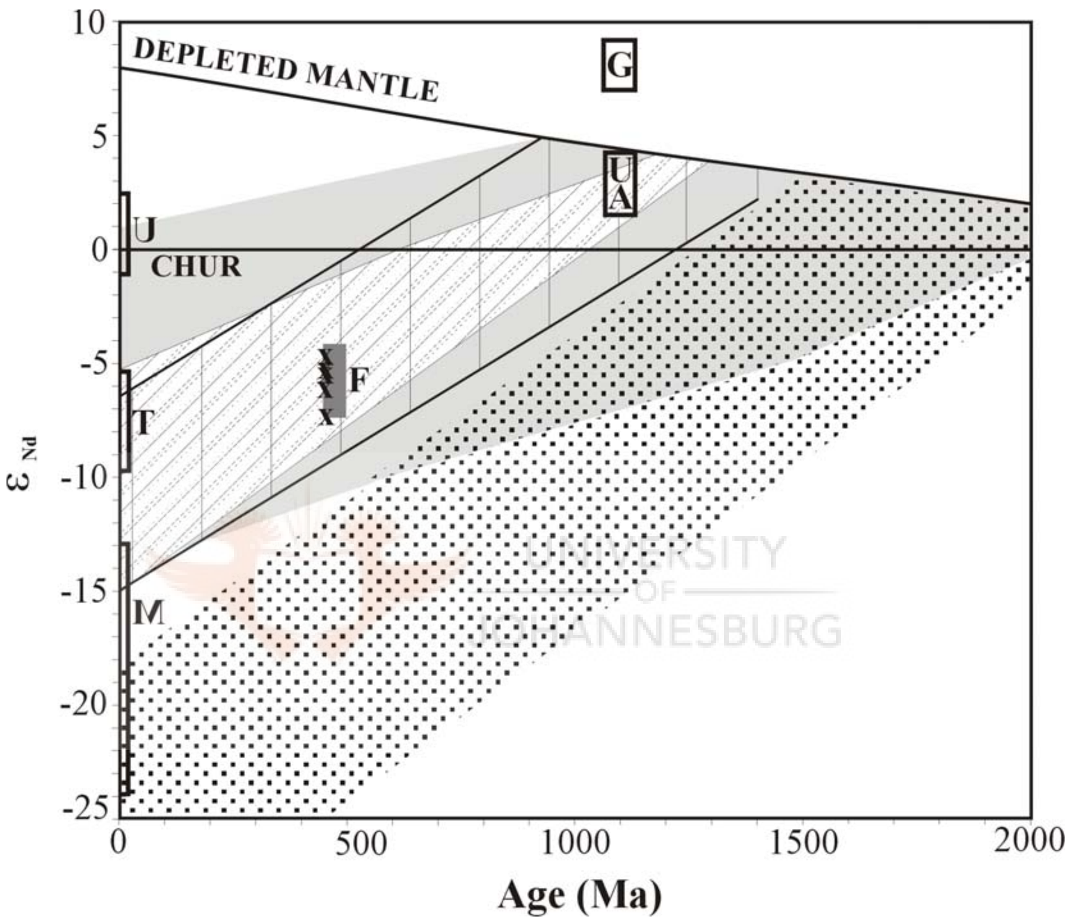

Figure 5.15: ε_{Nd} versus age of the Yerba Loca Formation (crosses) and of areas evaluated as probable sources. Dotted area: range of ε_{Nd} for the Northern domain of the Arequipa-Antofalla Basement (AAB) and light grey area: Central and Southern domains of the Arequipa-Antofalla Basement (Loewy *et al.*, 2004). Field of vertical lines: Laurentian Grenville crust (Patchett and Ruiz, 1989). A: granulitic and amphibolitic, and G: acidic-gneissic, xenoliths from the inferred basement of the Precordillera (Kay *et al.*, 1996). F denoting dark grey rectangle: magmatic rocks from the Famatinian arc (Pankhurst *et al.*, 1998). U: Umango Range, T: El Taco Complex, and M: Maz Complex all from the Western Pampeanas Ranges (Vujovich *et al.*, 2005). White field with diagonal lines: Cerro La Ventana Formation (Cingolani *et al.*, 2005a and unpublished data).

5.6.2 Pb-Pb

The use of Pb isotopes is now well established as an important tool for evaluating both the provenance and in some cases the post-depositional alteration history of clastic sedimentary rocks. The relationship between Pb isotopic composition and tectonic setting is not straightforward, but it is possible to discriminate between ancient upper continental crust and younger terrains (especially in terms of $^{207}Pb/^{204}Pb$). Pb-isotopes on whole-sedimentary rocks might be affected by enrichment or leaching of U, selective sorting of mineral phases like zircon, monazite, xenotime and feldspar, mixture of sources, weathering and diagenesis (Hemming and McLennan, 2001) and therefore the comparison of the Pb-system of a sedimentary rock with that from the probable source(s) can be complex (e.g. McLennan *et al.*, 2000).

$^{206}Pb/^{204}Pb$, $^{207}Pb/^{204}Pb$ and $^{208}Pb/^{204}Pb$ range from 18.83 to 19.71, 15.67 to 15.84, and 39.08 to 39.99 respectively for the Yerba Loca Formation (see Table 4 in Appendix A and Figs. 5.16 and 5.17). Samples plot between the GLOSS (globally subducted sediments) and upper continental crust in all the diagrams. On an uranogenic- Pb space samples from the Yerba Loca Formation plot slightly above the Stacey and Kramers (1975) second stage Pb evolution curve for average crust (Fig. 5.16). A similar behaviour is observed for the samples on a thorogenic ($^{208}Pb/^{204}Pb$) versus $^{206}Pb/^{204}Pb$ composition (Fig. 5.17). Figures 5.16 and 5.17 and data from the literature indicate that the Pb isotopes of the Western tectofacies are similar to Middle Proterozoic rocks of the Arequipa - Antofalla Basement (Aitcheson *et al.*, 1995; Tosdal, 1996 and references therein; Loewy *et al.*, 2004).

The Arequipa-Antofalla Basement (Central Andes) comprises three domains (Loewy *et al.*, 2004): the Northern domain exists in southern Peru and western Bolivia. The Central domain extends from the Peru-Chile border to the northernmost part of Chile, while the Southern domain is extended from 23º S to the northernmost part of Argentina. The area comprised in the so-called Central and Southern domains in the sense of Loewy *et al.* (2004) is almost equivalent to the ca. 500 Ma Mobile Belt of the Pampean Cycle according to Lucassen *et al.* (2000). However, the terminology of Loewy *et al.* (2004) is followed for this discussion.

The dataset differs consistently from the Grenvillian xenoliths from the inferred basement of the Precordillera terrane (Kay *et al.*, 1996), Proterozoic rocks from Eastern North America and Early Proterozoic rocks from the Arequipa-Antofalla Basement (Tosdal, 1996; Loewy *et al.*, 2004). Mesoproterozoic granitoids and orthogneisses from the Natal-Namaqua Metamorphic belt (Mzumbe gneiss), Falkland/Malvinas Microplate (Cape Meredith Complex), West Antarctica (Haag Nunataks block) and East Antarctica (Kirwanveggan and Sverdrupfjella ranges, Maud Province) have different Pb isotopic signatures (Wareham *et al.*, 1998).

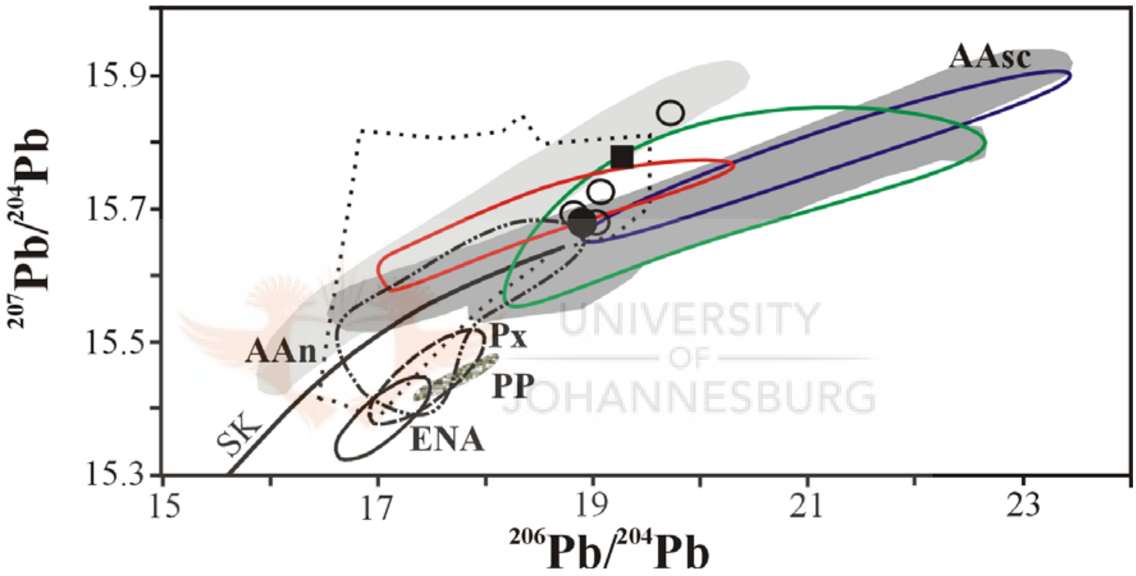

Figure 5.16: $^{207}Pb/^{204}Pb$ versus $^{206}Pb/^{204}Pb$ present-day ratios. Empty circles represent samples from the Yerba Loca Formation; solid square is the average value for the upper crust and solid circle the average value for Globally subducted sediments (GLOSS), both from Hemming and McLennan (2001). Fields obtained from several sources as indicated in the text. ENA denoting solid line: Eastern North America; Px denoting dashed line: xenoliths from the Precordillera terrane; AAsc and AAn: Arequipa-Antofalla Basement Southern and Central domains, and Northern domain respectively; PP: Pie de Palo Range; SK: Stacey and Kramers reference line; blue line: supracrustal Ordovician rocks from the Precordillera terrane (data from Gleason *et al.*, 2006); dotted line: Palaeozoic rocks from the Central Andes (Lucassen *et al.*, 2002); green line: Palaeozoic rocks from southern Central Andes (Bock *et al.*, 2000); red line: Ordovician rocks from south Bolivia (Egenhoff and Lucassen, 2003); double dotted-dashed line: Mesoproterozoic igneous and metamorphic rocks from Antarctica, Natal-Namaqua Metamorphic belt and the Falklands/Malvinas microplate (data from Wareham *et al.* 1998; see text).

The Pb signature is similar to supracrustal Palaeozoic rocks from the Central Andes (Bock *et al.*, 2000; Lucassen *et al.*, 2002), and Ordovician sedimentary rocks of south Bolivia (Egenhoff and Lucassen, 2003). The data obtained for the Alcaparrosa and Yerba Loca Formations by Gleason *et al.* (2006) indicate $^{206}Pb/^{204}Pb$, $^{207}Pb/^{204}Pb$ and $^{208}Pb/^{204}Pb$ ratios in the range from 20.22 to 23.33, 15.71 to 15.91, and 38.76 to 38.98 respectively (Figs. 5.16 and 5.17).

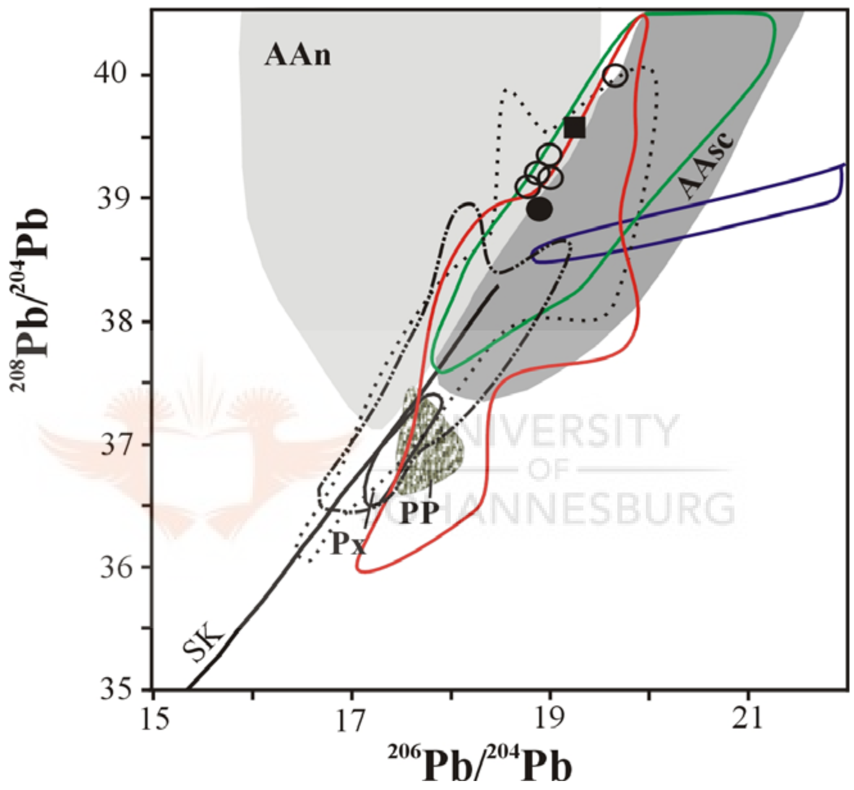

Figure 5.17: $^{208}Pb/^{204}Pb$ versus $^{206}Pb/^{204}Pb$ present-day ratios. Empty circles represent samples from the Yerba Loca Formation; solid square is the average value for the upper crust and solid circle the average value for GLOSS, both from Hemming and McLennan (2001). Fields obtained from several sources as indicated in the text. Px denoting dashed line: xenoliths from the Precordillera terrane; AAsc and AAn: Arequipa-Antofalla Basement Southern and Central domains, and Northern domain respectively; PP: Pie de Palo Range; SK: Stacey and Kramers reference line; blue line: supracrustal Ordovician rocks from the Precordillera terrane (Gleason *et al.*, 2006); dotted line: Palaeozoic rocks from the Central Andes (Lucassen *et al.*, 2002); green line: Palaeozoic rocks from southern Central Andes (Bock *et al.*, 2000); red line: Ordovician rocks from south Bolivia (Egenhoff and Lucassen, 2003); double dotted-dashed line: data from Wareham *et al.* (1998; see text).

5.7 DISCUSSION

Petrographic analyses showed that all the formations have similar characteristics, including the presence of texturally immature sandstones and greywackes composed of dominantly monocrystalline quartz, feldspars, biotite and sedimentary, volcanic (with typical textures of fine-grained rocks such as basalts and andesites) and metamorphic lithoclasts. Muscovite, chlorite and epidote resulted from the very low-grade metamorphism. A provenance from an upper continental crust component with the influence of a less fractionated component is therefore deduced, although the latter is more evident on certain samples and it is petrographically represented by coarse intergrowths of chlorite and muscovite and by volcanic lithoclasts with textures resembling those from basalts and/or andesites.

All the units studied have variable major element composition, which are characterized by enrichment in the mudstones of the K_2O concentration, compared with either the sandstones or the UCC. This enrichment is reflected in the A-CN-K diagram. Geochemical indicators of alteration (CIA, K/Cs, Th/U) suggest moderate to intense weathering. Geochemical data show that there were no important changes in the composition of the source area between the units studied. The Portezuelo del Tontal Formation shows a less negative Eu-anomaly (0.65 compared with 0.54 in average for the other three units) and a lower Th/Sc ratio (0.71 for the Portezuelo del Tontal Formation and 0.76 in average for the other three units), compared with the other units here studied. Even so, the Yerba Loca Formation has individual values as depleted as (and sometimes more depleted than) those from the Portezuelo del Tontal Formation. The enrichment of compatible elements together with the relatively high Cr/V and low Y/Ni ratios shown in some samples tend to support the influence of a source more depleted than the UCC. Further evidence regarding this depleted component is given by less negative Eu-anomalies (Eu_N/Eu^* of about 0.8) and by the Th/Sc ratios as low as expected for andesite- and basalt-like rocks. On the other hand, the UCC component is reflected by the predominance of negative Eu-anomalies. REE patterns are LREE depleted and HREE enriched compared with the PAAS for certain samples.

The Zr/Sc ratios demonstrate that the recycling was not an important process for the Portezuelo del Tontal and Sierra de la Invernada Formations, but a greater influence of recycling processes is evident for the Alcaparrosa and Yerba Loca Formations due to the increase in Zr concentrations (up to 570ppm). Nonetheless, recycling was not an important process affecting any of the units studied. Relationships between La, Th, Sc, Ti and Zr suggest a deposition on continental island arc or an active continental margin setting, rather than within a passive one (Merodio and Spalletti, 1990). The absence of the negative Nb and Ti anomalies (Hofmann, 1988) and the Eu_N/Eu^* values tend to rule out the influence of an arc. However, typical arc signatures are often not recorded in other than basins spatially closely related to the arc itself, and rocks derived from dissected arc terranes would show variable Eu_N/Eu^* values (McLennan *et al.*, 1990; Zimmermann, 2005). Furthermore, passive margin and foreland basin deposits cannot be easily discriminated using Th-Sc-Zr-La relationships (Zimmermann, 2005), and the active continental margin setting used by Bathia and Crook (1986) involves retro-arc foreland and pull-apart basins.

The ultramafic to mafic (SiO_2 between 37.6% and 49%) volcanic rocks interlayered within the Yerba Loca clastic rocks show phenocrysts of olivine, pyroxene and plagioclase embedded within a plagioclase-rich groundmass. Geochemical analyses indicate a sub-alkaline suite dominated by a basaltic composition but with subordinated andesitic-basaltic rocks. They also show sloping chondrite-normalized rare earth elements patterns characterized by no Eu-anomaly. The mantle-normalized diagram (Fig. 5.11) shows that the volcanic rocks have geochemical characteristics intermediate between enriched mid-ocean ridge basalts (E-MORB) and ocean island basalts (OIB). Regarding tectonic setting, the volcanic rocks are more likely related to a mid-ocean ridge.

Considering the several models that attempted to explain the geotectonic evolution of the Precordillera as an allochthonous terrane, certain probable source areas need to be evaluated: the Laurentian Grenville crust, the Arequipa-Antofalla Basement (*sensu* Loewy *et al.*, 2004), the Cerro La Ventana Formation and the Western Pampeanas Ranges. If the para-autochthonous models (Aceñolaza *et al*. 2002; Finney *et* *al.*, 2005) are taken into account, then the evaluation of Antarctica, Natal-Namaqua Metamorphic belt and the Falklands/Malvinas microplate is also required. Detrital zircon dating constrains the main source(s) as being Mesoproterozoic in age, whereas other zircon populations indicate the input from sources Neoproterozoic, Palaeoproterozoic, Cambrian and Ordovician in age (in order of abundance of dated grains). The scarcity of Famatinian-aged zircons is noteworthy and suggests the presence of an obstacle that prevented such detritus to have reached the basin (e.g. Pie de Palo Range of the Western Pampeanas Ranges; see below and Figs. 5.1 and 5.18). These ranges of ages are found within the Western Pampeanas Ranges and the Arequipa-Antofalla Basement, although partial age overlapping particularly regarding the main Mesoproterozoic population can be found with the Cerro La Ventana Formation, Grenville Province of Laurentia, Antarctica, Natal-Namaqua Metamorphic belt and Falkland/Malvinas Microplate.

The Sm-Nd isotope compositions of the Western tectofacies are characterized by ε_{Nd} (t) values between -4.81 and -7.28, T_{DM} of 1.59 ± 0.16 Ga on average and $f_{Sm/Nd}$ variations between -0.37 and -0.41. The Sm-Nd isotope compositions of the Yerba Loca Formation (this study and Gleason *et al.*, 2006) and the Alcaparrosa Formation (Gleason *et al.*, 2006) are similar. The comparison of the Sm-Nd signature with probable sources indicate similarities with the Laurentian Grenville crust, Central and Southern domains of the Arequipa-Antofalla Basement, the Cerro La Ventana Formation, the Western Pampeanas Ranges, Antarctica, Natal-Namaqua Metamorphic belt and the Falklands/Malvinas microplate. Data are similar to those from the Famatinian arc, but such a source can be neglected based on zircon dating.

Pb-isotopes give further constraints indicating an influence of a source with a "Gondwanan Pb-signature", emphasizing the input from a source such as the Arequipa-Antofalla Basement. However, Nd isotopes denoted similarities with the Southern and Central domains, whereas the Pb signatures show similarities with the Northern domain as well. The Pb composition excludes a provenance from the Laurentian Grenville crust, the Natal-Namaqua Metamorphic belt, Falkland/Malvinas Microplate, Antarctica and the xenoliths interpreted as the basement of the Precordillera terrane (Kay *et al.*, 1996). The only data available from the Western Pampeanas Ranges, (Pie de Palo Range) are dissimilar (Kay *et al.*, 1996).

In summary, the rocks that fit best all the constraints are found within the Western Pampeanas Ranges and the Arequipa-Antofalla Basement (Fig. 5.1a), despite age and Nd signature agreements with the Cerro La Ventana Formation. However, Pb data from the latter are not available and it does not account for the complete detrital zircon dataset of the Western tectofacies. Furthermore, a southern provenance is not supported by palaeocurrents, whereas a transport direction from north to south had been briefly described (Basilici *et al.*, 2005).

The Western Pampeanas Ranges comprise biotitic and dioritic-granodioritic gneisses, metamorphic rhyolites and amphibolites of Mesoproterozoic age (McDonough *et al.,* 1993). Greenschists facies metamorphic rocks such as carbonate marbles and schists, metaquartz-arenites and talc-, tremolite- and chlorite-serpentine schists are also present (Ramos *et al.*, 1993). The northernmost outcrops of the Western Pampeanas Ranges comprise marbles, calc-silicated rocks and quartz-mica schists, associated with amphibolites and ultramafic rocks, metapelites, metasandstones, metagabbros, metatonalites and tonalitic to granitic orthogneisses (Porcher *et al.*, 2004). The scarce Pb data available from the Western Pampeanas Ranges are dissimilar. However, the Sm-Nd signature is broadly coincident and the ages known from such rocks match very well with the detrital zircon range of the Western tectofacies, including Palaeoproterozoic ages (Maz Range; Casquet *et al.*, 2006). A source located to the east as the Western Pampeanas Ranges would also agree with east to west transport directions (Cingolani *et al.*, 1986; Banchig *et al.*, 1993), but an eastern source is doubtful due to the coeval sedimentation in shallow-marine environments of the Eastern tectofacies (Thomas *et al.*, 2001), unless detritus had been transported into the Western basin by funnelling through submarine canyons (Spalletti *et al.*, 1989).

The Arequipa-Antofalla Basement comprises igneous and high-grade metamorphic rocks. A provenance from the Arequipa-Antofalla Basement is in agreement with Sm-Nd (Southern and Central domains), Pb-Pb (all three domains), detrital zircon dating and palaeocurrents that indicate north to south transport directions

(Basilici *et al.*, 2005), although the lack of sedimentological details and information make such ascertain to be taken with caution. Furthermore, the northern termination of the Precordillera terrane (Jagüé area) is still under investigation and therefore the tectonic relationship with the Arequipa-Antofalla rocks is currently not well determined (Astini and Dávila, 2004). Several tectonic frameworks presented had located the Precordillera terrane immediately south of the Arequipa-Antofalla Basement for the Precambrian to Early Palaeozoic (Lucassen *et al.*, 2000; Rapela *et al.*, 2007), and current outcrops are located about 300 km north of the northernmost outcrops of the Western tectofacies.

A Laurentian derivation for the Neoproterozoic to Cambrian successions of the Precordillera terrane was recently deduced by Naipauer (2007), invoking an allochthonous model to understand such a provenance for the detrital record. The Mesoproterozoic basement of the Precordillera (Cuyania) terrane was at least partially exposed and provided detritus to a clastic level interlayered with the Angacos Formation (based on detrital zircon dating; Naipauer, 2007). Therefore, an allochthonous origin for the Precordillera terrane is here preferred. If the Western Pampeanas Ranges and the Arequipa-Antofalla Basement are accepted as sources of the Western tectofacies and since they might constitute a single continental crustal block since the Mesoproterozoic, autochthonous or para-autochthonous with respect to the pre-Famatinian margin of Gondwana (Casquet *et al.*, 2006), then the Precordillera terrane would have reached its present position by the time of the initiation of the deposition of the Western tectofacies (Figs. 5.18 and 5.19). The collision of the Precordillera terrane occurred due to the evolution of a subduction zone of the eastern Iapetus crust underneath the western margin of Gondwana (Thomas and Astini, 1996; Fig. 5.18), which produced the Famatinian magmatic arc towards west (480-460 Ma; Fig. 5.18). As a response to the accretion, the Western Pampeanas Ranges (and its probable continuation towards north) were uplifted at 460 Ma (Casquet *et al.*, 2001; Fig. 5.18), providing thus detritus to the basin and preventing that detrital material from the Famatinian arc reached the basin (Figs. 5.18 and 5.19) and implying a Late Arenig to Llanvirn final accretion age. To further support these areas as the sources, Pb data

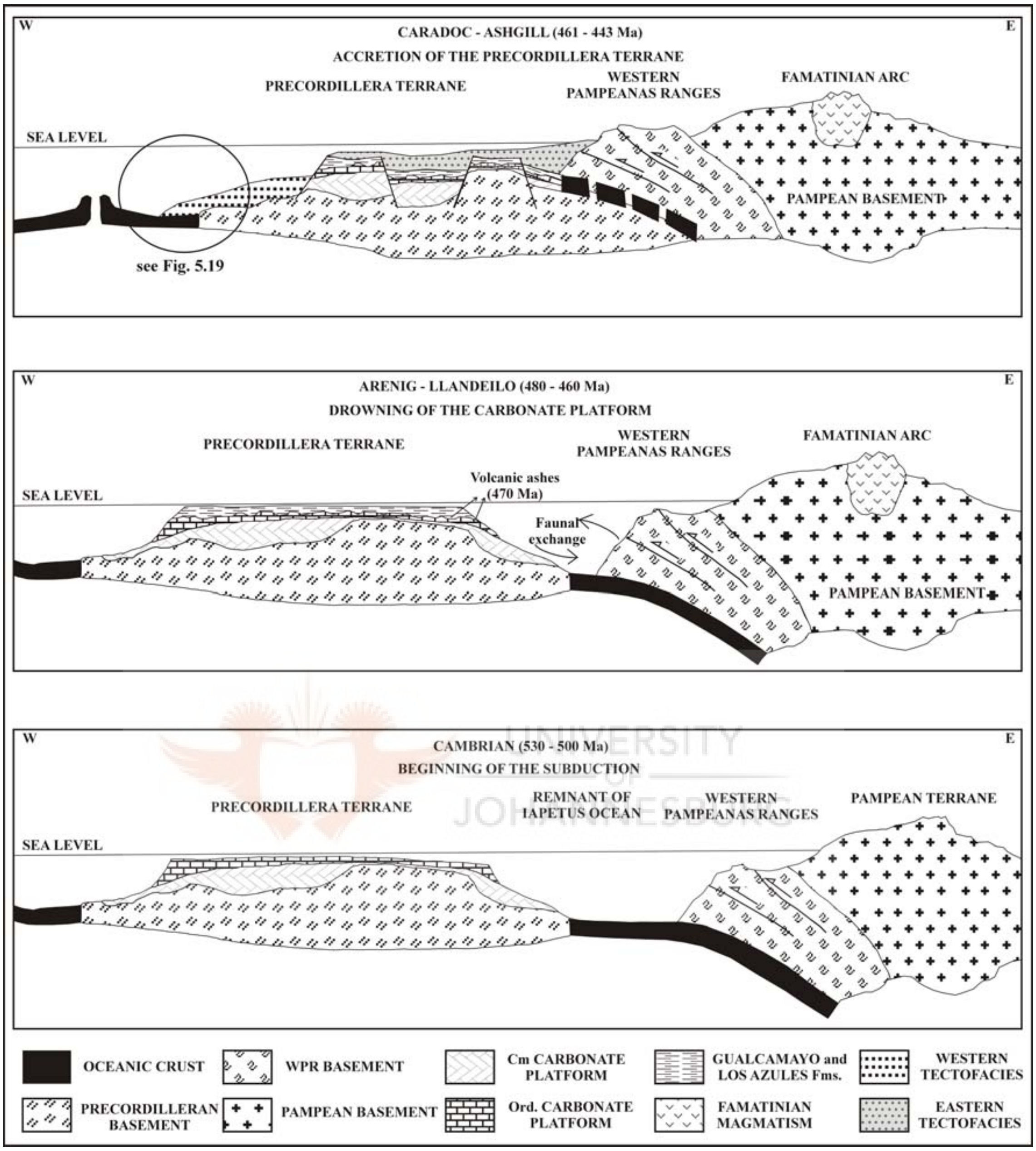

Figure 5.18: Geotectonic evolution of the Precordillera terrane. An eastern subduction was active since the Cambrian as documented by the magmatic arc (Famatina). The volcanic ashes (nowadays K-bentonites) found within the uppermost San Juan Formation and the lowermost Gualcamayo Formation record the activity of such magmatism in the context of the Precordillera terrane. A Late Arenig to Llanvirn final accretion age is estimated for the Precordillera terrane based on the provenance data presented (particularly regarding main detrital ages, Sm-Nd signatures and high $^{207}Pb/^{204}Pb$ ratios), which indicate that the Western Pampeanas Ranges and the Arequipa-Antofalla Basement are the more probable sources (see text for detailed discussion).

from the Western Pampeanas Ranges are needed, as well as a better knowledge of the rocks located immediately to the north of the Precordillera.

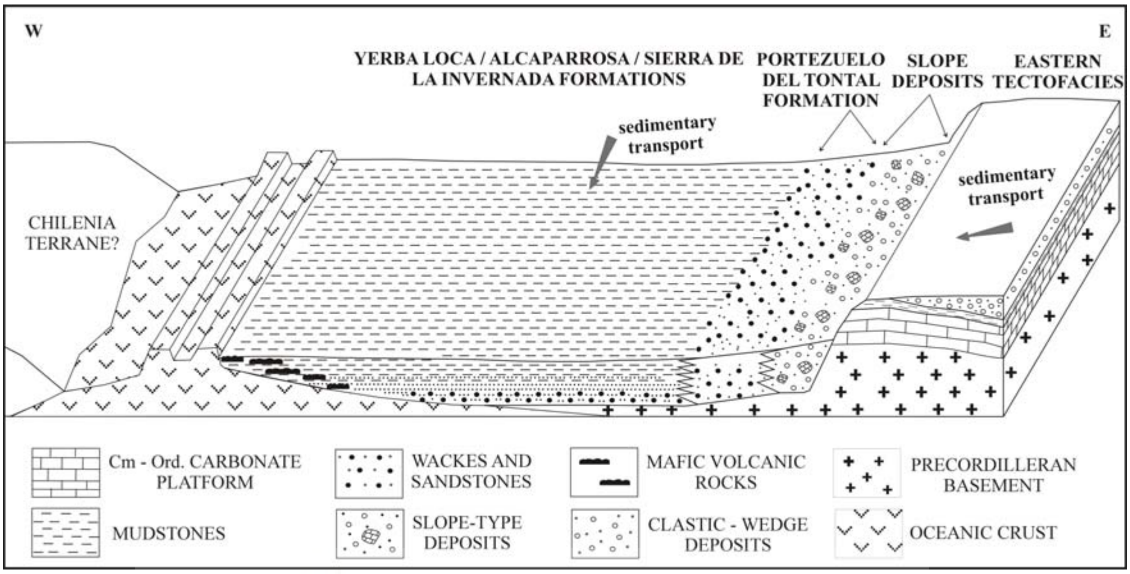

Figure 5.19: Schematic cross section (not to scale) showing the depositional setting of the Western Precordillera basin. The Western Pampeanas Ranges (WPR) and its probable continuation to the north named the Arequipa – Antofalla Basement are the most probable source areas of detritus. The existence of the Chilenia terrane to the west is nowadays debated. Two transport directions are known, one pointing to an eastern source and another one pointing to a northern source. The eastern source might imply funnelling across the coetaneous Eastern basin. The northern source is difficult to understand due to the sparse knowledge of the northern termination of the Precordillera terrane.

5.8 CONCLUSIONS

The provenance of the Western tectofacies of the Precordillera terrane is dominated by an upper continental crustal component (composed of igneous, metamorphic and sedimentary rocks), but the influence of a less fractionated than the upper continental crustal component is also evident. A sub-alkaline suite of a basaltic composition but with subordinated andesitic-basaltic rocks characterizes the ultramafic to mafic volcanic rocks interlayered within the Yerba Loca Formation. They have geochemical characteristics intermediate between enriched mid-ocean ridge basalts and ocean island basalts and are more likely related to a mid-ocean ridge setting.

The Sm-Nd and Pb isotope compositions are similar to several areas of Gondwana and Gondwanan-derived Palaeozoic rocks. In particular, Pb isotopes differ consistently with the Pb composition of Laurentia. Detrital zircon dating for the Alcaparrosa Formation constrains the sources as dominantly of Mesoproterozoic age, with other inputs from Neoproterozoic, Palaeoproterozoic, Pampean and Famatinian ages. The Western Pampeanas Ranges and the Arequipa-Antofalla Basement give the best fit to all the provenance constraints and remain the more likely source areas. However, the scarce known Pb data from the Western Pampeanas Ranges are dissimilar. The evaluation of the probable sources indicated by the para-autochthonous models suggests that such provenance is not likely.

If the Western Pampeanas Ranges and the Arequipa - Antofalla Basement were sources of the Western tectofacies, then a close spatial relationship between these three areas since the Middle Ordovician is obvious. Because both areas were autochthonous to Gondwana by that time, then the Precordillera terrane would have reached its present position with respect to them by the time of the initiation of the deposition of the Western tectofacies (Late Arenig to Early Llanvirn).

CHAPTER 6

PROVENANCE ANALYSIS OF ORDOVICIAN CLASTIC SEQUENCES OF THE SAN RAFAEL BLOCK, PRECORDILLERA TERRANE, WESTERN ARGENTINA.

6.1 INTRODUCTION

The Precordillera was initially considered as a north-south folded and thrusted elongated belt (Fig. 6.1; Precordillera *s.s.*) characterized by a Grenvillian-age basement, a Cambrian-Ordovician carbonate platform overlain by clastic deposits developed on the eastern margin, and deep-sea sedimentary rocks with interlayered mafic to ultramafic volcanic rocks on the western margin (compilation in Astini *et al.*, 1996). Since similar geological characteristics were found to the south, the Precordillera belt was extended in order to include the San Rafael and the Las Matras blocks (Fig. 6.1b). Within the San Rafael block, only two Ordovician units are known, the Ponón Trehué and Pavón Formations (Fig. 6.2).

Several authors have controversially discussed the geotectonic evolution of the Precordillera terrane. The proposed models imply either a para-autochthonous (Aceñolaza *et al.*, 2002; Finney *et al.*, 2005) or an allochthonous origin (i.e. Ramos *et al.*, 1986; Dalla Salda *et al.*, 1992a; Cingolani *et al.*, 1992; Dalziel *et al.*, 1994; Astini *et al.*, 1995; Thomas and Astini, 1996; Keller, 1999). No consensus has been reached yet since all the stratigraphical, palaeontological, palaeomagnetic and isotopic data available are thought to support the palaeogeographic proximity of this terrane to Laurentia (e.g. Benedetto, 1993; Lehnert and Keller, 1993; Buggisch *et al.*, 1993; Ramos *et al.*, 1998; Thomas *et al.*, 2001; Rapalini and Cingolani, 2004), and can also be interpreted as indicators of a Gondwanan signature (e.g. Aceñolaza *et al.*, 2002). Despite the general disagreement, comprehensive provenance analyses of the sedimentary record of the Precordillera terrane using modern techniques are scarce (e.g. Loske, 1994; Cingolani *et al.*, 2003a; Gleason *et al.*, 2006).

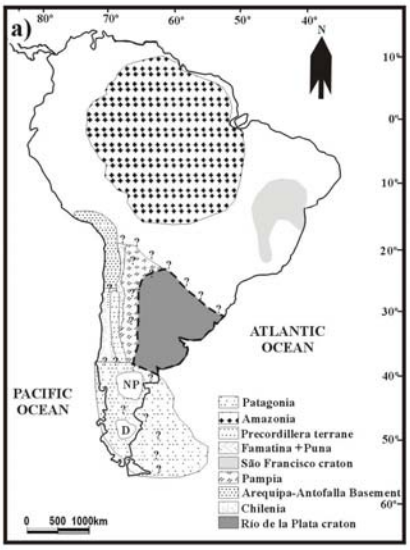

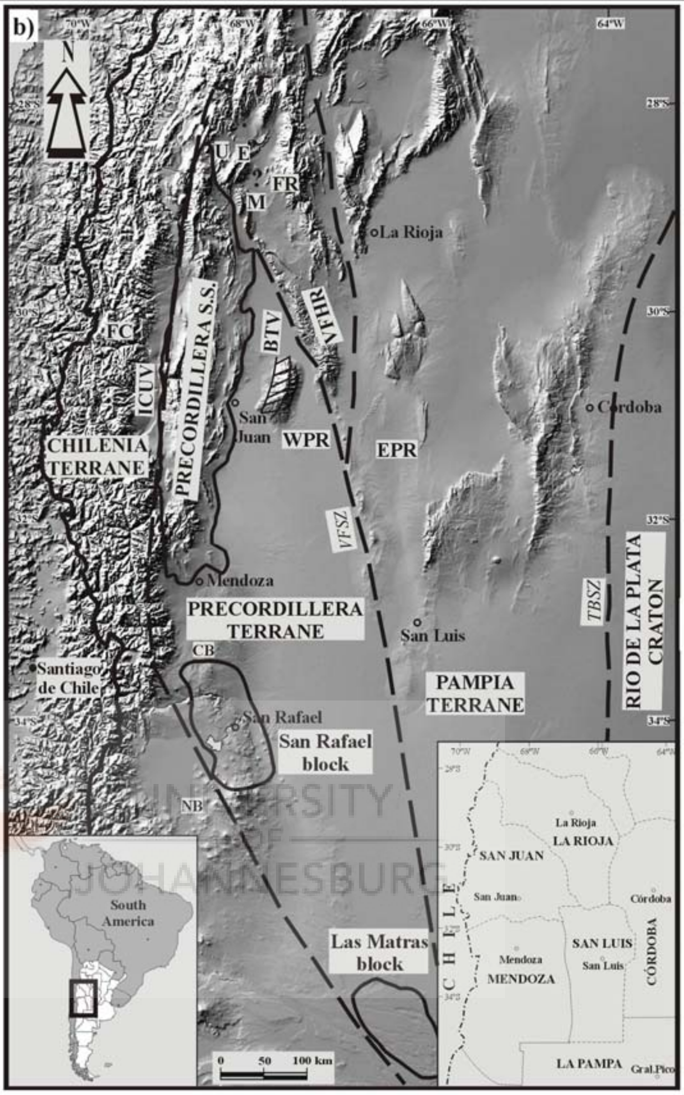

Figure 6.1: a) Main tectonostratigraphic units of South America (modified from Rapalini, 2005). NP: North Patagonian Massif; D: Deseado Massif. b) Satellite image based map showing terrane boundaries as dashed lines and blocks boundaries as continuum lines (based on Ramos *et al.*, 2000; Porcher *et al.*, 2004; Astini and Dávila, 2004). FR: Famatina Range; FC: Frontal Cordillera; ICUV: Iglesia Calingasta-Uspallata Valley; BTV: Bermejo-Tulum Valley; WPR: Western Pampeanas Ranges; EPR: Eastern Pampeanas Ranges; VFSZ: Valle Fértil Shear Zone; CB: Cuyo Basin; NB: Neuquén Basin; PP: Pie de Palo Range; E: Espinal Range; U: Umango Range; M: Maz Range; VFHR: Valle Fértil-La Huerta Range.

Since the San Rafael block comprises only two Ordovician units, and since the provenance of the Pavón Formation is known (Cingolani *et al.*, 2003a), this chapter focus in the evaluation of new data from the Ponón Trehué Formation, using a combination of different provenance techniques including petrography, whole-rock geochemistry, isotope geochemistry (Sm-Nd and Pb-Pb isotopes), and zircon dating. Specific information is obtained from each type of dataset and the integration of these different approaches allows the characterization of the probable source areas and the comparison with the known provenance of the younger Pavón Formation, focusing on the newly acquired detrital zircon dating for the later formation.

6.2 GEOLOGICAL BACKGROUND

The carbonate-siliciclastic Ponón Trehué Formation crops out at the Ponón Trehué locality, San Rafael block, Mendoza province (Fig. 6.2a), comprising one of the southernmost units of its characteristics of the Precordillera (Cuyania) terrane. The unit is exposed in three areas (Fig. 6.2b areas named 1, 2 and 3). The outcrops located to the south of the Ponón Trehué Creek (Fig. 6.2b areas 2 and 3) were simultaneously named as Ponón Trehué Formation (Criado Roqué and Ibañez, 1979) and as the Lindero Formation (Nuñez, 1979). Bordonaro *et al.* (1996) defined the Ponón Trehué Formation as to the outcrops located on the southern edge of the Ponón Trehué Creek as well as the outcrop located 1.5 km to the north of the mentioned creek (Fig. 6.2b areas 1 and 2). The name Lindero Fm. was retained for the outcrops to the south of the Ponón Trehué Creek (Fig. 6.2b area 3). Subsequent studies allowed Heredia (1996; 2006) to establish that all the abovementioned outcrops belong to an olistostromic sequence and the name Ponón Trehué Formation has since been used.

The Ponón Trehué Formation (Heredia, 1996; 2006) is separated from the underlying basement (Cerro La Ventana Formation; Criado Roqué, 1972) by an angular unconformity (Fig. 6.2c). The Pájaro Bobo Formation (Carboniferous in age) overlies the Ponón Trehué Formation through either an unconformity or a fault contact. The Ponón Trehué Formation is a fossil-rich sequence that contains trilobites, brachiopods, ostracods and conodonts, with a Darriwillian–Early Upper Ordovician (Caradoc) age (Heredia, 2006). The Ponón Trehué Formation is subdivided into two members. The lower one is known as the Peletay Member, and is composed of conglomerates and conglomeratic arkoses, limestones, quartz-arenites and black shales. The upper member is the Los Leones Member, and is composed of mudstones, siltstones, arenites and conglomeratic arenites.

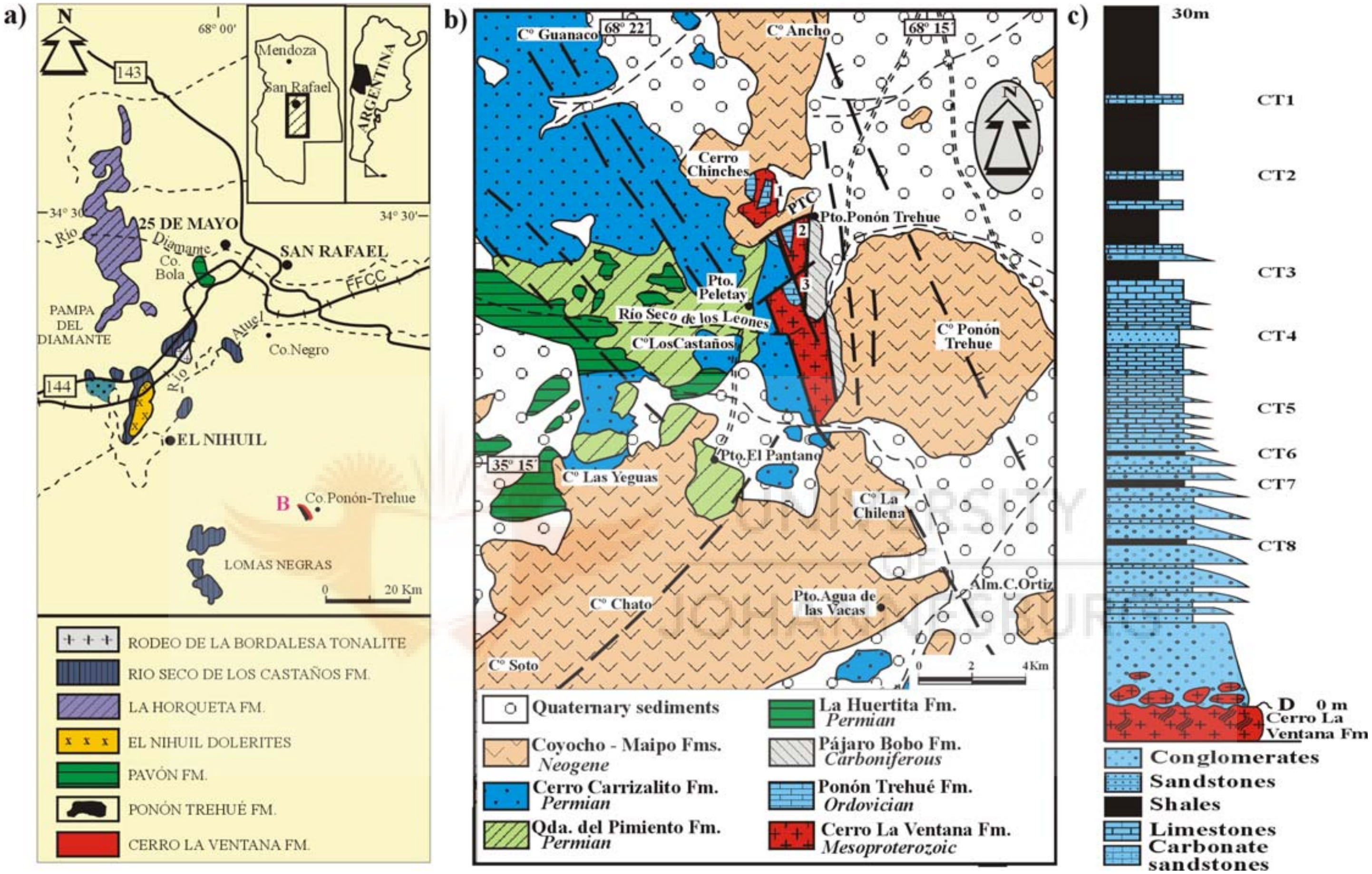

Figure 6.2: a) Location and geology of the San Rafael block. The pink letter (B) corresponds to the area of sampling and to the area expanded in b). b) Detailed geology of the Ponón Trehué area, with outcrops of the Ponón Trehué Formation in the central part (areas named 1, 2 and 3). PTC: Ponón Trehué Creek. c) Lithostratigraphic section of the Ponón Trehué Formation at the La Tortuga section, where samples used for the present study (numbered to the right of the section) were taken. Note that the complete sequence is thicker, as it is shown in Heredia (2006). Modified from Cingolani and Varela (1999), Cingolani *et al.* (2003a) and Heredia (2006).

Blocks of limestones, granitoids, gneisses and amphibolites are common. The limestone blocks resemble (compositionally and due to fossil content) the La Silla and San Juan Formations (Heredia, 2006 and references therein; Fig. 2.2).

This unit was interpreted as forming due to the extension undergone by the Precordillera terrane after its accretion to Gondwana, which produced the brecciation of parts of the carbonate platform that slumped down the slope, forming this breccia-type deposit (Astini, 2002) within a fine clastic matrix. Blocks of Cambrian the carbonate platform are absent, which indicates that for the time of deposition of the Ponón Trehué Formation, the basement was exposed (Heredia, 2006). Even when olistostromic successions are a common feature in the Ordovician of the Precordillera terrane, the age of the olistostromes varies along the terrane, being Lower Arenig for the Los Sombreros Formation (Benedetto and Vaccari, 1992; Chapter 4), Upper Arenig to Caradoc for the Ponón Trehué Formation (Heredia, 2006) and, Early Llanvirn for the Empozada Formation (Heredia and Gallardo, 1996; Chapter 4).

The Pavón Formation crops out in the central area of the San Rafael block (Fig. 6.2a). It is a sandy marine turbidite sequence composed of arenites, wackes, silicate-siltstones and claystones, which underwent very low-grade metamorphism (Manassero *et al.*, 1999; Cingolani *et al.*, 2003a). The graptolite fauna provides an Early Caradoc age (Cuerda and Cingolani, 1998). It is not in contact with the Ponón Trehué Formation.

At the La Tortuga section (Fig. 6.2c, area 3), the sedimentary succession known as the Ponón Trehué Formation unconformably overlies the Mesoproterozoic basement rocks from the Cerro La Ventana Formation (Cingolani and Varela, 1999; Beresi and Heredia, 2003; Cingolani *et al.*, 2005a). Sampling was done in this type section (35º 10' 53" S – 68 º 18' 13" W) of the Ponón Trehué Formation (Fig. 6.2). Zircons of the Pavón Formation were obtained from a subfeldspathic arenite and the sample was taken from outcrops located at the Cerro Bola section presented in figure 6.2a (sample QMOTO1; see details in Table 2 of the Appendix B and geochemical composition in Cingolani *et al.*, 2003a).

6.3 PETROGRAPHY OF FRAMEWORK AND HEAVY MINERALS

The samples studied from the Ponón Trehué Formation are claystones, siltstones and fine-grained arenites. The sandstones are moderately sorted and comprise a small amount of clay-rich matrix. Monocrystalline quartz is subrounded to subangular, with low sphericity and always displaying normal extinction. Fluid inclusions are common and very scarce grains display embayments, but the origin of the embayments could not be clarified. Subangular to subrounded polycrystalline quartz is sometimes present, but with normal extinction and no sutured boundaries. K-feldspar is rare and usually totally replaced by chlorite or clay minerals and subrounded. Sedimentary lithoclasts derived from siltstones, carbonates, mudstones and chert are present. Calcite is present as well as very scarce detrital muscovite lamellae. Zircon, apatite, spinel, tourmaline, rutile, Fe-oxides (including hematite) and other opaque minerals comprise the heavy mineral fraction of the Ponón Trehué Formation. XRD (X-ray diffraction) analyses indicate that clay minerals within the three lithotypes are mainly chlorite, sericite and illite (Table 3 in Appendix C).

As summarized by Cingolani *et al.* (2003a), sandstones of the Pavón Formation have 15% to 30% matrix, poor to moderate sorting and fine to very fine grain sizes. They are composed of quartz, K-feldspar, plagioclase, sedimentary and metamorphic lithoclasts, biotite, muscovite, zircon, apatite, magnetite and hematite. Petrographic provenance analysis suggests a recycled orogen and a continental block as the main source areas and palaeocurrents indicating a transport direction from east to the west (Manassero *et al.*, 1999).

A gabbro was found associated with the clastic rocks of the Ponón Trehué Formation, although its time-relationship to the sedimentary sequence is unclear. It is composed of coarse lath-like plagioclase crystals, forming a decussate texture. Opaque minerals are less than 10%, some of them being columnar-shaped while others are equidimensional. Plagioclase shows the typical polysynthetic twinning and it is slightly altered to clay minerals. The presence of chlorite, calcite and epidote in contact with each other and as secondary phases might indicate that this mafic rock was affected by greenschist facies metamorphism.

The illite crystallinity determinations on four fine-grained clastic samples of the Ponón Trehué Formation, shows that the unit was affected by very low-grade metamorphism (see Table 2 in Appendix A). The same was deduced for the Pavón Formation also based on illite crystallinity index (Manassero *et al.*, 1999).

6.4 GEOCHEMISTRY

Elements concentrated in mafic (Sc, Cr, Co) and silicic (La, Th, REE) rocks, REE (rare earth elements) patterns and the character of the Eu-anomaly have been used for provenance and tectonic determinations (Taylor and McLennan, 1985; McLennan and Taylor, 1991). The signature of the source rock may be modified by weathering, hydraulic sorting and diagenesis (Nesbitt and Young, 1982; Cullers *et al.*, 1987; Cox *et al.*, 1995; Nesbitt *et al.*, 1996; Andersson *et al.*, 2004). Therefore, the determination of the effects that these factors had on the geochemical composition of sedimentary rocks provides evidence for the correct interpretation of the provenance (e.g. Cox and Lowe, 1995). In Table 1 (Appendix A), the chemistry of all samples analyzed is shown.

6.4.1 Major elements and alteration

Major elements are easily mobilized during diagenesis and very low-grade metamorphism; although these processes are largely isochemical, some local redistribution of material may occur (Cox *et al.*, 1995). Weathering effects on sedimentary rocks can be quantitatively assessed using the Chemical Index of Alteration (CIA; Nesbitt and Young, 1982). This index uses molecular proportions as follows: CIA = $(Al_2O_3 / (Al_2O_3 + CaO^* + Na_2O + K_2O)) \times 100$, to measure the degree of alteration of feldspars (and volcanic glass) to clay minerals during weathering (Taylor and McLennan, 1985). CaO^* refers to the calcium associated with silicate minerals.

Samples from the Ponón Trehué Formation have SiO_2 concentrations ranging from 59% to 83.8%, Al_2O_3 is between 3.6% and 20.3%, Fe_2O_3 ranges from 3.1% to 8.1%, CaO and Na_2O are present in low concentrations (0.56% and 0.76% on average respectively), whereas K_2O is between 1% and 4.75%.

The CIA values for sandstones range from 69 to 77 and those for mudstones between 74 and 76 (see Table 1 in Appendix A). In the A-CN-K diagram (Fig. 6.3), samples are grouped towards the A-K boundary and close to the muscovite idealized composition, reflecting their low CaO and Na_2O concentrations compared with the upper continental crust (UCC) abundances of 4.2% and 3.9% respectively (Taylor and McLennan, 1985). Although only two samples are enriched in K_2O compared with the UCC value of 3.4% (McLennan *et al.*, 2006), the distribution of samples within the A-CN-K space cannot be easily explained by a normal weathering path (the field of vertical lines in Figure 6.3 indicates the predicted weathering trend for the average UCC; Bock *et al.*, 1998). Sorting of different grain sizes would lead to vertical spread with mudstones plotting closer to the A apex (Bock *et al.*, 1998), which is not the case in this unit. Diagenetic processes or mixing of sources should therefore explain the behaviour of samples from the Ponón Trehué Formation. Since the CIA values seem to have been modified, they can be recalculated using the expected weathering path of the UCC (Fedo *et al.*, 1995; Bock *et al.*, 1998). In Figure 6.3, the dashed lines go from the K apex through the samples with the lowest and highest CIA and towards the normal weathering path for the UCC. Dotted lines end on the CIA scale indicating the corresponding CIA value for that interval. Therefore, if the CIA values were recalculated to a normal weathering trend and assuming an average UCC composition for the source, then the CIA values would range from 76 to 81, indicating strong weathering (Fedo *et al.*, 1995).

CIA values of the Pavón Formation are plotted along with samples from the Ponón Trehué Formation (Fig. 6.3). The major elements composition of the Pavón Formation is similar to the distribution for the Ponón Trehué Formation, although the Pavón Formation have a wider range of SiO_2 concentrations (61% to 92%; Cingolani *et al.*, 2003a), and certain samples have higher CaO and Na_2O concentrations compared with the Ponón Trehué Formation. The CIA values of the Pavón Formation are between 67 and 85.5 (Cingolani *et al.*, 2003a), indicating intermediate to advanced weathering conditions. Contrary to the Ponón Trehué Formation distribution, samples from the Pavón Formation follow a general weathering trend parallel to the A-CN boundary and they do not show Potassium enrichments (Fig. 6.3).

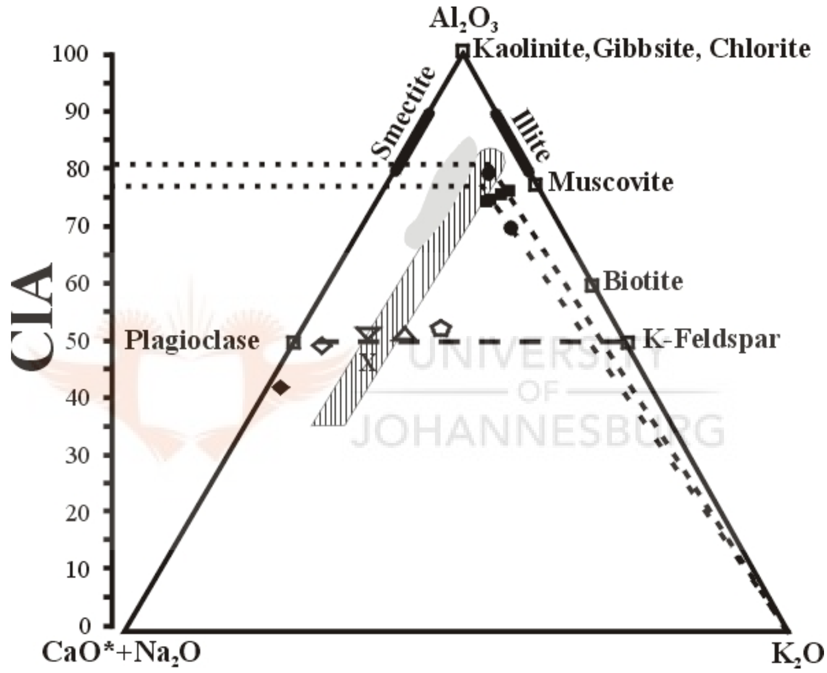

Figure 6.3: A-CN-K diagram based on molecular proportions. The CIA scale is shown on the left. The average upper continental crust is plotted (X; Taylor and McLennan, 1985), as well as idealized mineral compositions (empty squares). Empty pentagon: average granite; empty triangle: average adamellite; empty inverted triangle: average granodiorite; empty diamond: average tonalite; solid diamond: average gabbro (Nesbitt and Young, 1984). Mudstones are represented by solid squares whereas sandstones are represented by solid circles. Grey area represents the range of CIA values for the Pavón Formation (data from Cingolani *et al.*, 2003a). Field of vertical lines indicates the predicted weathering trend for the average upper crustal composition and it was used to recalculate the CIA values for the Ponón Trehué Formation. See text for discussion.

The K/Cs ratio is also an indicator of weathering, because Cs tends to be fixed in weathering profiles whereas the smaller cation of K tends to be lost in solution (McLennan *et al.*, 1990). Those samples from the Ponón Trehué Formation with SiO_2 concentrations above 70% (see Table 1 in Appendix A) are depleted in Cs and in K_2O compared with the UCC, and have K/Cs ratios higher than the UCC average value of 6136 (McLennan *et al.*, 2006). On the other hand, the two samples with SiO_2 abundances well below 70% have similar Cs concentrations (5ppm) to the UCC average of 4.6ppm (McLennan *et al.*, 2006).

These two samples are enriched in Potassium and their K/Cs ratios are higher than the upper continental crust average. The K/Cs ratio for the Pavón Formation ranges from 1322 to 6410, with an average value of 4621 indicating strong weathering conditions (calculated from data presented in Cingolani *et al.*, 2003a). Conclusively, both formations are rather strongly weathered.

Uranium and Thorium are both incompatible trace elements and have similar chemical properties. During weathering, there is a tendency for an increase in the ratio between Th and U to greater than upper crustal igneous values of 3.5 to 4.0, due to the oxidation of U^{4+} to the more soluble U^{6+}. A low Th/U ratio can be a consequence of U enrichment (McLennan, 1989).

Compared with upper continental crust averages of Th (10.7ppm) and U (2.8ppm) according to McLennan *et al.* (2006), most of the mudstones from the Ponón Trehué Formation have similar to enriched Th concentrations (between 11ppm and 14ppm), and depleted to enriched U concentrations (between 1.5ppm and 4.3ppm). Sandstones are depleted in Th (from 3.7ppm to 7.4ppm) or have similar Th concentrations compared with the UCC. U concentration of sandstones varies from 2ppm to 3.2ppm. The Th/U ratios (Fig. 6.4) for the mentioned unit are variable between 1.85 and 9.3, indicating loss of U due to weathering and/or recycling for some samples (e.g. sample CT7). However, some other samples have low Th/U ratios because of U gain (e.g. CT6). Other samples have Th/U ratios between 3.5 and 4, which is typical for unrecycled samples derived from the upper continental crust.

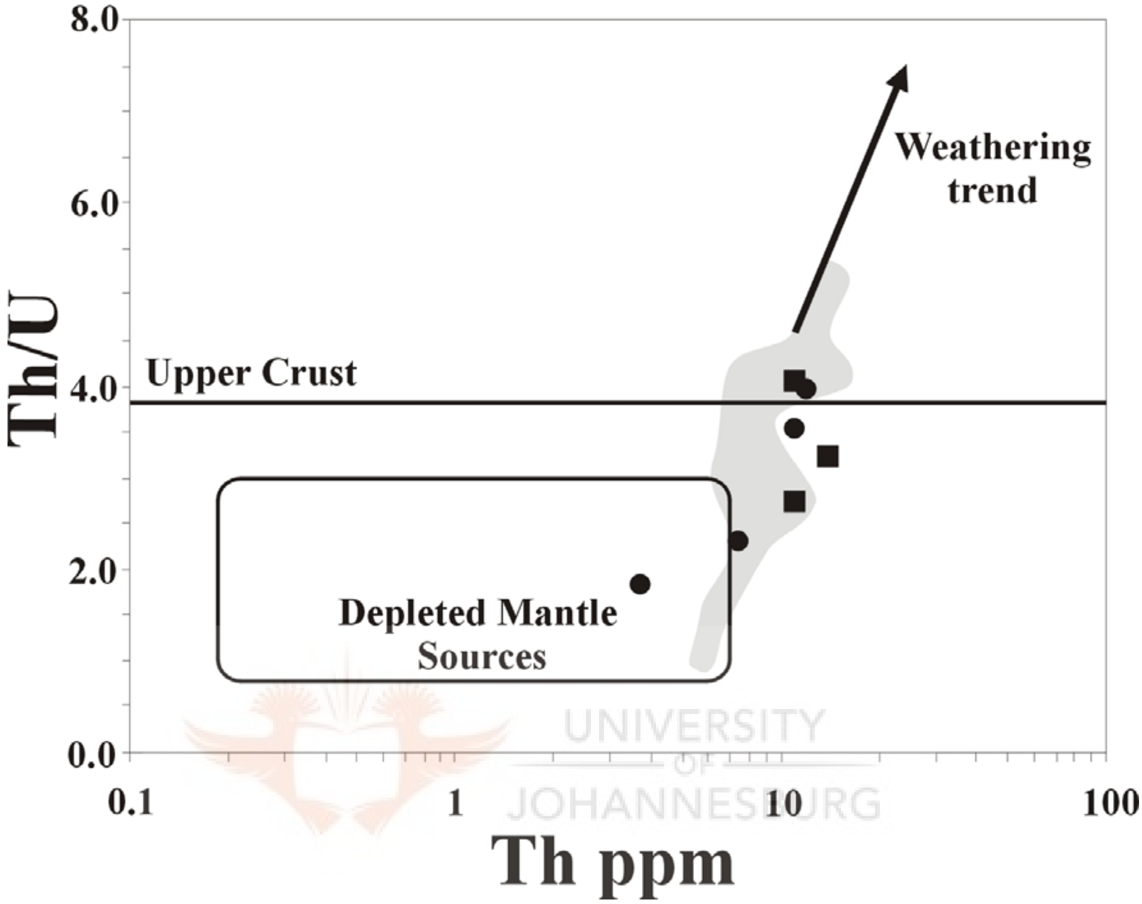

Figure 6.4: Plot of Th/U versus Th based on McLennan *et al.* (1993). Sandstones are represented by solid circles whereas mudstones are represented by solid squares. The distribution of the samples from the Pavón Formation is shown as a grey area and data were taken from Cingolani *et al.* (2003a).

The Pavón Formation have Thorium concentrations below the average for the upper continental crust (with Th concentrations as low as 5.77ppm; Cingolani *et al.*, 2003a), although a few samples are enriched. Regarding Uranium, some samples are depleted. Nonetheless, most of the samples are enriched in U compared with the upper continental crust. Average concentrations for the Pavón Formation are 9.3ppm and 3.2ppm of Th and U respectively (Cingolani *et al.*, 2003a). The Th/U ratios are either below 3.5 or between 3.5 and 4, although a very few samples have high Th/U ratios of up to 5.2 (Fig. 6.4).

Conclusively, both units show similar Th and U values ranging from depleted to enriched compared with UCC, where Th averages are of 10.5ppm for the Ponón Trehué Formation and 9.3ppm for the Pavón Formation and the U averages are of 2.98ppm and 3.2ppm respectively (Table 1 in Appendix A and Cingolani *et al.*, 2003a). Th/U ratios are similarly variable for both units (Fig. 6.4).

6.4.2 Trace elements

The immobile elements La and Th are more abundant in silicic rocks than mafic rocks, but the contrary is the case for Sc and Co. Therefore, La/Sc, Th/Sc and La/Co ratios may be useful for provenance determination (Taylor and McLennan, 1985). The high field strength elements (HFSE) such as Zr, Hf, Y, Th and U are enriched in felsic rather than mafic sources and they reflect provenance compositions because of their immobile behaviour (Taylor and McLennan, 1985). Mechanical processes transport the rare earth elements into a sedimentary basin. The redistribution of the REE abundances within weathering profiles would not have a significant effect on the REE patterns in well-mixed sedimentary rocks and would therefore represent reliable provenance indicators (Taylor and McLennan, 1985), as they would reflect the average REE composition of the source (Cullers *et al.*, 1979; McLennan, 1989). However, fractionations of non-redox-sensitive REE (plus Y) were reported and the fractionation is favoured by the presence of Fe-oxyhydroxides (i.e. Awwiller, 1994; Bau, 1999).

Compared with UCC values listed in Table 1 in Appendix C, the mudstones of the Ponón Trehué Formation are enriched in Sc, Cr, V (see below) and sandstones are depleted in Sc and depleted to enriched in Cr and V. Mudstones are also enriched in Y and Zr (with values up to 39.6ppm and 319ppm respectively) and sandstones are depleted to enriched in Y and Zr. The two sandstones with the highest SiO_2 concentration have lower Zr amounts (lower than UCC) than the other two sandstones with lower SiO_2 concentrations. Average values of the Pavón Formation compared with the UCC indicate that the unit is enriched in Sc and V (14ppm and 112ppm on average respectively; Cingolani *et al.*, 2003a), whereas it is strongly enriched in Cr, Y and Zr (average concentrations of 139ppm, 33ppm and 299ppm respectively; Cingolani *et al.*, 2003a).

The input of a mafic source could be discriminated using the Y/Ni and Cr/V ratios (McLennan *et al.*, 1993). The Y/Ni ratio indicates the concentration of ferromagnesian trace elements (e.g. Ni) compared with a proxy for heavy rare earth elements represented by Y. The Cr/V ratio indicates the enrichment of Cr over other ferromagnesian trace elements. The Cr/V and Y/Ni ratios for the UCC are 0.78 and 0.5 respectively (McLennan *et al.*, 2006), while for the PAAS (post- Archaean Australian Shales) is about 0.73 and 0.49 respectively (Taylor and McLennan, 1985). Ophiolitic components would have Cr/V ratios higher than 10 (discussion in McLennan *et al.*, 1993).

The Cr/V ratio for the Ponón Trehué Formation is between 0.41 and 1.95 and the Y/Ni ratio varies between 0.1 and 1.2 (Table 1 in Appendix A). Cr/V ratios higher than the UCC and Y/Ni ratios lower than the UCC, along with enrichment in compatible elements such as Sc (up to 20ppm), Cr (up to 240ppm) and V (up to 193ppm) compared with the UCC values might indicate the influence of a source with a composition less evolved than the average UCC (for example, mudstone CT8 and sandstone CT2, although the absolute concentrations of elements for the latter are low due to Si_2O dilution; Table 1 in Appendix A). An ophiolitic source can be neglected. For the Pavón Formation, the Cr/V ratio is between 0.83 and 2.5 whereas the Y/Ni ratio ranges from 0.07 to 1.26 from which the influence of a mafic source was deduced (Cingolani *et al.*, 2003a). Cr concentrations are as high as 292ppm for sandstones of the Pavón Formation. Noteworthy, samples used to obtain detrital chromian spinels display Cr concentrations of 152ppm in average. For both units, this depleted component could be represented by the detrital spinels (an extended discussion of spinels from the Pavón Formation is presented in Chapter 7).

The shape of the REE pattern can provide information on both bulk compositions of the provenance and the nature of the dominant igneous process affecting the provenance. Igneous differentiation processes commonly result in light rare earth elements (LREE) enrichment in more evolved felsic rocks. The shape of heavy rare earth elements (HREE) can be related to garnet content and its fractionation during igneous processes. Garnet fractionation occurs at considerable depths, suggesting a mantle origin and producing a depleted-HREE pattern in the rocks (McLennan and Taylor, 1991). Negative Eu-anomalies indicate that the ultimate igneous sources were strongly affected by intracrustal differentiation processes resulting from plagioclase fractionation (Taylor and McLennan, 1985). Eu_N/Eu^* is calculated as $Eu_N/Eu^* = Eu_N/\ (0.67Sm_N+0.33Tb_N)$, where subscript "N" denotes values normalized to chondrite. Recycling of sediment would enrich the ultrastable mineral zircon in relation to other detrital components. Zircon is enriched not only in Zr but has a typical concave REE pattern; therefore, it can lower the La_N/Yb_N ratio. Generally, first cycle deposits will reflect the composition of their source rocks without any loss despite climatic conditions (Basu *et al.*, 1990).

The chondrite normalized rare earth elements patterns for mudstones and sandstones of the Ponón Trehué Formation (Fig. 6.5) show a moderately enriched LREE pattern (La_N/Yb_N of about 5.8 on average), a negative Eu-anomaly (Eu_N/Eu^* of about 0.52 on average) and a flat HREE (Tb_N/Yb_N of 1.17 on average). The samples are enriched in HREE compared with the PAAS. Sample CT2 shows the effects of dilution in the REE concentration due to high silica (83.85%; Table 1 in Appendix A). Figure 6.5 shows that the Pavón Formation also displays REE patterns where an enrichment in HREE is also evident (Cingolani *et al.*, 2003a). The La/Th ratio falls between 2.58 and 4.05 for the Ponón Trehué Formation whereas it varies from 2.6 to 4.6 for the Pavón Formation. La/Th ratios of 2 to 4 are common values for upper crust composition and indicate felsic compositions (McLennan *et al.*, 1980).

6.4.3 Provenance and tectonic setting

The Zr/Sc ratio reflects reworking because Zr is strongly enriched in zircon whereas Sc is not, and zircon can be easily recycled (McLennan *et al.*, 1993). The Th/Sc

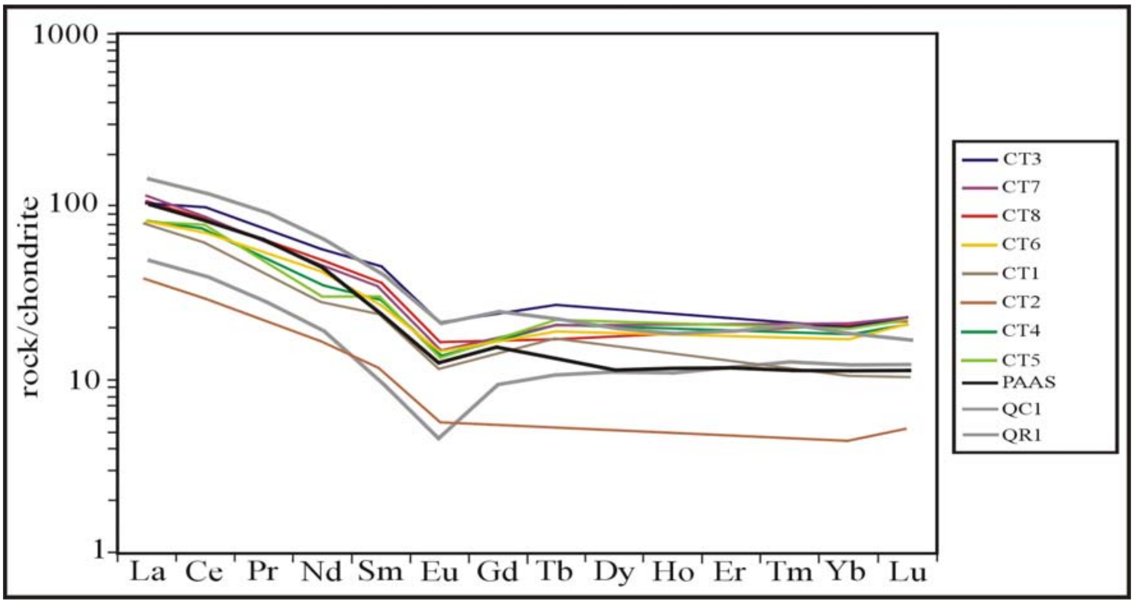

Figure 6.5: Chondrite normalized REE patterns for the Ponón Trehué Formation. PAAS= post-Archaean Australian shales pattern (after Nance and Taylor, 1976) is draw for comparison. Continuous grey lines (QC1 and QR1) correspond to the samples with the highest and the lowest sum of REE from the Pavón Formation (data from Cingolani *et al*., 2003a). REE patterns are drawn as a continuous line although certain elements of the Ponón Trehué Formation were not measured (see Table 1 in Appendix A). Chondrite normalization factors are those listed by Taylor and McLennan (1985).

ratio indicates the degree of igneous differentiation processes since Th is an incompatible element whereas Sc is compatible in igneous systems (McLennan *et al*., 1993). Therefore, both ratios are a powerful tool to decipher different source components of sedimentary rocks (Taylor and McLennan, 1985). In Figure 6.6, the Ponón Trehué Formation shows a spread for Zr/Sc ratios (11 to 36.22) but relatively small range in the Th/Sc ratios (0.7 to 1.08). Recycling played a subordinated role. The samples of the Pavón Formation have a similar range of the Zr/Sc ratios (11.7 to 40.1), whereas the Th/Sc ratios (0.43 to 0.89) include low values, which clearly point to a depleted source (Cingolani *et al*., 2003a).

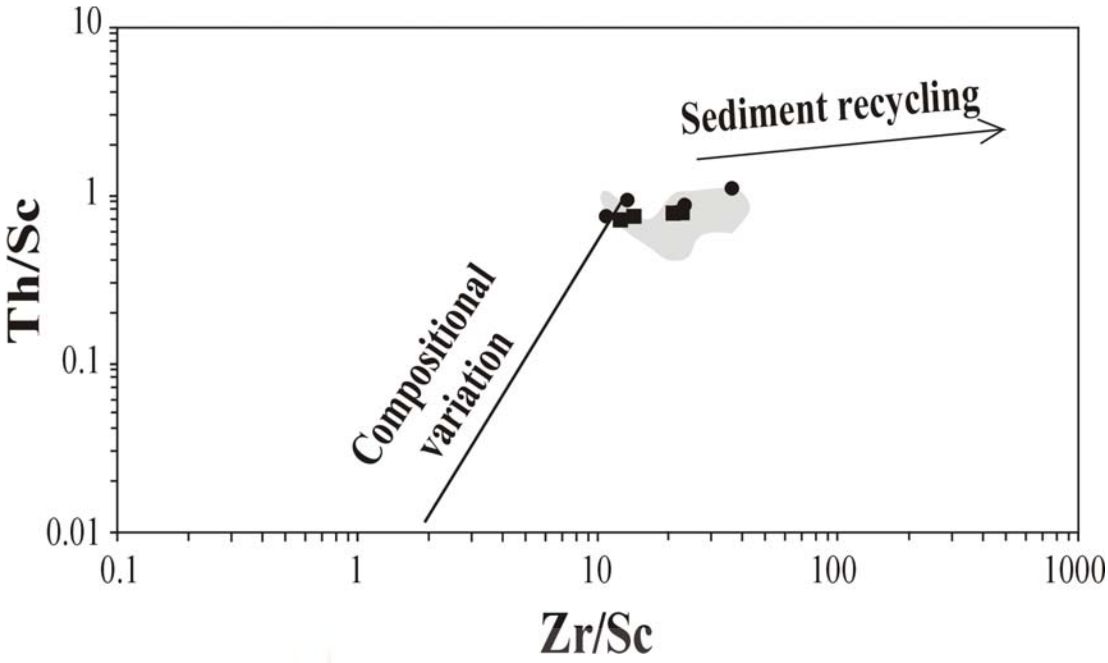

Figure 6.6: Th/Sc versus Zr/Sc diagram adapted from McLennan *et al.* (1990). Sandstones are represented by solid circles whereas mudstones are represented by solid squares. The distribution of the samples from the Pavón Formation is shown as a grey area and data were taken from Cingolani *et al.* (2003a).

When analyzing tectonic settings (e.g. using Bhatia and Crook diagrams) it is important to consider that the sediments can be transported across tectonic boundaries and thus may not necessarily be indicative of the tectonic setting of the deposition (McLennan, 1989). An example of the caution needed in the interpretation of tectonic settings based only on geochemistry is given by the distribution of samples from McLennan *et al.* (1990) drawn for comparison in Figures 6.7 and 6.8. Furthermore, Zimmermann (2005) stated that passive margin and foreland basin sequences cannot be discriminated using Th-Sc-Zr/10.

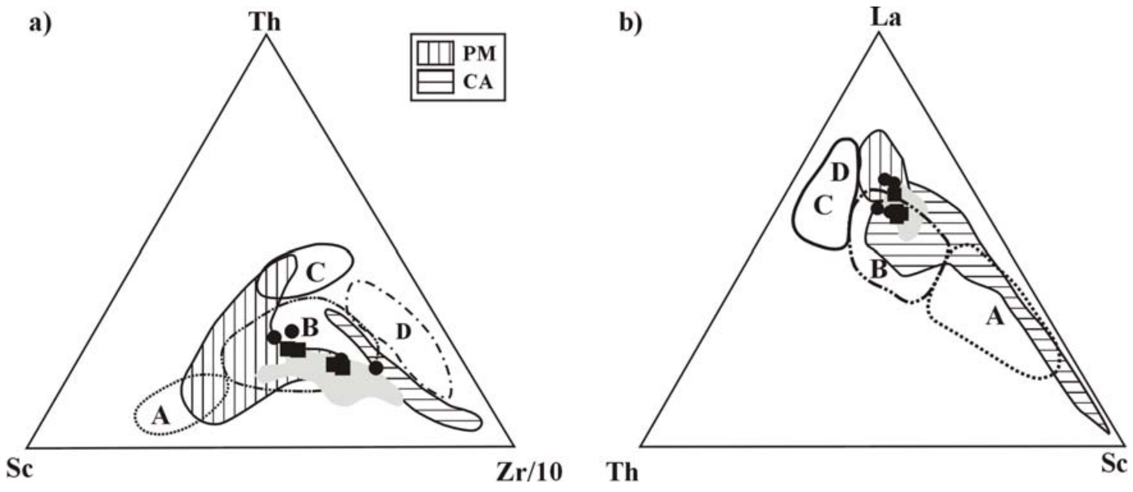

Figure 6.7: a) Th-Sc-Zr/10 and b) La-Th-Sc discriminatory plots after Bhatia and Crook (1986). A: Oceanic island arc; B: Continental island arc; C: Active continental margin; D: Passive margin. Mudstones are represented by solid squares whereas sandstones are solid circles. PM: recent deep-sea turbidites derived from and deposited at a passive margin. CA: recent deep-sea turbidites derived from and deposited at a continental arc margin (data from McLennan *et al.*, 1990). The Pavón Formation distribution (grey area) is according to Cingolani *et al.* (2003a).

According to the tectonic classification from Bhatia and Crook (1986), the oceanic island arc and continental arc settings represent convergent plate margins. The active continental margin setting comprises the Andean-type and strike-slip continental margins. The passive margin setting comprises rifted continental margins of the Atlantic-type. In Figures 6.7 and 6.8 samples from the Ponón Trehué Formation, display deposition in a basin associated with a continental arc or an active continental margin. Some samples of the Ponón Trehué Formation plot within the active continental margin, but other samples show higher Ti/Zr ratios trending towards the oceanic island arc setting (Fig. 6.8). A similar distribution is shown by the samples of the Pavón Formation (Figs. 6.7 and 6.8), which also plot within the continental island arc (Fig. 6.7a and b) and the active continental margin (Fig. 6.8) fields (Cingolani *et al.*, 2003a).

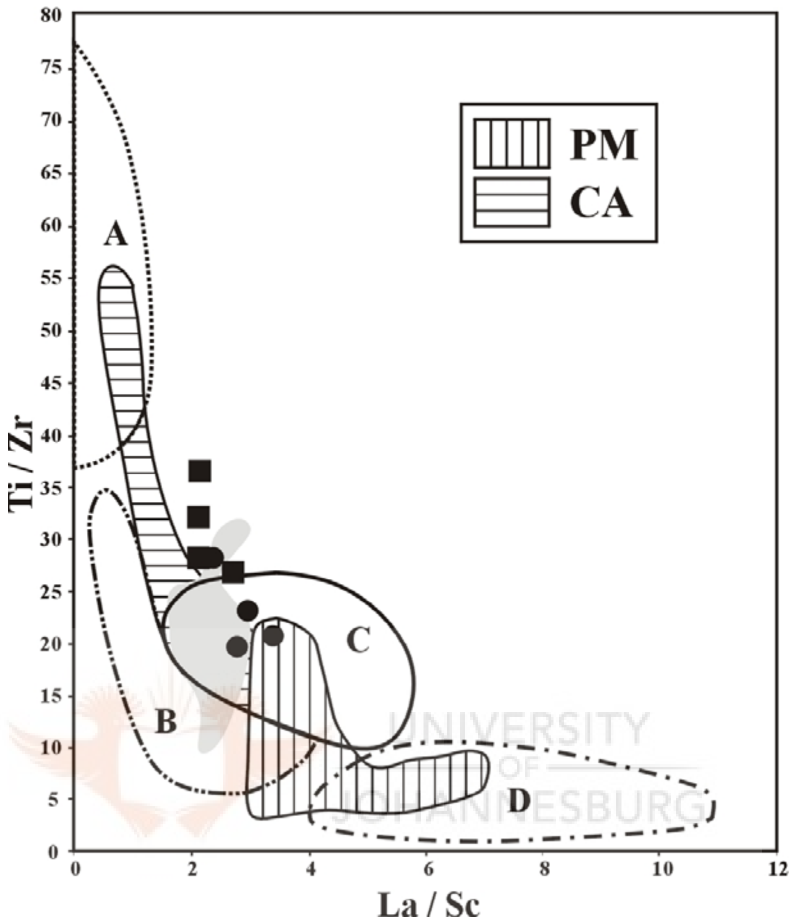

Figure 6.8: Ti/Zr versus La/Sc discriminatory plot (Bhatia and Crook, 1986). A: Oceanic island arc; B: Continental island arc; C: Active continental margin; D: Passive margin. Mudstones are represented by solid squares whereas sandstones are solid circles. PM and CA as indicated in previous figure The Pavón Formation distribution (grey area) is according to Cingolani *et al.* (2003a).

Low Th/Sc ratios, Eu_N/Eu^* of about 1 and strong negative Nb and Ti anomalies characterize continental arc components, although differentiated arcs would have variable Th/Sc ratios and Eu_N/Eu^* between 0.6 and 0.9 (Hofmann, 1988; McLennan *et al.*, 1993; Zimmermann, 2005). Therefore, the influence of an arc-provenance component might be decipher using trace elements ratios such as Th/Sc and Eu_N/Eu^* and element concentrations of Ti and Nb. Discarding those samples from the Ponón Trehué Formation with high Si_2O concentrations, the negative Nb and Ti anomalies are not observed and Eu_N/Eu^* ratios are below 0.56 for all samples analyzed. An input from an arc component seems improbable. The Nb and Ti anomalies are not observed for the Pavón Formation (based on data presented by Cingolani *et al.*, 2003a) if rocks with high Si_2O concentrations are discarded, and therefore the influence from an arc component seems unlikely. This is supported by chromian spinels analyses, which indicate a mafic provenance not linked to an arc (Chapter 7), but rather to mid-ocean ridge and intraplate rocks.

6.5 ISOTOPE GEOCHEMISTRY

6.5.1 Sm-Nd

The Sm-Nd isotope system is a good provenance indicator, but it should be used to complement other methods of provenance determination (Nelson and DePaolo, 1988). The application of the Sm-Nd isotopes to sedimentary rocks can refine the provenance information, as the grade of fractionation and the average crustal residence time of the detrital mix can be determined (McLennan *et al.*, 1990). One of the strengths of the Sm-Nd model age method, as applied to whole-rock systems, is that it provides the opportunity to view back in time through erosion, sedimentation, high-grade metamorphism and even crustal melting events, which usually re-set other isotope systems like K-Ar or Rb-Sr. (DePaolo, 1981).

Five selected samples from the Ponón Trehué Formation were analyzed for the present provenance study, which are compared with data from the Pavón Formation. Results are shown in Table 3 (Appendix A); data was calculated according to DePaolo (1981), although T_{DM} according to DePaolo *et al.* (1991) are also shown and were used to compare with data from the literature that was expressed according to the three-stage model (DePaolo *et al.,* 1991). For more details on methods and analytical techniques, see Appendix B.

ε_{Nd} (t) values, where t = 462 Ma (depositional age) range from -3.95 to -4.91 for the Ponón Trehué Formation (average -4.47 ± 0.39), while for the Pavón Formation are between -0.4 and -4.1 (Cingolani *et al.*, 2003a; considering a depositional age of 455 Ma). $f_{Sm/Nd}$ ranges from -0.34 to -0.40 (average -0.37 ± 0.02), whereas for the Pavón Formation it is between -0.34 and -0.52 (average -0.40 ± 0.06). The T_{DM} ages range from 1.3 to 1.52 Ga (average 1.44 ± 0.078 Ga) for the Ponón Trehué Formation and is between 1.1 and 1.51 Ga for the Pavón Formation (Cingolani *et al.*, 2003a). The T_{DM} ages are comparable to T_{DM} ages of rocks of Mesoproterozoic age and to supracrustal younger rocks, both of the Precordillera terrane (Kay *et al.*, 1996; Cingolani *et al.*, 2003a; Gleason *et al.*, 2006). They are also within the range of variation of the T_{DM} ages of Neoproterozoic to Palaeozoic sequences from northwestern Argentina, such as the igneous rocks of the Pampia terrane (Rapela *et al.*, 1998; Bock *et al.*, 2000; Lucassen *et al.*, 2000; Zimmermann and Bahlburg, 2003).

Figure 6.9a shows the relationship between ε_{Nd} (t) and Th/Sc ratio of samples from the Ponón Trehué Formation where it is seen that the ε_{Nd} (t) values obtained are neither typical of UCC nor of a juvenile input. The Th/Sc ratio is indicative of a source less fractionated than the UCC but not clearly mafic in composition, in coincides with geochemical proxies. The same can be deduced using the plot of $f_{Sm/Nd}$ versus ε_{Nd} (see Fig. 6.9b), where the $f_{Sm/Nd}$ values could be assigned to an old upper crust or an arc component but the ε_{Nd} (t) values are between the two fields. The Pavón Formation shows a similar ε_{Nd} (t) versus Th/Sc relationship (Fig. 6.9a), although some samples have lower Th/Sc ratios. One sample shows a less negative ε_{Nd} (t) of -0.4 and a low Th/Sc ratio (0.43) which could be indicating the input from a juvenile source. A $f_{Sm/Nd}$ of -0.34 tend to indicate that the Sm-Nd system from this sample is not fractionated.

Figure 6.9b shows the wider spread of the $f_{Sm/Nd}$ shown by the Pavón Formation with respect to the Ponón Trehué Formation, where such vertical array indicates that the sample with a $f_{Sm/Nd}$ of -0.52 could have been affected by isotope fractionation.

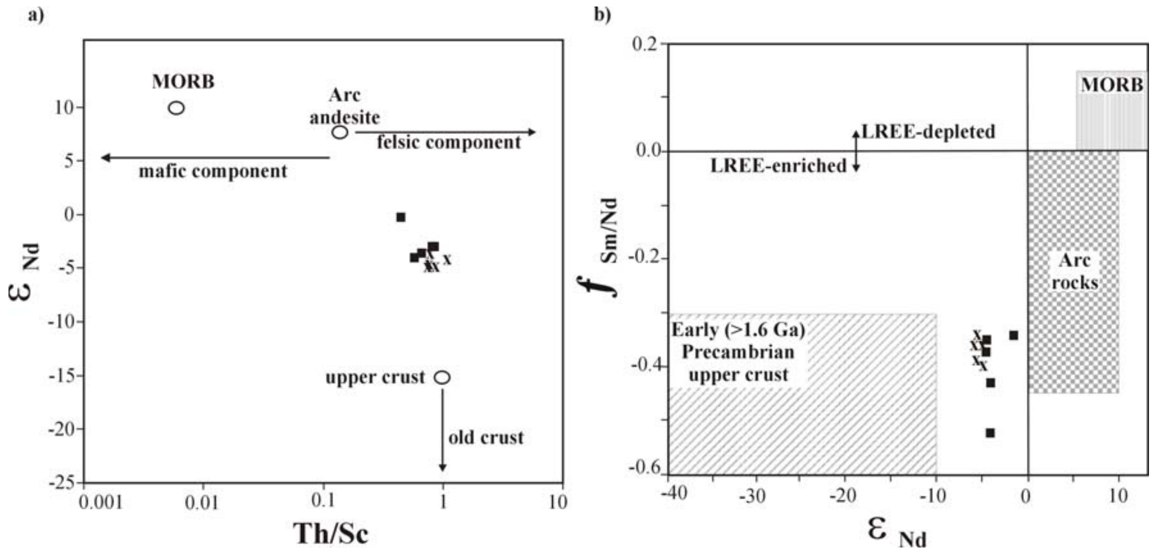

Figure 6.9: a) ε_{Nd} (t) versus Th/Sc ratio of samples from the Ponón Trehué Formation (crosses) and Pavón Formation (squares). b) Plots $f_{Sm/Nd}$ (the fractional deviation of the sample $^{147}Sm/^{144}Nd$ from a chondritic reference) versus ε_{Nd} (t). $f_{Sm/Nd}$ values for the Ponón Trehué Formation (crosses) range from -0.34 to -0.40, whereas the Pavón Formation (squares) shows a vertical array. $f_{Sm/Nd} = (^{147}Sm/^{144}Nd)_{sample} / (^{147}Sm/^{144}Nd)_{CHUR} - 1$. $\varepsilon_{Nd}\ (t) = \{[(^{143}Nd/^{144}Nd)_{sample\ (t)} / (^{143}Nd/^{144}Nd)_{CHUR\ (t)}] - 1\} * 10000$. $(^{147}Sm/^{144}Nd)_{CHUR} = 0.1967$. $(^{143}Nd/^{144}Nd)_{CHUR} = 0.512638$.

6.5.2 Pb-Pb

The use of Pb isotopes is an established tool for evaluating both the provenance and in some instances, the post-depositional alteration history of clastic sedimentary rocks. Pb isotopes from five selected samples from the Ponón Trehué Formation were analyzed. Results are shown in Table 4 (Appendix A). For more details about methods and analytical techniques, see Appendix B. $^{206}Pb/^{204}Pb$ range from 19.028 to 19.303 and $^{208}Pb/^{204}Pb$ range from 38.83 and 38.99. The radiogenic lead ($^{207}Pb/^{204}Pb$) is interesting since most terrestrial ^{207}Pb was produced early in the Earth's history and therefore the high $^{207}Pb/^{204}Pb$ ratio of these samples (15.66 to 15.71) might suggest the input from an old Pb component to the sedimentary succession (Hemming and McLennan, 2001). Pb-isotopes of the Ponón Trehué Formation are more similar to those from the globally subducted sediment

(GLOSS) average than the upper continental crust composition (Figs. 6.10 and 6.11) and they are more comparable with samples from trailing edges and continental collision zones (Hemming and McLennan, 2001).

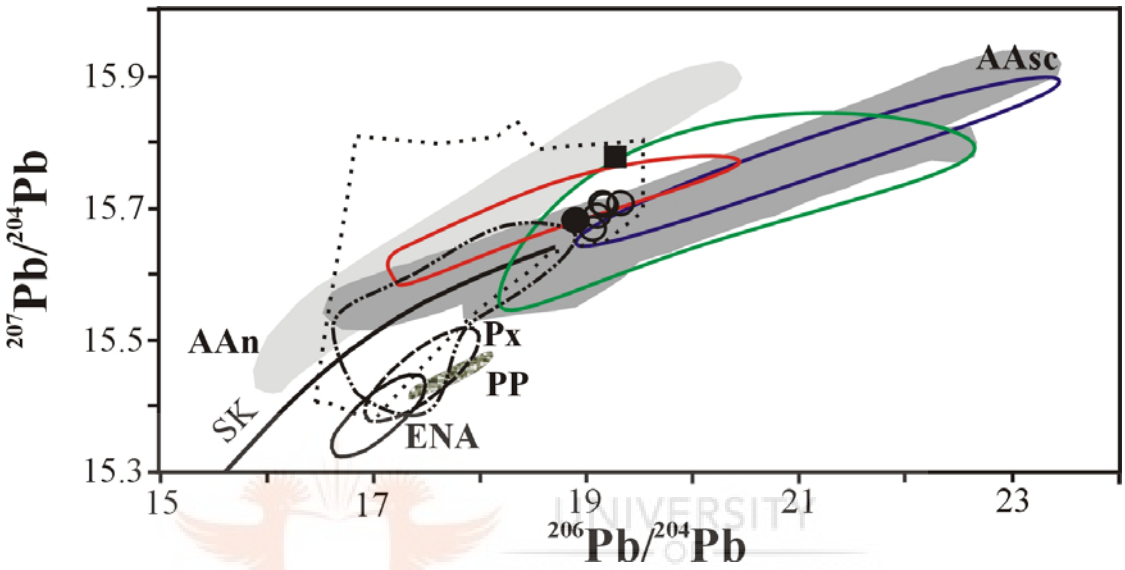

Figure 6.10: $^{207}Pb/^{204}Pb$ versus $^{206}Pb/^{204}Pb$ present-day ratios. Empty circles represent samples from the Ponón Trehué Formation; solid square is the average value for the upper crust and solid circle the average value for GLOSS, both from Hemming and McLennan (2001). Fields obtained from several sources as indicated in the text. ENA denoting solid line: Eastern North America; Px denoting dashed line: xenoliths from the Precordillera terrane; AAsc and AAn: Arequipa-Antofalla Basement Southern and Central domains, and Northern domain respectively; PP: Pie de Palo Range; SK: Stacey and Kramers reference line; blue line: supracrustal Ordovician rocks from the Precordillera terrane (Gleason *et al.*, 2006); dotted line: Palaeozoic rocks from the Central Andes (Lucassen *et al.*, 2002); green line: Palaeozoic rocks from southern Central Andes (Bock *et al.*, 2000); red line: Ordovician rocks from south Bolivia (Egenhoff and Lucassen, 2003); double dotted-dashed line: data from Wareham *et al.* (1998; see text).

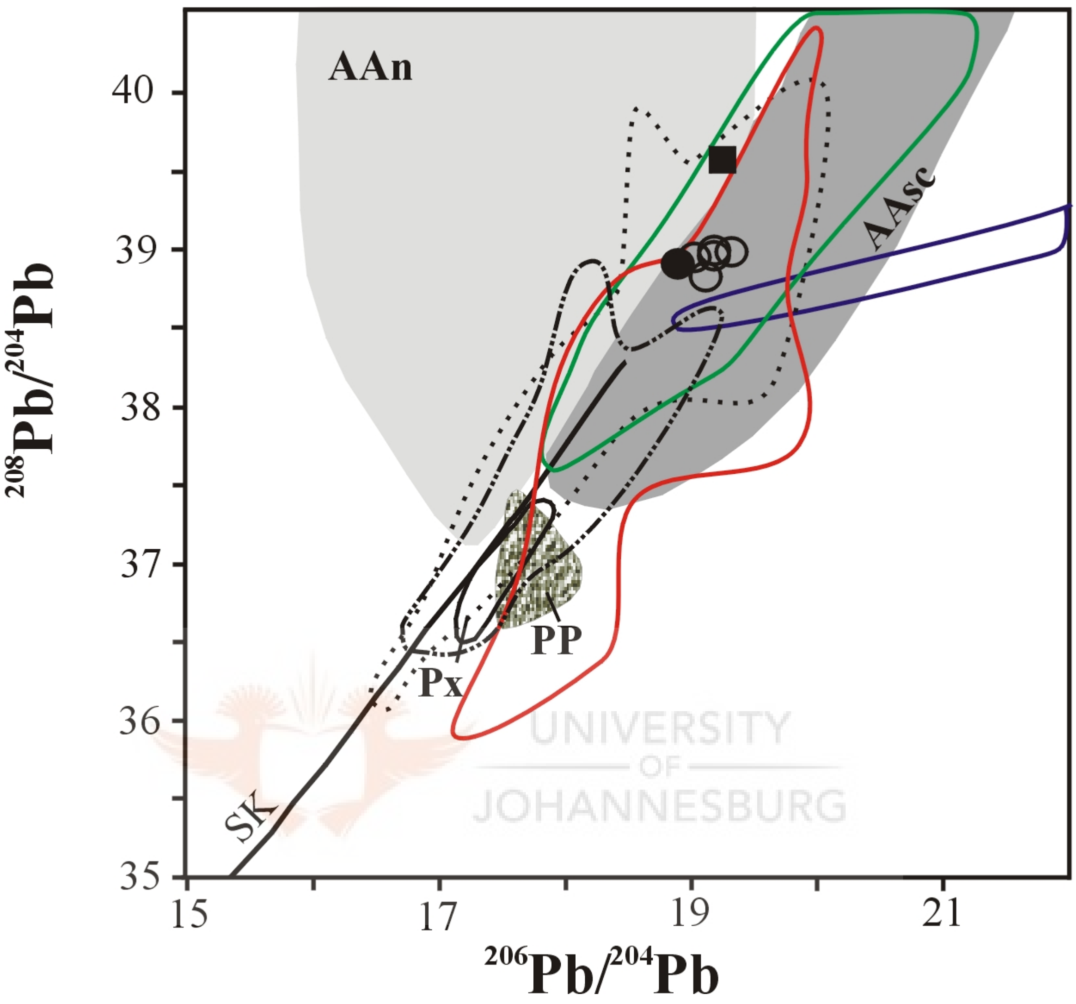

Figure 6.11: $^{208}Pb/^{204}Pb$ versus $^{206}Pb/^{204}Pb$ present-day ratios. Empty circles represent samples from the Ponón Trehué Formation; solid square is the average value for the upper crust and solid circle the average value for GLOSS, both from Hemming and McLennan (2001). Fields obtained from several sources as indicated in the text. Px denoting dashed line: xenoliths from the Precordillera terrane; AAsc and AAn: Arequipa-Antofalla Basement Southern and Central domains, and Northern domain respectively; PP: Pie de Palo Range; SK: Stacey and Kramers reference line; blue line: supracrustal Ordovician rocks from the Precordillera terrane (Gleason *et al.*, 2006); dotted line: Palaeozoic rocks from the Central Andes (Lucassen *et al.*, 2002); green line: Palaeozoic rocks from southern Central Andes (Bock *et al.*, 2000); red line: Ordovician rocks from south Bolivia (Egenhoff and Lucassen, 2003); double dotted-dashed line: data from Wareham *et al.* (1998; see text).

On an uranogenic-Pb plot (Fig. 6.10), samples from the Ponón Trehué Formation plot slightly above the Stacey and Kramers (1975) second stage Pb evolution curve for average crust, similarly to Proterozoic rocks of the Southern and Central domains of the Arequipa-Antofalla Basement (Aitcheson *et al.*, 1995; Tosdal, 1996; Loewy *et al.*, 2004). A similar behaviour is observed for the samples on a thorogenic ($^{208}Pb/^{204}Pb$) versus $^{206}Pb/^{204}Pb$ present-day composition (Fig. 6.11). In both diagrams, it is also evident that the Pb system of the Ponón Trehué Formation differs consistently from the Grenvillian xenoliths from the basement of the Precordillera terrane (Kay *et al.*, 1996), from Proterozoic rocks from Eastern North America and from rocks from the Northern domain of the Arequipa-Antofalla Basement (Tosdal, 1996; Loewy *et al.*, 2004). Mesoproterozoic granitoids and orthogneisses from the Natal-Namaqua Metamorphic belt (Mzumbe gneiss), Falkland/Malvinas Microplate (Cape Meredith Complex), West Antarctica (Haag Nunataks block) and East Antarctica (Kirwanveggan and Sverdrupfjella ranges, Maud Province) have different Pb isotopic signatures (Wareham *et al.*, 1998).

The Arequipa-Antofalla Basement comprises three domains (Loewy *et al.*, 2004): the Northern domain exists in southern Peru and western Bolivia. The Central domain extends from the Peru-Chile border to the northernmost part of Chile, while the Southern domain is extended from 23º S to the northernmost part of Argentina. The area comprised in the so-called Central and Southern domains in the sense of Loewy *et al.* (2004) is almost equivalent to the ca. 500 Ma Mobile Belt of the Pampean Cycle according to Lucassen *et al.* (2000). However, the terminology of Loewy *et al.* (2004) is followed for this discussion.

Compared with supracrustal rocks of the Precordillera terrane (Gleason *et al.*, 2006) the data here presented have higher $^{208}Pb/^{204}Pb$ and lower $^{206}Pb/^{204}Pb$ ratios (Figs. 6.10 and 6.11). They are similar to the Palaeozoic gneisses comprising the radiogenic source of the Central Andes from Lucassen *et al.* (2002) and they are comparable to the data from Palaeozoic rocks of southern Central Andes (Bock *et al.*, 2000), as well as to Ordovician sedimentary rocks of south Bolivia (Egenhoff and Lucassen, 2003).

6.6 DETRITAL ZIRCON DATING

Detrital zircon geochronology is a powerful tool for understanding the ages of source terranes, and when combined with Nd isotopes and whole rock geochemistry, even the compositions of source rocks can be elucidated. Zircons were obtained for the Ponón Trehué (sample CT1; Fig. 6.2c) and the Pavón Formations (sample QMOTO1), and details on the methodology used for zircon extraction and analysis are explained in Appendix B whereas analytical data are shown on Table 5 in Appendix A and in Figures 6.12 and 6.13.

Although the reasons are not well understood yet, it has been demonstrated that the Th/U ratio of metamorphic zircons is of about 0.1 or lower, whereas the Th/U ratio of igneous zircons is >0.2 or >0.5 (Vavra *et al.*, 1999; Hoskin and Schaltegger, 2003). The detrital zircon dating of the Ponón Trehué Formation shows that all the zircon grains analyzed except four, have a Th/U ratio >0.2, and are therefore most likely magmatic (Table 5 in Appendix A; e.g. Vavra *et al.*, 1999). For the Pavón Formation, all the zircon grains except one have Th/U ratios indicative of a magmatic origin (Table 5 in Appendix A). The analysis of cathodoluminescence images for both units shows that most of the grains are subhedral and display oscillatory zoning interpreted as magmatic zoning, whereas only a few have patchy metamorphic zoning (e.g. the zircon C-III-85 from Fig. 6.12).

Detrital zircon dates (n= 38) of the Ponón Trehué Formation cluster between 1065 and 1277 Ma with a main peak at about 1200 Ma. Only one discordant grain has a younger age (834 Ma). The very narrow range of detrital zircon ages implies a local and restricted provenance, most likely from the underlying Cerro La Ventana Formation (see discussion in section 6.7). The local provenance is in agreement with the low Zr/Sc ratio of that specific sample, which is the less recycled sandstone from this unit.

The zircon dating of the Pavón Formation (n= 53) indicate a main population between 1000 and 1300 Ma comprising 35 grains (about 69% of the total measured grains), a population with ages between 1.3 and 1.6 which comprise 13 grains (about

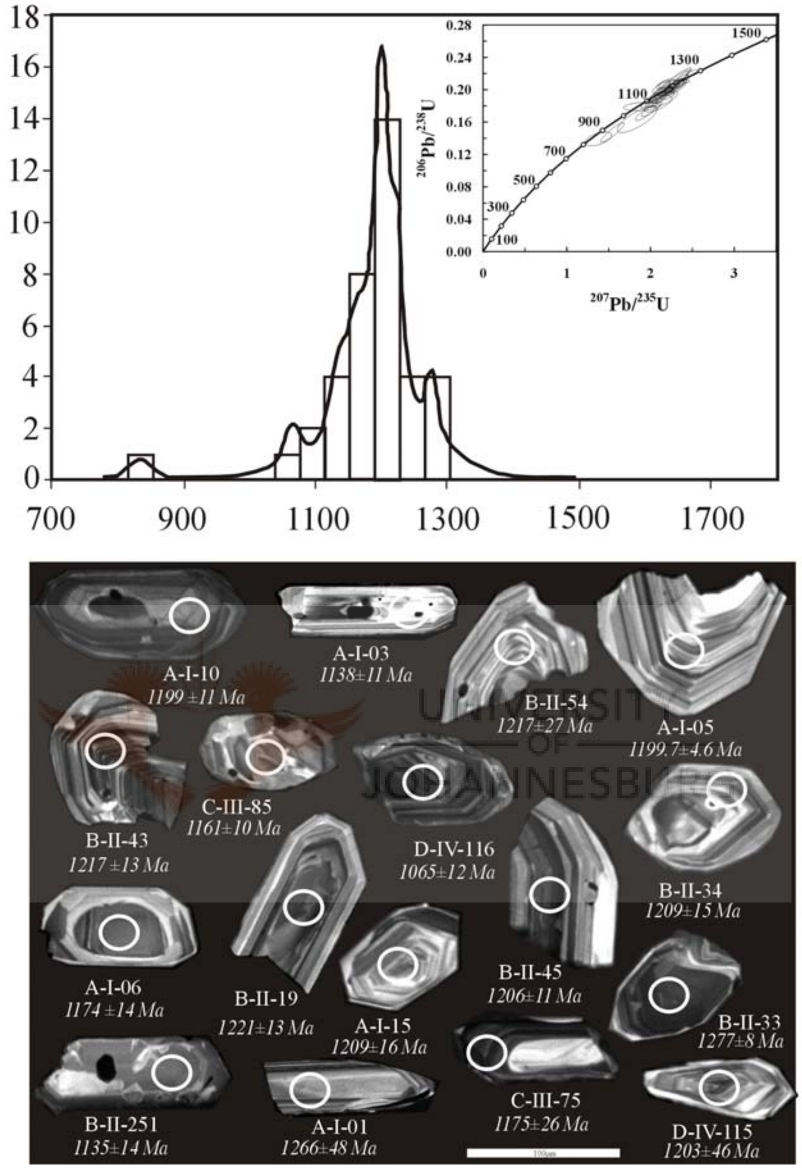

Figure 6.12: U-Pb distribution of analyzed detrital zircons with probability curves for the Ponón Trehué Formation (above). Histogram bars represent time intervals of 40 Ma. Concordia plot diagram in the inset area. Isoplot/Ex (Ludwig, 2001) was used for age calculations. Representative CL microphotographs of selected zircon grains used for detrital dating showing the predominance of magmatic internal textures (below). White circles denote dated areas. Bar length is 100µm.

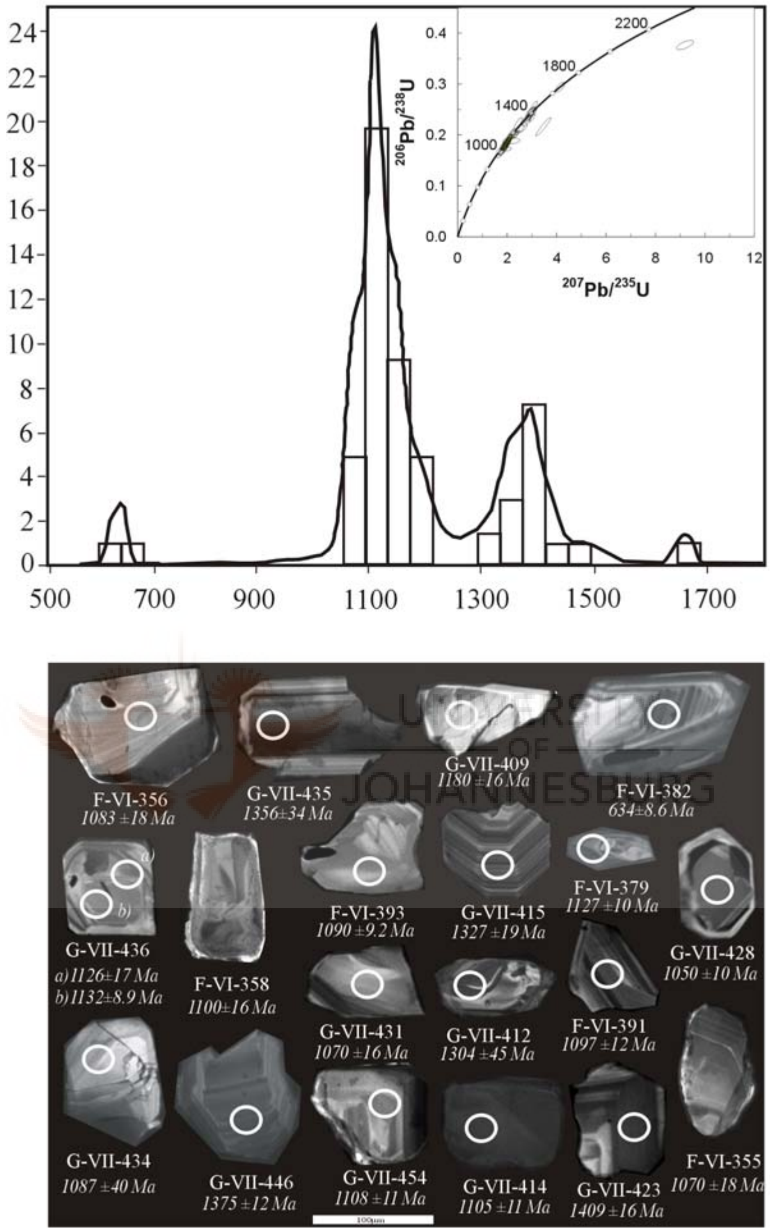

Figure 6.13: U-Pb distribution of analyzed detrital zircons with probability curves for the Pavón Formation (above). Histogram bars represent time intervals of 40 Ma. Concordia plot diagram in the inset area. Isoplot/Ex (Ludwig, 2001) was used for age calculations. Representative CL microphotographs of selected zircon grains used for detrital dating showing the predominance of magmatic internal textures (below). White circles denote dated areas. Bar length is 100µm.

25%), whereas two grains are Neoproterozoic (634 and 615 Ma) and one grain is Palaeoproterozoic (1652 Ma).

Mesoproterozoic rocks that could have contributed to the more important cluster of detrital zircons as well as Palaeoproterozoic rocks are present in several neighbouring areas. For example, in the basement of the Precordillera (Cerro La Ventana Formation, San Rafael block; Cingolani and Varela, 1999; Cingolani *et al.*, 2005a), in Western Pampeanas Ranges (Varela and Dalla Salda, 1992; McDonough *et al.*, 1993; Varela *et al.*, 1996; Casquet *et al.*, 2006) and in the Arequipa-Antofalla Basement (Bahlburg and Hervé, 1997 and references therein). The Neoproterozoic zircons could be linked to the Pampean/Brazilian Orogen.

6.7 DISCUSSION

The petrographic analyses of the Ponón Trehué Formation showed the dominance of monocrystalline quartz and K-feldspar and the presence of sedimentary lithoclasts (siltstones, carbonates, mudstones and chert) and spinels, which point to an upper continental crustal component (including the recycling of sedimentary rocks) and the influence of a source less evolved than the UCC. The lack of plagioclase and igneous and metamorphic lithoclasts (besides polycrystalline quartz) contrasts with the diversity in composition of the basement rocks. On the contrary, sandstones from the Pavón Formation are more immature (e.g. due to higher matrix contents), and show a variability of lithoclasts which includes those derived from metamorphic rocks. Input from a depleted component is also denoted by the presence of detrital chromian spinels (see below).

The major elements distribution of the Ponón Trehué Formation appears to be affected by weathering and other secondary processes, since high CIA values are present and Potassium enrichments were detected. K/Cs ratios are higher than the UCC values for some samples. However, Th/U ratios indicate weathering and/or recycling for only a few samples. Although the Pavón Formation displays CIA values, K/Cs and Th/U ratios indicative of strong weathering, effects of Potassium metasomatism are not evident. Instead, in the A-CN-K diagram the samples plot along a normal weathering trend. Geochemical analyses of mudstones and sandstones of the Ponón Trehué and Pavón Formations reflect the dominance of an upper continental crustal component, but relative high abundances of compatible elements along with low Th/Sc ratios suggest a mafic input, as it was indicated by petrography and heavy minerals analysis. Both units show a similar range of variation of the Zr/Sc ratios, indicating that recycling was not important. An ophiolitic source can be neglected based on Y/Ni and Cr/V ratios from both units. Further assumptions regarding such mafic source where obtained via chemical analyses of detrital chromian spinels from the Pavón Formation linked to mid-ocean ridge and intraplate basalts (Chapter 7).

Relationships between Th, Sc, Zr, La and Ti indicate an active continental margin or a continental island arc setting, although input from an arc component seems to be ruled out based on Eu_N/Eu^*, Nb, Ti and the Th/Sc ratios. However, typical arc signatures are often not recorded in other than basins spatially closely related to the arc itself, and rocks derived from dissected arc terranes would show variable Eu_N/Eu^* values (McLennan *et al.*, 1990; Zimmermann, 2005). Furthermore, passive margin and foreland basin deposits cannot be easily discriminated using Th-Sc-Zr-La relationships (Zimmermann, 2005), and the active continental margin setting used by Bathia and Crook (1986) involves retro-arc foreland and pull-apart basins. In summary, the main geochemical and petrographical differences between the Ponón Trehué and the Pavón Formations are the effects of Potassium enrichment observed in the first one (Fig. 6.3), and the general wider range of variation of the provenance composition for the Pavón Formation (as indicated by the presence of metamorphic lithoclasts and wider variability of geochemical proxies; Figs. 6.4 to 6.8).

Sm-Nd isotopes indicate a narrow range of variation with ε_{Nd} value of about -4.5, a $f_{Sm/Nd}$ of about -0.37 and T_{DM} of 1.44 Ga for the Ponón Trehué Formation. The Sm-Nd isotopic characteristics of the Pavón Formation are similar to the Ponón Trehué Formation, but a juvenile input is denoted by a sample with a ε_{Nd} of -0.4 and some isotope fractionation is also detected. Pb isotopes for the Ponón Trehué Formation indicate that at least a part of the components has a "Gondwanan Pb-signature", characterized by high $^{207}Pb/^{204}Pb$ ratios. Zircon dating for both units constrains the age of the main sources to the Mesoproterozoic. However, the Pavón Formation shows two peaks, one at 1.1 Ga and another at 1.4 Ga whereas the Ponón Trehué Formation shows only a main peak at 1.2 Ga. Minor contributions from Palaeoproterozoic and Neoproterozoic sources were also detected for the Pavón Formation which are absent in the Ponón Trehué sequence. These differences in the zircon populations and in the Sm-Nd signature as well, are consistent with petrography and geochemistry, which also suggest a more restricted source for the Ponón Trehué Formation compared with the Pavón Formation. The dissimilarities are related to deposition of olistostromic sequences within a subsiding basin for the Ponón Trehué Formation (Astini, 2002; Heredia, 2006) and to deposition of turbidites for the Pavón Formation (Fig. 6.15; Cingolani *et al*., 2003a).

Isotope geochemistry indicates similarities with several probable sources. Further constraints are provided by sedimentologic characteristics which indicates for the Ponón Trehué Formation a dominant provenance from the underlying Mesoproterozoic Cerro La Ventana Formation (Heredia, 2006), while palaeocurrents point to an eastern provenance for the detritus of the Pavón Formation (Manassero *et al*., 1999; Cingolani *et al*., 2003a). The absence of an important recycling (with some exceptions) tend to ruled out sources located further afield with respect to the depositional basin for both units. However, the models proposed to explain the tectonic evolution of the Precordillera terrane imply the evaluation of sources for the Ponón Trehué and Pavón Formations such as the Famatinian arc and the Grenville Province of Laurentia. The para-autochthonous models (Aceñolaza *et al*. 2002; Finney *et al*., 2005) placed the Precordillera surrounded by Antarctica, Falklands/Malvinas Microplate and the Natal-Namaqua Metamorphic belt (SAFRAN), being therefore important to evaluate these areas as probable sources as well.

A provenance from the Famatinian magmatic arc is not supported by detrital zircon dating. Although the Grenville Province of Laurentia comprises rocks with a range of ages that could account for the detrital zircon ages and the Nd-isotope signature (Fig. 6.14) of the Ordovician clastic rocks of the San Rafael block here studied, the Pb isotope composition differs consistently. Probable source rocks from Antarctica, Falklands/Malvinas Microplate and the Natal-Namaqua Metamorphic belt accomplish for Mesoproterozoic ages and have comparable T_{DM} ages, but they have different Pb isotopes composition.

When analyzing the Ponón Trehué Formation, the basement rocks known as the Cerro La Ventana Formation provides the best fit regarding sedimentology (Heredia, 2006), Nd signature and zircon ages. The Cerro La Ventana Formation consists of mafic to intermediate gneisses, foliated quartz-diorites and tonalites that partially graded to amphibolites and migmatites, as well as acidic to intermediate granitoids and pegmatitic and aplitic veins (Cingolani *et al.*, 2005a). However, metamorphic and plutonic derived rock fragments were not observed within the Ponón Trehué Formation. Only some of all the basement rock types had been studied until today (diorites and tonalites). Sm-Nd, Rb-Sr and U-Pb on zircons indicate Mesoproterozoic ages (1.1 to 1.2 Ga; Cingolani and Varela, 1999; Cingolani *et al.*, 2005a). Samples analyzed showed geochemical and isotopic characteristics of primitive (depleted) rocks (e.g. positive ε_{Nd} values; Cingolani *et al.*, 2005a). Detrital zircon dating restricts the provenance to a Mesoproterozoic source (between 1065 and 1277 Ma). Nd data presented by Cingolani *et al.* (2005a) of the Cerro La Ventana Formation show ε_{Nd} values in the range of variation of data calculated to the time of deposition of the Ponón Trehué Formation (Fig. 6.14). Unfortunately, the Pb composition of the Cerro La Ventana Formation remains unknown. If these basement rocks were the only source providing detritus to the Ponón Trehué Formation then the Pb-isotopic composition of the Cerro La Ventana Formation might have a high $^{207}Pb/^{204}Pb$ signature similar to that of Gondwanan areas.

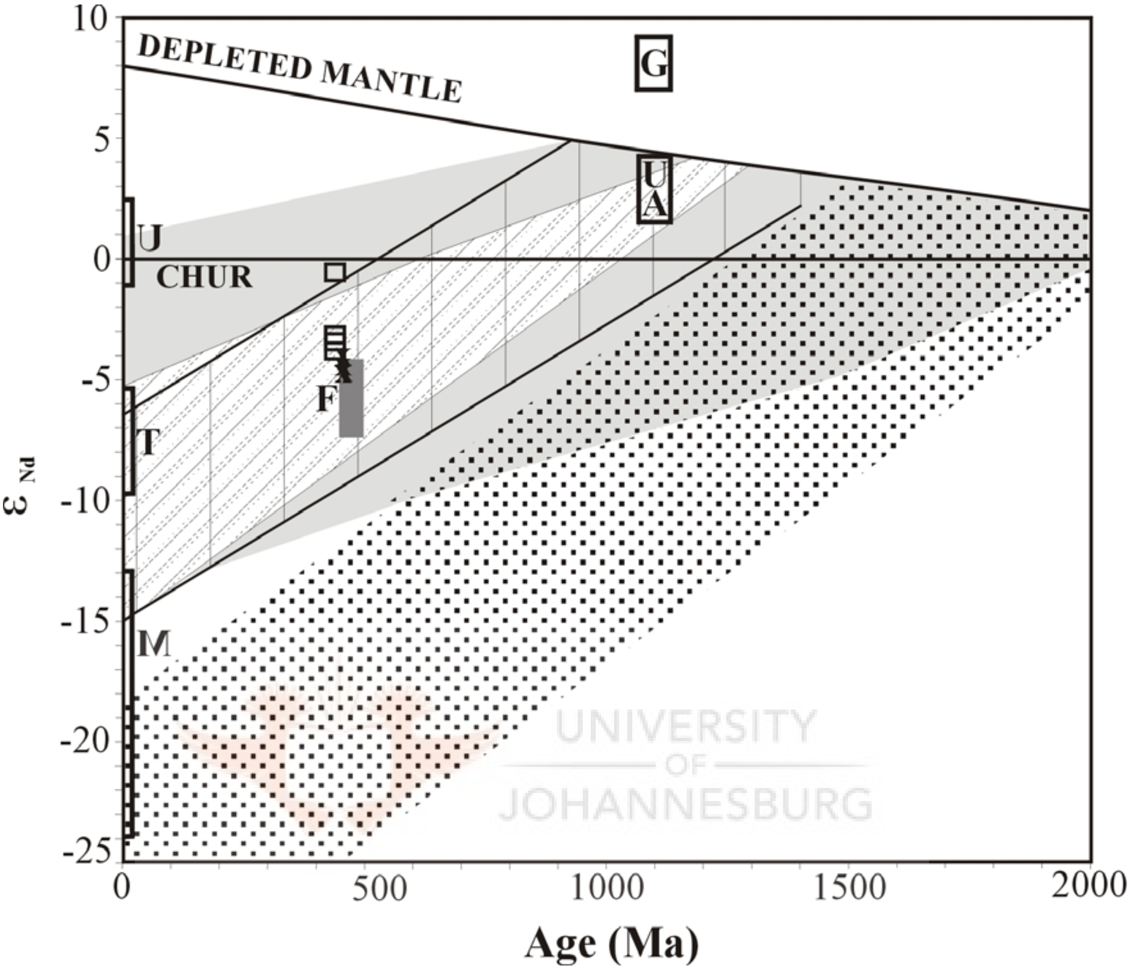

Figure 6.14: ε_{Nd} versus age of the Ponón Trehué (crosses) and the Pavón (empty squares) Formations and of areas evaluated as probable sources. Dotted area: range of ε_{Nd} for the Northern domain of the Arequipa-Antofalla Basement and light grey area: Central and Southern domains of the Arequipa-Antofalla Basement (sensu Loewy *et al.*, 2004). Field of vertical lines: the Laurentian Grenville crust (Patchett and Ruiz, 1989). A: granulitic and amphibolitic, and G: acidic-gneissic, xenoliths from the inferred basement of the Precordillera terrane (Kay *et al.*, 1996). F indicating dark grey area: Famatinian magmatic rocks (Pankhurst *et al.*, 1998). U: Umango Range, T: El Taco Complex, and M: Maz Complex from the Western Pampeanas Ranges (Vujovich *et al.*, 2005). White field with diagonal lines: the Cerro La Ventana Formation (Cingolani *et al.*, 2005a). Data for the Pavón Formation is from Cingolani *et al*. (2003a).

The wider range of detrital zircon ages of the Pavón Formation might indicate that although the Cerro La Ventana Formation could have been an important source, another source was also providing detritus to the basin. However, it might also reflect the fact that not all the rock types comprising the basement were already studied. In Figure 6.14 it can be observed that the range of variation of ε_{Nd} values of the Cerro La Ventana Formation does not explain the -0.4 value displayed by one sample of the Pavón Formation, implying inputs from other sources. A provenance from ocean floor basalts (mid-ocean ridge) and flood basalts in oceanic or continental intraplate settings are indicated by detrital chromian spinels. Pb data from the Pavón Formation are still not existent.

Source areas towards the east are likely (Manassero *et al.*, 1999; Cingolani *et al.*, 2003a), but outcrops of Mesoproterozoic sources are not found nowadays. However, extension of similar basement rocks from the northern outcrops of the Western Pampeanas Ranges and towards the Las Matras block (Fig. 6.1) had been used as the milestone to the definition of the Cuyania (Precordillera) terrane (compilation in Ramos, 2004). Therefore, another source (besides the Cerro La Ventana Formation) that could have contributed detrital material to this basin is represented by the Western Pampeanas Ranges. Sm-Nd data available from the Western Pampeanas Ranges are scarce (Vujovich *et al.*, 2005), but particularly noteworthy are the positive ε_{Nd} values found within the Umango Range (Fig. 6.14). The T_{DM} ages of the Pavón Formation are comparable to T_{DM} ages for Mesoproterozoic xenoliths interpreted as the basement of the Precordillera terrane (Kay *et al.*, 1996). However, the few Pb isotopes from the Pie de Palo Range are dissimilar (Kay *et al.*, 1996). Since the Western Pampeanas Ranges and the Arequipa-Antofalla Basement might constitute a single crustal block para-autochthonous with respect to the pre-Famatinian margin of Gondwana (Casquet *et al.*, 2006), then a minor contribution from the Central and Southern Domains can also be invoked to explain the Sm-Nd signature of the Pavón Formation (Fig. 6.14). However, a northern provenance is not supported by palaeocurrents, and immaturity of the sedimentary rocks including the subhedral character of the zircons tends to dismiss long transports.

The evidence here presented undoubtedly link the Cerro La Ventana Formation as a provenance component to the Ordovician sedimentary deposition within the San Rafael block. However, extensive petrographical, geochemical and isotopic studies of all the rock types comprised in the Cerro La Ventana Formation are needed to further support this. Considering the current information available, another source is needed to explain composition of the Pavón Formation. Comparisons made with several probable source areas ruled out the Grenville Province of Laurentia. Antarctica, Falklands/Malvinas Microplate, the Natal-Namaqua Metamorphic belt and the Western Pampeanas Ranges showed similarities in age and Nd-signature but different Pb compositions.

The dataset analyzed from the Antarctica, Falklands/Malvinas Microplate, the Natal-Namaqua Metamorphic belt comprises mafic, intermediate and felsic ortho- and paragneisses intruded by mafic dykes and granitoid suites all of Mesoproterozoic age; minor calc-silicate rocks and metapelites are also present (Wareham *et al.*, 1998). The Western Pampeanas Ranges also comprise a very wide range of igneous and metamorphic rocks including biotitic and dioritic-granodioritic gneisses, metamorphic rhyolites and amphibolites of Mesoproterozoic age (McDonough *et al.*, 1993). Greenschists facies metamorphic rocks such as carbonate marbles and schists, metaquartz-arenites and talc-, tremolite- and chlorite-serpentine schists are also present (Ramos *et al.*, 1993). The northernmost outcrops of the Western Pampeanas Ranges comprise marbles, calc-silicated rocks and quartz-mica schists, associated with amphibolites and ultramafic rocks, metapelites, metasandstones, metagabbros, metatonalites and tonalitic to granitic orthogneisses (Porcher *et al.*, 2004). Such a diversity of rock compositions contrast with the lithoclasts composition of the Ponón Trehué and Pavón Formations which show low proportions of sedimentary and metamorphic lithoclasts. Based on petrographical features it is not possible to discriminate the source rock.

Therefore, a para-autochthonous or allochthonous origin for the Precordillera terrane cannot be resolved, until more data from the probable sources is added. However, Naipauer (2007) deduced a Laurentian derivation for the Neoproterozoic to Cambrian successions of the Precordillera terrane, invoking an allochthonous model to understand such a provenance for the detrital record. The Mesoproterozoic basement of the Precordillera (Cuyania) terrane was at least partially exposed and provided detritus to a clastic level interlayered with the Angacos Formation (based on detrital zircon dating; Naipauer, 2007). Therefore, an allochthonous origin for the Precordillera terrane is here preferred.

The Cerro La Ventana Formation was probably a source for both units, but another eastern source such as the Western Pampeanas Ranges is needed to understand the provenance of the Pavón Formation. These differences might indicate that even though the Cerro La Ventana Formation was a source since the Darriwillian (Ponón Trehué Formation), towards younger ages (Caradoc) other sources such as the Western Pampeanas Ranges were available to provide detritus to the Pavón Formation (Fig. 6.15). However, this change in provenance may indicate that the restricted provenance of the Ponón Trehué Formation is due to the deposition within a restricted extensional basin (Astini, 2002; Heredia, 2006) whereas the Pavón Formation was deposited by turbidite currents within a foreland basin (Fig. 6.15; Cingolani *et al.*, 2003a). In this scenario, the depositional basins resulted from the extensional regime that followed the accretion during the Middle Ordovician of the Precordillera terrane to Gondwana (Astini, 2002).

6.8 CONCLUSIONS

Petrographical and geochemical analyses of the Ponón Trehué Formation indicate a main provenance component with an upper continental crust composition but with a subordinate input from a less evolved source. Similar characteristics were observed comparing the dataset with the Pavón Formation provenance. Main differences between the two units are the presence of metamorphic lithoclasts and the absence of Potassium metasomatism within the latter. Both formations are however, strongly weathered. Th/Sc ratios indicate no important recycling.

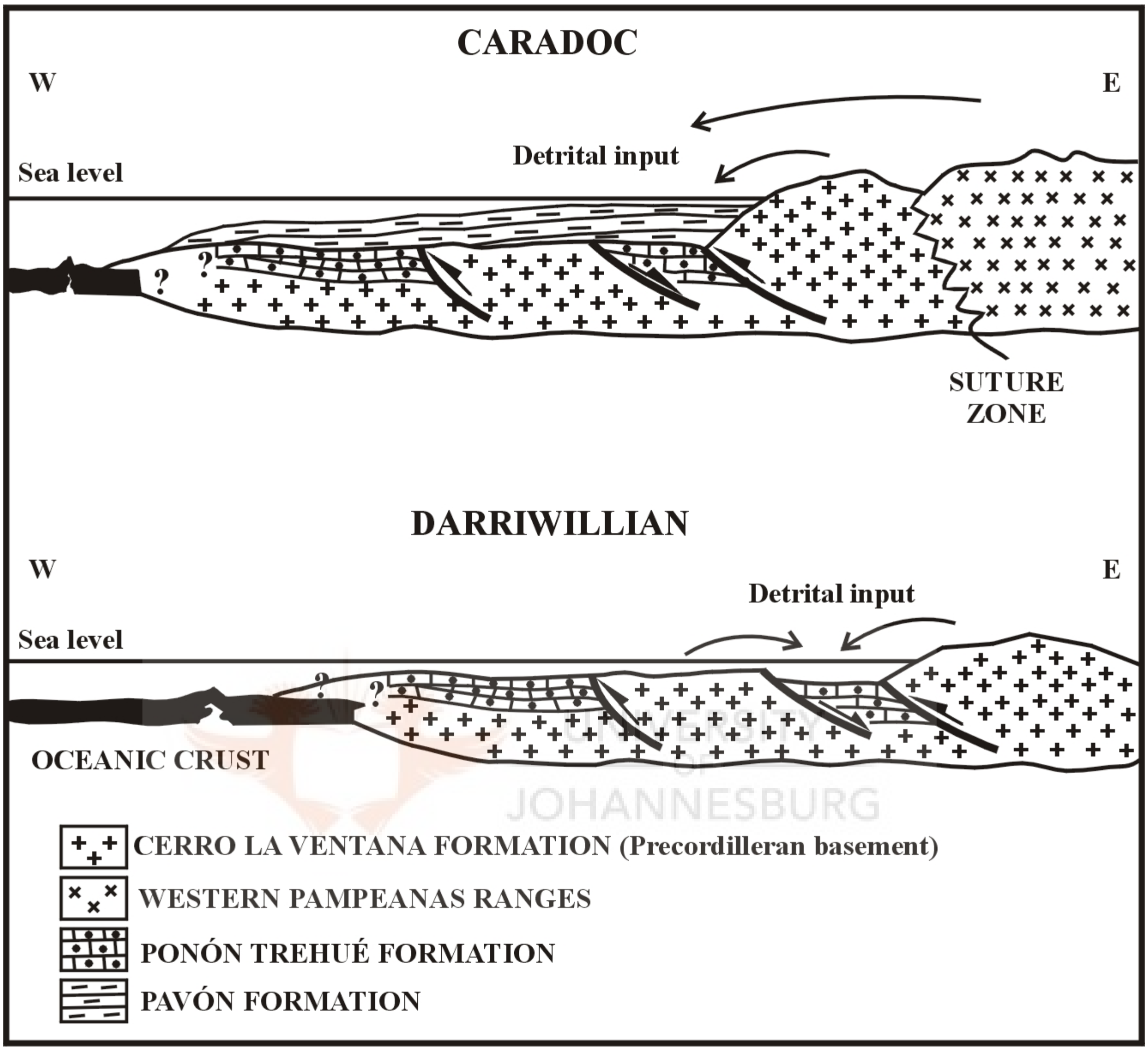

Figure 6.15: Interpretative schematic cross section showing the depositional setting of the two Ordovician units from the San Rafael block (the Pavón and Ponón Trehué Formations). The Ponón Trehué Formation received an input restricted to the Cerro La Ventana Formation (basement of the Precordillera terrane located within the San Rafael block). The progressive subsidence of the basin and the uplift of areas in the Western Pampeanas Ranges provided other eastern sources for the Pavón Formation, apart for the input from the Cerro La Ventana Formation. The basins were most probable generated as a response of the extension that followed the accretion of the Precordillera terrane to Gondwana (Astini, 2002; Heredia, 2006). The contact between the Ponón Trehué and the Pavón Formations is unknown. Modified from Cingolani *et al.* (2003a).

The Nd isotopes of the Ponón Trehué Formation are similar to those from the Pavón Formation, as well as to the Mesoproterozoic basement of the San Rafael block (Cerro La Ventana Formation). Pb isotopes of the Ponón Trehué Formation clearly account for an important influence of a source with high Pb-ratios, particularly $^{207}Pb/^{204}Pb$. Detrital zircon dating further constrains the ages of the sources as almost exclusively Mesoproterozoic (peak at 1.2 Ga), in coincidence with a dominant provenance from the Cerro La Ventana Formation. However, detrital zircon age dating of the Pavón Formation displays Palaeoproterozoic and Neoproterozoic detrital grains, besides two main Mesoproterozoic peaks (at 1.0 and 1.4 Ga).

The comparison between the two Ordovician clastic sequences of the San Rafael block (the Ponón Trehué and Pavón Formations) indicates a similar provenance composition, but the Pavón Formation shows wider ranges of variation of all the provenance indicators. These differences are interpreted in terms of basin evolution, where the Ponón Trehué Formation is an olistostromic sequence deposited within a restricted basin and the sediment supply was from a local source (the Cerro La Ventana Formation), whereas turbidite currents deposited the Pavón Formation within a more open basin and received sedimentary inputs from other sources as well. Following the different models proposed to explain the geotectonic evolution of the Precordillera terrane, several probable sources were tested and the Western Pampeanas Ranges seems to fit better all the provenance constraints. In these regard, an allochthonous origin for the Precordillera terrane is preferred, although extensive studies of the basement rocks are needed, as well as the Pb-isotopic characterization of the Pavón Formation, to further support this.

CHAPTER 7

DETRITAL CHROMIAN SPINELS FROM UPPER ORDOVICIAN DEPOSITS IN THE PRECORDILLERA TERRANE, ARGENTINA: A MAFIC CRUST INPUT.

7.1 INTRODUCTION

The origin and evolution of the Precordillera terrane has been debated for years. Although there is a general consensus about its allochthonous (or para-autochthonous) character, it has not been proved whether the Precordillera is a crustal block derived from Laurentia (Ramos *et al.*, 1986; Dalla Salda *et al.*, 1992ab; Cingolani *et al.*, 1992; Dalziel *et al.*, 1994; Astini *et al.*, 1995; Kay *et al.*, 1996; Keller, 1999), or a block located southwards (present coordinates) in West Gondwana during the Lower Palaeozoic and later displaced by strike-slip movements along the Gondwana margin (Baldis *et al.*, 1982; Aceñolaza *et al.*, 2002; Finney *et al.*, 2003a; 2005).

Several lines of research (sedimentology, biostratigraphy, geochronology, palaeomagnetism, isotope geochemistry) support the palaeogeographic proximity of this terrane to Laurentia (Benedetto, 1993; Lehnert and Keller, 1993; Buggisch *et al.*, 1993; Ramos *et al.*, 1998; Thomas *et al.*, 2001; Rapalini and Cingolani, 2004). Different models were developed to explain the transference from Laurentia to Gondwana (Ramos *et al.*, 1986; Dalla Salda *et al.*, 1992a; Astini *et al.*, 1995; Thomas and Astini, 1996; Dalziel, 1997; Ramos *et al.*, 1998; Keller, 1999; Buggisch *et al.*, 2000). Although all these models assume a collision between the two continents, they differ primarily in the time and type of collision. However, a Gondwana affinity for the Early Palaeozoic was recently provided by U-Pb ages on detrital zircons (Finney *et al.*, 2003a; 2003b; 2004; 2005), focusing the discussion again on the origin of the Precordillera terrane.

The Precordillera *sensu stricto* (see Fig. 7.1a) was initially defined as a geological Province of western Argentina. Since it was considered as a probable exotic mass, the term changed slightly to "Precordillera terrane" (Ramos *et al.*, 1986). The terrane was later expanded to include other exotic blocks, which share the same

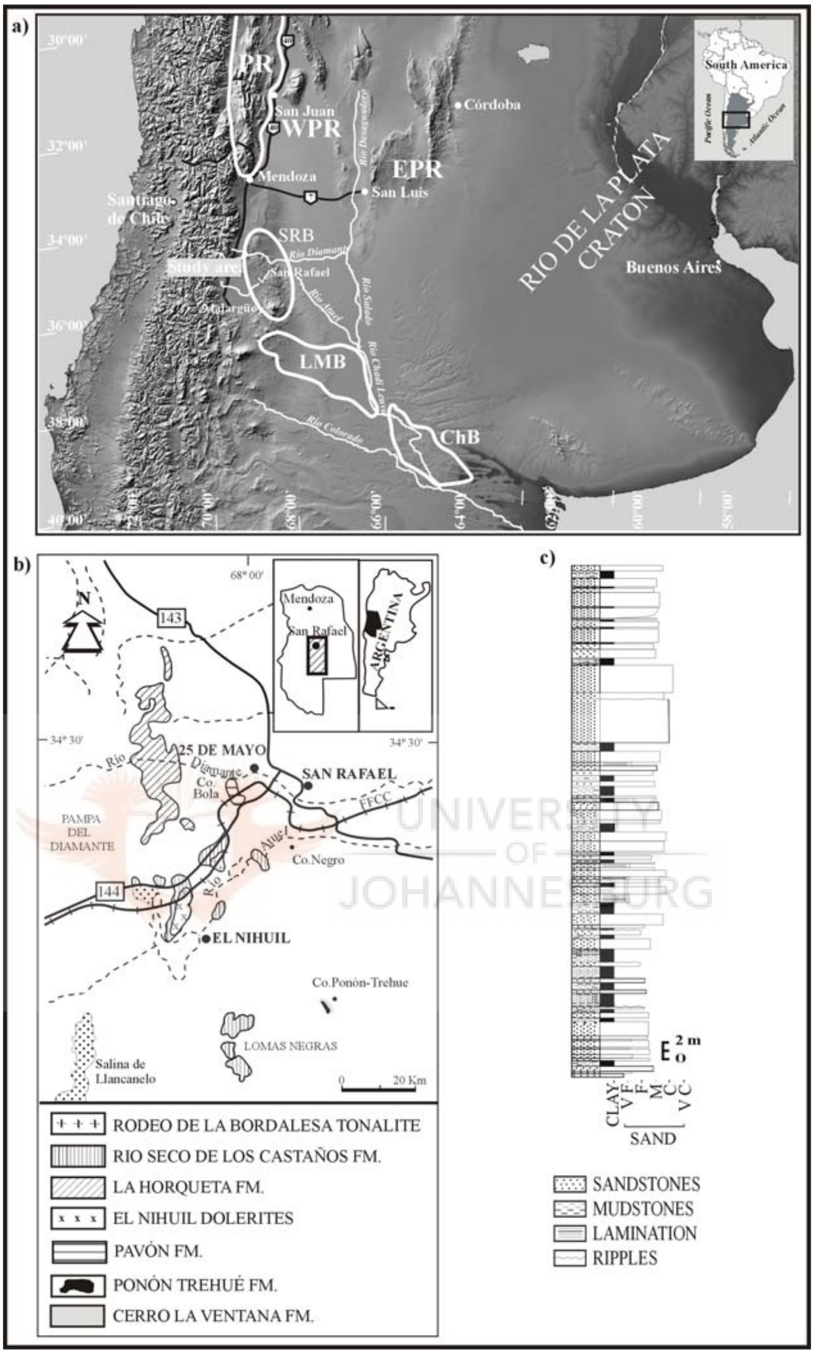

Figure 7.1: a) Location of the Precordillera *s.s.* and San Rafael block, central Argentina. PR= Precordillera *s.s.*; SRB= San Rafael block; LMB= Las Matras block; ChB= Chadileuvú block; EPR= Eastern Pampeanas Ranges; WPR= Western Pampeanas Ranges. b) Geological sketch map of the San Rafael block (SRB area of map a); see outcrops of the Pavón Formation in the central part. c) Simplified stratigraphic section of the Pavón Formation (integrated column) showing the coarsening and thickening upward trend (modified from Manassero *et al.*, 1999); VF: very fine; F: fine; M: medium; C: coarse; VC: very coarse.

characteristics for the Lower Palaeozoic as well as a Grenvillian-type basement, and are currently accepted as the continuation of the Precordillera *sensu stricto* (Astini *et al.*, 1995). It was also named as the "Cuyania composite terrane" (Ramos *et al.*, 1996) including the Western Pampeanas Ranges and the San Rafael and Las Matras blocks (Fig. 7.1a). The existence of the Cuyania or Precordillera terrane was argued by Dalla Salda *et al.* (1992b), who proposed the alternative concept of the Occidentalia terrane, which includes the Precordillera terrane and all the surrounding areas with a Grenvillian-age basement (from Arequipa to Northern Patagonia). The use of the term "Precordillera terrane" in the sense of Astini *et al.* (1995) is preferred throughout this study.

Notwithstanding the relevance in the understanding of the evolution of the Western Gondwana margin, provenance studies of its sedimentary record are scarce. One example is that of Cingolani *et al.* (2003a), who studied the Upper Ordovician Pavón Formation clastic sequence. This unit is part of the San Rafael block, in central western Mendoza Province, Argentina, which represents the southward continuation of the Precordillera *s.s.* These authors stated that the Pavón Formation had a complex provenance history. QFL data indicate an upper continental crust composition source but relative high abundances of V, Cr, Ni, Ti and Sc suggest a mafic input. However, the techniques used did not allow identification of the nature of that mafic source, since it could be derived from a MORB (Mid-Ocean Ridge Basalt) ophiolite, island arc or ultramafic volcanic rocks such as kimberlites or komatiites. In order to decipher the provenance and constrain the tectonic setting and continental evolution, the heavy mineral assemblage was studied.

Heavy minerals are a reliable tool in determining the nature of sedimentary source areas, especially when other techniques (geochemistry, petrography and Nd isotopes) show source mixing, but the origin of these sources are indecipherable. They are particularly useful in studies of sedimentation related to tectonic uplift, as the evolution and unroofing episodes of orogenic belts are reflected in adjacent basin sediments. Analysis of heavy minerals in foreland basins sequences may thus prove valuable in constraining the structural histories of both the basin and the source areas (Mange and Maurer, 1992) and give important clues to the composition of the sources.

Detrital heavy minerals species from the Pavón Formation were identified using a binocular microscope and energy dispersive system (EDS). Spinel chemistry was determined by electron microprobe analysis. Other associated mineral species, e.g. zircon, rutile and apatite have been described previously (Abre *et al.*, 2003) and are not discussed in detail here, as they do not contribute to the characterization of the mafic source. The discovery of detrital chromian spinel (Abre *et al.*, 2005) provides a new insight into the palaeogeographic evolution of the Precordillera terrane, since the spinels represent a remnant of a pre-Caradoc mafic source(s) in Ordovician sedimentary rocks of the southern limb of the Precordillera terrane.

The objective of the present chapter is to describe the composition of the chromian spinels in the heavy mineral assemblage, in order to determine the tectonic setting of their initial host rocks. Different areas surrounding the Precordillera terrane are tested as probable sources in relation to the models that attempt to explain the geotectonic evolution of this terrane.

7.2 GEOLOGICAL BACKGROUND

The Pavón Formation crops out in the central region of the San Rafael block, Mendoza province, central Argentina (Fig. 7.1a). It is bounded by the Cuyo and Neuquén oil basins to the north and southwest respectively, by the Andean Cordillera to the west and is overlain by modern cover towards the east. The San Rafael block comprises Precambrian and Lower-Middle Palaeozoic rocks (Fig. 7.1b), which are clearly separated from Upper Palaeozoic strata by a regional unconformity. Permian-Triassic magmatism and Cenozoic volcanism are present. The San Rafael block is a key area in the evolution of the proto-Andean margin of south western Gondwana, as it is considered a southward continuation of the proposed Laurentian-derived Precordillera terrane.

As summarized by Cingolani *et al.* (2003a) and references therein, the Pavón Formation is a massive, thick (700 m) clastic series composed of arenites, greywackes, silicate-siltstones and claystones (Fig. 7.1c). Illite Crystallinity Index suggests very low-grade metamorphic conditions (Manassero *et al.*, 1999). A rich graptolite fauna found in several levels provides an Early Caradoc age (*Climacograptus bicornis* Biozone; Cuerda *et al.*, 1998). The sequence was deposited as sandy marine turbidites (Manassero *et al.*, 1999). Sandstones have 15% to 30% matrix, poor to moderate sorting and fine to very fine grain sizes. They are composed of quartz, K-feldspar, plagioclase, sedimentary and metamorphic lithoclasts, biotite, muscovite, zircon, apatite, magnetite and hematite (Cingolani *et al.*, 2003a). Petrographic provenance analysis suggests a recycled orogen and a continental block as the main source areas (Manassero *et al.*, 1999). Geochemical data demonstrated that the Pavón Formation displays detrital components of an upper continental crust composition mixed with a less fractionated component (Cingolani *et al.*, 2003a). Th/Sc and Zr/Sc ratios reflect significant reworking with most input from upper crustal sources. However, Cr, Ni, V, Ti and Sc concentrations are enriched relative to average continental crust composition. The general character of the less fractionated source was interpreted as a mafic to ultramafic component (Cingolani *et al.*, 2003a). Nd model ages of Pavón sandstones scatter around 1.4 Ga, with an affinity to Grenvillian-age crust, and they differ significantly from the general Gondwana-like signature in northwestern Argentina (Cingolani *et al.*, 2003a).

The Pavón Formation clastic sequence was deposited in a foreland basin at latitude of 25.7º ± 2.9º S (Rapalini and Cingolani, 2004). This basin was related to the accretion of the Precordillera terrane located west of Gondwana; this accretion caused uplift by thrusting of the Grenvillian-age crust to the east at c. 460 Ma (Ramos *et al.*, 1996; Cingolani *et al.*, 2003a).

7.3 ANALYTICAL TECHNIQUES

Five wacke samples were crushed and sieved to less than 100µm. The size of the fraction was selected in order to avoid confusing results because of the hydrodynamic fractionation shown by samples with different grain sizes (Morton and Hallsworth, 1994). From the less than 100µm population a pre-concentrate of the heaviest fraction was obtained by settling in a back current of water active in a glass tube. This pre-concentrate was treated with bromoform (δ = 2.89) to obtain the complete heavy minerals fraction. The heavy minerals separation laboratory of the Centro de Investigaciones Geológicas (La Plata University, Argentina) was used for work.

The heavy mineral fraction was embedded randomly into epoxy resin, polished and carbon coated. The identification and characterization (shape, size, fractures, inclusions) of the heavy minerals were done using a binocular microscope, scanning and backscattered electron microscope using energy dispersive spectrometry (SEM-BSE-EDS). A JEOL JSM-5600 with a tungsten filament was used and EDS analyses were undertaken using a Noran X-ray detector and Noran Vantage software. The SEM-BSE-EDS system was set at 15 keV, a working distance of 20 mm and a live time of 60 s per spot.

Quantitative analyses of the spinels were carried out with a Cameca 355 electron microprobe equipped with an Oxford link integrated WDS/EDS, set at a voltage of 15 keV, and with a JEOL 733 with WDS/EDS set at a voltage of 15 keV. Beam current diameter in both microprobes was between 8 to 10 microns; ZAF corrections were effected under standard procedures. Chromite standard on MAC certified standard no. 2590 was used for analysis. The Centralized Analytical Facility (SPECTRAU), University of Johannesburg, South Africa, provided all the abovementioned analytical equipment.

As only total iron is measured with the electron microprobe, the stoichiometric compositions of the spinels were calculated using Visual Basic macro in Microsoft Excel based on the stoichiometric formula of spinels, in order to discriminate Fe^{2+} and Fe^{3+}. Accuracy and precision of such calculations are imperfect (i.e. Wood and Virgo, 1989). However, these errors become significant for calculating oxygen fugacity, but are precise and accurate enough to obtain Fe^{3+} and Fe^{2+} concentrations (Wood and Virgo, 1989). Each grain was measured several times (two to five spots) depending on grain size and then an average composition was computed (Table 7 in Appendix A), as differences due to fractionation could not be observed in any one grain.

7.4 ANALYTICAL RESULTS

The detrital heavy mineral assemblage is predominantly composed of zircon, spinel and rutile in order of abundance; these are widely known as ultrastable phases since they are mechanically and chemically resistant to sedimentary degradation (Morton and Hallsworth, 1999). Less abundant are apatite and sphene (Abre *et al.*, 2003). Only few heavy minerals could be used for provenance studies using microprobe analytical techniques. In this chapter, the focus is on spinels as indicators of a mafic to ultramafic source, which could give some important insights on the palaeotectonic setting of Ordovician deposits from the Precordillera terrane.

Spinel grains contained in sedimentary rocks can provide important information regarding source areas closely related to the depositional site (Arai, 1992; Oberhänsli *et al.*, 1999; Asiedu *et al.*, 2000; Garzanti *et al.* 2000; 2002; Zhu *et al.*, 2004). The main tool to decipher the nature of the source is geochemical analysis of individual grains, as melting and crystallization processes depend on tectonic setting, and can be recorded in the chemistry of a single grain (Dick and Bullen, 1984; Kamenetsky *et al.*, 2001; Barnes and Roeder, 2001). In this study, mafic to ultramafic rocks are known to be the source of detrital record for the Pavón Formation and the spinels will give some important clues regarding the nature of this source.

The spinels occur in fine grained, poor to moderate sorted wackes of the Pavón Formation. The Cr concentration of this unit varies between 65 ppm and 292ppm and has an average of 139ppm (Cingolani *et al.*, 2003a), which represents an enrichment compared with the average Cr concentration of wackes and shales (Cr = 67ppm and 88ppm respectively according to Taylor and McLennan, 1985). The layers sampled for this study show elevated Cr concentrations of 152ppm in average.

Spinel is a mineralogical group of oxides with a general formula AB_2O_4, were A= Fe^{2+}, Mg, Mn, Zn, Ni, Ca and B= Fe^{3+}, Al, Cr, Ti, V, Si. It is subdivided according to whether the trivalent ion is Al (spinel series), Fe^{3+} (magnetite series) or Cr (chromite series). The chromite series is known as chromian spinel or brown spinel, and consists of two minerals: magnesiochromite and chromite. Pure end-members of the spinel group are rare in nature. Chromites have a wide range in composition because of the substitutions of Mg for Fe^{2+} and of Al and Fe^{3+} for Cr. Based on their chemical composition the term chromian spinel is used here for the spinels in the Pavón Formation. "Spinel" is used to name the entire group (in a broad sense) and spinel *sensu stricto* (*s.s.*) to refer to the Al-rich series.

The chemical composition of the separated chromian spinels varies markedly: the Cr# = Cr/ (Cr+Al) atomic ratios range from 0.40 to 0.77 and the Mg# = Mg/ (Mg+Fe^{2+}) atomic ratios range from 0.2 to 0.8 (Table 7 in Appendix A). Cr concentration has an average of 41.1%, the Fe^{2+}/Fe^{3+} ratio ranges between 1.7 and 5.0. Spinels with highest Cr# have also high TiO_2 (up to 4.7%) and total Fe concentrations, while Al_2O_3 and MgO are low (Table 7 in Appendix A).

Based on chemistry, the data could be separated into two groups. Group 1 involves 60% of the grains (plotted as crosses in Figures 7.3 to 7.7), has a narrow range in Cr# (0.47 to 0.58) but an expanded range in Mg# (0.50 to 0.80); they have lower TiO_2 (less than 0.60%) and Fe^{3+}# ratio (Fe^{3+}# = Fe^{3+}/ (Cr+Al+Fe^{3+})) compared with Group 2. MnO, V_2O_5, NiO and ZnO concentrations are very low (Table 7 in Appendix A). Both groups of chromian spinels were found together within the same sampled layers.

Group 2 comprises 40% of the spinel grains with a distinctive chemical composition (represented as squares in Figures 7.3 to 7.7); they show very high TiO_2 (between 1.7% and 4.7%, average = 2.97%) and Fe^{2+} concentrations (average 23.2%), and display the highest Cr# (average 0.72) and the lowest Mg# (average 0.39). MnO, V_2O_5, NiO and ZnO concentrations are also very low (see Table 7 in Appendix A).

Morphologically the two groups are indistinguishable, since SEM and BSE microphotographs (Figs. 7.2a and b) show sizes ranging from 40µm to 110µm with an average of 60µm for both, and the proportion of subhedral, anhedral and euhedral grains are also equal in both groups. They do not show any visible zonation, intergrowth or inclusions. Under the binocular microscope, high- and low-TiO_2 chromites are black.

7.5 SPINEL PROVENANCE

Detrital chromian spinel is an abundant and important heavy mineral in sedimentary rocks. It is chemically and mechanically stable and is often the only remnant of tectonic slabs of oceanic crust involved in collision zones (Pober and Faupl, 1988). Chromite is the only igneous mineral that is commonly preserved in metamorphosed serpentinite (Proenza *et al.*, 2004; Ahmed *et al.*, 2005). Chromian spinel is an important petrogenetic indicator in mafic and ultramafic rocks, because it contains several cations whose atomic ratios vary according to physico-chemical conditions of the parent magma such as composition, cooling rate, crystallization temperature and f_{O2} (Irvine, 1965; 1967; Evans and Frost, 1975; Dick and Bullen, 1984; Sack and Ghiorso, 1991; Arai, 1992). Because the degree of magma melting determines the chemistry of chromites, and melting conditions depend on geotectonic setting, chromites are widely used in classifying mantle-derived peridotites according to their origin and tectonic setting (Dick and Bullen, 1984; Kamenetsky *et al.*, 2001). Detrital chromian spinel grains are also used in provenance studies of the sedimentary record (Pober and Faupl, 1988; Arai, 1992; Oberhänsli *et al.*, 1999; Asiedu *et al.*, 2000; Garzanti *et al.*, 2000; 2002; Zhu *et al.*, 2004).

Chromian spinel might exhibit chemical zoning due to changes in the composition of both melt and solid phases during crystallization. Assuming that the well-developed crystal boundaries of subhedral grains may preserve the original chemical zonation in detrital grains, microprobe profiles were constructed in order to determine any type of variation. No compositional variations were determined, as there is no difference between core and rim, neither intergrowths nor exsolution of other mineral species. These can be seen in Figure 7.2a and b where high- and low-TiO_2

spinels (Group 2 and Group 1 respectively) are shown. A microprobe profile on a spinel from Group 2 is shown in order to demonstrate that there is no chemical zoning (Fig. 7.2a). However, no spinels from Group 1 show any chemical zoning either. This homogeneous pattern indicates that there was no sub-solidus re-equilibration between spinels and other minerals (Scowen *et al.*, 1991).

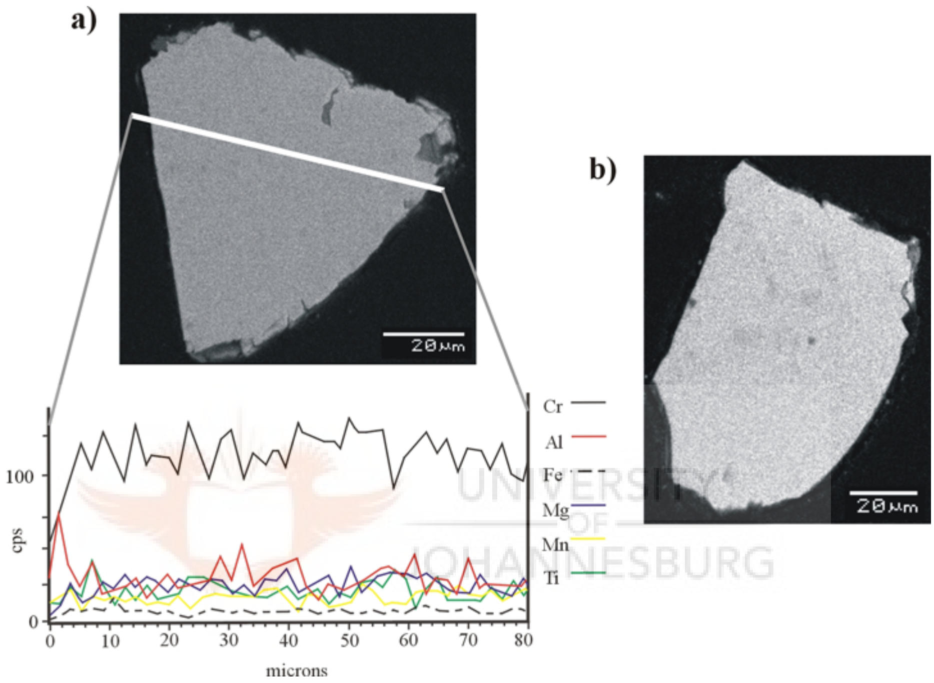

Figure 7.2: a) High TiO_2 chromian spinel from Group 2 under SEM and its microprobe profile showing no chemical zoning. b) Detrital spinel of Group 1 under SEM, which do not show any chemical zoning either. Bar length is 20µm; cps: counts per second.

Kamenetsky *et al.* (2001) proposed a differentiation between volcanic and so-called "mantle" spinels based on chemical parameters. Mantle spinels have TiO_2 less than 0.2% and Fe^{2+}/Fe^{3+} more than 2 while those of volcanic origin have higher TiO_2 concentrations and Fe^{2+}/Fe^{3+} less than 2. TiO_2 concentrations of Group 1 scatter around 0.4% while Group 2 is well above the 0.2% limit (Table 7 in Appendix A). Based on only such a value (Zhu *et al.*, 2004), a volcanic origin is preferable for the whole dataset.

Tri- and tetravalent cations in spinel experience almost no variation due to re-equilibration after entrapment because of their low diffusivity in minerals (like olivine), thus they are useful to discriminate mantle source of the host rocks of the spinels (Kamenetsky *et al.*, 2001). For example, spinel Al_2O_3 and TiO_2 concentrations depend on the parental melt composition and therefore, their relationship allows the discrimination between different tectonic settings (Kamenetsky *et al.*, 2001). In Figure 7.3, Group 1 plots entirely as MORB-related and an arc environment can be discounted. Group 2 displays a continuous array from LIP (Large Igneous Provinces) to OIB (Oceanic Island Basalt) fields.

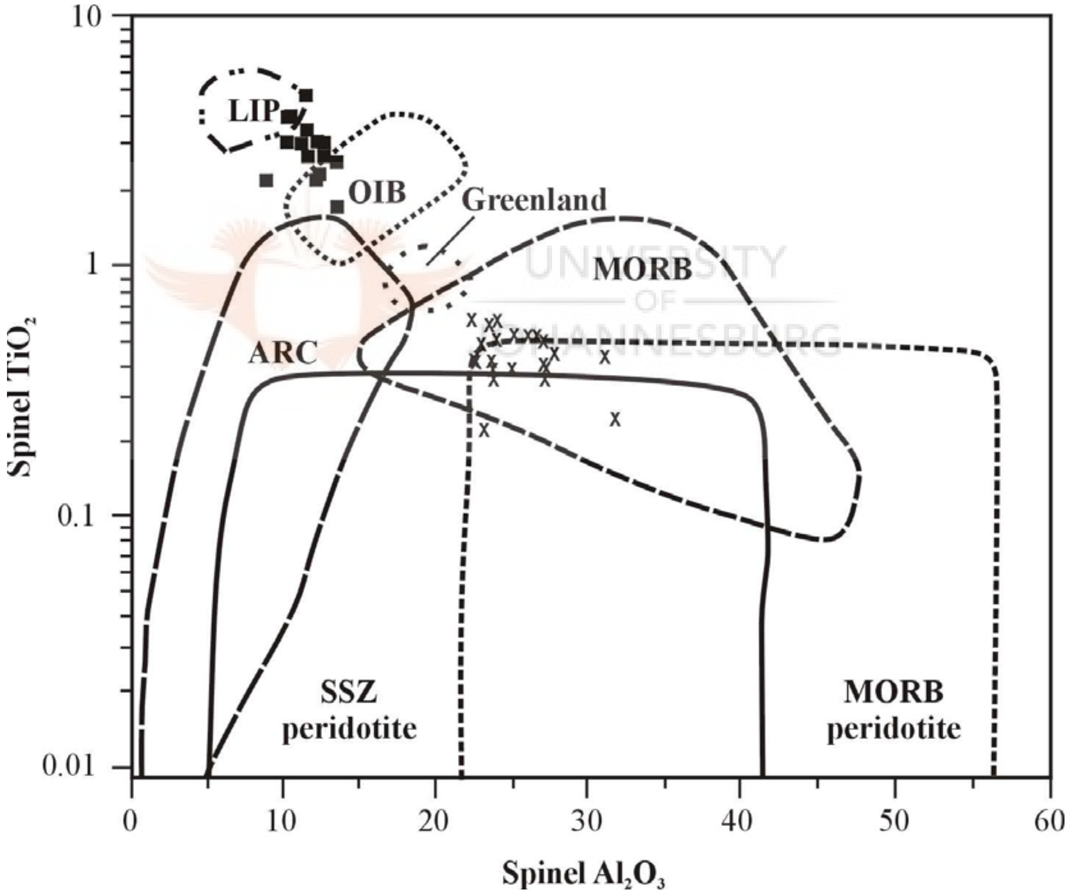

Figure 7.3: Spinel TiO_2 vs. Spinel Al_2O_3 after Kamenetsky *et al.* (2001). Group 1 is represented by crosses and it plots as MORB, while Group 2 is represented by squares and it plots in the LIP and OIB fields and between them. SSZ: supra-subduction zone; OIB: ocean island basalts; LIP: large igneous provinces; MORB: mid-ocean ridge basalt.

Chromian spinels from the Pavón Formation have the same composition as the 'tholeiitic basalts and boninites' group from Barnes and Roeder (2001). They are in particular, especially comparable to MORB (Group 1) and to continental flood basalts (Group 2; equivalent to LIP in the sense of Kamenetsky *et al.*, 2001), while they differ significantly from ophiolitic basalts, boninites, ocean islands, Hawaiian lava lakes and island arcs. In the Fe^{3+}# - Fe^{2+}# diagram (Fig. 7.4) spinels from Group 1 plot mainly in the ocean floor basalts field within the 50th percentile line (Fig. 7.4a), while Group 2 plots in the flood basalts field and within the 90th percentile (Fig. 7.4b).

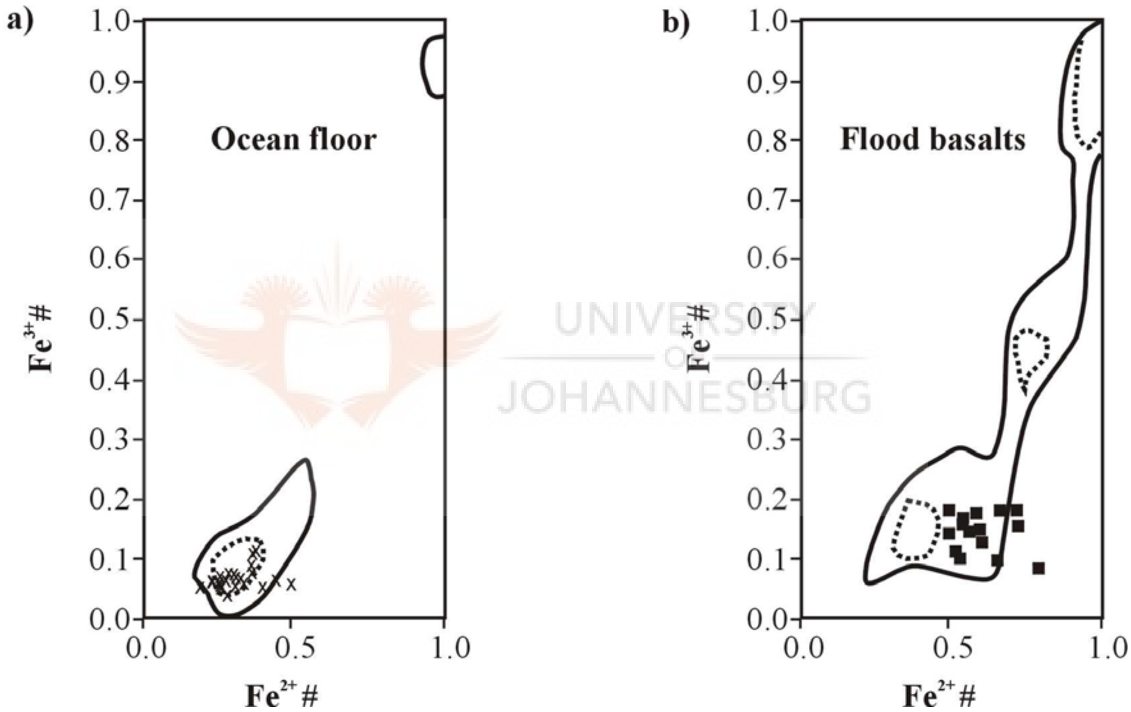

Figure 7.4: Fe^{3+}# - Fe^{2+}# relationships based on Barnes and Roeder (2001). The continuous line represents the 90th percentile while the dotted line encloses the 50th percentile. a) Spinels from Group 1 (crosses) and ocean floor basalts fields for comparison. b) Spinels from Group 2 (squares) and flood basalts fields for comparison.

In the TiO_2-Fe^{3+}# diagram (Fig. 7.5), Group 1 plots in the ocean floor basalts field again and within the 50th percentile (Fig. 7.5a); Group 2 plots slightly above the 50th percentile line of the continental flood basalts field, due to their higher Ti concentration (Fig. 7.5b). In the Cr-Fe^{2+}# diagram (Fig. 7.6), spinels from Group 1 plot in the ocean floor field, within the 50th percentile line (Fig. 7.6a); Group 2 plots in the continental flood basalts field, within both, 50th and 90th percentiles (Fig. 7.6b).

In the Fe^{3+}-Cr-Al triangular diagram (Fig. 7.7), Group 1 plots within the 90th percentile of the ocean floor field (Fig. 7.7a) whereas Group 2 plots within the 90th percentile of the flood basalts field (Fig. 7.7b). However, in all diagrams, Group 1 has a close similarity to basalt xenoliths, but this is not important in the case of provenance analysis, due to their scarcity and low probability of being an important source. Furthermore, spinels from Group 2 correlate with continental flood basalts and are similar to continental mafic intrusions; this is because the dataset for this latter category includes data from some subvolcanic intrusions in flood basalt provinces (Barnes and Roeder, 2001).

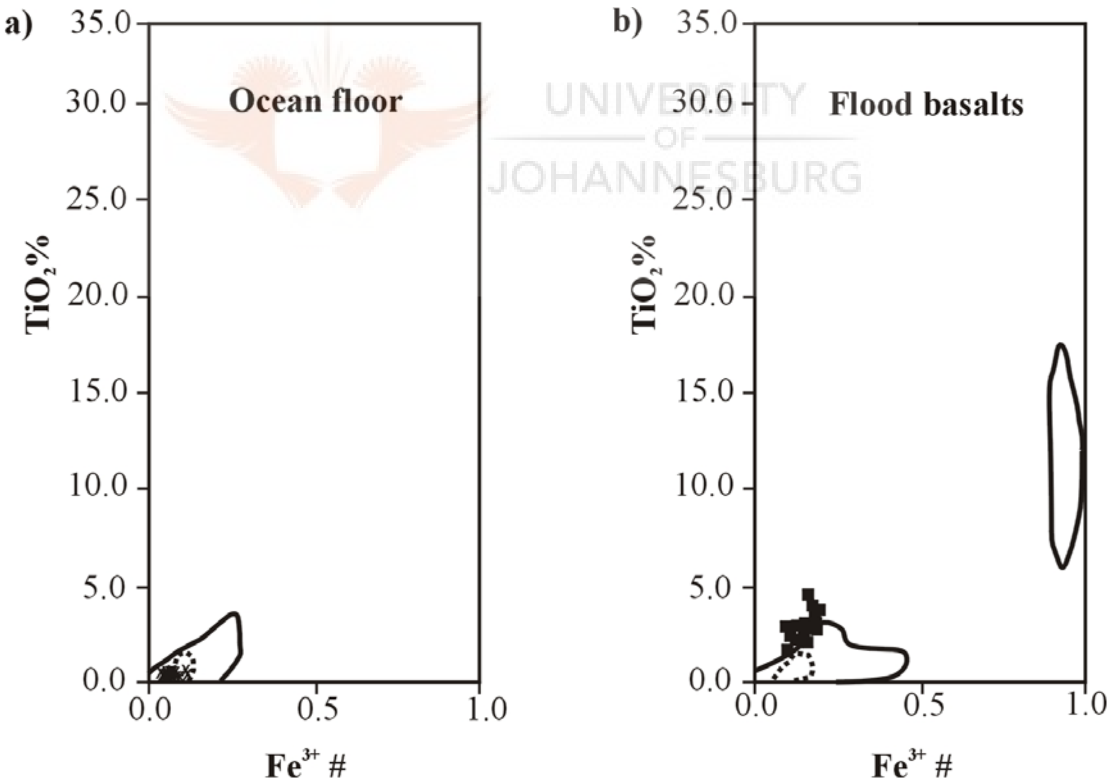

Figure 7.5: TiO_2% – Fe^{3+}# diagram from Barnes and Roeder (2001). Sample references are as in Figure 7.3 and field references as in previous Figure. a) Spinels from Group 1 plot as ocean floor related. b) Spinels from Group 2 plot as continental flood basalts.

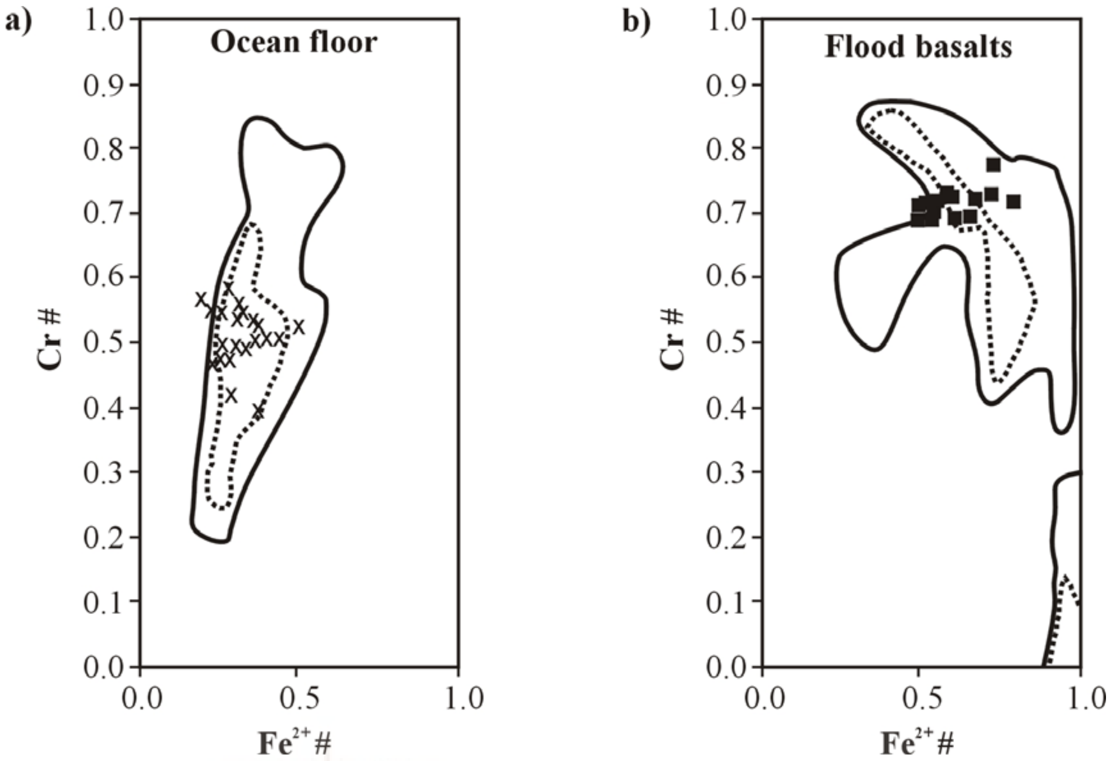

Figure 7.6: Cr# - Fe^{2+}# based on Barnes and Roeder (2001). References are as in Figures 7.3 and 7.4. a) Group 1 is clearly ocean floor related while Group 2 plots as flood basalts (b).

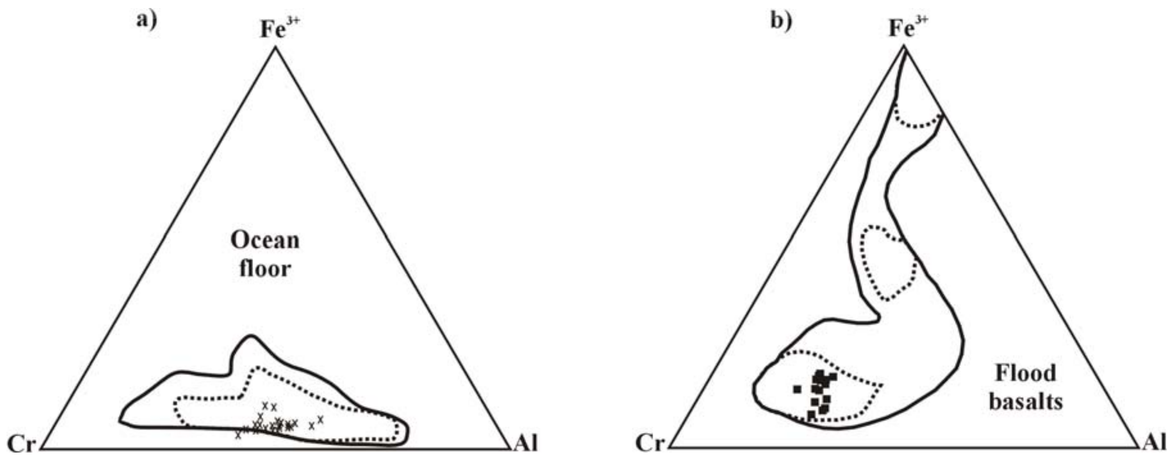

Figure 7.7: Fe^{3+} - Cr – Al triangular diagram from Barnes and Roeder (2001). References are as in Figures 7.3 and 7.4. The detrital spinels from the Pavón Formation plot within the ocean floor fields (a) and within the flood basalts field (b).

7.6 SOURCE ROCKS

Previous provenance studies (Cingolani *et al.*, 2003a) have shown that the Pavón Formation is of upper continental crust composition mixed with a less fractionated component. The upper continental crustal component is represented by recycled sedimentary rocks and metamorphic fragments, as well as by the product of erosion of igneous rocks (for example, as determined by the analyses of cathodoluminescence images on zircons; Abre *et al.*, 2003). The mafic or ultramafic element is represented by detrital spinels, and is responsible for the less fractionated component in the geochemistry and probably in the Nd-isotope geochemistry (Cingolani *et al.*, 2003a).

The detrital chromian spinels of the Pavón Formation were formed within a mid-ocean ridge basalt (Group 1) and continental flood basalts (Group 2). The location of the source rocks of these detrital spinels is important regarding the tectonic history and the debated origin of the Precordillera terrane. Possible source areas of mafic to ultramafic rocks that are older than Caradoc from the Precordillera and adjacent areas are shown in Figure 7.8 (terrane boundaries are based on Ramos *et al.* (2000) and Porcher *et al.* (2004) among others).

i) In the Western Precordillera ("a" in Fig. 7.8), a series of discontinuous outcrops of mafic and ultramafic rocks were first assigned to a 'Famatinian Ophiolite' sequence (Haller and Ramos, 1984) and interpreted as the suture between the Chilenia and Precordillera terranes (Ramos *et al.*, 1986). However, detailed studies carried out by Davis *et al.* (1999) show the presence of a number of ophiolite-like units with ages ranging from Middle Proterozoic to Early Palaeozoic and juxtaposed in the Early to Middle Devonian.

Despite these interpretations, the Western Precordillera Belt is composed of a Late Proterozoic ophiolite (Davis *et al.*, 1999), Ordovician basalts and pillow lavas interlayered with Caradoc wackes (Kay *et al.*, 1984; 2005) which form a belt extending into the San Rafael block (Cingolani *et al.*, 2000; see below), as well as Late Silurian basaltic flows and dykes. More recently, the Chuscho Formation was also considered as part of the Belt (Fauqué and Villar, 2003). This unit is interlayered with Ordovician

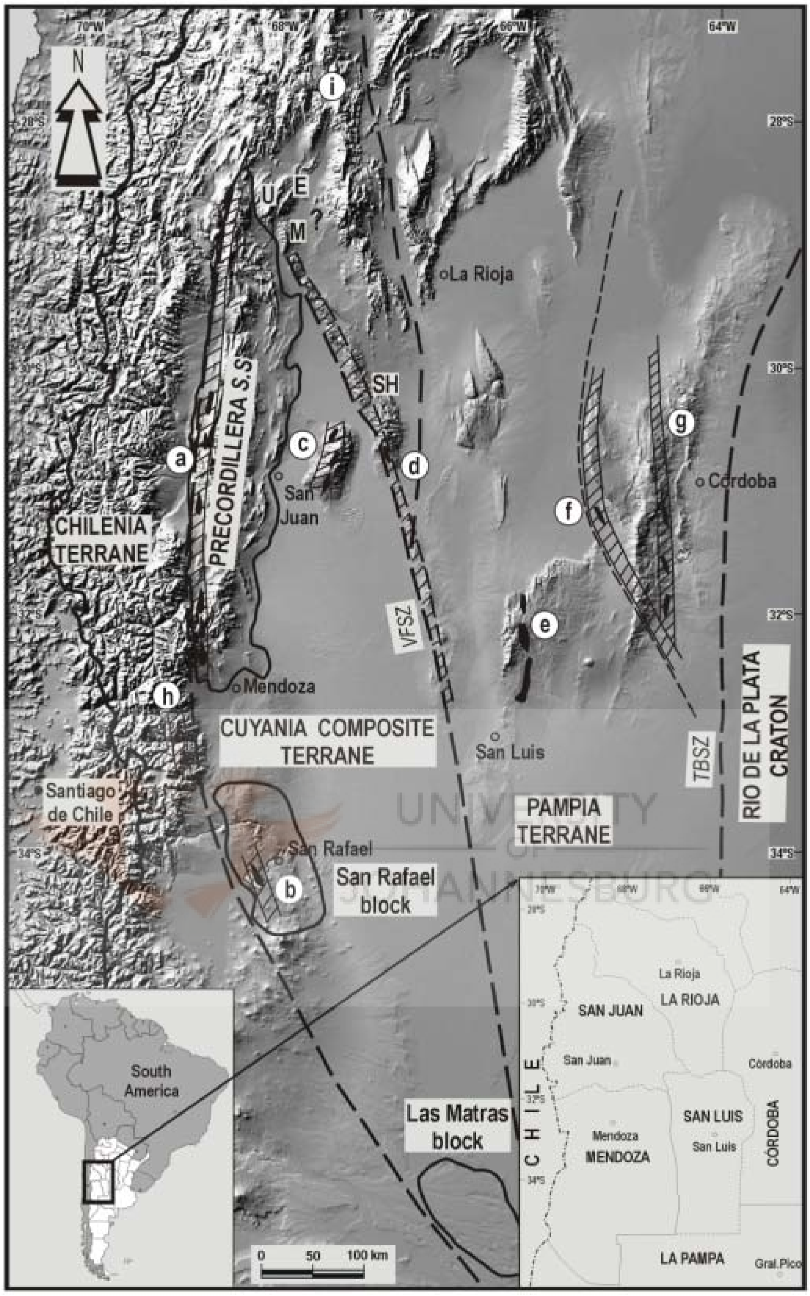

Figure 7.8: Mafic to ultramafic belts considered as possible source areas of detrital chromian spinels. Terrane boundaries based on Ramos *et al.* (2000) and Porcher *et al.* (2004). a: Western Precordillera Belt; b: El Nihuil mafic body; c: Pie de Palo Belt; d: Valle Fértil Shear Zone; e: Virorco – Las Águilas Belt; f: Western Córdoba Belt; g: Eastern Córdoba Belt; h: Cordillera Frontal Belt; i: Fiambalá Range complex. In black: mafic and ultramafic outcrops; sutures zones are marked by hatched lines while terranes boundaries by dashed lines. VFSZ= Valle Fértil Shear Zone; TBSZ= Trans-Brazilian Shear Zone; U= Umango Range; M= Maz Range; E= Espinal Range; SH= Sierra de la Huerta. Right side inset shows detail of the geographic location within Argentina and Chile.

phyllites of the Río Bonete Formation and it is composed of diabase sills, basalts and tholeiitic pillow lavas. All these units were formed in different extensional settings and at different times (Davis *et al.*, 1999; 2000). However, all have ε_{Nd} ranging from +6 to +9 (Kay *et al.*, 2005) and were interpreted as E-MORB related (e.g. Kay *et al.*, 1984). The northern part of the Western Precordillera Belt was interpreted as a segment of a transitional to plume-type mid-ocean ridge or unevolved back-arc basalts, whereas the southern part has a within plate origin or a plume or plateau setting (Ramos *et al.*, 2000 and references therein).

Spinels and chromites were described from certain areas (Davis *et al.*, 1999; Villar, 2003) but no chemical analyses are published. Although it is not possible to accept or reject this Belt as a potential source area, the fact that some mafic rocks are interlayered with Caradoc clastic rocks suggests cannibalistic processes that reworked detritus (specifically chromian spinels) from the magmatic rocks into the sedimentary sequence. The high TiO_2 concentration of these volcanic rocks supports this argument.

ii) In the San Rafael block, Mendoza Province, a mafic body known as El Nihuil ("b" in Fig. 7.8) has been described by Cingolani *et al.* (2000). It is Pre to Upper Ordovician with MORB affinities and contains ultramafic differentiates associated with tholeiitic diabases. Chromites were not described from these rocks. As the San Rafael block is a southern continuation of the Precordillera terrane, this mafic body was interpreted as a part of the Western Precordillera Belt (Haller and Ramos, 1984; Cingolani *et al.*, 2000; "a" in Fig. 7.8).

iii) Pie de Palo Belt ("c" in Fig. 7.8), Western Pampeanas Ranges, San Juan Province, where a Grenville-age ophiolite assemblage with island arc or back-arc affinities containing chromites and successively high concentrations of chromium have been described (Vujovich and Kay, 1998). This Belt was interpreted as the amalgamation of the Precordillera and the Pie de Palo terranes (Cuyania composite terrane), before their accretion to Gondwana (Vujovich and Kay, 1998) or as part of the pre-Famatinian Gondwanan autochthonous (Casquet *et al.*, 2006). It has been subjected to high-grade metamorphism. Although two main, different protoliths were distinguished, (ultramafic cumulates and lava flows, both related to an arc environment), different rock types were associated to different oceanic settings and different crustal thicknesses. A magmatic arc on a thin continental crust or oceanic crust, a magmatic arc on a thick crust related to compression, or a magmatic arc and oceanic back-arc (Vujovich and Kay, 1996). No spinel chemistry is currently available for any of the lithologies. However, it is known that the ultramafic cumulate chromites are Cr-rich (Vujovich and Kay, 1998). Based on these facts, it is expected that the composition of the chromite would be rather different from those from the Pavón Formation. The unit with protolith lava flows has normal MORB characteristics, but no information about spinels content is available.

iv) Valle Fértil shear zone ("d" in Fig. 7.8), is a lineament associated with mafic to ultramafic bodies. At Sierra de La Huerta (Western Pampeanas Ranges; see Fig. 7.8) a high grade metamorphic Precambrian to Lower Palaeozoic basement is composed of metasedimentary and meta-igneous rocks whose protoliths formed in an island arc or a back-arc (Vujovich and Kay, 1996). The mafic and ultramafic rocks contain green spinels with high Al, Fe and Mg concentrations but very low Cr. Some grains present a magnetite-rich rim due to metamorphism (Castro de Machuca *et al.*, 1996). Therefore, they differ from the detrital spinels found in the Pavón Formation.

The Umango, Maz and Espinal Ranges were considered part of Western Pampeanas Ranges, although their association with the Precordillera terrane is still under investigation (Porcher *et al.*, 2004; Vujovich *et al.*, 2005). They are composed of amphibolites and rare ultramafic rocks and were interpreted as an arc or back-arc unit (Vujovich and Kay, 1996). However, some amphibolites were interpreted as less evolved lavas with transitional composition between alkaline and tholeiitic and from an intraplate or back-arc environment. Others are related to an oceanic arc developed on a continental crust. They are Grenville in age (Varela *et al.*, 1996). No chromites have been described.

v) Virorco – Las Águilas Belt, San Luis Province ("e" in Fig. 7.8), where a mafic to ultramafic Precambrian to Palaeozoic layered intrusion is present. It contains chromian spinels classified by Ferracutti *et al.* (2004) according to Barnes and Roeder (2001) as crystallized in a mafic-layered intrusion. Comparing the diagrams presented by Ferracutti *et al.* (2004) with the dataset from Pavón Formation, there is a clear difference between them, since our dataset shows less Al and more TiO_2 concentrations and less Fe^{2+}# for a given Cr#. Furthermore, the spinels from this Belt show ferritchromite and chromium-rich magnetite rims produced by metamorphism (Ferracutti *et al.*, 2004). According to von Gosen and Prozzi (1998), the mafic to ultramafic Belt underwent several phases of metamorphism and deformation, reaching amphibolite facies during Middle to Late Ordovician.

vi) Western Córdoba Belt ("f" in Fig. 7.8), where ultramafic serpentinised peridotites contain magmatic chromite, ferritchromite and spinels *sensu stricto*. These rocks underwent amphibolite to granulite facies metamorphism, but the spinels have preserved cores whose chemical compositions define them as from podiform bodies (Mutti *et al.*, 2000). It should be noted that Pavón Formation lacks ferritchromite and spinels *s.s.* On the other hand, the chromites from the Western Córdoba Belt have a variable chemical composition (Cr_2O_3 = 11% to 47%, Al_2O_3 = 2% to 32%, total FeO = 18% to 81%, MgO 2% to 17%) and it should be ruled out as a source area.

vii) In Eastern Córdoba Belt ("g" in Fig. 7.8), there is an ophiolitic sequence developed in the Sierra Grande de Córdoba (Eastern Pampeanas Ranges), with chromian spinels, chromium-rich magnetite and iron-rich spinels, all of a magmatic origin and overprinted metamorphic characteristics. According to chromian spinels chemical data presented by Villar *et al.* (2001), they differ from the detrital grains found in the Pavón Formation mainly because the former have lower Cr_2O_3 (16% to 32%) and FeO (7% to 16%) concentrations and higher Al_2O_3 (38% to 48%) and MgO (15% to 20%) concentrations.

viii) In the Cordillera Frontal ("h" in Fig. 7.8), the Guarguaráz Complex contains bodies of ultramafic serpentinised rocks fault-emplaced into a metasedimentary sequence (López and Gregori, 2004). These ultramafic rocks contain zoned spinels, which show a different composition in two different localities. At Las Tunas, the chromites have Zn-rich Al-chromite cores (interpreted as relict magmatic cores) and ferritchromite rims surrounded by outer Cr-magnetite rims while those spinels from Salamanca (Cuchilla de Guarguaráz) district have a ferritchromite core and a chromium-rich magnetite rim (Bjerg *et al.*, 1993). Although the metamorphism that affected these rocks is considered to be Devonian in age (which means, after the deposition of the Pavón Formation), their cores are interpreted as relict magmatic, so they could still be used for comparison with the detrital grains from the Pavón Formation. Therefore, both groups of spinels are completely different to the detrital ones from the Pavón Formation. Tholeiitic basalts and metabasites with E-MORB affinities were also described in the Guarguaráz Complex. This Complex was also considered the continuation of the Western Precordillera Belt (Haller and Ramos, 1984, and others), but provenance analyses indicate that the Guarguaráz Complex and equivalent units from the Precordillera terrane share a common evolution (López and Gregori, 2004).

ix) The Early Cambrian gabbroic complex from the Fiambalá Range ("i" in Fig. 7.8), contains magmatic chromian spinels that were metamorphosed and has been interpreted as a stratified arc complex (Villar and Escayola, 1996). Chemical data presented by Villar *et al.* (2001) shows that their composition is characterized by very low Cr_2O_3 concentrations (3% to 6%), high Al_2O_3 (43% to 56%), low FeO and Fe_2O_3 (12% to 15% and 1.2% respectively). Although they have similar MgO concentration compared with chromian spinels from Pavón wackes, they are rather different (see Table 7 in Appendix A).

In summary, chemical analyses of spinels provided from the Valle Fértil shear zone, Virorco – Las Águilas Belt, Western and Eastern Córdoba Belts, Guarguaráz Complex of the Cordillera Frontal and the gabbroic complex from the Fiambalá Range, show differences with the chemical composition of spinels from the Pavón Formation, making these rocks unlike sources. On the other hand, the Western Precordillera Belt and its southern extension ('El Nihuil mafic body'), and the mafic rocks of the eastern side of the Precordillera (Pie de Palo Belt, Umango, Maz and Espinal Ranges) cannot be ruled out as source. However, chemical analyses of the spinels described are needed, as well as a better knowledge of the mafic rocks within certain areas, to definitively either accept or reject these rocks as sources.

Palaeocurrents (not palinspastically restored) indicate an eastern provenance for the detritus of the Pavón Formation (Manassero *et al.*, 1999), which would therefore might point to a provenance from those sources located towards east (present coordinates). Cingolani *et al.* (2003a) also implied an eastern provenance for the Pavón basin. However, the spinels from Pavón Formation could result from cannibalistic processes of the lavas and sills interfingered with the clastic Caradoc rocks, this means the mafic rocks outcropping to the west (Western Precordillera Belt and its southern extension). The 'El Nihuil mafic body' (Fig. 7.1) was tectonically emplaced and its primary relationship with the Pavón Formation sedimentary rocks is unknown. Nevertheless, its proximity to the basin might explain the subhedral character of the grains. The last possibility is to consider that the mafic and ultramafic source rocks of the detrital chromian spinels of the Pavón Formation were eroded away. Probable sources located further afield are excluded based on grains shape, which suggest rather a short transport of detrital material. This is supported by petrography which indicates relatively high amounts of matrix and subangular to angular framework minerals (Cingolani *et al.*, 2003a), as well as by interpretations of the sequence as non-fan, sandy, marine turbidites deposited on a linear trough located close to the source areas and fed by turbidite and granular flows (Manassero *et al.*, 1999).

7.7 IMPLICATIONS FOR THE TECTONIC SETTING

The entire detrital chromian spinel dataset is subdivided into two different groups, notwithstanding their preferable volcanic origin and their association with an extensional tectonic environment. Group 1 is related to ocean floor basalts from a mid-ocean ridge, while Group 2 was derived from flood basalts in an oceanic or continental intraplate setting. No ages are presently available from the chromian spinel grains apart from their Caradoc minimum age. Therefore, each group may or may not represent different source rocks temporally separated from each other. Furthermore, the source area was not detected. It is important to note that both varieties of chromian spinels were found together within the same sampled layers.

Based on this information, it is possible to explain the compositional variations of the two groups of spinel in terms of tectonic evolution of the source area and associated host rocks. An extrusion of intraplate basalts occurred first, leading to the crystallization of spinels from Group 2, followed by a well developed oceanic floor (Group 1) forming a mid-ocean ridge. More information is needed to support this, as the detrital grains could also come from two unrelated tectonic settings that were completely separated in time and space. However, it is known that continental flood basalts related to the break-up of continents have a wide range of TiO_2 concentration even within the same region depending on whether the mantle source is a plume or lithospheric mantle (Hisada *et al.*, 1998).

This simple tectonic evolution represented by the chromian spinels could be correlated in a broad sense to those tectonic models that proposed a Laurentian origin for the Precordillera terrane. The microcontinent model assumes an initial rifting stage related to the opening of the Iapetus Ocean, followed by a well-developed oceanic crust leading to the separation of the Precordillera terrane from Laurentia (Astini *et al.*, 1995; Thomas and Astini, 1996). If this were the case, then the initial host rocks of the detrital spinels from Pavón Formation would be within the units surrounding the Ouachita embayment. The more likely unit is the Catoctin Formation (c. 570 Ma), which is composed of tholeiitic flood metabasalts as well as metarhyolites and scarce interlayered metasedimentary rocks (Aleinikoff *et al.*, 1995). The unit is metamorphosed to greenschist facies and is related to the continental rifting and opening of the Iapetus Ocean (Badger and Sinha, 1988). However, these source areas would imply a western provenance that seems unlikely (Manassero *et al.*, 1999; Cingolani *et al.*, 2003a).

On the other hand, the continental collision model (Dalla Salda *et al.*, 1992a) interpreted the Western Precordillera Belt (and its southern extension into the San Rafael block) as formed within the interior rift-basin through which Laurentia separated from Gondwana. However, as mentioned above, chemical analyses of the spinels from the Western Precordillera Belt are still needed and a provenance from an eastern source seems to be more likely (Manassero *et al.*, 1999; Cingolani *et al.*, 2003a).

If an eastern provenance is assumed, the mafic and ultramafic rocks located on the eastern side of the Precordillera terrane are the most likely sources. The provenance from Gondwanan areas further afield cannot be completely ruled out, but it is not likely due to the subhedral character of the detrital chromian spinels from the Pavón Formation, which along with petrography and facies analyses suggest rather a short transport. In this regard, it could be that either the Precordillera has a para-autochthonous origin (Aceñolaza *et al.*, 2002; Finney *et al.*, 2005, and others), or that the terrane collided to Gondwana prior to the Caradoc. The later is emphasized when considering the Pie de Palo and probably other minor Ranges such as Umango as part of the Gondwanan autochthonous prior to the Lower Palaeozoic (Casquet *et al.*, 2006). Lately, it could be speculated that the mafic source is no longer outcropping.

7.8 CONCLUSIONS

The Early Caradoc Pavón Formation (Precordillera terrane) contains a low-diversity detrital heavy mineral population, characterized by a zircon-rich assemblage with minor but significant amounts of rutile and chromian spinels. Because these more stable heavy mineral phases can be recycled, a provenance from areas not closely related to the depositional basin cannot be excluded. However, the subhedral shape of the detrital spinels might indicate a close spatially related source. The proposal of a mafic to ultramafic source that influenced the Pavón Formation chemistry can now be explained by the discovery of chromian spinels in the heavy mineral fraction.

These detrital chromian spinels are divided into two groups based on their chemical characteristics. Group 1 is characterized by intermediate Cr# values, low TiO_2, Fe^{3+}# and Fe^{2+}#, and indicates a mid-ocean ridge emplacement of their initial host rocks. Group 2 has Cr# values of c. 0.7, high TiO_2, Fe^{3+}# and Fe^{2+}# and suggests an intraplate environment.

No known mafic to ultramafic rocks could be identified as the definite source. However, this case study shows a direct influence of two mafic sources shedding detrital heavy minerals into the Precordilleran Ordovician rocks. Chemical analyses of spinels from several probable source areas are needed to further constrain the provenance. However, a provenance from source rocks located toward east (present coordinates) seems to be more likely, although an input from the Western Precordillera Belt (and its southern continuation within the San Rafael block) cannot be completely ruled out.

Notwithstanding the uncertainties and assuming a source located towards east (present coordinates) and spatially closely related to the Pavón basin, the Precordillera terrane might had reached its present position before the Caradoc. However, neither the autochthonous nor the para-autochthonous models can be supported.

CHAPTER 8

CONCLUSIONS

8.1 INTRODUCTION

Allochthonous terranes are fundamental to the growth of continents and commonly have two components to their tectonic history, one relating to their original tectonic setting and the other reflecting their subsequent histories of dispersal and accretion. Because the latter tend to mask the former, considerable uncertainty might exist (McLennan *et al.*, 2006). One example is the Precordillera terrane, characterized by a mainly Mesoproterozoic (Grenvillian-age) basement and a Cambrian-Ordovician carbonate platform (summary in Ramos, 2004). These characteristics and its distinct geologic history mark a difference between this suspected exotic-to-Gondwana terrane and the Gondwanan autochthonous.

The geological characteristics along with sedimentological, palaeontological, and palaeomagnetic data, as well as isotope data from the basement (e.g. Benedetto, 1993; Lehnert and Keller, 1993; Buggisch *et al.*, 1993; Ramos *et al.*, 1998; Thomas *et al.*, 2001; Rapalini and Cingolani, 2004), lead to speculation that the Precordillera was derived from Laurentia (Ramos *et al.*, 1986; Dalla Salda *et al.*, 1992a; Dalziel *et al.*, 1994; Astini *et al.*, 1995; Keller, 1999). However, there are models that attempt to interpret the origin of the Precordillera terrane as being para-autochthonous (Baldis *et al.*, 1989; Loske, 1992; Aceñolaza *et al.*, 2002; Finney *et al.*, 2005). All these models are still controversial and recent detrital zircon dating and Nd-isotope data suggest that the origin of the Precordillera terrane will remain unresolved at least until more useful provenance data from both, the Precordilleran successions and the probable source rocks are added (Gleason *et al.*, 2006).

A combination of several methodologies including petrography and heavy minerals, geochemistry, Sm-Nd and Pb-Pb isotopes and zircon dating was applied to several clastic Ordovician and Ordovician to Silurian units of the Precordillera terrane. Both the Precordillera *s.s.* and the San Rafael block were studied. The combination of these different approaches can give accurate information in order to constrain the probable sources that provided detritus to the Precordillera terrane and ultimately to constrain the existing models about its origin. The complete dataset acquired is presented in Appendix A, whereas details of the sampling, methodologies and analytical techniques are given in Appendix B and detailed petrographic and geochemical descriptions along with additional data (e.g. X-ray diffractions patterns) for each unit can be found in Appendix C.

8.2 GEOLOGICAL SETTING

Several morphostructural units form the Precordillera (Astini *et al.*, 1995) or the Cuyania composite terrane (Ramos *et al.*, 1996): The Precordillera *s.s.* (*sensu stricto*), the Western Pampeanas Ranges and the San Rafael and Las Matras blocks (Criado Roqué and Ibañez, 1979; Sato *et al.*, 2000). As it was discussed in Chapter 2, the boundaries of the terrane are still not well-constrained (Ramos *et al.*, 1996; Porcher *et al.*, 2004; Astini and Dávila, 2004; Vujovich *et al.*, 2005; Casquet *et al.*, 2006). Particularly important regarding provenance is the inclusion or not of the Western Pampeanas Ranges within the Precordillera terrane.

A Mesoproterozoic basement (Leveratto, 1968; Abruzzi *et al.*, 1993; Kay *et al.*, 1996; Cingolani and Varela, 1999; Sato *et al.*, 2004; Cingolani *et al.*, 2005a) and a sedimentary Palaeozoic cover characterize the Precordillera. The thick Lower Palaeozoic sedimentary sequence starts with very thin Lower Cambrian rift-type deposits followed by a thick Cambrian-Ordovician carbonate platform. Mainly clastic sedimentary rocks were deposited from the Lower Ordovician until the end of the Palaeozoic (Baldis *et al.*, 1982; 1984).

The Upper Palaeozoic is clearly separated from the previous rocks by a regional unconformity. Continental, glacial-marine and marine deposits characterize the Carboniferous to Permian, while continental sedimentary and volcanic rocks compose the Permian-Triassic record. During a long period within the Mesozoic, the Precordillera acted as a positive topographic area providing sediments to marginal basins. The Tertiary sequences are mainly composed of alluvial sediments (Peralta, 2003a) with less extensive extrusive and subvolcanic rocks (Baldis *et al.*, 1984). The Cambrian-Ordovician carbonate platform is absent within southwestern Gondwana.

The Precordillera *s.s.* is subdivided into two synchronic tectofacies (Astini, 1991) delineated by differences in deposition, deformation and metamorphism during the Lower Palaeozoic. The Eastern tectofacies (Chapter 3) was deposited in a shallow basin, while the Western tectofacies (Chapter 5) was deposited in a deep-sea basin with high subsidence and sedimentation rates (although more recently questioned and re-interpreted as shallow marine deposits; see Chapter 5). A continent-ocean transition zone (so-called slope-type deposits adjacent to the continental rise; Keller *et al.*, 1998) was developed in between them (Chapter 4). A carbonate platform is overlaid by predominately clastic deposits and characterize the Eastern tectofacies, while the Western tectofacies is characterized by turbidite successions overprinted by low-grade metamorphism and with interlayered and intruded mafic to ultramafic igneous rocks. The slope-type deposits comprise olistostromic sequences.

The Eastern tectofacies comprises the Gualcamayo and Los Azules Formations (Fig. 8.1), which represent the drowning of the Cambrian-Ordovician carbonate platform. They also record evidence of contemporaneous explosive volcanism nowadays represented by K-bentonites beds (Huff *et al.*, 1998). The Las Vacas, Las Plantas, Trapiche and La Cantera Formations were deposited as a clastic-wedge that formed within faulted blocks in an extensional tectonic environment (Astini *et al.*, 1996; Thomas and Astini, 2003). The Don Braulio and La Chilca Formations record the Ordovician to Silurian transition within the Eastern tectofacies of the Precordillera terrane. The glacial deposits of the Don Braulio Formation along with faunal contents of the La Chilca Formation are interpreted as evidence of the final accretion of the terrane to Gondwana, because similar deposits and faunas are found within Gondwanan areas (e.g. Astini, 1993a).

The Western tectofacies comprises the Yerba Loca, Alcaparrosa, Portezuelo del Tontal and Sierra de la Invernada Formations (Fig. 8.1), which host mafic to ultramafic rocks. The Empozada and Los Sombreros Formations (Fig. 8.1) are olistostromic sequences developed on the western slope of the thick Cambrian-Ordovician carbonate platform of the Precordillera terrane, and are known as the slope-type deposits.

Within the San Rafael block, two units are developed: the Ponón Trehué Formation (Chapter 6), which is an olistostromic sequence (Heredia, 2006), and turbidite deposits known as the Pavón Formation (Chapters 6 and 7; Cingolani *et al.*, 2003a).

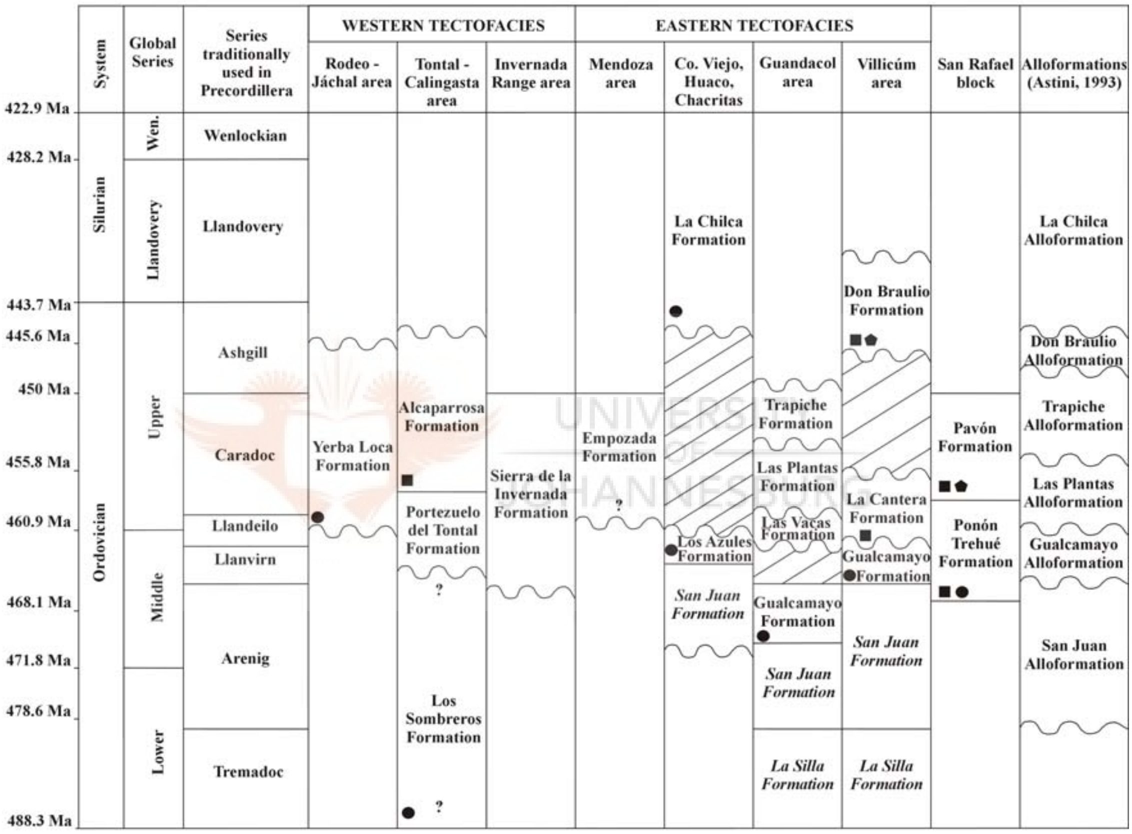

Figure 8.1: Stratigraphy of the Precordillera terrane based on Keller (1999). Absolute ages are as recommended by the International Commission on Stratigraphy (International Stratigraphic Chart 2004; Gradstein *et al.*, 2004). Except for the La Silla and San Juan Formations (in italics), all the units mentioned were analyzed petrographically and geochemically (see details in Appendixes B and C). Circles indicate units analyzed for Sm-Nd and Pb-Pb isotopes. Squares indicate units analyzed for detrital zircon age dating (U-Pb techniques). Pentagons indicate chemical analyses of single detrital chromian spinels using a microprobe. Crossed lines indicate hiatus.

8.3 PROVENANCE OF ORDOVICIAN TO SILURIAN SEQUENCES

8.3.1 Petrography of framework and heavy minerals

A number of 188 samples from sixteen Ordovician and Ordovician to Silurian units (see compilation in Fig. 8.1) from the Precordillera terrane were analyzed for provenance determinations.

The Gualcamayo and Los Azules Formations (Eastern tectofacies) comprise claystones, whereas the La Cantera, Las Vacas, Las Plantas and Trapiche Formations are composed of rather immature arenites with low matrix content as well as carbonate-cemented arenites. The Las Plantas and Trapiche Formations also contain mature quartz-arenites with neither cement nor matrix. The La Chilca Formation is composed of coarse siltstones and minor mature very fine arenites. It is clear that towards younger depositional ages the detrital grains tend to be more rounded, better sorted, and finer grained, and sandstones are more quartz-rich, with less matrix and cement, with less polycrystalline quartz and a more restricted lithoclast composition (mainly chert). Samples of the Empozada Formation range from limestones/silicate-sandstones (carbonate-cemented arenites where cement is almost 50%) to carbonate-cemented sandstones with 10% carbonate cement. Most of the rocks composing the matrix of the olistoliths within the Los Sombreros Formation are mudstones. The samples studied from the Ponón Trehué Formation are claystones, siltstones and fine-grained arenites. The Western tectofacies is composed of moderately well to very poorly sorted and immature to submature arenites and greywackes. A group of sandstones are carbonate-cemented (dominantly by calcite and less commonly by dolomite).

Petrographic analyses of all the different units indicate a main provenance from an upper continental crust (UCC) component and a mafic input. The presence of sedimentary (derived from mudstones, siltstones, chert, very fine-grained sandstones and carbonates) and metamorphic (derived from phyllites, quartz-mica schists and gneisses) lithoclasts indicate that the provenance component is not only represented by an igneous-metamorphic complex (OUC in the sense of McLennan *et al.*, 1993), but also by a recycled sedimentary component (RSR in the sense of McLennan *et al.*, 1993). Volcanic lithoclasts with a very fine crystalline matrix are present as well. A main difference of the Western tectofacies is the presence of greywackes; muscovite, chlorite and epidote are present as large crystals, and are the result of the greenschist facies metamorphism affecting this area. Intergrowths of muscovite and chlorite are frequent within the Western tectofacies.

The heavy minerals fraction of all the units studied is composed of zircon, tourmaline, epidote, muscovite, biotite, hematite, titanite, chlorite, apatite, brown spinels and other opaque minerals. Inclusions of Ti-bearing oxides were also observed. Apart from these minerals, the Western tectofacies also comprises staurolite and monazite, while spinels were not observed. Zircon, apatite, muscovite, spinel, tourmaline, rutile, Fe-oxides (including hematite) and other opaque minerals comprise the heavy mineral fraction of the Ponón Trehué Formation.

The less evolved component is represented by the chromian-spinels found within the heavy minerals fractions of the Eastern tectofacies (Don Braulio Formation), the slope-type deposits (Empozada Formation) and the San Rafael block (Ponón Trehué and Pavón Formations). Within the Western tectofacies, the less evolved component is petrographically represented by the volcanic lithoclasts with textures resembling those from basalts and/or andesites.

The spinels from the Don Braulio Formation have the same composition as the 'tholeiitic basalts and boninites' group from Barnes and Roeder (2001); they are especially comparable to spinels from ocean islands basalts (OIB in the sense of Kamenetsky *et al.*, 2001), while they differ significantly from ophiolitic basalts, boninites, mid-ocean ridge basalts (MORB), Hawaiian lava lakes and island arcs. The detrital chromian spinels of the Pavón Formation are divided into two groups based on their chemical characteristics. One group indicates a MORB emplacement of their initial host rocks whereas the other group suggests an intraplate environment. Ages of the initial host rocks of the detrital chromian spinels are unknown.

A chemical and textural comparison of these spinels with those hosted in probable source rocks is limited by the scarcity of spinels chemical analyses and descriptions within the surrounding rocks. No known mafic to ultramafic rocks could be identified as the definite source. However, a provenance from source rocks located toward east (present coordinates) such as the Western Pampeanas Ranges seems likely, but still speculative. This ascertain is made based on the tectonic settings deduced for the mafic and ultramafic rocks found within the Western Pampeanas Ranges, and because an eastern source is suggested by palaeocurrents of both formations. Furthermore, such a source is in accordance with other provenance indicators (see below).

8.3.2 Geochemistry

A summary of important geochemical provenance-indicators is given in Table 8.1. Geochemical data for the Eastern tectofacies, the slope-type deposits, the Western tectofacies and the Ponón Trehué Formation indicate a variable major element composition, which for the first two areas is influenced by highly variable CaO and SiO_2 concentrations. Geochemical indicators of alteration (CIA, K/Cs and Th/U) suggest rather moderately to advanced weathering and the effects of potassium metasomatism. Th concentrations of certain samples are disturbed in CaO-rich rocks of the Eastern tectofacies and the slope-type deposits.

In general, rare earth elements (REE) patterns of all the units studied (Fig. 8.2) are similar to the Post-Archaean Australian Shales pattern (PAAS). However, certain samples from the Los Sombreros Formation (slope-type deposits) showed disturbances of the rare earth elements, caused probably by secondary processes. Negative Eu-anomalies, Th/Sc ratios of approximately 0.8 and low Zr/Sc ratios indicate that the main provenance component has a relatively unrecycled upper continental crust (McLennan *et al.*, 2006) composition. An input from a less evolved source was detected by high abundances of compatible elements (Cr, V, and Sc) and Cr/V ratios, less negative Eu-anomalies (0.8) and low Th/Sc and Y/Ni ratios.

An arc-provenance component might be deciphered using Th/Sc, Eu_N/Eu^* and Ti and Nb concentrations. Low Th/Sc ratios, Eu_N/Eu^* of about 1 and strong negative Nb and Ti anomalies characterize continental arc components, although differentiated arcs would have variable Th/Sc ratios and Eu_N/Eu^* between 0.6 and 0.9 (Hofmann, 1988; McLennan *et al.*, 1993; Zimmermann, 2005). Relationships between La, Th, Sc, Ti and Zr suggest a deposition on continental island arc or an active continental margin setting. The absence of the negative Nb and Ti anomalies (Hofmann, 1988) and the Eu_N/Eu^* values tend to rule out the influence of an arc. However, typical arc signatures are often not recorded in other than basins spatially closely related to the arc itself, and rocks derived from dissected arc terranes would show variable Eu_N/Eu^* values (McLennan *et al.*, 1990; Zimmermann, 2005). Furthermore, passive margin and foreland basin deposits cannot be easily discriminated using Th-Sc-Zr-La relationships (Zimmermann, 2005), and the active continental margin setting used by Bathia and Crook (1986) involves retro-arc foreland and pull-apart basins. Nevertheless, certain samples from the slope-type deposits display negative Nb and Ti anomalies, very low Th/Sc ratios (between 0.34 and 0.62) and Eu_N/Eu^* ranging from 0.65 and 0.87. Therefore, they seem to indicate a provenance from a differentiated arc. However, these samples showed fractionation of REE. Other samples from this area do not indicate a provenance from an arc component.

Formation	Th/Sc	Zr/Sc	Th/U	Cr/V	Nb	La_N/Yb_N	Tb_N/Yb_N	Eu_N/Eu^*
La Chilca	0.87±0.17	43.1±22.0	3.4±1.2	1.1±0.2	12±2	6.1±1.1	1.5±0.2	0.61±0.06
Don Braulio	0.77±0.19	30.7±29.8	3.7±0.6	1.6±1.9	15±5	6.7±1.2	1.6±0.3	0.63±0.15
Las Plantas-Trapiche	0.75±0.11	62.8±66.7	3.4±0.9	1.9±1.4	10±6	6.7±1.4	1.3±0.3	0.53±0.06
La Cantera	0.64±0.08	23.4±14.6	3.8±0.8	1.1±0.2	18±2	7.0±1.4	1.3±0.2	0.59±0.10
Las Vacas	0.55±0.10	15.2±3.7	4.1±0.7	0.8±0.1	12±2	7.6±0.7	1.6±1.9	0.66±0.04
Los Azules	0.73±0.15	11.2±3.4	1.9±0.6	0.6±0.2	16±3	7.9±0.5	1.5±0.1	0.57±0.10
Gualcamayo	0.82±0.23	11.7±3.9	2.0±0.4	0.5±0.1	14±3	8.1±0.9	1.2±0.1	0.53±0.09
Empozada	0.89±0.32	40.0±39.2	2.8±1.5	1.6±1.0	12±5	6.5±1.3	1.5±0.2	0.61±0.15
Los Sombreros	0.68±0.14	11.5±4.1	4.9±0.9	0.9±0.1	15±5	6.9±1.9	1.6±0.9	0.63±0.12
Portezuelo del Tontal	0.71±0.11	16.9±3.8	4.6±0.9	0.9±0.1	16±2	7.2±1.0	1.3±0.2	0.65±0.08
Sierra de la Invernada	0.75±0.06	16.7±7.5	4.2±0.7	0.9±0.1	18±2	7.6±0.5	1.4±0.2	0.53±0.05
Yerba Loca	0.72±0.20	18.6±9.3	4.5±1.1	0.7±0.4	16±2	6.9±1.5	1.4±0.2	0.55±0.07
Alcaparrosa	0.81±0.10	23.8±9.6	3.8±0.4	0.9±0.1	18±3	6.8±0.5	1.3±0.2	0.54±0.04
Ponón Trehué	0.82±0.12	19.2±7.8	3.9±2.2	1.3±0.4	20±7	5.8±1.4	1.2±0.2	0.52±0.02

Table 8.1: Summary of averages of important geochemical proxies from a provenance point of view, of all the units studied from the Precordillera terrane (see also Fig. 8.1). $Eu_N/Eu^* = Eu_N/(0.67Sm_N+0.33Tb_N)$. Nb is expressed in ppm. The high Nb concentrations seem to indicate either that the mafic input is not linked to arc related rocks or that the influence of an arc provenance component is masked by dominant inputs of non-arc mafic rocks.

Within the Eastern tectofacies and towards younger depositional ages, the increase in recycling resulted in sandstones characterized by more rounded clasts, greater quartz content, better sorting, and with less labile components (matrix, cement, polycrystalline quartz and lithoclasts). Similarly, within the Western tectofacies towards younger ages the sedimentary rocks are more recycled.

In summary, it seems apparent that all the Formations studied received an input from at least two source components. The dominant source has an unrecycled upper continental crust composition whereas the other component is more depleted.

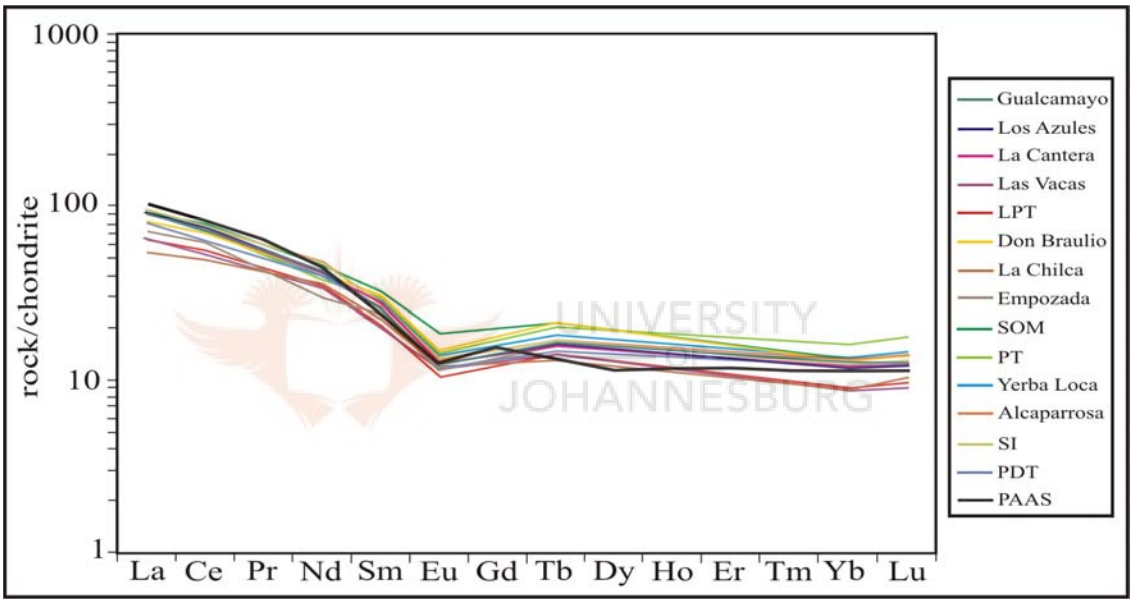

Figure 8.2: Average chondrite normalized REE patterns for units studied from the Precordillera terrane. PAAS= post-Archaean Australian Shales pattern is draw for comparison (Nance and Taylor, 1976). Chondrite normalization factors are those listed by Taylor and McLennan (1985). REE patterns are drawn as a continuous line although certain elements were not measured (see Table 1 in Appendix A). SI: Sierra de la Invernada Formation; PT: Ponón Trehué Formation; SOM: Los Sombreros Formation; PDT: Portezuelo del Tontal Formation; LPT: Las Plantas and Trapiche Formations.

8.3.3 Sm-Nd isotopes

Nd isotopes account for values between those typical of the UCC average or old continental crust and those typical of a juvenile input. The uniform Nd isotopes displayed by the different Ordovician and Ordovician to Silurian sedimentary rocks from the Precordillera terrane (Fig. 8.3) indicate ε_{Nd} values of about -5.36 ± 1.05, a $f_{Sm/Nd}$ of about -0.38 ± 0.05 and T_{DM} (model ages) of 1495 ± 137 Ma in average for the six units studied (see Fig. 8.1). However, certain anomalously high Sm/Nd ratios and T_{DM} ages are related to disturbances of the Sm-Nd isotopic system for some samples of the slope-type deposits and the Eastern tectofacies (Fig. 8.3a). The homogeneous Nd isotopes can be caused either by complete recycling of older basement material or by the mixing of different components of different model ages.

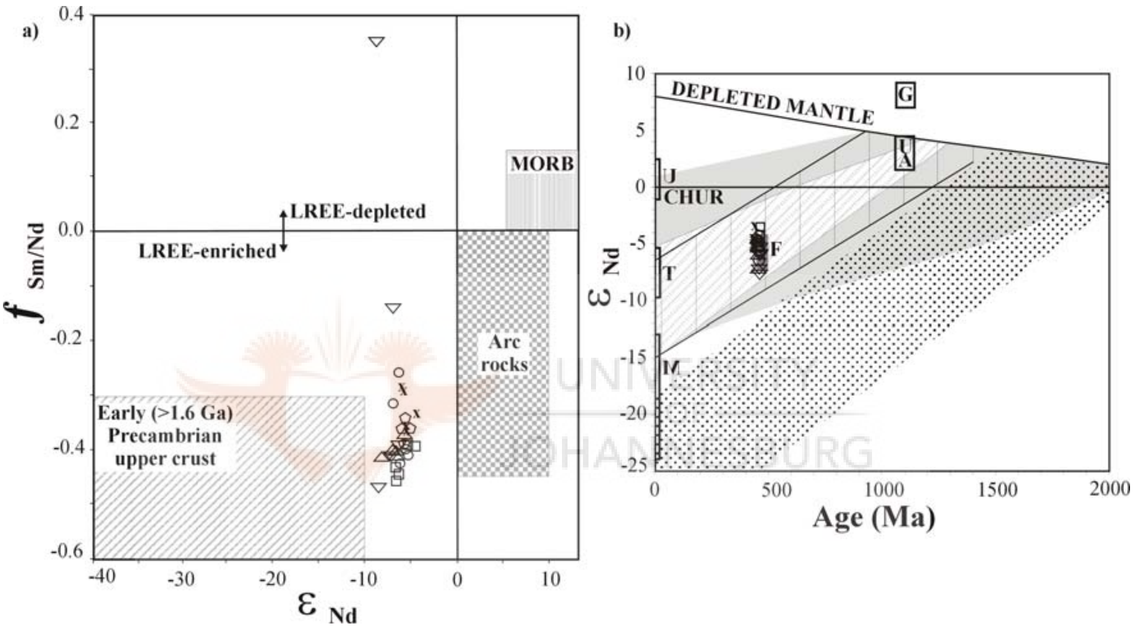

Figure 8.3: a) Plot of $f_{Sm/Nd}$ vs. ε_{Nd} (t) showing some remobilization of REE that fractionated the Sm/Nd ratios giving a vertical array of the $f_{Sm/Nd}$. ε_{Nd} values are neither typical of arc-related rocks nor of old crust; MORB: mid-ocean ridge basalts. b) ε_{Nd} versus age of the unit studied and of areas evaluated as probable sources. Dotted area: range of ε_{Nd} for the Northern domain of the Arequipa-Antofalla Basement and light grey area: Central and Southern domains of the Arequipa-Antofalla Basement (*sensu* Loewy *et al.*, 2004). Field of vertical lines: Laurentian Grenville crust (Patchett and Ruiz, 1989). A: granulitic and amphibolitic, and G: acidic-gneissic, xenoliths from the inferred basement of the Precordillera (Kay *et al.*, 1996). F denoting dark grey area: Famatinian magmatic rocks (Pankhurst *et al.*, 1998). U: Umango Range, T: El Taco Complex, and M: Maz Complex from the Western Pampeanas Ranges (Vujovich *et al.*, 2005). White field with diagonal lines: Cerro La Ventana Formation (Cingolani *et al.*, 2005a). Squares: Gualcamayo Formation; circles: Los Azules Formation; crosses: La Chilca Formation; pentagons: Ponón Trehué Formation; triangles: Yerba Loca Formation; inverted triangles: Los Sombreros Formation; LREE: light rare earth elements; CHUR: Chondritic uniform reservoir.

The models proposed to explain the tectonic evolution of the Precordillera terrane imply the evaluation of sources such as the Famatinian arc and the Grenville Province of Laurentia. The para-autochthonous models (Aceñolaza *et al*. 2002; Finney *et al*., 2005) placed the Precordillera surrounded by Antarctica, Falklands/Malvinas Microplate and the Natal-Namaqua Metamorphic belt (SAFRAN), being therefore important to evaluate these areas as probable sources as well. Comparing the model ages (T_{DM}) from the Precordillera terrane with those from other neighbouring rocks (Fig. 8.3), there are clear similarities with the values found within the Famatinian arc, the basement of Chilenia (Bahlburg *et al*., 2001), north-western Argentina and the igneous rocks of the Pampia terrane (Rapela *et al*., 1998; Bock *et al*., 2000; Lucassen *et al*., 2000; Zimmermann and Bahlburg, 2003). The T_{DM} ages are also comparable to T_{DM} ages for Mesoproterozoic basement rocks of the Precordillera terrane (Kay *et al*., 1996) and Antarctica, Natal-Namaqua Metamorphic belt and the Falklands/Malvinas microplate (Wareham *et al*., 1998).

The ε_{Nd} values are within the range of variation of the Laurentian Grenville crust (Patchett and Ruiz, 1989), Central and Southern domains of the Arequipa-Antofalla Basement (Central Andes; Loewy *et al*., 2004), the basement of the Precordillera terrane known as the Cerro La Ventana Formation (Cingolani, unpublished data) and the Famatinian arc (Pankhurst *et al*., 1998; Fig. 8.3b). They are also similar to those from other Ordovician sedimentary rocks from the Precordillera terrane (Cingolani *et al*., 2003a; Gleason *et al*., 2006). ε_{Nd} values from the Western Pampeanas Ranges are scarce, but a broad similarity with data here presented is evident (Fig. 8.3b).

8.3.4 Pb-Pb isotopes

The same six units studied for Nd isotopes were also analyzed for Pb isotopes (Fig. 8.1). $^{206}Pb/^{204}Pb$, $^{207}Pb/^{204}Pb$ and $^{208}Pb/^{204}Pb$ range from 18.82 to 21.20, 15.66 to 17.27, and 38.7 to 42.93 respectively, for the Precordillera terrane (Figs. 8.4 and 8.5). Pb isotopes indicate that a source with high $^{207}Pb/^{206}Pb$ was important. In the present-day Pb ratios diagrams (Fig. 8.4 and 8.5), the samples from the Precordillera terrane plot slightly above the Stacey and Kramers (1975) second stage Pb evolution curve for average crust, and along a trend from values similar to the UCC and globally subducted sedimentary rocks (GLOSS), and towards higher values for all the Pb-ratios.

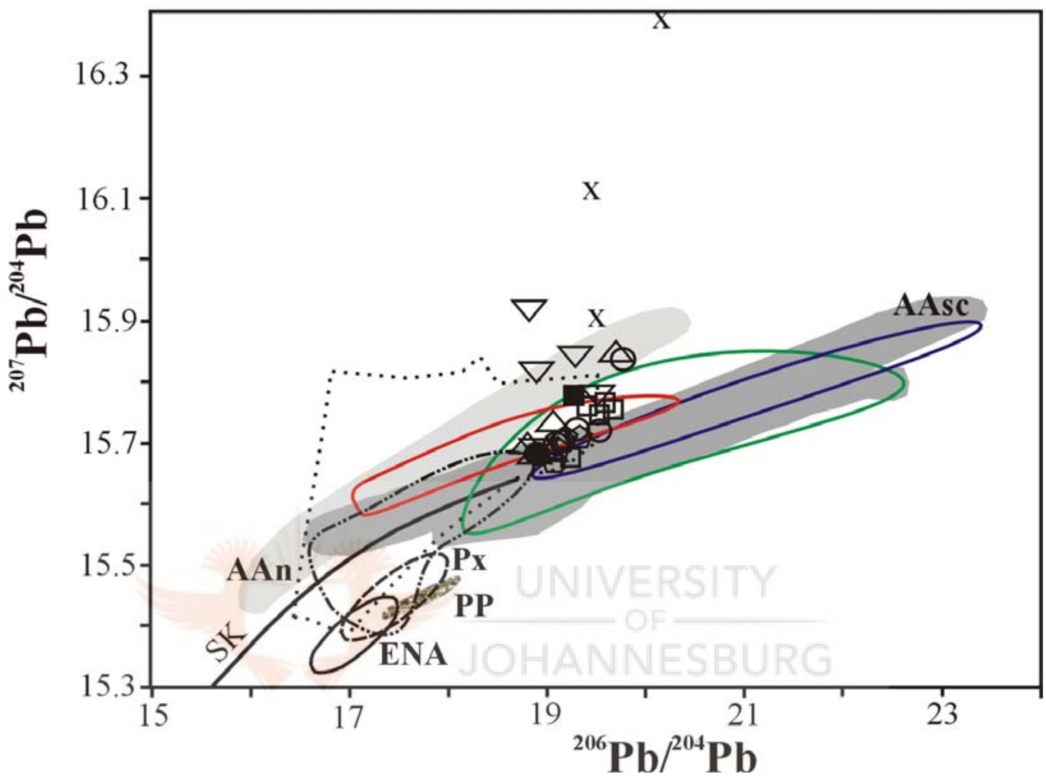

Figure 8.4: $^{207}Pb/^{204}Pb$ versus $^{206}Pb/^{204}Pb$ present-day ratios. Empty circles: Los Azules Formation; empty squares: Gualcamayo Formation; crosses: La Chilca Formation; pentagons: Ponón Trehué Formation; triangles: Yerba Loca Formation; inverted triangles: Los Sombreros Formation; solid square is the average value for the upper crust and solid circle the average value for GLOSS (globally subducted sedimentary rocks), both from Hemming and McLennan (2001). Fields obtained from several sources as indicated in the text. ENA: Eastern North America; Px: xenoliths from the Precordillera terrane, AAsc Arequipa-Antofalla Basement Southern and Central domains; AAn: Arequipa-Antofalla Basement Northern domain; PP: Pie de Palo Range (Western Pampeanas Ranges); SK: Stacey and Kramers reference line; blue line: supracrustal Ordovician rocks from the Precordillera terrane (Gleason *et al.*, 2006); dotted line: Palaeozoic rocks from the Central Andes (Lucassen *et al.*, 2002); green line: Palaeozoic rocks from southern Central Andes (data from Bock *et al.*, 2000); red line: Ordovician rocks from south Bolivia (Egenhoff and Lucassen, 2003); double dotted-dashed line: data from Wareham *et al.* (1998; see text).

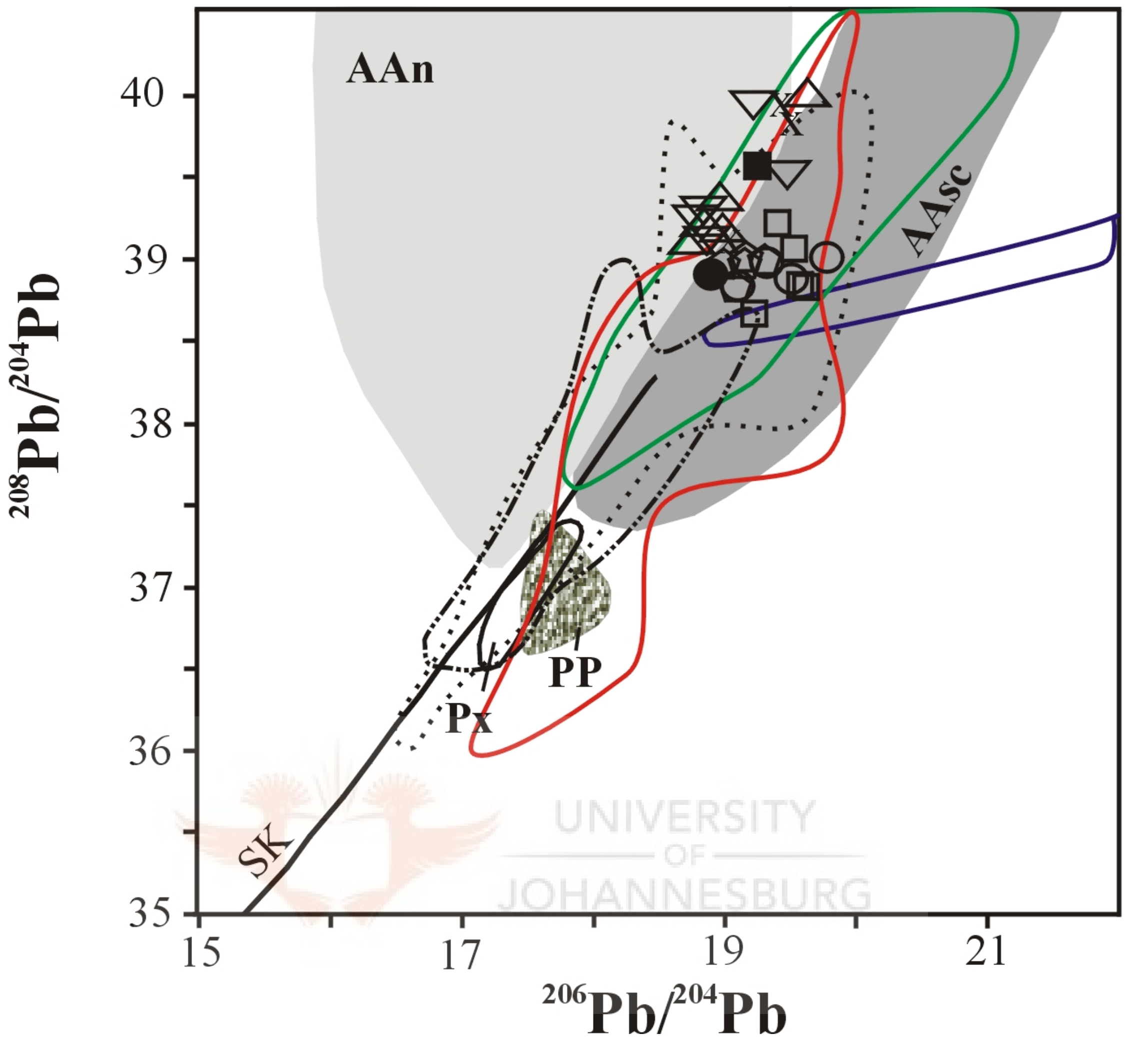

Figure 8.5: $^{208}Pb/^{204}Pb$ versus $^{206}Pb/^{204}Pb$ present-day ratios. Empty circles: Los Azules Formation; empty squares: Gualcamayo Formation; crosses: La Chilca Formation; pentagons: Ponón Trehué Formation; triangles: Yerba Loca Formation; inverted triangles: Los Sombreros Formation; solid square is the average value for the upper crust and solid circle the average value for GLOSS (globally subducted sedimentary rocks), both from Hemming and McLennan (2001). Fields obtained from several sources as indicated in the text. ENA: Eastern North America; Px: xenoliths from the Precordillera terrane, AAsc and AAn: Arequipa-Antofalla Basement Southern and Central domains, and Northern domain respectively; PP: Pie de Palo Range; SK: Stacey and Kramers reference line; blue line: supracrustal Ordovician rocks from the Precordillera terrane (Gleason *et al.*, 2006); dotted line: Palaeozoic rocks from the Central Andes (Lucassen *et al.*, 2002); green line: Palaeozoic rocks from southern Central Andes (Bock *et al.*, 2000); red line: Ordovician rocks from south Bolivia (Egenhoff and Lucassen, 2003); double dotted-dashed line: data from Wareham *et al.* (1998; see text).

Comparing the lead isotopic system with that from probable source areas (Figs. 8.4 and 8.5), it is evident that the dataset here presented is similar to Middle Proterozoic rocks of the Arequipa-Antofalla Basement (Central Andes; Aitcheson *et al.*, 1995; Tosdal, 1996 and references therein). However, data from the latter are widespread and therefore their use for discriminatory purposes is limited. On the other hand, they differ consistently from the xenoliths interpreted as the basement of the Precordillera terrane (Kay *et al.*, 1996) and from Proterozoic rocks from Eastern North America. They are also different compared with data from the Natal-Namaqua Metamorphic belt (Mzumbe gneiss), Falkland/Malvinas Microplate (Cape Meredith Complex), West Antarctica (Haag Nunataks block) and East Antarctica (Kirwanveggan and Sverdrupfjella ranges, Maud Province; Wareham *et al.*, 1998).

The lead signature is similar to supracrustal Palaeozoic rocks from the Central Andes (Bock *et al.*, 2000; Lucassen *et al.*, 2002) and from Ordovician sedimentary rocks of south Bolivia (Egenhoff and Lucassen, 2003). The Pb isotopic composition from the Cerro La Ventana Formation (Precordillera terrane) and the Famatinian arc are unknown. Regarding Western Pampeanas Ranges, the only Pb-data available from the Pie de Palo Range are dissimilar. Compared with Pb data from Ordovician sedimentary rocks of the Precordillera terrane (Gleason *et al.*, 2006), these samples have higher $^{207}Pb/^{204}Pb$ and $^{208}Pb/^{204}Pb$ ratios and a narrower range of $^{206}Pb/^{204}Pb$ variation.

8.3.5 Zircon dating

Five samples had been used for detrital zircon dating of Ordovician and Ordovician to Silurian sequences of the Precordillera terrane (n= 230 in total), as indicated in Figure 8.1. Detrital zircon dating for the Don Braulio (n= 42), La Cantera (n=38) and Alcaparrosa (n= 49) Formations constrain the sources as being dominantly of Mesoproterozoic age (but with a main peak in the range 1.0 to 1.3 Ga and a subordinate peak between 1.3 and 1.6 Ga), with inputs from both older (1.6 to 2.0 Ga) and younger (Neoproterozoic, Cambrian and Ordovician) sources (Fig. 8.6). Gleason *et al.* (2006) obtained similar zircon patterns for the Las Vacas, La Cantera and Empozada

Formations. However, these authors did not find Famatinian-aged zircons within the La Cantera Formation. The detrital zircon population for the Ponón Trehué Formation (n= 38) is even more restricted with a main Mesoproterozoic peak (and concentrated in the range 1.0 to 1.3 Ga) and one Neoproterozoic discordant zircon grain (Fig. 8.6). The more restricted detrital zircon age range from the latter unit agree well with a local provenance, most likely from the underlying Cerro La Ventana Formation as indicated by sedimentological features (Heredia, 2006). The age distribution of the Pavón Formation (n= 53) indicates a main population of Mesoproterozoic zircons (with one peak between 1.0 and 1.3 Ga and another one about 1.4 Ga), and only two Neoproterozoic zircons and one Palaeoproterozoic grain (Fig. 8.6).

Therefore, detrital zircon geochronology indicates that there were no important changes in the ages of the source areas neither within the Eastern tectofacies, nor within the Western tectofacies. Furthermore, both tectofacies as well as the sequences from the San Rafael block have a provenance from rocks of similar age, although the more restricted ages for the southern outcrops seems to obey to a local source (might be the exposed basement).

Mesoproterozoic rocks that could have been the main source of zircons for the Precordilleran sequences are found within the basement of the Precordillera terrane (Kay *et al.*, 1996; Cingolani and Varela, 1999; Sato *et al.*, 2004; Cingolani *et al.*, 2005a), the Western Pampeanas Ranges (Varela and Dalla Salda, 1992; McDonough *et al.*, 1993; Varela *et al.*, 1996; Casquet *et al.*, 2006), the Arequipa-Antofalla Basement (Bahlburg and Hervé, 1997 and references therein), the Grenville Province of Laurentia (summary from Carrigan *et al.*, 2003), and Antarctica, Natal-Namaqua Metamorphic belt and Falklands/Malvinas microplate (Wareham *et al.*, 1998).

Palaeoproterozoic rocks are present within the Arequipa-Antofalla Basement (Bahlburg and Hervé, 1997 and references therein), within Laurentia (summary from Carrigan *et al.*, 2003), but also at certain areas of the Western Pampeanas Ranges (Maz Range; Casquet *et al.*, 2006). The Ordovician zircons could be derived from the Famatinian arc (Pankhurst *et al.*, 1998; Fanning *et al.*, 2004). Famatinian-age granites are intruded within both, the Western Pampeanas Ranges and the Arequipa-Antofalla

Basement (Casquet *et al.*, 2001). The Neoproterozoic and Cambrian zircons most likely derived from the Pampean/Brazilian orogen. Neoproterozoic igneous rocks are found intruded within the Western Pampeanas Ranges (McDonough *et al.*, 1993; Baldo *et al.*, 2006).

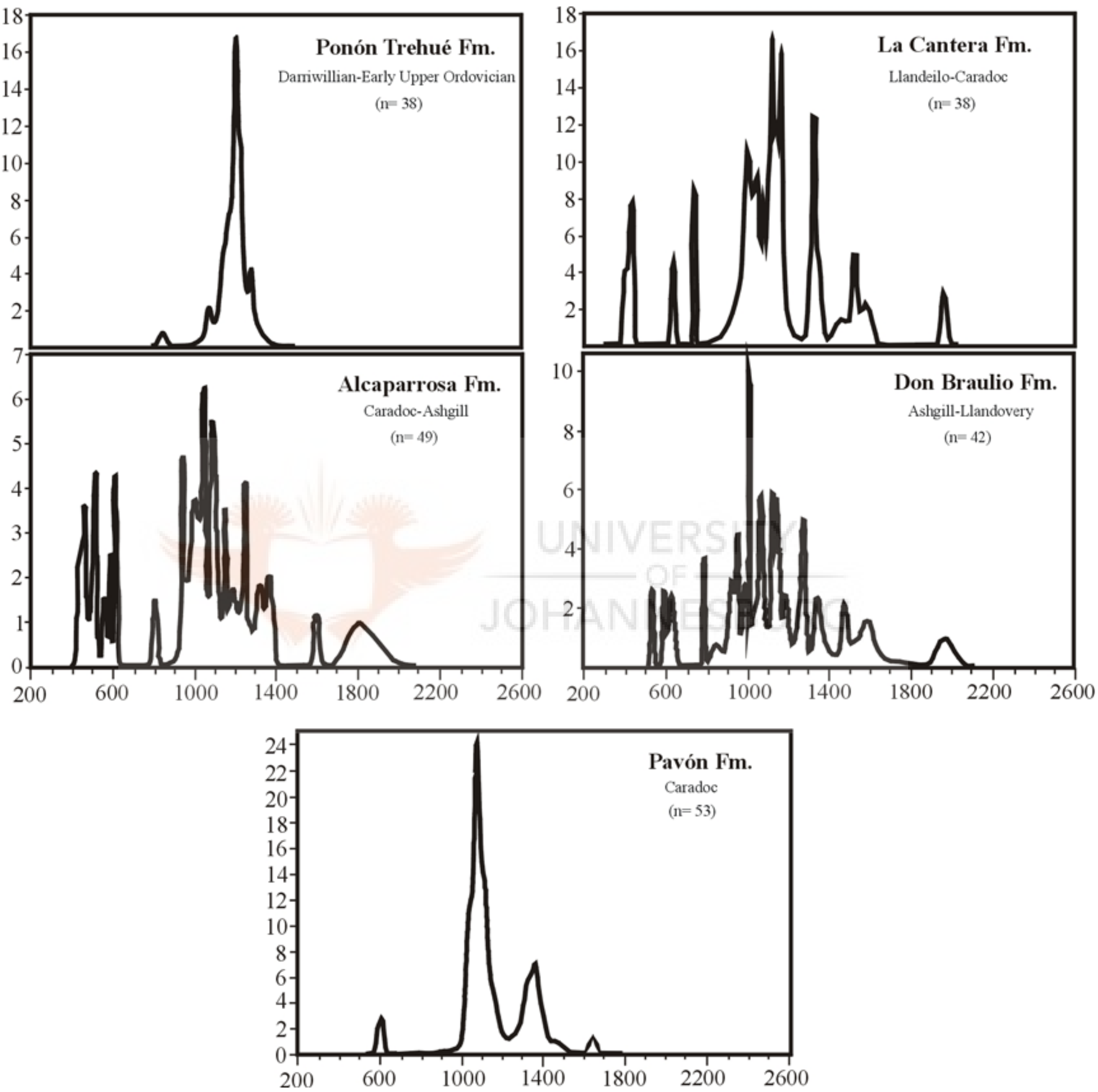

Figure 8.6: U-Pb distribution of analyzed detrital zircons with probability curves for the San Rafael block (the Ponón Trehué and Pavón Formations), the Eastern tectofacies (the La Cantera and Don Braulio Formations), and the Western tectofacies (the Alcaparrosa Formation). A main Mesoproterozoic source is observed for all samples, although inputs from Palaeoproterozoic, Neoproterozoic, Cambrian and Ordovician sources were also detected.

8.3.6 Source rocks

In summary, it was shown that the source rocks of the Ordovician and Ordovician to Silurian sedimentary sequences of the Precordillera terrane have a dominant unrecycled UCC composition as well as an input from a less fractionated component, which seems not to be arc related. Sm-Nd isotopes indicate negative ε_{Nd} values and Pb isotopes indicate that at least a part of the components has a signature characterized by high $^{207}Pb/^{204}Pb$ ratios. Zircon dating constrain the age of the main sources to the Mesoproterozoic (but with a main peak between 1.0 and 1.3 Ga), and with minor inputs from Palaeoproterozoic, Neoproterozoic, Cambrian and Ordovician sources.

The similarities shown by provenance data from the Eastern tectofacies and the slope-type deposits might indicate that despite the faulted contacts between them, they could have been derived from the same sources. However, similar provenance proxies might be produced by mixing of different sources. The provenance indicators of the Western tectofacies are also similar to those from the Eastern tectofacies and the slope-type deposits, which although it could be interpreted as a similar mix produced from mixing different sources it is more probably indicating that the sources for the three areas were basically the same. Despite processes that could have imprint minor differences in the chemical and mineralogical compositions of all the rocks studied (such as degree of weathering and alteration, metasomatism), main differences observed regarding the characteristics of the provenance are found particularly when analyzing detrital zircon ages. The Eastern and Western tectofacies contain detrital zircon ages dominated by a Mesoproterozoic population, but they also comprise Palaeoproterozoic, Neoproterozoic, Cambrian and Ordovician populations. Instead, with the San Rafael block, the ages are restricted to the Mesoproterozoic despite the presence of two Neoproterozoic zircons and one Palaeoproterozoic grain for the Pavón Formation. Another striking difference is shown by the detrital chromian spinels, that indicate inputs from mafic rocks related to ocean islands basalts for the Eastern tectofacies (Don Braulio Formation), whereas host rocks linked to continental flood basalts from an intraplate environment and mid-ocean ridge rocks are deduced for the southern outcrops (Pavón Formation, San Rafael block).

Several areas should be evaluated as sources in relation to the more relevant geotectonic models proposed until today (Fig. 8.7): the Famatinian magmatic arc, Antarctica, Falklands/Malvinas Microplate and the Natal-Namaqua Metamorphic belt, the Grenville Province of Laurentia, the Western Pampeanas Ranges, the basement of the Precordillera terrane, and the Arequipa-Antofalla Basement (Central Andes). Sedimentological characteristics such as palaeocurrents and the lack of important recycling tend to indicate that areas located far away of the Precordillera or those located to the west can be ruled out as sources (e.g. the Amazon craton and the Chilenia terrane).

A main provenance from the Famatinian magmatic arc is not supported by detrital zircon dating, except for a very few detrital zircons which could had been funnelled from the Famatinian magmatic arc (located towards east; Fig. 8.7) into the Precordilleran basin.

Rocks from Antarctica, Falklands/Malvinas Microplate and the Natal-Namaqua Metamorphic belt accomplish for Mesoproterozoic ages and have comparable T_{DM} ages, but have different Pb isotopes composition (Wareham *et al.*, 1998), which allow discarding such areas as sources.

Several models assigned a Laurentian (Southern Appalachian) origin for the Precordillera terrane. The time of detaching of the Precordillera from Laurentia varies according to different authors, but a link to Laurentia is considered even until the end of the Ordovician (e.g. Keller, 1999; see Chapter 2 for a detailed discussion). If the Precordillera was attached to Laurentia during the Ordovician (as a marginal plateau; Dalziel, 1997) then a Laurentian signature could be recorded within (and/or reworked into) the sedimentary sequences, as interpreted for the Cambrian clastic record (Naipauer, 2007). The Appalachian belt comprises Grenvillian-age igneous-metamorphic rocks (and minor Palaeoproterozoic and Neoproterozoic rocks), and since it was elevated during most of the Palaeozoic, it acted as a major source (Boghossian *et al.*, 1996). Even though these rocks could account for the detrital zircon ages and the

Sm-Nd signature (Patchett and Ruiz, 1989) of the clastic rocks here studied, the Pb isotopes do not show a Laurentian signature.

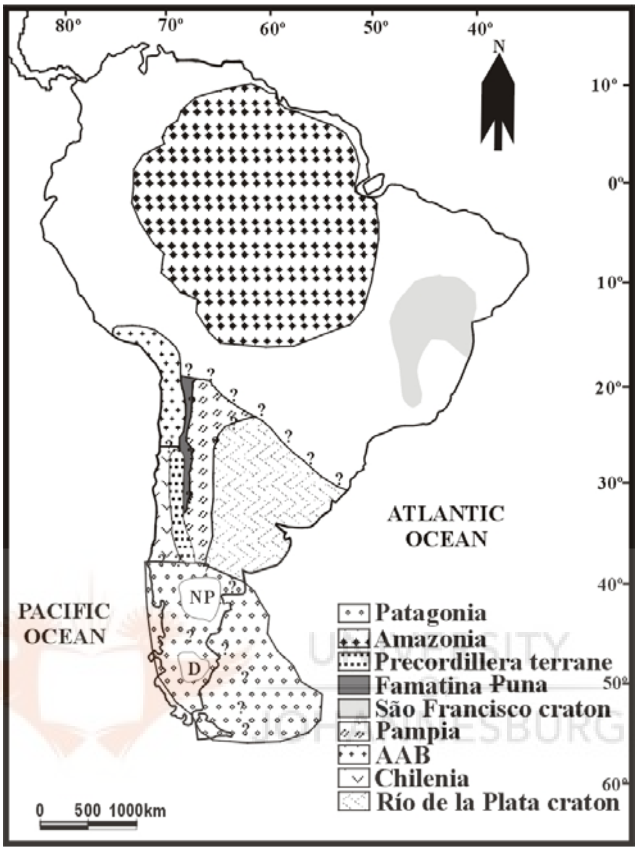

Figure 8.7: The Precordillera terrane and main tectonostratigraphic units of South America (modified from Rapalini, 2005). NP: North Patagonian Massif; D: Deseado Massif; AAB: Arequipa-Antofalla Basement.

The basement of the Precordillera terrane (Fig. 8.7) is known from xenoliths exhumed within Cenozoic volcanic rocks (Kay *et al.*, 1996). However, within the southern extensions of the terrane two more areas are known to comprise Mesoproterozoic basement rocks: the Cerro la Ventana Formation of the San Rafael block (Cingolani *et al.*, 2005a), and the Las Matras pluton of the Las Matras block (Sato *et al.*, 2004). The xenoliths and the rocks from the Las Matras block are characterized by positive ε_{Nd} (t) values (Kay *et al.*, 1996; Sato *et al.*, 2004), which are therefore dissimilar to values from the sedimentary record here studied. However, ε_{Nd} (0) values are also needed, because for a correct comparison the data from the sources need to be recalculated to the age of deposition of the sedimentary rocks (e.g. Bock *et al.*, 1998). Nd data presented by Cingolani *et al.* (2005a and also unpublished data provided by C.A. Cingolani) for the Cerro La Ventana Formation show ε_{Nd} values in the range of variation of data calculated to the time of deposition of the Ordovician and Ordovician to Silurian sedimentary rocks (Fig. 8.3). Pb isotopes are only available from a few xenoliths and they differ consistently from those of the sedimentary sequences here studied. Unfortunately, the Pb composition of the Cerro La Ventana Formation and from basement rocks of the Las Matras block remains unknown. Since the basement was already uplifted by the time of deposition of the clastic sequences studied (since the Darriwillian; Heredia, 2006), a provenance from the Mesoproterozoic basement is very likely, at least for the San Rafael block sedimentary sequences. However, a provenance from this basement is more difficult to reconcile when analyzing the Precordillera *s.s.*, since no basement outcrops are currently found northwards and palaeocurrents do not indicate a southern source. Pb data from the Cerro La Ventana Formation and the Las Matras block as well as complete Sm-Nd signatures from the xenoliths and the Las Matras block are needed to further support these areas as the sources.

The Arequipa-Antofalla Basement (Fig. 8.7) in the sense of Loewy *et al.* (2004; Central Andes) contains Mesoproterozoic plutons with ages between 0.97 to 1.2 Ga, older rocks ranging between 1.5 and 1.6 Ga and high-grade metamorphic rocks with Palaeoproterozoic ages (c. 1.9 Ga). The Arequipa-Antofalla Basement comprises three domains (Loewy *et al.*, 2004): the Northern domain exists in southern Peru and western Bolivia. The Central domain extends from the Peru-Chile border to the northernmost part of Chile, while the Southern domain is extended from 23º S to the northernmost part of Argentina. The area comprised in the so-called Central and Southern domains in the sense of Loewy *et al.* (2004) is almost equivalent to the ca. 500 Ma Mobile Belt of the Pampean Cycle according to Lucassen *et al.* (2000). However, the terminology of Loewy *et al.* (2004) is followed for this discussion.

Nd and Pb isotopic values from the Arequipa-Antofalla Basement agree well with values obtained for the Ordovician sedimentary record of the Precordillera terrane (Figs. 8.3, 8.4, 8.5) particularly when considering the Central and Southern domains. Detrital zircon age dating also agrees well with rock ages from the Central Andes. However, data from the latter are widespread and therefore their use for discriminatory purposes is limited.

The location of source rocks towards north of the Precordillera is supported by palaeocurrents from several units (e.g. La Cantera Formation according to Peralta, 1993 in Gleason *et al.*, 2006; La Chilca Formation following Astini and Maretto, 1993). However, such a northern provenance is problematic considering the palaeogeography of adjacent Ordovician basins. Furthermore, details of the northern termination of the Precordillera terrane at the Jagué area are still unknown. Sinistral strike-slip movements along an important fault located at the Jagué area (Astini and Dávila, 2004) was interpreted as a result of indenting during the collision of the Precordillera terrane against Gondwana. The motion along this fault is poorly constrained between the early Palaeozoic and pre-Carboniferous (Martina *et al.*, 2005). Nevertheless, several tectonic frameworks presented had located the Precordillera terrane immediately south of the Arequipa-Antofalla Basement for the Precambrian to Early Palaeozoic (Lucassen *et al.*, 2000; Rapela *et al.*, 2007), and current outcrops are located about 300 km north of the northernmost outcrops of the Precordillera terrane. A contribution from the Arequipa-Antofalla Basement to the clastic sequences of the Precordillera terrane might have been possible according to the provenance proxies, but it is still highly controversial. If the Arequipa-Antofalla Basement constituted a single crustal block along with the Western Pampeanas Ranges (Casquet *et al.*, 2006), then a similar isotopic signature would be expected for the latter.

The Pie de Palo, Maz, Umango and Espinal are the main mountain ranges that constitute the so-called Western Pampeanas Ranges (Fig. 8.7). They comprise metamorphosed igneous and sedimentary rocks from 0.9 to 1.2 Ga, meta-rhyolites, amphibolites, carbonate marbles and schists, mafic and ultramafic cumulates, shoshonitic magmatic rocks, metapelites and metasandstones, metagabbros, metatonalites, tonalitic to granitic orthogneisses associated with mafic rocks and a few pegmatites (McDonough *et al.*, 1993; Ramos *et al.*, 1993; Vujovich and Kay, 1996; 1998; Porcher *et al.*, 2004). Famatinian-age granites are intruded in Mesoproterozoic rocks (e.g. El Peñón Granite, which has a crystallization age of 473 Ma; Varela *et al.*, 2003). Grenvillian massif-type anorthosites are also described (Casquet *et al.*, 2005), as well as Neoproterozoic magmatic rocks (Baldo *et al.*, 2006).

Sm-Nd isotopic values from the Western Pampeanas Ranges are scarce and mostly ε_{Nd} (0) values are known, which vary from positive to highly negative (Vujovich *et al.*, 2005). Pb data from the Western Pampeanas Ranges (Pie de Palo Range; Kay *et al.*, 1996) are dissimilar to the Pb composition of the Precordillera terrane. Zircon age dating from the clastic record agrees with the ages found within the Western Pampeanas Ranges.

Palaeocurrents and facies analyses from several units support the location of an important source immediately east of the Precordillera. Furthermore, conglomerate clasts that resemble rocks from several areas of the Western Pampeanas Ranges have been described in a few Ordovician and Ordovician to Silurian units from the Precordillera (Hünicken and Pensa, 1989; Mendoza *et al.*, 1997). Zircon dating of selected clasts from the conglomerates of the clastic-wedge of the Eastern tectofacies showed mainly Mesoproterozoic and Neoproterozoic ages with minor older peaks that can be attributed to a Western Pampeanas Ranges origin (Astini *et al.*, 2005). The lithoclast composition of the Ordovician and Ordovician to Silurian sandstones studied from the Precordillera also matches the lithological descriptions of several rocks from the Western Pampeanas Ranges. Chemical analyses of detrital chromian spinels from the Eastern tectofacies (Don Braulio Formation) tend to point to an oceanic island (intraplate) setting such as that described by Vujovich and Kay (1996) from the Western Pampeanas Ranges. The mafic rocks from the Western Pampeanas Ranges could have provided chromian spinels to the Pavón Formation basin as well. However, the provenance of the spinels from both units (Don Braulio and Pavón Formations) is still highly speculative. Detailed Sm-Nd and Pb-Pb studies, as well as chemical analyses of the spinels from the Western Pampeanas Ranges are needed to support this area as a source.

8.4 GEOTECTONIC IMPLICATIONS

Based on data available up to now, the neighbouring rocks that best fit all the provenance constraints are found within the basement of the Precordillera terrane, the Western Pampeanas Ranges and less probably the Arequipa-Antofalla Basement (Central Andes). The basement of the Precordillera terrane and at least some of the Western Pampeanas Ranges (such as Pie de Palo and Umango Ranges) most likely derived from Laurentia (e.g. Ramos *et al.*, 1996; Dalla Salda *et al.*, 1992a; Astini *et al.*, 1995; Porcher *et al.*, 2004). Other areas of the Western Pampeanas Ranges (Maz and Espinal Ranges) are interpreted as representing the active Gondwana margin during the Lower Palaeozoic (Porcher *et al.,* 2004). However, the eastern boundary of the Precordillera (e.g. Pie de Palo Range), has been recently questioned and interpreted as autochthonous to Gondwana prior to the Lower Palaeozoic (Casquet *et al.*, 2006). In their discussion, Casquet *et al.* (2006) proposed that the Western Pampeanas Ranges and the Arequipa - Antofalla Basement (Fig. 8.7) might constitute a Mesoproterozoic continental crustal block autochthonous or para-autochthonous with respect to the pre-Famatinian margin of Gondwana.

A Laurentian origin for the Precordillera terrane cannot be accepted nor rejected with the data acquired for the Ordovician and Ordovician to Silurian sequences. Such a discussion can only be solved by examining the basement and pre-Ordovician rocks. However, a Laurentian provenance has been deduced for Cambrian sedimentary sequences based on detrital zircon dating (Naipauer, 2007), supporting the allochthonous character of the terrane.

Current lines of thinking had focus the discussion on either the Precordillera derived from Laurentia as a microplate (Thomas and Astini, 1996; 1999; 2003) or it was transferred by strike-slip movements from a southwards location (Aceñolaza *et al.*, 2002; Finney *et al.*, 2005). Therefore, these models would be tested with the provenance data acquired. Furthermore, as stated in Chapter 2, other models had been discussed and dismissed because, in general terms, they do not match palaeontological data, metamorphic events, etc.

The para-autochthonous model propose that the Lower Palaeozoic sequences of the Precordillera terrane were deposited within a pull-apart extensional basin developed along the transcurrent fault that transported the Precordillera to its present position adjacent to the Famatina Range (Finney *et al.*, 2003c). A Cambrian age is proposed for the initiation of the strike-slip movements along the border of the Precordillera, which ended in the Devonian (Aceñolaza *et al.*, 2002). Before transcurrence, the terrane was spatially related to South America, Africa and Antarctica (SAFRAN). Isotopic comparisons of the probable Mesoproterozoic sources indicated in the para-autochthonous models do not match the signatures of the Ordovician to Silurian successions of the Precordillera terrane. This fact could however been explained if the Precordillera would have reached its present position before the initiation of the sedimentation of the oldest unit studied (Arenig-Llanvirn). If this would had been the case, it would imply that the Precordillera was attached or at least close enough to the source (Western Pampeanas Ranges, Cerro La Ventana Formation and the Arequipa-Antofalla Basement) in order to get their detritus. However, the strike-slip model cannot explain neither the deep burial metamorphism undergone by the Pie de Palo Complex during the Middle Ordovician (Vujovich *et al.*, 2004; Casquet *et al.*, 2001), nor the Ordovician continental magmatic arc. The Famatinian magmatic arc was not related to the docking of the Precordillera due to the lack of Famatinian aged zircons within the Ordovician detrital record (Finney *et al.*, 2005), although the presence of a positive area acting as a barrier would have been enough to prevent those detritus to reach the Ordovician basin.

The geotectonic evolution of the Precordillera as an allochthonous terrane implies in summary that the Precordillera was attached to Laurentia, rifted away during the opening of the Iapetus ocean (ca. 550 – 570 Ma) and travelled as a microcontinent at ca. 470 Ma (Thomas and Astini, 1996). During Llanvirn-Llandeilo, an eastward subduction was active leading to the collision (Guandacol Orogenic event) of the

Precordillera with Gondwana (Thomas and Astini, 1996). At Caradoc-Ashgill times a forebulge was developed, a new foreland basin was formed and glacial sediments were deposited which clearly link the Precordillera to Gondwana (Thomas and Astini, 1996). However, according to the provenance data here presented, the Precordillera terrane must have been attached to Gondwana probably since before the Arenig-Llanvirn.

Naipauer (2007), based mainly on detrital zircon dating, deduced a Laurentian derivation for the Neoproterozoic to Cambrian successions of the Precordillera terrane, therefore supporting the allochthonous model. The Mesoproterozoic basement (Western Pampeanas Ranges) of the Precordillera (Cuyania) terrane was at least partially exposed and provided detritus to a clastic level interlayered with the Angacos Formation (Naipauer, 2007). Following this assertion, the same rocks could have provided detritus to the Ordovician to Silurian record. Provenance indicators applied to the Ordovician to Silurian successions of the Precordillera terrane have not indicated typical Laurentian signatures, particularly concerning the Pb-Pb composition (due to the dissimilarities shown by the scarce Pb isotopes known from the Pie de Palo Range from the Western Pampeanas Ranges).

Nevertheless, comparisons of several provenance indicators strongly suggested that the Western Pampeanas Ranges, the Cerro La Ventana Formation and the Arequipa-Antofalla Basement are the most probable source areas and indicated that the Precordillera terrane would have reached its present position before deposition of the oldest unit. Therefore, the probable sources would have been uplifted since at least the Late Arenig-Early Llanvirn (or probably before this time according to Naipauer, 2007), in order to provide detritus to the Ordovician Precordilleran basin.

In such scenario, the geotectonic evolution implies that a subduction towards east of the Iapetus crust beneath Gondwana was active since the Cambrian as documented by the Famatinian magmatic arc (530-500 Ma; Pankhurst *et al.*, 1998; Fig. 8.8). During the Cambrian to Lower Ordovician, the Precordillera terrane travelled as a microplate (Thomas and Astini, 1996) and comprised a carbonate platform (e.g. Keller, 1996). Before the Arenig-Llandeilo (480 – 460 Ma) the subduction progressed enough to develop the Famatinian magmatic arc towards west (Fig. 8.8). The drowning of the carbonate platform and deposition of very fine clastic successions denoted the deepening of the basin. The proximity of the Precordillera terrane to Gondwana is further constrained by the presence of volcanic ashes (nowadays K-bentonites) with Famatinian affinities within Arenig to Llanvirn units of the Precordillera terrane such as the San Juan, Gualcamayo and Los Azules Formations (Huff *et al.*, 1995; Baldo *et al.*, 2003; Fanning *et al.*, 2004; Astini *et al.*, 2006). Faunal exchange between the two areas could have been also possible. As a response to the accretion, the Western Pampeanas Ranges were uplifted developing an accretionary prism (since the Late Arenig to Early Llanvirn), that might have prevented that massive quantities of Famatinian and Pampean detritus (and any other eastern source) reached the Precordilleran basin (Fig. 8.8). The uplifting is documented by U-Pb SHRIMP data on nine detrital zircons from schists belonging to the Difunta Correa metasedimentary sequence, which indicate a crystallization age for the zircons of 1.03 to 1.22 Ga and a metamorphic overprint at 460 Ma and linked to the ductile thrusting (Casquet *et al.*, 2001). Furthermore, a thermal event during the Middle Ordovician (455-470 Ma) was also recognized in dated zircon rims, and interpreted as due to the collision of Precordillera (Cuyania) terrane against Gondwana (Vujovich *et al.*, 2004). The lack of metamorphic overprints on the eastern Precordilleran sedimentary deposits is coherent with an accretion that ended before the deposition of the Ordovician units here studied. The metamorphism overprinted instead the Western Pampeanas Ranges.

During the Middle Ordovician to Early Silurian, clastic sediments were mainly deposited within the Precordillera. The provenance proxies of these sedimentary sequences indicate inputs from the Precordilleran basement (particularly within the San Rafael block) and the Western Pampeanas Ranges. Input of detrital material from the Arequipa-Antofalla Basement is suggested by matching of several isotopic provenance indicators (Sm-Nd, Pb-Pb, detrital zircon age dating). However, such provenance is still speculative because palaeocurrents from the north are scarce and the northern termination of the Precordillera terrane is not well known, meaning that the Jagué area could have acted either as source and/or as barrier.

The Western Pampeanas Ranges provided detritus to the basin and it acted as a

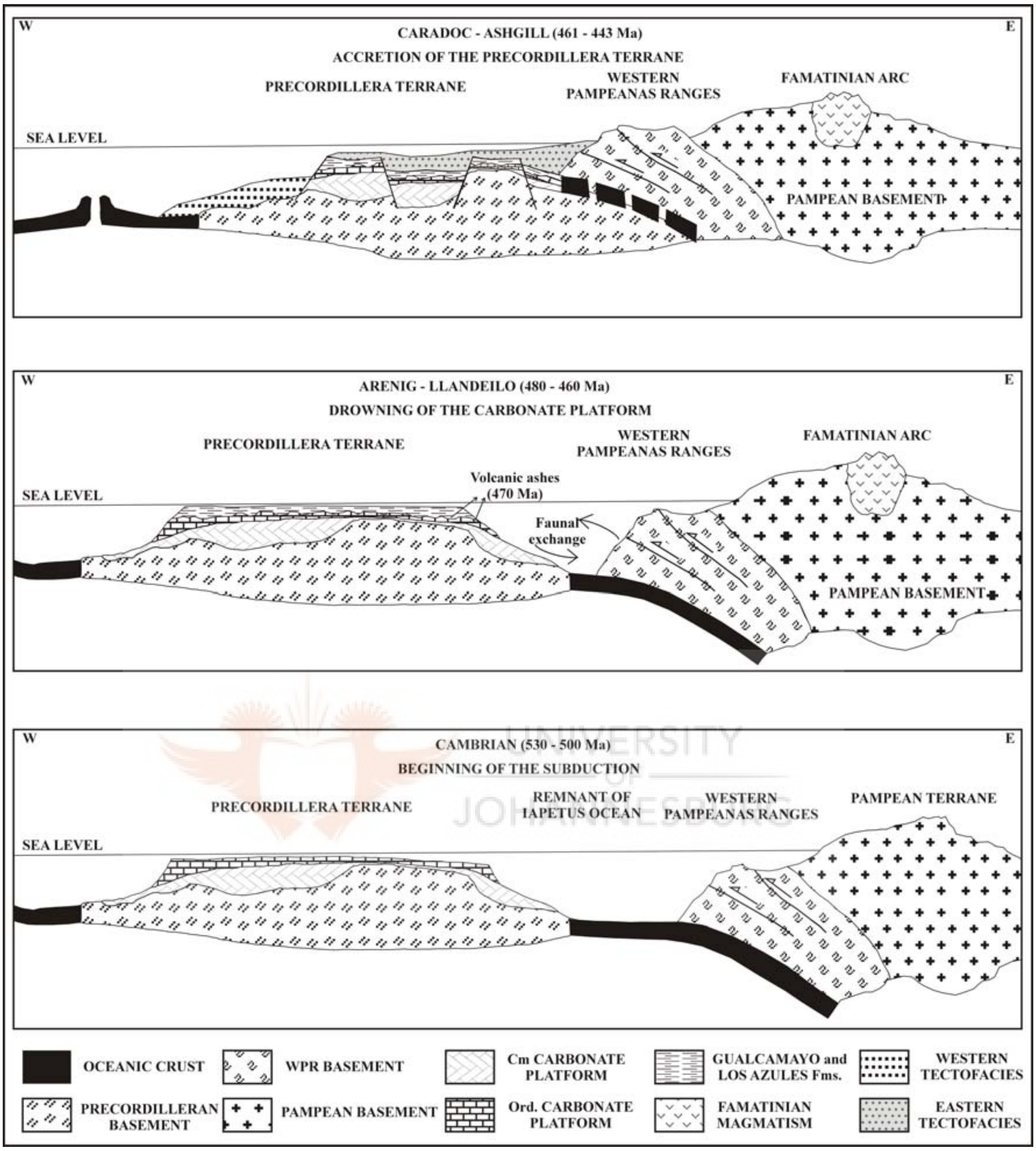

Figure 8.8: Geotectonic evolution of the Precordillera terrane. The subduction was active since the Cambrian as documented by the magmatic arc (Famatina). The volcanic ashes (nowadays K-bentonites) found within the uppermost San Juan Formation and the lowermost Gualcamayo Formation record the activity of such magmatism in the context of the Precordillera terrane. The basement of the Precordillera, the Western Pampeanas Ranges and the Arequipa-Antofalla Basement are the most probable sources. Irrespectively of their autochthonous or allochthonous character, a close spatial relationship between these sources and the Precordilleran basin is evident since at least the Late Arenig to Early Llanvirn.

positive area preventing that detrital material from the Famatinian arc reached the basin (Fig. 8.8). If the Western Pampeanas Ranges and the Arequipa-Antofalla Basement were autochthonous or para-autochthonous (Casquet *et al.,* 2006) to Gondwana, then the Precordillera terrane might have collided at least immediately before the beginning of the Ordovician clastic deposition (Late Arenig-Early Llanvirn; Fig. 8.8). Either if these areas were autochthonous to Gondwana or not, a close spatial relationship between them and the Precordilleran units studied in this thesis is deduced since the Late Arenig to Early Llanvirn (based on all the provenance indicators, particularly detrital zircon age dating). If at least a part of the sources were autochthonous to Gondwana, then the maximum age of accretion is Late Arenig to Early Llanvirn.

Because provenance indicators (mainly detrital zircon age dating and Pb-Pb isotopes) tend to exclude sources such as the Natal-Namaqua Metamorphic belt, the Falkland/Malvinas Microplate and Antarctica, those models proposing a para-autochthonous to Gondwana origin for the Precordillera terrane (e.g. Aceñolaza *et al.*, 2002; Finney *et al.*, 2005; Finney, 2007) need to be re-evaluated. The isotopic signatures from those areas were not found imprinted within the sedimentary successions from the Precordillera terrane here studied.

8.5 CONCLUDING REMARKS

Petrography, geochemistry, Sm-Nd and Pb-Pb isotopes, and detrital zircon dating analyses of the Ordovician to Silurian sedimentary rocks of sixteen different Formations deposited along the entire Precordillera terrane indicate a relatively uniform provenance, even though the unconformities that developed during this time interval. The homogeneous provenance signals are interpreted as produced by inputs from the same sources. Differences observed in the detrital zircon age populations are assigned to more restricted sources for the San Rafael block, compared with the Eastern and Western tectofacies. The different tectonic settings deduced for the host rocks of the detrital chromian spinels indicate mafic source rocks originated at several tectonic settings. Although the source rocks could not be detected, geotectonic settings similar to those indicated by the detrital spinels had been described for mafic to ultramafic rocks within the Western Pampeanas Ranges.

From the provenance point of view, the data obtained for the Precordilleran sequences analyzed indicate that a close relationship of the sedimentary record with the basement of the Precordillera terrane (e.g. the Cerro La Ventana Formation), the Western Pampeanas Ranges and less probably the Arequipa-Antofalla Basement is very likely. Furthermore, contributions to the detrital record from areas such as the Grenville Province of Laurentia, the Natal-Namaqua Metamorphic belt, the Falkland/Malvinas Microplate and Antarctica can be discounted.

The new constraints provided by the multi-disciplinary provenance analyses of the Ordovician and Ordovician to Silurian of the Precordillera terrane, together with palaeocurrent data and the geotectonic evolution of the main source areas, permitted constraining the proposed geotectonic models with regard to the evolution of the Precordillera terrane. Since at least the Late Arenig to Early Llanvirn, the sedimentary sequences of the Precordillera were spatially related to the Western Pampeanas Ranges and less probably to the Arequipa-Antofalla Basement (Central Andes). If these two areas are autochthonous to Gondwana, the collision between the Precordillera terrane and Gondwana is constrained to the Late Arenig to Early Llanvirn as the youngest age of collision. This has important implications for the proposed models regarding the geotectonic evolution of the Precordillera terrane. The lack of Famatinian zircons cannot be understood in terms of absence of a continental magmatic arc. The Western Pampeanas Ranges could have acted as positive area preventing the arrival of detritus from rocks located eastwards, such as the Famatinian magmatic arc.

APPENDIX A

GEOCHEMICAL AND ISOTOPE GEOCHEMICAL DATA

Gualcamayo Formation

	claystones													
Sample	**020454**	**020455**	**GUAL1**	**G 7**	**G 8**	**G 9**	**G 10**	**G 11**	**G 12**	**G 13**	**G 5**	**G 6**	**Aver**	**SD**
SiO_2	65.92	67.78	64.4	59.15	60.77	60.01	71.37	73.4	70.7	70.67	25.77	35.6	60.46	14.19
TiO_2	0.81	0.82	0.73	0.65	0.65	0.67	0.49	0.45	0.48	0.51	0.23	0.54	0.58	0.16
Al_2O_3	13.48	13.76	13.88	16.5	17.01	17.01	12.34	12.6	13.02	12.41	5.84	9.44	13.11	3.04
Fe_2O_3	5.78	3.54	5.14	6.65	5.2	6.04	1.49	2.2	0.49	2.28	4.89	6.95	4.22	2.06
MnO	0.02	b.d.l.	0.05	0.03	0.03	0.01	0.25	0.03	0.03	0.03	0.34	0.22	0.09	0.11
MgO	1.43	1.51	1.82	1.6	1.33	1.3	0.8	0.7	0.83	0.8	8.64	8.21	2.41	2.71
CaO	0.19	0.08	0.82	0.79	0.16	0.3	0.23	0.06	0.4	0.11	23.26	15.25	3.47	7.25
Na_2O	1.71	1.19	1.18	0.1	0.55	0.1	1.78	1.6	1.21	1.18	0.19	0.8	0.97	0.59
K_2O	3.4	3.42	3.37	5.16	5.22	5.11	3.11	2.76	3.2	2.95	1.97	3.24	3.57	0.99
P_2O_5	0.14	0.1	0.15	0.1	0.1	0.1	0.06	0.1	0.06	0.08	0.61	0.2	0.15	0.14
LOI	7.82	7.52	7.55	7.82	6.72	7.08	6.95	4.14	7.13	6.8	27.17	20.32	9.75	6.48
Σ	100.69	99.72	99.09	98.54	97.74	97.73	98.87	98.04	97.55	97.82	98.91	100.76	98.79	1.07
CIA	67	71	67		72		65	69	68	71			68.75	2.28
Sc	15.7	15.8	13.9	17.6	17.7	17.6	13.1	11.1	9.2	11.6	n.d.	n.d.	14.33	2.88
Cr	72	77	64	110	110	110	65	68	56	57	44	68	75.08	21.7
Ni	22	26	42	60	54	55	21	27	15	26	30	45	35.16	14.58
Cs	8	7	8	9	8	8	7	7	7	8	n.d.	n.d.	7.7	0.64
Rb	134	142	147	162	189	173	156	137	170	150	58	86	142	35.3
Ba	742	803	2133	534	569	554	2078	2312	2343	1958	264	380	1222.6	812.7
Hf	5	5	5	4	4	4	4	4	6	5	n.d.	n.d.	6.8	4.99
Th	12	13	12	10	10	10	10	11	12	12	3.5	5.7	10.1	2.69
U	7.2	8.6	4.2	4.3	4.6	6.1	4.6	5.5	7.3	5.8	n.d.	n.d.	5.82	1.41
V	175	252	100	196	175	221	141	199	117	142	71	111	158.33	51.54
Sr	66	60	116	244	149	162	131	134	141	144	214	485	170.5	106.97
Y	31.9	35.2	34.6	36.1	36.9	33.8	29.3	31.2	34.6	31.6	29.1	46	34.19	4.31
Zr	160	158	159	153	151	156	131	130	202	182	73	126	148.42	30.63
Nb	16	15	14	15	16	16	13	12	18	14	7	9	13.8	3.0
Pb	49.9	52.7	31.1	55.6	42.4	68.9	22.6	21	35	54.1	19.5	30.5	40.28	15.33
Zn	53	100	112	227	127	202	35	56	27	99	109	101	104	58.45
La	41	44	35	32	29	33	34	34	47	36	n.d.	n.d.	36.5	5.39
Ce	84	87	72	64	58	67	68	69	98	74	n.d.	n.d.	74.1	11.47
Nd	40	39	32	32	27	32	33	32	44	31	n.d.	n.d.	34.2	4.85
Sm	6.6	6.9	6.3	5.9	5.2	5.8	5.3	5.7	7.4	5.6	n.d.	n.d.	6.07	0.68
Eu	1	1.1	1.1	1.4	1.1	0.9	0.9	1	1	0.8	n.d.	n.d.	1.03	0.16
Tb	0.8	0.9	0.8	0.8	0.9	0.9	0.8	0.8	1	0.9	n.d.	n.d.	0.86	0.07
Yb	3.1	3.2	3.1	3.1	3	2.9	2.7	2.7	3.4	3.1	n.d.	n.d.	3.03	0.21
Lu	0.52	0.55	0.52	0.52	0.51	0.5	0.47	0.44	0.57	0.52	n.d.	n.d.	0.51	0.03
ΣREE	177.02	182.65	150.82	139.72	124.71	143	145.17	145.64	202.37	151.92			156.3	22.32
Eu/Eu*	0.49	0.5	0.55	0.74	0.63	0.47	0.52	0.55	0.42	0.43			0.53	0.09
Ce/Ce*	0.94	0.92	0.96	0.91	0.93	0.93	0.92	0.94	0.96	0.97			0.94	0.02
K/Cs	3525	4053	3497	4755	5420	5298	3688	3273	3797	3063			4037	793
Th/Sc	0.76	0.82	0.86	0.57	0.56	0.57	0.76	0.99	1.3	1.03			0.82	0.23
Zr/Sc	10.19	10	11.44	8.69	8.53	8.86	10	11.71	21.96	15.69			11.71	3.95
Th/U	1.67	1.51	2.86	2.33	2.17	1.64	2.17	2	1.64	2.07			2.01	0.39
La/Sc	2.61	2.78	2.52	1.82	1.64	1.88	2.6	3.06	5.11	3.1			2.71	0.93
La/Th	3.42	3.38	2.92	3.2	2.9	3.3	3.4	3.09	3.92	3			3.25	0.29
Cr/V	0.41	0.31	0.64	0.56	0.63	0.5	0.46	0.34	0.48	0.4	0.62	0.61	0.5	0.11
Y/Ni	1.46	1.37	0.83	0.60	0.68	0.61	1.40	1.16	2.31	1.22	0.97	1.02	1.14	0.46
Ti/Nb	305	329.5	303.9	254.7	243.9	254.2	220.3	222.9	159.9	215.3	193.5	367.8	255.9	57.7
La_N/Yb_N	8.94	9.29	7.63	6.98	6.53	7.69	8.51	8.51	9.34	7.85			8.13	0.9
La_N/Sm_N	3.91	4.01	3.5	3.41	3.51	3.58	4.04	3.75	4	4.05			3.78	0.24
Tb_N/Yb_N	1.1	1.2	1.1	1.1	1.28	1.33	1.27	1.27	1.26	1.24			1.22	0.08
Cr/Th	6	5.92	5.33	11	11	11	6.5	6.18	4.67	4.75	12.57	11.93	8.07	2.97
Ti/Zr	30.31	31.08	27.52	25.47	25.69	25.75	22.20	20.75	14.25	16.8	18.56	25.69	23.67	5.02

Table 1: Chemical analyses of sedimentary clastic rocks of the Precordillera terrane. Major elements are in % whereas trace elements are in ppm. N denotes normalized to chondrite values (after Taylor and McLennan, 1985). Aver: average; SD: standard deviation; b.d.l.: below detection limits; n.d.: not determined.

Los Azules Formation

	claystones							siltstones			
Sample	**020406**	**020407**	**020409**	**020411**	**020412**	**020413**	**020414**	**020405**	**020408**	**Aver**	**SD**
SiO_2	73.41	65.70	56.95	54.10	62.38	62.93	67.84	79.52	33.07	61.77	12.52
TiO_2	0.71	0.81	1.13	0.78	1.09	1.12	0.99	0.51	0.33	0.83	0.27
Al_2O_3	13.15	14.02	19.37	10.75	14.81	14.59	13.24	9.46	7	12.93	3.35
Fe_2O_3	0.76	5.07	8.24	7.06	6.75	6.6	5.53	1.59	2.81	4.93	2.47
MnO	0.01	0.04	0.09	0.08	0.02	0.07	0.05	b.d.l.	0.85	0.15	0.26
MgO	1.05	1.25	4.22	1.82	2.29	2.08	1.58	0.54	1.31	1.79	1
CaO	0.04	0.12	0.73	11.07	0.57	0.29	0.48	0.13	33.37	5.2	10.51
Na_2O	1.1	1.35	2.4	2.04	1.68	2.49	1.69	0.75	2.78	1.81	0.64
K_2O	3.14	3.02	4.34	2.46	3.23	3.12	2.98	1.75	1.5	2.84	0.8
P_2O_5	0.04	0.14	0.17	0.17	0.18	0.18	0.15	0.1	0.62	0.19	0.16
LOI	5.96	6.81	5.02	12.35	5.68	5.58	5.52	3.05	25.3	8.36	6.44
Σ	99.37	98.33	102.67	102.69	98.66	99.04	100.04	97.38	108.92	100.79	3.35
CIA	72	72	67		68	66	67	75		69.6	3.2
Sc	13.4	15.8	18.7	13.3	16.9	16.7	14.8	7.8	7.4	13.87	3.72
Cr	68	75	100	77	110	100	96	40	35	77.89	25.21
Ni	45	86	44	48	77	76	76	31	15	55.16	23.07
Cs	9	8	12	3	6	5	5	5	4	6.34	2.67
Rb	163	133	171	73	115	115	117	94	41	102.4	49
Ba	1570	1779	920	886	773	761	826	1489	657	1073.4	394.2
Hf	4	4	3	5	5	6	5	4	2	4.22	1.13
Th	8.5	12	13	8.4	10	11	11	8.8	5.1	9.76	2.23
U	4.8	5.9	3.7	5	7	5.3	4.9	7.3	3.4	5.26	1.24
V	154	125	107	218	173	164	140	108	41	136.89	47.07
Sr	114	140	108	178	126	118	121	178	215	144.22	35.11
Y	30.8	45.9	21.3	40.1	39.9	35.3	28.3	24.2	45	34.53	8.39
Zr	133	150	88	155	180	189	178	144	93	145.56	34.11
Nb	15	14	23	14	17	18	18	12	10	15.6	3.5
Pb	19.5	37.9	19.2	146.4	35.1	33.1	34.8	157.2	8.1	54.59	52.83
Zn	106	336	136	137	197	168	140	106	29	150.56	78.95
La	32	38	25	34	40	38	37	27	30	33.44	4.99
Ce	63	72	54	69	79	82	75	52	61	67.44	10.03
Nd	29	35	25	35	43	38	31	28	27	32.33	5.52
Sm	5.2	7.4	4.5	6.7	8.3	7.9	6.6	5	5.8	6.38	1.26
Eu	0.9	1.4	0.8	1.2	1.5	1.6	1	0.8	1.4	1.18	0.29
Tb	b.d.l.	1.3	b.d.l.	1.1	1.2	1.3	1	0.8	0.7	1.06	0.22
Yb	2.8	3.4	2.1	3.1	3.4	3.2	2.9	2.6	2.3	2.87	0.44
Lu	0.47	0.57	0.33	0.5	0.55	0.55	0.48	0.44	0.37	0.47	0.08
ΣREE	132.87	159.07	111.23	150.6	176.95	172.55	154.98	116.64	128.57	144.83	22.29
Eu/Eu*		0.56		0.54	0.56	0.61	0.46	0.48	0.77	0.57	0.1
Ce/Ce*	0.92	0.88	0.99	0.92	0.89	0.98	0.96	0.87	0.95	0.93	0.04
K/Cs	2895	3128	3002	6815	4462	5185	4949	2910	3102	4050	1308
Th/Sc	0.63	0.76	0.7	0.63	0.59	0.66	0.74	1.13	0.69	0.73	0.15
Zr/Sc	9.93	9.49	4.71	11.65	10.65	11.32	12.03	18.46	12.57	11.2	3.37
Th/U	1.77	2.03	3.51	1.68	1.43	2.08	2.24	1.21	1.5	1.94	0.64
La/Sc	2.39	2.41	1.34	2.56	2.37	2.28	2.5	3.46	4.05	2.59	0.72
La/Th	3.76	3.17	1.92	4.05	4	3.45	3.36	3.07	5.88	3.63	1
Cr/V	0.44	0.59	0.93	0.35	0.64	0.61	0.69	0.37	0.85	0.61	0.19
Y/Ni	0.69	0.53	0.48	0.84	0.52	0.47	0.37	0.78	3.1	0.87	0.8
Ti/Nb	288	341.9	297.1	335.3	386.3	377.9	338.2	256.6	192	312.6	57.98
La_N/Yb_N	7.72	7.55	8.04	7.41	7.95	8.02	8.62	7.02	8.81	7.91	0.53
La_N/Sm_N	3.87	3.23	3.5	3.19	3.03	3.03	3.53	3.4	3.26	3.34	0.25
Tb_N/Yb_N		1.63		1.52	1.51	1.74	1.47	1.32	1.3	1.5	0.15
Cr/Th	8	6.25	7.69	9.17	11	9.09	8.73	4.55	6.86	7.93	1.78
Ti/Zr	32.05	32.37	76.64	30.28	36.27	35.4	33.44	21.02	21.27	35.42	15.49

Table 1 (cont): Chemical analyses of sedimentary clastic rocks of the Precordillera terrane. Major elements are in % whereas trace elements are in ppm. N denotes normalized to chondrite values (after Taylor and McLennan, 1985). Aver: average; SD: standard deviation; b.d.l.: below detection limits; n.d.: not determined.

La Cantera Formation

	mudstones					sandstones								
Sample	**020442**	**020446**	**020448**	**020450**	**020452**	**020441**	**020444**	**020445**	**020447**	**020449**	**020451**	**020453**	**Aver**	**SD**
SiO_2	56.48	55.15	59.37	59.44	57.60	63.28	55.40	53.18	72.99	63.67	71.2	77.29	62.09	7.5
TiO_2	1.12	1.04	1.24	1.1	1.24	1.09	1.09	0.72	1.14	0.89	1	1.11	1.06	0.14
Al_2O_3	17.64	18.76	16.03	17.06	17.22	10.75	17.81	6.33	9.29	8.1	6.06	8.27	12.78	4.82
Fe_2O_3	8.14	8.49	7.48	7.74	7.72	4.22	8.52	3.09	4.58	3.91	3.48	3.88	5.94	2.12
MnO	0.05	0.08	0.05	0.05	0.05	0.07	0.09	0.39	0.03	0.14	0.11	0.05	0.1	0.09
MgO	3.66	3.58	3.09	3.13	3.11	1.96	3.95	1.35	2	1.53	1.26	1.73	2.53	0.94
CaO	0.65	0.49	1.14	0.46	0.66	5.27	1.54	19.04	1.17	8.82	7.5	2.47	4.1	5.28
Na_2O	1.6	1.87	1.87	1.57	1.67	2.8	1.94	2.55	2.14	2.75	2.04	1.81	2.05	0.41
K_2O	4.1	4.68	3.44	4.08	3.94	1.67	4.26	0.98	1.27	1.12	0.86	1.04	2.62	1.5
P_2O_5	0.17	0.16	0.19	0.16	0.18	0.17	0.17	0.13	0.15	0.14	0.12	0.13	0.16	0.02
LOI	5.23	4.94	5.13	4.97	5.63	6.4	6.35	15.9	2.65	9.05	7.24	3.64	6.43	3.26
Σ	98.84	99.25	99.03	99.76	99	97.68	101.12	103.68	97.4	100.11	100.87	101.42	99.85	1.67
CIA	69	68	65	69	69		63		58				65.86	3.87
Sc	19.1	20.2	18.1	18.8	19.6	11.8	19.4	7.5	11.3	8.8	7.4	9.2	14.27	5.1
Cr	120	120	110	110	120	85	120	68	96	78	100	91	101.5	17.33
Ni	59	64	57	58	55	41	61	24	48	38	38	47	49.31	11.53
Cs	8	9	6	7	8	2	8	1	1	b.d.l.	1	1	4.73	3.3
Rb	134	157	118	140	132	56	136	30	48	39	31	39	88.3	49
Ba	602	767	538	529	549	325	607	268	260	248	211	234	428.2	181.6
Hf	5	5	7	6	6	10	5	8	11	11	12	12	8.17	2.73
Th	11	11	11	11	12	8.1	10	5.5	7.3	5.9	6	6.3	8.76	2.37
U	2.8	3	3	2.9	3.1	2.6	3	1.5	1.2	1.5	2.2	1.8	2.38	0.68
V	108	121	108	110	113	83	111	62	83	70	63	71	91.92	21.03
Sr	65	71	75	63	67	133	79	207	77	146	123	91	99.67	42.15
Y	31.7	30.6	33.5	33.1	32.5	29.7	32.6	49.6	19.9	32.6	21.8	17.9	30.46	7.86
Zr	181	176	230	184	219	319	167	287	316	338	390	332	261.58	74.04
Nb	19	20	21	19	21	19	18	14	17	16	16	17	18.0	2.1
Pb	24.4	23.4	23.5	37.5	22.7	6.6	15.3	4.8	7.5	7.7	7.2	7.1	15.64	10
Zn	111	132	120	130	127	74	124	35	67	53	47	61	90.08	35.47
La	40	37	38	41	42	29	39	34	28	22	18	20	32.33	8.28
Ce	83	76	78	85	86	71	82	65	64	55	45	51	70.08	13.44
Nd	41	38	38	39	39	34	38	29	31	29	22	24	33.5	6.1
Sm	6.9	6.3	6.9	7.1	7.3	7.3	7.3	6.5	6.1	5.9	4.5	5	6.43	0.88
Eu	1.3	1	1.4	1.2	1.3	1.5	1.5	1.6	1.1	1.3	0.6	1.1	1.24	0.26
Tb	0.8	1	1	0.9	0.9	b.d.l.	1.2	0.9	1	1.2	0.8	0.7	0.95	0.15
Yb	3.2	3.1	3.5	3.2	3.5	3.2	3.3	2.8	2.8	3.2	2.8	2.4	3.08	0.31
Lu	0.51	0.5	0.55	0.53	0.57	0.53	0.53	0.46	0.46	0.5	0.47	0.42	0.5	0.04
ΣREE	176.71	162.9	167.35	177.93	180.57	146.03	172.83	140.26	134.46	118.1	94.17	104.62	147.99	28.74
Eu/Eu*	0.61	0.48	0.63	0.54	0.57		0.62	0.77	0.54	0.62	0.39	0.68	0.59	0.1
Ce/Ce*	0.94	0.93	0.94	0.96	0.95	1.08	0.96	0.90	1.02	1.07	1.09	1.12	1	0.07
K/Cs	4254	4317	4759	4842	4086	6911	4424	8143	10526		7139	8608	6183	2101
Th/Sc	0.58	0.54	0.61	0.59	0.61	0.69	0.52	0.73	0.65	0.67	0.81	0.68	0.64	0.08
Zr/Sc	9.48	8.71	12.71	9.79	11.17	27.03	8.61	38.27	27.96	38.41	52.7	36.09	23.41	14.66
Th/U	3.93	3.67	3.67	3.79	3.87	3.12	3.33	3.67	6.08	3.93	2.73	3.5	3.77	0.78
La/Sc	2.09	1.83	2.1	2.18	2.14	2.46	2.01	4.53	2.48	2.5	2.43	2.17	2.41	0.67
La/Th	3.64	3.36	3.45	3.73	3.5	3.58	3.9	6.18	3.84	3.73	3	3.17	3.76	0.77
Cr/V	1.11	0.99	1.02	1	1.06	1.02	1.08	1.1	1.16	1.11	1.59	1.28	1.13	0.16
Y/Ni	0.53	0.48	0.59	0.57	0.59	0.72	0.53	2.04	0.41	0.86	0.57	0.38	0.69	0.43
Ti/Nb	357.5	312.6	359.4	348.9	349.2	344.2	358.4	312.9	390.5	335.8	385.5	397	354.4	25.99
La_N/Yb_N	8.45	8.07	7.34	8.66	8.11	6.12	7.99	8.21	6.76	4.65	4.34	5.63	7.03	1.44
La_N/Sm_N	3.65	3.7	3.47	3.63	3.62	2.5	3.36	3.29	2.89	2.35	2.52	2.52	3.12	0.51
Tb_N/Yb_N	1.07	1.38	1.22	1.2	1.1		1.55	1.37	1.53	1.6	1.22	1.25	1.32	0.17
Cr/Th	10.91	10.91	10	10	10	10.49	12	12.36	13.15	13.22	16.67	14.44	12.01	1.99
Ti/Zr	37.13	35.53	32.35	35.94	33.81	20.39	39.06	14.94	21.63	15.7	15.42	19.97	26.82	9.15

Table 1 (cont.): Chemical analyses of sedimentary clastic rocks of the Precordillera terrane. Major elements are in % whereas trace elements are in ppm. N denotes normalized to chondrite values (after Taylor and McLennan, 1985). Aver: average; SD: standard deviation; b.d.l.: below detection limits; n.d.: not determined.

Las Vacas Formation

	mudstones		sandstones						
Sample	**VACAS0**	**VACAS4**	**VACAS1**	**VACAS3**	**LV 5**	**LV 10**	**LV 11**	**Aver**	**SD**
SiO_2	43.97	42	76.09	69.78	67.88	64.97	66.3	61.57	12.22
TiO_2	0.54	0.56	0.94	0.47	0.76	0.79	0.74	0.69	0.15
Al_2O_3	8.49	9.45	8.89	5.25	9.96	9.77	9.43	8.75	1.5
Fe_2O_3	4.34	3.41	3.55	2.66	5.71	6.72	5.9	4.61	1.4
MnO	0.09	0.06	0.02	0.1	0.05	0.08	0.06	0.07	0.03
MgO	3.4	2.07	0.8	1.02	2.8	3.86	3.81	2.54	1.18
CaO	19.57	22.44	0.94	9.58	2.63	2.34	2.94	8.63	8.27
Na_2O	0.75	0.55	1.7	1.07	2.81	2.8	2.29	1.71	0.88
K_2O	2.38	2.48	1.68	1.11	1.21	1.36	1.23	1.64	0.53
P_2O_5	0.13	0.1	0.09	0.07	0.12	0.11	0.1	0.1	0.02
LOI	21.65	21.38	3.07	10.21	5.14	4.96	5.01	10.2	7.44
Σ	105.32	104.5	97.74	101.33	99.08	97.77	97.79	100.5	3.03
CIA			59					59	0
Sc	10	11	10.3	6.6	15.3	15.5	15	11.96	3.14
Cr	61	69	65	39	87	87	83	70.14	16.1
Ni	37	33	40	23	41	43	39	36.54	6.27
Cs	4	5	2	2	1	2	1	2.43	1.4
Rb	73	72	67	45	39	431	42	109.9	131.8
Ba	1598	973	728	681	327	260	249	688	450
Hf	3	3	8	5	7	7	6	5.57	1.84
Th	6.2	7	6.1	4.4	6.6	6.5	6.8	6.23	0.8
U	2	1.8	1.8	1.1	1.4	1.2	1.5	1.54	0.31
V	87	76	76	55	97	103	95	84.14	15.25
Sr	538	606	88	219	106	101	89	249.57	208.99
Y	32.3	40.5	22.7	19.8	21.5	19.7	19.1	25.09	7.57
Zr	130	139	217	140	195	204	192	173.86	33.45
Nb	9	10	14	10	15	15	14	12.43	2.3
Pb	14.2	13.4	6.5	4.4	10	6.7	8.2	9.06	3.4
Zn	73	63	68	36	71	73	72	65.14	12.35
La	24	28	29	17	26	25	22	24.43	3.74
Ce	50	57	63	37	56	54	49	52.29	7.59
Nd	25	30	24	15	27	27	23	24.43	4.4
Sm	4.6	5.6	5	3.2	5.1	5	4.6	4.73	0.7
Eu	1	1.2	1.1	0.7	1.2	1.1	1.1	1.06	0.16
Tb	0.7	0.6	b.d.l.	0.8	0.9	0.9	0.9	0.8	0.12
Yb	2	2.2	2.4	1.5	2.4	2.4	2.4	2.19	0.31
Lu	0.32	0.36	0.39	0.25	0.39	0.39	0.37	0.35	0.05
ΣREE	107.62	124.96	124.89	75.45	118.99	115.79	103.37	110.15	16.05
Eu/Eu*	0.66	0.7		0.58	0.69	0.64	0.68	0.66	0.04
Ce/Ce*	0.94	0.92	1.03	1.02	0.98	0.97	1.01	0.98	0.04
K/Cs	4943	4124	6956	4620	10019	5645	10210	6645	2347
Th/Sc	0.62	0.64	0.59	0.67	0.43	0.42	0.45	0.55	0.1
Zr/Sc	13	12.64	21.07	21.21	12.75	13.16	12. 8	15.23	3.74
Th/U	3.1	3.89	3.39	4	4.71	5.42	4.53	4.15	0.74
La/Sc	2.4	2.55	2.82	2.58	1.7	1.61	1.47	2.16	0.51
La/Th	3.87	4	4.75	3.86	3.94	3.85	3.24	3.93	0.41
Cr/V	0.7	0.91	0.86	0.71	0.9	0.84	0.87	0.83	0.08
Y/Ni	0.88	1.23	0.57	0.86	0.52	0.46	0.49	0.72	0.26
Ti/Nb	346.9	329.7	396	289.9	309.9	324.4	312.5	329.9	31.59
La_N/Yb_N	8.11	8.6	8.17	7.66	7.32	7.04	6.19	7.58	0.75
La_N/Sm_N	3.28	3.15	3.65	3.34	3.21	3.15	3.01	3.26	0.19
Tb_N/Yb_N	1.5	1.17		2.28	1.6	1.6	1.6	1.63	1.99
Cr/Th	9.84	9.86	10.66	8.86	13.18	13.38	12.21	11.14	1.65
Ti/Zr	25.09	24.2	25.91	20.3	23.37	23.22	22.95	23.57	1.67

Table 1 (cont.): Chemical analyses of sedimentary clastic rocks of the Precordillera terrane. Major elements are in % whereas trace elements are in ppm. N denotes normalized to chondrite values (after Taylor and McLennan, 1985). Aver: average; SD: standard deviation; b.d.l.: below detection limits; n.d.: not determined.

Las Plantas – Trapiche Formations

Sample	mudstones									VF conglomerate	
	PLANT2	LPT 6	LPT 7	LPT 9	LPT 10	LPT 17	LPT 19	LPT 21	LPT 22	LPT 25	LPT 26
SiO_2	62.02	60.42	63.73	62.59	64.91	60.29	63.59	83.45	84.63	62.95	61.11
TiO_2	1.11	0.63	0.75	0.55	0.53	0.8	0.89	0.21	0.21	0.4	0.37
Al_2O_3	16.08	12.46	13.74	9.98	9.27	15.5	16.15	4.46	4.19	5.53	5.42
Fe_2O_3	6.58	5.86	6.53	4.85	3.57	7.92	5.09	3.38	2.88	2.49	2.17
MnO	0.04	0.05	0.05	0.06	0.02	0.02	0.01	0.01	0.01	0.05	0.07
MgO	2.47	2.34	2.09	2.06	1.78	1.43	0.81	0.43	0.38	2.83	2.4
CaO	0.35	3.85	0.65	5.89	6.65	0.13	0.09	0.14	0.11	10.53	13.15
Na_2O	1.14	2.18	2.31	2.18	1.9	2.16	1.82	1.8	1.38	1.21	1.24
K_2O	3.61	2.74	2.94	2.08	1.78	3.23	3.57	0.29	0.2	1.06	1.07
P_2O_5	0.13	0.09	0.11	0.1	0.09	0.1	0.07	0.08	0.07	0.1	0.1
LOI	5.32	7.53	5.21	8.62	8.35	7.06	6.03	4.62	4.35	11.96	13.31
Σ	98.84	98.14	98.11	98.95	98.85	98.64	98.11	98.88	98.42	99.09	100.4
CIA	72		63			69	70	57	62		
Sc	19.3	15.3	15.2	12.9	11.8	18.4	15.9	3.8	3.7	n.d.	6.2
Cr	100	85	93	73	59	110	120	24	27	51	59
Ni	51	37	40	39	43	27	31	30	25	24	28
Cs	6	7	6	5	4	7	8	b.d.l.	1	n.d.	2
Rb	132	110	119	84	74	123	141	15	12	43	42
Ba	946	591	571	491	455	1130	1577	253	380	650	614
Hf	7	7	8	10	8	9	11	10	10	n.d.	3
Th	13	10	11	9.1	8.4	12	13	3.3	3.1	4.1	4.5
U	3.8	2.4	2.3	2.4	2	3.4	3.9	1.1	0.8	n.d.	1.5
V	127	80	90	68	63	107	115	21	21	50	50
Sr	86	169	108	209	223	173	143	92	116	273	246
Y	32.6	30.9	30.4	30.4	30.7	29	34.4	7.7	7.1	22.2	21.1
Zr	221	223	249	318	275	284	330	261	282	123	115
Nb	19	16	19	15	14	20	22	7	7	8	8
Pb	28.7	21.1	25.1	19.2	15.1	30.5	20.9	2.8	4.4	4.5	4.5
Zn	142	83	89	86	80	81	79	58	50	41	41
La	44	36	39	32	31	41	46	14	13	n.d.	14
Ce	92	78	87	72	69	91	100	34	35	n.d.	30
Nd	44	38	39	33	31	38	47	18	17	n.d.	16
Sm	7.5	7.1	7.6	6.9	6.6	6.8	7.7	3.2	3.3	n.d.	2.9
Eu	1.4	1.2	1.4	1.3	1.2	1	1.1	0.5	0.7	n.d.	0.6
Tb	1.2	0.7	1.1	0.8	1	0.8	1	0.6	b.d.l.	n.d.	
Yb	3.4	3.2	3.2	3	2.9	3.4	4.1	1.4	1.4	n.d.	1.5
Lu	0.54	0.51	0.54	0.5	0.5	0.57	0.68	0.26	0.25	n.d.	0.23
ΣREE	194.04	164.71	178.84	149.5	143.2	182.57	207.58	71.96	70.15	n.d.	64.73
Eu/Eu*	0.56	0.56	0.57	0.61	0.56	0.47	0.45	0.45			
Ce/Ce*	0.95	0.98	1.02	1.02	1.02	1.03	0.99	1.05	1.16		0.95
K/Cs	4989	3246	4073	3450	3694	3830	3704		1685		4445
Th/Sc	0.67	0.65	0.72	0.71	0.71	0.65	0.82	0.87	0.84		0.73
Zr/Sc	11.45	14.58	16.38	24.65	23.31	15.43	20.75	68.68	76.22		18.55
Th/U	3.42	4.17	4.78	3.79	4.2	3.53	3.33	3	3.88		3
La/Sc	2.28	2.35	2.57	2.48	2.63	2.23	2.89	3.68	3.51		2.26
La/Th	3.38	3.6	3.55	3.52	3.69	3.42	3.54	4.24	4.19		3.11
Cr/V	0.79	1.06	1.03	1.07	0.94	1.03	1.04	1.14	1.29	1.02	1.18
Y/Ni	0.64	0.84	0.76	0.78	0.71	1.07	1.11	0.26	0.28	0.92	0.75
Ti/Nb	346.8	231.3	234.8	225.1	231.5	239.8	244.7	187.9	188	283.3	257.2
La_N/Yb_N	8.74	7.6	8.24	7.21	7.22	8.15	7.58	6.76	6.27		6.31
La_N/Sm_N	3.69	3.19	3.23	2.92	2.96	3.8	3.76	2.75	2.48		3.04
Tb_N/Yb_N	1.51	0.94	1.47	1.14	1.47	1.01	1.04	1.83			
Cr/Th	7.69	8.5	8.45	8.02	7.02	9.17	9.23	7.27	8.71	12.44	13.11
Ti/Zr	29.98	16.91	18.01	10.41	11.53	16.97	16.17	4.82	4.4	19.35	19.24

Table 1 (cont.): Chemical analyses of sedimentary clastic rocks of the Precordillera terrane. Major elements are in % whereas trace elements are in ppm. N denotes normalized to chondrite values (after Taylor and McLennan, 1985). Aver: average; SD: standard deviation; b.d.l.: below detection limits; n.d.: not determined; V.F.: very fine.

Las Plantas – Trapiche Formations (cont.)

Sample	sandstones												Aver	SD
	PLANT1	LPT1	LPT2	LPT3	LPT5	LPT12	LPT13	LPT14	LPT15	LPT16	LPT23	LPT24		
SiO_2	67.51	69.59	70.44	70.50	72.25	70.53	67.28	95.23	89.92	92.57	78.92	68.17	71.42	10.5
TiO_2	1.04	0.12	0.16	0.08	0.09	0.18	0.34	0.07	0.07	0.09	0.61	0.17	0.41	0.32
Al_2O_3	11.76	0.83	1.96	0.85	0.06	1.39	5.61	0.53	1.15	0.87	6.25	1.47	6.33	5.46
Fe_2O_3	5.98	0.43	0.97	0.74	0.49	0.32	2.66	0.24	0.74	1.16	3.76	1.31	3.05	2.33
MnO	0.08	0.03	0.05	0.05	0.01	0.05	0.04	0.04	0.04	0.01	0.04	0.07	0.04	0.02
MgO	2.04	0.55	0.67	0.35	0.31	0.98	1.25	0.28	0.66	0.31	1.04	0.52	1.22	0.83
CaO	2.01	14.52	13.12	14.86	14.26	12.95	9.72	0.35	1.08	0.37	1.42	14.57	6.12	5.92
Na_2O	1.8	0.68	1.85	1.36	0.31	1.1	1.54	0.31	0.49	0.73	2.19	0.47	1.4	0.64
K_2O	2.12	0.08	0.13	0.09	0.03	0.06	1.1	0.09	0.05	0.08	0.74	0.13	1.19	1.26
P_2O_5	0.13	0.09	0.13	0.09	0.06	0.06	0.09	0.09	0.06	0.1	0.14	0.08	0.09	0.02
LOI	4.22	12.8	11.27	11.57	12.62	11.64	9.96	0.81	3.5	1.9	2.9	12.33	7.73	3.85
Σ	98.68	99.73	100.75	100.53	100.48	99.26	99.6	98.03	97.76	98.2	98	99.29	98.99	0.88
CIA													65.5	5.25
Sc	14.8	n.d.	n.d.	1.7	n.d.	n.d.	n.d.	1.3	1.2	1.3	7.7	3	9.03	6.46
Cr	77	22	41	14	25	23	22	29	12	34	65	25	51.74	32.25
Ni	41	16	15	13	14	36	63	41	36	41	36	21	32.58	12.13
Cs	3	n.d.	n.d.	b.d.l.	n.d.	n.d.	n.d.	b.d.l.	b.d.l.	b.d.l.	b.d.l.	b.d.l.	4.9	2.21
Rb	79	6	6	5	4	5	7	6	6	6	32	8	46.3	48.3
Ba	556	119	86	83	44	406	1109	301	327	306	296	285	503.3	370.6
Hf	8	n.d.	n.d.	6	n.d.	n.d.	n.d.	10	6	12	13	4	9.63	3.56
Th	10	2.7	2.2	1.4	2	2.3	2.2	0.6	0.9	1.2	7	2.5	5.5	4.19
U	2.9	n.d.	n.d.	b.d.l.	n.d.	n.d.	n.d.	1	b.d.l.	b.d.l.	2.1	0.9	2.18	1.01
V	90	12	11	8	6	11	12	5	7	6	58	21	45.17	39.28
Sr	129	356	277	312	389	368	78	77	164	84	123	234	192.57	96.81
Y	26.1	34.2	30.4	34.8	20.8	28.4	1.7	1.2	7.4	1.3	19.2	18.8	21.77	11.39
Zr	237	291	377	205	358	573	426	273	126	306	357	132	275.74	103.42
Nb	17	6	5	4	3	5	7	4	4	5	13	5	10.15	6.08
Pb	5.8	1.3	3.2	1.9	1.3	2	2.2	4.8	5.3	0.5	8.8	2	9.39	9.55
Zn	84	b.d.l.	b.d.l.	b.d.l.	b.d.l.	12	20	b.d.l.	5	b.d.l.	43	4	58.71	35.73
La	31	n.d.	n.d.	14	n.d.	n.d.	n.d.	5.6	7.8	6.7	28	12	24.42	13.68
Ce	71	n.d.	n.d.	38	n.d.	n.d.	n.d.	15	21	19	72	32	56.24	28.27
Nd	32	n.d.	n.d.	18	n.d.	n.d.	n.d.	10	13	9	31	14	26.35	12.18
Sm	6.2	n.d.	n.d.	3.8	n.d.	n.d.	n.d.	1.8	2.6	2.1	6.1	2.9	5.01	2.14
Eu	1.2	n.d.	n.d.	0.6	n.d.	n.d.	n.d.	0.5	0.6	0.5	1.2	0.7	0.92	0.33
Tb	0.9	n.d.	n.d.	0.7	n.d.	n.d.	n.d.	b.d.l.	b.d.l.	b.d.l.	1	b.d.l.	0.89	0.18
Yb	2.9	n.d.	n.d.	2.1	n.d.	n.d.	n.d.	1.1	0.7	1	2.6	1.4	2.31	1.01
Lu	0.45	n.d.	n.d.	0.33	n.d.	n.d.	n.d.	0.16	0.11	0.18	0.45	0.23	0.38	0.17
ΣREE	145.65			77.53				33.66	45.31	37.98	142.35	62.73	116.03	58.17
Eu/Eu*	0.6			0.46							0.59		0.53	0.06
Ce/Ce*	1.04			1.17				1.05	1.08	1.21	1.15	1.18	1.06	0.08
K/Cs	5863												3898	1048
Th/Sc	0.68			0.82				0.46	0.75	0.92	0.91	0.83	0.75	0.11
Zr/Sc	16.01			120.59				210	105	235.38	46.36	44	62.79	66.73
Th/U	3.45							0.6			3.33	2.78	3.38	0.93
La/Sc	2.09			8.24				4.31	6.5	5.15	3.64	4	3.58	1.64
La/Th	3.1			10				9.33	8.67	5.58	4	4.8	4.81	2.19
Cr/V	0.86	1.83	3.73	1.75	4.17	2.09	1.83	5.8	1.71	5.67	1.12	1.19	1.88	1.45
Y/Ni	0.64	2.11	1.97	2.68	1.49	0.79	0.03	0.03	0.21	0.03	0.53	0.9	0.85	0.66
Ti/Nb	367.5	121.9	196.1	128	181.9	201.3	301.7	92.6	104.9	114.8	271.6	189.7	214.9	71.45
La_N/Yb_N	7.22			4.5				3.44	7.53	4.53	7.28	5.79	6.73	1.4
La_N/Sm_N	3.15			2.32				1.96	1.89	2.01	2.89	2.6	2.86	0.58
Tb_N/Yb_N	1.33			1.43							1.64		1.35	0.27
Cr/Th	7.7	8.15	18.64	10	12.5	10	10	48.33	13.33	28.33	9.29	10	12.43	8.89
Ti/Zr	26.36	2.47	2.5	2.31	1.47	1.86	4.82	1.49	3.33	1.76	10.19	7.9	10.18	8.4

Table 1 (cont.): Chemical analyses of sedimentary clastic rocks of the Precordillera terrane. Major elements are in % whereas trace elements are in ppm. N denotes normalized to chondrite values (after Taylor and McLennan, 1985). Aver: average; SD: standard deviation; b.d.l.: below detection limits; n.d.: not determined.

Don Braulio Formation								
	mudstones		sandstones					
Sample	**020436**	**020439**	**020437**	**020438**	**020440**	**DB1**	**Aver**	**SD**
SiO_2	59.13	60.32	74.13	70.23	62.95	77.42	67.37	6.98
TiO_2	1.39	1.07	0.73	0.96	1.09	0.13	0.9	0.39
Al_2O_3	18.43	15.68	5.42	3.32	13.63	b.d.l.	11.29	5.89
Fe_2O_3	6.92	7.32	5.09	7.94	6.44	0.52	5.70	2.48
MnO	0.04	0.09	0.02	0.11	0.06	0.09	0.07	0.03
MgO	2	2.89	0.72	1.48	2.62	0.14	1.64	0.98
CaO	0.21	1.51	5.36	5.6	2	12.26	4.49	3.99
Na_2O	1.52	2.16	1.42	1.84	1.91	0.22	1.51	0.63
K_2O	4.57	3.44	0.38	1.19	2.55	0.08	2.03	1.63
P_2O_5	0.12	0.2	3.78	0.15	0.19	0.11	0.76	1.35
LOI	5.63	5.19	2.94	6.34	5.24	9.38	5.79	1.91
Σ	99.95	99.85	99.98	99.15	98.67	100.14	99.62	0.53
CIA	71	62	61				64.8	4.4
Sc	21.7	18.1	5.9	9	17	1.6	12.22	7.19
Cr	98	90	40	59	88	59	72.33	20.89
Ni	39	42	26	34	41	16	32.88	9.28
Cs	7	7	b.d.l.	2	4	n.d.	5	2.12
Rb	162	118	16	47	91	3	72.8	56.4
Ba	868	420	203	432	444	75	407	247.2
Hf	8	6	6	8	8	5	6.83	1.21
Th	15	12	6.8	5.9	10	1.4	8.52	4.41
U	3.8	2.6	1.9	2.2	2.6	b.d.l.	2.62	0.65
V	156	98	72	75	108	10	86.5	44.01
Sr	92	79	103	101	88	128	98.5	15.44
Y	37.4	32.3	44	22.4	29.2	14.9	30.03	9.51
Zr	250	202	144	242	245	154	206.17	43.43
Nb	23	18	12	14	18	6	15.02	5.4
Pb	50.3	17.3	31.2	12.3	18.4	4.3	22.3	14.87
Zn	119	106	53	69	97	2	74.33	39.22
La	47	40	30	22	35	8.1	30.35	12.63
Ce	110	86	89	48	76	19	71.33	29.8
Nd	46	39	33	22	35	17	32	9.83
Sm	10	7.3	7.9	4.8	6.8	2.1	6.48	2.49
Eu	1.7	1.5	2.2	0.9	1.2	0.4	1.32	0.58
Tb	1.3	1.5	1	b.d.l.	1.2	b.d.l.	1.25	0.18
Yb	4.5	3.3	3.2	2.4	3	1.2	2.93	1
Lu	0.7	0.55	0.45	0.37	0.5	0.2	0.46	0.15
ΣREE	221.2	179.15	166.75	99.97	158.7	47.5	145.55	56.52
Eu/Eu*	0.54	0.58	0.88		0.52		0.63	0.15
Ce/Ce*	1.07	0.99	1.33	1	0.99	0.88	1.04	0.14
K/Cs	5413	4077		4918	5286		4924	521
Th/Sc	0.69	0.66	1.15	0.66	0.59	0.88	0.77	0.19
Zr/Sc	11.52	11.16	24.41	26.89	14.41	96.25	30.77	29.9
Th/U	3.95	4.62	3.58	2.68	3.85		3.73	0.63
La/Sc	2.17	2.21	5.08	2.44	2.06	5.06	3.17	1.35
La/Th	3.13	3.33	4.41	3.73	3.5	5.79	3.98	0.9
Cr/V	0.63	0.92	0.56	0.79	0.81	5.9	1.6	1.93
Y/Ni	0.95	0.78	1.72	0.65	0.72	0.93	0.96	0.36
Ti/Nb	368.2	354.7	375.1	396.1	371.9	142.4	334.7	86.9
La_N/Yb_N	7.06	8.19	6.34	6.19	7.88	4.56	6.7	1.21
La_N/Sm_N	2.96	3.45	2.39	2.88	3.24	2.43	2.89	0.39
Tb_N/Yb_N	1.24	1.94	1.34		1.71		1.56	0.29
Cr/Th	6.53	7.5	5.88	10	8.8	42.14	13.48	12.89
Ti/Zr	33.28	31.79	30.47	23.73	26.72	5.18	25.2	9.5

Table 1 (cont.): Chemical analyses of sedimentary clastic rocks of the Precordillera terrane. Major elements are in % whereas trace elements are in ppm. N denotes normalized to chondrite values (after Taylor and McLennan, 1985). Aver: average; SD: standard deviation; b.d.l.: below detection limits; n.d.: not determined.

La Chilca Formation									
	mudstone	**sandstones**							
Sample	**020401**	**020402**	**020403**	**020404**	**020410**	**020415**	**020416**	**Aver**	**SD**
SiO_2	75.06	81.53	76.78	84.7	84.82	86.36	88.77	82.57	4.68
TiO_2	0.87	0.81	0.93	0.41	0.57	0.58	0.56	0.68	0.18
Al_2O_3	10.61	7.38	8.78	3.34	4.96	4.88	4.34	6.33	2.46
Fe_2O_3	3.98	2.43	4.07	1.75	3.15	1.61	0.51	2.5	1.22
MnO	0.02	b.d.l.	0.03	0.07	0.02	0.01	b.d.l.	0.03	0.02
MgO	1.17	0.74	1.31	0.48	0.21	0.27	0.14	0.62	0.44
CaO	0.21	0.22	0.31	2.88	0.66	0.17	0.17	0.66	0.92
Na_2O	0.8	2.09	1.45	1.38	0.96	1.59	1.32	1.37	0.39
K_2O	2.84	0.88	1.9	0.45	0.29	0.83	0.47	1.09	0.87
P_2O_5	0.11	0.07	0.06	0.07	0.11	0.07	0.07	0.08	0.02
LOI	4.32	1.4	2.58	2.99	2.51	1.33	1.25	2.34	1.04
Σ	99.98	97.53	98.19	98.53	98.25	97.69	97.58	98.25	0.79
CIA	70	61	64		64	57	60	62.7	4.01
Sc	11.5	7.9	10.4	4.3	5.5	5.7	3.6	6.99	2.81
Cr	65	49	68	45	43	39	33	48.86	12.1
Ni	32	35	36	21	20	26	31	28.59	5.99
Cs	5	2	3	b.d.l.	b.d.l.	2	b.d.l.	3	1.23
Rb	116	21	70	21	15	43	25	44.4	34.1
Ba	312	140	451	116	181	236	150	226.6	110.5
Hf	4	14	8	5	12	7	9	8.43	3.33
Th	7.6	6.9	8.1	3.4	5.2	4.7	4.5	5.77	1.64
U	1.6	2.6	1.4	1.3	2.3	1.7	1.5	1.77	0.45
V	65	51	66	28	45	43	32	47.14	13.66
Sr	66	72	96	82	114	114	72	88	18.7
Y	25.6	23.9	19.9	16.2	11.9	11.5	8.2	16.74	6.14
Zr	140	420	238	143	379	199	274	256.14	101.52
Nb	15	14	13	8	10	11	11	12.0	2.35
Pb	35	17.4	13.6	9.6	18.6	15.5	10.7	17.2	7.88
Zn	84	b.d.l.	57	30	15	19	9	35.67	26.58
La	28	26	28	13	16	17	14	20.29	6.25
Ce	59	67	62	34	40	39	36	48.14	12.89
Nd	35	35	31	18	22	22	18	25.86	7.04
Sm	7.6	7.7	6.2	3.8	4.4	4	3.5	5.31	1.68
Eu	1.4	1.6	1	0.8	0.9	0.8	0.8	1.04	0.3
Tb	1.1	1	0.9	0.6	0.8	0.7	0.5	0.8	0.2
Yb	2.4	3.2	2.6	1.7	2.2	1.7	1.9	2.24	0.5
Lu	0.41	0.57	0.48	0.28	0.42	0.32	0.34	0.4	0.09
ΣREE	134.91	142.07	132.18	72.18	86.72	85.52	75.04	104.09	28.51
Eu/Eu*	0.57	0.66	0.5	0.64	0.6	0.59	0.71	0.61	0.06
Ce/Ce*	0.92	1.1	0.99	1.11	1.06	0.99	1.11	1.04	0.07
K/Cs	4708	3636	5266			3457		4267	749
Th/Sc	0.66	0.87	0.78	0.79	0.95	0.82	1.25	0.87	0.17
Zr/Sc	12.17	53.16	22.88	33.26	68.91	34.91	76.11	43.06	21.99
Th/U	4.75	2.65	5.79	2.62	2.26	2.76	3	3.4	1.23
La/Sc	2.43	3.29	2.69	3.02	2.91	2.98	3.89	3.03	0.43
La/Th	3.68	3.77	3.46	3.82	3.08	3.62	3.11	3.51	0.28
Cr/V	1	0.96	1.03	1.61	0.96	0.91	1.03	1.07	0.22
Y/Ni	0.81	0.68	0.55	0.77	0.6	0.44	0.27	0.59	0.18
Ti/Nb	340.2	338	438.5	298.3	335.9	325.2	315	341.61	41.9
La_N/Yb_N	7.88	5.49	7.28	5.17	4.91	6.76	4.98	6.07	1.13
La_N/Sm_N	2.32	2.13	2.84	2.15	2.29	2.68	2.52	2.42	0.25
Tb_N/Yb_N	1.96	1.34	1.48	1.51	1.55	1.76	1.13	1.53	0.25
Cr/Th	8.55	7.1	8.4	13.24	8.27	8.3	7.33	8.74	1.91
Ti/Zr	37.43	11.59	23.4	17.31	8.95	17.32	12.19	18.31	8.97

Table 1 (cont.): Chemical analyses of sedimentary clastic rocks of the Precordillera terrane. Major elements are in % whereas trace elements are in ppm. N denotes normalized to chondrite values (after Taylor and McLennan, 1985). Aver: average; SD: standard deviation; b.d.l.: below detection limits; n.d.: not determined.

Empozada Formation

	mudstones				sandstones						
Sample	**E2**	**E4**	**E5**	**E7**	**E1**	**E3**	**E6**	**E8**	**E10**	**Aver**	**SD**
SiO_2	30.61	46.44	59.03	64.89	46.22	46.55	76.54	69.21	50.85	54.48	13.38
TiO_2	0.33	0.76	1.2	0.71	0.11	0.16	0.34	0.04	1.43	0.56	0.47
Al_2O_3	7.76	13.09	15.3	14.2	1.35	3.24	5.93	3.62	10.7	8.36	4.88
Fe_2O_3	2.42	5.58	8.49	7.1	1.39	1.01	1.52	1.56	6.73	3.98	2.79
MnO	0.05	0.07	0.09	0.02	0.06	0.01	0.07	0.4	0.09	0.09	0.11
MgO	1.53	2.1	2.38	2.23	3.69	0.52	0.88	0.71	4.4	2.05	1.25
CaO	29.31	10.93	2.34	0.53	34.67	24.21	5.38	12.33	9.74	14.38	11.48
Na_2O	2.74	2.95	1.82	0.8	1.23	1.96	2.73	1.78	3.68	2.19	0.86
K_2O	1.39	2.56	3.85	4.07	0.29	0.15	0.26	1.07	0.67	1.59	1.45
P_2O_5	0.13	0.18	0.24	0.27	0.23	0.16	0.13	3.79	0.78	0.66	1.12
LOI	27.66	12.9	6.19	4.6	10.17	21.46	4.89	3.1	10.58	11.28	7.85
Σ	103.92	97.56	100.93	99.42	99.42	99.42	98.67	97.63	99.65	99.62	1.81
CIA				70						70	0.0
Sc	6.4	13.7	18	15.3	2.5	1.8	3.6	2.7	17.8	9.1	6.6
Cr	36	75	100	57	26	34	84	52	220	76	56
Ni	8	30	51	46	5	3	b.d.l.	17	30	23.8	17.3
Cs	3	6	8	10	b.d.l.	b.d.l.	1	b.d.l.	b.d.l.	5.6	3.26
Rb	34	95	150	161	5	4	16	22	30	57.4	58.3
Ba	274	541	762	1441	204	132	127	4933	717	1014.6	1440.9
Hf	3	5	6	4	8	10	10	1	5	5.8	2.9
Th	5.3	10	12	13	2.6	2.2	4.7	3.1	3.4	6.3	4
U	2.3	2.5	3.2	2.3	1.4	1.3	1.6	10	b.d.l.	3.1	2.7
V	34	89	139	94	15	11	23	54	130	65.4	46.4
Sr	142	140	97	97	170	182	155	548	175	189.6	130
Y	0.9	19.2	34.4	24.4	2.1	0.4	19.8	37.2	8.3	16.3	13.4
Zr	72	159	219	153	174	213	324	74	181	174.3	72.4
Nb	10	15	19	16	7	7	12	5	21	12.3	5.2
Pb	b.d.l.	10.4	22.4	22.6	b.d.l.	1.2	11	35.9	8.2	16	10.8
Zn	26	64	108	105	6	4	12	22	32	42.1	38.3
La	18	34	44	39	16	14	22	34	22	27	10.3
Ce	39	68	87	86	35	34	53	100	45	60.8	23.8
Nd	19	27	34	21	14	15	21	23	20	21.6	5.7
Sm	3.7	6.8	8.6	5.6	3.9	3.5	5.7	7.5	5.7	5.7	1.7
Eu	0.7	1.2	1.4	0.9	0.8	0.7	1.1	1.6	1.9	1.1	0.4
Tb	0.6	1	1.4	0.8	0.6	0.7	1.1	1.4	0.9	0.9	0.3
Yb	1.7	3.3	4.1	2.9	2	1.9	2.6	4.9	2.1	2.8	1
Lu	0.28	0.53	0.62	0.52	0.34	0.33	0.45	0.78	0.35	0.5	0.2
ΣREE	82.98	141.83	181.12	156.72	72.64	70.13	106.95	173.18	97.95	120.4	41
Eu/Eu*	0.57	0.54	0.49	0.5	0.62	0.57	0.55	0.62	1.01	0.61	0.15
Ce/Ce*	0.98	0.95	0.95	1.11	1.02	1.09	1.11	1.44	0.95	1.07	0.15
K/Cs	3843	3547	3997	3375			2158			3384	651
Th/Sc	0.83	0.73	0.67	0.85	1.04	1.22	1.31	1.15	0.19	0.89	0.32
Zr/Sc	11.25	11.61	12.17	10	69.6	118.33	90	27.41	10.17	40.06	39.25
Th/U	2.3	4	3.75	5.65	1.86	1.69	2.94	0.31		2.81	1.54
La/Sc	2.81	2.48	2.44	2.55	6.4	7.78	6.11	12.59	1.24	4.93	3.44
La/Th	3.4	3.4	3.67	3	6.15	6.36	4.68	10.97	6.47	5.34	2.38
Cr/V	1.06	0.84	0.72	0.61	1.73	3.09	3.65	0.96	1.69	1.6	1.03
Y/Ni	0.11	0.64	0.68	0.53	0.42	0.12		2.19	0.28	0.62	0.63
Ti/Nb	204.7	310.3	376.3	270.1	95.1	139	173.6	46.9	414.8	225.67	118.93
La_N/Yb_N	7.15	6.96	7.25	9.09	5.41	4.98	5.72	4.69	7.08	6.48	1.32
La_N/Sm_N	3.06	3.15	3.22	4.38	2.58	2.52	2.43	2.85	2.43	2.96	0.58
Tb_N/Yb_N	1.51	1.3	1.46	1.18	1.28	1.58	1.81	1.22	1.83	1.46	0.23
Cr/Th	6.79	7.5	8.33	4.38	10	15.45	17.87	16.77	64.71	16.87	17.5
Ti/Zr	27.39	28.69	32.77	27.9	3.82	4.5	6.22	3.4	47.36	20.23	15.17

Table 1 (cont.): Chemical analyses of sedimentary clastic rocks of the Precordillera terrane. Major elements are in % whereas trace elements are in ppm. N denotes normalized to chondrite values (after Taylor and McLennan, 1985). Aver: average; SD: standard deviation; b.d.l.: below detection limits; n.d.: not determined.

Los Sombreros Formation

	mudstones							sandstones			
Sample	**020418**	**LRAT1**	**SOM 5**	**SOM 6**	**SOM 7**	**SOM 8**	**SOM 9**	**020419**	**LRAT2**	**Aver**	**SD**
SiO_2	59.68	63.60	56.54	56.60	66.41	56.61	57.01	69.29	70.67	61.82	5.46
TiO_2	1.13	1.11	0.66	0.64	0.27	0.59	0.24	0.51	0.84	0.67	0.3
Al_2O_3	18.97	15.39	21.01	19.54	11.08	18.18	2.98	7.1	11.45	13.97	5.85
Fe_2O_3	6.97	7.09	5.92	7.34	6.03	9.09	8.33	7.64	5.44	7.09	1.11
MnO	0.05	0.07	0.01	0.04	0.04	0.08	0.71	0.34	0.06	0.16	0.22
MgO	1.86	2.28	1.81	1.58	1.8	2.39	5.36	1.58	1.8	2.27	1.12
CaO	0.16	0.43	0.19	0.25	2.25	0.39	10.44	4.01	0.6	2.08	3.2
Na_2O	1.74	2.78	1.43	1.9	0.64	1.99	0.5	0.79	2.43	1.58	0.76
K_2O	4	2.76	4.51	4.21	1.38	3.52	0.45	0.73	1.53	2.57	1.48
P_2O_5	0.07	0.2	0.1	0.15	1.38	0.17	0.05	1.35	0.13	0.4	0.52
LOI	4.08	3.59	5.86	6.09	6.59	6.87	11.86	5.13	2.83	5.88	2.49
Σ	98.7	99.3	98.04	98.32	97.86	99.87	97.93	98.45	97.79	98.47	0.67
CIA	72	66	74	71	77	71			64	70.7	4.14
Sc	21	16.3	19.7	19.4	10	19.1	10	10	11.4	15.21	4.52
Cr	110	89	110	100	47	89	18	40	63	74	31.38
Ni	44	41	38	39	61	41	25	31	37	39.62	9.29
Cs	12	5	12	10	5	8	1	2	2	6.34	4.08
Rb	165	105	198	184	65	136	19	31	64	107.4	473.6
Ba	517	546	868	818	295	602	142	148	326	62.8	251.1
Hf	6	9	5	6	3	5	3	3	8	5.33	2.05
Th	14	12	17	16	6.2	14	3.4	6.1	8.1	10.76	4.63
U	3	2.4	3.2	2.7	1.1	2.7	0.8	2.2	1.5	2.18	0.81
V	102	95	111	115	59	107	23	55	69	81.78	29.87
Sr	89	81	81	80	130	67	256	114	77	108.33	55.45
Y	26.9	35.3	33.6	40.2	60.6	33.4	19.3	67	25.3	37.96	15.05
Zr	192	281	173	176	91	144	112	107	232	167.56	58.59
Nb	19	20	19	19	10	16	6	12	15	15.11	4.74
Pb	76.6	23.8	25.8	26.5	15.8	26.1	26	45.3	19.7	31.73	17.59
Zn	111	108	137	115	88	152	48	82	88	103.22	29.26
La	42	43	48	47	22	38	9.2	31	31	34.58	12.02
Ce	94	94	100	100	49	85	19	78	69	76.44	25.63
Nd	42	43	45	45	25	38	5	30	30	33.67	12.27
Sm	7.4	8.3	7.3	7.6	11.8	7.1	2.3	10	6.1	7.54	2.46
Eu	1.5	1.4	1.3	1.3	3.8	1.2	0.6	2.6	1.2	1.66	0.9
Tb	1	1.6	0.7	0.8	2.8	1.1	0.7	1.6	0.9	1.24	0.64
Yb	3.3	4.1	3.5	3.6	3	3.4	1.9	3.7	3.1	3.29	0.58
Lu	0.56	0.65	0.59	0.6	0.45	0.55	0.33	0.54	0.48	0.53	0.09
ΣREE	191.76	196.05	206.39	205.9	117.85	174.35	39.03	157.44	141.78	158.95	51.11
Eu/Eu*	0.63	0.49	0.59	0.56	0.87	0.51	0.65	0.78	0.6	0.63	0.12
Ce/Ce*	1.02	1	0.96	0.98	0.99	1.02	1.04	1.16	1.02	1.02	0.05
K/Cs	2764	4589	3120	3496	2294	3655	3744	3009	6367	3671	1136
Th/Sc	0.67	0.74	0.86	0.82	0.62	0.73	0.34	0.61	0.71	0.68	0.14
Zr/Sc	9.14	17.24	8.78	9.07	9.1	7.54	11.2	10.7	20.35	11.46	4.11
Th/U	4.67	5	5.31	5.93	5.64	5.19	4.25	2.77	5.4	4.91	0.89
La/Sc	2	2.64	2.44	2.42	2.2	1.99	0.92	3.1	2.72	2.27	0.58
La/Th	3	3.58	2.82	2.94	3.55	2.71	2.71	5.08	3.83	3.36	0.72
Cr/V	1.08	0.94	0.99	0.87	0.8	0.83	0.78	0.73	0.91	0.88	0.1
Y/Ni	0.62	0.86	0.88	1.03	0.99	0.81	0.77	2.18	0.68	0.98	0.44
Ti/Nb	350.4	324.3	212.4	202.5	160.3	223.2	256.9	264.6	324.9	257.7	60.9
La_N/Yb_N	8.6	7.09	9.27	8.82	4.96	7.55	3.27	5.66	6.76	6.89	1.86
La_N/Sm_N	3.57	3.26	4.14	3.89	1.17	3.37	2.52	1.95	3.2	3.01	0.9
Tb_N/Yb_N	1.3	1.67	0.86	0.95	3.99	1.38	1.58	1.85	1.24	1.65	0.88
Cr/Th	7.86	7.42	6.47	6.25	7.58	6.36	5.29	6.56	7.78	6.84	0.82
Ti/Zr	35.41	23.66	22.84	21.63	17.79	24.65	12.85	28.69	21.71	23.25	5.99

Table 1 (cont.): Chemical analyses of sedimentary clastic rocks of the Precordillera terrane. Major elements are in % whereas trace elements are in ppm. N denotes normalized to chondrite values (after Taylor and McLennan, 1985). Aver: average; SD: standard deviation; b.d.l.: below detection limits; n.d.: not determined.

Yerba Loca Formation

	mudstones						sandstones						
Sample	**YL1**	**YL2**	**YL441**	**YL449**	**YL451**	**YL450**	**YL3**	**YL4**	**YL5**	**YL 411**	**YL426**	**YL431**	**YL432**
SiO_2	60.87	57.37	58.75	60.24	56.27	69.54	70.21	65.29	70.84	48.08	72.49	74.8	61.19
TiO_2	0.97	0.95	1.07	0.91	0.96	0.84	0.88	0.69	1.38	2.17	0.83	0.89	0.84
Al_2O_3	16.82	18.43	17.83	19.66	18.59	12.11	11.33	16.13	10.73	10.15	9.97	9.74	10.74
Fe_2O_3	6.45	7.39	6.44	8.26	9.27	6.1	5.75	4.78	5.6	14.38	6.03	5.37	5.73
MnO	0.06	0.12	0.08	0.07	0.14	0.1	0.12	0.06	0.06	0.18	0.09	0.07	0.1
MgO	2.33	2.65	2.42	2.95	2.81	1.92	1.68	2.69	1.72	7.64	2.03	1.83	3.22
CaO	0.42	0.56	0.82	0.2	0.3	0.38	1.36	0.83	1.62	11.4	0.49	0.45	4.29
Na_2O	2.18	2.13	3.28	0.97	2.23	2.52	2.49	4.25	2.05	1.94	1.69	1.59	2.39
K_2O	3.42	3.85	3.4	4.86	4.56	1.92	1.74	1.82	1.76	0.25	1.62	1.64	2.04
P_2O_5	0.2	0.16	0.19	b.d.l.	0.17	0.2	0.15	b.d.l.	0.2	0.2	0.09	0.09	0.12
LOI	4.68	4.5	3.8	3.1	4.45	3.24	3.46	2.17	2.28	2.4	2.9	1.99	7.84
Σ	98.4	98.1	98.08	101.22	99.75	98.85	99.16	98.7	99.72	98.79	98.22	98.46	98.5
CIA	69	69	64	73	68	65	58	61	58		66	66	
Sc	19	20.7	18.8	19.4	20.8	11.9	12.2	13.5	n.d.	35.6	12.9	12.1	13.5
Cr	89	86	94	89	100	54	69	72	64	130	70	69	140
Ni	46	50	44	51	51	34	37	41	34	59	78	38	41
Cs	7	8	6	8	8	4	4	3	n.d.	b.d.l.	3	3	3
Rb	155	165	150	206	209	89	79	67	73	4	73	72	93
Ba	638	493	526	678	719	371	396	494	328	133	802	702	613
Hf	6	5	6	5	5	6	8	6	n.d.	3	6	7	7
Th	14	14	14	14	14	10	10	13	17.9	0.8	8.1	8.5	10
U	3.4	3.3	2.5	2.5	2.2	2.4	2.6	3.2	n.d.	b.d.l.	1.6	1.2	3.9
V	128	130	132	124	137		94	89	126	230	112	107	127
Sr	72	66	65	34	39	73	67	204	59	308	56	46	84
Y	34.6	33.5	33.2	37.8	40.6	33.5	23.5	20.1	28.8	32.5	29.2	17.5	27
Zr	202	177	206	173	173	217	278	231	449	167	217	233	235
Nb	18	19	20	19	19	18	16	16	19	16	15	14	15
Pb	17.7	23.9	25.6	17	18.1	27.9	15.2	21.1	16.9	b.d.l.	8	9.3	14.9
Zn	107	100	107	123	134	106	77	72	73	79	273	68	108
La	44	43	43	45	43	39	28	38	n.d.	11	34	42	33
Ce	83	83	84	89	81	77	64	68	n.d.	26	68	53	65
Nd	31	31	32	35	31	32	26	28	n.d.	17	29	26	24
Sm	7.9	7.4	8.1	7.9	7.8	7.4	5.9	6.1	n.d.	4.8	7.9	6	6.5
Eu	1.2	1.2	1.4	1.4	1.4	1.6	1.1	1.2	n.d.	1.4	1.4	0.9	1.1
Tb	1.1	1.2	1.2	1.1	1.1	1.2	1	1.2	n.d.	1.3	1.2	0.8	1.2
Yb	3.8	3.7	3.7	3.7	3.9	3.2	3.3	3	n.d.	2.6	3.4	2.6	3.4
Lu	0.61	0.62	0.63	0.6	0.61	0.58	0.52	0.44	n.d.	0.42	0.54	0.42	0.57
ΣREE	172.61	171.12	174.03	183.7	169.81	161.98	129.82	145.94		64.52	145.44	131.72	134.77
Eu/Eu*	0.47	0.49	0.53	0.55	0.56	0.65	0.55	0.56		0.75	0.54	0.47	0.49
Ce/Ce*	0.92	0.93	0.94	0.95	0.91	0.94	1.06	0.86		0.97	0.94	0.62	0.95
K/Cs	4060	3992	4708	5042	4731	3989	3607	5022			4474	4546	5653
Th/Sc	0.74	0.68	0.74	0.72	0.67	0.84	0.82	0.96		0.02	0.63	0.7	0.74
Zr/Sc	10.63	8.55	10.96	8.92	8.32	18.24	22.79	17.11		4.69	16.82	19.26	17.41
Th/U	4.12	4.24	5.6	5.6	6.36	4.17	3.85	4.06			5.06	7.08	2.56
La/Sc	2.32	2.08	2.29	2.32	2.07	3.28	2.3	2.81		0.31	2.64	3.47	2.44
La/Th	3.14	3.07	3.07	3.21	3.07	3.9	2.8	2.92		13.75	4.2	4.94	3.3
Cr/V	0.7	0.66	0.71	0.72	0.73		0.73	0.81	0.51	0.57	0.63	0.64	1.1
Y/Ni	0.75	0.67	0.75	0.74	0.8		0.64	0.49	0.85	0.55	0.37	0.46	0.66
Ti/Nb	319.3	291	313.1	291.5	303.1		322.5	255.8	428.4	823.4	328.2	381.6	339.9
La_N/Yb_N	7.82	7.85	7.85	8.22	7.45	8.24	5.73	8.56		2.86	6.76	10.92	6.56
La_N/Sm_N	3.51	3.66	3.34	3.59	3.47	3.32	2.99	3.92		1.44	2.71	4.41	3.2
Tb_N/Yb_N	1.24	1.39	1.39	1.27	1.21	1.6	1.3	1.71		2.14	1.51	1.32	1.51
Cr/Th	6.36	6.14	6.71	6.36	7.14	5.4	6.9	5.54	3.57	162.5	8.64	8.12	14
Ti/Zr	28.82	32.11	31.11	31.67	33.41	23.15	18.87	17.87	18.48	77.9	23.04	22.87	21.4

Table 1 (cont.): Chemical analyses of sedimentary clastic rocks of the Precordillera terrane. Major elements are in % whereas trace elements are in ppm. N denotes normalized to chondrite values (after Taylor and McLennan, 1985). Aver: average; SD: standard deviation; b.d.l.: below detection limits; n.d.: not determined.

Yerba Loca Formation (cont.)

	sandstones											
Sample	**YL433**	**YL4341**	**YL439**	**YL440**	**YL442**	**YL445**	**YL446**	**YL448**	**YL452**	**YL454**	**Aver**	**SD**
SiO_2	73.92	72.73	70.66	66.28	73.03	73.07	73.72	69.72	73.05	57.71	66.51	7.11
TiO_2	0.85	0.75	0.89	1.15	0.78	1	0.95	1.17	0.84	1.02	0.99	0.29
Al_2O_3	10.07	8.51	11.14	12.81	9.22	9.04	8.86	10.51	9.47	13.8	12.42	3.45
Fe_2O_3	5.4	4.68	4.73	6.82	5.63	5.98	5.91	6.25	5.55	8.53	6.57	1.98
MnO	0.07	0.06	0.07	0.11	0.13	0.11	0.11	0.11	0.11	0.16	0.1	0.03
MgO	1.67	1.87	1.55	2.23	1.5	1.58	1.53	1.79	1.48	4.03	2.4	1.26
CaO	0.48	2.63	1.14	1.52	2.24	1.65	1.56	1.35	2.09	4.31	1.83	2.27
Na_2O	1.37	1.31	2.67	1.67	2.23	2.39	2.01	2.56	2.25	2.61	2.21	0.65
K_2O	1.94	1.64	1.55	2.14	1.27	1.4	1.36	1.4	1.32	1.25	2.09	1.09
P_2O_5	0.08	0.08	0.16	0.19	0.13	0.15	0.14	0.18	0.13	0.2	0.14	0.06
LOI	3.18	5.99	3.89	2.9	3.79	3.7	3.7	3.86	4.02	4.9	3.77	1.24
Σ	99.03	100.25	98.45	97.83	99.93	100.05	99.83	98.9	100.31	98.52	99.09	0.84
CIA	67		59	63		53	55	58	52		62.44	5.82
Sc	12.5	10.5	11.8	11.6	10.2	11.5	11.5	n.d.	11	24.7	15.51	5.94
Cr	67	65	49	50	220	50	53	58.5	52	130	83.5	38.29
Ni	77	35	29	b.d.l.	29	28	27	31	28	47	42.5	14.1
Cs	3	3	3	5	3	4	4	n.d.	4	3	4.45	1.83
Rb	88	70	69	71	60	67	66	67	60	66	92.1	49
Ba	753	576	279	289	255	299	285	281	237	290	453.8	193.1
Hf	6	5	9	11	9	13	12	n.d.	9	5	7.1	2.45
Th	8.6	7.4	10	10	8.8	10	10	20.3	9.4	6.7	10.85	3.83
U	2.9	1.7	1.7	2.7	1.5	3	2.3	n.d.	2.8	b.d.l.	2.49	0.68
V	123	98	96	105	93	116	115	122	97	145	120.27	28.52
Sr	64	61	77	63	98	65	56	72	96	197	87.91	62.09
Y	23.9	11.1	21.9	27	19.8	24.5	25.8	28.1	19.7	19.9	26.37	6.83
Zr	203	184	272	389	300	430	391	570	316	185	269.48	105.33
Nb	14	13	15	17	14	16	14	19	14	15	16.30	2.17
Pb	13.7	4.9	13.4	21.5	24	15.2	17.5	18.3	23.6	13.2	16.8	5.17
Zn	136	92	77	74	68	66	68	83	66	91	97.74	42.98
La	33	22	35	27	31	32	29	n.d.	31	25	33.71	8.14
Ce	66	44	67	54	64	67	61	n.d.	65	50	65.67	14.26
Nd	23	20	24	23	23	27	30	n.d.	31	21	26.86	4.5
Sm	6.6	4.8	6.7	5.7	6	6.6	6.1	n.d.	6.1	5.5	6.56	0.97
Eu	1.2	0.7	1.2	1.1	1.1	1.3	1.1	n.d.	1.1	1.1	1.2	0.19
Tb	1.1	0.9	1	1.1	0.9	1.1	0.9	n.d.	0.7	0.9	1.06	0.15
Yb	3.1	2.2	3.4	3.6	3.1	3.5	3.6	n.d.	2.9	3.1	3.28	0.42
Lu	0.51	0.37	0.55	0.59	0.52	0.64	0.64	n.d.	0.54	0.5	0.54	0.07
ΣREE	134.51	94.97	138.85	116.09	129.62	139.14	132.34		138.34	107.1	138.88	27.21
Eu/Eu*	0.54	0.42	0.55	0.55	0.56	0.59	0.55		0.58	0.6	0.55	0.07
Ce/Ce*	0.97	0.93	0.93	0.94	0.99	0.99	0.95		0.96	0.94	0.93	0.07
K/Cs	5354	4530	4292	3550	3500	2901	2812		2737	3470	4148	815
Th/Sc	0.69	0.7	0.85	0.86	0.86	0.87	0.87		0.85	0.27	0.72	0.2
Zr/Sc	16.24	17.52	23.05	33.53	29.41	37.39	34		28.73	7.49	18.62	9.32
Th/U	2.97	4.35	5.88	3.7	5.87	3.33	4.35		3.36		4.55	1.16
La/Sc	2.64	2.1	2.97	2.33	3.04	2.78	2.52		2.82	1.01	2.41	0.67
La/Th	3.84	2.97	3.5	2.7	3.52	3.2	2.9		3.3	3.73	3.68	2.31
Cr/V	0.54	0.66	0.51	0.48	2.37	0.43	0.46	0.48	0.54	0.9	0.72	0.39
Y/Ni	0.31	0.32	0.76		0.68	0.87	0.96	0.91	0.70	0.42	0.62	0.23
Ti/Nb	357.2	350.4	355.7	392.6	333.5	370.5	407.8	377	360.1	412.1	368.8	107.8
La_N/Yb_N	7.19	6.76	6.96	5.07	6.76	6.18	5.44		7.22	5.45	6.95	1.53
La_N/Sm_N	3.15	2.88	3.29	2.98	3.25	3.05	2.99		3.2	2.86	3.2	0.53
Tb_N/Yb_N	1.52	1.75	1.26	1.31	1.24	1.34	1.07		1.03	1.24	1.4	0.24
Cr/Th	7.79	8.78	4.9	5	25	5	5.3	2.88	5.53	19.4	14.65	31.24
Ti/Zr	24.98	24.44	19.57	17.66	15.49	13.87	14.57	12.35	15.88	33.12	24.9	13

Table 1 (cont.): Chemical analyses of sedimentary clastic rocks of the Precordillera terrane. Major elements are in % whereas trace elements are in ppm. N denotes normalized to chondrite values (after Taylor and McLennan, 1985). Aver: average; SD: standard deviation; b.d.l.: below detection limits; n.d.: not determined.

Yerba Loca Formation (cont.)

	volcanic rocks										
Sample	**YL408**	**YL413**	**YL417**	**YL418**	**YL419**	**YL420**	**YL421**	**YL422**	**YL455**	**Media**	**SD**
SiO_2	48.98	42.05	41.96	33.80	44.74	44.84	46.21	45.93	37.57	42.9	4.44
TiO_2	2.06	1.71	1.85	2.12	1.99	2.16	2.14	1.95	1.35	1.93	0.25
Al_2O_3	13.08	13.72	9.97	14.87	15.61	13.94	14.35	14.75	16.48	14.09	1.74
Fe_2O_3	13.66	12.76	15.1	17.06	13.87	11.13	12.45	12.07	14.29	13.6	1.68
MnO	0.17	0.18	0.18	0.18	0.17	0.14	0.16	0.17	0.25	0.18	0.03
MgO	6.33	6.46	7.69	10.69	6.43	4.59	5.22	6.25	12.38	7.34	2.42
CaO	10.13	13.23	9.42	7.64	9.71	11.84	10.41	12.79	10.52	10.63	1.65
Na_2O	2.43	2.68	1.71	1.08	2.9	4.44	3.82	2.18	2.17	2.6	0.97
K_2O	0.27	0.81	0.27	0.53	0.8	0.14	0.53	0.32	b.d.l.	0.41	0.26
P_2O_5	0.2	0.18	0.17	0.11	0.25	0.23	0.21	0.2	0.26	0.2	0.04
LOI	2.6	6.1	7.2	6.9	3.4	6.5	4.4	3.3	4.77	5.02	1.62
Σ	99.91	99.88	95.53	94.99	99.87	99.95	99.9	99.91	100.04	98.89	1.95
Sc	37	32	40.3	35.1	37	35	36	37	55.4	38.31	6.39
Cr	212	246	160	220	287	144	137	287	170	207	54.73
Ni	43	93	48	67	116	47	38	111	56	68.88	28.36
Cs	0.4	0.3	b.d.l.	b.d.l.	0.5	0.2	0.2	0.3	1	0.41	0.3
Rb	4	10	5	13	11	3	15	4	6	7.81	4.17
Ba	72	340	101	170	347	36	119	73	53	145.6	112.1
Hf	3.4	2.9	4	4	3.2	4	3.6	3.8	3	3.54	0.4
Ta	0.6	0.6	0.9	b.d.l.	0.7	0.8	0.7	0.7	0.6	0.70	0.1
Th	0.5	0.7	0.9	0.6	1	0.9	0.5	0.6	0.6	0.7	0.18
U	0.3	0.3	b.d.l.	0.8	0.5	0.4	0.2	0.4	b.d.l.	0.41	0.2
V	331	298	219	227	346	335	338	346	211	294.6	55.15
Sr	285	255	317	305	276	113	3142	303	438	289.5	79.1
Y	26.8	25.7	30.3	25.1	28.9	31.9	28.9	28	39.8	29.49	4.17
Zr	115	103	150	149	109	135	122	120	118	124.64	15.6
Nb	9	9	14	14	10	11	11	10	9	10.82	1.95
Pb	0.4	0.8	b.d.l.	b.d.l.	0.8	0.5	0.7	0.4	8.9	1.79	2.91
Zn	77	71	75	125	92	106	85	73	88	88	16.74
La	10.1	7.4	11	9.1	9.6	11.8	10.7	9.9	6.6	9.58	1.58
Ce	25.3	20.1	24	16	24.9	29.1	25.6	24.8	11	22.31	5.32
Pr	3.6	3	n.d.	n.d.	3.6	4.1	3.7	3.5	n.d.	3.59	0.32
Nd	17	15.8	14	16	16.9	20.5	17.7	18.3	12	16.47	2.32
Sm	4.8	4	5	3.8	4.6	5.1	4.8	4.8	3.6	4.5	0.52
Eu	1.7	1.3	1.6	1.6	1.5	1.8	1.8	1.7	1.3	1.59	0.18
Gd	5.6	4.8	n.d.	n.d.	5.2	6.3	5.6	5.4	n.d.	5.47	0.45
Tb	0.9	0.8	1.2	1	0.9	1.1	1	0.9	1.7	1.05	0.25
Dy	5.1	4.7	n.d.	n.d.	5.1	5.9	5.4	5.1	n.d.	5.22	0.35
Ho	1	0.9	n.d.	n.d.	1	1.1	1	1	n.d.	1.01	0.07
Er	2.7	2.5	n.d.	n.d.	2.9	3.4	2.9	2.8	n.d.	2.85	0.26
Tm	0.4	0.4	n.d.	n.d.	0.4	0.5	0.4	0.4	n.d.	0.41	0.02
Yb	2.4	2.1	2.8	2.2	2.4	2.8	2.5	2.3	3.7	2.58	0.45
Lu	0.32	0.3	0.43	0.34	0.34	0.39	0.36	0.34	0.53	0.37	0.07
ΣREE	80.9	68.18	60.03	50.04	79.48	93.76	83.42	81.12	40.43	70.82	16.49
Eu/Eu*	1.02	0.93	0.86	1.1	0.93	1.02	1.03	1.04	0.74	0.96	0.1

Table 1 (cont.): Chemical analyses of sedimentary volcanic rocks of the Precordillera terrane. Major elements are in % whereas trace elements are in ppm. N denotes normalized to chondrite values (after Taylor and McLennan, 1985). Aver: average; SD: standard deviation; b.d.l.: below detection limits; n.d.: not determined.

Alcaparrosa Formation

	mudstones					sandstones							
Sample	**A2**	**020457**	**020459**	**020461**	**A1**	**A3**	**A4**	**020456**	**020458**	**020460**	**020462**	**Aver**	**SD**
SiO_2	61.07	62.3	63.38	65.5	67.83	72.4	74.36	76.15	62.39	76.48	77.52	69.04	6.15
TiO_2	1.09	1.14	1.02	1.03	0.93	0.86	0.74	0.74	1.11	0.72	0.78	0.92	0.15
Al_2O_3	16.81	16.33	15.89	14.75	13.04	10.98	10.51	8.59	15.87	9.43	8.55	12.79	3.12
Fe_2O_3	6.67	7.12	7.88	7.12	6.48	5.6	5.19	4.76	6.93	3.79	3.8	5.94	1.33
MnO	0.04	0.06	0.06	0.08	0.08	0.07	0.08	0.05	0.05	0.03	0.05	0.06	0.02
MgO	2.25	2.31	2.28	2.07	1.91	1.53	1.35	0.74	2.25	1.24	1.19	1.74	0.52
CaO	0.45	0.39	0.32	0.33	0.39	0.48	0.82	0.86	0.35	0.42	0.4	0.47	0.18
Na_2O	2.15	1.52	1.67	1.85	1.93	2.35	2.53	2.06	1.66	1.61	1.59	1.9	0.32
K_2O	3.32	3.56	3.42	3.12	2.21	1.81	1.69	1.43	3.35	1.56	1.3	2.43	0.87
P_2O_5	0.2	0.19	0.15	0.15	0.18	0.13	0.11	0.11	0.18	0.1	0.11	0.15	0.03
LOI	4.71	4.7	3.66	3.38	4.29	1.8	1.83	3.66	4.33	1.58	1.86	3.25	1.19
Σ	98.76	99.6	99.72	99.37	99.26	98	99.22	99.16	98.46	96.95	97.14	98.69	0.91
CIA	69	71	70	69	69	63	59	58	71	66	66	66.45	4.4
Sc	16.6	18	16.8	15.4	13.1	11.3	10.5	7.8	16.7	9.1	8.8	13.1	3.6
Cr	98	97	88	84	79	73	63	53	88	53	64	76.4	15.6
Ni	46	42	40	41	45	46	37	36	41	37	42	41.2	3.4
Cs	7	7	6	5	5	2	2	3	6	2	2	4.28	2
Rb	151	133	130	121	107	81	75	60	126	73	61	101.64	31
Ba	566	550	648	698	486	497	432	278	521	360	338	488.5	123.2
Hf	8	9	6	8	10	12	8	11	9	8	13	9.3	2
Th	13	13	12	12	10	9.1	8.4	7.5	12	8.2	8.9	10.4	2
U	3.5	3.4	3.1	3.2	2.4	2.1	2.3	2.5	3	2.4	2	2.7	0.5
V	114	107	91	94	93	75	67	54	102	65	63	84.1	19.2
Sr	73	61	50	49	69	66	81	70	61	48	44	61.1	11.4
Y	38.9	33.3	30.6	28.1	30	28.1	28.2	18.7	35.3	20.7	20.3	28.4	6.1
Zr	278	289	189	226	345	366	250	316	273	222	349	282.1	55
Nb	22	20	19	19	19	18	16	14	20	14	15	18.0	2.6
Pb	21.9	29.3	24.6	26.5	27.4	28.5	21.6	47	25.3	21.8	17.8	26.5	7.3
Zn	112	114	116	107	97	68	62	79	112	b.d.l.	66	93.3	21
La	41	42	39	35	35	33	29	25	41	26	29	34.09	5.92
Ce	88	92	85	77	78	77	64	56	90	59	64	75.45	12.27
Nd	43	43	36	32	39	40	32	29	40	28	32	35.82	5.22
Sm	7.6	7.7	7.2	6.3	6.9	6.7	5.8	5.1	7.8	5	5.5	6.51	0.99
Eu	1.4	1.4	1.1	1.1	1.2	1.3	1.1	1	1.4	0.7	1	1.15	0.21
Tb	1.4	1.3	0.7	1.2	1	0.8	1	0.9	1.3	0.7	0.9	1.02	0.24
Yb	3.7	4	3.4	3.2	3.6	3.4	3.1	2.7	4	2.7	3.2	3.36	0.42
Lu	0.62	0.66	0.54	0.54	0.59	0.57	0.48	0.46	0.63	0.42	0.53	0.55	0.07
ΣREE	186.72	192.06	172.94	156.34	165.29	162.77	136.48	120.16	186.13	122.52	136.13	157.96	24.7
Eu/Eu*	0.54	0.54	0.51	0.5	0.54	0.62	0.56	0.58	0.54	0.44	0.55	0.54	0.04
Ce/Ce*	0.97	0.99	1.01	1.02	0.99	1.02	0.99	0.99	1.01	1.02	0.99	1	0.02
K/Cs	3932	4217	4736	5172	3672	7492	7023	3968	4632	6458	5375	5152	1248
Th/Sc	0.78	0.72	0.71	0.78	0.76	0.81	0.8	0.96	0.72	0.9	1.01	0.81	0.1
Zr/Sc	16.75	16.06	11.25	14.68	26.34	32.39	23.81	40.51	16.35	24.4	39.66	23.83	9.62
Th/U	3.71	3.82	3.87	3.75	4.17	4.33	3.65	3	4	3.42	4.45	3.83	0.39
La/Sc	2.47	2.33	2.32	2.27	2.67	2.92	2.76	3.21	2.46	2.86	3.3	2.69	0.34
La/Th	3.15	3.23	3.25	2.92	3.5	3.63	3.45	3.33	3.42	3.17	3.26	3.3	0.19
Cr/V	0.86	0.91	0.97	0.89	0.85	0.97	0.94	0.98	0.86	0.82	1.02	0.92	0.06
Y/Ni	0.85	0.8	0.76	0.68	0.67	0.61	0.76	0.52	0.85	0.56	0.49	0.69	0.12
Ti/Nb	296.7	336.1	312.7	317.3	291.9	282.6	269.6	325.6	333.5	306.9	308.5	307.4	19.9
La_N/Yb_N	7.49	7.1	7.75	7.39	6.57	6.56	6.32	6.26	6.93	6.51	6.12	6.82	0.52
La_N/Sm_N	3.4	3.43	3.41	3.5	3.19	3.1	3.15	3.09	3.31	3.27	3.32	3.29	0.13
Tb_N/Yb_N	1.62	1.39	0.88	1.6	1.19	1.01	1.38	1.43	1.39	1.11	1.2	1.29	0.22
Cr/Th	7.54	7.46	7.33	7	7.9	8.02	7.5	7.07	7.33	6.46	7.19	7.35	0.41
Ti/Zr	23.48	23.61	32.26	27.38	16.16	14.05	17.79	14.11	24.31	19.5	13.35	20.55	5.87

Table 1 (cont.): Chemical analyses of sedimentary clastic rocks of the Precordillera terrane. Major elements are in % whereas trace elements are in ppm. N denotes normalized to chondrite values (after Taylor and McLennan, 1985). Aver: average; SD: standard deviation; b.d.l.: below detection limits; n.d.: not determined.

Portezuelo del Tontal Formation

	mudstones		sandstones										
Sample	**PDT3**	**020464**	**PDT1**	**PDT2**	**020463**	**020465**	**020466**	**020467**	**020468**	**020469**	**020470**	**Aver**	**SD**
SiO_2	51.02	69.59	73.27	68.10	71.83	72.99	72.72	74.55	73.39	67.81	69.67	69.54	6.25
TiO_2	1.16	0.84	0.85	1.22	1.15	0.82	1.1	0.74	0.78	1.12	0.7	0.95	0.19
Al_2O_3	20.2	12.05	10.32	11.73	10.38	9.96	10.35	10.17	10.43	11.84	9.44	11.53	2.86
Fe_2O_3	10.02	5.97	5.38	5.85	6.3	4.39	4.64	4.56	4.17	6.5	3.27	5.55	1.7
MnO	0.11	0.07	0.08	0.05	0.07	0.1	0.05	0.05	0.04	0.08	0.03	0.07	0.02
MgO	3.59	2.01	1.64	2.44	2.01	1.56	1.82	1.41	1.69	2.36	1.33	1.99	0.61
CaO	0.89	0.38	1.13	1.76	0.56	1.6	1.21	0.59	0.63	1.5	0.77	1	0.45
Na_2O	1.59	2.54	2.62	2.06	2.21	2.12	1.45	2.29	2.05	2.25	2.45	2.15	0.35
K_2O	4.98	2.22	1.61	1.86	1.67	1.71	1.94	1.71	1.61	1.98	1.57	2.08	0.94
P_2O_5	0.16	0.17	0.17	0.17	0.17	0.15	0.13	0.15	0.13	0.17	0.13	0.15	0.02
LOI	5.59	2.43	1.79	2.9	2.18	3.27	2.59	2.56	2.67	3.29	2.16	2.86	0.97
Σ	99.3	98.26	98.86	98.13	98.54	98.65	98	98.77	97.58	98.9	91.52	97.87	2.06
CIA	69	64	57	59	63	56	62	62	64	59	58	61.18	3.64
Sc	24.9	12.6	11.3	16.1	14.5	11.6	14.5	11.8	12.3	16.1	11.9	14.33	3.74
Cr	120	61	51	87	76	55	77	64	68	79	73	73.73	17.88
Ni	74	39	b.d.l.	52	38	36	46	42	39	43	31	43.92	11.43
Cs	10	4	3	3	3	3	3	2	2	3	2	3.46	2.15
Rb	214	92	72	78	70	74	78	72	68	76	80	88.5	40.1
Ba	915	341	272	412	273	269	407	384	426	385	288	397.5	173.8
Hf	5	6	8	8	9	7	7	8	9	8	9	7.64	1.23
Th	15	10	9.2	9.3	9.1	8.6	7.7	10	10	10	10	9.9	1.76
U	4.7	2.1	1.5	2.5	2.5	2.3	1.8	1.8	2.4	1.8	1.8	2.29	0.83
V	149	72	71	125	98	71	94	63	68	88	65	87.64	26.31
Sr	62	43	88	84	47	79	67	75	97	86	59	71.55	16.62
Y	39.2	24.6	25	25.4	23.1	20.1	23.8	17	17.1	28.2	21.9	24.13	5.79
Zr	192	183	254	279	254	204	207	222	237	248	252	230.18	29.13
Nb	23	16	16	18	16	14	16	13	13	18	16	16.41	2.51
Pb	43.8	24.9	17	15.1	22	16.3	13.2	13.6	13	14	42.3	21.38	10.83
Zn	149	85	75	84	74	68	79	66	55	76	70	80.09	23.25
La	32	32	33	31	34	28	27	20	26	37	28	29.82	4.43
Ce	46	71	72	72	72	63	63	48	61	83	62	64.82	10.4
Nd	33	30	30	31	32	29	29	23	30	40	28	30.45	3.89
Sm	6.9	6.3	6	6.6	6.1	5.2	5.4	4	4.6	7.2	5.1	5.76	0.95
Eu	1.2	1.2	1.1	1.5	1.3	1	1	0.9	0.9	1.3	1	1.13	0.18
Tb	b.d.l.	1	b.d.l.	b.d.l.	0.8	b.d.l.	0.6	0.6	b.d.l.	b.d.l.	0.9	0.78	0.16
Yb	3.8	2.7	2.6	3.2	2.7	2.3	2.7	2.4	2.5	3.2	2.7	2.8	0.42
Lu	0.61	0.43	0.46	0.51	0.44	0.37	0.43	0.4	0.4	0.51	0.43	0.45	0.06
ΣREE	123.01	144.63	144.66	145.31	149.34	128.37	129.13	99.3	124.9	171.71	128.13	135.32	17.81
Eu/Eu*	0.8	0.58			0.67		0.6	0.69			0.58	0.65	0.08
Ce/Ce*	0.65	1.03	1.01	1.06	0.98	1.02	1.05	1.06	1.04	1.01	1.01	0.99	0.11
K/Cs	4136	4605	4447	5141	4624	4729	5360	7093	6666	5465	6500	5342	949
Th/Sc	0.6	0.79	0.81	0.58	0.63	0.74	0.53	0.85	0.81	0.62	0.84	0.71	0.11
Zr/Sc	7.71	14.52	22.48	17.33	17.52	17.59	14.28	18.81	19.27	15.4	21.18	16.92	3.8
Th/U	3.19	4.76	6.13	3.72	3.64	3.74	4.28	5.56	4.17	5.56	5.56	4.57	0.94
La/Sc	1.29	2.54	2.92	1.93	2.34	2.41	1.86	1.69	2.11	2.3	2.35	2.16	0.43
La/Th	2.13	3.2	3.59	3.33	3.74	3.26	3.51	2	2.6	3.7	2.8	3.08	0.58
Cr/V	0.81	0.85	0.72	0.7	0.78	0.77	0.82	1.02	1	0.9	1.12	0.86	0.13
Y/Ni	0.53	0.63		0.48	0.62	0.56	0.52	0.41	0.44	0.66	0.71	0.56	0.09
Ti/Nb	306.6	323.2	309.9	408.4	429.7	347	404.6	332.4	355.6	365.6	255.9	349	48.98
La_N/Yb_N	5.69	8.01	8.58	6.55	8.51	8.23	6.76	5.63	7.03	7.81	7.01	7.25	1
La_N/Sm_N	2.92	3.2	3.46	2.96	3.51	3.39	3.15	3.15	3.56	3.23	3.46	3.27	0.21
Tb_N/Yb_N		1.58			1.27		0.95	1.07			1.43	1.26	0.23
Cr/Th	8	6.1	5.54	9.35	8.35	6.4	10	6.4	6.8	7.9	7.3	7.47	1.33
Ti/Zr	36.09	27.55	20.13	26.11	27.24	24.16	31.86	20.06	19.81	27.12	16.65	25.16	5.5

Table 1 (cont.): Chemical analyses of sedimentary clastic rocks of the Precordillera terrane. Major elements are in % whereas trace elements are in ppm. N denotes normalized to chondrite values (after Taylor and McLennan, 1985). Aver: average; SD: standard deviation; b.d.l.: below detection limits; n.d.: not determined.

Sierra de la Invernada Formation

	mudstones				sandstones					
Sample	**020421**	**020423**	**020431**	**020433**	**SI1**	**020425**	**020428**	**020432**	**Aver**	**SD**
SiO_2	57.77	61.42	56.53	56.62	71.21	71.65	68.59	72.56	64.54	6.69
TiO_2	0.94	1.07	1.06	1.12	1.24	0.84	1.16	0.79	1.03	0.15
Al_2O_3	18.2	16.04	18.36	18.55	9.61	10.87	12.07	9.59	14.16	3.77
Fe_2O_3	8.34	6.62	7.67	8.26	6.1	5.33	5.65	4.71	6.59	1.29
MnO	0.06	0.06	0.07	0.1	0.09	0.07	0.06	0.07	0.07	0.01
MgO	2.98	2.29	2.76	2.86	1.79	1.54	1.75	1.3	2.16	0.61
CaO	0.33	0.93	0.88	0.78	1.46	0.89	0.92	1.25	0.93	0.31
Na_2O	1.45	2.04	1.46	1.89	2.43	2.64	2.25	2.58	2.09	0.44
K_2O	4.42	3.53	4.57	4.74	1.45	1.94	2.23	1.63	3.06	1.31
P_2O_5	0.13	0.2	0.17	0.18	0.17	0.17	0.19	0.15	0.17	0.02
LOI	4.43	4.53	5.85	5.32	2.57	2.54	2.98	2.96	3.9	1.22
Σ	99.05	98.71	99.38	100.42	98.1	98.48	97.84	97.6	98.7	0.86
CIA	71	66	68	67	55	59	62	55	62.88	5.7
Sc	20.2	16.8	20.2	21.3	12.8	11.5	13.9	10.5	15.9	4.02
Cr	93	83	94	99	94	53	70	48	79.25	18.64
Ni	40	40	43	43	39	32	36	33	38.35	4.05
Cs	7	6	9	9	2	4	4	3	5.5	2.5
Rb	160	130	162	166	62	79	91	60	113.8	42.9
Ba	635	459	498	525	303	290	430	250	423.8	124.7
Hf	5	8	5	6	11	7	11	8	7.63	2.23
Th	13	13	14	15	9.2	9.2	11	8.8	11.65	2.26
U	2.8	2.4	3.1	3.7	2.7	2	3.2	2.5	2.8	0.49
V	101	92	104	113	103	64	87	65	91.13	17.03
Sr	46	91	73	68	100	85	91	95	81.13	16.7
Y	24.8	36	35.5	35.7	24.8	24.2	29.2	20.8	28.88	5.72
Zr	148	245	180	193	375	218	328	232	239.88	71.43
Nb	17	20	20	20	18	15	18	14	17.88	2.21
Pb	19.2	30.1	27.1	27.9	16.4	24.1	14.8	20.5	22.51	5.27
Zn	121	112	127	116	68	75	b.d.l.	b.d.l.	103.17	22.94
La	36	45	37	38	33	29	37	27	35.25	5.26
Ce	76	91	84	88	74	65	82	59	77.38	10.42
Nd	36	44	38	36	34	28	34	28	34.75	4.89
Sm	6.4	8.1	7.5	7.3	6.2	5.7	7.3	5.2	6.71	0.93
Eu	1	1.5	1.3	1.1	1.1	1.1	1.2	1	1.16	0.16
Tb	0.8	1.1	1	1.4	b.d.l.	1.1	0.9	0.8	1.01	0.2
Yb	3	3.5	3.4	3.6	2.9	2.7	3.5	2.4	3.13	0.41
Lu	0.47	0.57	0.56	0.59	0.5	0.42	0.56	0.38	0.51	0.07
ΣREE	159.67	194.77	172.76	175.99	151.2	133.02	166.46	123.78	159.71	21.75
Eu/Eu*	0.5	0.58	0.54	0.43		0.55	0.52	0.59	0.53	0.05
Ce/Ce*	0.96	0.93	1.03	1.07	1.02	1.03	1.03	0.99	1.01	0.04
K/Cs	5240	4877	4214	4374	5997	4032	4632	4510	4735	594
Th/Sc	0.64	0.77	0.69	0.7	0.72	0.8	0.79	0.84	0.75	0.06
Zr/Sc	7.33	14.58	8.91	9.06	29.3	18.96	23.6	22.1	16.73	7.52
Th/U	4.64	5.42	4.52	4.05	3.41	4.6	3.44	3.52	4.2	0.67
La/Sc	1.78	2.68	1.83	1.78	2.58	2.52	2.66	2.57	2.3	0.39
La/Th	2.77	3.46	2.64	2.53	3.59	3.15	3.36	3.07	3.07	0.37
Cr/V	0.92	0.9	0.9	0.88	0.91	0.83	0.8	0.74	0.86	0.06
Y/Ni	0.62	0.9	0.82	0.83	0.64	0.76	0.8	0.64	0.75	0.1
Ti/Nb	325.7	328.5	316.7	326.4	408.4	332.1	379.7	341.9	344.9	29.99
La_N/Yb_N	8.11	8.69	7.35	7.13	7.69	7.26	7.14	7.6	7.62	0.51
La_N/Sm_N	3.54	3.5	3.11	3.28	3.35	3.2	3.19	3.27	3.3	0.14
Tb_N/Yb_N	1.14	1.34	1.26	1.66		1.74	1.1	1.43	1.38	0.23
Cr/Th	7.15	6.38	6.71	6.6	10.22	5.76	6.36	5.45	6.83	1.37
Ti/Zr	38.08	26.28	35.37	34.67	19.82	23.16	21.18	20.34	27.36	7.03

Table 1 (cont.): Chemical analyses of sedimentary clastic rocks of the Precordillera terrane. Major elements are in % whereas trace elements are in ppm. N denotes normalized to chondrite values (after Taylor and McLennan, 1985). Aver: average; SD: standard deviation; b.d.l.: below detection limits; n.d.: not determined.

Ponón Trehué Formation

	mudstones				sandstones					
Sample	**CT3**	**CT7**	**CT8**	**CT6**	**CT1**	**CT2**	**CT4**	**CT5**	**Aver**	**SD**
SiO_2	74.36	59.11	60.3	70.61	78.99	83.85	75.32	77.67	72.53	8.22
TiO_2	1.42	1.54	1.46	1.4	0.42	0.19	1.39	1.32	1.14	0.49
Al_2O_3	13	20.28	18.32	13.23	7.77	3.59	10.86	8.67	11.96	5.15
Fe_2O_3	3.62	5.76	8.09	6.03	3.09	1.82	4.31	4.83	4.69	1.83
MnO	0.01	0.04	0.04	0.08	0.02	0.06	0.04	0.03	0.04	0.02
MgO	1.04	1.44	1.42	1.23	0.52	0.23	0.91	0.81	0.95	0.4
CaO	0.27	0.21	0.26	0.16	0.55	2.67	0.17	0.21	0.56	0.8
Na_2O	0.62	0.64	1.29	0.85	0.48	1.02	0.78	0.37	0.76	0.28
K_2O	2.93	4.75	3.81	2.78	2.4	1.04	2.34	1.5	2.69	1.11
P_2O_5	0.17	0.07	0.11	0.08	0.4	0.17	0.09	0.11	0.15	0.1
LOI	3.26	4.67	5	3.33	3.52	3.54	2.79	3.74	3.73	0.69
Σ	100.7	98.52	100.09	99.78	98.15	98.16	98.98	99.26	99.2	0.87
CIA	75	76	74	74	69		74	77	74.1	2.36
Sc	14.3	20.1	19.3	14.3	10	4.1	12.9	11.1	13.26	4.81
Cr	240	150	150	150	80	140	150	170	153.75	40.91
Ni	47	49	75	45	87	23	31	25	49.56	20.92
Cs	3	5	5	3	3	b.d.l.	3	2	3.43	1.05
Rb	110	178	153	107	83	36	89	61	102.1	43.3
Ba	1109	1145	763	756	4969	3824	964	575	1763.1	1557.2
Hf	10	7	7	9	3	1	9	12	7.25	3.42
Th	11	14	14	11	7.4	3.7	11	12	10.51	3.23
U	2.7	1.5	4.3	4	3.2	2	3.1	3	2.98	0.87
V	123	158	148	119	193	83	117	115	132	31.26
Sr	45	66	85	45	70	41	38	36	53.25	16.84
Y	39.6	38.6	38.2	25.9	23.4	2.4	25.7	30.3	28.02	11.41
Zr	319	253	272	299	110	55	295	402	250.63	106.30
Nb	25	27	25	24	10	7	23	22	20.39	7.21
Pb	11.3	11.9	19.9	14	39.6	15.6	10.2	13.7	17.03	9
Zn	65	86	117	84	154	52	69	60	85.88	31.92
La	39	43	42	31	30	14	31	31	32.63	8.64
Ce	95	85	83	70	59	28	71	75	70.75	19.12
Nd	41	34	36	31	20	12	25	22	27.63	8.96
Sm	10.7	8.1	8.6	6.4	5.6	2.7	6.7	7.2	7	2.19
Eu	1.9	1.3	1.5	1.1	1	0.5	1.2	1.2	1.21	0.38
Tb	1.6	1.2	1	1.1	1	b.d.l.	1.2	1.3	1.2	0.19
Yb	5	5.3	5.2	4.3	2.6	1.1	4.6	4.8	4.11	1.39
Lu	0.89	0.88	0.84	0.8	0.4	0.2	0.79	0.83	0.7	0.24
ΣREE	195.09	178.78	178.14	145.7	119.6	58.5	141.49	143.33	145.08	40.14
Eu/Eu*	0.54	0.49	0.56	0.51	0.52		0.53	0.49	0.52	0.02
Ce/Ce*	1.1	0.94	0.93	1.03	0.96	0.94	1.09	1.17	1.02	0.09
K/Cs	8107	7879	6322	7698	6627		6461	6234	7047	751
Th/Sc	0.77	0.7	0.73	0.77	0.74	0.9	0.85	1.08	0.82	0.12
Zr/Sc	22.31	12.59	14.09	20.91	11	13.41	22.87	36.22	19.17	7.8
Th/U	4.07	9.33	3.26	2.75	2.31	1.85	3.55	4	3.89	2.18
La/Sc	2.73	2.14	2.18	2.17	3	3.41	2.4	2.79	2.6	0.43
La/Th	3.55	3.07	3	2.82	4.05	3.78	2.82	2.58	3.21	0.49
Cr/V	1.95	0.95	1.01	1.26	0.41	1.69	1.28	1.48	1.25	0.44
Y/Ni	0.84	0.79	0.51	0.58	0.27	0.1	0.83	1.21	0.64	0.33
Ti/Nb	343	337.4	342.9	353.1	263.2	165.9	358.1	359.9	315.46	63.57
La_N/Yb_N	5.27	5.48	5.46	4.87	7.8	8.6	4.55	4.36	5.8	1.45
La_N/Sm_N	2.29	3.34	3.07	3.05	3.37	3.26	2.91	2.71	3	0.34
Tb_N/Yb_N	1.37	0.97	0.82	1.09	1.64		1.12	1.16	1.17	0.25
Cr/Th	21.82	10.71	10.71	13.64	10.81	37.84	13.64	14.17	16.67	8.69
Ti/Zr	26.63	36.54	32.07	28.11	22.89	20.71	28.29	19.67	26.86	5.36

Table 1 (cont.): Chemical analyses of sedimentary clastic rocks of the Precordillera terrane. Major elements are in % whereas trace elements are in ppm. N denotes normalized to chondrite values (after Taylor and McLennan, 1985). Aver: average; SD: standard deviation; b.d.l.: below detection limits; n.d.: not determined.

air-dried samples

Sample	Formation	FWHM	CIS	Diagenesis/Metamorphism
020457	Alcaparrosa	0.495	0.498	late diagenesis
020459	Alcaparrosa	0.314	0.367	low anchizone
020461	Alcaparrosa	0.262	0.33	low anchizone
A2	Alcaparrosa	0.445	0.462	late diagenesis
CT3	Ponón Trehué	0.328	0.378	low anchizone
CT6	Ponón Trehué	0.318	0.370	low anchizone
CT7	Ponón Trehué	0.274	0.339	low anchizone
CT8	Ponón Trehué	0.334	0.382	low anchizone
E2	Empozada	0.379	0.414	low anchizone
E4	Empozada	0.498	0.500	late diagenesis
E5	Empozada	0.534	0.526	late diagenesis
E7	Empozada	0.674	0.627	late diagenesis
LRAT1	Los Sombreros	0.350	0.393	low anchizone
020464	Portezuelo del Tontal	0.205	0.289	late anchizone
PDT3	Portezuelo del Tontal	0.206	0.290	late anchizone
YL424	Yerba Loca	0.236	0.311	low anchizone
YL437	Yerba Loca	0.218	0.298	late anchizone
YL438	Yerba Loca	0.258	0.327	low anchizone
YL1	Yerba Loca	0.372	0.409	low anchizone
YL2	Yerba Loca	0.205	0.289	late anchizone

ethylene-glycol attacked sample

Sample	Formation	FWHM	CIS	Diagenesis/Metamorphism
020457	Alcaparrosa	0.482	0.489	late diagenesis
020459	Alcaparrosa	0.309	0.364	low anchizone
020461	Alcaparrosa	0.288	0.349	low anchizone
A2	Alcaparrosa	0.424	0.447	late diagenesis
CT3	Ponón Trehué	0.322	0.373	low anchizone
CT6	Ponón Trehué	0.313	0.367	low anchizone
CT7	Ponón Trehué	0.275	0.339	low anchizone
E2	Empozada	0.376	0.412	low anchizone
E4	Empozada	0.379	0.414	low anchizone
E7	Empozada	0.641	0.603	late diagenesis
LRAT1	Los Sombreros	0.303	0.360	low anchizone
020464	Portezuelo del Tontal	0.212	0.294	late anchizone
PDT3	Portezuelo del Tontal	0.201	0.286	late anchizone
YL424	Yerba Loca	0.230	0.307	low anchizone
YL437	Yerba Loca	0.220	0.300	late anchizone
YL438	Yerba Loca	0.249	0.321	low anchizone
YL1	Yerba Loca	0.369	0.407	low anchizone
YL2	Yerba Loca	0.200	0.285	late anchizone

Table 2: Illite crystallinity index measured to determine the grade of diagenesis and/or very low-grade metamorphism of sedimentary clastic rocks of the Precordillera terrane. FWHM: full-width-height-maximum. CIS: crystallization index corrected according to standardized values. For details on methodology, see Appendix B. The term anchizone is equivalent to very-low grade metamorphism according to the recommendations of the Subcommission on the Systematics of Metamorphic Rocks from the IUGS (Árkai *et al.*, 2003).

sample	age (Ma)	Sm (ppm)	Nd (ppm)	$^{147}Sm/^{144}Nd$	$^{143}Nd/^{144}Nd$ (t=0)	error (ppm)	ε_{Nd} (0)	ε_{Nd} (t)	T_{DM}^{1} (Ma)	T_{DM}^{2} (Ma)	$f_{Sm/Nd}$
Yerba Loca Formation											
YL451	455	5.03	25.82	0.11785	0.512109	20	-10.32	-5.74	1476	1631	-0.40
YL449	455	5.08	26.55	0.11578	0.512024	19	-11.97	-7.28	1576	1739	-0.41
YL3	455	3.76	18.26	0.12434	0.512176	13	-9.01	-4.81	1469	1563	-0.37
YL2	455	4.77	24.82	0.11620	0.512110	20	-10.30	-5.63	1450	1622	-0.41
YL1	455	5.07	25.88	0.11844	0.512089	17	-10.70	-6.16	1516	1661	-0.40
Ponón Trehué Formation											
CT8	462	5.47	27.32	0.12102	0.512161	14	-9.31	-4.84	1442	1569	-0.38
CT5	462	4.54	21.68	0.12676	0.512217	14	-8.20	-4.08	1438	1513	-0.36
CT4	462	4.50	21.56	0.12613	0.512173	36	-9.07	-4.91	1504	1574	-0.36
CT3	462	6.22	28.87	0.13016	0.512203	13	-8.48	-4.56	1522	1549	-0.34
CT1	462	4.29	21.88	0.11858	0.512230	18	-7.96	-3.95	1298	1985	-0.40
Gualcamayo Formation											
GUAL1	467	4.25	21.43	0.12000	0.512181	13	-8.91	-4.34	1394	1536	-0.39
020455	467	4.65	25.07	0.11213	0.512088	15	-10.74	-5.70	1425	1635	-0.43
020454	467	4.38	24.58	0.10764	0.512075	17	-10.97	-5.67	1383	1633	-0.45
G12	467	4.98	27.56	0.10933	0.512087	16	-10.75	-5.54	1389	1624	-0.44
G5	467	1.81	9.14	0.11989	0.512224	14	-8.08	-3.50	1324	1472	-0.39
Los Sombreros Formation											
LRAT1	465	5.54	27.96	0.11986	0.512128	11	-9.95	-5.37	1477	1612	-0.39
020418	465	5.01	26.18	0.11561	0.512081	16	-10.86	-6.05	1486	1660	-0.41
SOM5	465	4.90	28.22	0.10489	0.511970	13	-13.03	-7.58	1494	1767	-0.47
SOM7	465	7.95	18.16	0.26456	0.512440	10	-3.85	-7.90	-2490	1789	0.34
SOM9	465	1.54	5.54	0.16862	0.512251	11	-7.54	-5.99	2699	1647	-0.14
La Chilca Formation											
020401	436	5.02	21.72	0.13960	0.512223	13	-8.10	-4.92	1674	1557	-0.29
020402	436	5.02	21.54	0.14086	0.512213	32	-8.29	-5.19	1723	1577	-0.28
020403	436	4.14	20.01	0.12510	0.512197	16	-8.60	-4.61	1445	1534	-0.36
020415	436	2.63	12.58	0.12631	0.512201	18	-8.52	-4.60	1458	1533	-0.36
020416	436	2.36	10.85	0.13141	0.512276	14	-7.07	-3.44	1412	1446	-0.33
Los Azules Formation											
020405	462	3.48	17.14	0.12272	0.512135	33	-9.82	-5.46	1501	1614	-0.26
020406	462	3.49	18.63	0.11330	0.512112	24	-10.25	-5.34	1405	1606	-0.42
020407	462	4.89	21.86	0.13523	0.512123	19	-10.05	-6.42	1774	1684	-0.31
020409	462	2.88	14.68	0.11855	0.512163	16	-9.27	-4.67	1402	1556	-0.40
020414	462	4.28	22.24	0.11645	0.512178	15	-8.97	-4.24	1348	1525	-0.41

Table 3: Sm-Nd isotopes of sedimentary clastic rocks of the Precordillera terrane. See Appendix B for details on methodology and analytical techniques applied. Calculated according to DePaolo (1981) except for T_{DM}^{2} that is calculated according to DePaolo *et al.* (1991).

sample	$^{206}Pb/^{204}Pb$	$^{207}Pb/^{204}Pb$	$^{208}Pb/^{204}Pb$	$^{208}Pb/^{206}Pb$	$^{207}Pb/^{206}Pb$
Yerba Loca Formation					
YL451	19.042375	15.676560	39.358725	2.0668557	0.82323272
YL449	18.929203	15.674350	39.201005	2.0709597	0.82807240
YL3	19.075712	15.727532	39.166689	2.0533489	0.82452272
YL2	18.828934	15.687246	39.084801	2.0757807	0.83313447
YL1	19.706384	15.839169	39.994669	2.0295229	0.80375530
Ponón Trehué Formation					
CT8	19.027669	15.666211	38.948940	2.0469290	0.82333189
CT6	19.100324	15.689129	38.833531	2.0331038	0.82139061
CT5	19.160300	15.703960	38.975361	2.0341752	0.81960700
CT4	19.173025	15.703028	38.970501	2.0325439	0.81902006
CT3	19.303141	15.706133	38.989437	2.0198499	0.81364848
Gualcamayo Formation					
GUAL1	19.373456	15.760460	39.225151	2.0247125	0.81349013
020455	19.601049	15.754774	38.817697	1.9803865	0.80377072
020454	19.552706	15.748809	38.865992	1.9877671	0.80545188
G12	19.505572	15.768741	39.081363	2.0036251	0.80842121
G5	19.198924	15.676245	38.696522	2.0155446	0.81650453
Los Sombreros Formation					
LRAT1	19.496023	15.782430	39.523273	2.0272789	0.80953024
020418	18.902289	15.689646	39.116128	2.0694154	0.83005634
SOM5	19.252671	15.847305	39.937921	2.0744693	0.82314671
SOM7	18.887147	15.824926	39.297977	2.0806795	0.83787425
SOM9	18.819950	15.921354	39.243822	2.0783595	0.84319903
La Chilca Formation					
020401	19.037480	15.693332	39.113453	2.0545695	0.82434112
020402	20.164236	16.417603	40.859648	2.0263223	0.81419221
020403	19.498234	15.904639	39.830771	2.0427358	0.81567180
020415	19.429056	16.114116	39.938218	2.0555495	0.82935600
020416	21.191455	17.267178	42.926558	2.0256563	0.81482005
Los Azules Formation					
020405	19.759557	15.834524	39.006425	1.9740804	0.80137917
020406	19.089215	15.695964	38.831680	2.0342082	0.82224763
020407	19.501651	15.718090	38.874025	1.9933965	0.80599880
020409	19.089215	15.695964	38.831680	2.0342082	0.82224763
020414	19.298011	15.722089	38.969906	2.0193963	0.81469408

Table 4: Pb-Pb isotopes of sedimentary clastic rocks of the Precordillera terrane. Pb data are corrected for mass fractionation. Details regarding methodology and analytical techniques are given in Appendix B.

Alcaparrosa Formation

		Isotopic ratios				Apparent age (Ma)						Concordant age
Sample	**$^{232}Th/^{238}U$**	**$^{207}Pb/^{235}U$**	**error**	**$^{206}Pb/^{238}U$**	**error**	**$^{206}Pb/^{238}U$**	**error**	**$^{207}Pb/^{235}U$**	**error**	**$^{207}Pb/^{206}Pb$**	**error**	**Ma**
A-I-01a	*0.46*	*2.14369*	*1.23*	*0.19176*	*0.81*	*1131*	*9*	*1163*	*14*	*1223*	*11*	*1223 ± 37*
A-I-04	0.52	0.65158	3.46	0.08314	1.94	515	10	509	18	485	14	512 ± 6.3
A-I-06	0.68	2.69548	2.50	0.22628	1.39	1315	18	1327	33	1347	28	1319 ± 15
B-II-08	*0.35*	*0.88067*	*5.78*	*0.09975*	*1.16*	*613*	*7*	*641*	*37*	*743*	*42*	*616 ± 6.6*
B-II-15	0.28	1.74963	2.81	0.17319	1.37	1030	14	1027	29	1021	25	1029 ± 13
B-II-16	*0.67*	*4.83490*	*1.72*	*0.30450*	*1.22*	*1714*	*21*	*1791*	*31*	*1882*	*23*	*1882 ± 43*
B-II-18	0.45	1.54664	4.38	0.15767	0.73	944	7	949	42	962	42	944 ± 6.4
B-II-21	0.19	0.53124	2.09	0.06928	1.84	432	8	433	9	437	4	432 ± 7.3
B-II-29	0.32	1.80195	2.43	0.17750	0.79	1053	8	1046	25	1031	24	1053 ± 7.6
B-II-33	0.44	1.20922	1.74	0.13397	1.48	810	12	805	14	789	7	805 ± 9.7
B-II-34	*0.27*	*1.48581*	*2.54*	*0.14945*	*2.07*	*898*	*19*	*925*	*23*	*989*	*15*	*989 ± 59*
B-II-35	0.53	0.66716	3.85	0.08218	1.81	509	9	519	20	563	19	510 ± 8.8
B-II-37	0.61	0.63891	4.14	0.07965	2.62	494	13	502	21	536	17	495 ± 12
B-II-39	0.32	1.54000	3.44	0.15757	1.47	943	14	947	33	954	30	944 ± 13
B-II-51	0.30	2.23634	2.98	0.20212	1.88	1187	22	1193	35	1203	28	1189 ± 19
B-II-63	0.68	1.79572	2.32	0.17537	1.25	1042	13	1044	24	1049	21	1042 ± 11
B-II-73	0.55	3.88560	2.01	0.28017	0.89	1592	14	1611	32	1635	30	1597 ± 12
B-II-76	*0.92*	*1.70988*	*2.74*	*0.16538*	*1.12*	*987*	*11*	*1012*	*28*	*1068*	*27*	*989 ± 10*
B-II-81	*0.37*	*1.69988*	*6.14*	*0.16610*	*2.63*	*991*	*26*	*1008*	*62*	*1048*	*58*	*993 ± 24*
B-II-82a	*0.56*	*4.50253*	*1.40*	*0.29646*	*0.56*	*1674*	*9*	*1731*	*24*	*1802*	*23*	*1802 ± 44*
B-II-82b	*0.37*	*4.30896*	*1.85*	*0.28751*	*1.03*	*1629*	*17*	*1695*	*31*	*1778*	*27*	*1778 ± 55*
B-II-83	*0.69*	*1.71632*	*6.54*	*0.16552*	*2.30*	*987*	*23*	*1015*	*66*	*1074*	*66*	*989 ± 21*
B-II-84	0.59	1.92108	1.84	0.18173	1.22	1076	13	1088	20	1113	15	1082 ± 11
B-II-86	0.59	1.84449	1.66	0.17547	0.54	1042	6	1061	18	1101	17	1044 ± 5.1
B-II-87a	*0.53*	*2.32873*	*1.33*	*0.20262*	*0.95*	*1189*	*11*	*1221*	*16*	*1278*	*12*	*1278 ± 37*
B-II-88	0.37	1.71924	3.46	0.17204	2.12	1023	22	1016	35	999	27	1020 ± 19
B-II-89a	0.40	1.69516	1.98	0.16969	1.50	1010	15	1007	20	999	13	1008 ± 12
B-II-92	0.90	0.78188	1.55	0.09505	1.00	585	6	587	9	591	7	586 ± 5.5
B-II-94	0.81	1.92563	2.42	0.18422	0.96	1090	10	1090	26	1090	24	1090 ± 9.4
C-III-101	*0.56*	*0.56893*	*5.07*	*0.07240*	*2.39*	*451*	*11*	*457*	*23*	*491*	*22*	*451 ± 10*
C-III-102	*0.47*	*1.87138*	*1.52*	*0.17590*	*1.23*	*1045*	*13*	*1071*	*16*	*1125*	*10*	*1125 ± 37*
C-III-103	0.33	1.92043	1.25	0.18210	0.85	1078	9	1088	14	1108	10	1083 ± 7.7
C-III-104	*0.61*	*4.55339*	*1.59*	*0.30300*	*0.87*	*1706*	*15*	*1741*	*28*	*1783*	*24*	*1783 ± 48*
C-III-106	0.50	1.83814	1.50	0.17564	1.03	1043	11	1059	16	1092	12	1051 ± 240
C-III-109	0.58	2.05246	2.99	0.19464	0.51	1146	6	1133	34	1108	33	1146 ± 5.3
C-III-112	0.27	2.87863	1.96	0.23732	1.11	1373	15	1376	27	1382	22	1374 ± 13
C-III-115	0.60	0.81552	4.79	0.09900	0.79	609	5	606	29	594	28	608 ± 4.6
C-III-117	0.36	2.67855	3.26	0.23004	2.83	1335	38	1323	43	1303	21	1318 ± 23
C-III-118	1.26	0.57330	6.44	0.07412	5.33	461	25	460	30	456	16	461 ± 23
C-III-119	0.47	2.01171	2.23	0.18754	1.50	1108	17	1119	25	1142	19	1114 ± 14
C-III-120	0.17	2.39253	1.94	0.20904	1.48	1224	18	1240	24	1269	16	1238 ± 14
C-III-122	0.51	0.57359	2.46	0.07405	1.69	460	8	460	11	460	8	460 ± 7.4
C-III-125	0.51	2.44303	1.00	0.21323	0.49	1246	6	1255	13	1271	11	1248 ± 5.3
C-III-127	0.56	1.92954	2.13	0.18603	1.06	1100	12	1091	23	1075	20	1098 ± 10
C-III-128	0.53	0.73722	2.56	0.09034	1.71	558	10	561	14	574	11	558 ± 8.9
C-III-129	*0.25*	*2.00449*	*0.79*	*0.18381*	*0.60*	*1088*	*6*	*1117*	*9*	*1174*	*6*	*1174 ± 21*
C-III-134	*0.73*	*5.22287*	*2.36*	*0.32557*	*1.32*	*1817*	*24*	*1856*	*44*	*1901*	*37*	*1901 ± 68*
C-III-136	0.30	1.56535	1.61	0.15903	1.08	951	10	957	15	969	12	954 ± 8.9
C-III-140	0.48	2.81381	1.74	0.23390	1.16	1355	16	1359	24	1366	18	1358 ± 12

Table 5: Detrital zircon dating on selected samples from Ordovician units of the Precordillera terrane. Isotope ratios corrected for fractionation by comparison with standard GJ-1. Analyses with large errors were excluded (about 8% of the grains). Highly discordant samples (of up to 15% discordance) are shown in italics since a medium age was anchored. Errors are at one sigma.

Pavón Formation

		Isotopic ratios				Apparent age (Ma)						Concordant age
Sample	$^{232}Th/^{238}U$	$^{207}Pb/^{235}U$	error	$^{206}Pb/^{238}U$	error	$^{206}Pb/^{238}U$	error	$^{207}Pb/^{235}U$	error	$^{207}Pb/^{206}Pb$	error	Ma
G-VII-458	0.58	1.81152	2.31	0.17440	1.88	1036	19	1050	24	1077	15	1049 ± 15
G-VII-456	0.66	1.83079	3.89	0.17622	1.74	1046	18	1057	41	1078	37	1048 ± 16
G-VII-454	0.44	1.98432	1.66	0.18713	1.17	1106	13	1110	18	1119	13	1108 ± 11
G-VII-449	0.78	2.86412	2.09	0.23598	1.38	1366	19	1373	29	1383	22	1375 ± 12
G-VII-446	0.44	2.90877	2.44	0.24167	1.95	1395	27	1384	34	1367	20	1375 ± 12
G-VII-439	0.67	1.96370	1.52	0.18602	1.12	1100	12	1103	17	1110	11	1090 ± 7.7
G-VII-438	0.52	1.89188	1.87	0.17881	1,37	1060	15	1078	20	1114	14	1090 ± 7.7
G-VII-437	0.86	2.09490	2.97	0.19529	1.92	1150	22	1147	34	1142	26	1149 ± 18
G-VII-436a	0.26	2.02791	2.74	0.19107	1.84	1127	21	1125	31	1121	23	1126 ± 17
G-VII-436b	0.50	2.03482	1.95	0.19228	0.89	1134	10	1127	22	1115	19	1132 ± 8.9
G-VII-435	*0.90*	*2.57362*	*2.77*	*0.21294*	*1.71*	*1244*	*21*	*1293*	*36*	*1375*	*30*	*1356 ± 34*
G-VII-434	*0.68*	*1.78238*	*4.06*	*0.17078*	*2.72*	*1016*	*28*	*1039*	*42*	*1087*	*33*	*1087 ± 40*
G-VII-432	*0.47*	*3.04117*	*1.70*	*0.25658*	*1.37*	*1472*	*20*	*1418*	*24*	*1337*	*13*	*1356 ± 34*
G-VII-431	0.61	1.87367	2.57	0.18004	1.73	1067	18	1072	28	1081	20	1070 ± 16
G-VII-429	0.51	2.79883	2.18	0.23342	1.31	1352	18	1355	30	1360	24	1354 ± 14
G-VII-428	0.29	1.82389	1.65	0.17585	1.16	1044	12	1054	17	1075	13	1050 ± 10
G-VII-426	*0.89*	*1.98214*	*3.10*	*0.16918*	*0.84*	*1008*	*8*	*1109*	*34*	*1315*	*39*	*1361 ± 66*
G-VII-424	0.45	2.90639	2.81	0.24215	1.47	1398	21	1384	39	1362	33	1393 ± 17
G-VII-423	0.72	2.96160	2.52	0.24593	1.39	1417	20	1398	35	1368	29	1409 ± 16
G-VII-417	0.40	1.87287	2.61	0.17763	1.46	1054	15	1072	28	1107	24	1059 ± 14
G-VII-415	0.44	2.73001	2.63	0.22594	1.76	1313	23	1337	35	1374	27	1327 ± 19
G-VII-414	0.43	1.95331	1.99	0.18756	1.11	1108	12	1100	22	1083	18	1105 ± 11
G-VII-413	*0.40*	*2.45500*	*2.61*	*0.21043*	*1.51*	*1231*	*19*	*1259*	*33*	*1307*	*28*	*1304 ± 45*
G-VII-412	*0.71*	*2.35359*	*1.64*	*0.20218*	*0.76*	*1187*	*9*	*1229*	*20*	*1302*	*19*	*1304 ± 45*
G-VII-411	*0.69*	*1.90578*	*1.96*	*0.17675*	*1.19*	*1049*	*12*	*1083*	*21*	*1152*	*18*	*1167 ± 35*
G-VII-409	0.41	2.16132	2.70	0.20232	1.56	1188	19	1169	32	1134	25	1180 ± 16
G-VII-404	0.45	1.83630	2.58	0.17594	1.40	1045	15	1059	27	1087	24	1048 ± 13
G-VII-408	0.96	2.07574	2.36	0.19212	1.55	1133	18	1141	27	1156	21	1137 ± 14
F-VI-402	0.59	4.08749	1.89	0.29270	1.35	1655	22	1652	31	1648	22	1652 ± 15
F-VI-401	*1.46*	*1.87702*	*2.48*	*0.17151*	*1.99*	*1020*	*20*	*1073*	*27*	*1181*	*17*	*1167 ± 35*
F-VI-400	*0.87*	*2.00281*	*2.60*	*0.18453*	*2.17*	*1092*	*24*	*1116*	*29*	*1165*	*17*	*1167 ± 35*
F-VI-397	0.51	1.90289	2.04	0.18074	1.67	1071	18	1082	22	1105	13	1082 ± 14
F-VI-396	0.49	1.98944	2.14	0.18645	1.27	1102	14	1112	24	1131	20	1106 ± 12
F-VI-395	0.46	1.92244	2.48	0.18328	1.24	1085	13	1089	27	1097	24	1086 ± 12
F-VI-393	0.55	1.94213	2.60	0.18404	0.93	1089	10	1096	28	1109	27	1090 ± 9.2
F-VI-391	0.32	1.95343	2.64	0.18551	1.19	1097	13	1100	29	1105	26	1097 ± 12
F-VI-390	*0.56*	*2.37360*	*3.01*	*0.21921*	*2.51*	*1278*	*32*	*1235*	*37*	*1160*	*19*	*1126 ± 32*
F-VI-389	*0.42*	*1.82514*	*1.93*	*0.17191*	*1.17*	*1023*	*12*	*1055*	*20*	*1121*	*17*	*1126 ± 32*
F-VI-387	*0.66*	*1.83003*	*1.75*	*0.17121*	*1.25*	*1019*	*13*	*1056*	*18*	*1135*	*14*	*1126 ± 32*
F-VI-385	0.55	2.00671	2.54	0.19225	1.73	1134	20	1118	28	1087	20	1124 ± 16
F-VI-384	0.49	1.99576	2.23	0.18650	1.30	1102	14	1114	25	1137	21	1106 ± 12
F-VI-382	0.51	0.87311	2.50	0.10328	1.45	634	9	637	16	650	13	634 ± 8.6
F-VI-379	0.44	2.02631	1.53	0.19214	1.11	1133	13	1124	17	1108	12	1127 ± 10
F-VI-376	0.46	1.93860	2.50	0.18484	1.41	1093	15	1095	27	1097	23	1094 ± 13
F-VI-375	*0.67*	*2.94807*	*1.62*	*0.23155*	*1.38*	*1343*	*19*	*1394*	*23*	*1474*	*13*	*1474 ± 32*
F-VI-372	0.97	1.87010	3.22	0.18052	1.25	1070	13	1071	34	1072	32	1070 ± 12
F-VI-368	0.36	1.94540	1.82	0.18206	1.17	1078	13	1097	20	1134	16	1086 ± 11
F-VI-363	0.50	2.73140	2.34	0.23087	1.37	1339	18	1337	31	1334	25	1338 ± 15
F-VI-359	0.02	0.82952	2.59	0.10018	1.73	615	11	613	16	605	12	615 ± 9.9
F-VI-358	0.52	1.95880	2.52	0.18562	1.77	1098	19	1101	28	1109	20	1100 ± 16
F-VI-356	0.39	1.93119	3.42	0.18232	1.89	1080	20	1092	37	1117	32	1083 ± 18
F-VI-355	0.29	1.87360	2.94	0.18019	2.05	1068	22	1072	32	1080	23	1070 ± 18

Table 5 (cont.): Detrital zircon dating on selected samples from Ordovician units of the Precordillera terrane. Isotope ratios corrected for fractionation by comparison with standard GJ-1. Analyses with large errors were excluded (about 5% of the grains). Highly discordant samples (of up to 15% discordance) are shown in italics since a medium age was anchored. Errors are at one sigma.

Ponón Trehué Formation

		Isotopic ratios				Apparent age (Ma)						Concordant age
Sample	$^{232}Th/^{238}U$	$^{207}Pb/^{235}U$	error	$^{206}Pb/^{238}U$	error	$^{206}Pb/^{238}U$	error	$^{207}Pb/^{235}U$	error	$^{207}Pb/^{206}Pb$	error	Ma
A-I-01	*0.49*	*1.99744*	*2.52*	*0.17479*	*2.20*	*1038*	*23*	*1115*	*28*	*1266*	*15*	*1266 ± 48*
A-I-01b	*0.45*	*2.19197*	*1.55*	*0.19149*	*1.01*	*1129*	*11*	*1178*	*18*	*1270*	*15*	*1270 ± 45*
A-I-03	0.48	2.13908	1.97	0.19915	1.39	1171	16	1162	23	1144	16	1165 ± 13
A-I-02a	0.33	1.34998	4.87	0.13708	2.64	828	22	868	42	970	40	834 ± 20
A-I-03	0.16	2.05176	1.64	0.18954	1.44	1119	16	1133	19	1160	9	1138 ± 11
A-I-05	0.50	2.26971	1.04	0.20442	0.43	1199	5	1203	12	1210	11	1199.7 ± 4.6
A-06	0.41	2.17768	2.00	0.19888	1.60	1169	19	1174	23	1183	14	1174 ± 14
A-I-10	0.31	2.33728	2.38	0.21279	2.30	1244	29	1224	29	1189	7	1199 ± 11
A-I-12	0.16	2.27266	2.60	0.20182	1.92	1185	23	1204	31	1238	22	1199 ± 18
A-I-15	0.16	2.29091	2.33	0.20389	1.86	1196	22	1209	28	1233	17	1209 ± 16
A-I-19	0.48	2.33586	1.90	0.21036	1.63	1231	20	1223	23	1210	12	1221 ± 13
B-II-25	0.26	2.06161	2.12	0.19312	1.85	1138	21	1136	24	1132	12	1135 ± 14
B-II-29	0.49	2.33317	2.16	0.20909	0.60	1224	7	1222	26	1220	25	1224 ± 7
B-II-33	0.40	2.49116	1.20	0.22019	0.73	1283	9	1269	15	1247	12	1277 ± 8
B-II-34	0.47	2.28317	2.09	0.20436	1.79	1199	21	1207	25	1222	13	1209 ± 15
B-II-40	0.42	2.24650	1.84	0.20312	1.63	1192	19	1196	22	1202	10	1197 ± 12
B-II-43	0.49	2.32042	1.84	0.20716	1.31	1214	16	1219	22	1227	16	1217 ± 13
B-II-48	0.23	2.29776	1.70	0.20492	1.06	1202	13	1212	21	1229	16	1206 ± 11
B-II-54	*0.47*	*2.20956*	*1.06*	*0.19828*	*0.82*	*1166*	*10*	*1184*	*13*	*1217*	*8*	*1217 ± 27*
B-II-55	0.27	2.25312	1.45	0.20223	0.97	1187	12	1198	17	1217	13	1193 ± 9.5
B-II-56	0.34	2.19581	1.51	0.19473	0.46	1147	5	1180	18	1240	18	1149 ± 100
C-III-63	0.15	2.11401	3.82	0.18815	2.35	1111	26	1153	44	1233	37	1126 ± 23
B-II-61	*0.17*	*2.17676*	*2.36*	*0.19250*	*2.28*	*1135*	*26*	*1174*	*28*	*1246*	*8*	*1246 ± 25*
B-II-65	*0.37*	*1.97031*	*1.90*	*0.18117*	*1.25*	*1073*	*13*	*1105*	*21*	*1169*	*17*	*1169 ± 59*
C-III-66	*0.49*	*2.10575*	*1.44*	*0.19080*	*1.15*	*1126*	*13*	*1151*	*17*	*1198*	*10*	*1200 ± 17*
C-III-69	*0.25*	*1.92456*	*2.61*	*0.16934*	*2.27*	*1008*	*23*	*1090*	*28*	*1256*	*16*	*1256 ± 59*
B-II-75	0.34	2.21532	4.84	0.20399	4.59	1197	55	1186	57	1166	18	1175 ± 26
C-III-73	0.37	2.21646	4.21	0.20352	4.02	1194	48	1186	50	1172	15	1177 ± 22
B-II-85	0.36	2.16012	1.69	0.19643	1.03	1156	12	1168	20	1191	16	1161 ± 10
D-IV-109a	*0.45*	*1.82395*	*5.42*	*0.16150*	*4.22*	*965*	*41*	*1054*	*57*	*1243*	*42*	*1243 ± 100*
D-IV-109b	*0.47*	*2.05928*	*1.98*	*0.18466*	*1.66*	*1092*	*18*	*1135*	*23*	*1219*	*13*	*1241 ± 44*
D-IV-112	*0.32*	*2.07703*	*3.32*	*0.18123*	*2.32*	*1074*	*25*	*1141*	*38*	*1272*	*30*	*1272 ± 94*
D-IV-116	0.53	1.87917	4.81	0.17799	1.22	1056	13	1074	52	1110	52	1065 ± 12
D-IV-118	*0.34*	*2.11591*	*2.07*	*0.20177*	*1.43*	*1185*	*17*	*1154*	*24*	*1097*	*16*	*1097 ± 60*
D-IV-120	*0.37*	*1.52118*	*3.84*	*0.14503*	*3.47*	*873*	*30*	*939*	*36*	*1097*	*18*	*1097 ± 69*
D-IV-126	0.58	2.14267	1.66	0.20534	1.03	1204	12	1163	19	1087	14	1170 ± 100
D-IV-131	0.76	2.17900	1.83	0.20721	1.10	1214	13	1174	21	1102	16	1184 ± 100
D-IV-115	*0.43*	*2.12890*	*2.51*	*0.19237*	*2.28*	*1134*	*26*	*1158*	*29*	*1203*	*13*	*1203 ± 46*

Table 5 (cont.): Detrital zircon dating on selected samples from Ordovician units of the Precordillera terrane. Isotope ratios corrected for fractionation by comparison with standard GJ-1. Analyses with large errors were excluded (about 5% of the grains). Highly discordant samples (of up to 15% discordance) are shown in italics since a medium age was anchored. Errors are at one sigma.

Don Braulio Formation

		Isotopic ratios				Apparent age (Ma)						Concordant age
Sample	^{232}Th/^{238}U	^{207}Pb/^{235}U	error	^{206}Pb/^{238}U	error	^{206}Pb/^{238}U	error	^{207}Pb/^{235}U	error	^{207}Pb/^{206}Pb	error	Ma
E-V-153	0.94	5.46664	1.20	0.32891	0.82	1833	15	1895	23	1964	17	1964 ± 30
E-V-155	0.97	1.46309	6.52	0.15163	3.41	910	31	915	60	928	52	911 ± 28
E-V-157	1.06	0.81316	6.17	0.09421	1.27	580	7	604	37	695	42	581 ± 7
E-V-159	0.50	1.23956	5.92	0.13914	3.35	840	28	819	48	762	37	834 ± 25
E-V-161	0.41	2.15990	1.74	0.19933	1.18	1172	14	1168	20	1162	15	1170 ± 11
E-V-167	0.35	1.43298	2.81	0.15081	1.58	906	14	903	25	896	21	905 ± 13
F-VI-202	*0.85*	*5.29321*	*2.03*	*0.32576*	*1.87*	*1818*	*34*	*1868*	*38*	*1924*	*16*	*1924 ± 29*
G-VII-196	*0.25*	*2.15170*	*1.23*	*0.19424*	*0.68*	*1144*	*8*	*1166*	*14*	*1205*	*12*	*1205 ± 41*
F-VI-192	*0.27*	*1.75712*	*2.08*	*0.16546*	*1.44*	*987*	*14*	*1030*	*21*	*1122*	*17*	*1122 ± 58*
E-V-186	*0.26*	*1.75304*	*1.67*	*0.16546*	*1.44*	*987*	*14*	*1028*	*17*	*1117*	*10*	*1117 ± 34*
G-VII-173	0.82	1.87527	5.45	0.17530	2.02	1041	21	1072	58	1136	58	1044 ± 19
G-VII-169	*0.64*	*3.04664*	*1.39*	*0.23586*	*0.97*	*1365*	*13*	*1419*	*20*	*1502*	*15*	*1502 ± 35*
G-VII206b	*0.50*	*3.35083*	*2.61*	*0.24956*	*2.42*	*1436*	*35*	*1493*	*39*	*1575*	*15*	*1575 ± 35*
F-VI-211	0.56	1.75105	1.27	0.16923	0.84	1008	9	1028	13	1070	10	1070 ± 37
G-VII-226	0.71	1.64110	2.08	0.16241	1.07	970	10	986	21	1022	18	973 ± 9.4
G-VII-237	*0.45*	*2.49062*	*4.44*	*0.19924*	*2.64*	*1171*	*31*	*1269*	*56*	*1440*	*51*	*1440 ± 130*
G-VII-242	0.24	1.84569	9.60	0.16295	2.69	973	26	1062	102	1249	115	976 ± 24
G-VII-206	*0.78*	*3.48156*	*0.89*	*0.26016*	*0.68*	*1491*	*10*	*1523*	*14*	*1568*	*9*	*1567 ± 24*
G-VII-243	0.09	1.99625	1.91	0.19057	0.52	1124	6	1114	21	1094	20	1124 ± 5.4
G-VII-248	0.40	2.38608	2.00	0.21118	1.48	1235	18	1238	25	1244	17	1238 ± 14
G-VII-253	0.37	1.73063	2.90	0.17005	2.11	1012	21	1020	30	1036	21	1017 ± 18
G-VII-256	0.36	3.19519	1.38	0.25622	1.10	1470	16	1456	20	1435	12	1454 ± 11
G-VII-258	0.30	3.68330	1.78	0.28117	0.34	1597	5	1568	28	1528	27	1596 ± 130
G-VII-260	0.80	0.84416	3.65	0.10099	2.45	620	15	621	23	626	17	621 ± 14
G-VII-262	1.11	2.14694	3.61	0.19302	0.66	1138	8	1164	42	1213	43	1138 ± 7
G-VII-263	1.71	4.44660	1.94	0.29576	0.70	1670	12	1721	33	1783	32	1679 ± 400
G-VII-265	0.30	1.86209	1.95	0.17680	1.03	1049	11	1068	21	1105	18	1054 ± 9.6
H-VIII-268	0.23	2.44061	1.26	0.21513	0.70	1256	9	1255	16	1252	13	1256 ± 7.4
H-VIII-272	0.45	1.51173	3.54	0.15317	1.62	919	15	935	33	974	31	921 ± 14
H-VIII-275	0.77	2.72202	2.00	0.22605	1.18	1314	16	1334	27	1368	22	1322 ± 13
H-VIII-279	0.41	2.45132	1.95	0.21498	1.05	1255	13	1258	24	1262	21	1256 ± 11
H-VIII-280	0.55	1.65969	2.08	0.16301	1.45	973	14	993	21	1037	15	993 ± 2
H-VIII-285	0.59	1.98999	1.34	0.18602	0.61	1100	7	1112	15	1136	14	1105 ± 5
H-VIII-286	0.52	1.94660	1.31	0.18031	0.82	1069	9	1097	14	1154	12	1091 ± 150
H-VIII-289	0.53	0.82931	3.22	0.09963	2.47	612	15	613	20	617	13	613 ± 14
H-VIII-293	*0.39*	*2.53188*	*2.35*	*0.21168*	*1.26*	*1238*	*16*	*1281*	*30*	*1355*	*27*	*1355 ± 85*
H-VIII-296	0.43	2.77032	4.56	0.22963	2.09	1333	28	1348	61	1371	56	1336 ± 24
H-VIII-297	0.53	0.68047	1.93	0.08443	1.35	522	7	527	10	547	8	524 ± 6.6
H-VIII-298	*0.37*	*1.99103*	*1.76*	*0.18685*	*1.45*	*1104*	*16*	*1112*	*20*	*1129*	*11*	*1113 ± 12*
H-VIII-299	0.48	1.52968	2.31	0.15334	1.48	920	14	942	22	996	18	938 ± 5.5
H-VIII-300	0.44	1.83807	2.27	0.17553	0.99	1043	10	1059	24	1094	22	1049 ± 7.4
H-VIII-303	0.63	1.13096	1.30	0.12605	1.28	765	10	768	10	777	2	774 ± 4.8

Table 5 (cont.): Detrital zircon dating on selected samples from Ordovician units of the Precordillera terrane. Isotope ratios corrected for fractionation by comparison with standard GJ-1. Analyses with large errors were excluded (less than 5% of the grains). Highly discordant samples (of up to 15% discordance) are shown in italics since a medium age was anchored. Errors are at one sigma.

La Cantera Formation

		Isotopic ratios				Apparent age (Ma)						Concordant age
Sample	**$^{232}Th/^{238}U$**	**$^{207}Pb/^{235}U$**	**error**	**$^{206}Pb/^{238}U$**	**error**	**$^{206}Pb/^{238}U$**	**error**	**$^{207}Pb/^{235}U$**	**error**	**$^{207}Pb/^{206}Pb$**	**error**	**Ma**
H-VIII303	0.63	1.13096	1.30	0.12605	1.28	765	10	768	10	777	2	774 ± 4.8
I-IX-309	0.49	1.90938	1.63	0.18188	1.18	1077	13	1084	18	1099	12	1082 ± 10
I-IX-310	0.85	2.82982	2.11	0.23173	1.86	1344	25	1363	29	1395	14	1373 ± 15
I-IX-316	0.83	2.07780	1.29	0.19125	0.78	1128	9	1142	15	1167	12	1133 ± 7.5
I-IX-319	0.16	1.89200	2.10	0.18481	1.97	1093	21	1078	23	1048	8	1065 ± 12
I-IX-330	0.35	2.81581	2.33	0.23659	1.63	1369	22	1360	32	1345	22	1362 ± 17
I-IX-331	0.23	2.15664	1.49	0.19829	1.14	1166	13	1167	17	1169	11	1167 ± 10
I-IX-334	0.31	2.69512	2.04	0.23075	0.97	1338	13	1327	27	1309	23	1335 ± 11
I-IX-336	0.27	2.23513	2.42	0.20116	1.52	1182	18	1192	29	1211	23	1186 ± 15
I-IX-338	0.27	2.23023	2.40	0.20089	1.25	1180	15	1191	29	1210	25	1183 ± 13
J-X-342	0.23	1.74908	2.32	0.17251	1.50	1026	15	1027	24	1029	18	1026 ± 13
J-X-373	0.58	2.80315	0.75	0.23239	0.44	1347	6	1356	10	1371	8	1351 ± 5
J-X-375	*0.72*	*5.81635*	*0.84*	*0.34726*	*0.74*	*1922*	*14*	*1949*	*16*	*1978*	*8*	*1978 ± 14*
J-X-376	*0.30*	*1.54284*	*1.16*	*0.15308*	*0.73*	*918*	*7*	*948*	*11*	*1017*	*9*	*1017 ± 38*
K-XI-382	*0.30*	*1.52442*	*1.52*	*0.15075*	*1.08*	*905*	*10*	*940*	*14*	*1023*	*11*	*1023 ± 45*
K-XI384a	0.47	0.59882	3.60	0.07687	1.94	477	9	476	17	472	14	477 ± 6.3
K-XI384b	0.64	0.57663	3.41	0.07450	1.91	463	9	462	16	458	13	463 ± 8.5
J-X-345	0.32	3.59879	1.40	0.27011	1.03	1541	16	1549	22	1560	15	1548 ± 11
J-X-348	*0.21*	*3.16520*	*1.24*	*0.24779*	*0.86*	*1427*	*12*	*1449*	*18*	*1481*	*13*	*1481 ± 34*
J-X-357	*0.20*	*1.58673*	*1.42*	*0.15359*	*1.03*	*921*	*10*	*965*	*14*	*1067*	*10*	*1067 ± 39*
J-X-360	0.48	1.91826	1.30	0.17876	0.68	1060	7	1087	14	1142	13	1075 ± 170
J-X-363	1.44	0.55172	4.88	0.07058	2.27	440	10	446	22	480	21	440 ± 9.6
J-X-372	0.38	2.55808	3.10	0.20911	0.67	1224	8	1289	40	1398	42	1226 ± 270
K-XI-400	0.37	2.37864	1.49	0.21727	1.28	1267	16	1236	18	1182	9	1182 ± 29
K-XI-401	0.55	1.76947	2.12	0.17480	1.57	1038	16	1034	22	1026	15	1036 ± 13
K-XI-404	0.47	2.23552	1.10	0.20397	0.47	1197	6	1192	13	1184	12	1195 ± 5
K-XI-408	0.50	2.09592	3.98	0.19753	3.13	1162	36	1147	46	1120	28	1149 ± 27
K-XI-412	*0.70*	*3.68574*	*1.11*	*0.26947*	*0.89*	*1538*	*14*	*1568*	*17*	*1609*	*11*	*1609 ± 24*
K-XI-415	0.61	2.08370	1.84	0.19573	1.16	1152	13	1143	21	1127	16	1148 ± 11
L-XII-427	0.42	0.93938	2.11	0.10972	1.44	671	10	673	14	677	10	672 ± 8.9
L-XII-419	0.48	1.98310	1.33	0.18770	0.85	1109	9	1110	15	1112	11	1109 ± 8
L-XII-431	*0.36*	*2.01652*	*2.44*	*0.18300*	*1.86*	*1083*	*20*	*1121*	*27*	*1195*	*19*	*1110 ± 640*
L-XII-433	*0.38*	*1.21189*	*1.71*	*0.12249*	*1.15*	*745*	*9*	*806*	*14*	*979*	*12*	*979 ± 52*
L-XII-434	0.31	2.12426	2.23	0.19524	0.51	1150	6	1157	26	1170	25	1150 ± 5.4
L-XII-436	*0.68*	*1.70924*	*3.36*	*0.16057*	*1.41*	*960*	*14*	*1012*	*34*	*1126*	*34*	*1126 ± 110*
L-XII-438	*0.25*	*1.50823*	*1.01*	*0.14803*	*0.57*	*890*	*5*	*934*	*9*	*1039*	*9*	*1049 ± 33*
L-XII-445	*0.22*	*1.86735*	*1.14*	*0.17076*	*0.77*	*1016*	*8*	*1070*	*12*	*1180*	*10*	*1180 ± 35*
L-XII-450	*1.24*	*3.25886*	*1.12*	*0.24443*	*0.62*	*1410*	*9*	*1471*	*17*	*1561*	*15*	*1561 ± 36*

Table 5 (cont.): Detrital zircon dating on selected samples from Ordovician units of the Precordillera terrane. Isotope ratios corrected for fractionation by comparison with standard GJ-1. Analyses with large errors were excluded (less than 10% of the grains). Highly discordant samples (of up to 15% discordance) are shown in italics since a medium age was anchored. Errors are at one sigma.

sample	SiO_2	TiO_2	Al_2O_3	Cr_2O_3	Fe_2O_3	FeO	MnO	MgO	CaO	V_2O_5	ZnO	Σ
a1-3	0.24	1.56	14.07	50.14	5.64	14.98	0.25	13.56	0.16	0.16	b.d.l.	100.74
a2-4	0.27	1.64	13.69	50.71	4.11	15.63	b.d.l.	12.82	0.12	0.33	0.65	99.95
c1-h	b.d.l.	1.46	13.95	50.02	5.97	14.22	0.49	13.07	0.07	b.d.l.	0.78	100.03
a6-8	0.11	1.79	14.56	43.30	9.24	23.50	0.10	8.20	0.05	0.39	0.33	101.57
c2-b	0.58	1.72	14.30	42.93	8.45	25.10	0.17	7.25	b.d.l.	0.20	0.58	101.28
c3-a	0.13	1.52	13.90	46.27	6.80	18.42	0.54	10.42	b.d.l.	0.64	0.61	99.24
c3-b	0.54	1.67	13.82	46.91	6.41	18.62	0.12	11.25	0.10	0.06	0.22	99.72
c3-c	0.25	1.86	13.73	45.80	7.51	19.52	0.31	10.26	b.d.l.	b.d.l.	0.59	99.83
c4-d	0.28	1.25	13.21	46.43	7.80	24.50	0.61	6.85	b.d.l.	0.10	0.37	101.40
c5-a	0.37	1.70	12.54	46.71	7.90	22.00	b.d.l.	9.31	0.08	0.34	b.d.l.	100.95
c5-c	0.10	1.64	12.60	48.07	7.60	19.90	0.40	9.60	b.d.l.	0.28	1.01	101.20
c6-a	0.42	1.81	13.95	48.09	5.40	20.50	b.d.l.	10.48	0.10	0.09	b.d.l.	100.84
c6-b	0.07	1.60	13.81	47.09	7.66	19.03	b.d.l.	10.86	b.d.l.	0.25	0.24	100.62
c7-a	0.37	1.69	14.21	47.60	6.32	18.50	0.12	11.37	0.03	0.29	0.49	100.99
a28-29	0.35	1.83	13.84	46.41	7.30	19.50	b.d.l.	10.40	0.12	0.17	1.03	100.95
c7-d	0.57	1.59	13.53	47.52	7.10	17.30	b.d.l.	11.37	0.02	0.27	1.60	100.87
c7-e	0.29	1.64	13.49	47.26	7.33	18.10	0.29	11.55	0.02	0.47	b.d.l.	100.44
a32-36	0.68	0.67	10.11	58.71	b.d.l.	21.52	0.53	7.62	0.06	0.35	0.56	100.80
c9-b	0.38	2.43	13.55	41.89	10.80	20.90	b.d.l.	9.94	0.01	0.18	0.90	100.98
c9-c	0.26	2.63	13.29	40.83	12.30	19.80	b.d.l.	10.50	0.12	0.19	1.00	100.92
c9-d	0.18	2.22	13.75	41.39	11.62	19.76	0.09	10.78	0.02	0.39	b.d.l.	100.19
c10-b	0.46	1.36	14.36	46.65	5.75	21.80	0.10	9.46	0.06	0.71	b.d.l.	100.71
c10-d	0.21	1.26	14.28	48.78	5.93	16.65	b.d.l.	12.00	0.03	b.d.l.	0.54	99.68
c10-e	0.06	1.17	13.91	49.20	6.75	16.76	b.d.l.	12.05	0.13	0.12	0.00	100.15
c12-a	0.20	1.28	14.81	44.15	7.24	25.78	0.93	5.48	0.17	0.00	0.72	100.76
c14-a	0.40	1.02	19.79	41.95	5.68	20.28	b.d.l.	10.54	0.03	0.31	0.19	100.19
c14-d	0.26	1.21	20.19	42.40	5.80	19.90	0.06	10.93	0.03	b.d.l.	0.16	100.94
c15-a	0.18	2.30	10.83	46.08	9.21	22.41	0.00	8.64	0.20	0.37	0.27	100.49
c15-c	0.11	2.26	11.17	45.34	9.63	22.87	0.37	8.05	0.05	0.13	0.42	100.39
c16-b	0.26	1.52	9.62	41.27	12.20	31.80	1.43	0.37	b.d.l.	0.56	1.80	100.83
c16-c	0.12	2.16	9.32	42.07	11.60	33.22	1.15	0.32	0.21	0.17	0.77	101.11
c17-a	0.37	1.69	12.06	48.07	7.17	20.32	0.36	9.97	b.d.l.	0.17	b.d.l.	100.18
c17-c	0.13	1.77	12.11	47.42	8.55	18.05	0.46	10.89	b.d.l.	0.15	0.49	100.02
average	0.29	1.66	13.53	46.29	7.77	20.64	0.40	9.58	0.08	0.27	0.63	100.57

Table 6: Detrital chromian spinels microprobe analyses from the Don Braulio Formation, Eastern tectofacies of the Precordillera terrane. Oxides are in percentages. Number of ions based on four oxygen atoms. b.d.l.: below detection limits.

sample	Si	Ti	Al	Cr	Fe^{3+}	Fe^{2+}	Mn	Mg	Ca	V	Zn
a1-3	0.008	0.037	0.523	1.250	0.134	0.395	0.007	0.638	0.005	0.004	b.d.l.
a2-4	0.009	0.039	0.516	1.281	0.099	0.418	0.000	0.611	0.004	0.008	0.015
c1-h	b.d.l.	0.035	0.525	1.262	0.143	0.379	0.013	0.622	0.002	b.d.l.	0.018
a6-8	0.004	0.044	0.557	1.113	0.226	0.638	0.003	0.397	0.002	0.010	0.008
c2-b	0.019	0.042	0.553	1.111	0.208	0.689	0.005	0.354	b.d.l.	0.005	0.014
c3-a	0.004	0.037	0.536	1.197	0.167	0.504	0.015	0.508	b.d.l.	0.017	0.015
c3-b	0.017	0.041	0.527	1.200	0.156	0.504	0.003	0.542	0.003	0.002	0.005
c3-c	0.008	0.046	0.528	1.181	0.184	0.532	0.009	0.499	b.d.l.	b.d.l.	0.014
c4-d	0.009	0.031	0.512	1.211	0.194	0.676	0.017	0.338	b.d.l.	0.003	0.009
c5-a	0.012	0.043	0.482	1.204	0.195	0.600	b.d.l.	0.452	0.003	0.009	b.d.l.
c5-c	0.003	0.040	0.484	1.234	0.188	0.542	0.011	0.466	b.d.l.	0.007	0.024
c6-a	0.013	0.044	0.528	1.222	0.133	0.552	b.d.l.	0.502	0.003	0.002	b.d.l.
c6-b	0.002	0.039	0.525	1.201	0.186	0.513	b.d.l.	0.522	0.000	0.006	0.006
c7-a	0.012	0.041	0.535	1.201	0.152	0.496	0.003	0.541	0.001	0.007	0.012
a28-29	0.011	0.044	0.525	1.181	0.178	0.528	b.d.l.	0.499	0.004	0.004	0.025
c7-d	0.018	0.038	0.508	1.201	0.171	0.462	b.d.l.	0.554	0.001	0.007	0.039
c7-e	0.009	0.040	0.511	1.201	0.177	0.487	0.008	0.554	0.001	0.012	b.d.l.
a32-36	0.023	0.017	0.395	1.540	b.d.l.	0.597	0.015	0.377	0.002	0.009	0.014
c9-b	0.012	0.059	0.517	1.072	0.264	0.567	b.d.l.	0.481	b.d.l.	0.005	0.023
c9-c	0.008	0.065	0.506	1.043	0.300	0.537	b.d.l.	0.508	0.004	0.005	0.024
c9-d	0.006	0.054	0.525	1.061	0.283	0.536	0.002	0.521	0.001	0.010	b.d.l.
c10-b	0.015	0.033	0.546	1.197	0.144	0.588	0.003	0.455	0.002	0.018	b.d.l.
c10-d	0.007	0.030	0.541	1.241	0.144	0.448	b.d.l.	0.575	0.001	b.d.l.	0.013
c10-e	0.002	0.028	0.526	1.248	0.163	0.449	b.d.l.	0.576	0.004	0.003	b.d.l.
c12-a	0.007	0.032	0.581	1.161	0.181	0.717	0.026	0.272	0.006	b.d.l.	0.018
c14-a	0.013	0.024	0.736	1.047	0.135	0.535	b.d.l.	0.496	0.001	0.008	0.004
c14-d	0.008	0.028	0.743	1.047	0.136	0.521	0.002	0.509	0.001	b.d.l.	0.004
c15-a	0.006	0.057	0.424	1.209	0.230	0.622	b.d.l.	0.428	0.007	0.010	0.007
c15-c	0.004	0.057	0.439	1.195	0.242	0.638	0.010	0.400	0.002	0.003	0.010
c16-b	0.009	0.040	0.408	1.151	0.326	0.940	0.043	0.019	b.d.l.	0.016	0.047
c16-c	0.004	0.057	0.394	1.169	0.310	0.982	0.034	0.017	0.008	0.005	0.020
c17-a	0.012	0.042	0.466	1.245	0.177	0.557	0.010	0.487	b.d.l.	0.004	b.d.l.
c17-c	0.004	0.043	0.466	1.224	0.210	0.493	0.013	0.530	b.d.l.	0.004	0.012
average	0.01	0.04	0.52	1.19	0.19	0.56	0.01	0.46	0.003	0.010	0.020

Table 6 (cont.): Detrital chromian spinels microprobe analyses from the Don Braulio Formation, Eastern tectofacies of the Precordillera terrane. Number of ions based on four oxygen atoms. b.d.l.: below detection limits.

sample	Cr#	Mg#	Fe^{2+}#	Fe^{3+}#	Fe^{2+}/Fe^{3+}
a1-3	0.71	0.62	0.38	0.07	2.95
a2-4	0.71	0.59	0.41	0.05	4.23
c1-h	0.71	0.62	0.38	0.07	2.64
a6-8	0.67	0.38	0.62	0.12	2.82
c2-b	0.67	0.34	0.66	0.11	3.31
c3-a	0.69	0.50	0.50	0.09	3.01
c3-b	0.69	0.52	0.48	0.08	3.23
c3-c	0.69	0.48	0.52	0.10	2.89
c4-d	0.70	0.33	0.67	0.10	3.49
c5-a	0.71	0.43	0.57	0.10	3.08
c5-c	0.72	0.46	0.54	0.10	2.88
c6-a	0.70	0.48	0.52	0.07	4.16
c6-b	0.70	0.50	0.50	0.10	2.76
c7-a	0.69	0.52	0.48	0.08	3.26
a28-29	0.69	0.49	0.51	0.09	2.96
c7-d	0.70	0.55	0.45	0.09	2.70
c7-e	0.70	0.53	0.47	0.09	2.74
a32-36	0.80	0.39	0.61		
c9-b	0.67	0.46	0.54	0.14	2.15
c9-c	0.67	0.49	0.51	0.16	1.79
c9-d	0.67	0.49	0.51	0.15	1.89
c10-b	0.69	0.44	0.56	0.08	4.09
c10-d	0.70	0.56	0.44	0.07	3.12
c10-e	0.70	0.56	0.44	0.08	2.76
c12-a	0.67	0.27	0.73	0.09	3.96
c14-a	0.59	0.48	0.52	0.07	3.97
c14-d	0.58	0.49	0.51	0.07	3.82
c15-a	0.74	0.41	0.59	0.12	2.70
c15-c	0.73	0.39	0.61	0.13	2.64
c16-b	0.74	0.02	0.98	0.17	2.89
c16-c	0.75	0.02	0.98	0.17	3.17
c17-a	0.73	0.47	0.53	0.09	3.15
c17-c	0.72	0.52	0.48	0.11	2.35
average	0.70	0.45	0.55	0.10	3.05

Table 6 (cont.): Detrital chromian spinels microprobe analyses from the Don Braulio Formation, Eastern tectofacies of the Precordillera terrane. Number of ions based on four oxygen atoms. See text for more explanations (Chapter 3).

Sample	SiO_2	TiO_2	Al_2O_3	Cr_2O_3	FeO_t	MnO	MgO	CaO	V_2O_5	NiO	ZnO	Σ	Fe_2O_3	FeO
Group 1														
2	0.13	0.51	26.81	36.19	17.61	0.17	15.69	0.04	0.16	0.25	0.31	97.86	6.70	11.58
23	0.01	0.39	24.97	38.41	22.17	0.24	11.88	0.01	0.09	0.27	0.28	98.72	5.63	17.11
c1	0.06	0.54	25.31	38.75	19.99	0.05	13.07	0.00	0.23	0.00	0.30	98.29	4.61	15.84
c2	0.02	0.35	27.49	37.47	15.70	0.00	16.61	0.01	0.16	0.02	0.11	97.93	5.63	10.63
48	0.09	0.37	23.79	41.47	17.73	0.33	15.17	0.02	0.19	0.28	0.00	99.45	5.97	12.36
c3	0.07	0.44	27.83	36.38	14.66	0.05	16.93	0.02	0.17	0.31	0.43	97.29	5.73	9.51
37	0.17	0.39	27.34	40.38	15.47	0.22	16.85	0.06	0.07	0.32	0.04	101.30	4.92	11.04
45	0.28	0.60	22.47	46.82	14.87	0.51	16.08	0.17	0.18	0.46	0.03	102.45	3.66	11.58
a	0.16	0.40	27.23	38.85	16.56	0.18	16.85	0.01	0.00	0.42	0.12	100.77	6.42	10.78
e	0.22	0.22	23.16	39.88	21.17	0.51	13.65	0.12	0.17	0.29	0.17	99.56	7.73	14.22
c	0.15	0.41	22.78	37.94	23.44	0.20	13.45	0.17	0.34	0.44	0.12	99.44	9.72	14.69
b	0.19	0.43	31.12	33.33	17.05	0.35	16.46	0.05	0.53	0.29	0.14	99.93	5.95	11.69
s	0.44	0.50	24.12	39.60	24.11	0.43	11.01	0.13	0.07	0.20	0.13	100.71	5.15	19.48
i	0.12	0.41	23.07	43.74	17.14	0.14	15.09	0.10	0.00	0.55	0.00	100.35	5.10	12.55
m	0.17	0.51	26.30	38.65	18.42	0.43	15.57	0.08	0.00	0.07	0.25	100.45	6.57	12.51
q	0.29	0.57	23.56	42.30	18.85	0.47	15.16	0.09	0.00	0.00	0.00	101.26	6.05	13.40
n	0.18	0.24	31.77	31.04	21.34	0.10	14.06	0.04	0.01	0.35	0.80	99.93	7.17	14.89
r	0.18	0.48	23.11	45.30	12.36	0.39	18.03	0.12	0.00	0.57	0.06	100.58	4.93	7.92
u	0.08	0.40	23.76	43.26	14.14	0.58	16.82	0.09	0.07	0.76	0.06	100.00	5.55	9.15
t	0.13	0.51	27.08	38.97	18.57	0.50	14.82	0.05	0.11	0.27	0.07	101.07	5.26	13.84
ae	0.23	0.35	23.96	43.19	15.01	0.59	16.38	0.00	0.00	0.07	0.11	99.88	4.82	10.67
af	0.01	0.58	24.14	36.91	22.99	0.38	13.73	0.00	0.00	0.47	0.08	99.29	9.52	14.42
Average	0.15	0.43	25.51	39.49	18.15	0.31	15.15	0.06	0.12	0.30	0.16	99.84	6.04	12.72
Group 2														
23-6	0.05	3.10	11.77	45.06	35.22	0.41	4.29	0.18	0.18	0.27	0.45	100.94	6.51	29.36
38	0.16	3.99	10.39	40.53	38.18	0.29	7.37	0.10	0.27	0.60	0.01	101.88	13.46	26.07
40	0.16	2.26	11.97	45.66	27.68	0.13	10.22	0.02	0.11	0.38	0.13	98.71	8.92	19.65
14	0.02	3.43	11.15	40.37	32.54	0.18	9.90	0.00	0.21	0.05	0.00	97.85	12.71	21.10
ad	0.01	2.73	12.71	41.84	32.94	0.19	11.12	0.06	0.00	0.00	0.07	101.67	14.39	19.99
f	0.13	2.73	11.76	44.42	32.10	0.50	9.26	0.12	0.35	0.36	0.24	101.97	11.23	22.00
w	0.06	3.94	10.40	42.11	35.18	0.29	9.15	0.14	0.00	0.00	0.22	101.49	13.11	23.38
d	0.09	3.01	10.21	40.75	38.83	0.88	5.64	0.03	0.00	0.20	0.17	99.81	13.39	26.78
g	0.11	4.70	11.44	40.78	32.89	0.35	10.31	0.11	0.33	0.45	0.00	101.45	11.84	22.23
h	0.16	2.15	8.88	45.36	36.76	0.43	5.49	0.13	0.21	0.00	0.37	99.94	11.43	26.48
p	0.15	1.66	13.63	46.33	31.30	0.32	7.06	0.10	0.02	0.49	0.45	101.51	7.67	24.40
o	0.17	2.27	12.35	45.43	30.11	0.24	11.01	0.09	0.11	0.00	0.17	101.95	11.50	19.76
v	0.18	3.03	11.22	44.13	33.05	0.69	8.37	0.12	0.00	0.39	0.79	101.97	11.30	22.88
aa	0.16	2.49	13.52	45.46	27.87	0.37	9.73	0.11	0.16	0.41	0.72	101.00	8.01	20.67
ac	0.01	3.02	12.69	42.60	32.25	0.36	8.28	0.09	0.51	0.00	0.26	100.07	9.59	23.62
Average	0.11	2.97	11.61	43.39	33.13	0.37	8.48	0.09	0.16	0.24	0.27	100.81	11.00	23.23

Table 7: Detrital chromian spinels microprobe analyses from the Pavón Formation, San Rafael block, Precordillera terrane. Oxides are in percentages. Number of ions based on four oxygen atoms.

Sample	Si	Ti	Al	Cr	Fe^{3+}	Fe^{2+}	Mn	Mg	Ca	V	Ni	Zn
Group 1												
2	0.004	0.011	0.952	0.862	0.152	0.292	0.004	0.705	0.001	0.004	0.006	0.007
23	0.000	0.009	0.910	0.939	0.131	0.442	0.006	0.548	0.000	0.002	0.007	0.006
c1	0.002	0.012	0.917	0.942	0.107	0.407	0.001	0.599	0.000	0.006	0.000	0.007
c2	0.000	0.008	0.968	0.885	0.127	0.266	0.000	0.740	0.000	0.004	0.000	0.002
48	0.003	0.008	0.847	0.990	0.136	0.312	0.008	0.683	0.000	0.005	0.007	0.000
c3	0.002	0.010	0.982	0.861	0.129	0.238	0.001	0.755	0.001	0.004	0.007	0.010
37	0.005	0.009	0.936	0.928	0.108	0.268	0.005	0.730	0.002	0.002	0.007	0.001
45	0.008	0.013	0.781	1.091	0.081	0.285	0.013	0.707	0.005	0.004	0.011	0.001
a	0.005	0.009	0.936	0.896	0.141	0.263	0.004	0.733	0.000	0.000	0.010	0.003
e	0.007	0.005	0.833	0.962	0.177	0.363	0.013	0.621	0.004	0.004	0.007	0.004
c	0.005	0.009	0.822	0.918	0.224	0.376	0.005	0.614	0.006	0.008	0.011	0.003
b	0.006	0.009	1.064	0.764	0.130	0.284	0.008	0.711	0.002	0.012	0.007	0.003
s	0.013	0.011	0.871	0.959	0.119	0.499	0.011	0.503	0.004	0.002	0.005	0.003
i	0.004	0.009	0.818	1.041	0.116	0.316	0.004	0.677	0.003	0.000	0.013	0.000
m	0.005	0.011	0.917	0.904	0.146	0.309	0.011	0.687	0.003	0.000	0.002	0.005
q	0.008	0.013	0.827	0.996	0.135	0.334	0.012	0.673	0.003	0.000	0.000	0.000
n	0.005	0.005	1.100	0.721	0.158	0.366	0.002	0.616	0.001	0.000	0.008	0.017
r	0.005	0.011	0.803	1.056	0.109	0.195	0.010	0.792	0.004	0.000	0.014	0.001
u	0.002	0.009	0.834	1.018	0.124	0.228	0.015	0.747	0.003	0.002	0.018	0.001
t	0.004	0.011	0.942	0.909	0.117	0.341	0.012	0.652	0.002	0.003	0.006	0.002
ae	0.007	0.008	0.843	1.019	0.108	0.266	0.015	0.729	0.000	0.000	0.002	0.002
af	0.000	0.013	0.866	0.889	0.218	0.367	0.010	0.623	0.000	0.000	0.012	0.002
Average	0.005	0.010	0.898	0.934	0.136	0.319	0.008	0.675	0.002	0.003	0.007	0.004
Group 2												
23-6	0.002	0.079	0.468	1.202	0.165	0.828	0.012	0.216	0.006	0.005	0.007	0.011
38	0.005	0.098	0.402	1.052	0.332	0.716	0.008	0.361	0.004	0.007	0.016	0.000
40	0.005	0.056	0.465	1.189	0.221	0.541	0.004	0.502	0.001	0.003	0.010	0.003
14	0.001	0.086	0.438	1.064	0.319	0.588	0.005	0.492	0.000	0.006	0.001	0.000
ad	0.000	0.065	0.475	1.050	0.344	0.531	0.005	0.526	0.002	0.000	0.000	0.002
f	0.004	0.066	0.447	1.132	0.272	0.593	0.014	0.445	0.004	0.009	0.009	0.006
w	0.002	0.096	0.399	1.083	0.321	0.636	0.008	0.444	0.005	0.000	0.000	0.005
d	0.003	0.077	0.408	1.092	0.341	0.759	0.025	0.285	0.001	0.000	0.005	0.004
g	0.003	0.114	0.434	1.037	0.287	0.598	0.009	0.494	0.004	0.009	0.012	0.000
h	0.005	0.055	0.357	1.223	0.293	0.755	0.012	0.279	0.005	0.006	0.000	0.009
p	0.005	0.041	0.524	1.196	0.188	0.666	0.009	0.344	0.003	0.001	0.013	0.011
o	0.005	0.054	0.462	1.141	0.275	0.525	0.006	0.521	0.003	0.003	0.000	0.004
v	0.006	0.074	0.430	1.134	0.276	0.622	0.019	0.406	0.004	0.000	0.010	0.019
aa	0.005	0.060	0.513	1.158	0.194	0.557	0.010	0.467	0.004	0.004	0.011	0.017
ac	0.000	0.075	0.492	1.108	0.237	0.650	0.010	0.406	0.003	0.013	0.000	0.006
Average	0.003	0.073	0.448	1.124	0.271	0.638	0.010	0.412	0.003	0.004	0.006	0.007

Table 7 (cont.): Detrital chromian spinels microprobe analyses from the Pavón Formation, San Rafael block, Precordillera terrane. Number of ions based on four oxygen atoms.

Sample	Cr#	Mg#	Fe^{2+}#	Fe^{3+}#	Fe^{2+}/Fe^{3+}
Group 1					
2	0.48	0.71	0.29	0.08	1.92
23	0.51	0.55	0.45	0.07	3.38
c1	0.51	0.60	0.40	0.05	3.82
c2	0.48	0.74	0.26	0.06	2.10
48	0.54	0.69	0.31	0.07	2.30
c3	0.47	0.76	0.24	0.07	1.84
37	0.50	0.73	0.27	0.05	2.49
45	0.58	0.71	0.29	0.04	3.51
a	0.49	0.74	0.26	0.07	1.87
e	0.54	0.63	0.37	0.09	2.05
c	0.53	0.62	0.38	0.11	1.68
b	0.42	0.71	0.29	0.07	2.18
s	0.52	0.50	0.50	0.06	4.20
i	0.56	0.68	0.32	0.06	2.73
m	0.50	0.69	0.31	0.07	2.11
q	0.55	0.67	0.33	0.07	2.46
n	0.40	0.63	0.37	0.08	2.31
r	0.57	0.80	0.20	0.06	1.79
u	0.55	0.77	0.23	0.06	1.83
t	0.49	0.66	0.34	0.06	2.92
ae	0.55	0.73	0.27	0.05	2.46
af	0.51	0.63	0.37	0.11	1.68
Average	0.51	0.68	0.32	0.07	2.44
Group 2					
23-6	0.72	0.21	0.79	0.09	5.01
38	0.72	0.34	0.66	0.19	2.15
40	0.72	0.48	0.52	0.12	2.45
14	0.71	0.46	0.54	0.18	1.84
ad	0.69	0.50	0.50	0.18	1.54
f	0.72	0.43	0.57	0.15	2.18
w	0.73	0.41	0.59	0.18	1.98
d	0.73	0.27	0.73	0.19	2.22
g	0.71	0.45	0.55	0.16	2.09
h	0.77	0.27	0.73	0.16	2.57
p	0.70	0.34	0.66	0.10	3.54
o	0.71	0.50	0.50	0.15	1.91
v	0.73	0.39	0.61	0.15	2.25
aa	0.69	0.46	0.54	0.10	2.87
ac	0.69	0.38	0.62	0.13	2.74
Average	0.72	0.39	0.61	0.15	2.49

Table 7 (cont.): Detrital chromian spinels microprobe analyses from the Pavón Formation, San Rafael block, Precordillera terrane. Number of ions based on four oxygen atoms. See text (Chapter 7) for more explanations.

APPENDIX B

METHODOLOGIES AND ANALYTICAL TECHNIQUES

B.1 INTRODUCTION

Provenance analysis aims not only at described the detrital composition of a sedimentary rock, but also to decipher the characteristics of the source rocks. On its way to its final deposition and even once deposited, detritus suffers several different processes such as chemical and physical weathering, grain-size sorting, diagenesis and metamorphism, that might modify its original composition, and hence, the signal provided by the source rocks (Nesbitt and Young, 1982; Taylor and McLennan, 1985; Cullers *et al.*, 1987; McLennan *et al.*, 1990; 1993; Cox *et al.*, 1995; Andersson *et al.*, 2004). Therefore, the understanding of such processes provides clues to decipher the characteristics of the source rocks and to reconstruct the history of the sedimentary rock. Provenance analysis is undoubtedly a multidisciplinary approach, because different aspects of the sedimentary rock needs to be evaluated at the same time and several techniques are used, such as petrography, geochemistry, Sm-Nd and Pb-Pb isotopes, detrital zircon dating, heavy mineral analyses and measurements of the illite crystallization index. A brief discussion of the information given by each of these methodologies is presented as follows, as well as the analytical techniques applied to obtain the corresponding data.

B.2 METHODOLOGY

B.2.1 Petrography

Petrologic information can help to identify the main source rock types. However, the composition of the sedimentary rocks depend not only on the rock type of the source area but also on other factors such as weathering (and its relationship to climate and relief), sorting, intrastratal solution during diagenesis and mixing of different source rocks. The changes in the bulk mineralogy that all these factors might provoke make the characterization of the provenance using only petrography a problematic task. Therefore, to understand these factors and to enhance provenance determinations the petrographic data should be used together with geochemical and isotope geochemical analyses.

Framework grains were identified under the microscope based on their optical properties, with special attention on those features that have provenance significance such as: quartz types (polycrystalline, monocrystalline, undulose), feldspar composition, lithoclast types (sedimentary, metamorphic, igneous), detrital minerals present in minor amounts (micas, tourmaline, zircon, apatite, Ti-oxides). The composition of the matrix or any very fine-grained mineral and the interrelations between certain grains were determined on polished thin sections using a scanning and backscattered electron microscope with energy dispersive spectrometry (SEM-BSE-EDS). X-Ray Diffraction (XRD) patterns on whole-rocks were also processed to check the presence of certain species and to help in the determination of clay minerals and cements.

B.2.2 Geochemistry

The composition of sedimentary rocks changes through time, reflecting changes in the average composition of the crystalline source rocks (Taylor and McLennan, 1985). Therefore, geochemical analysis is a valuable tool for provenance studies of sedimentary rocks as long as the bulk composition is not affected by weathering, diagenesis and metamorphism (McLennan *et al.*, 1993).

B.2.2.1 Major elements and alteration

Major elements are strongly affected by weathering and diagenesis (e.g. Nesbitt and Young, 1982; McLennan, 1993; Fedo *et al.*, 1995; 1997). The chemical weathering can be quantified using the Chemical Index of Alteration (CIA = $\{Al_2O_3 / (Al_2O_3 + CaO^* + Na_2O + K_2O)\} \times 100$; Nesbitt and Young, 1982), but also some diagenetic processes that involve for instance K-metasomatism can be assessed (Fedo *et al.*, 1995). In an A-CN- K (Al_2O_3 - CaO^* + Na_2O - K_2O) diagram, unaltered igneous rocks will plot on or close to the feldspar tie line but closer to the CN apex. Expected weathering trends start in the average composition of the source rock and progress parallel to the A-CN join towards the A apex, as a result of the alteration of feldspars and volcanic glass to clay minerals (Nesbitt and Young, 1982; Fedo *et al.*, 1995; Nesbitt, 2003). Deviations towards the K apex suggest K-metasomatism (Nesbitt and Young, 1989; Fedo *et al.*, 1995) or mixing of different sources (McLennan *et al.*, 1993), but postdepositional metasomatic sodium enrichment and grain size sorting may modified the CIA as well (McLennan *et al.*, 1993).

Further assumptions of chemical weathering can be made using the K/Cs ratio, because during weathering the Cs tends to be fixed in the weathering profile whereas the potassium is more likely lost in solution. Therefore, low K/Cs ratios might indicate weathering (McLennan *et al.*, 1990).

The ratio between two incompatible trace elements with similar properties as Th and U can also be analyzed in terms of alteration. The Th/U ratio in average upper continental crust (UCC) is 3.8, and for most sedimentary rocks derived from average crust, the Th/U ratio is around 3.5-4.0, indicating that they have not undergone weathering and/or recycling (McLennan *et al.*, 1993). However, under oxidizing conditions the U^{4+} oxidizes to U^{6+}, which is more soluble than the first one and tends to be lost in solution during weathering and recycling. The loss of U increases the Th/U ratios to values above 4.0 (McLennan *et al.*, 1993). Notwithstanding, a low Th/U ratio can be also due to U enrichment (McLennan and Taylor, 1991).

Several works have documented the disturbances that weathering and diagenesis might produce to the distribution of rare earth elements (REE) in sedimentary rocks (McDaniel *et al.*, 1994; Bock *et al.*, 1994), and therefore a better understanding of the alteration processes through the study of the REE and the Sm-Nd isotopes can be obtained (see sections B.2.2.2 and B.2.3).

B.2.2.2 Trace elements

As discussed in section B.2.2.1, some trace elements as Th, U and Cs are useful to evaluate the changes in composition of a sedimentary rock produced during weathering and/or recycling. The use of trace elements for provenance determinations is based on the immobile character and low residence time in seawater of certain elements, particularly high field strength elements (HFSE) and REE, and it is also based on the fact that compatible elements (e.g. Sc, Cr, V, Co and Ni) concentrate in mafic rocks whereas incompatible elements (such as Th, Zr, La, Y, U and Hf) concentrate in felsic rocks (Taylor and McLennan, 1985). Therefore, ratios like La/Sc, Th/Sc, La/Th, and Zr/Sc may be useful for provenance determination (Taylor and McLennan, 1985). The concentration of trace elements in sedimentary rocks compared with the concentration of the same elements in the UCC can ideally give an indication of the composition of the average source rocks (McLennan *et al.*, 1993; Cox and Lowe, 1995).

The input of a mafic source could be discriminated using the Cr/V and Y/Ni ratios. The Cr/V ratio indicates the enrichment of Cr over other ferromagnesian trace elements. The main minerals that concentrate Cr over other ferromagnesian are chromites. The Y/Ni ratio indicates the concentration of ferromagnesian trace elements (such as Ni) compared with Y that represents a proxy for heavy rare earth elements. The Cr/V and Y/Ni ratios for PAAS (post-Archaean Australian shales) is about 0.73 and 0.49 respectively (Taylor and McLennan, 1985), while for the UCC are 0.78 and 0.5 respectively (McLennan *et al.*, 2006). However, ophiolitic components would have Cr/V ratios higher than 10 (discussion in McLennan *et al.*, 1993). In this regard, it is also important to consider that certain elements such as V, Cr, Cd and Mo are sensitive to anoxic environment and tend to be enriched (Calvert and Pedersen, 1993) or fractionated from each other during sedimentary processes like diagenesis (Feng and Kerrich, 1990).

Mechanical processes are responsible for the transport of REE into a sedimentary basin and therefore REE represent reliable provenance indicators (Cullers *et al.*, 1979; Taylor and McLennan, 1985; McLennan, 1989). However, mobility of REE (plus Y) had been widely reported (i.e. Awwiller, 1994; McDaniel *et al.*, 1994; Bock *et al.*, 1994; Bau, 1999). The shape of the REE pattern (including the presence or not of a Eu-anomaly) can provide information about both bulk composition of the provenance and about the nature of the dominant igneous process affecting the provenance (McLennan *et al.*, 1990; McLennan and Taylor, 1991).

Felsic rocks tend to be enriched in light rare earth elements (LREE) due to igneous differentiation processes. Intracrustal differentiation processes result in plagioclase fractionation within the igneous sources and the concomitant Eu-anomaly characteristic for any post-Archaean sedimentary rock, with some exceptions (Taylor and McLennan, 1985). However, cases of sorting that concentrate plagioclase in a sedimentary rock, with a concomitant less negative Eu-anomaly have been described (discussion in McLennan *et al.*, 1990). Eu_N/Eu^* is calculated by the formula $Eu_N/Eu^* = Eu_N / (0.67\ Sm_N + 0.33\ Tb_N)$, where the subscript N denotes normalized to chondrite. The shape of heavy rare earth elements (HREE) can be related to garnet content in the parental rock and its fractionation during igneous processes. Garnet fractionation occurs at considerable depths, suggesting a mantle origin and leaving a depleted-HREE pattern in the rocks (McLennan and Taylor, 1991).

The Ce-anomaly is calculated as $Ce_N/Ce^* = Ce_N / (0.67\ La_N + 0.33\ Nd_N)$, where N denotes normalized to chondrite. Since Ce is dissolved under anoxic conditions, it tends to be depleted in the sediments and hence resulting in a negative Ce-anomaly. On the other hand, the Ce is enriched if the environment conditions are oxic resulting in a positive Ce-anomaly in the sedimentary rock (Taylor and McLennan, 1985).

B.2.2.3 Provenance and tectonic setting

The ultrastable heavy mineral zircon can be recycled and consequently the Zr concentration would be enriched in a sedimentary rock. On the other hand, Th is an incompatible element whereas Sc is compatible in igneous systems (McLennan *et al.*, 1993). Furthermore, Sc is present in labile phases. Therefore, the Zr/Sc and Th/Sc ratios are very useful for provenance analysis, since the first ratio reflects reworking and the latter indicates the degree of igneous differentiation processes (McLennan *et al.*, 1990; 1993). The Th/Sc ratio for the UCC is 0.79 (McLennan *et al.*, 2006).

Trace element ratios such as La/Th, La/Sc, Zr/Sc, Th/Sc and Ti/Zr have been applied to characterize the tectonic settings of the source (e.g. Bhatia and Crook, 1986).

However, the sediments can be transported across tectonic boundaries and thus may not necessarily be indicative of the tectonic setting of the deposition (McLennan, 1989). The diagram Ti/Zr versus La/Sc along with the triangular diagrams Th-Sc-Zr/10 and La-Th-Sc could help to discriminate between oceanic island arc, continental island arc, active continental margin and passive margin settings (Bhatia and Crook, 1986). The influence of an arc-provenance component might be decipher using trace elements ratios such as Th/Sc and Eu_N/Eu^* and element concentrations of Ti and Nb. Low Th/Sc ratios, Eu_N/Eu^* of about 1 and strong negative Nb and Ti anomalies characterize continental arc components, although differentiated arcs would have variable Th/Sc ratios and Eu_N/Eu^* between 0.6 and 0.9 (Hofmann, 1988; McLennan *et al.*, 1993; Zimmermann, 2005).

B.2.3 Sm-Nd isotopes

Nd isotopes have been widely used as provenance indicators (e.g. McLennan *et al.*, 1989; 1993) and their utility for provenance studies stems from the coherent behaviour of the rare earth elements during sedimentary processes. Nd isotopic signatures of terrigenous sedimentary rocks average those of the various sources from which the sediments were derived (McLennan *et al.*, 1989). Since the Sm/Nd ratio is modified during processes of differentiation mantle-crust it is possible to estimate the time at which the initial magma was separated from the upper mantle, also called the model age or T_{DM} (DePaolo, 1981; Nelson and DePaolo, 1988). When studying sedimentary rocks, the model age should be interpreted as the model age of that rock which has contributed in a higher degree to the Sm-Nd relationship of that sediment, because the Nd isotopic composition is the result of mixing Nd signatures of different source rocks. Furthermore, since mafic rocks are depleted in REE their contribution to the Sm-Nd system could be masked by the stronger isotopic signal imprinted by the felsic sources.

One of the strengths of the Sm-Nd model age method applied to whole-rock systems is that it allows seeing back through processes such as erosion, sedimentation, metamorphism and even crustal melting events, which usually re-set other dating tools

(McLennan et *al.*, 1989). However, various studies have addressed processes that might alter the Sm-Nd isotopic signatures in sedimentary rocks. These include the alteration of Sm/Nd ratios and Nd isotopic signatures during weathering, diagenesis or sorting (McDaniel *et al.*, 1994; Bock *et al.*, 1994). Since these processes may cause complications in the interpretation of model ages, the emphasis is on the ε_{Nd} values (i.e. McLennan *et al.*, 1989; 1993). The ε_{Nd} (0) indicates the deviation of the $^{143}Nd/^{144}Nd$ value of the sample from that of CHUR (Chondritic Uniform Reservoir; DePaolo and Wasserburg, 1976), and it is expressed as ε_{Nd} (0) = $\{[(^{143}Nd/^{144}Nd)_{sample\ (0)} / (^{143}Nd/^{144}Nd)_{CHUR\ (0)}] - 1\}$ *10000. The ε_{Nd} (t) can be calculated in the same way but considering t as the age of sedimentation. The $f_{Sm/Nd}$ is the fractional deviation of the $^{147}Sm/^{144}Nd$ ratio of the sample from a chondritic reference ($f_{Sm/Nd} = (^{147}Sm/^{144}Nd)_{sample} / (^{147}Sm/^{144}Nd)_{chondrite} - 1$). T_{DM} were calculated based on the depleted mantle model (DePaolo, 1981). This model implies that the mantle suffered fractionation that leads to a residual mantle enriched in Sm/Nd ratio but geochemically depleted in large ions lithophile elements (LILE; DePaolo, 1981).

B.2.4 Pb-Pb isotopes

Pb isotopes provide a different view of sediment provenance compared to other isotope systems. The relationship between Pb isotopic composition and tectonic setting is not straightforward, but it is possible to discriminate between ancient upper continental crust and younger terrains (especially in terms of $^{207}Pb/^{204}Pb$). Studying Pb-isotopes on whole-sedimentary rocks might be complex due to the effect that several processes can have on the Pb system. Uranogenic-Pb (^{207}Pb and ^{206}Pb) would be affected by enrichment of U by sedimentary processes that more likely occur on black shales. Furthermore, weathering could leach U from the sedimentary rock and therefore affecting the Pb-isotopes (Hemming and McLennan, 2001). Sedimentary selective sorting of mineral phases such as zircon, monazite, xenotime and feldspar might fractionate the Pb isotopes. The effects of sedimentary sorting might be complex because even though U and Th are enriched in heavy minerals, their ratios are different in different minerals (Hemming and McLennan, 2001). Moreover, common Pb (^{204}Pb)

is not in the same mineral phases as the other three Pb isotopes, but is rather concentrated within feldspars (and particularly K-feldspar). In general, sandstones with no or very low matrix contents and not altered will tend to preserve the Pb-isotope composition (because resistant minerals will contain most of the radiogenic Pb and the non-radiogenic Pb would be in feldspars), whereas fine-grained rocks would reflect a complicated mixture of source, weathering and diagenetic characteristics, more probably related to the break-down of feldspars, U enrichment or leaching, etc. (Hemming and McLennan, 2001).

The discrimination of an 'ancient' component using Pb data reside in the observation that most terrestrial ^{207}Pb was produced early in the history of the Earth, due to the short half-life of ^{235}U. Therefore, ^{207}Pb/^{204}Pb is relatively insensitive to Meso-Neoproterozoic and younger U/Pb variations (Asmerom and Jacobsen, 1993). The half-life of ^{238}U is about the same as the age of the Earth, so ^{206}Pb/^{204}Pb has grown more linearly over Earth's history. Consequently, relatively high ^{207}Pb/^{204}Pb ratios of any given crustal block require the presence of an old Pb-component (Asmerom and Jacobsen, 1993). Further complications may arise by comparing Pb isotopes from a sedimentary rock with Pb isotopes from the probable source(s), since disturbances in the Pb system during erosion and deposition or due to post-depositional processes can change the Pb-ratios giving ratio values very dissimilar to those from the source rock (e.g. McLennan *et al.*, 2000). Therefore, comparisons between Pb-system of a sedimentary rock and the Pb-system of the sources is not straightforward and erroneous results can easily be obtained, particularly when constraints on the interpretations based on Pb-isotopes through other provenance approaches are missing (e.g. McLennan *et al.*, 2000).

B.2.5 Detrital zircon dating

Zircon is an ultrastable heavy mineral and hence, it survives processes of erosion, transport and deposition. U–Pb dating of single detrital zircons is a very important dating tool that allows the identification of provenance components in clastic sedimentary rocks. However, the detrital zircon approach to sedimentary provenance is controlled by several factors (transport and deposition, recycling, sorting, drainage basin, but also artificial biasing during sampling and sample preparation). Therefore, detrital zircon ages alone can only be used to evaluate the overall mass balance of source components in a sedimentary rock when the number of grains analyzed is large enough to be statistically significant and in combination with other provenance approaches (e.g. Sircombe and Stern, 2002). Nevertheless, for zircon samples randomly selected if more than 30 zircons are analyzed then the probability of sampling an age group that represents at least 10% of the population is of about 95% (Dodson *et al.*, 1988). Other authors estimate that 117 zircon grains are needed to have statistically meaningful results, particularly when the absence of a certain population is to be proved (Vermeersch, 2004). However, it has been proved that a combination of random and non-random selection of detrital zircon grains could give accurate results when measuring lower amounts of grains (Andersen, 2004).

Since the selection of zircon grains for this study included each morphological type observed (despite grain size), then the possibility of omission of zircons from rare age groups had been minimize (e.g. applied by Thomas *et al.*, 2004). The zircon geochronologic dataset of a sedimentary rock is generally biased towards magmatic zircon grains because the metamorphic zircons (or metamorphic portions of grains) are more susceptible to disintegration during erosion and transport, due to the presence of decay-induced defects (e.g. Hartmann and Santos, 2004).

B.2.6 Heavy minerals

Heavy minerals are a reliable tool in determining the nature of sedimentary source areas, especially when other techniques (geochemistry, petrography and Nd isotopes) show source mixing or are dominated by felsic derived debris, but the origin of these sources are indecipherable. They are particularly useful in studies of sedimentation related to tectonic uplift, as the evolution and unroofing episodes of orogenic belts are reflected in adjacent basins. Analysis of heavy minerals in foreland basins sequences may thus prove valuable in constraining the structural histories of both the basin and the source areas (Mange and Maurer, 1992) and give important clues to the composition of the sources. The heavy minerals analyses in combination with petrography and geochemistry provide constraints on the mineralogical nature of the source rocks (Morton and Hallsworth, 1999). Particularly useful are those species which occur under specific paragenesis, and further refinement to provenance can be provided by chemical analysis of individual grains, as for example on spinels (Morton, 1991).

The composition of heavy mineral assemblages is not only controlled by the composition of the source, but the processes that operate during sedimentation (sorting, abrasion, dissolution) would modify the original provenance signal (Morton and Hallsworth, 1999) and therefore the combination of heavy minerals analyses with other provenance approaches is needed to characterize the sources. Changes in the heavy mineral assemblages will affect also the geochemical and isotope composition of the whole rock, and therefore the evaluation of those processes causing the changes of the heavy minerals distribution is very important to understand the provenance (Morton and Hallsworth, 1999).

B.2.7 Illite Crystallinity Index

The 'illite crystallinity index' (ICI; Kübler, 1966 in Warr and Rice, 1994) is defined as the width of the (001) XRD peak at half of its height. A well-crystallized illite, characteristic of a relatively high-temperature history, has sharp peaks, and therefore a low index, while low-temperature illite is more disordered, and has irregular peaks with large indexes. The objective of analyzing the illite crystallinity index is to determine either the degree of diagenesis or the very low-grade metamorphism that the clastic rocks from the Precordillera terrane could have suffered.

The standardization procedures applied over the samples allowed the comparison of the data with the worldwide established values used to separate diagenesis from very low-grade metamorphism. However, it was demonstrated by several authors that the correspondence of the different zones (diagenesis, low and high anchizone and epizone) and theirs diagnostic mineral facies (zeolite facies, prehnite-pumpellyite, pumpellyite-actinolite and green-schist respectively) is not always correct.

The reason for this is that the concept of facies is based on thermodynamic laws, where the mineral reactions are reversible and the associated equilibrium is maintained over certain P-T conditions, independently of the P-T-t path. On the other hand, the ICI method is based on continuous and non-reversible chemical and structural transformations that occurred in the pro-grade series illite-muscovite, which in turn are much more dependent on the P-T-t conditions suffered by the rock (Warr, 1996). Furthermore, the Subcommission on the Systematic of Metamorphic Rocks (SCMR) from the IUGS recommended the use of 'very low-grade metamorphism' as a rough equivalent of 'anchizone' and 'low-grade metamorphism' as the equivalent of 'epizone' (Árkai *et al.*, 2003).

B.3 ANALYTICAL TECHNIQUES

B.3.1 Petrography

A thin section from each siltstone, sandstone (including conglomerate matrix) and volcanic rock sampled was made at the Centro de Investigaciones Geológicas (CIG), La Plata, Argentina. Mineralogical and textural studies were conducted by optical methods using a LEICA petrographic microscope. The electron microscope (SEM-BSE-EDS) used to aid in the mineralogical identification is a JEOL JSM-5600 with a tungsten filament and EDS analyses were done using a Noran X-ray detector and Noran Vantage software. The SEM-BSE-EDS system was set at 15 keV, a working distance of 20 mm and a live time of 60 s per spot. The XRD used is a Philips PW1729 equipped with a PANanalytical X-Pert Pro diffractometer. All these equipment was available at the University of Johannesburg, South Africa. A detailed petrographic description for each unit studied and the XRD results are given in Appendix C (Part 1 and Table 3 respectively).

B.3.2 Geochemistry

The samples were crushed with a jaw-crusher and milled with a tungsten carbide mill at Centro de Investigaciones Geológicas, La Plata, Argentina. The type of container used can contaminate samples with Nb and Ta, among other elements; however, the absence of notorious contamination had been checked since eleven selected mudstones and sandstones of different grain sizes and compositions were analyzed as well after milling using an agata mill at ACME Laboratories (Canada). To measure the major elements, fusion beads using a 50/50 lithium metaborate/ lithium tetraborate as flux were made. Trace elements such as Ni, V, Cu, Ga, Sr, Y, Zr, Zn, Nb, Rb, Ba and Pb were measured on pressed powder tablets, made using a 8:4 grams ratio between sample and Herzog binder pellets (composed of 90% cellulose and 10% wax). The fusion beads and the pressed tablets were analyzed by X-Ray Fluorescence (XRF) using a Phillips wavelength-dispersive XRF spectrometer operating with PANalytical MagiX PRO software at SPECTRAU (the Central Analytical Facilities of the University of Johannesburg, South Africa). The loss on ignition (LOI) was calculated by difference in weight sample prior and after heating (around 1 gram of sample) for two hours at 1100 ºC in an electric oven. Possible Th interferences in Tb had not been taken into account.

Certain trace elements such as Sc, Cr, Co, Cs, Hf, Ta, W, Th, U, As and Sb as well as rare earth elements (La, Ce, Nd, Sm, Eu, Tb, Yb and Lu) were obtained by INAA (Instrumental Neutron Activation Analysis) at ACME Laboratories (Canada). Geochemical data (major, trace and rare earth elements) from the volcanic rocks interlayered with the Yerba Loca Formation (see Chapter 5) were determined by ICP-MS (Inductively Coupled Plasma – Mass Spectrometer) at ACME Laboratories (Canada), except for sample YL417, Yl418 and YL455. Major and certain trace elements of the latter three samples were measured by XRF (the abovementioned equipment) and other trace elements (including REE) by INAA at ACME Laboratories (Canada).

Standards used for the XRF determinations of major and the certain trace elements mentioned are SARM-1, GS-N, JG-1, AC-E and JA-1. Detection limits using the XRF are Si_2O = 250ppm, Al_2O_3 = 145ppm,, CaO = 40ppm, MgO and Na_2O = 65ppm, K_2O = 47ppm, MnO = 15ppm, TiO_2 = 20ppm, Fe_2O_3 = 150ppm, P_2O_5 = 9ppm, Ni, Rb, Sr, Cu, Y and Zr = 1ppm, V = 3ppm, Nb and Pb = 0.5, Ba = 13ppm. Detection limits for elements analyzed by INNA are Sc, Sm and Sb = 0.1ppm, Cr and Nd = 5ppm, Co, Cs, Hf and W = 1ppm, Ta, U, As, La and Tb,= 0.5ppm, Th, Eu and Yb = 0.2ppm, Ce = 3ppm, Lu = 0.05ppm. Detection limits for elements analyzed by ICP-MS are: Si_2O, Al_2O_3, CaO, MgO, Na_2O, K_2O, MnO, TiO_2 and P_2O_5 = 0.01%, Fe_2O_3 = 0.04%, LOI = 0.1%, Cs, Rb, Hf, Ta, U, Y, Zr, Nb, Pb, La and Ce, = 0.1ppm, Ba and Zn = 1ppm, Th = 0.2ppm, V = 8ppm, Sr = 0.5 ppm, Nd = 0.3ppm, Sm, Gd, Dy and Yb = 0.05ppm, Pr, Eu and Ho = 0.02, Tb, Tm and Lu = 0.01ppm, Er = 0.03ppm.

The calculation of the CIA implies that only the CaO (CaO*) associated to silicate minerals should be used. Therefore, corrections to the measured CaO content for the presence of Ca in carbonates (calcite and dolomite) and phosphates (apatite) are needed. This can be accomplished using the measured CO_2 and P_2O_5 contents. For this study, CaO was corrected for phosphate assuming that all the P_2O_5 content is associated to apatite. Because CO_2 data were unavailable, if the remaining number of CaO moles obtained after deducing those moles associated with apatite are less than the number of Na_2O moles, then this CaO value was adopted to calculate the CIA (McLennan, 1993). If the number of CaO moles is greater than the moles of Na_2O, then those samples were discarded.

B.3.3 Sm-Nd isotopes

To measure the Sm and Nd isotopes the whole-rock samples were digested in acids (HF/HNO_3) after the addition of a combined spike $^{149}Sm/^{150}Nd$. The preliminary separation of Sm and Nd along with other REE was performed on cation exchange columns with an AG-50x-X8 resin and eluting the elements with dilute acids (Sato *et al.*, 1995). The Sm and the Nd were separated in turn from the other REE using cation exchange techniques in teflon columns with a HDEHPLN-B50 anion resin (Sato *et al.*, 1995).

For the quantification on a thermal ionization mass spectrometer (TIMS) each sample was evaporated to desiccation, and then the samarium concentrate was placed on simple Ta-Re filaments while the neodymium concentrate was placed on triple Ta-Re filaments. In both cases, the sample was dissolve in H_3PO_4 0.25N. To obtain a measurement with a TIMS the sample loaded in a filament needs to be ionized by heating it under vacuum. Sm-Nd analyses were performed using static mode on a VG sector 54 multicollector TIMS at the Laboratório de Geologia Isotópica da Universidade Federal do Rio Grande do Sul (LGI-CPGq/UFRGS), Porto Alegre, Brazil. Neodymium crustal residence ages (T_{DM}) were calculated according to the depleted mantle model of DePaolo (1981), but results according to DePaolo *et al.* (1991) were used to compare with data from the literature. ε_{Nd} (t) values were calculated based on average ages according to palaeontological ages for each unit. Nd ratios were normalized to $^{146}Nd/^{144}Nd = 0.72190$ and calculated assuming a $^{143}Nd/^{144}Nd_{(0)} = 0.512638$. Measurements for the La Jolla standard gave $^{143}Nd/^{144}Nd = 0.511859 \pm 0.000010$. $\varepsilon_{Nd}(0) = \{[(^{143}Nd/^{144}Nd)_{sample\ (t=0)} / 0.512638] - 1\} * 10000$. $\varepsilon_{Nd}(t) = \{[(^{143}Nd/^{144}Nd)_{sample\ (t)} / (^{143}Nd/^{144}Nd)_{CHUR\ (t)}] - 1\} * 10000$. $^{147}Sm/^{144}Nd_{CHUR} = 0.1967$. Values obtained for the samples analyzed are listed on Table 3 in Appendix A.

B.3.4 Pb-Pb isotopes

The samples were digested in acids (HF/HNO_3) and the lead was separated in anionic resin (AG-1 X8) exchange microcolumns using HBr 0.6N and HCl 6N. After complete desiccation of each sample on a hot plate, the samples were mounted on filaments and the different Pb isotopes were measured using a VG sector 54 multicollector a thermal ionization mass spectrometer at the Laboratório de Geologia Isotópica da Universidade Federal do Rio Grande do Sul (LGI-CPGq/UFRGS), Porto Alegre, Brazil. The NBS-981 standard was used as recommended (variation from accepted values was less than 0.01% / a.m.u.) and samples were corrected for mass fractionation. Values obtained for the samples analyzed are listed on Table 4 in Appendix A.

B.3.5 Detrital zircon dating

To obtain detrital zircon ages the zircons were handpicked from heavy-concentrates. An explanation of the methodology used to concentrate heavy minerals before the handpicking of the zircons is given below in section B.3.6. The zircons were mounted on epoxy resin and the mounts were polished down to approximately their centres. Cathodoluminescence (CL) photographs were taken prior to dating analyses. Detrital zircon dating was carried out with a Finnigan ThermoElectron Neptune LA-MC-ICP/MS (laser ablation multicollector inductively coupled plasma mass spectrometer) at the Laboratório de Geologia Isotópica da Universidade Federal do Rio Grande do Sul (LGI-CPGq/UFRGS), Porto Alegre, Brazil. The spot size was of 25µm and the crater depth of 15µm. The zircon standard GJ-1 was measured every five measurements on grains from the sample.

Samples with large errors were excluded from the results. Samples with discordance less than 15% (where the discordance is defined by 100* [1- ($^{206}Pb/^{238}U$ age) /($^{207}Pb/^{206}Pb$ age)]) were anchored to get a medium age and they are shown in italics in Table 5 of Appendix A. The cathodoluminescence pictures were used to determine the best area to focus the laser spot of the LA-MC-ICP/MS. Cathodoluminescence microphotographs were obtained with a JEOL JSM-5600 set at a voltage of 15 kV with a working distance of 20mm, at the Centralized Analytical Facility (SPECTRAU, University of Johannesburg, South Africa). Values obtained for the samples analyzed are listed on Table 5 in Appendix A.

B.3.6 Heavy minerals

The separation of heavy minerals was done only over selected fine to medium-grained sandstones. The samples were crushed and sieved to less than 100µm. The <100µm fraction was analyzed in order to avoid confusing results because of the hydrodynamic fractionation shown by samples with different grain sizes (Morton and Hallsworth, 1994) and also to prevent the bias toward coarse source rocks (Gehrels, 2000). The heaviest fraction was then separated by hydraulic processes. This pre-concentrate was treated with bromoform (δ = 2.89) to obtain the complete heavy mineral fraction. Methylene iodide (δ = 3.32) was used in certain samples to obtain a fraction enriched in zircons, followed by an electromagnetic separation with a Frantz Isodynamic Separator. However, the zircon population of some samples was extracted from the δ>2.89. In either case, zircon grains were hand-picked under binocular microscope for dating porpoises (for details on zircon dating see section B.3.5), and grains representing all sizes and morphological types were selected.

Each of these different fractions was embedded randomly into epoxy resin, avoiding a preference for a certain population, polished and carbon coated. The identification and characterization (shape, size, fractures, inclusions) of the heavy minerals were done under a binocular microscope, scanning and backscattered electron microscope using energy dispersive spectrometry (SEM-BSE-EDS). The SEM-BSE-EDS system was set at 15 keV, a working distance of 20mm and a live time of 60 s per spot, and is the same equipment as described above (see section B.3.1).

Quantitative analyses of the spinels were carried out at the Central Analytical Facility (SPECTRAU, University of Johannesburg, South Africa) with a Cameca 355 electron microprobe equipped with an Oxford link integrated WDS/EDS, set at a voltage of 15 keV, and with a JEOL 733 with WDS/EDS set at a voltage of 15 keV. Beam current diameter in both microprobes was between 8 to 10 microns; ZAF corrections were effected under standard procedures. Chromite standard on MAC certified standard no. 2590 was used for analysis. Values obtained for each grain analyzed are listed in Tables 6 and 7 in Appendix A. Pictures to illustrate the heavy mineral content of the units studied are shown in Appendix C.

B.3.7 Illite Crystallization Index

Twenty samples from different clastic units of the Precordillera terrane were analyzed by X-rays diffraction, and results are listed in Table 2 in Appendix A. Sample preparation was done according to Kisch (1991). Claystones were milled on a porcelain mill trying to avoid over-milling. Organic matter was eliminated with H_2O_2 and carbonates were removed with acetic acid. The less than 2μm fraction of each sample was obtained by repeating series of ultrasound dispersion and centrifugation. This fraction was analyzed at the Centro de Investigaciones Geológicas (La Plata, Argentina), in a Philips PW 2233/20, at 36 kV and 18 mA, Cu Kα radiation, Ni-filter, λ 1.54 A (vertical goniometer). Samples were studied on the range from 2° to 32° 2θ at a 2° 2θ/min. scanning velocity and with a time constant of 1 second. At the same time and under the same procedures already explained, the international standards were analyzed as well in order to determine the standardized illite crystallization index for the samples.

Three different X-ray diffraction patterns were obtained per sample: air-dried, ethylene glycol attacked, obtained after the exposition of the sample to ethylene glycol vapours for 24 hours; and the heated sample, obtained after warming the samples to 550°C for 2 hours (X-ray diffraction patterns are shown in Part 2 of Appendix C). The thickness of sample on each glass-slide is a clue parameter (Krumm and Warr, 1994). This parameter was controlled weighing 0.058 grams of sample, diluting it in 2 millilitres of distilled water and ultrasound dispersed before spreading it onto the glass-slide. The illite crystallinity values (IC) were determined measuring the full-width at high-maximum (FWHM) of the peak (001) on the air-dried and ethylene glycol X-ray diffraction patterns using the WinFit software (Krumm, 1994). These IC values obtained were standardized (CIS) according to the regression curve obtained with the standards ($y = 1.3877x - 0.1959$, $R^2 = 0.9316$; where R^2 is the correlation coefficient; Fig. B.1). Values are shown below (Table 1). The identification of the mineralogy was done manually reading each diffraction pattern and comparing with tables of clay minerals.

B.4 SAMPLING

The sampling was done preferably in well-known type-sections of the different sixteen units. Columnar sections found in the literature were used to position the samples. The sampling was attempted to cover all different lithologic types in each section. At the same time, efforts to sample the complete stratigraphy of each unit in an equidistant way were made. Each sample was large enough to make a thin section, as well as to mill for geochemical and isotopic analyses and to apply XRD techniques, although not all samples were geochemically analyzed. Between two and four samples weighing around 5 kg each of all the different formations were taken to obtain heavy mineral concentrates. A total of 188 samples from the Ordovician and the transition

Ordovician-Silurian clastic record from the Precordillera terrane were taken and analyzed. In Figures B.2 and B.3 the sampling locations within the San Rafael block and the Precordillera *s.s.* respectively are shown (letters correspond to samples in Table 2), whereas in Table 2 a compilation of the precise geographic locations and rock type for each sample are given.

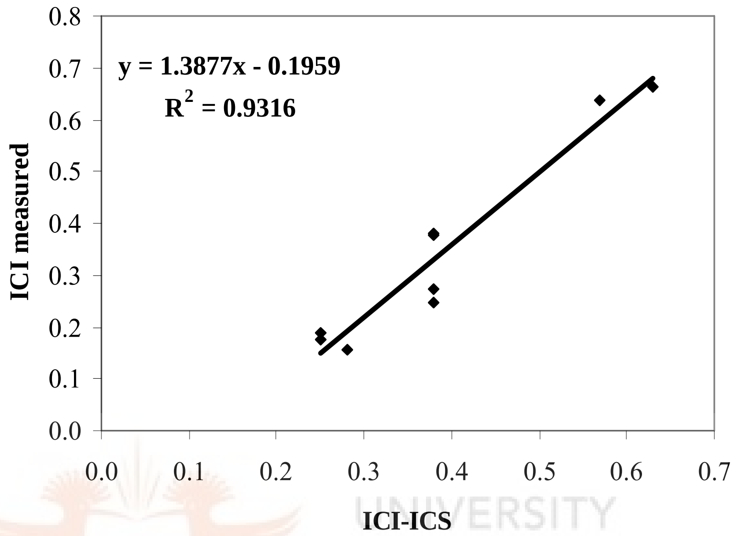

Figure B.1: Relationship between the ICI values of the standards as obtained at CIG (ICI measured) and the recommended ICI values of the standards (ICI-ICS). The regression curve obtained was used to recalculate the ICI values of all the samples in order to standardize the results and make them comparable to the worldwide establish values used to separate diagenesis from very low-grade metamorphism.

standard	ICI-ICS	ICI measured
n ILC2	0.28	0.156
n SW1-0	0.63	0.663
n SW4	0.38	0.272
n SW4-0	0.38	0.376
n SW6	0.25	0.187
g SW1-0	0.57	0.637
g SW4	0.38	0.248
g SW4-0	0.38	0.380
g SW6	0.25	0.175

Table 1: ICI-ICS values of the standards and ICI values of the standards measured at CIG. g= ethylene-glycol attacked sample; n= air-dried sample.

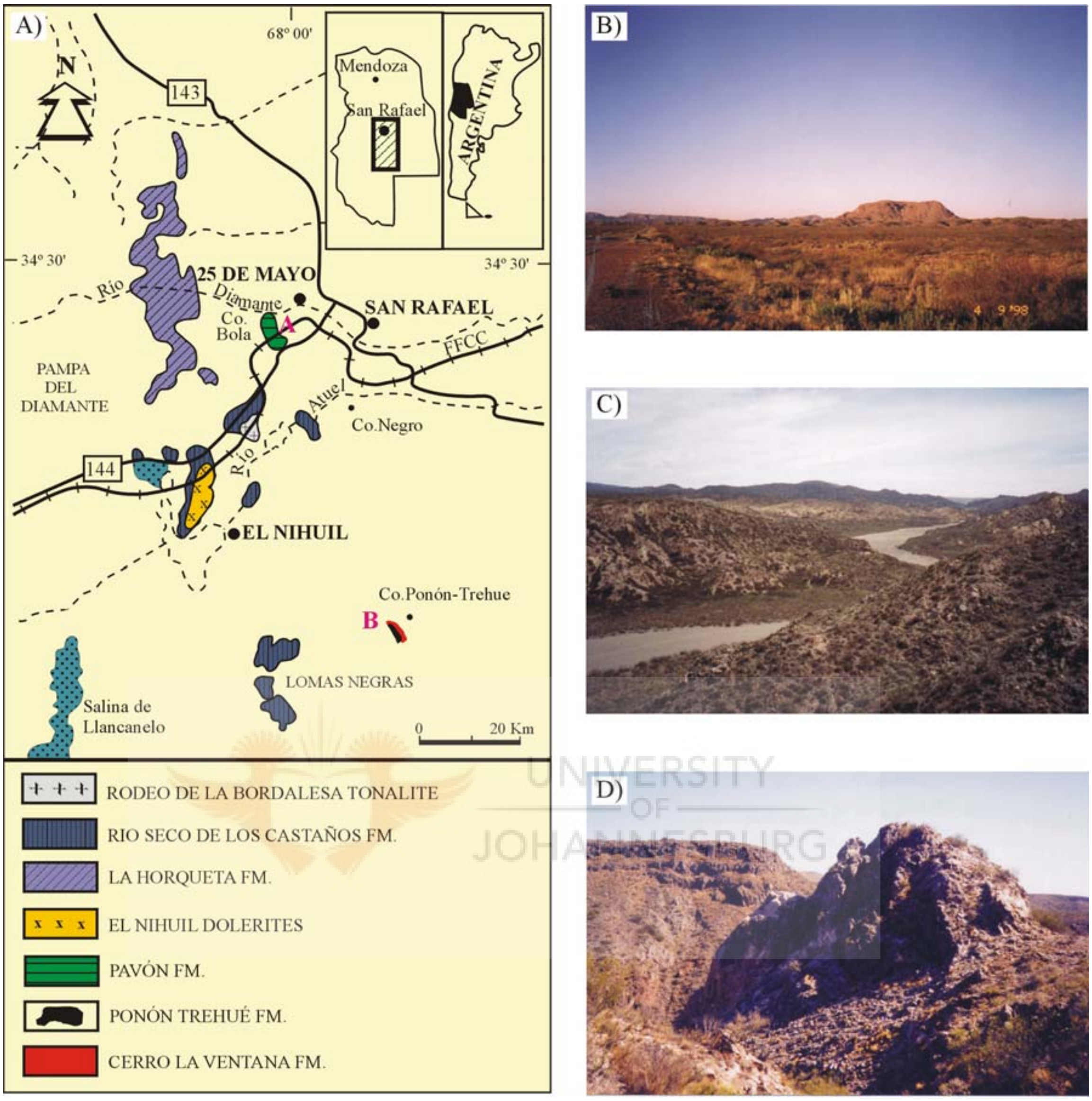

Figure B.2: A) Sampling locations within the San Rafael block (pink letters correspond to samples in Table 1). Modified from Cingolani *et al.* (2003a). B) The Pavón Formation outcrops on the eastern slope of the Cerro Bola hill (in the centre of the picture). C) General view of the Cerro Ponón Trehué area, where the Ponón Trehué Formation overlaps the basement rocks of the Cerro La Ventana Formation (Mesoproterozoic basement of the Precordillera terrane). D) A carbonate olistolith is outstanding from the olistostromic matrix within the Ponón Trehué Formation, in the Ponón Trehué Creek area.

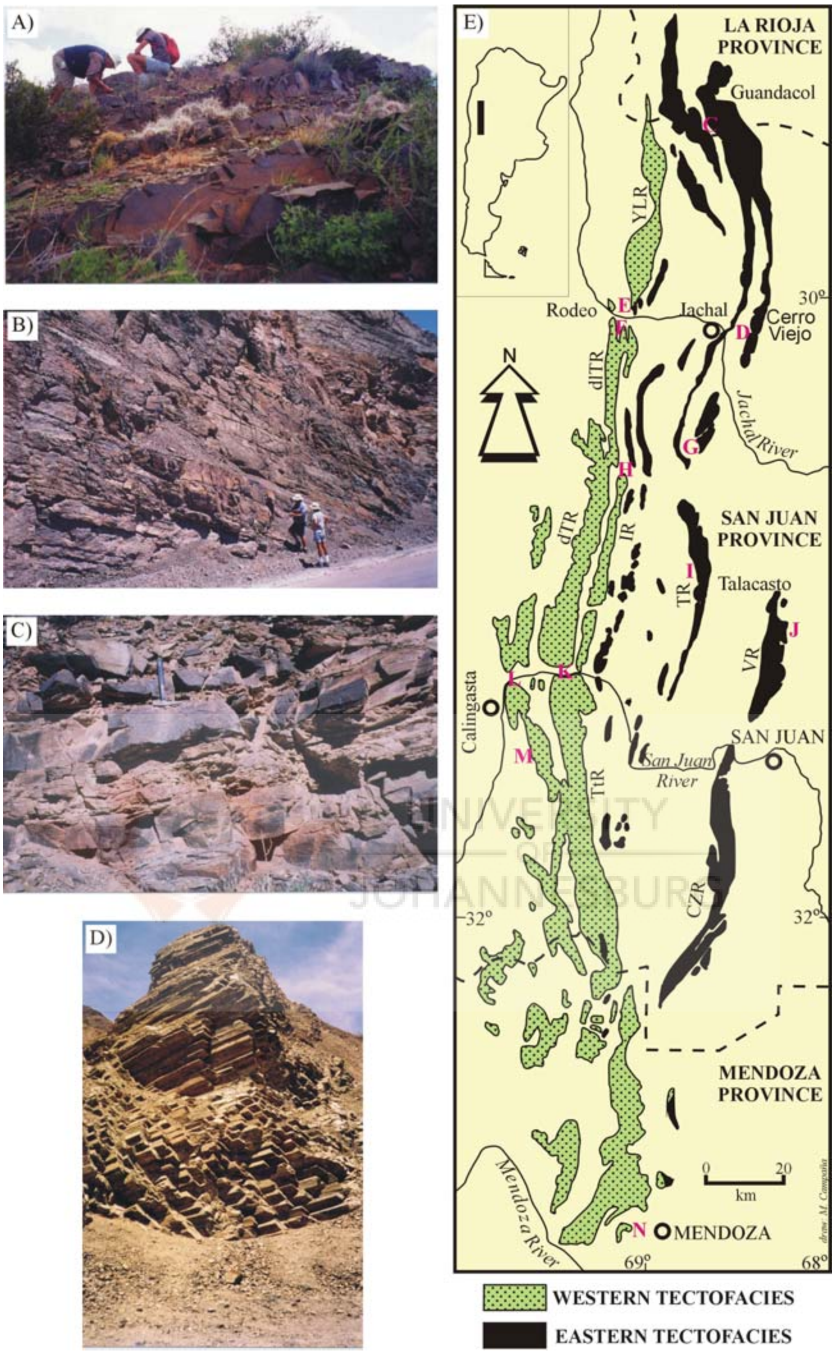

Figure B.3: A) Interlayered sandstones and mudstones of the Sierra de la Invernada Formation. B) Wackes and mafic volcanic rocks of the Alcaparrosa Formation. C) Interlayered sandstones and mudstones of the Portezuelo del Tontal Formation. D) Mafic volcanic rocks with columnar junction within the Alcaparrosa Formation. The outcrop is about 3m high. E) Sampling locations within the Precordillera *s.s.* (pink letters correspond to samples in Table 1). IR: Invernada Range; dTR: del Tigre Range; dlTR: de la Tranca Range; YLR: Yerba Loca Range; TR: Talacasto Range; TtR: del Tontal Range; CZR: Chica de Zonda Range; VR: Villicúm Range. Modified from Astini (1991).

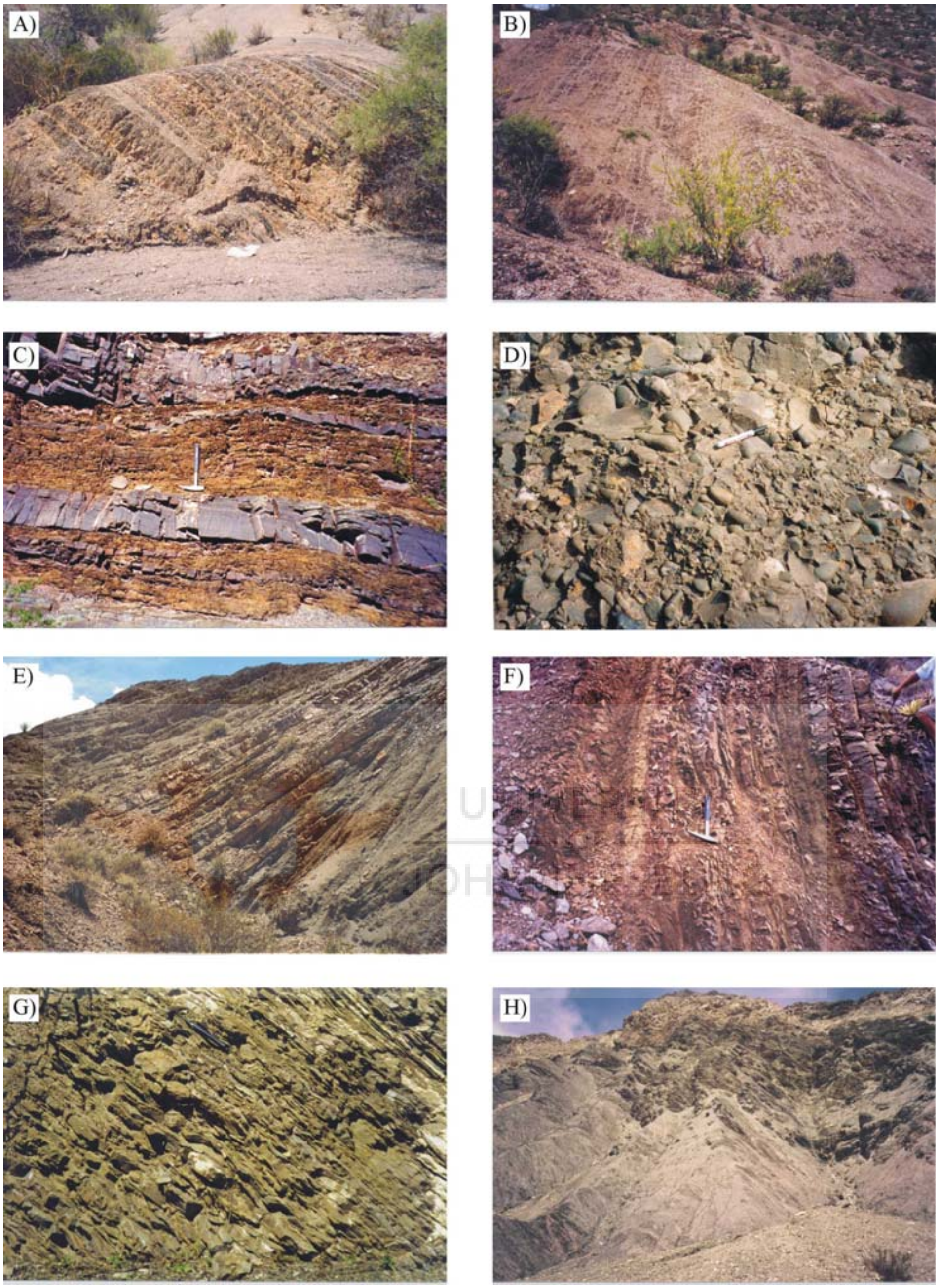

Figure B.4: A) Lower section of the Gualcamayo Formation where the black shales are interlayered with K-bentonites (orange levels); the white notebook on the floor is 20cm long. B) Mudstones of the Los Azules Formation from the Cerro Viejo area (see Fig. B.2 E); the plant in the centre is about 60cm high. C) Interlayering of sandstones (dark) and mudstones (orange) of the La Cantera Formation D) Las Vacas Conglomerate. E) Outcrop of the Las Plantas Formation F) Mudstones and very fine sandstones of the La Chilca Formation at the Talacasto area (see Fig. B.2 E). G) Thin layered section of the Empozada Formation H) Mudstones of the Los Sombreros Formation (grey) containing a Cambrian olistolith (white rocks in the upper part of the section).

sample	Formation	rock type	latitude (S)	longitude (W)	letter in map
QMOTO1	Pavón	m sf-arenite	34° 38´ 15"	68° 35´ 25"	A
QMOTO2	Pavón	arenite	34° 38´ 15"	68° 35´ 25"	A
QCB1	Pavón	f arenite	34° 38´ 45"	68° 35´ 20"	A
QCB3	Pavón	f arenite	34° 38´ 45"	68° 35´ 20"	A
QCB6	Pavón	arenite	34° 38´ 45"	68° 35´ 20"	A
CT 1	Ponón Trehué	vf sf-arenite	35º 10´ 53"	68º 18´ 13"	B
CT 2	Ponón Trehué	vf sf-arenite	35º 10´ 53"	68º 18´ 13"	B
CT 3	Ponón Trehué	mudstone	35º 10´ 53"	68º 18´ 13"	B
CT 4	Ponón Trehué	vf sf-arenite	35º 10´ 53"	68º 18´ 13"	B
CT 5	Ponón Trehué	vf sf-arenite	35º 10´ 53"	68º 18´ 13"	B
CT 6	Ponón Trehué	mudstone	35º 10´ 53"	68º 18´ 13"	B
CT 7	Ponón Trehué	mudstone	35º 10´ 53"	68º 18´ 13"	B
CT 8	Ponón Trehué	mudstone	35º 10´ 53"	68º 18´ 13"	B
CT 9	Ponón Trehué	volcanic rock	35º 10´ 53"	68º 18´ 13"	B
VACAS0	Las Vacas	mudstone	29° 40´ 09"	68° 41´ 44"	C
VACAS1	Las Vacas	vf sf-arenite	29° 40´ 09"	68° 41´ 44"	C
VACAS3	Las Vacas	f sf-arenite	29° 40´ 09"	68° 41´ 44"	C
VACAS4	Las Vacas	mudstone	29° 40´ 09"	68° 41´ 44"	C
LV 5	Las Vacas	m sl-arenite	29° 45´ 08"	68° 37´ 55"	C
LV 7	Las Vacas	c sl-arenite	29° 45´ 08"	68° 37´ 55"	C
LV 8	Las Vacas	m sl-arenite	29° 45´ 08"	68° 37´ 55"	C
LV 9	Las Vacas	m sf-arenite	29° 45´ 08"	68° 37´ 55"	C
LV 10	Las Vacas	m sf-arenite	29° 45´ 08"	68° 37´ 55"	C
LV 11	Las Vacas	m sf-arenite	29° 45´ 08"	68° 37´ 55"	C
PLANT1	Las Plantas	arenite	29° 38´ 14"	68° 42´ 23"	C
PLANT2	Las Plantas	mudstone	29° 38´ 14"	68° 42´ 23"	C
LPT 1	Las Plantas - Trapiche	vf q-arenite	29° 45´ 32"	68° 39´ 38"	C
LPT 2	Las Plantas - Trapiche	m q-arenite	29° 45´ 32"	68° 39´ 38"	C
LPT 3	Las Plantas - Trapiche	m q-arenite	29° 45´ 32"	68° 39´ 38"	C
LPT 4	Las Plantas - Trapiche	m q-arenite	29° 45´ 32"	68° 39´ 38"	C
LPT 5	Las Plantas - Trapiche	m q-arenite	29° 45´ 32"	68° 39´ 38"	C
LPT 6	Las Plantas - Trapiche	mudstone	29° 45´ 32"	68° 39´ 38"	C
LPT 7	Las Plantas - Trapiche	mudstone	29° 45´ 32"	68° 39´ 38"	C
LPT 8	Las Plantas - Trapiche	m q-arenite	29° 45´ 32"	68° 39´ 38"	C
LPT 9	Las Plantas - Trapiche	mudstone	29° 45´ 32"	68° 39´ 38"	C
LPT 10	Las Plantas - Trapiche	mudstone	29° 45´ 32"	68° 39´ 38"	C
LPT 11	Las Plantas - Trapiche	m q-arenite	29° 45´ 32"	68° 39´ 38"	C
LPT 12	Las Plantas - Trapiche	m q-arenite	29° 45´ 30"	68° 39´ 34"	C
LPT 13	Las Plantas - Trapiche	f q-arenite	29° 45´ 30"	68° 39´ 34"	C
LPT 14	Las Plantas - Trapiche	m q-arenite	29° 45´ 30"	68° 39´ 34"	C
LPT 15	Las Plantas - Trapiche	f q-arenite	29° 45´ 30"	68° 39´ 34"	C
LPT 16	Las Plantas - Trapiche	m q-arenite	29° 45´ 30"	68° 39´ 34"	C
LPT 17	Las Plantas - Trapiche	mudstone	29° 45´ 30"	68° 39´ 34"	C
LPT 18	Las Plantas - Trapiche	mudstone	29° 45´ 30"	68° 39´ 34"	C
LPT 19	Las Plantas - Trapiche	mudstone	29° 45´ 30"	68° 39´ 34"	C
LPT 20	Las Plantas - Trapiche	vf conglomerate	29° 45´ 30"	68° 39´ 34"	C
LPT 21	Las Plantas - Trapiche	mudstone	29° 45´ 30"	68° 39´ 34"	C
LPT 22	Las Plantas - Trapiche	mudstone	29° 45´ 30"	68° 39´ 34"	C
LPT 23	Las Plantas - Trapiche	f q-arenite	29° 45´ 29"	68° 39´ 30"	C

Table 2: Location and rock-type (including mean size) of samples. Letters correspond to location in map (Figs. B.2 and B.3). vf: very fine; f: fine; m: medium; c: coarse; vc: very coarse; sf: subfeldspathic-; sl: sublithic-; q: quartz-. Classification of rocks adapted from Pettijohn *et al.* (1987).

sample	Formation	rock type	latitude (S)	longitude (W)	letter in map
LPT 24	Las Plantas - Trapiche	f q-arenite	29° 45´ 29"	68° 39´ 30"	C
LPT 25	Las Plantas - Trapiche	vf conglomerate	29° 45´ 29"	68° 39´ 30"	C
LPT 26	Las Plantas - Trapiche	vf conglomerate	29° 45´ 29"	68° 39´ 30"	C
GUAL1	Gualcamayo	claystone	29° 45´ 20"	68° 38´ 51"	C
020454	Gualcamayo	claystone	31° 12´ 30"	68° 29´ 12"	J
020455	Gualcamayo	claystone	31° 12´ 30"	68° 29´ 12"	J
G 5	Gualcamayo	claystone	29° 45´ 20"	68° 38´ 51"	C
G 6	Gualcamayo	claystone	29° 45´ 20"	68° 38´ 51"	C
G 7	Gualcamayo	claystone	29° 45´ 20"	68° 38´ 51"	C
G 8	Gualcamayo	claystone	29° 45´ 20"	68° 38´ 51"	C
G 9	Gualcamayo	claystone	29° 45´ 20"	68° 38´ 51"	C
G 10	Gualcamayo	claystone	29° 45´ 35"	68° 39´ 24"	C
G 11	Gualcamayo	claystone	29° 45´ 35"	68° 39´ 24"	C
G 12	Gualcamayo	claystone	29° 45´ 23"	68° 39´ 20"	C
020405	Los Azules	c siltstone	30° 11´ 04"	68° 35´ 05"	D
020406	Los Azules	claystone	30° 11´ 03"	68° 35´ 05"	D
020407	Los Azules	claystone	30° 11´ 03"	68° 35´ 05"	D
020408	Los Azules	c siltstone	30° 10´ 59"	68° 35´ 09"	D
020409	Los Azules	claystone	30° 10´ 59"	68° 35´ 09"	D
020411	Los Azules	claystone	30° 36´ 04"	68° 47´ 26"	G
020412	Los Azules	claystone	30° 36´ 04"	68° 47´ 26"	G
020413	Los Azules	claystone	30° 36´ 04"	68° 47´ 26"	G
020414	Los Azules	claystone	30° 36´ 03"	68° 47´ 31"	G
020418	Los Sombreros	mudstone	30° 13´ 00"	68° 58´ 18"	E
020419	Los Sombreros	vf sf-arenite	30° 13´ 00"	68° 58´ 18"	E
LRAT1	Los Sombreros	mudstone	31° 17´ 10"	69° 11´ 20"	K
LRAT2	Los Sombreros	vf sf-arenite	31° 17´ 10"	69° 11´ 20"	K
SOM 5	Los Sombreros	mudstone	30° 13´ 00"	68° 57´ 56"	E
SOM 6	Los Sombreros	mudstone	30° 13´ 00"	68° 57´ 56"	E
SOM 7	Los Sombreros	mudstone	30° 13´ 00"	68° 57´ 56"	E
SOM 8	Los Sombreros	mudstone	30° 13´ 00"	68° 57´ 56"	E
SOM 9	Los Sombreros	mudstone	30° 13´ 00"	68° 57´ 56"	E
YL 1	Yerba Loca	mudstone	30° 13´ 08"	68° 58´ 27"	E
YL 2	Yerba Loca	mudstone	30° 13´ 08"	68° 58´ 54"	E
YL 3	Yerba Loca	m sf-wacke	30° 13´ 09"	68° 59´ 44"	E
YL 4	Yerba Loca	f sf-arenite	30° 35´ 14"	69° 06´ 24"	H
YL 5	Yerba Loca	carbonate-arenite	30° 38´ 40"	69° 04´ 20"	H
YL 6	Yerba Loca	vf sf-wacke	30° 13´ 04"	68° 59´ 28"	E
YL 408	Yerba Loca	volcanic rock	30° 12´ 20"	69° 03´ 57"	F
YL 411	Yerba Loca	m sl-wacke	30° 12´ 20"	69° 03´ 57"	F
YL 413	Yerba Loca	volcanic rock	30° 12´ 20"	69° 03´ 57"	F
YL 417	Yerba Loca	volcanic rock	30° 12´ 20"	69° 03´ 57"	F
YL 418	Yerba Loca	volcanic rock	30° 12´ 17"	69° 03´ 29"	F
YL 419	Yerba Loca	volcanic rock	30° 12´ 17"	69° 03´ 29"	F
YL 420	Yerba Loca	volcanic rock	30° 12´ 17"	69° 03´ 29"	F
YL 421	Yerba Loca	volcanic rock	30° 12´ 17"	69° 03´ 29"	F
YL 422	Yerba Loca	volcanic rock	30° 12´ 17"	69° 03´ 29"	F
YL 423	Yerba Loca	volcanic rock	30° 12´ 17"	69° 03´ 29"	F
YL 426	Yerba Loca	m sf-wacke	30° 12´ 17"	69° 03´ 29"	F

Table 2: Location and rock-type (including mean size) of samples. Letters correspond to location in map (Figs. B.2 and B.3). vf: very fine; f: fine; m: medium; c: coarse; vc: very coarse; sf: subfeldspathic-; sl: sublithic-; q: quartz-. Classification of rocks adapted from Pettijohn *et al.*, 1987.

sample	Formation	rock type	latitude (S)	longitude (W)	letter in map
YL 431	Yerba Loca	f sf-arenite	30° 12´ 17"	69° 03´ 29"	F
YL 432	Yerba Loca	m sf-arenite	30° 12´ 24"	69° 03´ 13"	F
YL 433	Yerba Loca	vf sf-wacke	30° 12´ 24"	69° 03´ 13"	F
YL 434/1	Yerba Loca	m sf-arenite	30° 12´ 24"	69° 03´ 13"	F
YL 439	Yerba Loca	m sf-arenite	30° 12´ 24"	69° 03´ 13"	F
YL 440	Yerba Loca	m sl-arenite	30° 12´ 24"	69° 03´ 13"	F
YL 441	Yerba Loca	mudstone	30° 12´ 24"	69° 03´ 13"	F
YL 442	Yerba Loca	m sf-wacke	30° 12´ 24"	69° 03´ 13"	F
YL 445	Yerba Loca	c sf-arenite	30° 12´ 24"	69° 03´ 13"	F
YL 446	Yerba Loca	m sf-arenite	30° 12´ 24"	69° 03´ 13"	F
YL 448	Yerba Loca	m sf-arenite	30° 12´ 24"	69° 03´ 13"	F
YL 449	Yerba Loca	mudstone	30° 12´ 24"	69° 03´ 13"	F
YL 450	Yerba Loca	mudstone	30° 12´ 24"	69° 03´ 13"	F
YL 451	Yerba Loca	mudstone	30° 12´ 24"	69° 03´ 13"	F
YL 452	Yerba Loca	c sf-arenite	30° 12´ 24"	69° 03´ 13"	F
YL 454	Yerba Loca	m sf-wacke	30° 12´ 24"	69° 03´ 13"	F
YL 455	Yerba Loca	volcanic rock	30° 13´ 04"	68° 59´ 44"	E
020401	La Chilca	mudstone	31° 01´ 30"	68° 44´ 58"	I
020402	La Chilca	vf sf-arenite	31° 01´ 30"	68° 44´ 58"	I
020403	La Chilca	vf sf-arenite	31° 01´ 30"	68° 44´ 58"	I
020404	La Chilca	vf sf-arenite	31° 01´ 30"	68° 44´ 58"	I
020410	La Chilca	f q-arenite	30° 36´ 14"	68° 47´ 34"	G
020415	La Chilca	vf q-arenite	30° 36´ 19"	68° 47´ 37"	G
020416	La Chilca	vf q-arenite	30° 36´ 19"	68° 47´ 37"	G
020420	Sierra de la Invernada	limestone	30° 41´ 47"	69° 01´ 14"	H
020421	Sierra de la Invernada	mudstone	30° 41´ 47"	69° 01´ 14"	H
020422	Sierra de la Invernada	m sf-wacke	30° 42´ 39"	68° 59´ 37"	H
020423	Sierra de la Invernada	mudstone	30° 42´ 39"	68° 59´ 37"	H
020424	Sierra de la Invernada	f sf-wacke	30° 42´ 39"	68° 59´ 37"	H
020425	Sierra de la Invernada	f sf-wacke	30° 42´ 39"	68° 59´ 37"	H
020426	Sierra de la Invernada	m sf-wacke	30° 42´ 39"	68° 59´ 37"	H
020427	Sierra de la Invernada	m sf-arenite	30° 42´ 39"	68° 59´ 37"	H
020428	Sierra de la Invernada	f sf-arenite	30° 42´ 38"	68° 59´ 41"	H
020429	Sierra de la Invernada	m sf-arenite	30° 42´ 38"	68° 59´ 41"	H
020430	Sierra de la Invernada	f sf-arenite	30° 42´ 38"	68° 59´ 41"	H
020431	Sierra de la Invernada	mudstone	30° 42´ 38"	68° 59´ 41"	H
020432	Sierra de la Invernada	f sf-arenite	30° 42´ 38"	68° 59´ 41"	H
020433	Sierra de la Invernada	mudstone	30° 42´ 38"	68° 59´ 41"	H
SI 1	Sierra de la Invernada	m sf-wacke	31° 16´ 13"	69° 11´ 39"	K
020436	Don Braulio	mudstone	31° 12´ 58"	68° 29´ 14"	J
020437	Don Braulio	f q-arenite	31° 12´ 58"	68° 29´ 14"	J
020438	Don Braulio	f sf-arenite	31° 12´ 50"	68° 29´ 10"	J
020439	Don Braulio	mudstone	31° 12´ 50"	68° 29´ 10"	J
020440	Don Braulio	m sf-arenite	31° 12´ 50"	68° 29´ 10"	J
DB 1	Don Braulio	m sf-arenite	31° 12´ 50"	68° 29´ 10"	J
020441	La Cantera	vf sf-arenite	31° 12´ 50"	68° 29´ 10"	J
020442	La Cantera	mudstone	31° 12´ 50"	68° 29´ 10"	J
020443	La Cantera	m arenite	31° 12´ 50"	68° 29´ 10"	J
020444	La Cantera	mudstone	31° 12´ 50"	68° 29´ 10"	J

Table B.2: Location and rock-type (including mean size) of samples. Letters correspond to location in map (Figs. B.2 and B.3). vf: very fine; f: fine; m: medium; c: coarse; vc: very coarse; sf: subfeldspathic-; sl: sublithic-; q: quartz-. Classification of rocks adapted from Pettijohn *et al.*, 1987.

sample	Formation	rock type	latitude (S)	longitude (W)	letter in map
020445	La Cantera	f sf-arenite	31° 12′ 50"	68° 29′ 10"	J
020446	La Cantera	mudstone	31° 12′ 50"	68° 29′ 10"	J
020447	La Cantera	m sf-arenite	31° 12′ 47"	68° 29′ 13"	J
020448	La Cantera	mudstone	31° 12′ 47"	68° 29′ 13"	J
020449	La Cantera	m sf-arenite	31° 12′ 47"	68° 29′ 13"	J
020450	La Cantera	mudstone	31° 12′ 47"	68° 29′ 13"	J
020451	La Cantera	m sf-arenite	31° 12′ 47"	68° 29′ 13"	J
020452	La Cantera	mudstone	31° 12′ 47"	68° 29′ 13"	J
020453	La Cantera	m sf-arenite	31° 12′ 47"	68° 29′ 13"	J
020456	Alcaparrosa	f sf-arenite	31° 15′ 14"	69° 19′ 41"	K
020457	Alcaparrosa	mudstone	31° 15′ 14"	69° 19′ 41"	K
020458	Alcaparrosa	vf sf-arenite	31° 15′ 14"	69° 19′ 41"	K
020459	Alcaparrosa	mudstone	31° 36′ 01"	69° 21′ 00"	L
020460	Alcaparrosa	m sf-arenite	31° 36′ 01"	69° 21′ 00"	L
020461	Alcaparrosa	mudstone	31° 36′ 01"	69° 21′ 00"	L
020462	Alcaparrosa	f sf-wacke	31° 36′ 01"	69° 21′ 00"	L
A 1	Alcaparrosa	mudstone	31° 14′ 54"	69° 20′ 17"	K
A 2	Alcaparrosa	mudstone	31° 14′ 54"	69° 20′ 17"	K
A 3	Alcaparrosa	f sf-wacke	31° 14′ 45"	69° 21′ 44"	K
A 4	Alcaparrosa	m sf-arenite	31° 14′ 45"	69° 21′ 44"	K
020463	Portezuelo del Tontal	vf sf-wacke	31° 35′ 54"	69° 14′ 03"	M
020464	Portezuelo del Tontal	mudstone	31° 35′ 54"	69° 14′ 03"	M
020465	Portezuelo del Tontal	f sf-wacke	31° 35′ 05"	69° 13′ 37"	M
020466	Portezuelo del Tontal	vc sf-arenite	31° 31′ 24"	69° 12′ 04"	M
020467	Portezuelo del Tontal	m sf-arenite	31° 31′ 24"	69° 12′ 04"	M
020468	Portezuelo del Tontal	f sf-arenite	31° 31′ 24"	69° 12′ 04"	M
020469	Portezuelo del Tontal	m sf-wacke	31° 31′ 24"	69° 12′ 04"	M
020470	Portezuelo del Tontal	f sf-arenite	31° 31′ 24"	69° 12′ 04"	M
PDT 1	Portezuelo del Tontal	vf sf-arenite	31° 15′ 09"	69° 12′ 22"	K
PDT 2	Portezuelo del Tontal	vf sf-wacke	31° 15′ 13"	69° 13′ 53"	K
PDT 3	Portezuelo del Tontal	mudstone	31° 15′ 13"	69° 13′ 53"	K
E1	Empozada	vf sf-arenite	32° 52′ 22"	69° 00′ 54"	N
E2	Empozada	mudstone	32° 52′ 22"	69° 00′ 54"	N
E3	Empozada	vf sf-arenite	32° 52′ 22"	69° 00′ 54"	N
E4	Empozada	mudstone	32° 52′ 22"	69° 00′ 54"	N
E5	Empozada	mudstone	32° 52′ 22"	69° 00′ 54"	N
E6	Empozada	m sf-arenite	32° 52′ 26"	69° 00′ 50"	N
E7	Empozada	mudstone	32° 52′ 26"	69° 00′ 50"	N
E8	Empozada	m sf-arenite	32° 52′ 28"	69° 00′ 44"	N
E9	Empozada	c sf-arenite	32° 52′ 28"	69° 00′ 44"	N
E10	Empozada	c sf-arenite	32° 52′ 28"	69° 00′ 44"	N

Table B.2: Location and rock-type (including mean size) of samples. Letters correspond to location in map (Figs. B.2 and B.3). vf: very fine; f: fine; m: medium; c: coarse; vc: very coarse; sf: subfeldspathic-; sl: sublithic-; q: quartz-. Classification of rocks adapted from Pettijohn *et al.*, 1987.

APPENDIX C

PART 1: DETAILED PETROGRAPHIC AND GEOCHEMICAL DESCRIPTIONS

C.1 Gualcamayo Formation

C.1.1 Petrography

As the Gualcamayo Formation is a claystone-dominated sequence, its main mineralogical composition was determined by XRD (X-ray diffraction) and SEM (scanning electron microscope) techniques. Rocks from this unit are composed of quartz, plagioclase, muscovite, illite, scarce microcline and very rare dolomite, kaolinite, chlorite and biotite (Table 3).

C.1.2 Geochemistry

Mudstones from the Gualcamayo Formation have a major elements distribution similar to post-Archaean Australian Shales (PAAS; Taylor and McLennan, 1985; see Table 1), except for two samples that show CaO enrichment with values up to 23.2% and consequently SiO_2 concentrations as low as 25.8%. The high MgO concentration (about 8%) of these two samples is also in agreement with XRD data, which indicate dolomite. This unit shows variable Cs concentrations ranging from 7ppm to 9ppm, and the K/Cs ratio ranges from 3063 to 5420.

The CIA (Chemical Index of Alteration) values for mudstones range from 65 to 72 (see Table 1 in Appendix A), indicating moderate to strong weathering. Samples follow a general weathering trend, although one sample (G8) could be showing some potassium metasomatism (Fedo *et al.*, 1995). XRD data of this sample show that quartz and muscovite are the main constituents and differ from the rest of the samples, as it does not contain any plagioclase.

The mudstones from the Gualcamayo Formation cluster well below the 3.8 Th/U limit. The Th concentration of all these samples is similar to values for the upper continental crust (UCC; McLennan *et al.*, 2006). The low Th/U ratio is due to enrichment of the U concentration of this unit to values up to 8.6ppm (see Table 1 in Appendix A).

In the Th/Sc versus Zr/Sc diagram it is evident that the Gualcamayo Formation received a major input from an average upper crust composition and that the recycling was not important in this unit. The La/Th ratios for this unit are between 2.9 and 3.9, indicating a provenance from a source with an acid arc composition.

The Cr/V ratio of the Gualcamayo Formation is between 0.31 and 0.64 and the Cr/Th ratio is 8.1 on average, indicating no mafic input. The Y/Ni ratio varies between 0.60 and 2.31. However, three samples (G7, G8 and G9) have Cr concentrations of 110ppm that represent an enrichment compared with the 83ppm found in the UCC (McLennan *et al.*, 2006). These samples are also enriched in Sc (with values about 17.65ppm) and in V (with values between 175ppm and 221ppm) compared with the UCC (Sc=13.6ppm; V=107ppm; McLennan *et al.*, 2006). These characteristics are accompanied by low Th/Sc ratios (about 0.57), low Zr/Sc ratios (about 8.7), high Cr/Th ratios (11) and Y/Ni ratios of 0.60, 0.68 and 0.61 respectively. The Sc/Th ratio ranges from 0.77 to 1.77 (Table 2).

The chondrite normalized rare earth elements (REE) patterns for mudstones of the Gualcamayo Formation (Fig. C.8) show a moderately enriched light REE (LREE) pattern (La_N/Yb_N about 8.13 on average), a negative Eu anomaly (Eu_N/Eu^* about 0.53 on average) and a rather flat heavy REE (Tb_N/Yb_N of 1.22 on average). All these features match with the PAAS (Nance and Taylor, 1976) pattern, which is considered in turn to reflect the average composition of the upper crust.

Samples from the Gualcamayo Formation plot within the fields of continental island arc and active continental margin settings according to Bhatia and Crook (1986).

C.2 Los Azules Formation

C.2.1 Petrography

Because the Los Azules Formation is a claystone-dominated sequence, their main mineralogical components were determined by XRD and SEM techniques. Rocks from this unit are composed of quartz, plagioclase, muscovite, illite, scarce microcline, calcite, kaolinite and chlorite (Table 3).

C.2.2 Geochemistry

Mudstones from the Los Azules Formation have a major elements distribution similar to the PAAS (Taylor and McLennan, 1985; see Table 1), except for two samples that show CaO enrichment with values up to 33.4% and consequently SiO_2 concentrations as low as 33%. The low MgO concentration of these two samples is also in agreement with XRD data that indicate calcite. The CIA value ranges from 66 to 75 (see Table 1 in Appendix A), indicating moderate weathering. Samples follow a general weathering trend (Fedo *et al.*, 1995). This unit shows variable Cs concentrations ranging from 3ppm to 12ppm, and the K/Cs ratios range from 2895 to 6815.

The mudstones of the Los Azules Formation cluster well below the 3.8 Th/U limit. The Th concentration of all these samples ranges from values similar to the UCC to deplete compared with the UCC. The low Th/U ratio is due to enrichment of the U concentration of this unit to values up to 7.3ppm (see Table 1 in Appendix A). The low Th abundance of certain samples seems to be link to high SiO_2 or CaO concentrations.

In the Th/Sc versus Zr/Sc diagram, it is evident that the Los Azules Formation received a major input from an average upper crust composition and from a slightly less evolved component. The recycling was not important in this unit. The La/Th ratios for this unit are between 1.9 and 5.9, indicating a source with an acid arc composition.

The Cr/V ratio for Los Azules Formation is between 0.35 and 0.93, while the Cr/Th ratio is 7.9 and the Y/Ni ratio is between 0.37 and 3.1 on average indicating no mafic input. However, samples 020409, 020412 and 020413 show high Cr (about 100ppm) and V (between 107ppm and 173ppm) concentrations along with low Th/Sc and Zr/Sc ratios (between 0.59 and 0.7 for the first and between 5 and 11 for the latter) allowing the estimation of the influence of a depleted source. The Sc/Th ratio ranges from 0.89 to 1.69 (Table 2).

The chondrite normalized rare earth elements patterns for the Los Azules Formation (Fig. C.9) show a moderately enriched light REE pattern (La_N/Yb_N of about 7.91 on average), a negative Eu anomaly (Eu_N/Eu^* of about 0.57 on average) and a rather flat heavy REE distribution (Tb_N/Yb_N of 1.50 on average). All these features match with the PAAS pattern.

Using the La-Th-Sc and Th-Sc-Zr/10 discriminatory plots after Bhatia and Crook (1986) siltstones and claystones from the Los Azules Formation could be related to an active continental margin or a continental island arc setting.

C.3 La Cantera Formation

C.3.1 Petrography

La Cantera Formation is composed of arenites with low matrix contents (5% to 10%), and carbonate-cemented arenites (10% to 20% cement contents). Arenites are moderately to poorly sorted and their detrital components are subrounded to subangular, but also ranging to rounded in certain samples. Grain sizes range from very fine to coarse sand, but silt sizes are also represented. Main minerals are monocrystalline quartz with normal extinction while undulose grains are scarce. Apart from fluid inclusions, apatite, muscovite, zircon and booklets of kaolinite are included in quartz. Pressure dissolution effects could be observed on quartz boundaries. Graphic quartz is present as a coarse detrital grain. Polycrystalline undulose quartz is less frequent than monocrystalline quartz, although it is normally present in higher quantities compared with all the lithoclast-types. Plagioclase always shows polysynthetic twinning and no alteration. K-feldspar (abundant microcline and scarce anorthoclase) is either partially altered to clay minerals or totally replaced by chlorite. Plagioclase is less abundant than K-feldspar. Different twin-types were observed: polysynthetic, Carlsbad, grid and perthitic. Muscovite, biotite and chlorite are present as detrital lamellae. Accessory minerals are in order of abundance opaque (including hematite), zircon, tourmaline and very scarce detrital epidote. The matrix is composed of white mica and quartz. The cement is composed predominantly of calcite, although dolomite is also a component (Table 3). Sedimentary lithoclasts are mudstones, siltstones, chert, very fine-grained sandstones and carbonates, in order of abundance. The volcanic lithoclasts are mainly very fine volcanic rocks and less common from coarser rocks (altered plagioclase within a pilotaxitic texture). Within the metamorphic lithoclasts, the commonest are derived from low-grade rocks like phyllites, followed by quartz-mica schists and very scarce gneisses. The lithoclast population is dominated by sedimentary lithoclasts. The order of abundance regarding lithoclast type is followed by volcanic lithoclasts and being the metamorphic lithoclasts the less abundant.

C.3.2 Geochemistry

Samples from the La Cantera Formation have a variable major elements distribution, with SiO_2 concentrations ranging from 53.2% to 77.3%, Al_2O_3 vary from 6% to 18.8%, Fe_2O_3 ranges from 3.1% to 8.5%, CaO from 0.5% to 19%, K_2O is between 1% and 4.7% and Na_2O is between 1.6% and 2.8%. Most of the sandstones have high CaO concentrations, thus only two samples could be used to calculate the CIA value. The CIA value ranges from 58 to 69 indicating a moderately weathering. They follow a general weathering trend, particularly if sample 020447 is discarded due to its high SiO_2 concentration. This unit shows variable Cs concentrations ranging from 1ppm to 9ppm, and the K/Cs ratios range from 4086 to 10526.

Mudstones from the La Cantera Formation show Th/U values between 3.5 and 4, which is normal for rocks derived from the UCC. The sandstones instead are more scattered because their Th concentrations (between 5.5ppm and 10ppm) are depleted compared with the UCC. The U concentrations vary from values similar to lower than the UCC. The Th/U ratio for the sandstones ranges from 2.7 to 6. Some sandstones show the loss of U due to weathering and/or recycling.

In the Th/Sc versus Zr/Sc diagram, it is evident a separation of the samples according to grain size, since all the mudstones have a Th/Sc ratio below 0.61 and Zr/Sc ratio below 12.7 indicating no recycling and a depleted source. The sandstone

020444 shows the same characteristics. On the other hand, the other sandstones of the La Cantera Formation have higher Th/Sc and Zr/Sc ratios, indicating more recycling (although not very important) and an input from an average upper continental crust composition. The La/Th ratios for this unit are between 3 and 3.9, indicating a source with an acid arc composition. Only one sample has a La/Th ratio of 6.2 that coincides with very low Th concentration for this sample compared with the UCC (Table 1).

The Cr/V ratio for this unit is between 0.99 and 1.60 while the Cr/Th ratio is 12 on average. The Y/Ni ratios vary from 0.38 to 2.04. The sandstone 020444 shows high Sc (19.4ppm), Cr (120ppm) and V (111ppm), which along with low Th/Sc (0.52) and Zr/Sc (8.6) ratios indicate the influence of a depleted source. The Sc/Th ratio ranges from 1.23 to 1.94 (Table 2).

The chondrite normalized rare earth elements patterns for mudstones and sandstones of the La Cantera Formation (Fig. C.10) show a moderately enriched LREE pattern (La_N/Yb_N about 7.03 on average), a negative Eu anomaly (Eu_N/Eu^* about 0.59 on average) and a flat HREE (Tb_N/Yb_N of 1.32 on average). All these features match with the PAAS pattern. La_N/Yb_N ratios slightly lower than PAAS might however, indicate the provenance from a slightly less evolved source than the one that feed the PAAS.

Samples from the La Cantera Formation plot within the field of continental island arc setting in the La-Th-Sc and Th-Sc-Zr/10 discriminatory plots after Bhatia and Crook (1986). However, some deviations towards the Zr apex are consistent with recycling and with the depletion of Th observable for the sandstones. In the Ti/Zr versus La/Sc discriminatory plot (Bhatia and Crook, 1986), the same samples plot either within the active continental margin or completely out of any field. In a broad sense, this unit could be link to an active margin.

C.4 Las Vacas Formation

C.4.1 Petrography

Samples from the Las Vacas Formation are arenites with low matrix contents (up to 15%), and carbonate-cemented arenites (10% to 20% cement concentrations). Arenites are moderately to poorly sorted and their detrital components are subangular to subrounded and with low sphericity. Grain sizes range from very fine to coarse sand, but silt sizes are also represented. Main minerals are monocrystalline quartz with normal extinction while undulose grains are scarce. Apart from fluid inclusions, muscovite and booklets of kaolinite are included in quartz. Polycrystalline quartz is also present and very scarce graphic quartz was observed. Plagioclase always shows polysynthetic twinning and no alteration. K-feldspar (abundant microcline and scarce anorthoclase) is partially altered to clay minerals. Plagioclase is more abundant than K-feldspar. Muscovite and biotite are present as detrital lamellae. Accessory minerals are in order of abundance opaque (including hematite), zircon, tourmaline and very scarce detrital epidote. The matrix is composed of white mica and quartz. The cement is composed predominantly of calcite, although dolomite and ankerite are also a component (Table 3). Sedimentary lithoclasts are derived from mudstones, siltstones, chert, very fine-grained sandstones and carbonates, in order of abundance. The volcanic lithoclasts are mainly from very fine volcanic rocks and less common from coarser rocks (altered plagioclase within a pilotaxitic texture). Within the metamorphic lithoclasts, the commonest are derived from low-grade rocks like phyllites, followed by quartz-mica schists and very scarce gneisses. The lithoclast population is dominated by sedimentary lithoclasts. The order of abundance regarding lithoclast types is followed by metamorphic lithoclasts that predominate over the volcanic lithoclasts.

C.4.2 Geochemistry

Samples from the Las Vacas Formation have a variable major elements distribution, with SiO_2 concentrations ranging from 42% to 76%, Al_2O_3 varies from 5.2% to 10%, Fe_2O_3 ranges from 2.7% to 6.7%, CaO from 1% to 22.4%, K_2O is between 1.1% and 2.5% and Na_2O is between 0.5% and 2.8%. Most of the samples have high CaO concentrations, thus only one sample could be used to calculate the CIA value. A CIA value of 59 indicates a slight weathering (Table 1). This unit shows Cs concentrations ranging from 1ppm to 5ppm, and the K/Cs ratios ranges from 4124 to 10210.

The Th concentration of all the samples from the Las Vacas Formation is depleted compared with the UCC, showing values as low as 4.4ppm. The U concentration is also depleted compared with UCC and have values between 1.1ppm and 2ppm. A link between low Th concentrations and high CaO concentrations is evident for several samples of different units of the Precordillera terrane. Although the Th/U ratios might be affected by the high CaO concentration, a loss of U due to weathering and/or recycling seems evident.

The relationship between the Th/Sc and the Zr/Sc ratios of the Las Vacas Formation shows a cluster of data indicating no recycling and a provenance from a source slightly less evolved than the typical UCC composition. Th/Sc ratios of three samples are as low as 0.41 indicating the presence of a less evolved source, although Sc abundances are similar to upper continental crustal compositions and Th is diminished (McLennan *et al.*, 2006). The La/Th ratios for this unit are between 3.2 and 4.7.

The Cr/V ratio for this unit is between 0.7 and 0.9, and the Cr/Th ratio of 11.1 on average indicates no clear mafic input. Furthermore, Sc, Cr and V abundances are similar to deplete compared with UCC values. The Y/Ni ratio varies between 0.46 and 1.23. The Sc/Th ratio ranges from 1.5 to 2.38 (Table 2).

The chondrite normalized rare earth elements patterns for mudstones and sandstones of the Las Vacas Formation (Fig. C.11) show a moderately enriched LREE pattern (La_N/Yb_N of about 7.58 on average), a negative Eu anomaly (Eu_N/Eu^* of about 0.66 on average) and a rather flat HREE (Tb_N/Yb_N of 1.63 on average). All these features match with the PAAS pattern. However, slight deviations (La_N/Yb_N lower than PAAS, Eu_N/Eu^* values up to 0.7 as well as a less depleted HREE pattern) of these parameters compared with PAAS and UCC compositions imply the input from a less differentiated source.

Using the La-Th-Sc, Th-Sc-Zr/10 and Ti/Zr versus La/Sc discriminatory plots after Bhatia and Crook (1986) samples from the Las Vacas Formation could be related to an active margin tectonic setting.

C.5 Las Plantas and Trapiche Formations

C.5.1 Petrography

Las Plantas and Trapiche Formations are composed of arenites with low matrix contents (5% to 10%), and carbonate-cemented arenites (10% to 20% cement concentrations). Arenites are moderately to poorly sorted and their detrital components are subrounded to subangular. Detrital high-sphericity grains form approximately the half of the detrital population. Grain sizes range from very fine to coarse sand. Main minerals are monocrystalline non-undulose and undulose quartz that are present approximately in equal proportions. Apart from fluid inclusions, apatite, muscovite, zircon and booklets of kaolinite are included in quartz. Warped monocrystalline quartz grains were also observed as well as quartz-overgrowths. Plagioclase always shows polysynthetic twinning and no alteration, but partial replacement by calcite could be observed. K-feldspar (abundant microcline and scarce anorthoclase) is partially altered to clay minerals. Plagioclase is less abundant than K-feldspar. Different twin-types were observed: polysynthetic, Carlsbad, grid and perthitic. Muscovite, biotite and chlorite are present as detrital lamellae. Accessory minerals are in order of abundance opaque (including hematite), zircon, tourmaline and very scarce detrital epidote and titanite. The matrix is composed of white mica and quartz. The cement is composed predominantly of calcite, although dolomite and ankerite are also a component (Table 3). Veins of calcite and hematite are a feature present in almost all samples. Sedimentary lithoclasts are chert, siltstones, mudstones, very fine-grained sandstones and carbonates, in order of abundance. The volcanic lithoclasts are mainly very fine volcanic rocks and less common coarser rocks (altered plagioclase within a pilotaxitic texture). Within the metamorphic lithoclasts, the commonest are derived from low-grade rocks like phyllites, followed by quartz-mica schists and very scarce gneisses. The lithoclast population is dominated by sedimentary lithoclasts, followed by volcanic lithoclasts and being the metamorphic lithoclasts the less abundant.

The Las Plantas and the Trapiche Formations also show quartz-arenites with neither cement nor matrix. This arenites have detrital components ranging from fine to medium in size, well sorted and subangular to well rounded. Framework minerals show both low and high sphericity. Monocrystalline undulose quartz is the main constituent. Warped grains and overgrowths are common, as well as sutured contact between grains. Fluid inclusions within quartz form trends and mineral inclusions are zircon, muscovite and booklets of kaolinite. Polycrystalline quartz is very scarce. K-feldspar is more abundant than plagioclase and is represented by microcline and less abundant anorthoclase. Microcline shows the grid twinning and perthitic texture, and is partially altered to clay minerals. Plagioclase is normally not altered. Zircon, tourmaline and opaque minerals represent the heavy minerals fraction. Lithoclasts are represented almost exclusively by chert, although siltstone fragments were observed as well.

C.5.2 Geochemistry

Mudstones from the Las Plantas and Trapiche Formations have SiO_2 concentrations ranging from 60% to 84.6%. Al_2O_3 concentrations vary strongly from 4.2% to 16%, Fe_2O_3 ranges from 2.9% to 7.9%, CaO from 0.1% to 6.6%, K_2O is between 0.2% and 3.6% and Na_2O is between 1.1% and 2.3%. Sandstones have a major elements distribution showing SiO_2 concentrations ranging from 67% to 95%, Al_2O_3 concentrations vary from 0.5% to 11.7%, Fe_2O_3 ranges from 0.2% to 6%, CaO from 0.3% to 14.6%, K_2O is between 0.1% and 2.1% and Na_2O is between 0.3% and 2.2%. The CIA values for mudstones range between 57 and 72 (see Table 1 in Appendix A), indicating moderately weathering. The lowest CIA values of 57 and 62 are apparent and due to a high SiO_2 concentration and therefore low Al_2O_3 concentration. Excluding these two samples, the rest of the mudstones follow a normal weathering trend (Fedo *et al.*, 1995). Although several sandstones were studied, it was not possible to calculate their CIA values since they are either carbonate cemented or quartz-rich arenites. This unit shows Cs concentrations ranging from 1ppm to 8ppm, and the K/Cs ratios range from 1685 to 5863.

Compared with the UCC (Table 1) values for Th (10.7ppm) and U (2.8ppm), the Th concentration of mudstones from the Las Plantas and Trapiche Formations varies from slightly enriched (with values up to 13ppm) to very depleted (with values as low as 3ppm). The U concentrations also vary from depleted (0.8ppm) to enriched

(3.9ppm). The Th/U ratios range from 3 to 4.8. Sandstones instead are greatly depleted in Th (with concentrations ranging from 0.6ppm to 2.7ppm, with two exceptional values of 7ppm and 10ppm) and in U. The Th/U ratios are also low.

Analyzing the relationship between the Th/Sc and Zr/Sc ratios it is evident that samples from the Las Plantas and Trapiche Formations could be subdivided into two groups. One group do not show any recycling and reflect an input from the UCC while the second group show an important process of recycling (also shown by their high SiO_2 concentration) although the source was of about the same composition. It is noteworthy that samples from this second group do not follow a normal recycling trend, since the more recycled samples show lower Th/Sc ratios than the less recycled ones. The La/Th ratio is between 3.4 and 4.2 for mudstones and between 3 and 10 for sandstones.

The Cr/V ratio is between 0.79 and 1.29, whereas the Cr/Th ratio ranges from 7 to 9.2 for mudstones. Compared with UCC concentrations Sc is generally enriched in the mudstones, while Cr and V are enriched in samples PLANT2 and LPT19, but sample LPT17 is enriched in Cr but the V concentration is the same as the UCC. The Cr/V ratio for sandstones is between 0.86 and 5.8 and the Cr/Th ratio ranges from 7.7 to 48.3. Compared with UCC concentrations Sc is enriched only in one sandstone but is depleted in the others (with values from 1.2ppm to 7.7ppm). Cr and V are depleted. The Y/Ni ratio varies between 0.03 and 2.68. The Sc/Th ratio ranges from 1.08 to 2.17 (Table 2).

The chondrite normalized rare earth elements patterns for mudstones (Fig. C.12) and sandstones (Fig. C.13) of the Las Plantas and Trapiche Formations show a moderately enriched LREE pattern (La_N/Yb_N of 6.7 on average), a negative Eu anomaly (Eu_N/Eu^* of 0.53 on average) and a rather flat HREE (Tb_N/Yb_N of 1.35 on average). All these features match with the PAAS pattern. However, two mudstones and some sandstones show a low sum of REE, low La_N/Yb_N ratios but at the same time, their very low abundances of transition trace elements (Sc, Cr, and V) inhibit to assume a depleted rock as a source. Instead, these features are clearly related to dilution due to high SiO_2 (samples LPT21, LPT22, LPT14 and LPT16) or CaO concentrations (LPT3).

If these samples are removed then the La_N/Yb_N, Eu_N/Eu^* and Tb_N/Yb_N ratios will average 7.4, 0.55 and 1.24 respectively, which is typical for an UCC composition.

Using the La-Th-Sc, Th-Sc-Zr/10 and La/Sc versus Ti/Zr discriminatory plots after Bhatia and Crook (1986), samples from the Las Plantas and Trapiche Formations plot within the field of active margin settings. Some samples however, plot either towards the La or Zr apexes or towards the passive margin field. When analyzing the absolute values (see Table 1 in Appendix A), no enrichment in La is observed, but instead an important depletion of Sc and Th. The same samples show instead high Zr absolute values.

C.6 Don Braulio Formation

C.6.1 Petrography

Petrographical studies shown that the Don Braulio Formation is composed of calcite-cemented quartz-arenites, with rounded to subrounded, moderately sorted and low sphericity detrital components. The sizes ranges from medium to fine grained. The main framework mineral is quartz, which only rarely has undulose extinction, but normally contains fluid inclusions and less commonly mineral inclusions such as muscovite and booklets of kaolinite. Quartz does not show overgrowths. Occasionally, well rounded and high spherical grains are present. Unaltered plagioclase is more frequent than K-feldspar, being the latter normally altered to sericite or chlorite, or replaced by calcite. Lithic fragments are mainly sedimentary and derived from chert, siltstones and mudstones (in order of abundance). Less common are metamorphic lithoclasts, from quartz-rich schists. Polycrystalline quartz is also present but scarce. Matrix, when present, is less than 10% and composed of white mica and chlorite (Table 3). Epidote is detrital and very scarce. Hematite and other opaque minerals are also present.

C.6.2 Geochemistry

Samples from the Don Braulio Formation have SiO_2 concentrations ranging from 59.1% to 77.42%. Al_2O_3 concentrations vary strongly from 3.3% to 18.4%, Fe_2O_3 ranges from 0.52% to 7.94%, CaO from 0.21% to 12.26%, K_2O is between 0.1% and 4.6% and Na_2O is between 0.22% and 2.16%. Most of the samples from the Don Braulio Formation are CaO-rich. The latter is associated with the carbonate cement of sandstones. Due to the high CaO concentrations the CIA could be calculated for three samples only, showing values between 61 and 71. This unit shows Cs concentrations ranging from 2ppm to 7ppm, and the K/Cs ratios range from 4077 to 5413.

The Th and U concentrations of the mudstones are similar to slightly enriched compared with UCC values (Table 1). The Th/U ratios are typical for rocks derived from the UCC but some samples show U loss due to weathering and/or recycling. Sandstones instead have depleted Th and U concentrations compared with UCC and the Th/U ratios are between 2.7 and 3.8.

Regarding the Zr/Sc and the Th/Sc ratios, samples from the Don Braulio Formation could be subdivided into two groups. One group does not show any recycling while the second group shows processes of recycling. All the samples show a provenance from an upper continental crust composition and a subordinate mafic component. The La/Th ratio ranges from 3.1 to 5.8.

The Cr/V ratio for this unit is between 0.63 and 0.92 for mudstones and 0.56 to 6.2 for sandstones. The sample with the highest Cr/V ratio (sample DB1) has the lowest Sc and V abundances (1.6ppm and 10ppm respectively). Since the chemical composition of this unit is strongly affected by the high SiO_2 and CaO concentrations, caution in its geochemical interpretation is needed, particularly when considering absolute values. Cr/Th ratio of 7.7 on average (excluding sample DB1) does not indicate a mafic input. Sample DB1 has a Cr/Th ratio of about 42. The Sc/Th ratio ranges from 0.87 to 1.7 (Table 2) and the Y/Ni ratios vary between 0.65 and 1.72.

The chondrite normalized rare earth elements patterns for mudstones and sandstones of the Don Braulio Formation (Fig. C.14) show a moderately enriched LREE pattern (La_N/Yb_N of 6.7 on average), a negative Eu anomaly (Eu_N/Eu^* of 0.63 on average) and a rather flat HREE (Tb_N/Yb_N of 1.56 on average). All these features match with the PAAS pattern. The effects of dilution due to high SiO_2 and high CaO concentration on sample DB1 is evident.

The Don Braulio Formation plots within the field of continental island arc setting in the Th-Sc-Zr/10 and La-Th-Sc diagrams of Bhatia and Crook (1986). Only one important deviation towards the Zr apex is shown, but it is also related to a continental arc margin. In the La/Sc versus Ti/Zr diagram (Bhatia and Crook, 1986), the same samples scatter but in general show a tendency towards an active continental margin setting.

C.7 La Chilca Formation

C.7.1 Petrography

The La Chilca Formation is composed of coarse siltstones and minor very fine arenites, moderately well sorted and with subrounded grains. Certain samples are partially carbonate-cemented. They are characterized by monocrystalline quartz (with low sphericity) that predominates over the polycrystalline quartz. Chert is very scarce. Plagioclase is unaltered and with the typical polysynthetic twinning. K-feldspar (microcline and anorthoclase) is also present, and partially altered to clay minerals (mainly sericite). Accessory detrital minerals are tourmaline, zircon, chlorite, epidote, muscovite, biotite, titanite, apatite, hematite and other opaque minerals. The carbonate cement is composed of calcite (Table 3).

C.7.2 Geochemistry

Samples from the La Chilca Formation have SiO_2 concentrations ranging from 75% to 88.8%. Al_2O_3 concentrations vary from 3.3% to 10.6%, Fe_2O_3 ranges from 0.5% to 4%, CaO from 0.17% to 2.8%, K_2O is between 0.3% and 2.8% and Na_2O is between 0.8% and 2.1%. The CIA value is between 57 and 70 (see Table 1 in Appendix A), indicating moderately weathering. They do not follow a general weathering trend and samples plot erratically in the A-CN-K diagram. This unit shows Cs concentrations ranging from 2ppm to 5ppm, and the K/Cs ratios range from 3457 to 5266.

All samples from the La Chilca Formation are depleted in Th (average 5.8ppm) and in U (average 1.8ppm) compared with the UCC (Table 1). The Th/U ratios are between 2.3 and 5.8, indicating that some samples had loss U due to weathering and/or recycling.

Th/Sc ratio between 0.66 and 1.25, and Zr/Sc ratio between 12.2 and 76.1 indicate processes of recycling (in accordance to their high SiO_2 concentration) and a source from an upper continental crust composition. The La/Th ratios are between 3.1 and 3.8.

The Cr/V ratio for this unit is between 0.90 and 1.6 and the Cr/Th ratio is 8.7 on average. No enrichments of Sc, Cr and V along with Th/Sc ratios above 0.79 (except for the mudstone) indicate none mafic input. The Y/Ni ratio is between 0.27 and 0.81. The Sc/Th ratio ranges from 0.8 to 1.51 (Table 2).

The chondrite normalized rare earth elements patterns for mudstones and sandstones of the La Chilca Formation (Fig. C.15) show a moderately enriched LREE pattern (La_N/Yb_N of 6.07 on average), a negative Eu anomaly (Eu_N/Eu^* of 0.61 on average) and a rather flat HREE (Tb_N/Yb_N of 1.53 on average). All these features match with the PAAS pattern. The abundances of HREE might be controlled by the concentration of zircon (and less importantly titanite) due to recycling processes.

Using the diagrams to discriminate tectonic settings from Bhatia and Crook (1986), the La Chilca Formation can be linked to an active tectonic setting. Deviations towards the Zr apex are consistent with recycling and consequently enrichment in zircon.

C.8 Empozada Formation

C.8.1 Petrography

Samples of the Empozada Formation are ranging from limestones/silicate-sandstones (carbonate-cemented arenites where cement is almost 50%) to carbonate-cemented sandstones with 10% carbonate cement. The carbonate cement is present in sparitic and micritic sizes and is mainly calcite in composition, but ankerite was also found (Table 3). However, chlorite is present also as cement in a few samples. Their siliciclastic framework components are in general subangular to subrounded, with low sphericity and moderately to well sorted. Poorly sorted samples are also present. Grain sizes are between very fine and medium, but the poorly sorted samples have even granule sizes grains. Monocrystalline non-undulose quartz is the more abundant framework mineral and frequently presents fluid and mineral inclusions (booklets of kaolinite, muscovite and monazite). Some grains show undulose extinction. Polycrystalline quartz is also common. Rounded quartz grains with high sphericity were also observed, and in most cases, they do not show any overgrowth. However, overgrowths of quartz are present in a few cases. K-feldspar is more abundant than plagioclase. The latter varies from unaltered to partial replaced by calcite, and shows the typical polysynthetic twinning. K-feldspar (microcline and anorthoclase) is either altered to clay minerals or calcite replaced, or does not show any alteration; they show the typical grid twin-type and perthites are present as well. Both feldspars present overgrowths. Lithoclasts are predominantly sedimentary from chert and siltstones, but volcanic lithoclasts with a very fine crystalline matrix are present as well (Fig. C.2). Calcite and quartz veins, hematite and other opaque minerals are frequent.

The heavy mineral fraction of the Empozada Formation is composed of apatite, zircon, brown spinels, rutile, tourmaline and detrital muscovite, epidote, chlorite and biotite in order of abundance. Apatite is in major proportion than zircon and subhedral; it ranges in size from 50µm to 250µm. Zircon is subhedral and ranging in size from 50µm to 100µm. The chromian spinels do not show any rim or visible zonation; they are subhedral and ranging in size from 80µm to 200µm. Ti-oxides included in quartz, calcite and feldspar were also observed, as well as barite included in carbonate lithoclasts.

C.8.2 Geochemistry

Samples from the Empozada Formation have a variable major elements distribution, with SiO_2 concentrations ranging from 30% to 76.4%, Al_2O_3 varies from 1.3% to 15.3%, Fe_2O_3 ranges from 1.01% to 8.5%, CaO from 2.3% to 34.7%, K_2O is between 0.26% and 3.85% and Na_2O is between 0.8% and 3.68%. Most of the samples from the Empozada Formation have high CaO concentrations, thus only one sample could be used to calculate the CIA value. Although it is not statistically meaningful, it is worth noting that this mudstone has a CIA value of about 70, indicating a moderately weathering (Table 1). This unit shows variable Cs concentrations ranging from 1ppm to 10ppm, and the K/Cs ratios range from 2158 to 3997.

Compared with the UCC averages of Th (10.7ppm) and U (2.8ppm) according to McLennan *et al.* (2006), most of the samples from the Empozada Formation are depleted in U and have depleted to similar Th concentrations (Table 1 in Appendix A). However, certain samples have higher U concentrations compared with UCC, with values up to 10ppm. Low Th concentrations seem to be link to high CaO and SiO_2 concentrations. The Th/U ratios are highly variable, with lower, similar and higher values compared with the UCC. The group of samples showing low Th/U ratios have also low Th and U concentrations. The group of samples with normal Th/U ratios and normal Th and U abundances for the UCC (McLennan *et al.*, 2006) is entirely made up by mudstones. Sample E7 reflects the effects of weathering and/or recycling under oxidizing conditions, with the concomitant loss of U but maintaining a normal Th value for the UCC.

Samples from the Empozada Formation could be subdivided into two groups in terms of their Th/Sc versus Zr/Sc ratios. One group does not show any recycling and reflect an input from the upper continental crust while the second group shows an important process of recycling. The Zr concentration is lower than the UCC value of 190ppm for the first group. However, the Zr concentration of the recycled samples ranges from enriched (with values up to 323ppm) to deplete compared with the UCC. The high Zr/Sc ratio of those samples with low Zr concentration is affected by the very low Sc concentrations (less than 3ppm) compared with the UCC rather than by an enrichment of Zr-rich phases (typically zircon) due to recycling. Sample E10 has a Th/Sc ratio of 0.19, indicating that a less evolved rock was also a source (Table 1 in Appendix A). The La/Th ratio ranges from 3 to 11, and it is affected by the very low Th concentration of certain samples.

The Cr/V ratio for this unit is between 0.61 and 1.06 for mudstones and 0.96 to 3.65 for sandstones, indicating a depleted input, although not ophiolitic. Cr/Th ratios of 17 on average for the Empozada Formation confirm the depleted input, although this ratio might be affected by the low Th concentrations. The enrichment in compatible elements (Sc, Cr and V) of the Empozada Formation have individual values as high as 18ppm of Sc, 220ppm of Cr and 139ppm of V. The Y/Ni ratio varies between 0.11 and 2.19. The Sc/Th ratio ranges from 0.77 to 1.5 with an exceptional value of 5.24 (Table 2).

The chondrite normalized rare earth elements patterns for mudstones and sandstones of the Empozada Formation (Chapter 4) show a moderately enriched LREE pattern (La_N/Yb_N of 6.48 on average), and a rather flat HREE (Tb_N/Yb_N of 1.46 on average). The Eu-anomaly is negative, with Eu_N/Eu^* of about 0.61 on average. All these features match with the PAAS pattern. Although REE patterns of the samples are parallel to the PAAS, they tend to be depleted in LREE and enriched in HREE compared with the PAAS. Notwithstanding the sample E10 shows the influence of a less evolved source since its Eu_N/Eu^* is of about 1 (no Eu-anomaly) and it also shows a low sum of REE (98ppm).

In the La-Th-Sc and Th-Sc-Zr/10 diagrams (Bhatia and Crook, 1986) mudstones from the Empozada Formation plot within the field of continental island arc setting. One sandstone shows the influence of a less evolved source plotting towards the oceanic island arc field. The rest of the sandstones plot either towards the La or Zr apexes. However, when analyzing the absolute values (Table 1 in Appendix A), no enrichment in La and Zr for those samples are observed, but instead an important depletion of Sc and Th (with absolute values of about 2ppm and 3ppm respectively). Two factors could be addressed to explain the deviations: dilution effects due to high concentrations of either CaO or SiO_2, or most probably sorting with the correspondent enrichment on certain heavy minerals, particularly apatite. In the La/Sc versus Ti/Zr diagram (Bhatia and Crook, 1986) the same samples show the same tendencies mainly indicating an active continental margin setting, as well as the influence of a less evolved source. Some samples plot in the passive margin field.

C.9 Los Sombreros Formation

C.9.1 Petrography

The Los Sombreros Formation is composed of olistoliths embedded in mudstones and subordinated siltstones and sandstones. The mudstones forming the matrix of the olistoliths were analyzed are and their compositions were determined mainly by XRD techniques. They are composed of quartz, plagioclase, muscovite, illite, and chlorite while hematite and carbonate phases (ankerite, calcite and dolomite) are minor components (Table 3). Petrographic analyses made on siltstones and fine sandstones confirm the presence of the abovementioned components. Detrital grains are subangular to subrounded and with low sphericity. Quartz is mainly monocrystalline, although polycrystalline grains are also present. Within the feldspar group, plagioclase is more abundant than K-feldspar and is not altered. Microcline instead is partially altered to clay minerals. Muscovite and chlorite as well as biotite are detrital phases, although chlorite has been identified as an alteration on biotite as well. Lithoclasts are derived from low-grade metamorphic rocks (phyllite) and less commonly from fine-grained volcanic rocks. Accessory minerals are zircon, apatite, tourmaline, detrital epidote and opaque minerals.

C.9.2 Geochemistry

The Los Sombreros Formation shows variable major elements composition. The SiO_2 concentration ranges from 56.5% to 70.7%, Al_2O_3 varies from 3% to 21%, Fe_2O_3 ranges from 5.4% to 9%, CaO from 0.16% to 10.4%, K_2O is between 0.45% and 4.5% and Na_2O is between 0.5% and 2.8%. The CIA value for the Los Sombreros Formation is between 64 and 77, indicating intermediate to strong weathering. Some mudstones are enriched in K_2O. This unit shows variable Cs concentrations ranging from 1ppm to 12ppm, and the K/Cs ratios range from 2294 to 6367.

Samples from the Los Sombreros Formation can be subdivided into two groups. One group have Th concentrations enriched compared with the UCC, and U concentrations similar to very slightly depleted compared with the UCC. Their Th/U ratios are higher than the UCC and seem to indicate weathering and/or recycling, but the ratios are affected by the Th concentrations since no U loss is observed. The other group of samples instead display a depletion in Th concentrations probably related to high CaO or SiO_2 concentrations (Table 1 in Appendix A), whereas their U concentrations are strongly depleted compared with the UCC (with values as low as 0.8ppm). Their Th/U ratios are higher than the UCC values (Table 1), and although the Th concentrations are depleted the loss of U of these samples is evident.

The Los Sombreros Formation show a cluster of data indicating no recycling (confirmed by the low Zr concentration on Table 1 in Appendix A) and a provenance from a typical UCC composition with the influence from a subordinate slightly less evolved source as well. The less evolved character of sample SOM9, with a Th/Sc ratio of 0.34 could be apparent and due to its CaO concentration. It can be seen in Table 1 (Appendix A) that the Sc concentration is about 10ppm (which is accompanied by very low concentrations of Cr and V as well), whereas the Th is highly depleted (3.4ppm), compared with the UCC. The La/Th ratio ranges from 3 to 5.1.

The Cr/V ratio for this unit is between 0.73 and 1.08. The slight enrichment of Sc, Cr and V (with maximum abundances of 19.7ppm, 110ppm and 115ppm respectively), compared with the UCC indicate a mafic input. Cr/Th ratio of 6.8 on average however does not indicate a mafic input. The Y/Ni ratio varies between 0.62 and 2.18. The Sc/Th ratio ranges from 1.16 to 2.94 (Table 2).

The chondrite normalized rare earth elements patterns for mudstones and sandstones of the Los Sombreros Formation (Chapter 4) show a moderately enriched LREE pattern (La_N/Yb_N of 6.9 on average), a negative Eu-anomaly (Eu_N/Eu^* of 0.63 on average) and a rather flat HREE (Tb_N/Yb_N of 1.65 on average). All these features match with the PAAS pattern. Although REE patterns of the samples are parallel to the PAAS, they tend to be depleted in LREE and enriched in HREE compared with the PAAS. Three samples have a different REE pattern and are therefore described below.

It is noteworthy the behaviour of samples 020419, SOM7 and SOM9 in the REE diagram. Sample 020419 shows a clear enrichment of MREE (medium rare earth elements) compared with PAAS and a disturbance of the REE composition is evident. Sample SOM7 shows a relatively low sum of REE (118ppm), high concentrations of Y

(60ppm), low Zr and Th concentrations (91ppm and 6ppm respectively), high P_2O_5 concentrations (1.38%) but very low TiO_2 concentrations (0.27%). The normalization of the REE to the PAAS values shows that La, Ce and Nd concentrations of sample SOM7 are moderately depleted with respect to the PAAS, Sm, Eu and Tb are two to three times enriched, whereas Yb and Lu have almost the same concentrations compared with the PAAS (Taylor and McLennan, 1985). Based on these geochemical considerations, the distribution of the REE is better explained by sorting of heavy minerals rich in MREE (Bock *et al.*, 1994). Apatite and titanite are both MREE-rich, but according to high P_2O_5 and low TiO_2 concentrations, the heavy mineral enriched in this sample is most probably apatite. On the other hand, the moderate depletion in LREE and Th might be due to the loss of phases like monazite and allanite, whereas Zr and HREE concentrations are in accordance with no important concentrations of zircon. A Sm/Nd ratio of 0.47 for sample SOM7 indicate that there is a fractionation of REE (Sm/Nd for the PAAS is of about 0.2), although more probably related to selective sorting of apatite (Bock *et al.*, 1994). However, the effects of the very low-grade metamorphism on the distribution of the rare earth elements cannot be excluded.

The sample SOM9 has a very low sum of REE (39ppm), high CaO (10.5%) and Fe_2O_3 concentrations (related to the presence of ankerite), and very low TiO_2, P_2O_5 and Th concentrations (0.24%, 0.05% and 3.4ppm respectively). The normalization of the REE to the PAAS values shows that La, Ce, Nd, Sm, and Eu concentrations of sample SOM9 are depleted with respect to the PAAS, whereas Tb, Yb and Lu are slightly depleted. The distribution of the REE is better explained by the presence of zircon, responsible for the Zr and HREE concentrations that approximate their abundances to the PAAS values (Taylor and McLennan, 1985), and the loss of heavy minerals characterized by high concentrations of LREE, MREE, P_2O_5, TiO_2 and Th such as monazite, allanite, apatite and titanite. A Sm/Nd ratio of 0.46 for sample SOM9 indicates that the REE were fractionated, most probably during the very low-grade metamorphism that affected this unit. The absence of a negative Ce-anomaly for samples SOM7 and SOM9 (Ce/Ce* of 0.99 and 1.04 respectively) also support that the remobilization was not during weathering (McDaniel *et al.*, 1994; Bock *et al.*, 1994).

The deposition in a basin linked to an active margin is evident in the diagrams of Bhatia and Crook (1986) applied to the Los Sombreros Formation.

C.10 Yerba Loca Formation

C.10.1 Petrography

Samples are mostly arenites and wackes. Their detrital components are moderately well to very poorly sorted and with sizes ranging from silt to coarse sand. Framework minerals are subrounded to subangular and with low sphericity, but rounded and high spherical grains (most commonly of quartz) are present. Some samples contain low amounts of matrix, while wackes with matrix content between 31% and 37% are also present. The matrix is predominantly composed of white mica (sericite and illite) and quartz, but chlorite is also present. A group of sandstones are calcite-cemented and less commonly dolomite-cemented (Table 3).

The main mineralogical component is monocrystalline quartz, with normal extinction; grains with undulose extinction are scarce. Fluid inclusions are present and in some cases, they even form warped quartz. Booklets of kaolinite and muscovite are frequently included in quartz whereas rare inclusions are zircon, apatite and biotite. Occasionally, grains with embayments were observed as well as polycrystalline quartz with sutured edges and undulose extinction. Graphic quartz had been observed.

Following order of abundance are feldspar grains, where K-feldspar is more abundant than plagioclase. The K-feldspar (microcline is dominant and less common is anorthoclase) is altered to chlorite, clay minerals and less frequently to calcite, while plagioclase is smaller and range from unaltered to partially or totally replaced by calcite and clay minerals. Inclusions in plagioclase are not frequent, but when present they are composed of apatite and Ti-oxides. Some quartz and K-feldspar grains are several times larger than the medium grain size of the detrital constituents.

Muscovite, chlorite and epidote are present as large crystals, and are probably the result of the greenschist facies metamorphism. Muscovite and biotite are also present as detrital lamellae, and chlorite is frequently replacing biotite. The lithoclastic composition include sedimentary lithoclasts (siltstone, mudstones, carbonate and chert), volcanic lithoclasts (with typical textures of fine-grained rocks like basalts and andesites), and metamorphic lithoclasts (fine flat-grained from phyllitic rocks and rarely from coarse-grained schist-type rocks or even gneisses).

Zircon, tourmaline, epidote, staurolite, rutile, apatite, monazite, titanite, hematite and other opaque minerals represent the detrital accessory assemblage. Sometimes, these heavy minerals are as big as the main light framework minerals. Ti-oxides are a frequent component of wackes, but are also common within mudstones. They are present as small (between 10µm and 20µm) anhedral to subhedral grains within the matrix or as lamellae included within other minerals such as chlorite, muscovite, quartz and plagioclase. In several cases, the lamellae are conspicuous and cover almost the whole grain. Fe-oxyhydroxides such as goethite or lepidocrocite were also observed.

The igneous rocks associated to the Yerba Loca sequence show the effects of metamorphism. They are dominantly mafic, but more differentiated compositions also exist. The phenocrystals of olivine, pyroxene and plagioclase are embedded within a plagioclase-rich groundmass forming a pilotaxitic texture. The intermediate rocks are similar to the previously described, but the groundmass of the pilotaxitic texture also contains minor amounts of quartz, apart from plagioclase. A greenschist facies assemblage is assumed due to the presence of chlorite, calcite and epidote.

C.10.2 Geochemistry

The Yerba Loca Formation is characterized by SiO_2 concentrations ranging from 56% to 75%, Al_2O_3 ranging from 8.5% to 19.7%, Fe_2O_3 is between 4.7% and 9.3%, MgO ranges from 1.5% to 3%. CaO from 0.2% to 4.3% and the Na_2O concentration is of 2.21±0.65 on average. Sandstones have a low K_2O concentration (between 1.4% and 2.1%) whereas mudstones are enriched in K_2O (between 3.4% and 4.9%) compared with the sandstones and with the UCC (McLennan *et al.*, 2006; Table 1). Two sandstones have a distinctive chemical composition and are therefore separately described and discussed from now on. Samples YL411 and YL454 (see

Table 1 in Appendix A) have lower SiO_2 and higher Fe_2O_3, MgO and CaO concentrations compared with the rest of the samples of the Yerba Loca Formation. Notwithstanding, these two samples have similar Al_2O_3 and Na_2O. Sample YL411 is depleted in K_2O (0.25%). Sample YL454 is depleted in K_2O (1.25%) compared with the UCC (McLennan *et al.*, 2006), but with a K_2O content similar to the rest of the sandstones from this unit.

The CIA value for sandstones range between 52 and 67 and for mudstones is between 64 and 73 (see Table 1 in Appendix A). Some samples from Yerba Loca Formation show the effects of potassium metasomatism while others follow a normal weathering path (Fedo *et al.*, 1995). Mudstones from the Yerba Loca Formation have Cs concentrations ranging from 4ppm to 8ppm, and they show K/Cs ratios between 3992 and 5042. Sandstones instead show Cs values between 3ppm and 5ppm and K/Cs ratios between 2737 and 5653.

A group of samples from the Yerba Loca Formation show Th/U values between 3.5 and 4, which is normal for rocks derived from the UCC. Some of the samples that seem to be affected by weathering and/or recycling have U concentrations around 2.8ppm, and their higher Th/U ratios are due to an increase in the Th concentration (with values up to 20ppm) rather than loss of U. However, some other samples show depletion in U along with a depletion of Th and enrichment in SiO_2, and therefore, effects of weathering and/or recycling should be addressed. On the other hand, some of the sandstones that show low Th/U ratios have U concentrations similar to the rest of the samples, but instead lower Th concentrations.

The Th/Sc ratio for this unit ranges from 0.63 to 0.96 whereas the Zr/Sc ratio is between 8.3 and 37.4 and a consequently increase in Zr concentrations (with values up to 570ppm) is observed indicating recycling. Two samples from the Yerba Loca Formation (YL411 and YL454) have very low Th/Sc ratios (0.02 and 0.27 respectively) and Zr/Sc ratios (4.69 and 7.5 respectively). One of these samples has a composition close to average andesite while the other one has a composition close to average basalt. The La/Th ratio for the Yerba Loca Formation is between 2.8 and 4.9, whereas samples YL411 and YL454 show values of 13.75 and 3.73 respectively.

The Cr/V ratio for the Yerba Loca Formation is between 0.66 to 0.73 for mudstones and 0.43 to 2.37 for sandstones, indicating an input from a source more depleted than the UCC in some samples. Accordingly, enrichment in Sc (with values up to 35.6ppm), Cr (up to 220ppm) and V (enrichments up to 230ppm) compared with the UCC averages of 13.6ppm, 83ppm and 107ppm respectively, indicate the influence of a depleted source. Cr/Th ratio of 14.65 on average confirms the mafic input. The Y/Ni ratio varies between 0.11 and 2.19. The Y/Ni ratio is between 0.31 and 0.96. The Sc/Th ratio ranges from 1.04 to 1.59, except for samples YL411 and YL454 which reach values of 44.5 and 3.69 respectively (Table 2).

The chondrite normalized rare earth elements patterns for mudstones (Fig. C.16) and sandstones (Fig. C.17) of the Yerba Loca Formation show a moderately enriched LREE pattern (La_N/Yb_N of 6.95 on average), a negative Eu anomaly (Eu_N/Eu^* of 0.55 on average) and a rather flat HREE (Tb_N/Yb_N of 1.4 on average). All these features match with the PAAS pattern. The two samples (YL411 and YL454) of the Yerba Loca Formation with a less fractionated composition also show low La_N/Yb_N (2.86 and 5.45 respectively) and La/Sc ratios (0.31 and 1.01 respectively) but a negative Eu-anomaly (0.75 and 0.6 respectively).

C.11 Alcaparrosa Formation

C.11.1 Petrography

The Alcaparrosa Formation is composed of arenites and wackes. Their detrital constituents are moderately well to very poorly sorted. They range in size from silt to coarse sand. Framework minerals are subrounded to subangular and with low sphericity. Some samples contain low amounts of matrix. The matrix is composed predominantly of white mica (sericite and illite) and quartz (Table 3). The main mineralogical component is monocrystalline quartz, with normal extinction; grains with undulose extinction and polycrystalline quartz are scarce. Fluid inclusions are present and in some cases, they even form warped quartz. Following order of abundance are feldspar grains, where plagioclase is more abundant than K-feldspar. The K-feldspar (microcline is dominant and less common is anorthoclase) is altered to chlorite, clay minerals and less frequently to calcite, while plagioclase is smaller and range from unaltered to partially or totally replaced by calcite and clay minerals.

Muscovite and biotite are present as detrital lamellae, and chlorite is frequently replacing biotite. The lithoclastic composition include sedimentary lithoclasts (chert, siltstone and mudstones), volcanic lithoclasts (with typical textures of fine-grained rocks such as basalts and andesites), and metamorphic lithoclasts (fine flat-grained from phyllitic rocks and rarely from coarse-grained schist-type rocks or even gneisses). Zircon, tourmaline, epidote, staurolite, rutile, hematite and other opaque minerals represent the detrital accessory assemblage. Sometimes, these heavy minerals are as big as the main light framework minerals.

C.11.2 Geochemistry

SiO_2 is the main oxide with abundances ranging from 61% to 77.5%. Al_2O_3 ranges from 8.5% to 16.8%, Fe_2O_3 ranges from 3.8% to 7.9%, MgO ranges from 0.74% to 2.3%, the Na_2O concentration is between 1.6% and 2.5%, CaO is between 0.3% and 0.86%, and K_2O ranges from 1.3% to 3.56%. Mudstones of the Alcaparrosa are enriched in K_2O compared with both the sandstones within the same unit and the UCC.

The CIA value for sandstones range between 58 and 71 and for mudstones is between 69 and 71 (see Table 1 in Appendix A), indicating moderately weathering. Samples from the Alcaparrosa Formation follow a general weathering trend, although a very slight potassium metasomatism can be attributed to the mudstones. The Cs concentration is between 2ppm and 7ppm and the K/Cs ratio ranges from 3672 to 7492.

The Th concentration of mudstones from the Alcaparrosa Formation varies from 10ppm to 13ppm. The U concentration varies from 2.4ppm to 3.5ppm. The Th/U ratios range from 3.7 to 4.17. Sandstones instead are depleted in Th (with concentrations ranging from 7.5ppm to 9.1ppm, with one exceptional value of 12ppm) and in U (with concentrations ranging from 2ppm to 2.5ppm, with one exceptional value of 3ppm). The Th/U ratios are between 3 and 4.4.

The Th/Sc ratio for this unit ranges from 0.71 to 1 whereas the Zr/Sc ratio is between 11.25 and 39.66 and an increase in the Zr concentrations (with values up to 366ppm) is observed indicating recycling. Th/Sc ratios do not show great variations indicating that the input was mostly from rocks with an average upper continental crust composition.

The Cr/V ratio for this unit is between 0.85 and 0.97 for mudstones, and between 0.82 and 1.02 for sandstones, whereas the Cr/Th ratio is of 7.35 on average. A depleted source is not clearly defined. The Y/Ni ratio is between 0.49 and 0.85. The Sc/Th ratio ranges from 0.99 to 1.4 (Table 2).

The chondrite normalized rare earth elements patterns for mudstones and sandstones of the Alcaparrosa Formation (Fig. C.18) show a moderately enriched LREE pattern (La_N/Yb_N of 6.8 on average), a negative Eu anomaly (Eu_N/Eu^* of 0.54 on average) and a rather flat HREE (Tb_N/Yb_N of 1.29 on average). All these features match with the PAAS (Table 1) pattern.

Sandstones and mudstones from the Alcaparrosa Formation indicate the deposition within a basin linked to an active margin (this study) rather than to a passive one (Merodio and Spalletti, 1990).

C.12 Portezuelo del Tontal Formation

C.12.1 Petrography

The Portezuelo del Tontal Formation is composed of arenites and wackes. Their detrital constituents are poorly to very poorly sorted, with sizes ranging from fine to coarse sand. Framework minerals are subangular to subrounded and with low sphericity. The matrix is composed predominantly of white mica (sericite and illite) and quartz, but chlorite is also present (Table 3). The arenites have matrix content up to 10%. The main mineralogical component is monocrystalline quartz, with normal extinction; grains with undulose extinction are scarce. Occasionally, grains with embayments were observed as well as polycrystalline quartz with sutured edges and undulose extinction. Graphic quartz had been observed.

Following order of abundance are feldspar grains, where K-feldspar is more abundant than plagioclase. The K-feldspar (microcline is dominant and less common is anorthoclase) is altered to clay minerals, while plagioclase is smaller and unaltered. Muscovite, chlorite and epidote are present as large crystals, and are probably the result of the greenschist facies metamorphism. Intergrowth of muscovite and chlorite are frequent. Muscovite and biotite are also present as detrital lamellae, and chlorite is frequently replacing biotite. The lithoclastic composition include sedimentary lithoclasts (mudstones, siltstone, very fine sandstones and very scarce chert), volcanic lithoclasts (with typical textures of fine-grained rocks such as basalts and andesites), and metamorphic lithoclasts (fine flat-grained from phyllitic rocks and rarely from coarse-grained schist-type rocks or even gneisses). Zircon, tourmaline, epidote, staurolite, rutile, apatite, monazite, titanite, hematite and other opaque minerals represent the detrital accessory assemblage.

C.12.2 Geochemistry

SiO_2 is the main oxide with abundances ranging from 67.8% to 74.5%. Al_2O_3 ranges from 9.4% to 12%, Fe_2O_3 range from 3.3% to 6.5%, MgO ranges from 1.3% to 2.4%, the Na_2O concentration is between 1.4% and 2.6%, CaO is between 0.4% and 1.76%, and K_2O ranges from 1.6% to 2.2%. Even though the mudstone of the Portezuelo del Tontal Formation has higher K_2O concentration compared with the sandstones of the same unit, it is not enriched compared with the UCC value of 3.4% (McLennan *et al.*, 2006; Table 1). Sample PDT3 from the Portezuelo del Tontal Formation has a major elements composition substantially different to the above described. This sample has lower SiO_2 (51%) and higher Al_2O_3 (20%), Fe_2O_3 (10%) and MgO (3.6%) concentrations compared with the rest of the samples of the Portezuelo del Tontal Formation. On the other hand, the CaO and Na_2O concentrations of sample PDT3 (0.89% and 1.6% respectively), are similar to the average values of the unit. K_2O is about 5% for this sample and therefore it is enriched compared with the other samples of the Portezuelo del Tontal Formation and the UCC.

The CIA value for sandstones ranges between 56 and 64 and that for mudstones is between 64 and 69 (Table 1 in Appendix A). According to average CIA values for sedimentary rocks, samples from the Portezuelo del Tontal Formation are slightly to moderately weathered. The samples follow a general weathering trend particularly if sample PDT3 is discarded due to it high Al_2O_3, Fe_2O_3 and K_2O concentrations. The Cs concentration of the Portezuelo del Tontal Formation is between 2ppm and 4ppm but it is 10ppm for sample PDT3. The K/Cs ratio ranges from 4447 to 7093, whereas for sample PDT3 is 4136.

The Th concentration for the Portezuelo del Tontal Formation varies from 7.7ppm to 10ppm. The U concentration varies from 1.5ppm to 2.5ppm. The Th/U ratios range from 3.72 to 6.13, indicating loss of U due to weathering and/or recycling. Sample PDT3 instead has a Th concentration of 15ppm, a U concentration of 4.7ppm and a Th/U ratio of 3.2.

The relationship between Th/Sc and Zr/Sc ratios for the Portezuelo del Tontal Formation shows a cluster of data indicating no important recycling and a provenance from a typical upper continental crust composition with a subordinate input from a slightly less evolved source. Sample PDT3 shows high Sc (25ppm), Cr (120ppm), V (150ppm) and Th (15ppm) concentrations but Zr values similar to the UCC. These characteristics indicate that a mafic source was closely related and implying that zircon was not the main mineral-host for Th.

The Cr/V ratio for this unit is between 0.81 and 0.85 for mudstones and between 0.7 and 1.12 for sandstones. Together with the high Sc, Cr and V concentration of certain samples, a mafic input is deduced. Cr/Th ratio of 7.4 on average however, does not clearly indicate a mafic input, although individual values are as high as 10. The Y/Ni ratio is between 0.41 and 0.71. The Sc/Th ratio ranges from 1.18 to 1.88 (Table 2).

The chondrite normalized rare earth elements patterns for mudstones and sandstones of the Portezuelo del Tontal Formation (Fig. C.19) show a moderately enriched LREE pattern (La_N/Yb_N of 7.25 on average), a negative Eu-anomaly (Eu_N/Eu^* of 0.65 on average) and a rather flat HREE (Tb_N/Yb_N of 1.26 on average). All these features match with the PAAS pattern. Sample PDT3 shows the lowest Eu-anomaly (Eu_N/Eu^* of 0.8) and a lower La_N/Yb_N (5.69) and La/Sc (1.3) ratios compared with the rest of the samples of the same unit.

Sandstones and mudstones from the Portezuelo del Tontal Formation indicate the deposition within a basin linked to an active margin (this study) rather than to a passive one (Merodio and Spalletti, 1990).

C.13 Sierra de la Invernada Formation

C.13.1 Petrography

The Sierra de la Invernada Formation is composed of arenites and wackes. Framework minerals are angular to subrounded and with low sphericity, but rounded and high spherical grains (most commonly of quartz) are present; they are poorly to very poorly sorted and range in size from very fine to fine sandstones, although medium grain sizes are also present. The matrix of the arenites (5% to 10%) and wackes (up to 35%) is composed of white mica, quartz, chlorite and calcite (Table 3).

The main mineralogical component is monocrystalline quartz, with normal extinction; grains with undulose extinction are scarce. Fluid inclusions are present and in some cases, they form trends. Zircon, apatite and muscovite are frequently included in quartz. Occasionally, grains with embayments were observed as well as polycrystalline quartz with sutured edges and undulose extinction. Graphic quartz had been observed. Following order of abundance are feldspar grains, where K-feldspar is more abundant than plagioclase. The K-feldspar (microcline is dominant and less common is anorthoclase) show grid and Carlsbad twinning as well as a perthitic texture; it is not altered, only partially altered to clay minerals or totally replaced by chlorite. Plagioclase range from unaltered to partially replaced by calcite.

Muscovite and biotite are also present as detrital lamellae, and chlorite is frequently replacing biotite. The lithoclastic composition include sedimentary lithoclasts (mudstones, siltstone, sandstones, carbonate and chert), volcanic lithoclasts (with typical textures of fine-grained rocks such as basalts and andesites), and metamorphic lithoclasts (fine flat-grained phyllitic rocks and rarely coarse-grained schist-type rocks or gneisses). Zircon, tourmaline, epidote, apatite, titanite, hematite and other opaque minerals represent the detrital accessory assemblage.

C.13.2 Geochemistry

SiO_2 is the main oxide with abundances ranging from 56.5% to 72.5%. Al_2O_3 ranges from 9.6% to 18.5%, Fe_2O_3 ranges from 4.7% to 8.3%, MgO ranges from 1.3% to 3%, the Na_2O concentration is between 1.4% and 2.64%, CaO is between 0.3% and 1.5%, and K_2O ranges from 1.5% to 4.74%. The higher concentrations of Fe_2O_3 and MgO of the mudstones compared with the sandstones of the Sierra de la Invernada Formation might be related to the presence of chlorite within the matrix-sized material. Higher concentrations of K_2O within mudstones compared with sandstones are link to the potassium metasomatism shown in the A-CN-K diagram.

The CIA value for sandstones range between 55 and 62 and for mudstones is between 66 and 71 (Table 1 in Appendix A), indicating slight to moderate weathering. The sandstones follow a general weathering trend but the mudstones show some deviations suggesting potassium metasomatism. The Cs concentration ranges from 2ppm to 9ppm and the K/Cs ratio is between 4032 and 5240.

Samples from Sierra de la Invernada Formation can be subdivided into two groups: one group shows Th/U ratios above 3.8, but these values are more likely related to an increase of Th rather than a loss of U due to weathering and/or recycling (see Table 1 in Appendix A). The other group of samples shows lower Th/U ratios but relatively the same U abundances than the first group of samples described. Their low Th/U ratios are a consequence of their low Th concentration.

The Th/Sc ratio is between 0.64 and 0.84, while the Zr/Sc ratio ranges from 7.3 to 29.3, indicating incipient recycling and an input from the UCC with a subordinate less evolved input. The La/Th ratio is between 2.5 and 3.6.

The Cr/V ratio for this unit is between 0.88 and 0.92 for mudstones whereas for the sandstones is between 0.74 and 0.91. The Cr/Th ratio is about 6.8 on average. Both ratios do not clearly indicate a mafic input. Furthermore, no important enrichment in Cr and V compared with the UCC is seen, although some enrichment in Sc is observable within the mudstones. The Y/Ni ratio is between 0.62 and 0.9. The Sc/Th ratio ranges from 1.19 to 1.55 (Table 2).

The chondrite normalized rare earth elements patterns for mudstones and sandstones of the Sierra de la Invernada Formation (Fig. C.20) show a moderately enriched LREE pattern (La_N/Yb_N of 7.62 on average), a negative Eu-anomaly (Eu_N/Eu^* of 0.53 on average) and a rather flat HREE (Tb_N/Yb_N of 1.38 on average). All these features match with the PAAS pattern.

The deposition in a basin related to an active margin as tectonic setting is evident for the Sierra de la Invernada Formation using the discriminatory diagrams from Bhatia and Crook (1986).

C.14 Ponón Trehué Formation

C.14.1 Petrography

The samples studied from the Ponón Trehué Formation are claystones, siltstones and fine arenites. XRD analyses indicate that clay minerals are mainly chlorite, sericite and illite (Table 3). The detrital constituents of the sandstones are moderately sorted. Monocrystalline quartz is subrounded to subangular, with low sphericity and always shows normal extinction. Fluid inclusions in quartz are common and very scarce grains have embayments. Polycrystalline quartz is sometimes present, but with normal extinction and no sutured boundaries. K-feldspar is scarce and almost always totally replaced by chlorite or clay minerals. Sedimentary lithoclasts derived from siltstones, carbonates, mudstones and chert are present. Calcite is present as well as very scarce detrital muscovite lamellae. Zircon, apatite, spinel, tourmaline, rutile, Fe-oxides (including hematite) and other opaque minerals compose the heavy minerals fraction of the Ponón Trehué Formation.

A gabbro associated to the siliciclastic record was found, although its time-relationship to the sedimentary sequence is not clear yet. It is mainly composed of coarse laths-like plagioclase crystals, forming a decussate texture; opaque minerals represent a 10%, being some of them columnar-shaped while others have an equidimensional-shape. Plagioclase shows the typical polysynthetic twinning and commonly contains inclusions; they are slightly altered to clay minerals in certain cases. Epidote is also present. Calcite is present as veins and as an alteration phase. The presence of chlorite, calcite and epidote in contact to each other and as secondary phases indicate that this mafic rock was affected by greenschist facies metamorphism.

C.14.2 Geochemistry

The SiO_2 concentration ranges from 59.1% to 83.85%, Al_2O_3 varies from 3.6% to 20.3%, Fe_2O_3 ranges from 1.8% to 8.1%, CaO from 0.16% to 2.67%, K_2O is between 1% and 4.75% and Na_2O is between 0.37% and 1.29%. The CIA value for the Ponón Trehué Formation is between 69 and 77, indicating intermediate to strong weathering. This unit shows Cs concentrations ranging from 2ppm to 5ppm, and the K/Cs ratios range from 6234 to 8107.

Compared with the UCC averages of Th (10.7ppm) and U (2.8ppm) according to McLennan *et al.* (2006), most of the mudstones from the Ponón Trehué Formation have similar to enriched Th concentrations (between 11ppm and 14ppm), and depleted to enriched U concentrations (between 1.5ppm and 4.3ppm). Sandstones are depleted in Th (from 3.7ppm to 7.4ppm) or have similar Th concentrations compared with the UCC. U concentration of sandstones varies from 2ppm to 3.2ppm. The Th/U ratios for the unit are variable (between 1.85 and 9.3), indicating loss of U due to weathering and/or recycling for some samples (e.g. sample CT7). However, some other samples have low Th/U ratios due to U gain (e.g. CT6). Other samples have Th/U ratios between 3.5 and 4, which is typical for unrecycled samples derived from the UCC.

The Th/Sc ratio is between 0.7 and 1.08, while the Zr/Sc ratio ranges from 11 to 36.22, indicating incipient recycling and an input from the UCC. The La/Th ratio is between 2.58 and 4.05.

The Cr/V ratio for the Ponón Trehué Formation is between 0.41 to 1.95 and the Cr/Th ratio of individual layers is up to 37.8 (Table 1 in Appendix A). Compatible elements like Cr, Sc and V are enriched compared with the UCC, with maximum values of 240ppm, 20.1ppm and 193ppm respectively. The Y/Ni ratio is between 0.1 and 1.21. The Sc/Th ratio ranges from 0.93 to 1.44 (Table 2).

The chondrite normalized rare earth elements patterns for mudstones and sandstones of the Ponón Trehué Formation (Chapter 6) show a moderately enriched LREE pattern (La_N/Yb_N of 5.8 on average), a negative Eu-anomaly (Eu_N/Eu^* of 0.52 on average) and a rather flat HREE (Tb_N/Yb_N of 1.17 on average). All these features match with the PAAS pattern, although most of the samples are enriched in HREE compared with PAAS. Sample CT2 is diluted in REE due to the high silica concentration (83.85%; Table 1 in Appendix A).

The deposition in a basin related to an active margin as tectonic setting is evident for the Ponón Trehué Formation using the discriminatory diagrams from Bhatia and Crook (1986).

	Gual	LAz	LCa	LV	LPT	DB	LCh	E	SOM	YL	A	PDT	SI	PT	UCC*	PAAS#
SiO_2	60.5	61.8	62.1	61.6	71.4	67.4	82.6	54.5	61.8	66.5	69	69.5	64.5	72.5	66	62.8
TiO_2	0.6	0.8	1.1	0.7	0.4	0.9	0.7	0.6	0.7	1	0.9	0.9	1	1.1	0.5	1
Al_2O_3	13.1	12.9	12. 8	8.7	6.3	5.9	6.3	8.3	14	12.4	12.6	11.5	14.2	12	15.2	18.9
Fe_2O_3	4.2	4.9	6	4.6	3.0	10.2	2.5	4	7.1	6.6	6	5.5	6.6	4.7	4.5	7.2
MnO	0.1	0.1	0.1	0.1	0.04	0.1	0.03	0.1	0.2	0.1	0.1	0.1	0.1	0.04	0.06	0.11
MgO	2.4	1.8	2.5	2.5	1.2	1.6	0.6	2.0	2.3	2.4	1.7	2	2.2	0.9	2.2	2.2
CaO	3.5	5.2	4.1	8.6	6.1	4.5	0.7	14.4	2.1	1.8	0.5	1	0.9	0.6	4.2	1.3
Na_2O	1	1.8	2.0	1.7	1.4	1.5	1.4	2.2	1.6	2.2	1.9	2.1	2.1	0.8	3.9	1.2
K_2O	3.6	2.8	2.6	1.6	1.2	2	1.1	1.6	2.6	2.1	2.4	2.1	3.1	2.7	3.4	3.7
P_2O_5	0.1	0.2	0.2	0.1	0.1	0.8	0.1	0.7	0.4	0.1	0.1	0.1	0.2	0.1	0.16	0.16
LOI	9.7	8.4	6.4	10.2	7.7	5.8	2.3	11.3	5.9	3.8	3.2	2.9	3.9	3.7		
Σ	98.8	100.8	99.8	100.5	99	99.6	98.2	99.6	98.5	99.1	98.7	97.9	98.7	99.2	100.1	
CIA	68.7	69.6	66.2	59.3	65.7	64.8	63	70.2	70.8	62.4	66.5	61.1	63	74.5	50	69
Sc	14.3	13.9	14.3	12	9	12.2	7	9.1	15.2	15.5	13.1	14.3	16	13.3	13.6	16
Cr	75.1	77.9	101.5	70.1	51.7	72.3	48.9	76	74	83.5	76.4	73.7	79.2	153.7	83	110
Ni	35	55	49	36.5	32.6	33	28.6	23.8	39.6	42.5	41.2	43.9	38.4	49.6	44	55
Cs	7.7	6.3	4.7	2.4	4.9	5	3	5.6	6.3	4.4	4.3	3.5	5.5	3.4	4.6	15
Rb	142	102.4	88.3	109.9	46.3	72.8	44.4	57.4	107.4	92.1	101.6	88.5	113.8	102.1	112	160
Ba	1223	1073	428	688	503	407	227	1015	62.8	454	488	397	424	1763	550	650
Hf	6.8	4.2	8.2	5.6	9.6	6.8	8.4	5.8	5.3	7.1	9.3	7.6	7.6	7.2	5.8	5
Th	10.1	9.8	8.8	6.2	5.5	8.5	5.8	6.3	10.8	10.8	10.4	9.9	11.6	10.5	10.7	14.6
U	5.8	5.3	2.4	1.5	2.2	2.6	1.8	3.1	2.2	2.5	2.7	2.3	2.8	3	2.8	3.1
V	158.3	137	92	84.1	45.3	86.6	47.1	65.4	81.8	120.3	84.1	87.5	91.2	131.8	107	150
Sr	170.5	144.4	99.7	249.6	192.8	98.5	88.1	189.5	108.4	88.5	61.2	71.7	81.3	53.2	350	200
Y	34.2	34.5	30.5	25.1	21.8	30	16.7	16.3	38	26.4	28.4	24.1	28.9	28	22	27
Zr	148.5	145.5	261.6	173.7	275.8	206.1	256.4	174.2	167.7	271.9	282.3	230.2	240	250.7	190	210
Nb	14	15.6	18	12.4	10	15	12	12.3	15.1	16.3	18	16.4	17.9	20.4	12	19
Pb	40.3	54.6	15.6	9.1	9.4	22.3	17.2	16	31.7	16.8	26.5	21.4	22.5	17	17	20
Zn	104.1	150.7	90.1	65.3	52.6	74.5	35.6	42.3	103.3	97.7	93.3	80.2	103.3	85.8	71	85
La	36.5	33.4	32.3	24.4	24.4	30.3	20.3	27	34.6	33.7	34.1	29.8	35.2	32.6	30	38^
Ce	74.1	67.4	70.1	52.3	56.2	71.3	48.1	60.8	76.4	65.7	75.4	64.8	77.4	70.7	64	80^
Nd	34.2	32.3	33.5	24.4	26.3	32	25.9	21.6	33.7	26.9	35.8	30.4	34.7	27.6	26	32^
Sm	6.1	6.4	6.4	4.7	5	6.5	5.3	5.7	7.5	6.6	6.5	5.8	6.7	7	4.5	5.6^
Eu	1	1.2	1.2	1.1	0.9	1.3	1	1.1	1.7	1.2	1.1	1.1	1.2	1.2	0.9	1.1^
Tb	0.9	1.1	0.9	0.8	0.9	1.2	0.8	0.9	1.2	1.1	1	0.8	1	1.2	0.64	0.77^
Yb	3	2.9	3.1	2.2	2.3	2.9	2.2	2.8	3.3	3.3	3.4	2.8	3.1	4.1	2.2	2.8^
Lu	0.5	0.5	0.5	0.3	0.4	0.5	0.4	0.5	0.5	0.5	0.5	0.4	0.5	0.7	0.32	0.43^
ΣREE	156.3	44.8	148	110.1	116	145.5	104.1	120.4	59	138.9	158	135.3	159.7	145.1	128.54	
Eu_N/Eu^*	0.53	0.57	0.59	0.66	0.53	0.63	0.61	0.61	0.63	0.55	0.54	0.65	0.53	0.52	0.63	0.66^
Ce_N/Ce^*	0.94	0.93	1	0.98	1.06	1.04	1.04	1.07	1.02	0.93	1	0.99	1.01	1.02	1.07	1.02
Th/Sc	0.82	0.73	0.64	0.55	0.75	0.77	0.87	0.89	0.68	0.72	0.81	0.71	0.75	0.82	0.79	0.91
Zr/Sc	11.7	11.2	23.4	15.2	62.8	30.7	43.1	40	11.5	18.6	23.8	16.9	16.7	19.2	14	13.13
Th/U	2	1.9	3.8	4.1	3.4	3.7	3.4	2.8	4.9	4.5	3.8	4.6	4.2	3.9	3.8	4.7
La/Sc	2.7	2.6	2.4	2.2	3.6	3.2	3	4.9	2.3	2.4	2.7	2.2	2.3	2.6	2.2	2.4
La/Th	3.2	3.6	3.8	3.9	4.8	4	3.5	5.3	3.4	3.7	3.3	3.1	3.1	3.2	2.8	2.6
Cr/V	0.5	0.6	1.1	0.8	1.9	1.6	1.1	1.6	0.9	0.7	0.9	0.9	0.9	1.3	0.77	0.73
Y/Ni	1.1	0.87	0.69	0.72	0.85	0.96	0.59	0.62	0.98	0.62	0.69	0.56	0.75	0.64	0.5	0.49
Ti/Nb	255.9	312.6	354.4	330	215	335	341.6	226.7	257.7	368.8	307.4	349	345	315.5		
La_N/Yb_N	8.1	7.9	7	7.6	6.7	6.7	6.1	6.5	6.9	6.9	6.8	7.2	7.6	5.8	9.3	9.2^
La_N/Sm_N	3.8	3.3	3.1	3.3	2.9	2.9	2.4	3	3	3.2	3.3	3.3	3.3	3	4.2	
Tb_N/Yb_N	1.2	1.5	1.3	1.6	1.3	1.6	1.5	1.5	1.6	1.4	1.3	1.3	1.4	1.2	1.24	
Cr/Th	8.1	7.9	12	11.1	12.4	13.5	8.7	16.9	6.8	14.6	7.3	7.5	6.8	16.7	7.76	7.53#
Ti/Zr	23.6	35.4	26.8	23.6	10.2	25.2	18.3	20.2	23.2	25	20.5	25.2	27.4	26.9	12.9	28.55
K/Cs	4037	4050	6183	6645	3898	4924	4267	3384	3671	4148	5152	5342	4735	7047	6136	2050

Table 1: Average geochemical data of following formations: Gual: Gualcamayo; LAz: Los Azules; LCa: La Cantera; LV: Las Vacas; LPT: Las Plantas and Trapiche; DB: Don Braulio; LCh: La Chilca; E: Empozada; SOM: Los Sombreros; YL: Yerba Loca; A: Alcaparrosa; PDT: Portezuelo del Tontal; SI: Sierra de la Invernada; PT: Ponón Trehué; UCC: upper continental crust; PAAS: Post-Archaean Australian Shales. Data from ^ Nance and Taylor (1976); # Taylor and McLennan (1985); *McLennan *et al.* (2006). Major elements are in % whereas trace elements are in ppm.

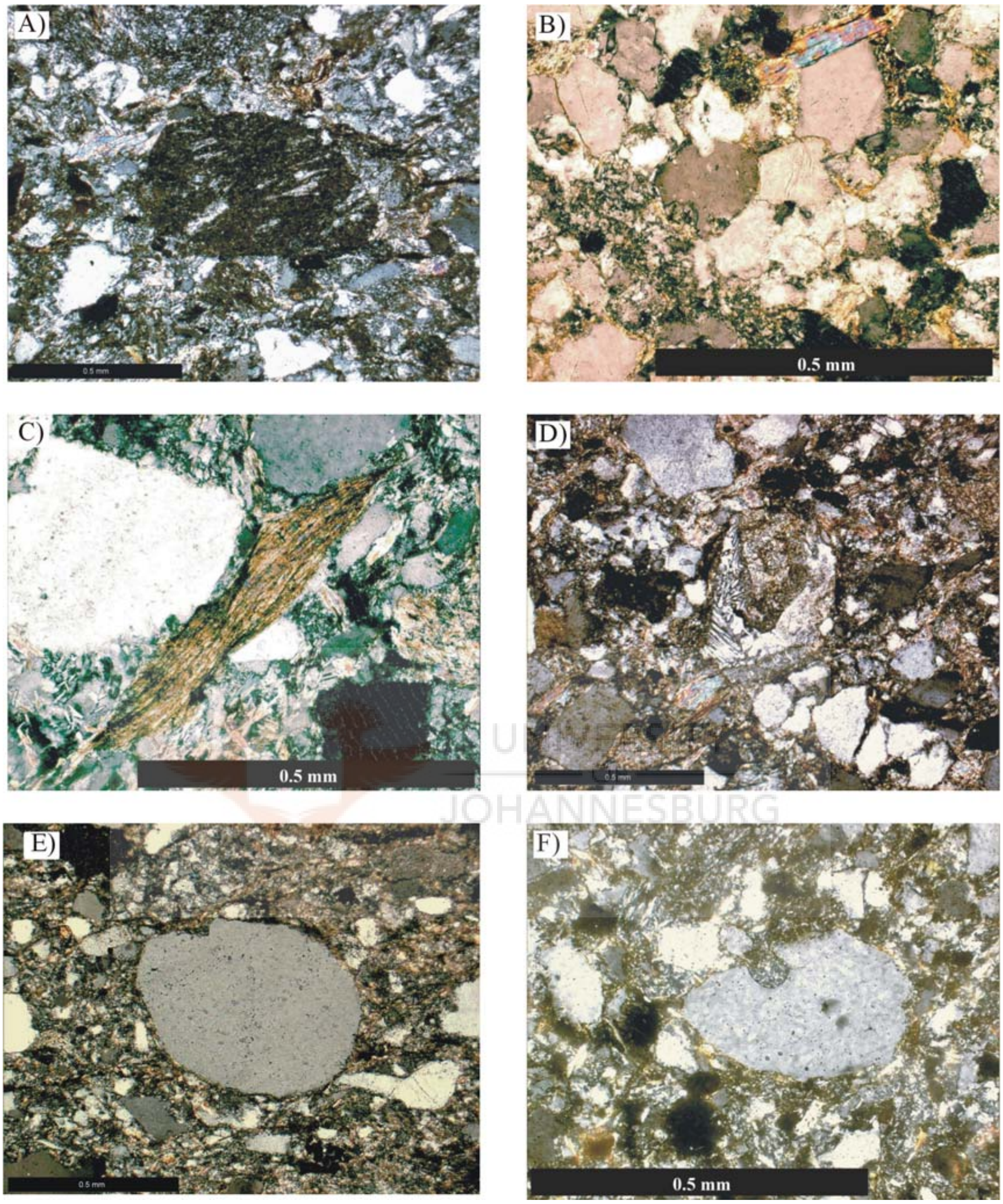

Figure C.1: Light microscope photographs from arenites and wackes to illustrate the petrography of the clastic record. A) Very fine mafic volcanic lithoclast with elongated phenocrystals of plagioclase. B) Subrounded to subangular quartz grains and detrital muscovite lamellae. C) Metamorphic lithoclast (phyllite). D) A large detrital grain of angular graphic quartz is shown in the centre of the image. E) Well rounded quartz grain several times bigger than the other detrital components. F) Detrital quartz with embayment that points to a volcanic origin for the grain, although it could have been produced by dissolution as well. Bar length is 0.5mm.

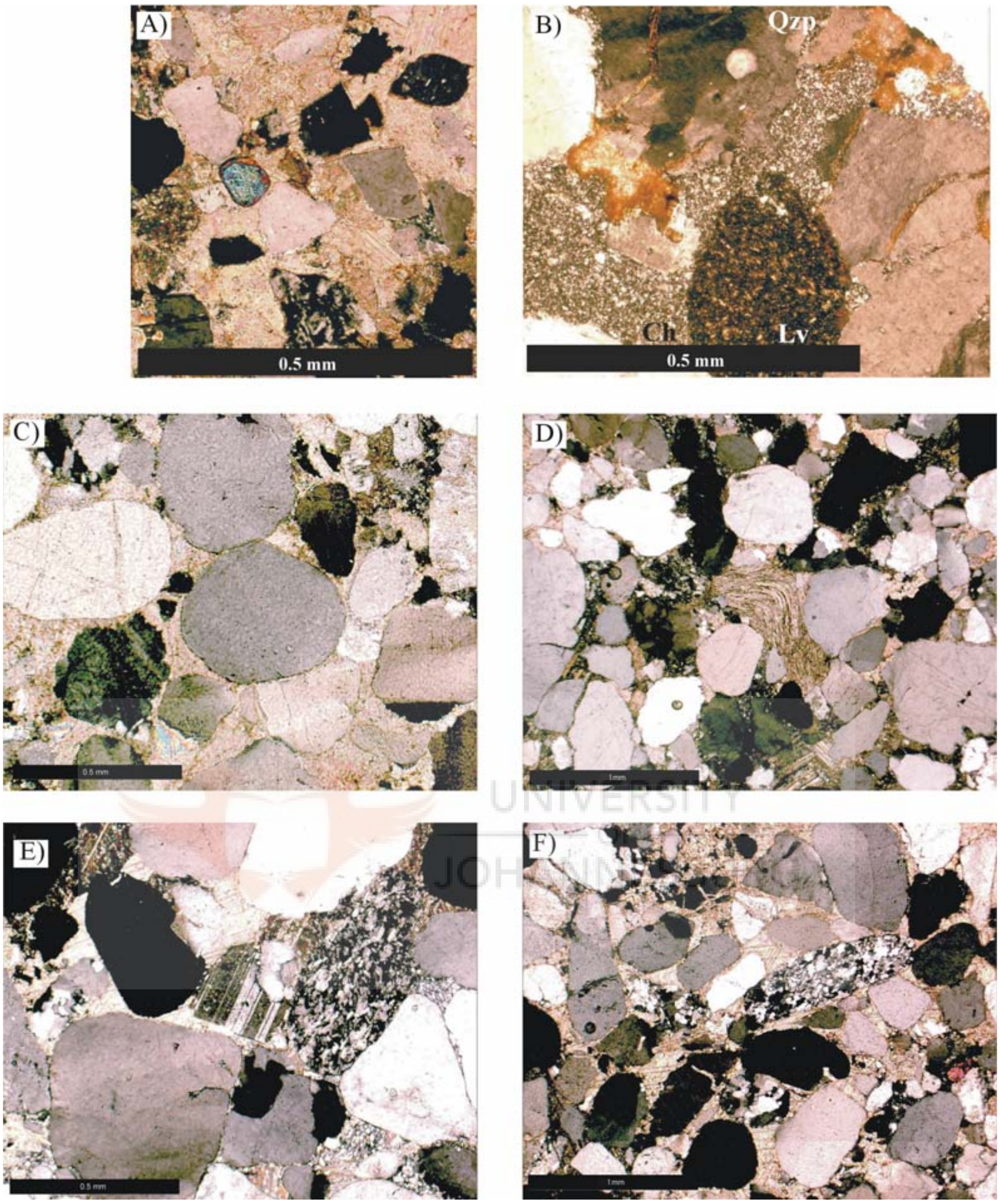

Figure C.2: Light microscope photographs from arenites and wackes to illustrate the petrography of the clastic record. A) General view of a carbonate-cemented sandstone of the Empozada Formation. Note the epidote grain in the centre-left area. B) Three types of lithoclasts are shown: Lv: volcanic lithoclast; Ch: chert; Qzp: polycrystalline quartz. Bar length is 0.5mm. C) Well rounded quartz-grains embedded in carbonate cement of the Don Braulio Fm. D) Deformed sedimentary lithoclast from a very fine grained rock is observable in the centre of the image. E) Subrounded and rounded quartz grains and a crystal of twinned plagioclase slightly altered to clay minerals in the centre. F) General view of a quartz-rich arenite of the Don Braulio Formation. Monocrystalline quartz is the more abundant mineral, but polycrystalline grains (centre-right) are also present. The cement is mainly calcite in composition.

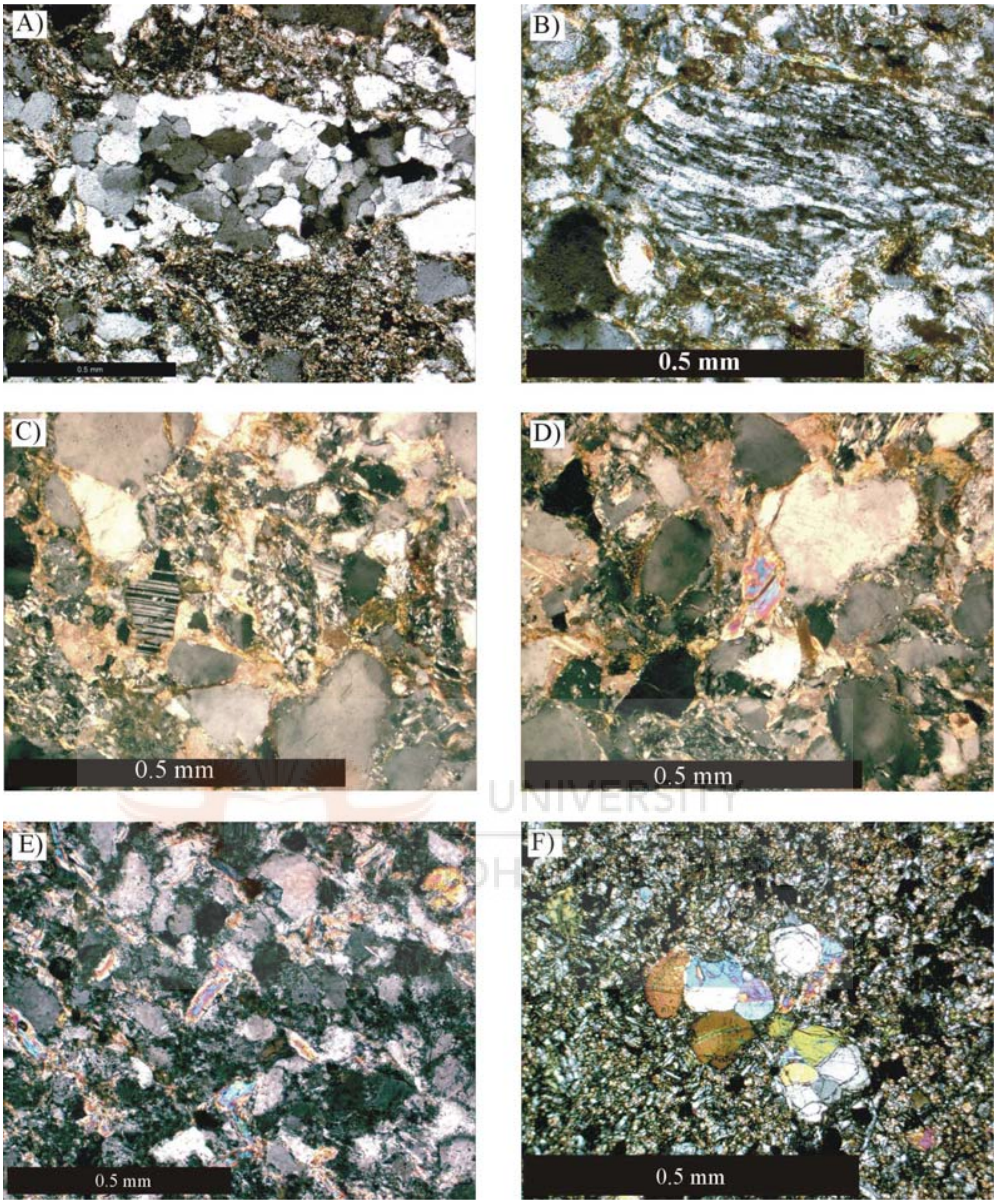

Figure C.3: Light microscope photographs from arenites and wackes to illustrate the petrography of the clastic and volcanic records. A) Polycrystalline grain within arenite from the Portezuelo del Tontal Formation. B) Metamorphic lithoclast derived from quartz-rich banded medium-grade rock; Portezuelo del Tontal Formation. C) General view of arenite from the Sierra de la Invernada Formation; an unaltered plagioclase and carbonate cement are observable. D) General view of arenite from the Sierra de la Invernada Formation. E) General view of fine arenite with matrix composed predominately of white micas from the Yerba Loca Formation. F) Phenocrystals of olivine within a pilotaxitic groundmass is the texture of the volcanic rocks interlayered with the Yerba Loca sequence.

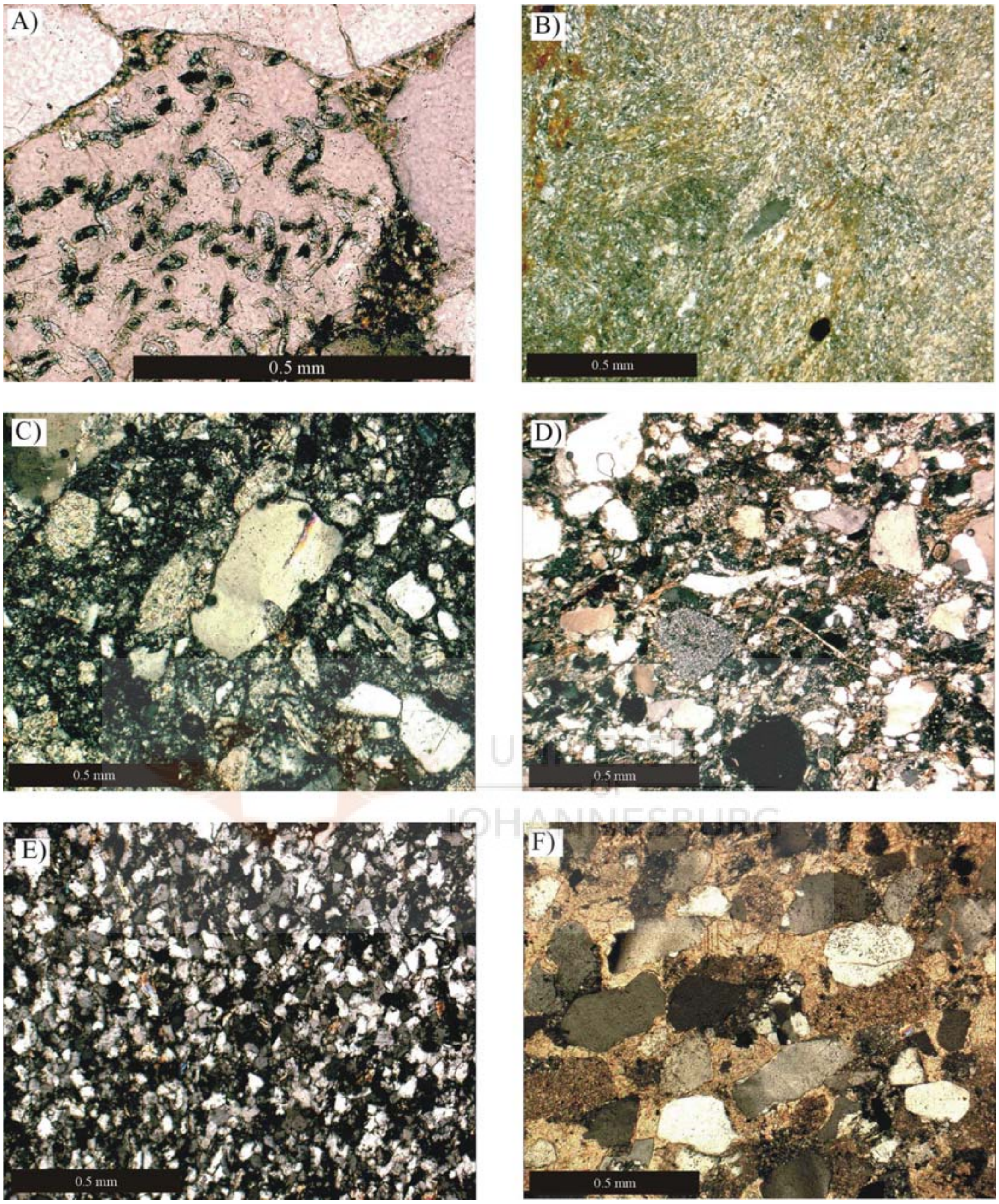

Figure C.4: Light microscope photographs from arenites and wackes to illustrate the petrography of the clastic record. A) A quartz-grain with inclusions of booklets of kaolinite from the Don Braulio Formation. B) Siltstone from the Ponón Trehué Formation. C) Quartz with embayments is shown in the centre of the image from a feldspathic-arenite of the Ponón Trehué Formation. D) Typical wacke from the Pavón Formation showing a lithoclast of chert in the centre-left area of the image. E) Quartz and feldspar compose the siltstones of the Los Sombreros Formation. F) Characteristic composition of arenites with carbonate cement of the La Cantera Formation.

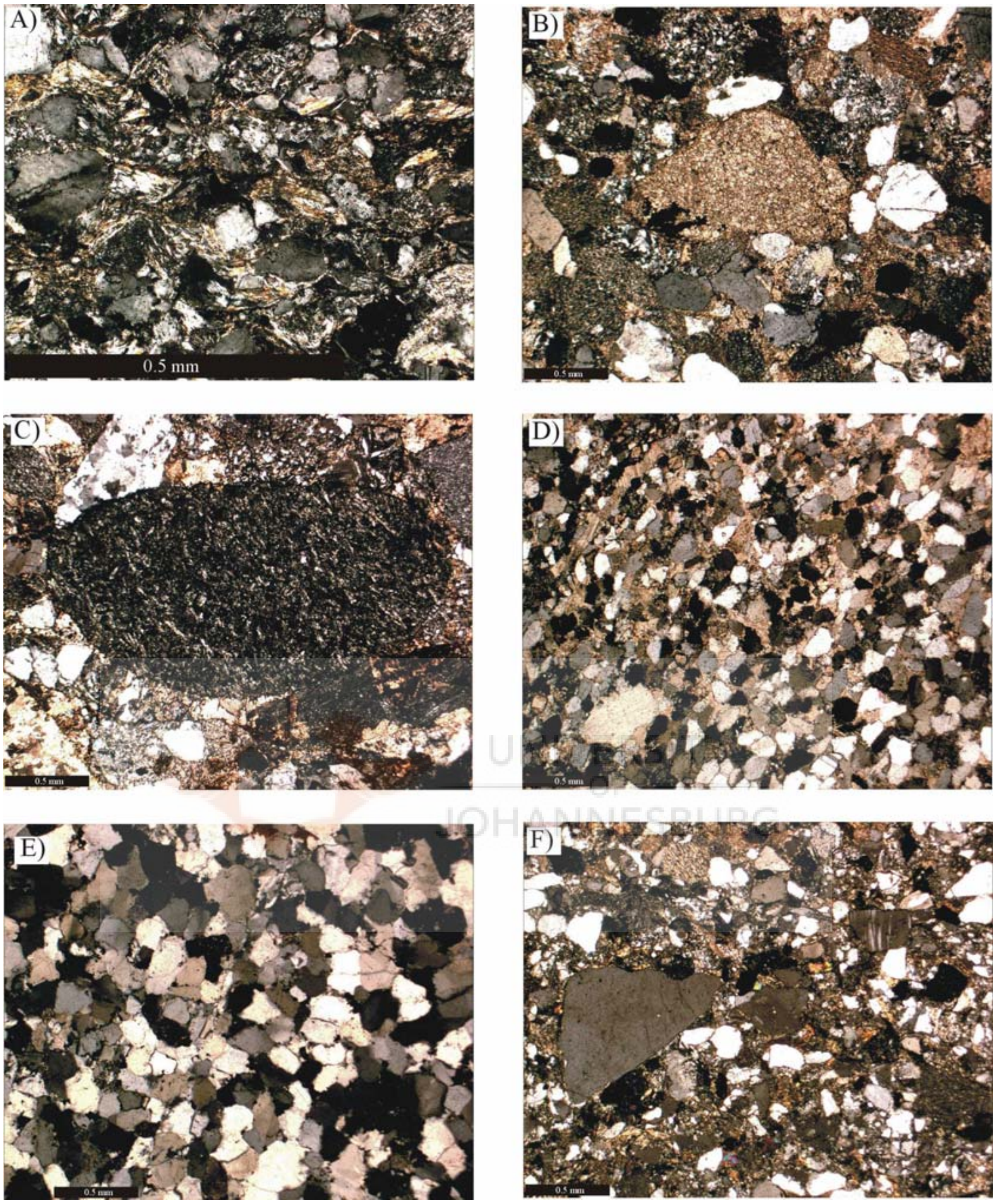

Figure C.5: Light microscope photographs from arenites and wackes to illustrate the petrography of the clastic record. A) Typical arenite from the Las Vacas Formation. B) A large carbonate lithoclast is shown in the centre of the arenite of the Las Plantas and Trapiche Formations. C) Large volcanic lithoclasts are also abundant in the latter mentioned units. D) General view of a quartz-arenite with abundant carbonate cement from the Las Plantas and Trapiche Formations. E) General view of a quartz-arenite without cement and matrix from the Las Plantas and Trapiche Formations. F) Poorly sorted arenite from the Las Vacas Formation.

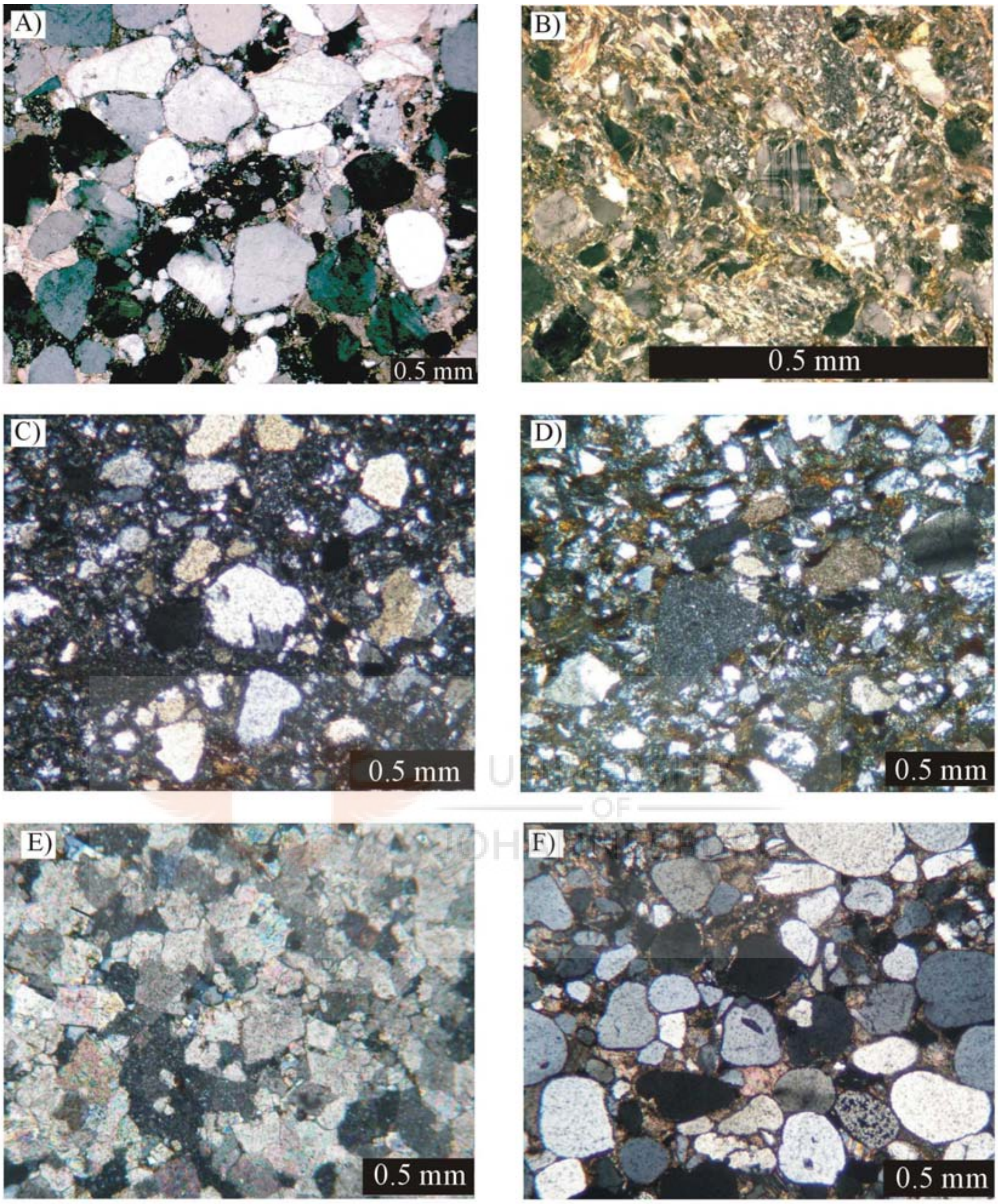

Figure C.6: Light microscope photographs from arenites and wackes to illustrate the petrography of the clastic record. A) Subfeldspathic arenite from the Don Braulio Formation; note the carbonate (light pink) cementing the detrital subrounded grains. B) Subfeldspathic wacke from the Sierra de la Invernada Formation; a microcline grain is present in the centre of the picture. C) Sublithic wacke from the Yerba Loca Formation. D) Sublithic arenite from the Las Vacas Formation showing fine-grained lithoclasts. E) Carbonate-arenite from the Yerba Loca Formation. F) Quartz-arenite from the Las Plantas-Trapiche Formation, showing rounded to subrounded quartz grains.

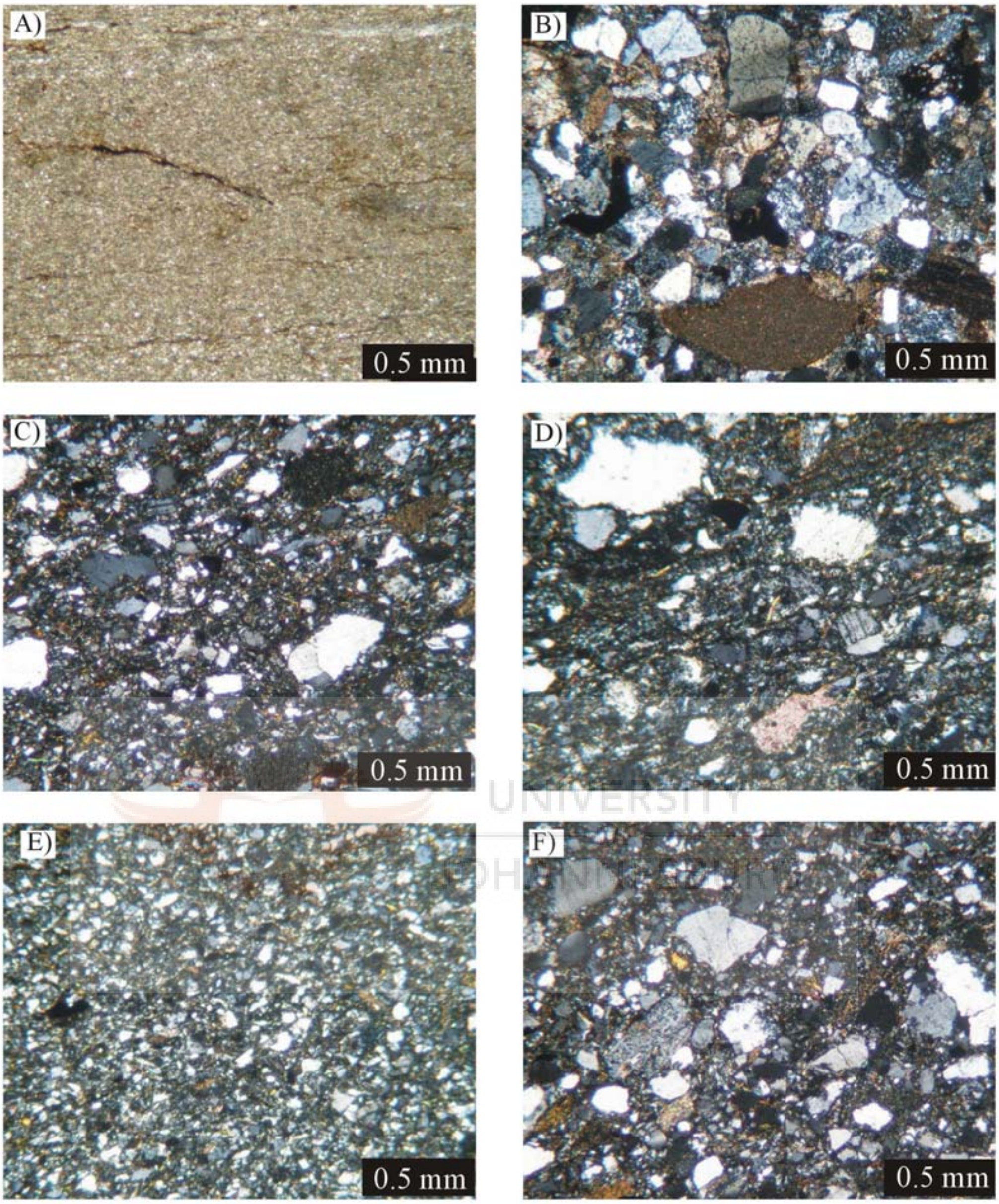

Figure C.7: Light microscope photographs to illustrate the petrography of the clastic record. A) Coarse siltstone from the Los Azules Formation. B) Very fine conglomerate from the Las Plantas and Trapiche Formations. C) The subfeldspathic arenites are the commonest lithotype found within the units studied. D) Subfeldspathic wacke from the Sierra de la Invernada Formation; a detrital plagioclase is shown in the centre-right part of the picture. E) and F) Fine to very fine grained subfeldspathic arenite from the Sierra de la Invernada Formation.

PART 2: ADDITIONAL DATA

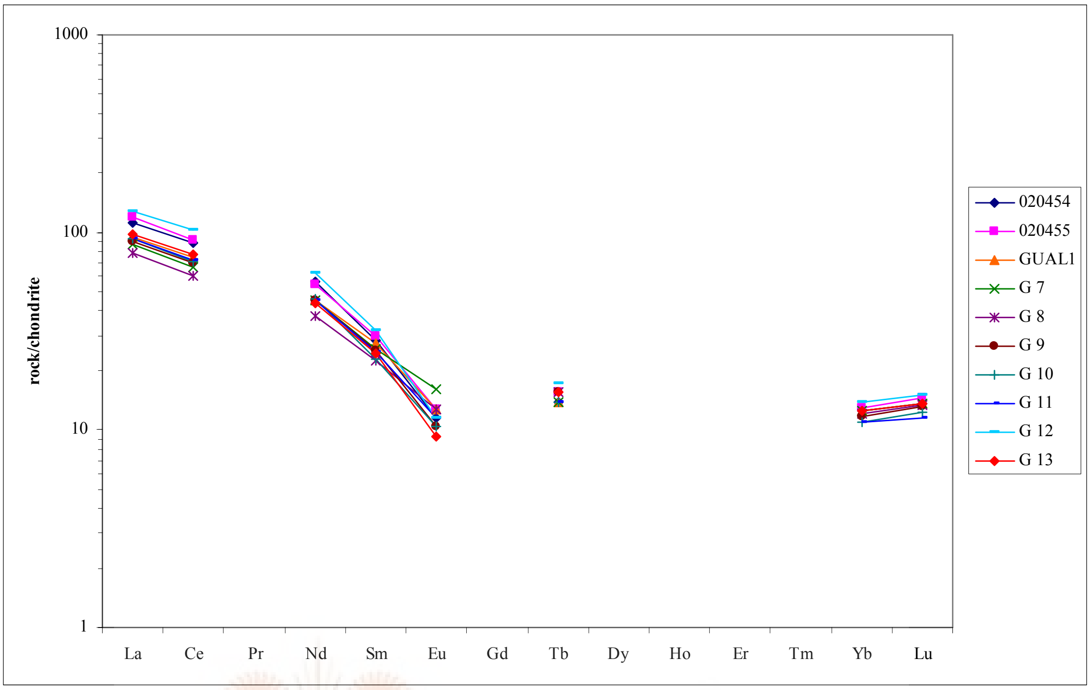

Figure C.8: Chondrite normalized rare earth elements (REE) patterns for the Gualcamayo Formation.

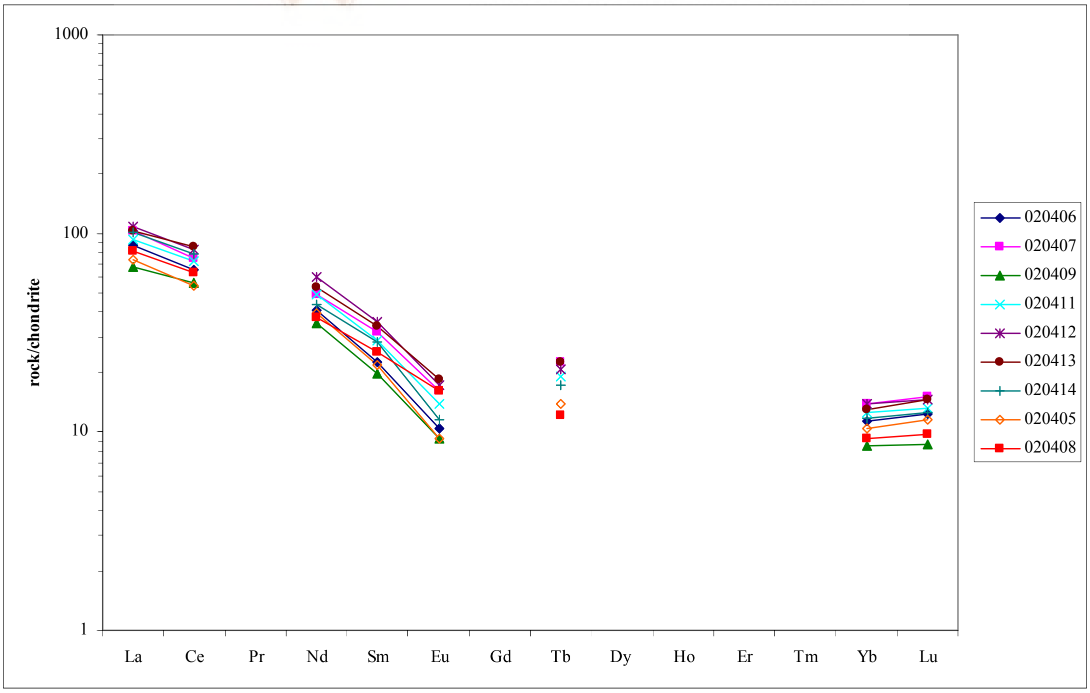

Figure C.9: Chondrite normalized REE patterns for the Los Azules Formation.

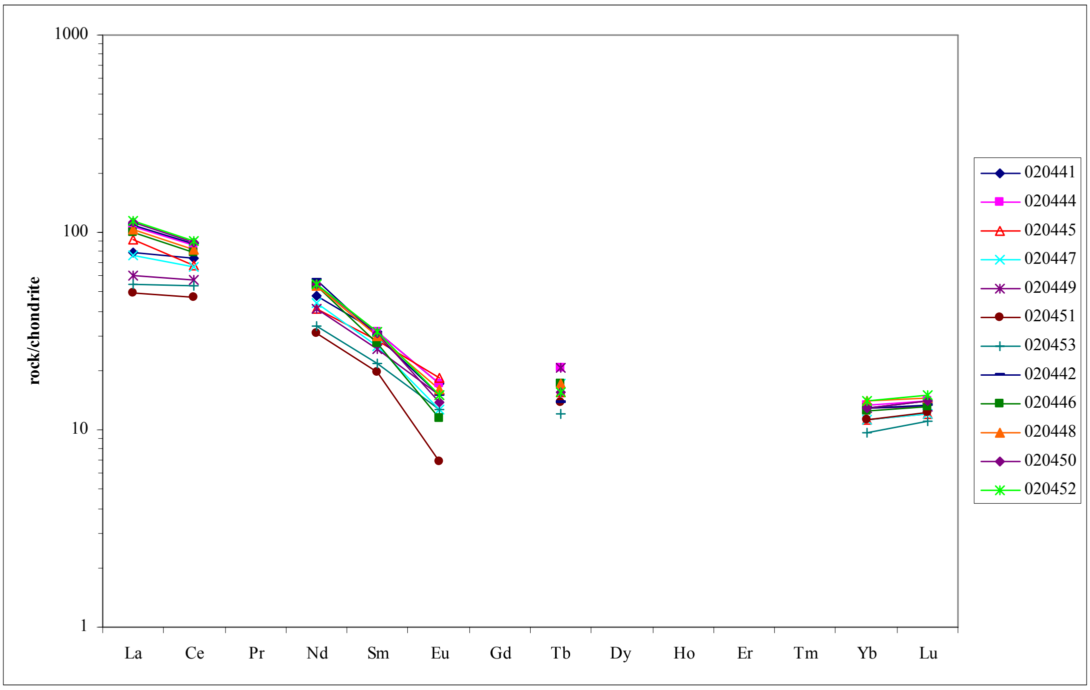

Figure C.10: Chondrite normalized REE patterns for the La Cantera Formation.

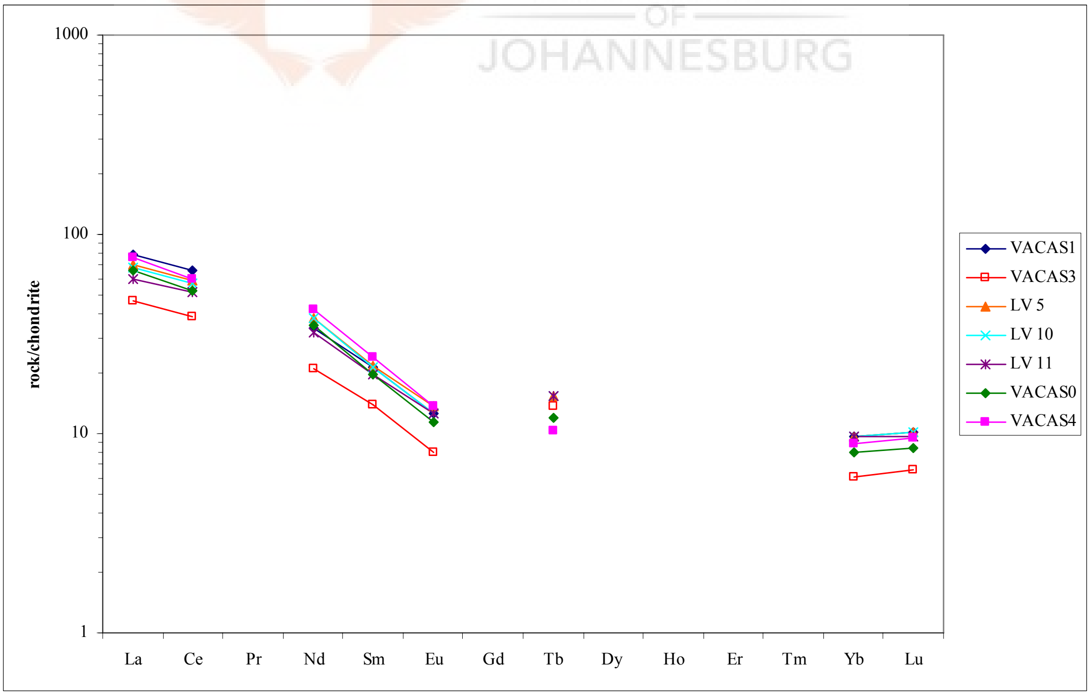

Figure C.11: Chondrite normalized REE patterns for the Las Vacas Formation.

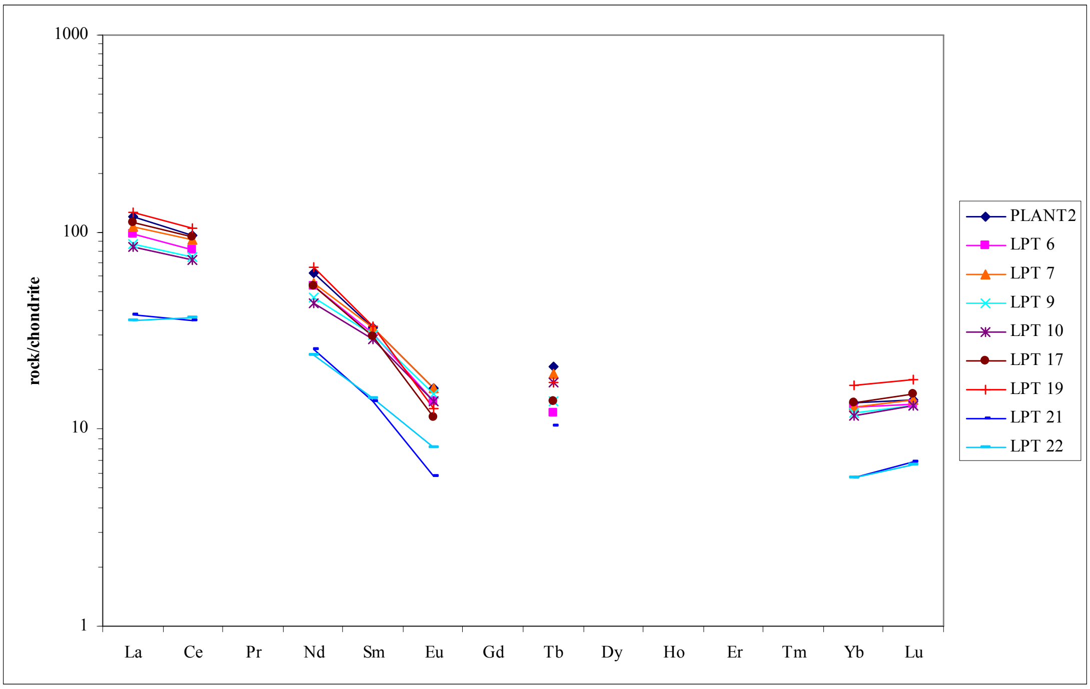

Figure C.12: Chondrite normalized REE patterns for mudstones of the Las Plantas and Trapiche Formations.

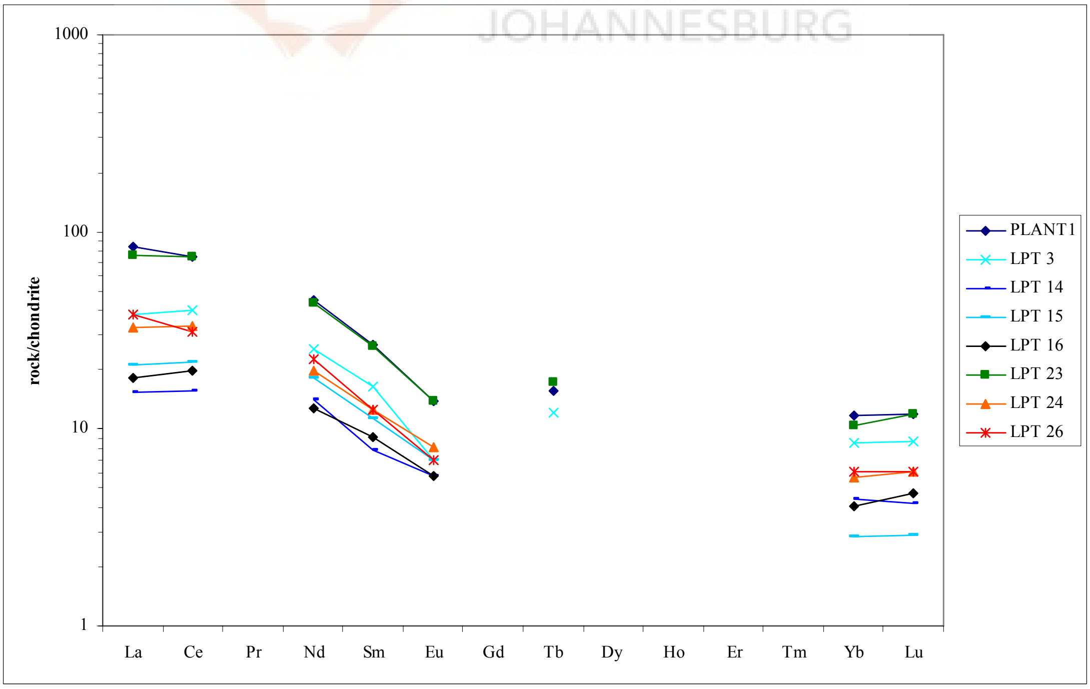

Figure C.13: Chondrite normalized REE patterns for sandstones of the Las Plantas and Trapiche Formations.

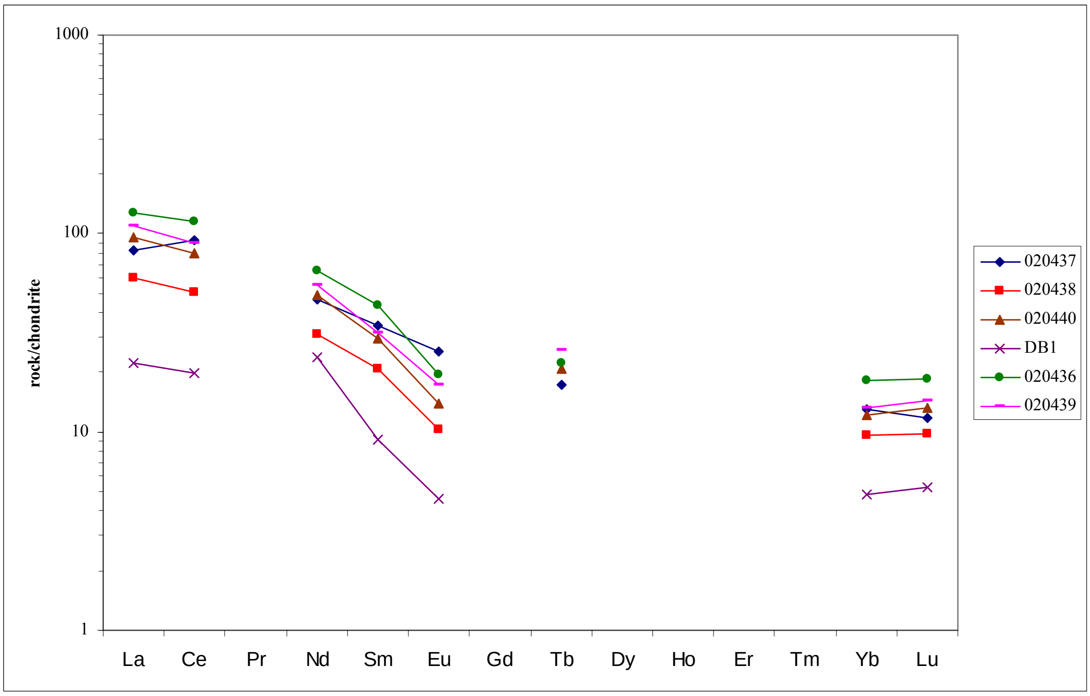

Figure C.14: Chondrite normalized REE patterns for the Don Braulio Formation.

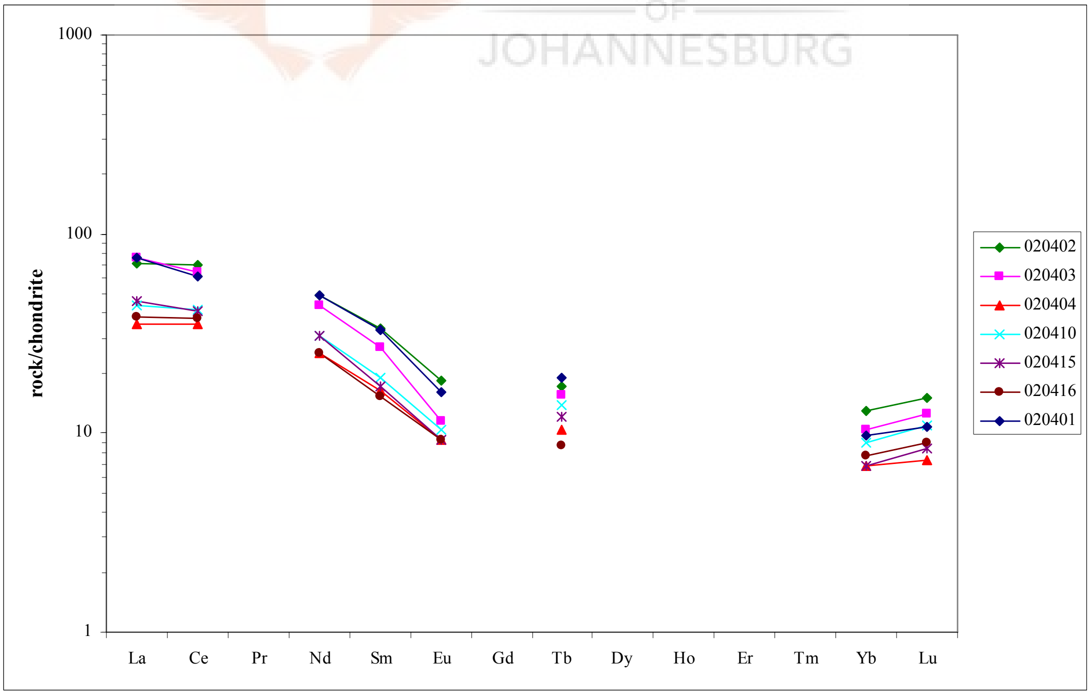

Figure C.15: Chondrite normalized REE patterns for the La Chilca Formation.

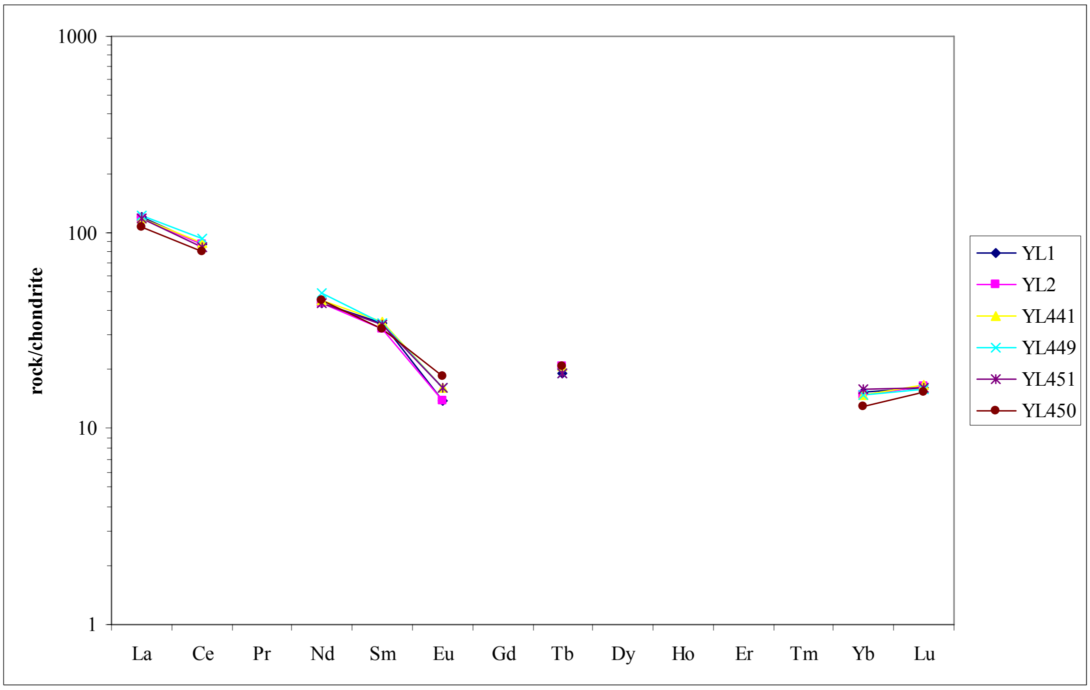

Figure C.16: Chondrite normalized REE patterns for mudstones of the Yerba Loca Formation.

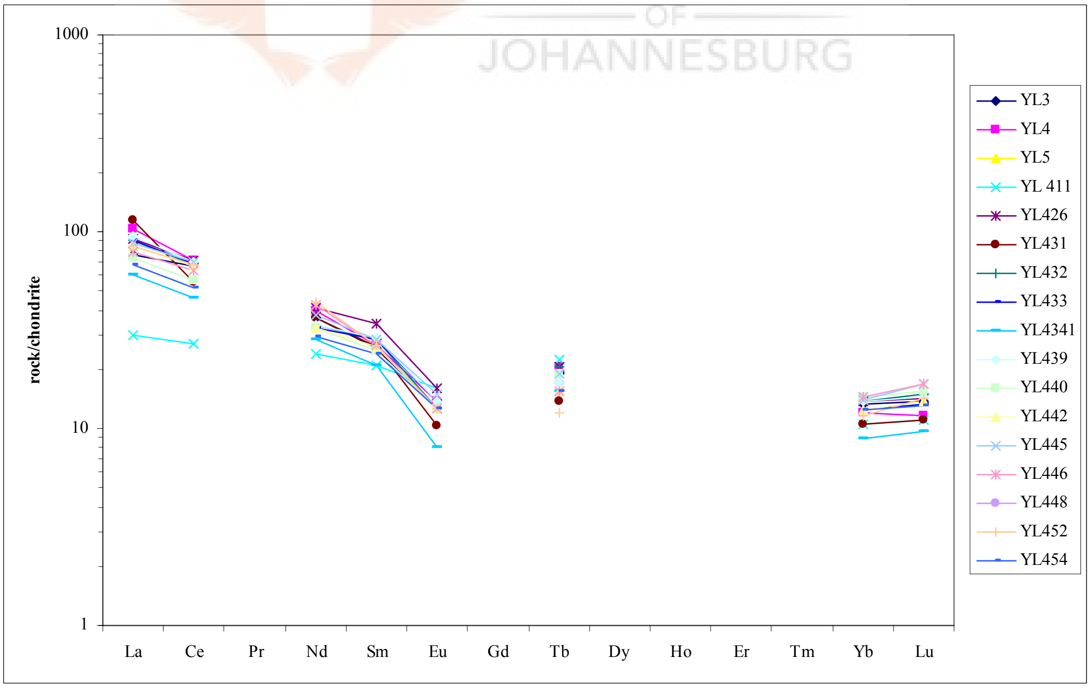

Figure C.17: Chondrite normalized REE patterns for sandstones of the Yerba Loca Formation.

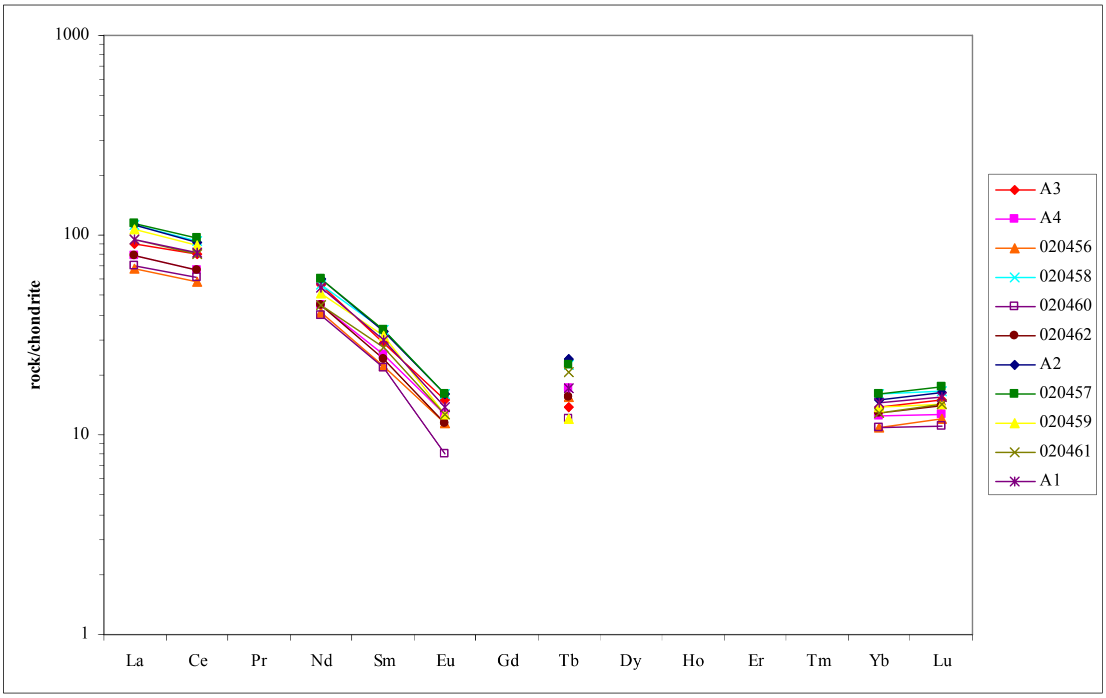

Figure C.18: Chondrite normalized REE patterns for the Alcaparrosa Formation.

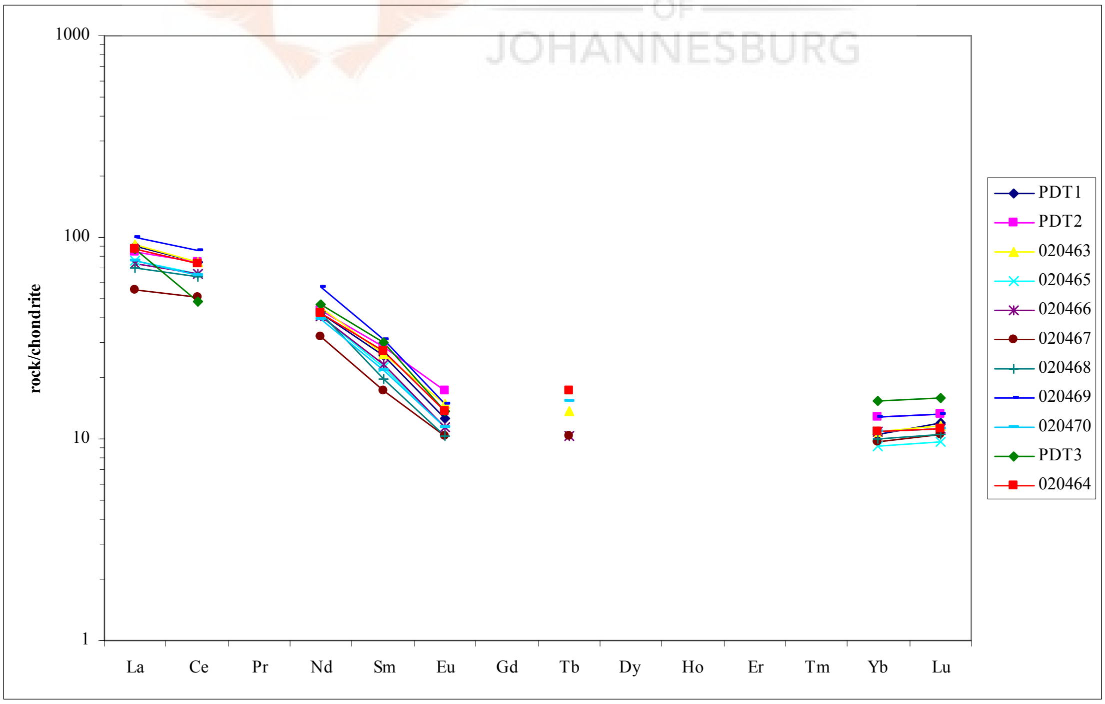

Figure C.19: Chondrite normalized REE patterns for the Portezuelo del Tontal Formation.

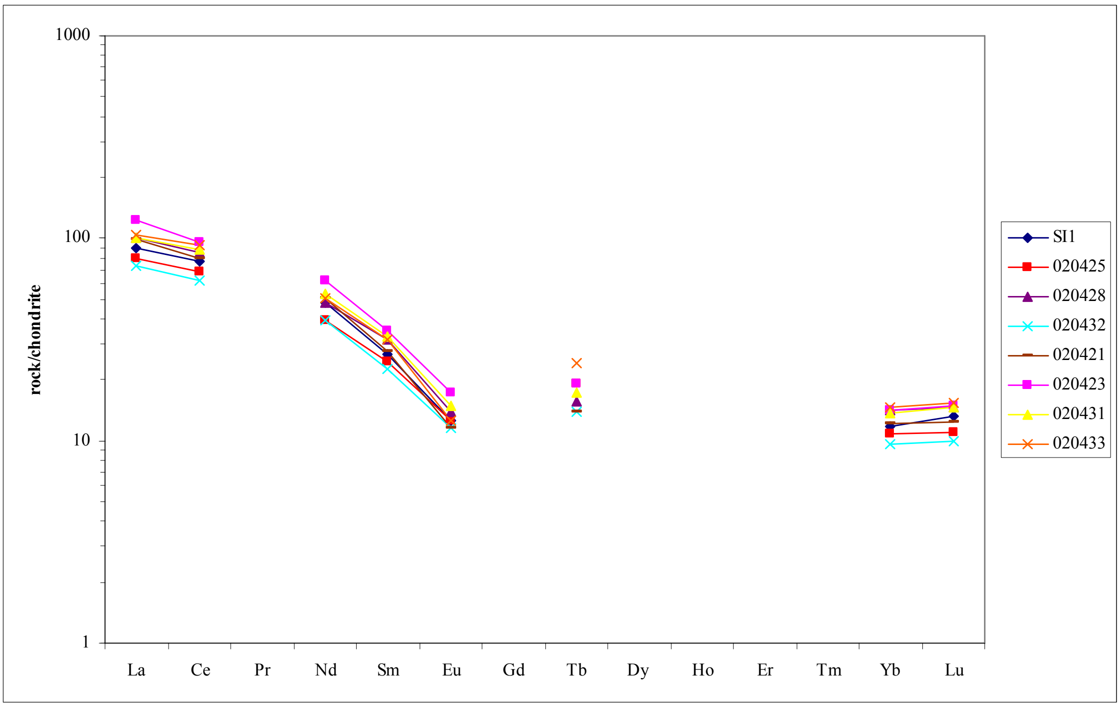

Figure C.20: Chondrite normalized REE patterns for the Sierra de la Invermada Formation.

Gualcamayo Formation

	claystones													
Sample	**020454**	**020455**	**GUAL1**	**G 7**	**G 8**	**G 9**	**G 10**	**G 11**	**G 12**	**G 13**	**G 5**	**G 6**	**Aver**	**SD**
Co	9	14	20	22	16	19	6	9	9	9	9	13.7	12.98	5.05
As	16	15	11	27	17	29	4.9	6	7	14	n.d.	n.d.	14.69	7.8
Sb	2.3	3.1	1.1	2	1.6	2.5	1.5	1.5	1.7	2.3	n.d.	n.d.	1.96	0.56
Ta	1.5	1.2	0.7	1	1.6	1	1.2	2	1.7	1.7	n.d.	n.d.	1.36	0.38
W	21	26	33	13	22	15	34	38	41	35	n.d.	n.d.	27.8	9.28
Cu	49	55.5	56.9	20.6	15.6	18.8	6.1	7	4.8	11.1	10.2	15.2	22.57	18.7
Nb/Y	0.50	0.42	0.42	0.42	0.43	0.47	0.45	0.39	0.52	0.45	0.24	0.19	0.41	0.09
Nb/Ta	10.6	12.42	20.57	15.3	9.94	15.8	11	6.05	10.59	8.35			12.06	3.96
Sc/Th	1.31	1.22	1.16	1.76	1.77	1.76	1.31	1.01	0.77	0.97			1.09	0.58

Table 2: Additional chemical analyses of sedimentary clastic rocks of the Precordillera terrane. Trace elements are in ppm. Aver: average; SD: standard deviation; b.d.l.: below detection limits; n.d.: not determined.

Los Azules Formation

	claystones							siltstones			
Sample	**020406**	**020407**	**020409**	**020411**	**020412**	**020413**	**020414**	**020405**	**020408**	**Aver**	**SD**
Co	15	28	25	19	19	31	15	21	10	20.33	6.34
As	3.6	12	4.8	94.6	13	12	11	65.6	1.5	24.23	30.88
Sb	1.6	2	0.3	4.5	1.7	1.2	1.2	5.3	b.d.l.	2.23	1.63
Ta	1.7	1.6	3	0.6	2.1	1.3	1.7	1.1	1.2	1.59	0.64
W	24	22	15	67	43	41	24	156	25	46.33	41.53
Cu	31.6	64.8	48.5	41.4	54	47.7	41.6	31.1	18.8	42.17	12.93
Nb/Y	0.48	0.31	1.07	0.35	0.42	0.5	0.62	0.49	0.23	0.5	0.23
Nb/Ta	8.71	8.88	7.57	23.33	8.05	13.62	10.35	10.73	8.58	11.09	4.66
Sc/Th	1.58	1.32	1.44	1.58	1.69	1.52	1.35	0.89	1.45	1.42	0.22

Table 2 (cont.): Additional chemical analyses of sedimentary clastic rocks of the Precordillera terrane. Trace elements are in ppm. Aver: average; SD: standard deviation; b.d.l.: below detection limits; n.d.: not determined.

La Cantera Formation

	mudstones					sandstones								
Sample	**020442**	**020446**	**020448**	**020450**	**020452**	**020441**	**020444**	**020445**	**020447**	**020449**	**020451**	**020453**	**Aver**	**SD**
Co	27	28	24	27	22	24	26	18	33	30	31	50	28.33	7.61
As	7.1	7	7.6	11	6.6	3.1	5.3	3.3	1.4	2	2.5	b.d.l.	5.17	2.83
Sb	0.6	0.7	0.6	1.3	0.6	0.4	0.6	0.2	0.2	0.2	b.d.l.	b.d.l.	0.54	0.31
Ta	1.8	1.2	1.7	1.3	2	1.3	1.2	1.8	2.3	1.9	2.1	3.5	1.84	0.61
W	30	19	66	32	36	143	13	105	264	299	352	547	158.83	163.06
Cu	54.6	57.1	49.7	48.7	48.9	21.3	52.5	16.9	20.6	17.7	14.9	17.3	35.02	17.11
Nb/Y	0.59	0.65	0.62	0.57	0.65	0.64	0.56	0.28	0.88	0.48	0.72	0.93	0.63	0.16
Nb/Ta	10.44	16.67	12.18	14.54	10.60	14.54	15.17	7.61	7.61	8.32	7.43	4.77	10.82	3.63
Sc/Th	1.74	1.84	1.65	1.71	1.63	1.46	1.94	1.36	1.55	1.49	1.23	1.46	1.59	0.19

Table 2 (cont.): Additional chemical analyses of sedimentary clastic rocks of the Precordillera terrane. Trace elements are in ppm. Aver: average; SD: standard deviation; b.d.l.: below detection limits; n.d.: not determined.

Las Vacas Formation

	mudstones		sandstones						
Sample	**VACAS0**	**VACAS4**	**VACAS1**	**VACAS3**	**LV 5**	**LV 10**	**LV 11**	**Aver**	**SD**
Co	13	16	31	29	33	33	29	26.29	7.65
As	4.2	5.1	1.2	1.1	3.2	2.2	2.3	2.76	1.39
Sb	0.5	0.7	0.3	0.2	0.3	0.3	0.4	0.39	0.16
Ta	1.3	0.9	1.7	1.5	2.2	2.7	1.8	1.73	0.55
W	24	23	284	255	225	211	149	167.29	98.74
Cu	25	31.9	25.4	16.1	11.6	12.6	13.1	19.39	7.38
Nb/Y	0.29	0.25	0.63	0.49	0.68	0.74	0.74	0.55	0.19
Nb/Ta	7.23	11.33	8.35	6.53	6.68	5.41	7.83	7.62	1.75
Sc/Th	1.61	1.57	1.69	1.5	2.32	2.38	2.21	1.9	0.36

Table 2 (cont.): Additional chemical analyses of sedimentary clastic rocks of the Precordillera terrane. Trace elements are in ppm. Aver: average; SD: standard deviation; b.d.l.: below detection limits; n.d.: not determined.

Las Plantas – Trapiche Formations

	mudstones									VF conglomerate	
Sample	**PLANT2**	**LPT 6**	**LPT 7**	**LPT 9**	**LPT 10**	**LPT 17**	**LPT 19**	**LPT 21**	**LPT 22**	**LPT 25**	**LPT 26**
Co	22	25	29	36	26	22	34	41	37	14.1	31
As	8.1	7.1	7.4	6.5	5.4	10	8.6	1.5	1.7	b.d.l.	2.9
Sb	1.2	0.4	0.4	0.4	0.4	0.6	0.6	b.d.l.	b.d.l.	b.d.l.	0.2
Ta	2	1.6	2.4	2.6	2.1	2.2	2.2	2.6	2.3	b.d.l.	2
W	64	138	185	296	182	167	328	536	458		322
Cu	54.5	9.3	10.1	7.3	6	11.5	6.3	4.8	4.8	6.1	7.3
Nb/Y	0.59	0.53	0.63	0.48	0.45	0.69	0.63	0.87	0.93	0.38	0.41
Nb/Ta	9.55	10.19	7.96	5.65	6.52	9.14	9.91	2.58	2.87		4.3
Sc/Th	1.48	1.53	1.38	1.42	1.4	1.53	1.22	1.15	1.19		1.38

Table 2 (cont.): Additional chemical analyses of sedimentary clastic rocks of the Precordillera terrane. Trace elements are in ppm. Aver: average; SD: standard deviation; b.d.l.: below detection limits; n.d.: not determined.

Las Plantas – Trapiche Formations (cont.)

	sandstones													
Sample	**PLANT1**	**LPT1**	**LPT2**	**LPT3**	**LPT5**	**LPT12**	**LPT13**	**LPT14**	**LPT15**	**LPT16**	**LPT23**	**LPT24**	**Aver**	**SD**
Co	26	22.4	19.1	17	21	27.1	80.3	58	50	63	38	30	33.43	15.73
As	2.7	b.d.l.	b.d.l.	1	b.d.l.	b.d.l.	b.d.l.	1.1	0.9	0.9	4	1.7	4.21	3.06
Sb	0.3	b.d.l.	b.d.l.	b.d.l.	b.d.l.	b.d.l.	b.d.l.	b.d.l.	b.d.l.	b.d.l.	b.d.l.	b.d.l.	0.5	0.27
Ta	2	b.d.l.	b.d.l.	1.1	b.d.l.	b.d.l.	b.d.l.	4	3.2	3.9	3.9	1.9	2.47	0.8
W	168	b.d.l.	b.d.l.	242	b.d.l.	b.d.l.	b.d.l.	864	721	898	445	438	379.53	244.35
Cu	35.8	2	2.7	4.7	1.5	1.3	3.6	1.7	3.1	1.7	4.2	3.8	8.44	11.97
Nb/Y	0.65	0.17	0.16	0.11	0.14	0.19	4	3.67	0.54	3.62	0.7	0.29	0.9	1.13
Nb/Ta	8.5			3.36				1.1	1.25	1.21	3.44	2.89	5.32	3.21
Sc/Th	1.48			1.21				2.17	1.33	1.08	1.1	1.2	1.37	0.25

Table 2 (cont.): Additional chemical analyses of sedimentary clastic rocks of the Precordillera terrane. Trace elements are in ppm. Aver: average; SD: standard deviation; b.d.l.: below detection limits; n.d.: not determined.

Don Braulio Formation

	mudstones		sandstones					
Sample	**020436**	**020439**	**020437**	**020438**	**020440**	**DB1**	**Aver**	**SD**
Co	16	21	32	33	24	55	30.17	12.59
As	15	2.1	10	4.2	5.9	2.8	6.67	4.53
Sb	0.4	0.4	b.d.l.	0.3	0.5	b.d.l.	0.4	0.07
Ta	1.6	1.7	2.3	2.9	2	4	2.42	0.83
W	25	39	326	296	65	739	248.33	250.46
Cu	35.8	40.4	18.6	22.1	35.1	9.2	26.87	11.06
Nb/Y	0.6	0.56	0.27	0.65	0.6	0.38	0.51	0.14
Nb/Ta	14.13	10.65	5.09	5	8.8	1.4	7.51	4.18
Sc/Th	1.45	1.51	0.87	1.53	1.7	1.14	1.37	0.28

Table 2 (cont.): Additional chemical analyses of sedimentary clastic rocks of the Precordillera terrane. Trace elements are in ppm. Aver: average; SD: standard deviation; b.d.l.: below detection limits; n.d.: not determined.

La Chilca Formation

	mudstone	sandstones							
Sample	**020401**	**020402**	**020403**	**020404**	**020410**	**020415**	**020416**	**Aver**	**SD**
Co	10	45	22	22	28	36	46	29.86	12.24
As	14	4.1	18	1.8	5.3	2.3	2.1	6.8	6.03
Sb	0.4	0.2	0.4	b.d.l.	b.d.l.	b.d.l.	b.d.l.	0.33	0.09
Ta	1.1	3.6	2.1	1.6	1.5	2.6	3.3	2.26	0.88
W	47	491	209	254	311	450	590	336	172.6
Cu	19.3	13.6	20	15.1	11	10.9	12	14.56	3.5
Nb/Y	0.6	0.6	0.64	0.51	0.85	0.92	1.29	0.77	0.25
Nb/Ta	14	4	6.05	5.19	6.73	4.08	3.21	6.18	3.39
Sc/Th	1.51	1.14	1.28	1.26	1.06	1.21	0.8	1.18	0.2

Table 2 (cont.): Additional chemical analyses of sedimentary clastic rocks of the Precordillera terrane. Trace elements are in ppm. Aver: average; SD: standard deviation; b.d.l.: below detection limits; n.d.: not determined.

Empozada Formation

	mudstones				sandstones						
Sample	**E2**	**E4**	**E5**	**E7**	**E1**	**E3**	**E6**	**E8**	**E10**	**Aver**	**SD**
Co	18	23	27	27	21	28	45	39	33	29	8.2
As	7.8	14	20	1.3	3	2.2	4.9	2.8	5.1	6.8	5.9
Sb	0.2	0.4	0.5	0.8	0.1	b.d.l.	b.d.l.	0.5	1.3	0.5	0.4
Ta	1	1.4	1.5	1	1.3	1.2	3.3	2.6	2.5	1.8	0.8
W	60	84	78	39	220	202	591	513	229	224	188.8
Cu	6.6	12.9	22.5	141.9	3.4	3.7	7.7	7.7	7	23.7	42.1
Nb/Y	10.7	0.77	0.55	0.65	3.33	18.82	0.59	0.14	2.49	4.23	6.03
Nb/Ta	9.63	10.5	12.71	15.8	5.38	5.75	3.52	2.06	8.27	8.18	4.2
Sc/Th	1.21	1.37	1.5	1.18	0.96	0.82	0.77	0.87	5.24	1.55	1.33

Table 2 (cont.): Additional chemical analyses of sedimentary clastic rocks of the Precordillera terrane. Trace elements are in ppm. Aver: average; SD: standard deviation; b.d.l.: below detection limits; n.d.: not determined.

Los Sombreros Formation

	mudstones							sandstones			
Sample	**020418**	**LRAT1**	**SOM 5**	**SOM 6**	**SOM 7**	**SOM 8**	**SOM 9**	**020419**	**LRAT2**	**Aver**	**SD**
Co	30	25	21	23	29	25	30	28	26	26.33	2.98
As	38	8.5	12	11	4.5	7.4	11	16	4.6	12.56	9.64
Sb	1	0.7	0.7	0.9	0.3	0.4	0.9	0.8	0.6	0.7	0.22
Ta	2.1	2.4	1.6	2.3	1.6	1.5	0.7	1.2	2.7	1.79	0.6
W	47	80	39	67	165	38	192	124	130	98	53.74
Cu	34.2	43.8	20.6	15.5	10.4	19.4	9	26.2	26.2	22.81	10.58
Nb/Y	0.72	0.58	0.55	0.47	0.17	0.48	0.29	0.17	0.61	0.45	0.19
Nb/Ta	9.24	8.54	11.63	8.17	6.31	10.6	8	9.67	5.74	8.66	1.78
Sc/Th	1.5	1.36	1.16	1.21	1.61	1.36	2.94	1.64	1.41	1.58	0.51

Table 2 (cont.): Additional chemical analyses of sedimentary clastic rocks of the Precordillera terrane. Trace elements are in ppm. Aver: average; SD: standard deviation; b.d.l.: below detection limits; n.d.: not determined.

Yerba Loca Formation

	mudstones						sandstones						
Sample	**YL1**	**YL2**	**YL441**	**YL449**	**YL451**	**YL450**	**YL3**	**YL4**	**YL5**	**YL 411**	**YL426**	**YL431**	**YL432**
Co	31	30	15	33	25	73	43	57	46	84	70	115	16
As	5.4	48	26	1.7	10	4.9	4.1	15	b.d.l.	b.d.l.	3.9	4.7	9.2
Sb	0.5	0.3	0.7	0.8	0.9	0.6	0.6	0.5	b.d.l.	b.d.l.	1.3	0.4	1.2
Ta	1.9	1.6	1.6	1.1	1.4	1.2	2.6	2.1	b.d.l.	1.1	0.9	0.8	1.2
W	114	52	2	44		307	380	246	b.d.l.	211	292	573	2
Cu	35	31.2	25.6	20.5	22.2		18.6	24.5	27	169.4	21.8	22.3	26.3
Nb/Y	0.53	0.58	0.62	0.5	0.47		0.69	0.8	0.67	0.49	0.52	1	0.55
Nb/Ta	9.6	12.21	12.79	17.09	13.62		6.26	7.68		14.36	16.93	17.46	12.33
Sc/Th	1.36	1.48	1.34	1.39	1.49	1.19	1.22	1.04		44.5	1.59	1.42	1.35

Table 2 (cont.): Additional chemical analyses of sedimentary clastic rocks of the Precordillera terrane. Trace elements are in ppm. Aver: average; SD: standard deviation; b.d.l.: below detection limits; n.d.: not determined.

Yerba Loca Formation (cont.)

	sandstones											
Sample	**YL433**	**YL4341**	**YL439**	**YL440**	**YL442**	**YL445**	**YL446**	**YL448**	**YL452**	**YL454**	**Aver**	**SD**
Co	21	101	14	14	12	104	91	151	195	27	59.49	47.69
As	7.1	4.2	13	4.6	8.9	5.2	4.2	b.d.l.	8.5	20	10.43	10.44
Sb	0.9	0.5	0.5	0.5	0.6	0.6	0.5	b.d.l.	0.5	1.2	0.68	0.27
Ta	0.9	1	1	1	0.8	1	1.1	b.d.l.	1	0.9	1.25	0.46
W	2	535	2	2	2	576	475	b.d.l.	1030	b.d.l.	255.11	275.58
Cu	22.5	14.2	19.9	32.9	28.3	19.1	21	22.8	17.2	55.8	31.73	31.17
Nb/Y	0.59	1.16	0.68	0.65	0.7	0.66	0.54	0.66	0.71	0.75	0.65	0.15
Nb/Ta	15.78	12.83	14.97	17.5	17.42	16.1	12.7		13.93	16.52	13.9	3.15
Sc/Th	1.45	1.42	1.18	1.16	1.16	1.15	1.15		1.17	3.69	3.47	9.19

Table 2 (cont.): Additional chemical analyses of sedimentary clastic rocks of the Precordillera terrane. Trace elements are in ppm. Aver: average; SD: standard deviation; b.d.l.: below detection limits; n.d.: not determined.

Alcaparrosa Formation

	mudstones					sandstones							
Sample	**A2**	**020457**	**020459**	**020461**	**A1**	**A3**	**A4**	**020456**	**020458**	**020460**	**020462**	**Aver**	**SD**
Co	24	24	19	25	29	40	34	31	25	28	50	29.9	8.3
As	6.8	11	7.9	7.2	8.7	10	7.1	17	8.9	5.7	4.1	8.6	3.2
Sb	0.6	0.6	0.8	1	0.5	0.9	0.6	0.8	0.7	0.8	0.5	0.7	0.2
Ta	2.4	2.2	1.8	1.8	2	3.9	3.5	2.3	1.7	2.1	4	2.5	0.8
W	93	53	35	118	174	584	355	257	82	231	586	233.5	189.3
Cu	38.4	36.7	38.3	35.5	29.4	24.6	23.4	18	34.6	23.1	19.9	29.3	7.4
Nb/Y	0.57	0.61	0.64	0.69	0.64	0.65	0.59	0.73	0.56	0.68	0.74	0.65	0.06
Nb/Ta	9.17	9.23	10.83	10.83	9.55	4.67	4.71	5.96	11.71	6.71	3.78	7.92	2.71
Sc/Th	1.28	1.38	1.4	1.28	1.31	1.24	1.25	1.04	1.39	1.11	0.99	1.24	0.13

Table 2 (cont.): Additional chemical analyses of sedimentary clastic rocks of the Precordillera terrane. Trace elements are in ppm. Aver: average; SD: standard deviation; b.d.l.: below detection limits; n.d.: not determined.

Portezuelo del Tontal Formation

	mudstones		sandstones										
Sample	**PDT3**	**020464**	**PDT1**	**PDT2**	**020463**	**020465**	**020466**	**020467**	**020468**	**020469**	**020470**	**Aver**	**SD**
Co	26	28	32	31	22	35	33	44	40	30	27	31.64	6.02
As	16	10	5.5	4.5	8.5	4.5	3.6	1.3	2.8	3.5	1.5	5.61	4.16
Sb	1.9	1	0.7	0.4	0.9	2.5	0.3	b.d.l.	0.3	0.5	0.3	0.88	0.71
Ta	2.1	2.7	2.3	2.5	1.7	1.4	2.4	2.4	2.6	1.4	2.2	2.15	0.44
W	20	222	263	192	138	287	278	469	419	159	244	244.64	119.25
Cu	102.7	35.5	32.9	26.8	31.2	28.8	31.3	24.1	21.6	35	19.3	35.38	21.88
Nb/Y	0.58	0.63	0.66	0.7	0.7	0.71	0.68	0.79	0.77	0.65	0.75	0.69	0.06
Nb/Ta	10.76	5.78	7.17	7.13	9.47	10.14	6.79	5.58	5.08	13.14	7.45	8.05	2.4
Sc/Th	1.66	1.26	1.23	1.73	1.59	1.35	1.88	1.18	1.23	1.61	1.19	1.45	0.24

Table 2 (cont.): Additional chemical analyses of sedimentary clastic rocks of the Precordillera terrane. Trace elements are in ppm. Aver: average; SD: standard deviation; b.d.l.: below detection limits; n.d.: not determined.

Sierra de la Invernada Formation

	mudstones				sandstones					
Sample	**020421**	**020423**	**020431**	**020433**	**SI1**	**020425**	**020428**	**020432**	**Aver**	**SD**
Co	24	24	21	24	32	21	28	29	25.38	3.67
As	6.6	8.6	11	13	5	6	2.9	3.6	7.09	3.32
Sb	0.7	0.8	1.1	1.1	0.6	0.5	0.4	0.3	0.69	0.28
Ta	0.9	2.7	1.8	1.9	2.4	1.3	2.5	2.6	2.01	0.61
W	28	54	24	23	289	104	151	212	110.63	92.86
Cu	53.2	46.4	59.5	42.4	32.6	31.4	31.8	25.1	40.3	11.28
Nb/Y	0.7	0.54	0.57	0.57	0.73	0.63	0.63	0.66	0.63	0.06
Nb/Ta	19.22	7.26	11.17	10.79	7.58	11.69	7.32	5.31	10.04	4.07
Sc/Th	1.55	1.29	1.44	1.42	1.39	1.25	1.26	1.19	1.35	0.11

Table 2 (cont.): Additional chemical analyses of sedimentary clastic rocks of the Precordillera terrane. Trace elements are in ppm. Aver: average; SD: standard deviation; b.d.l.: below detection limits; n.d.: not determined.

Ponón Trehué Formation

	mudstones				sandstones					
Sample	**CT3**	**CT7**	**CT8**	**CT6**	**CT1**	**CT2**	**CT4**	**CT5**	**Aver**	**SD**
Co	13	6	17	9	11	4	13	9	10.25	3.9
As	5.1	33	40	19	46	15	8.1	7.1	21.66	14.91
Sb	0.7	1.4	1.3	1.2	17.2	11	1.7	1.2	4.46	5.78
Ta	1.6	2	1.4	1.4	b.d.l.	b.d.l.	1.7	1.3	1.57	0.24
W	3	b.d.l.	b.d.l.	2	2	2	3	3	2.5	0.5
Cu	9.2	69.7	27.8	10.2	44.1	11.6	15.2	6.7	24.33	20.76
Nb/Y	0.63	0.71	0.67	0.92	0.41	2.86	0.91	0.72	0.98	0.73
Nb/Ta	15.48	13.7	18.17	17			13.71	16.9	15.82	1.69
Sc/Th	1.3	1.44	1.38	1.3	1.35	1.11	1.17	0.93	1.25	0.16

Table 2 (cont.): Additional chemical analyses of sedimentary clastic rocks of the Precordillera terrane. Trace elements are in ppm. Aver: average; SD: standard deviation; b.d.l.: below detection limits; n.d.: not determined.

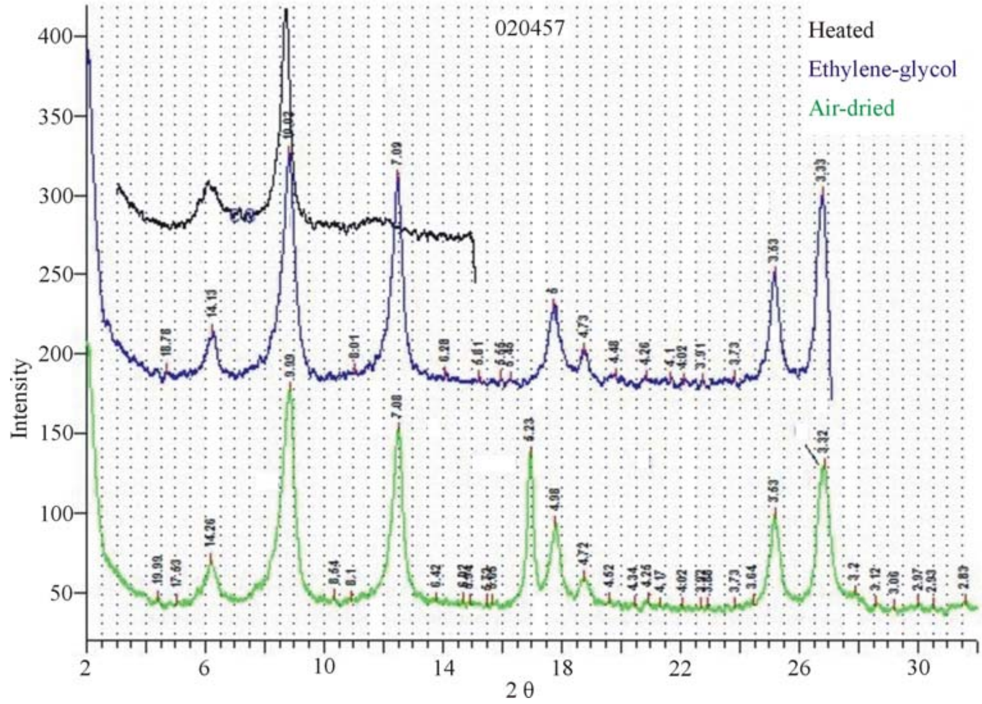

Figure C.21: Heated, ethylene glycol attacked and air-dried X-ray diffraction patterns of sample 020457, Alcaparrosa Formation. For more details, see Table 2 (Appendix A) and Appendix B.

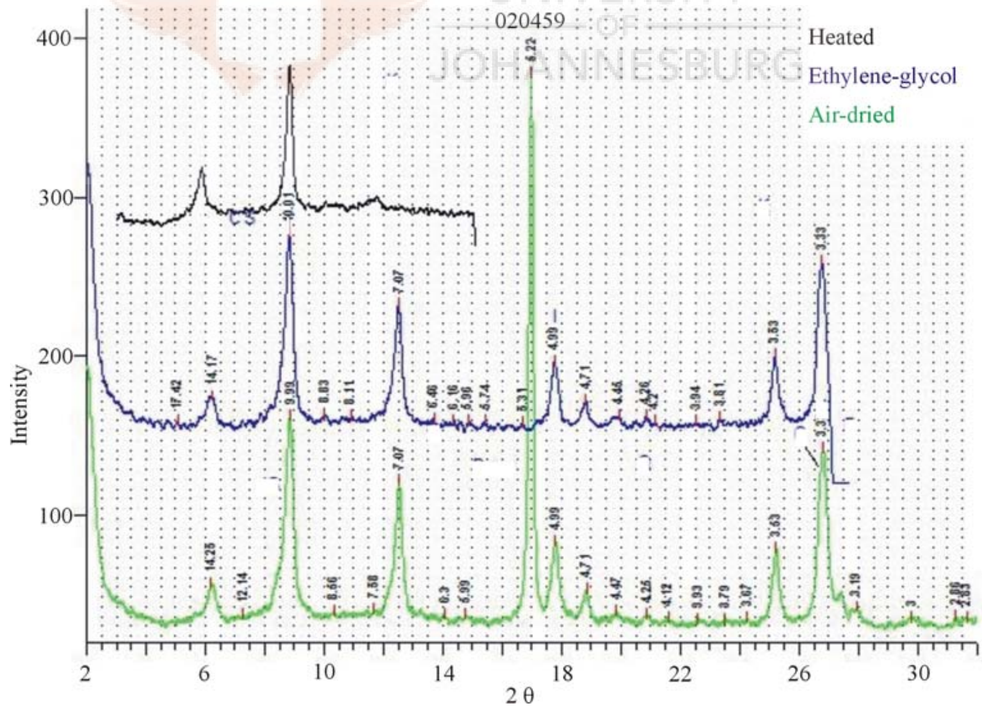

Figure C.22: Heated, ethylene glycol attacked and air-dried X-ray diffraction patterns of sample 020459, Alcaparrosa Formation. For more details, see Table 2 (Appendix A) and Appendix B.

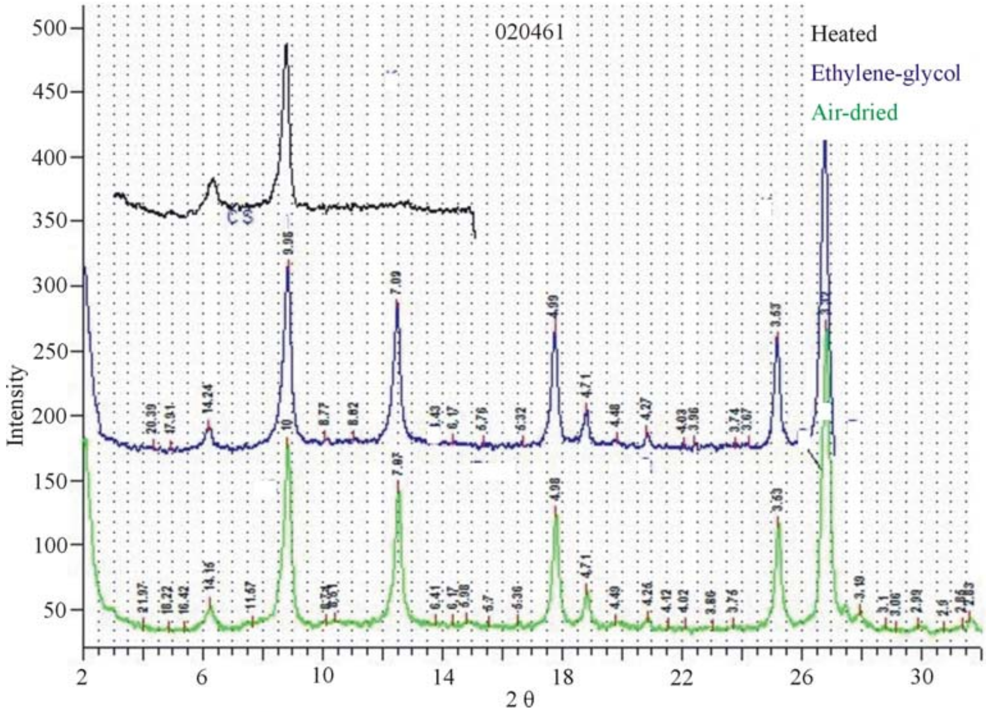

Figure C.23: Heated, ethylene glycol attacked and air-dried X-ray diffraction patterns of sample 020461, Alcaparrosa Formation. For more details, see Table 2 (Appendix A) and Appendix B.

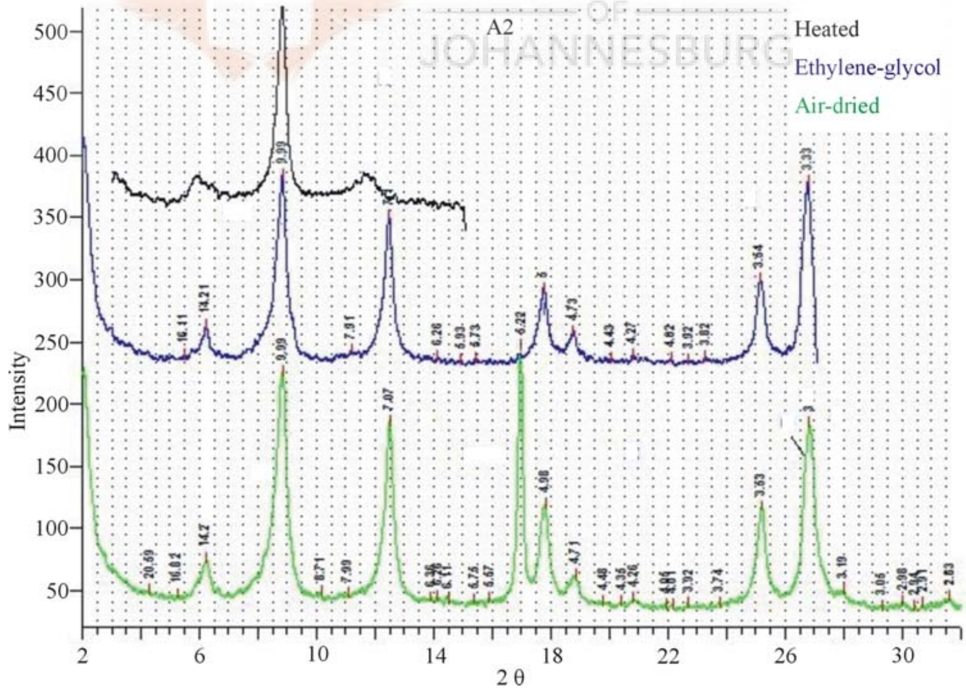

Figure C.24: Heated, ethylene glycol attacked and air-dried X-ray diffraction patterns of sample A2, Alcaparrosa Formation. For more details, see Table 2 (Appendix A) and Appendix B.

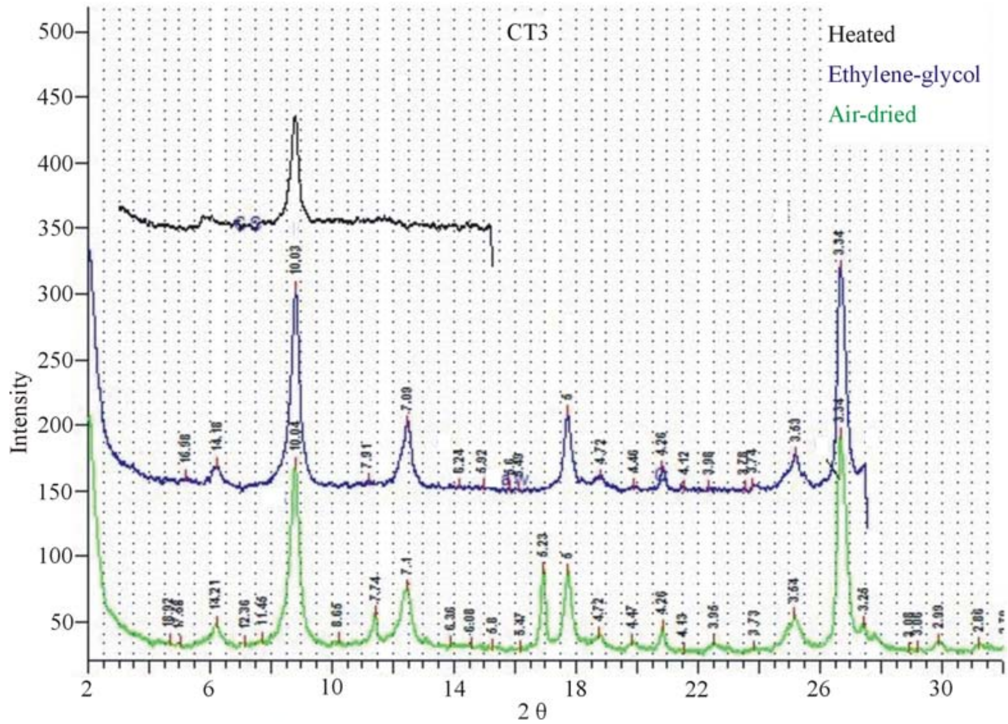

Figure C.25: Heated, ethylene glycol attacked and air-dried X-ray diffraction patterns of sample CT3, Ponón Trehué Formation. For more details, see Table 2 (Appendix A) and Appendix B.

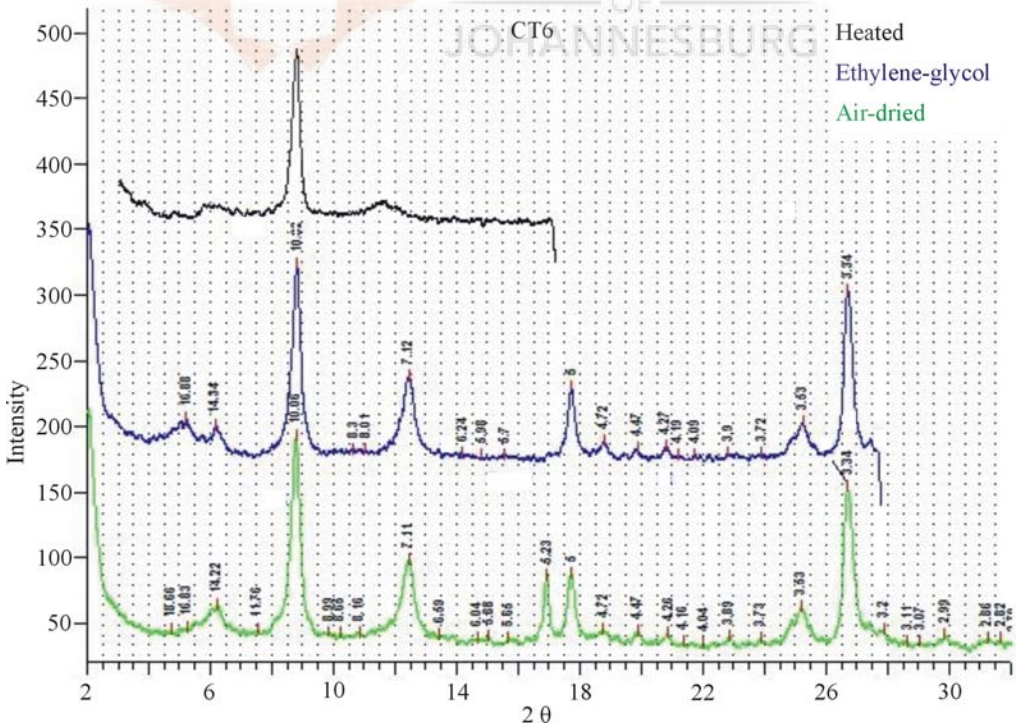

Figure C.26: Heated, ethylene glycol attacked and air-dried X-ray diffraction patterns of sample CT6, Ponón Trehué Formation. For more details, see Table 2 (Appendix A) and Appendix B.

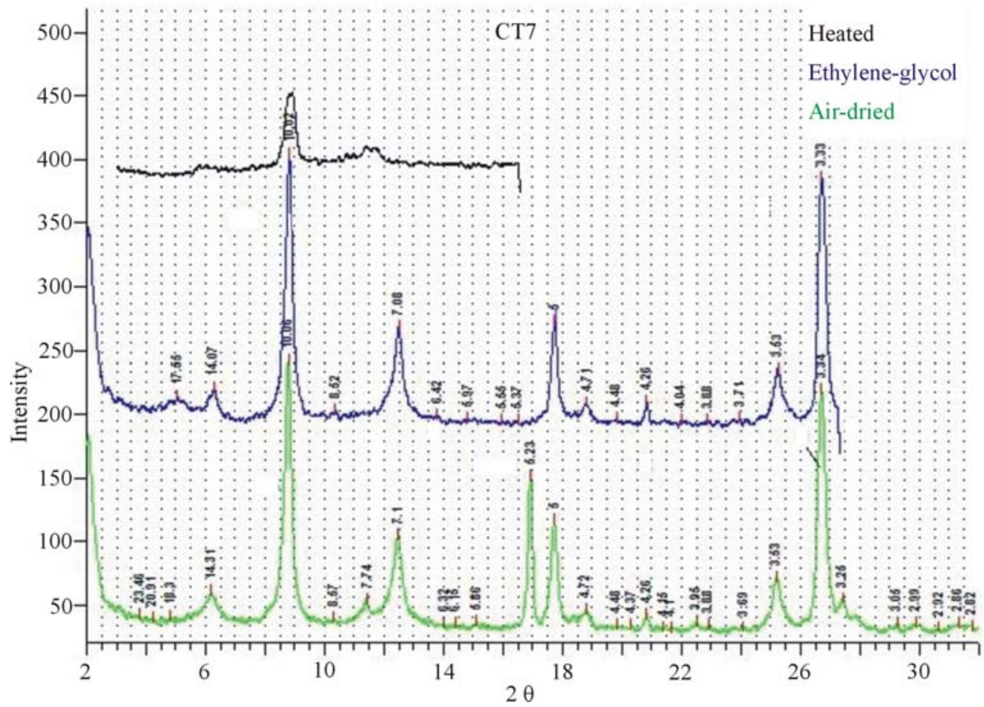

Figure C.27: Heated, ethylene glycol attacked and air-dried X-ray diffraction patterns of sample CT7, Ponón Trehué Formation. For more details, see Table 2 (Appendix A) and Appendix B.

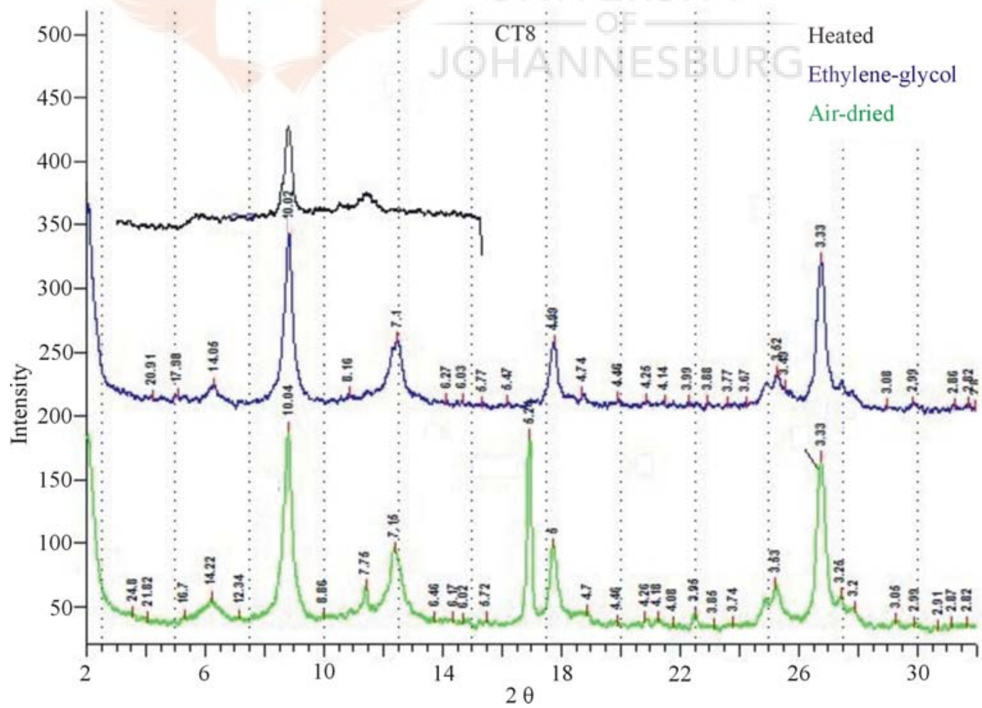

Figure C.28: Heated, ethylene glycol attacked and air-dried X-ray diffraction patterns of sample CT8, Ponón Trehué Formation. For more details, see Table 2 (Appendix A) and Appendix B.

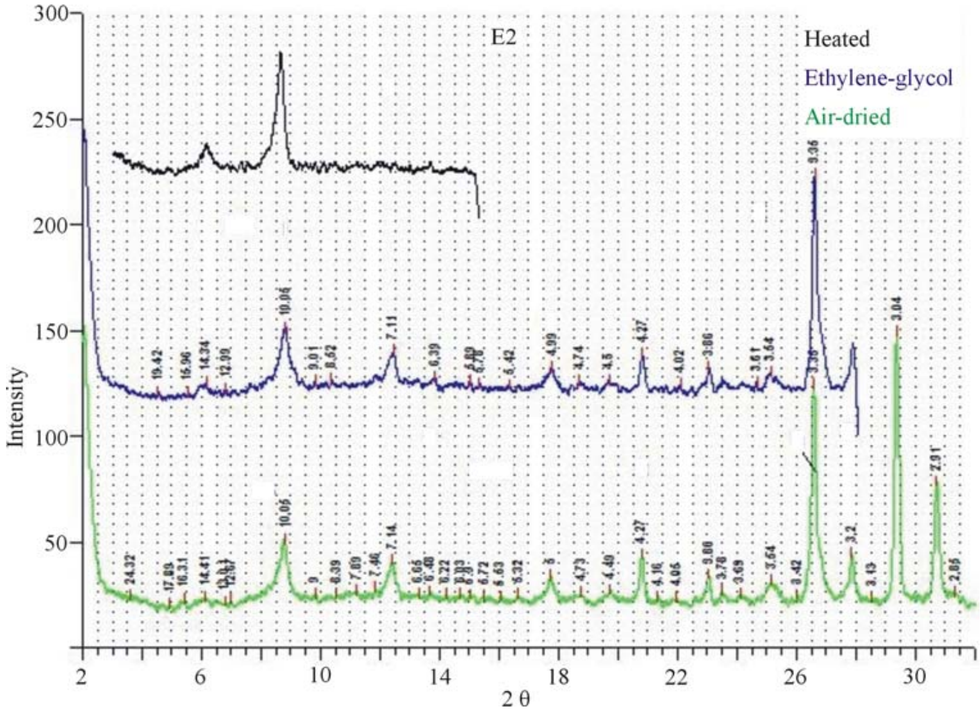

Figure C.29: Heated, ethylene glycol attacked and air-dried X-ray diffraction patterns of sample E2, Empozada Formation. For more details, see Table 2 (Appendix A) and Appendix B.

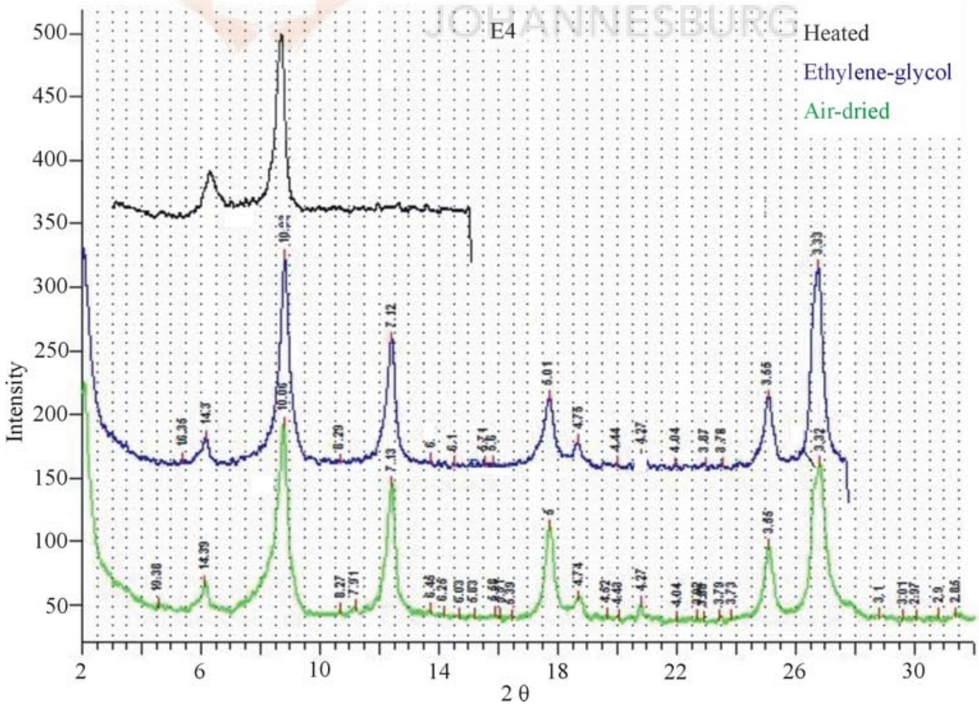

Figure C.30: Heated, ethylene glycol attacked and air-dried X-ray diffraction patterns of sample E4, Empozada Formation. For more details, see Table 2 (Appendix A) and Appendix B.

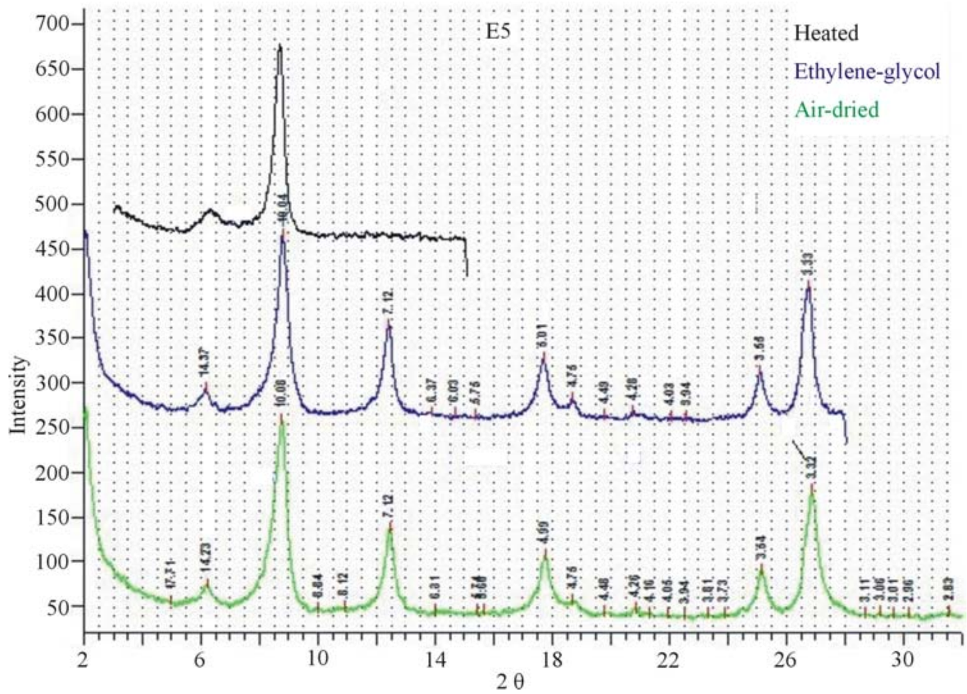

Figure C.31: Heated, ethylene glycol attacked and air-dried X-ray diffraction patterns of sample E5, Empozada Formation. For more details, see Table 2 (Appendix A) and Appendix B.

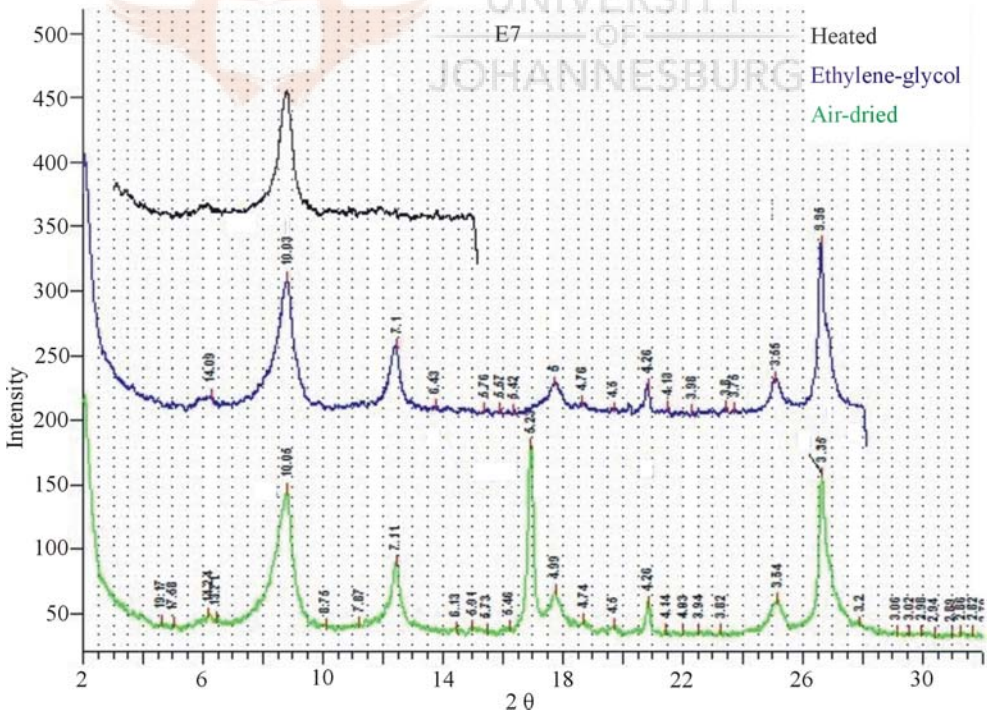

Figure C.32: Heated, ethylene glycol attacked and air-dried X-ray diffraction patterns of sample E7, Empozada Formation. For more details, see Table 2 (Appendix A) and Appendix B.

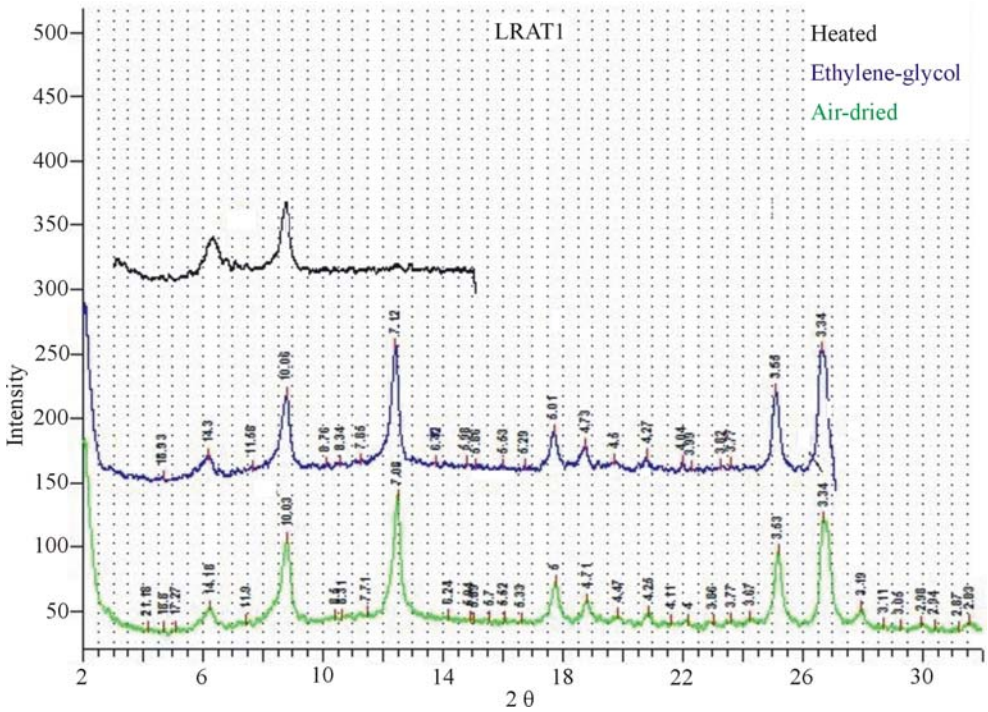

Figure C.33: Heated, ethylene glycol attacked and air-dried X-ray diffraction patterns of sample LRAT1, Los Sombreros Formation. For more details, see Table 2 (Appendix A) and Appendix B.

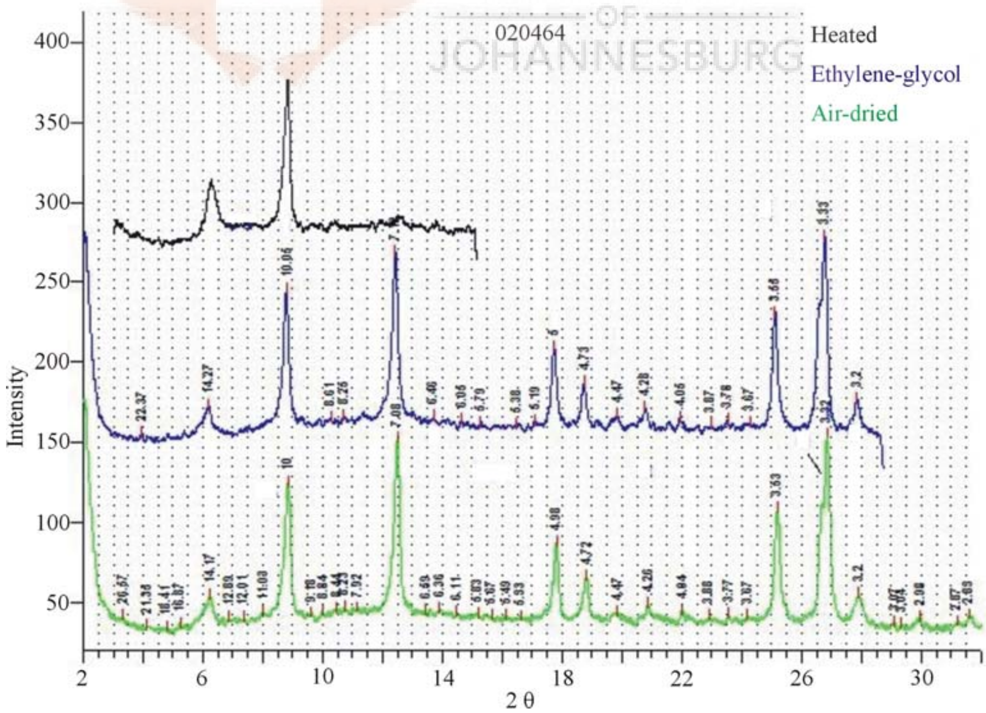

Figure C.34: Heated, ethylene glycol attacked and air-dried X-ray diffraction patterns of sample 020464, Portezuelo del Tontal Formation. For more details, see Table 2 (Appendix A) and Appendix B.

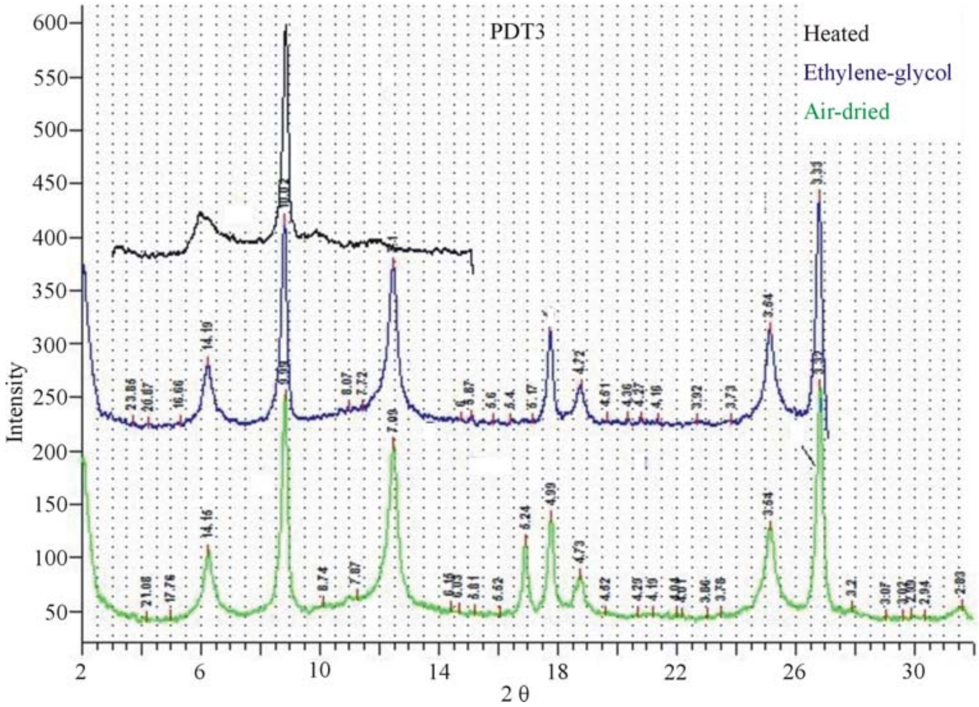

Figure C.35: Heated, ethylene glycol attacked and air-dried X-ray diffraction patterns of sample PDT3, Portezuelo del Tontal Formation. For more details, see Table 2 (Appendix A) and Appendix B.

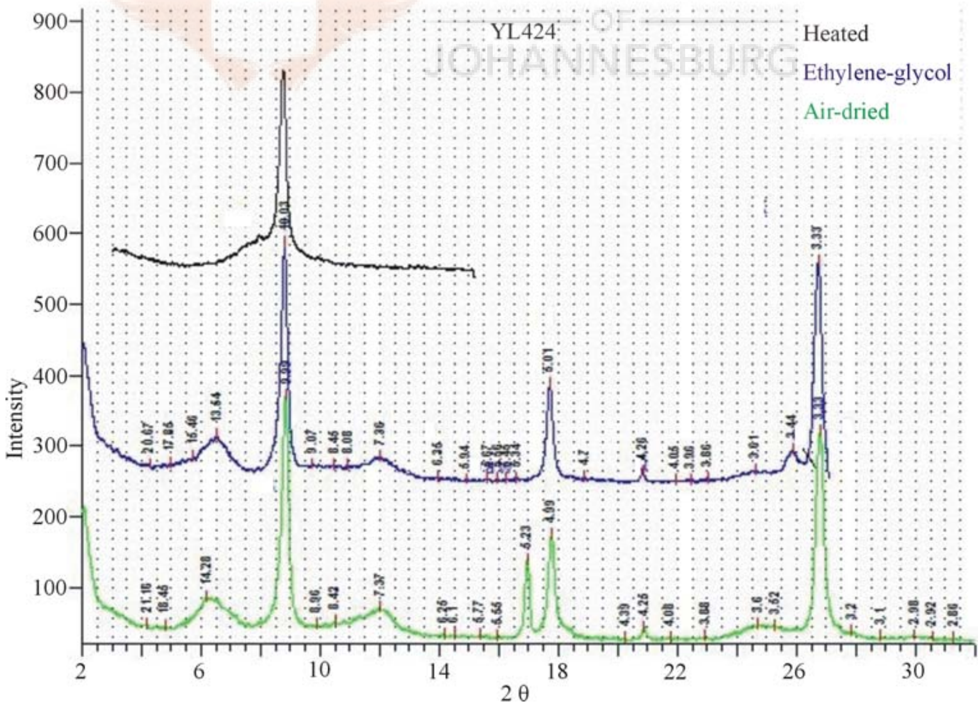

Figure C.36: Heated, ethylene glycol attacked and air-dried X-ray diffraction patterns of sample YL424, Yerba Loca Formation. For more details, see Table 2 (Appendix A) and Appendix B.

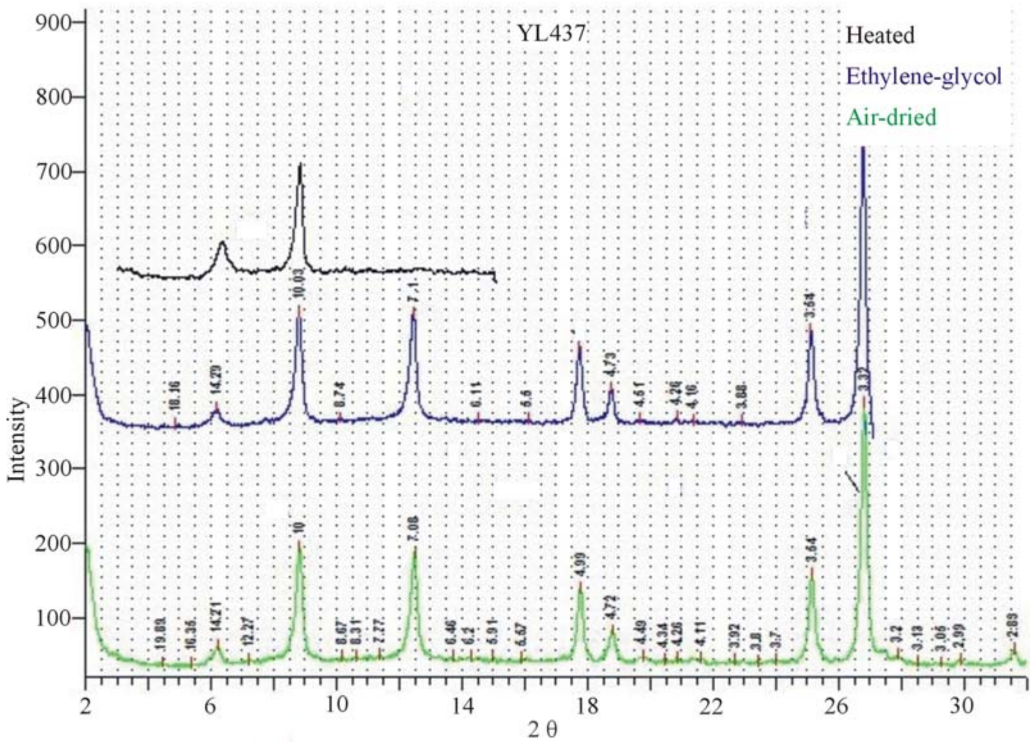

Figure C.37: Heated, ethylene glycol attacked and air-dried X-ray diffraction patterns of sample YL437, Yerba Loca Formation. For more details, see Table 2 (Appendix A) and Appendix B.

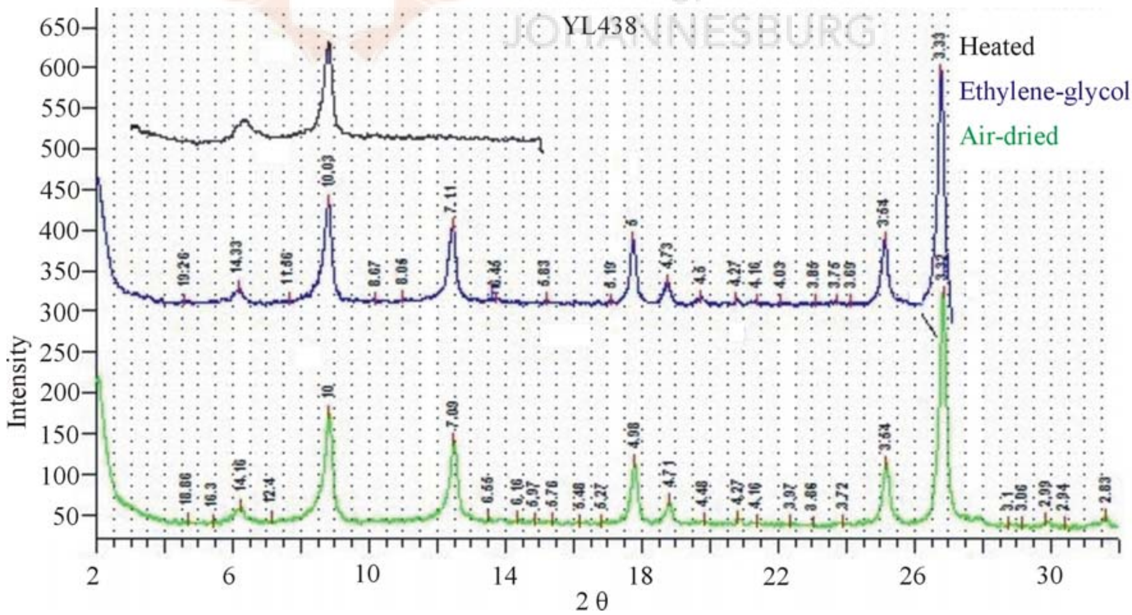

Figure C.38: Heated, ethylene glycol attacked and air-dried X-ray diffraction patterns of sample YL438, Yerba Loca Formation. For more details, see Table 2 (Appendix A) and Appendix B.

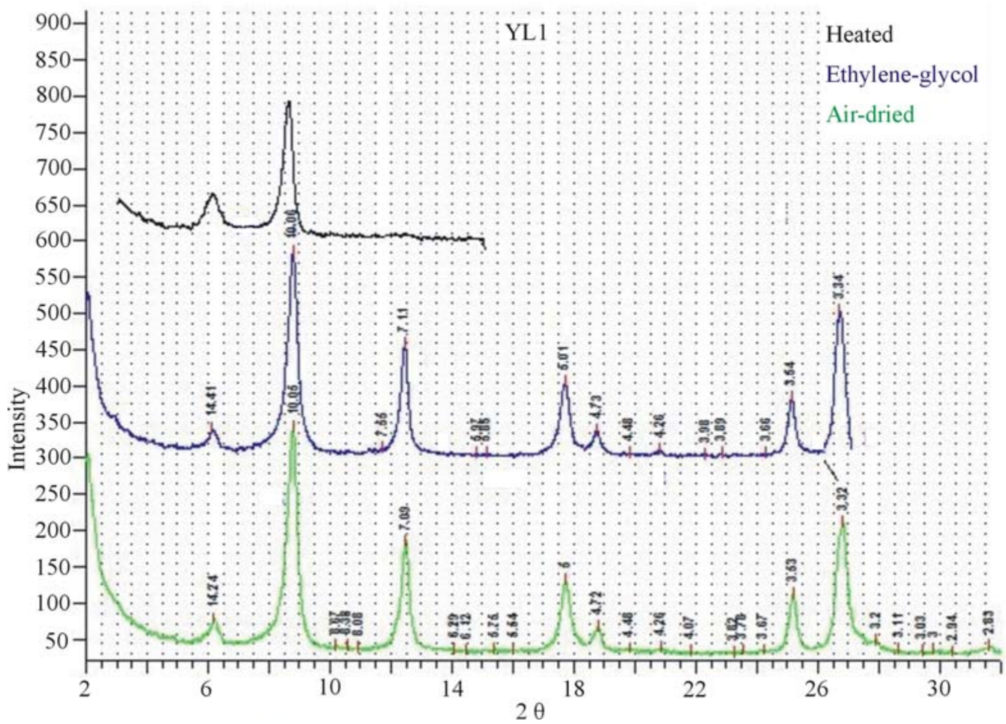

Figure C.39: Heated, ethylene glycol attacked and air-dried X-ray diffraction patterns of sample YL1, Yerba Loca Formation. For more details, see Table 2 (Appendix A) and Appendix B.

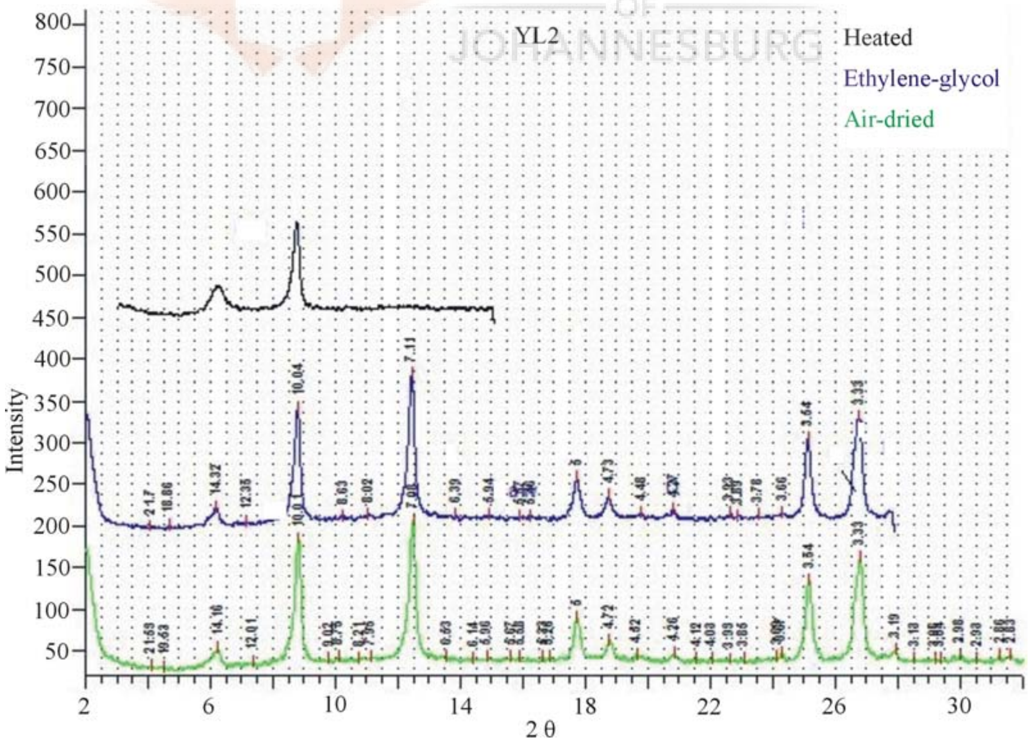

Figure C.40: Heated, ethylene glycol attacked and air-dried X-ray diffraction patterns of sample YL2, Yerba Loca Formation. For more details, see Table 2 (Appendix A) and Appendix B.

Gualcamayo Formation

Sample	Qz	Ank	Calc	Mg-Calc	Ab	Kaol	Rut	Dol	Dick	Clinochl	Il	Chl	Zinw	Musc	Seric	Gyp	Biot	Cham	Microc	Goeth	Hem
GUAL1	X				X	X								X							
020454	X				X									X							
020455	X				X					X			X								
G5	X							X			X		X	X							
G6	X							X			X			X							
G7	X						X	X			X			X							
G8	X													X							
G9	X					X							X	X							
G10	X				X						X			X			X		X		
G11	X				X						X		X	X					X		
G12	X				X								X	X							
G13	X				X									X					X		

Los Azules Formation

Sample	Qz	Ank	Calc	Mg-Calc	Ab	Kaol	Rut	Dol	Dick	Clinochl	Il	Chl	Zinw	Musc	Seric	Gyp	Biot	Cham	Microc	Goeth	Hem
020405	X				X	X					X										
020406	X				X									X							
020407	X				X									X							
020408	X		X		X					X	X								X		
020409	X				X					X	X								X		
020411	X		X		X									X							
020412	X				X					X			X								
020413	X				X					X				X							
020414	X				X					X				X					X		

La Cantera Formation

Sample	Qz	Ank	Calc	Mg-Calc	Ab	Kaol	Rut	Dol	Dick	Clinochl	Il	Chl	Zinw	Musc	Seric	Gyp	Biot	Cham	Microc	Goeth	Hem
020441	X		X		X					X				X							
020442	X				X					X	X			X					X		
020443	X		X		X			X		X				X							
020444	X		X		X					X				X					X		
020445	X		X	X	X					X				X							
020446	X		X		X					X				X							
020447	X		X		X					X			X				X				
020448	X		X		X					X	X			X			X				
020449	X		X		X					X				X					X		
020450	X				X					X				X	X						
020451	X		X		X	X				X				X							
020452	X				X					X				X			X				
020453	X		X		X					X			X								

Table 3: Mineralogy as indicated by whole-rock XRD patterns for the La Cantera Formation. Qz: Quartz; Ank: Ankerite; Calc: Calcite; Mg-Calc: Magnesium rich-calcite; Ab: Albite; Kaol: Kaolinite; Rut: Rutile; Dol: Dolomite; Dick: Dickite; Clinochl: Clinochlorite; Il: Illite; Chl: Chlorite; Zinw: Zinwaldite; Musc: Muscovite; Seric: Sericite; Gyp: Gypsum; Biot: Biotite; Cham: Chamosite; Microc: Microcline; Goeth: Goethite; Hem: Hematite.

Las Vacas Formation

Sample	Qz	Ank	Calc	Mg-Calc	Ab	Kaol	Rut	Dol	Dick	Clinochl	Il	Chl	Zinw	Musc	Serc	Gyp	Biot	Cham	Microc	Goeth	Hem
VACAS0	X	X	X			X								X			X				
VACAS1	X				X						X								X		
VACAS3	X		X		X	X		X					X								
VACAS4	X	X	X							X	X			X							
LV 5	X		X		X					X			X	X							
LV 10	X		X		X					X				X							
LV11	X		X		X					X	X										

Las Plantas – Trapiche Formations

Sample	Qz	Ank	Calc	Mg-Calc	Ab	Kaol	Rut	Dol	Dick	Clinochl	Il	Chl	Zinw	Musc	Serc	Gyp	Biot	Cham	Microc	Goeth	Hem
PLANT1	X		X		X					X				X					X		
PLANT2	X		X		X					X				X							
LPT1	X		X		X			X											X		
LPT2	X	X	X		X																
LPT3	X		X		X									X							
LPT5	X	X	X		X																
LPT6	X	X	X		X					X				X							
LPT7	X				X					X				X					X		
LPT9	X		X		X			X		X			X								
LPT10	X		X		X			X			X	X									
LPT12	X		X		X			X													
LPT13	X				X									X							
LPT14	X				X															X	
LPT15	X				X			X													
LPT16	X				X									X							
LPT17	X				X						X			X			X				
LPT18	X				X						X			X						X	
LPT19	X				X		X				X			X							
LPT21	X				X							X		X							
LPT22	X				X					X									X		
LPT23	X		X		X							X		X							
LPT24	X		X		X	X								X							
LPT25	X		X		X			X		X				X							
LPT26	X		X		X			X						X							

Don Braulio Formation

Sample	Qz	Ank	Calc	Mg-Calc	Ab	Kaol	Rut	Dol	Dick	Clinochl	Il	Chl	Zinw	Musc	Seric	Gyp	Biot	Cham	Microc	Goeth	Hem
020436	X				X					X	X			X							
020437	X				X					X							X		X		
020438	X		X		X					X				X							
020439	X		X		X					X	X			X							
020440	X		X		X					X	X			X							
DB 1	X		X		X																

Table 3 (cont.): Mineralogy as indicated by whole-rock XRD patterns for the Don Braulio Formation. Qz: Quartz; Ank: Ankerite; Calc: Calcite; Mg-Calc: Magnesium rich-calcite; Ab: Albite; Kaol: Kaolinite; Rut: Rutile; Dol: Dolomite; Dick: Dickite; Clinochl: Clinochlorite; Il: Illite; Chl: Chlorite; Zinw: Zinwaldite; Musc: Muscovite; Seric: Sericite; Gyp: Gypsum; Biot: Biotite; Cham: Chamosite; Microc: Microcline; Goeth: Goethite; Hem: Hematite.

La Chilca Formation

Sample	Qz	Ank	Calc	Mg-Calc	Ab	Kaol	Rut	Dol	Dick	Clinochl	Il	Chl	Zinw	Musc	Seric	Gyp	Biot	Cham	Microc	Goeth	Hem
020401	X				X									X							
020402	X				X					X				X							
020403	X				X					X				X							
020404	X		X		X					X				X							
020410	X		X		X				X					X							
020415	X				X									X					X		
020416	X				X								X	X							

Empozada Formation

Sample	Qz	Ank	Calc	Mg-Calc	Ab	Kaol	Rut	Dol	Dick	Clinochl	Il	Chl	Zinw	Musc	Seric	Gyp	Biot	Cham	Microc	Goeth	Hem
E1	X	X	X		X																
E2	X	X	X		X					X			X								
E3	X	X	X		X									X							
E4	X	X	X		X					X			X								
E5	X		X		X					X			X	X							
E6	X	X	X		X												X				
E7	X				X					X			X								
E8	X	X		X	X														X		
E10	X	X	X		X		X		X	X											

Los Sombreros Formation

Sample	Qz	Ank	Calc	Mg-Calc	Ab	Kaol	Rut	Dol	Dick	Clinochl	Il	Chl	Zinw	Musc	Seric	Gyp	Biot	Cham	Microc	Goeth	Hem
020418	X				X					X	X			X							
020419	X		X		X			X				X		X							
LRAT1	X				X					X				X					X		
LRAT2	X				X					X	X	X	X								
SOM 5	X				X							X		X							
SOM 6	X				X					X				X							X
SOM 7	X	X												X							X
SOM 8	X				X					X	X			X							
SOM 9	X	X												X							

Alcaparrosa Formation

Sample	Qz	Ank	Calc	Mg-Calc	Ab	Kaol	Rut	Dol	Dick	Clinochl	Il	Chl	Zinw	Musc	Seric	Gyp	Biot	Cham	Microc	Goeth	Hem
020456	X	X			X					X			X								
020457	X				X					X				X					X		
020458	X				X					X				X					X		
020459	X				X							X	X	X					X		
020460	X				X							X		X					X		
020461	X				X					X				X					X		
020462	X				X					X				X							
A 1	X				X					X	X										
A 2	X				X					X				X							
A 3	X				X							X	X								
A 4	X				X							X	X								

Table 3 (cont.): Mineralogy as indicated by whole-rock XRD patterns for the Alcaparrosa Formation. Qz: Quartz; Ank: Ankerite; Calc: Calcite; Mg-Calc: Magnesium rich-calcite; Ab: Albite; Kaol: Kaolinite; Rut: Rutile; Dol: Dolomite; Dick: Dickite; Clinochl: Clinochlorite; Il: Illite; Chl: Chlorite; Zinw: Zinwaldite; Musc: Muscovite; Seric: Sericite; Gyp: Gypsum; Biot: Biotite; Cham: Chamosite; Microc: Microcline; Goeth: Goethite; Hem: Hematite.

Yerba Loca Formation

Sample	Qz	Ank	Calc	Mg-Calc	Ab	Kaol	Rut	Dol	Dick	Clinochl	Il	Chl	Zinw	Musc	Serc	Gyp	Biot	Cham	Microc	Goeth	Hem
YL 1	X				X					X	X										
YL 2	X		X		X							X	X	X							
YL 3	X		X		X							X	X								
YL 4	X				X					X			X								
YL 5	X				X					X			X								
YL 6	X		X		X					X				X							
YL 425	X		X		X					X	X										
YL 426	X				X					X	X			X							
YL 428	X		X		X					X			X								
YL 429	X		X		X			X		X					X	X					
YL 429-2	X		X		X					X				X							
YL 430-1	X		X		X			X		X			X								
YL 431	X				X					X			X								
YL 432	X		X		X					X				X							
YL 433	X		X		X					X				X			X				
YL 434/1	X		X		X					X				X		X					
YL 436	X		X		X					X			X								
YL 439	X		X		X							X	X								
YL 440	X		X		X					X			X								
YL 441	X				X							X		X				X			
YL 442	X		X		X					X	X										
YL 443	X		X		X							X	X								
YL 444	X				X					X			X								
YL 445	X		X		X					X			X								
YL 446	X		X		X							X	X								
YL 447	X		X		X							X	X								
YL 449	X				X							X	X	X							
YL 450	X				X							X	X								
YL 451	X				X					X				X					X		
YL 452	X		X		X					X			X								
YL 454	X	X			X					X			X								

Portezuelo del Tontal Formation

Sample	Qz	Ank	Calc	Mg-Calc	Ab	Kaol	Rut	Dol	Dick	Clinochl	Il	Chl	Zinw	Musc	Seric	Gyp	Biot	Cham	Microc	Goeth	Hem
020463	X				X					X				X					X		
020464	X				X					X				X					X		
020465	X		X		X					X				X							
020466	X				X					X				X					X		
020467	X				X					X				X					X		
020468	X				X					X				X							
020469	X				X					X					X						
020470	X				X					X	X								X		
PDT 1	X				X					X			X								
PDT 2	X		X		X					X			X								
PDT 3	X				X					X				X							

Table 3 (cont.): Mineralogy as indicated by whole-rock XRD patterns for the Portezuelo del Tontal Formation. Qz: Quartz; Ank: Ankerite; Calc: Calcite; Mg-Calc: Magnesium rich-calcite; Ab: Albite; Kaol: Kaolinite; Rut: Rutile; Dol: Dolomite; Dick: Dickite; Clinochl: Clinochlorite; Il: Illite; Chl: Chlorite; Zinw: Zinwaldite; Musc: Muscovite; Seric: Sericite; Gyp: Gypsum; Biot: Biotite; Cham: Chamosite; Microc: Microcline; Goeth: Goethite; Hem: Hematite.

Sierra de la Invernada Formation

Sample	Qz	Ank	Calc	Mg-Calc	Ab	Kaol	Rut	Dol	Dick	Clinochl	Il	Chl	Zinw	Musc	Seric	Gyp	Biot	Cham	Microc	Goeth	Hem
020420	X		X	X	X																
020421	X				X					X				X							
020423	X				X					X				X					X		
020425	X				X					X	X			X					X		
020428	X				X					X	X		X	X					X		
020431	X				X									X							
020432	X		X		X					X			X								
020433	X				X					X			X						X		
SI 1	X				X					X			X								

Ponón Trehué Formation

Sample	Qz	Ank	Calc	Mg-Calc	Ab	Kaol	Rut	Dol	Dick	Clinochl	Il	Chl	Zinw	Musc	Seric	Gyp	Biot	Cham	Microc	Goeth	Hem
CT 1	X										X			X						X	
CT 2	X		X								X										
CT 3	X						X			X	X			X					X		
CT 4	X						X			X				X							
CT 5	X						X			X	X			X							
CT 6	X						X			X				X							
CT 7	X									X				X					X		
CT 8	X									X				X					X		

Table 3 (cont.): Mineralogy as indicated by whole-rock XRD patterns for the Ponón Trehué Formation. Qz: Quartz; Ank: Ankerite; Calc: Calcite; Mg-Calc: Magnesium rich-calcite; Ab: Albite; Kaol: Kaolinite; Rut: Rutile; Dol: Dolomite; Dick: Dickite; Clinochl: Clinochlorite; Il: Illite; Chl: Chlorite; Zinw: Zinwaldite; Musc: Muscovite; Seric: Sericite; Gyp: Gypsum; Biot: Biotite; Cham: Chamosite; Microc: Microcline; Goeth: Goethite; Hem: Hematite.

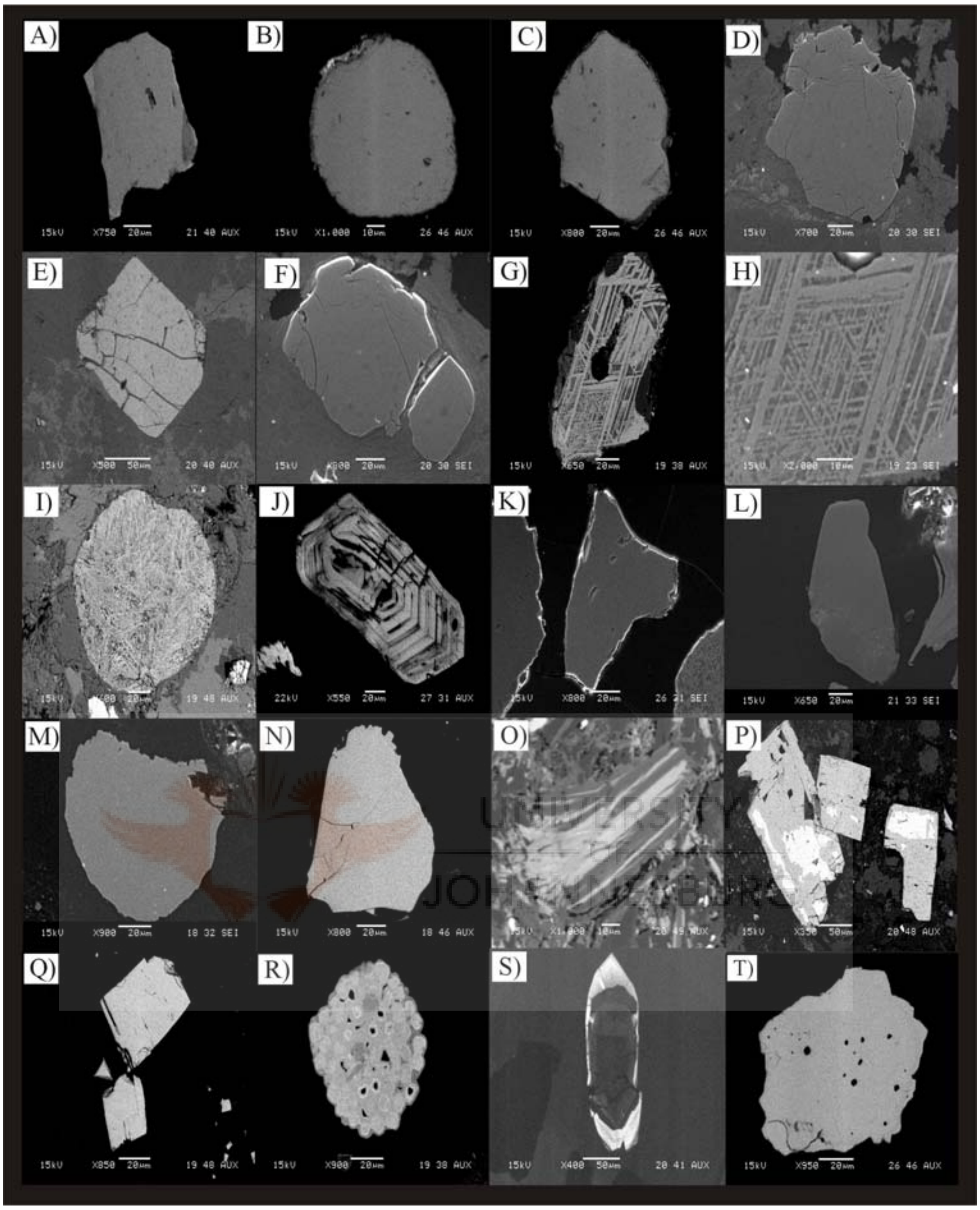

Figure C.41: Examples of minerals studied under SEM-BSE-EDS-CL. A) Chromian spinel of the Pavón Fm. under BSE. B) Chromian spinel of the Don Braulio Fm. under BSE. C) Chromian spinel of the Don Braulio Fm. under BSE. D) Chromian spinel of the Empozada Fm. (thin section) under SEM. E) Chromian spinel of the Empozada Fm. (thin section) under BSE. F) Chromian spinel of the Empozada Fm. (thin section) under SEM. G) Ti-oxides included in feldspar under BSE. This feature is present in several units. H) Detail of previous image but under SEM. I) Ti-oxides included in unidentified well-rounded mineral under BSE. Note how Ti-oxides do not affect the matrix. J) Zoned zircon under BSE. K) Anhedral apatite in the centre of the image under SEM. L) Subhedral tourmaline under SEM from the Yerba Loca Fm. M) Anhedral apatite under SEM from the Yerba Loca Fm. N) Subhedral apatite under BSE from the Yerba Loca Fm. O) intergrowth of muscovite(dark) and chlorite (grey) under BSE from the Yerba Loca Fm. P) Crystals of pyrite (grey) altered to Fe-oxyhydroxides (e.g. lepidocrocite, goethite; bright white areas) under BSE from the Las Vacas Fm. Q) Cubic pyrite under BSE from the Las Vacas Fm. R) Hematite under BSE. S) Elongated subhedral zircon showing under CL an internal dark zone and a thick bright overgrowth. T) Barite under BSE from the Don Braulio Fm.

REFERENCES

Abbruzzi, J.M., Kay, S.M., Bickford, S.M., 1993. Implications for the nature of the Precordilleran basement from the geochemistry and age of Precambrian xenoliths in Miocene volcanic rocks, San Juan province. XII Congreso Geológico Argentino y II Congreso de Exploración de Hidrocarburos, Actas III, 331-339.

Abre, P., Zimmermann, U., Cingolani, C., 2003. Pavón Formation zircons under scanning electronic microscope: preliminary results on the Ordovician siliciclastics from the San Rafael block, Mendoza. In: Albanesi, G.L., Beresi, M.S., Peralta, S.H. (Eds.), Ordovician from the Andes, INSUGEO, Tucumán, Serie Correlación Geológica 17, 217-221.

Abre, P., Cingolani, C., Zimmermann, U., Cairncross, B., 2005. Espinelas cromíferas detríticas en la Formación Pavón (Ordovícico): indicadoras de corteza oceánica en el terreno Precordillera, Argentina. XVI Congreso Geológico Argentino, CD version, La Plata.

Abre, P., Zimmermann, U., Cingolani, C., Cairncross, B., 2005. Provenance of Silurian successions in north-western Argentina. XVI Congreso Geológico Argentino, Actas en CD, La Plata.

Abre, P., Cingolani, C., Zimmermann, U., Cairncross, B., 2006. Detrital chromian spinels from Upper Ordovician deposits in the Precordillera terrane: a mafic crust input. Journal of South American Earth Sciences, Special Issue, submitted.

Aceñolaza, F.G., Baldis, B., 1986. The Ordovician System of South America. IUGS Publication, 64pp.

Aceñolaza, F.G., Peralta, S.H., 1985. Lophoctenium comosum Reinhold Ritcher (traza fósil) en la Formación Los Espejos (Silúrico), Precordillera de San Juan. Primeras Jornadas sobre Geología de la Precordillera, San Juan, Acta I, 145-150.

Aceñolaza, F.G., Toselli, A., 1976. Consideraciones estratigráficas y tectónicas sobre el Paleozoico inferior del noroeste argentino. II Congreso Latinoamericano de Geología, Actas 2, 755-763.

Aceñolaza, F.G., Toselli, A., 1988. El Sistema de Famatina, Argentina: su interpretación como orógeno de margen continental activo. V Congreso Geológico Chileno Actas 1, A55–A67.

Aceñolaza, F.G. Toselli, A., 1998. Precordillera argentina: alóctono o autóctono gondwánico? Terra Nostra 5, 2-3.

Aceñolaza, F.G., Toselli, A., 2000. Argentine Precordillera: allochthonous or autochthonous Gondwanic? Zentralblatt Geologie und Palaontologie 1999 (7/8), 743–756.

Aceñolaza, F.G., Miller, H., Toselli, A., 2002. Proterozoic – Early Paleozoic evolution in western South America – a discussion. Tectonophysics 354, 121-137.

ACTLABS. Service Guide 2006. www.actlabsint.com.

Adams, C.J., Pankhurst, R.J., Maas, R., Millar, I.L., 2005. Nd and Sr isotopic signatures of metasedimentary rocks around the South Pacific margin and implications for their provenance. In: Vaughan, A.P.M., Leat, P.T., Pankhurst, R.J. (Eds.), Terrane processes at the margins of Gondwana. Geological Society of London, Special Publications 246, 113-141.

Ahmed, A.H., Arai, S., Abdel-Aziz, Y.M., Rahimi, A., 2005. Spinel composition as a petrogenetic indicator of the mantle section in the Neoproterozoic Bou Azzer ophiolite, Anti-Atlas, Morocco. Precambrian Research 138, 225-234.

Aitcheson, S.J., Harmon, R.S., Moorbath, S., Schneider, A., Soler, P., Soria-Escalante, E., Steele, G., Swainbank, I., Wörner, G., 1995. Pb isotopes define basement domains of the Altiplano, central Andes. Geology 23 (6), 555-558.

Albanesi, G.L., Vaccari, N.E., 1994. Conodontos del Arenig en la Formación Suri, Sistema de Famatina, Argentina. Revista Española de Micropalentología 26 (2), 125-146.

Albanesi, G.L., Sansom, I.J., Davies, N.S., 2005. *Sacabambaspis janvieri* Gagnier *et al.*: records and paleogeographic implications for the late Middle Ordovician Gondwanan margin. Gondwana 12, Abstracts, 37.

Aleinikoff, J.N., Zartman, R.E., Walter, M., Rankin, D.W., Lyttle, P.T., Burton, W.C., 1995. U-Pb ages of metarhyolites of the Catoctin and Mount Rogers Formations, central and southern Appalachians: evidence for two pulses of Iapetan rifting. American Journal of Science 295, 428-454.

Andersen, T., 2004. Detrital zircons as tracers of sedimentary provenance: limiting conditions from statistics and numerical simulation. Chemical Geology, 216, 249-270.

Andersson, P.O.D., Worden, R.H., Hodgson, D.M., Flint, S., 2004. Provenance evolution and chemostratigraphy of a Paleozoic submarine fan-complex: Tanqua Karoo Basin, South Africa. Marine and Petroleum Geology 21, 555-577.

Arai, S., 1992. Chemistry of chromian spinel in volcanic rocks as a potential guide to magma chemistry. Mineralogical Magazine 56, 173-184.

Árkai, P., Sassi, F.P., Desmons, J., 2003. Very low- to low-grade metamorphic rocks. Recommendations by the IUGS Subcommission on the Systematics of Metamorphic Rocks. Web version of 01-02-07. www.bgs.ac.uk/scmr/home.html

Asiedu, D.K., Suzuki, S., Shibata, T., 2000. Provenance of sandstones from the Lower Cretaceous Sasayama Group, Inner Zone of southwest Japan. Sedimentary Geology 131, 9-24.

Asmerom, Y.S.B., Jacobsen, S., 1993. The Pb isotopic evolution of the Earth: inferences from river water suspended loads. Earth and Planetary Sciences Letters 115, 245-256.

Astini, R.A., 1986. Análisis petrológico, litofacial y estratigráfico de las unidades clásticas ordovícicas en el área de Guandacol, norte de la Precordillera y sus implicancias en la evolución paleogeográfica de la cuenca. Trabajo Final. Universidad Nacional de Córdoba, 68 pp. (unpublished).

Astini, R.A., 1991. Paleoambientes sedimentarios y secuencias depositacionales del Ordovícico clástico de la Precordillera Argentina. Tesis Doctoral. Universidad Nacional de Córdoba, 851 pp. (unpublished).

Astini, R.A., 1993a. Secuencias deposicionales y niveles del mar en el Sistema Ordovícico de la Precordillera argentina. Boletín Real Sociedad Española de Historia Natural (Sección Geología) 88 (1-4), 113-126.

Astini, R.A., 1993b. Facies glacigénicas del Ordovícico tardío (Hirnantiense) de la Precordillera Argentina. Boletín Real Sociedad Española de Historia Natural (Sección Geología) 88, 137-149.

Astini, R.A., 1994a. Las megaturbiditas de la Formación Trapiche (Ordovícico superior de la Precordillera): procesos sedimentarios y marco geológico. V Reunión Argentina de Sedimentología, Actas, 107-112.

Astini, R.A., 1994b. Geología e interpretación de la Formación Gualcamayo en su localidad clásica (suroeste de Guandacol y Cordón de Perico-Potrerillo), Precordillera septentrional. Revista de la Asociación Geológica Argentina 49 (1-2), 55-70.

Astini, R.A., 1994c. Análisis secuencial y paleoambientes de las pelitas negras (Aloformación Gualcamayo) que suprayacen a las sucesiones carbonáticas eo-ordovícicas en la Precordillera argentina. Revista de la Asociación Geológica Argentina 49 (1-2), 71-84.

Astini, R.A., 1994d. Sucesiones calcáreo-silicoclásticas coetáneas del Ordovícico inferior de la Precordillera y su significado en la evolución de la cuenca. V Reunión Argentina de Sedimentología, Actas, 113-118.

Astini, R.A., 1998a. Stratigraphical evidence supporting the rifting, drifting and collision of the Laurentian Precordillera terrane of western Argentina. In: Pankhurst, R.J., Rapela, C.W. (Eds.), The Proto-Andean Margin of Gondwana. Geological Society of London, Special Publication 142, 11-33.

Astini, R.A., 1998b. El conglomerado de Las Vacas y el Grupo Trapiche de la Precordillera: tectónica distensiva en el Ordovícico tardío. Revista de la Asociación Geológica Argentina 53 (4), 489-503.

Astini, R.A., 2002. Los conglomerados basales del Ordovícico de Ponón Trehué (Mendoza) y su significado en la historia sedimentaria del terreno exótico de Precordillera. Revista de la Asociación Geológica Argentina 57 (1), 19-34.

Astini, R.A., Benedetto, J.L., 1992. El Ashgilliano tardío (Hirnantiano) del Cerro La Chilca, Precordillera de San Juan, Argentina. Ameghiniana 29 (3), 249-264.

Astini, R.A., Brussa, E.D., 1996. Dos nuevas localidades fosilíferas en el Conglomerado de Las Vacas (Caradociano) en la Precordillera Argentina: importancia cronoestratigráfica. Reunión de Comunicaciones Paleontológicas, Asociación Paleontológica Argentina. Ameghiniana 34 (1), 114.

Astini, R.A., Buggisch, W., 1993. Aspectos sedimentológicos y paleoambientales de los depósitos glacigénicos de la Formación Don Braulio, Ordovícico tardío de la Precordillera argentina. Revista de la Asociación Geológica Argentina 48 (3-4), 217-232.

Astini, R.A., Dávila, F.M., 2004. Ordovician back arc foreland and Ocloyic thrust belt development on the Western Gondwana margin as a response to Precordillera terrane accretion. Tectonics 23, TC4008, doi:10.1029/2003TC001620.

Astini, R.A., Maretto, H.M., 1993. Análisis estratigráfico del Silúrico de la Precordillera Central de San Juan y consideraciones sobre la evolución de la cuenca. XIII Congreso Geológico Argentino y III Congreso de Exploración de Hidrocarburos, Actas I, 351-368.

Astini, R.A., Rapalini, A.E., 2003. Discussion to Proterozoic – Early Paleozoic evolution in western South America – a discussion. Tectonophysics 366, 143-148.

Astini, R.A., Thomas, W.A., 1999. Origin and evolution of the Precordillera terrane of western Argentina: A drifted Laurentian orphan. In: Ramos, V.A., Keppie, D. (Eds.), Laurentia-Gondwana connections before Pangea. Geological Society of America Bulletin, Special Paper 336, 1-20.

Astini, R.A., Cañas, F.L., Benedetto, J.L., 1988. The Ordovician in the Precordillera Basin, western Argentina. V International Symposium on the Ordovician System, Abstract 4. Newfoundland.

Astini, R.A., Benedetto, J.L., Vaccari, N.E., 1995. The Early Paleozoic evolution of the Argentine Precordillera as a Laurentian rifted, drifted and collided terrane: A geodynamic model. Geological Society of America Bulletin 107 (3), 253-273.

Astini, R.A., Ramos, V.A., Benedetto, J.L. Vaccari, N.E., Cañas, F.L., 1996. La Precordillera: un terreno exótico a Gondwana. XIII Congreso Geológico Argentino y III Congreso de Exploración de Hidrocarburos, Actas V, 293-324.

Astini, R.A., Brussa, E.D., Mitchell, C.E., 2000. Revisión estratigráfica y consideraciones paleogeográficas de la tectofacies occidental de la Precordillera argentina. Revista de la Asociación Geológica Argentina 55 (4), 378-386.

Astini, R.A., Thomas, W.A., Yochelson, E.L., 2004. *Salterella* in the Argentine Precordillera: an Early Cambrian palaeobiogeographic indicator of Laurentian affinity. Palaeogeography, Palaeoclimatology, Palaeoecology 213, 125-132.

Astini, R.A., Thomas, W.A., McClelland, W.C., 2005. Provenance of Middle Ordovician detritus in the Argentine Precordillera. Gondwana 12 Conference, Abstracts, 51.

Astini, R.A., Collo, G., Martina, F., 2006. Ordovician K-bentonites in the upper-plate active margin of Western Gondwana, (Famatina Range): Stratigraphic and palaeogeographic significance. Gondwana Research 9, 324-335.

Awwiller, D.N., 1994. Geochronology and mass transfer in Gulf Coast mudrocks (south-central Texas, USA): Rb-Sr, Sm-Nd and REE systematics. Chemical Geology 116, 61-84.

Badger, R.L., Sinha, A.K., 1988. Age and Sr isotopic signature of the Catoctin volcanic province: Implications for subcrustal mantle evolution. Geology 16, 692-695.

Bahlburg, H., Hervé, F., 1997. Geodynamic evolution and tectonostratigraphic terranes of northwestern Argentina and northern Chile. Geological Society of America Bulletin 109 (7), 869-884.

Bahlburg, H., Hervé, F., Bock, B., 2001. New Nd isotope data on the ?Devonian Chilenia terrane in northern Chile: implications for the Paleozoic accretionary history of the Andean Gondwana margin.

Baldis, B.A., Beresi, M., Bordonaro, O., Vaca, A., 1982. Síntesis evolutiva de la Precordillera Argentina. V Congreso Latinoamericano de Geología, Actas 4, 399-445.

Baldis, B.A., Beresi, M., Bordonaro, O., Vaca, A., 1984. The Argentine Precordillera as a key to Andean structure. Episodes 7 (3), 14-19.

Baldis, B.A., Peralta, S., Villegas, R., 1989. Esquematizaciones de una posible transcurrencia del terrane de Precordillera como fragmento continental procedente de áreas Pampeano-Bonaerenses. Correlación Geológica 5, 81-99.

Baldo, E., Casquet, C., Galindo, C., 1998. Datos preliminares sobre el metamorfismo de la Sierra de Pie de Palo, Sierras Pampeanas Occidentales (Argentina). Geogaceta 24, 39-42.

Baldo, E.G., Fanning, C.M., Rapela, C.W., Pankhurst, R.J., Casquet, C., Galindo, C., 2003. U-Pb SHRIMP dating of rhyolite volcanism in the Famatinian belt and K-bentonites in the Precordillera. In: Albanesi, G.L., Beresi, M.S., Peralta, S.H. (Eds.), Ordovician from the Andes. INSUGEO, Serie Correlación Geológica 17, 185-189.

Baldo, E., Dahlquist, J., Rapela, C.W., Casquet, C., Pankhurst, R.J., Galindo, C., Fanning, C.M., 2005. Early Ordovician peraluminous magmatism in the Sierra de Pie de Palo (Western Sierras Pampeanas): geotectonic implications. Gondwana 12 Conference, Abstracts 57.

Baldo, E., Casquet, C., Pankhurst, R.J., Galindo, C., Rapela, C.W., Fanning, C.M., Dahlquist, J.A., Murra, J., 2006. Neoproterozoic A-type magmatism in the Western Sierras Pampeanas (Argentina): evidence for Rodinia break-up along the proto-Iapetus rift? Terra Nova, doi: 10.1111/j.1365-3121.2006.00703.x.

Banchig, A.L., Ormeño, P.A., Lucero, C.G., 1993. Análisis de paleodirecciones en las brechas carbonáticas y conglomerados del talud continental ordovícico. Precordillera Occidental, San Juan. XII Congreso Geológico Argentino y II Congreso de Exploración de Hidrocarburos, Actas I, 121-127.

Banchig, A.L., Weidmann, C., Marchese, N., Sacci, F., 2004. Vulcanismo submarino y flujos sedimentarios asociados, sur de la Sierra de la Invernada, descripción e interpretación, Precordillera Occidental, San Juan. X Reunión Argentina de Sedimentología, Resúmenes, 25-26. San Luis.

Barnes, S.J., Roeder, P.L., 2001. The range of spinel compositions in terrestrial mafic and ultramafic rocks. Journal of Petrology 42 (12), 2279-2302.

Basilici, G., Cutolo, A., Gomes Borges, J.P., Henrique, A., Moretti, P.A. 2005. Ordovician storm-dominated basins and the evolution of the western Gondwana margin (Portezuelo del Tontal, Sierra de la Invernada and Yerba Loca formations, Argentine Precordillera). Gondwana 12 Conference, Abstracts, 63.

Bau, M., 1999. Scavenging of dissolved yttrium and rare earths by precipitating iron oxyhydroxide: Experimental evidence for Ce oxidation, Y-Ho fractionation, and lanthanide tetrad effect. Geochimica et Cosmochimica Acta 63, 67-77.

Benedetto, J.L., 1993. La hipótesis de la aloctonía de la Precordillera argentina: un test estratigráfico y biogeográfico. XII Congreso Geológico Argentino y II Congreso de Exploración de Hidrocarburos, Actas III, 375-384.

Benedetto, J.L., 1998. Early Paleozoic brachiopods and associated shelly faunas from western Gondwana: their bearing on the geodynamic history of the pre-Andean margin. In: Pankhurst, R.J., Rapela, C.W. (Eds.), The Proto-Andean Margin of Gondwana. Geological Society of London, Special Publication 142, 57-83.

Benedetto, J.L., 1999. Braquiópodos de la Formación Trapiche, Ordovícico tardío de la Precordillera de La Rioja y San Juan, Argentina. Ameghiniana 36 (3), 323-337.

Benedetto, J.L., 2004. The allochthony of the Argentine Precordillera ten years later (1993-2003): a new plaeobiogeographic test of the microcontinental model. Gondwana Research 7 (4), 1027-1039.

Benedetto, J.L., Herrera, Z.A., 1987. Primer hallazgo de braquiópodos y trilobites en la Formación Trapiche (Ordovícico superior) Precordillera argentina. X Congreso Geológico Argentino, Actas 3, 73-76.

Benedetto, J.L., Vaccari, E., 1992. Significado estratigráfico y tectónico de los complejos de bloques resedimentados Cambro-ordovícicos de la Precordillera Occidental, Argentina. Estudios Geológicos, 48, 305-313.

Benedetto, J.L., Ortega, G., Brussa, E., Toro, B., 1985. Estratigrafía y fauna de la secuencia neo-Ordovícica y Llandoveriana del Río Escondido (flanco occidental del Cerro del Fuerte), provincia de San Juan. Primeras Jornadas sobre Geología de Precordillera, Acta I, 128-133. San Juan.

Benedetto, J.L., Herrera, Z.A., Ortega, G., 1991. Bioestratigrafía del Ordovícico en el flanco occidental del Cerro Potrerillo, provincia de San Juan. Revista de la Asociación Geológica Argentina 46 (1-2), 60-68.

Benedetto, J.L., Sánchez, T.M., Carrera, M.G., Brussa, E.D., Salas, M.J., 1999. Paleontological constraints on successive paleogeographic positions of Precordillera terrane during the early Paleozoic. In: Ramos, V.A., Keppie, J.D. (Eds.), Laurentia-Gondwana Connections before Pangea. Geological Society of America, Special Paper 336, 21-42.

Beresi, M.S., 1978. Presencia de depósitos de hierro sedimentarios en el Paleozoico inferior de la Precordillera de San Juan. 1ª Reunión Nacional del Paleozoico de Argentina (Tucumán, 1975), Actas, 61-64.

Beresi, M.S., 1990. El Ordovícico de la Precordillera de San Juan. XI Congreso Geológico Argentino, Relatorio, 32-46.

Beresi, M.S., 1991. Caracterización de la Formación San Juan (Ordovícico inferior calcáreo) de la Precordillera de San Juan, Argentina. Congreso Geológico Chileno, Actas 1, 302-305.

Beresi, M.S., 1992. Ordovician cycles and sea-level fluctuation in the Precordillera Terrane, western Argentine. In: Webby, B.D., Laurie, J.R. (Eds.), Global perspectives on Ordovician Geology. Proceedings of the Sixth International Symposium on the Ordovician System, 337-344.

Bhatia, M.R., Crook, K.A.W., 1986. Trace Element Characteristics of Graywackes and Tectonic Setting Discrimination of Sedimentary Basins. Contributions to Mineralogy and Petrology 92, 181 193.

Bickford, M.E., Soegaard, K., Nielsen, K.C., McLelland, J.M., 2000. Geology and geochronology of Grenville-age rocks in the Van Horn and Franklin Mountains area, west Texas: Implications for the tectonic evolution of Laurentia during the Grenville. Geological Society of America Bulletin 112, 1134-1148.

Bjerg, E.A., Brodtkorb, M.K., Stumpfl, E.F., 1993. Compositional zoning in Zn-chromites from the Cordillera Frontal Range, Argentina. Mineralogical Magazine 57, 131-139.

Blasco, G., Ramos, V., 1976. Graptolitos caradocianos de la Formación Yerba Loca y del Cerro La Chilca – Dpto. Jáchal, provincia de San Juan. Ameghiniana 13 (3-4), 312-329.

Bock, B., McLennan, S.M., Hanson, G.N. 1994. Rare earth element redistribution and its effects on the neodymium isotope system in the Austin Glen Member of the Normanskill Formation, New York, USA. Geochimica et Cosmochimica Acta 58, 5245-5253.

Bock, B., Bahlburg, H., Wörner, G., Zimmermann, U., 2000. Tracing crustal evolution in the Southern Central Andes from Late Precambrian to Permian with geochemical and Nd and Pb isotope data. Journal of Geology 108, 515-535.

Boghossian, N.D., Patchett, P.J., Ross, G.M., Gehrels, G.E., 1996. Nd isotopes and the source of sediments in the Miogeocline of the Canadian Cordillera. Journal of Geology 104, 259-277.

Bond, G.C., Nickelson, P.A., Kominz, M.A., 1984. Breakup of a supercontinent between 625 Ma and 555 Ma: new evidence and implications for continental histories. Earth and Planetary Sciences Letters 70, 325-345.

Bordonaro, O., 1999. Cámbrico y Ordovícico de la Precordillera y Bloque de San Rafael. In: Caminos, R. (Ed.), Geología Regional Argentina. SEGEMAR, Anales 29, 189-204.

Bordonaro, O., Keller, M., Lehnert, O., 1996. El Ordovícico de Ponón Trehué en la provincia de Mendoza (Argentina): redefiniciones estratigráficas. XIII Congreso Geológico Argentino y III Congreso de Exploración de Hidrocarburos, Actas I, 541-550.

Borrello, A.V., 1969. Los geosinclinales de la Argentina. Dirección Nacional de Geología y Minería, Anales 14, 1-136.

Brussa, E.D., 1997. La biozona de *Paraglossograptus tentaculatus* (Graptolithina) en la Formación Sierra de la Invernada, Precordillera Occidental, Argentina. Geobios 30 (1), 15-29.

Brussa, E.D., Mitchell, C.E., Astini, R.A., 1999. Ashgillian (Hirnantian?) graptolites from the western boundary of the Argentine Precordillera. Acta Universitatis Carolinae, Geologica 43, 199-202. Praga.

Buggisch, W., von Gosen, W., Henjes-Kunst, F., Krumm. S., 1993. The age of Early Paleozoic deformation and metamorphism in the Argentine Precordillera - evidence from K-Ar data. Zentralblatt Geologie und Palaontologie, T I, H1/2, 275-286.

Buggisch, W., Bordonaro, O.L., Cañas, F.L., von Gosen, W., Keller, M., Krumm, S., Lehnert, O., Loske, W., 2000. Sedimentary and structural evolution of the Argentine Precordillera – A key to the history of an exotic terrane. In: The Geological Evolution of the Andes, Sonderheft ZAG, 355-362.

Burt, D.M., 1989. Compositional and phase relations among rare earth element minerals. In: Lipin, B.R., McKay, G.A. (Eds.): Geochemistry and mineralogy of rare earth elements. Reviews in Mineralogy 21, 259-307.

Caballé, M., Furque, P., Cuerda, A., Alfaro, M., 1992. Nuevos hallazgos de graptolitos en la Formación Sierra de la Invernada (Ordovícico), Precordillera de San Juan, Argentina. Ameghiniana 29 (1), 9-26.

Calvert, S.E., Pedersen, T.F., 1993. Geochemistry of recent oxic and anoxic marine sediments: Implications for the geological record. Marine Geology, 113, 67-88.

Cañas, F.L., 1995. Early Ordovician carbonate platform facies of the Argentine Precordillera: Restricted shelf to open platform evolution. In: Cooper, J.D., Droser, M.L., Finney, S.C. (Eds.), Ordovician Odyssey. Pacific Section, Society of Economic Paleontologists and Mineralogists, Book 77, 221-224.

Carrera, M.G., Astini, R.A., 1998. Valoración de las restricciones ambientales durante la transición Arenigiano-Llanvirniano, Ordovícico de la Precordillera argentina. Revista de la Asociación Geológica Argentina 53 (1), 41-56.

Carrigan, C.W., Miller, C.F., Fullagar, P.D., Bream, B.R., Hatcher Jr., R.D., Coath, C.D., 2003. Ion microprobe age and geochemistry of southern appalachian basement, with implications for Proterozoic and Paleozoic reconstructions. Precambrian Research 120, 1-36.

Casquet, C., Baldo, E., Pankhurst, R.J., Rapela, C., Galindo, C., Fanning, M., Saavedra, J., 2001. Involvement of the Argentine Precordillera terrane in the Famatinian mobile belt: U-Pb SHRIMP and metamorphic evidence from the Sierra de Pie de Palo. Geology 29 (8), 703-706.

Casquet, C., Rapela, C.W., Pankhurst, R.J., Galindo, C., Dahlquist, J.A., Baldo, E., Saavedra, J., González-Casado, J.M., Fanning, C.M., 2005. Grenvillin massif-type anorthosites in the Sierras Pampeanas. Journal of the Geological Society of London 162, 9-12.

Casquet, C., Pankhurst, R.J., Fanning, C.M., Baldo, E., Galindo, C., Rapela, C.W., González-Casado, J.M., Dahlquist, J.A., 2006. U-Pb SHRIMP zircon dating of Grenvillian metamorphism in Western Sierras Pampeanas (Argentina): Correlation with the Arequipa-Antofalla craton and constraints on the extent of the Precordillera terrane. Gondwana Research 9, 524-529.

Castro de Machuca, B., Conte-Grand, A., Meissi, E., Pontoriero, S., Sumay, C., 1996. Petrología de las asociaciones máficas-ultramáficas de la Sierra de La Huerta. XIII Congreso Geológico Argentino y III Congreso de Exploración de Hidrocarburos, Actas 3, 439-452. Buenos Aires.

Chernicoff, C.J., Zappettini, E.O., 2004. Geophysical evidence for terrane boundaries in south-central Argentina. Gondwana Research 7 (4), 1105-1116.

Cingolani, C., Varela, R., 1999. The San Rafael bock, Mendoza (Argentina). Rb-Sr isotopic age of basement rocks. II South American Symposium on Isotope Geology, Anales, 23-26.

Cingolani, C., Varela, R., Cuerda A.J., Schauer, O., 1986. El Paleozoico inferior de la Sierra del Tontal, Precordillera de San Juan, República Argentina. VIII Congreso Geológico de Bolivia.

Cingolani, C.A., Cuerda, A.J., Aceñolaza, F.G., 1992. El Paleozoico Inferior sedimentario de Argentina y Chile. In: Gutiérrez Marco, J.G., Saavedra, J., Rábano, I. (Eds.), Paleozoico Inferior de Ibero-América. Universidad de Extremadura, 255-277.

Cingolani, C.A., Varela, R., Dalla Salda, L., Kawashita, K., 1993. Los granitoides del Cerro Veladero, río de la Troya, provincia de La Rioja: estudio geocronológico e implicancias tectónicas. XII Congreso Geológico Argentino y II Congreso de exploración de Hidrocarburos, Actas 4, 68-74.

Cingolani, C.A., Cuerda, A.J., Manassero, M., 1999. Litoestratigrafía de los depósitos silicoclásticos ordovícicos del cerro Bola, bloque de San Rafael, Mendoza. XIV Congreso Geológico Argentino, Actas 1, 409-413.

Cingolani, C.A., Llambías, E., Ortiz, L., 2000. Magmatismo básico pre-carbónico del Nihuil, Bloque de San Rafael, provincia de Mendoza, Argentina. IX Congreso Geológico Chileno, Actas 2, International Symposium n 4, 717-721.

Cingolani, C.A., Manassero, M., Abre, P., 2002. Geoquímica de elementos traza y tierras raras de las sedimentitas de la Formación Pavón, Ordovícico del Bloque de San Rafael, Mendoza. XV Congreso Geológico Argentino, Actas 1, 667-673. El Calafate.

Cingolani, C., Manassero, M., Abre, P., 2003a. Composition, provenance and tectonic setting of Ordovician siliciclastic rocks in the San Rafael Block: Southern extension of the Precordillera crustal fragment, Argentina. Journal of South American Earth Sciences Special Issue on the Pacific Gondwana Margin 16 (1), 91-106.

Cingolani, C.A, Basei, M.A., Llambías, E.J., Varela, R., Chemale Jr., F., Siga Jr., O. and Abre, P. 2003b. The Rodeo Bordalesa Tonalite, San Rafael Block (Argentina): Geochemical and isotopic age constraints. 10° Congreso Geológico Chileno, Concepción, CD Rom, 10 p.

Cingolani, C.A., Llambías, E.J., Basei, M.A.S., Varela, R., Chemale Jr., F., Abre, P. 2005a. Grenvillian and Famatinian-age igneous events in the San Rafael Block, Mendoza Province, Argentina: geochemical and isotopic constraints. Gondwana 12 Conference, Abstracts 102.

Cingolani, A., Varela, R., Abre, P., 2005b. Geocronología Rb-Sr del Stock de Agua de La Chilena: Magmatismo Pérmico del Bloque de San Rafael, Mendoza. XVI Congreso Geológico Argentino, Actas en CD.

Cox R., Lowe D.R., 1995. Controls on sediment composition on a regional scale: a conceptual review. Journal of Sedimentary Research 65, 1-12.

Cox, R., Lowe, D.R., Cullers, R.L., 1995. The influence of sediment recycling and basement composition on evolution of mudrock chemistry in the southwestern U.S. Geochimica et Cosmochimica Acta 59 (14), 2919-2940.

Criado Roqué, P., 1972. Bloque de San Rafael. In: Leanza, A.F. (Ed.): Geología Regional Argentina. Academia Nacional de Ciencias, Córdoba, Argentina, 283-295.

Criado Roqué, P., Ibáñez, G., 1979. Provincia Geológica Sanrafaelino-Pampeana. In: Leanza, A.F. (Ed.): Segundo Simposio de Geología Regional Argentina, Academia Nacional de Ciencias, Córdoba, Argentina, 837-869.

Cuerda, A.J., 1966. Formación La Chilca, Silúrico inferior de San Juan. Notas CIC 4 (1).

Cuerda, A.J., 1969. El límite Silúrico – Devónico en el borde oriental de la Precordillera de San Juan. Cuartas Jornadas Geológicas Argentinas, Actas I. Buenos Aires.

Cuerda, A.J., 1986. Graptolitos del techo de la Formación San Juan, Precordillera de San Juan. IV Congreso Argentino de Paleontología y Bioestratigrafía, Actas I, 49-57. Mendoza.

Cuerda, A.J., Furque, G., 1975. Nuevos datos sobre la paleobiogeografía de la Formación Gualcamayo, Ordovícico de la Precordillera. Congreso Argentino de Paleontología y Bioestratigrafía, Actas I, 49-57. Tucumán.

Cuerda, A.J., Cingolani, C., 1998. El Ordovícico de la región del Cerro Bola en el Bloque de San Rafael, Mendoza: sus faunas graptolíticas. Ameghiniana 35 (4), 427-448.

Cuerda, A.J., Ortega, G.O., 1982. *Loganograptus logani* (Hall) en la Precordillera de San Juan y La Rioja. Ameghiniana 19 (3-4), 281-288.

Cuerda, A.J., Furque, G., Uliarte, E., 1982. Graptolitos de la base del Siluriano de Talacasto, Precordillera de San Juan. Ameghiniana 19 (3-4), 239-252.

Cuerda, A.J., Cingolani, C., Varela, R., 1983. Las graptofunas de la Formación Los Sombreros, Ordovícico inferior, de la vertiente oriental de la Sierra del Tontal, Precordillera de San Juan. Ameghiniana 20 (3-4), 239-260.

Cuerda A.J., Cingolani, C., Schauer, O., Varela, R., 1985. El Ordovícico de la Sierra del Tontal, Precordillera de San Juan, República Argentina. IV Congreso Geológico Chileno, Actas 1-15, 109-131.

Cuerda, A.J., Cingolani, C., Varela, R., Schauer, O., 1986a. Cámbrico y Ordovícico en la Precordillera de San Juan: Formación Los Sombreros. Ampliación de su conocimiento bioestratigráfico. IV Congreso Argentino de Paleontología y Bioestratigrafía, Actas 1, 5-17. Mendoza.

Cuerda A.J., Cingolani, C., Schauer, O., Varela, R., 1986b. Bioestratigrafía del Ordovícico (Llanvirniano-Llandeilliano) de la Sierra del Tontal, Precordillera de San Juan. Descripción de su fauna graptolítica. Ameghiniana 23 (1-2), 3-33.

Cuerda, A.J., Rickards, B., Cingolani, C., 1988a. A new Ordovician-Silurian boundary section in San Juan province, Argentina, and its definitive graptolite fauna. Journal of the Geological Society 145, 1-9.

Cuerda A.J., Varela, R., Cingolani, C., Schauer, O., 1988b. Nuevas localidades con graptolitos en la Formación Portezuelo del Tontal (Ordovícico), sector septentrional de la Sierra del Tontal, Precordillera de San Juan, Argentina. Ameghiniana 25 (2), 175-183.

Cuerda, A.J., Alfaro, M., Caballé, M., Furque, G., 1994. *Dichograptus fasciculatus* nov. sp. (Graptolithina) en la Formación Gualcamayo (Ordovícico), Precordillera de San Juan, República Argentina. Ameghiniana 31 (1), 67-71.

Cuerda, A., Cingolani, C.A., Manassero, M., 1998. Caradoc graptolite assemblages and facial relations from the Cerro Bola section, San Rafael Block, Mendoza Province, Argentina. 6th International Graptolite Conference, IUGS Subcomission on Silurian Stratigraphy 23, 170-175. Madrid.

Cullers, R.L., Podkovyrov, V.N., 2000. Geochemistry of the Mesoproterozoic Lakhanda shales in southeastern Yakutia, Russia: implications for mineralogical and provenance control, and recycling. Precambrian Research 104, 77-93.

Cullers, R.L., Chaudhuri, S., Kilbane, N., Koch, R., 1979. Rare-earths in size fractions and sedimentary rocks of Pennsylvanian – Permian age from the mid-continent of the U.S.A. Geochimica et Cosmochimica Acta 43, 1285-1301.

Cullers, R.L., Barrett, T., Carlson, R., Robinson, R., 1987. Rare-earth element and mineralogic changes in Holocene soil and stream sediment: a case study in the Wet Mountains, Colorado, U.S.A. Chemical Geology 63, 275-297.

Dalla Salda, L., 2005. The Appalachian-Famatinian orogenic belt. Gondwana 12 Conference, Abstracts, 125.

Dalla Salda, L., Cingolani, C.A., Varela, R., 1992a. Early Paleozoic orogenic belts of the Andes in southwestern South America. Results of Laurentia - Gondwana collision? Geology 20, 617-620.

Dalla Salda, L., Dalziel, I.W.D., Cingolani, C.A., Varela, R., 1992b. Did the Taconic Appalachians continue into South America? Geology 20, 1059-1062.

Dalla Salda, L., Varela, R., Cingolani, C.A., 1993. Sobre la colisión de Laurentia – Sudamérica y el Orógeno Famatiniano. XII Congreso Geológico Argentino y II Congreso de Exploración de Hidrocarburos, Actas III, 358-366.

Dalziel, I.W.D., 1993. Tectonic tracers and the origin of the proto-Andean margin. XII Congreso Geológico Argentino y II Congreso de Exploración de Hidrocarburos, Actas III, 367-374.

Dalziel, I.W.D., 1997. Neoproterozoic-Paleozoic geography and tectonics: review, hypothesis, environmental speculations. Geological Society of America Bulletin 109, 16-42.

Dalziel, I.W.D., Dalla Salda, L., Gahagan, L.M., 1994. Paleozoic Laurentia-Gondwana interaction and the origin of the Appalachian-Andean mountain system. Geological Society of America Bulletin 106, 243-252.

Davis, J.S., Roeske, S.M., McClelland, W.C., Snee, L., 1999. Closing the ocean between the Precordillera terrane and Chilenia: Early Devonian ophiolite emplacement and deformation in the SW Precordillera. In: Ramos, V.A., Keppie, D. (Eds.), Laurentia-Gondwana connections before Pangea. Geological Society of America Bulletin, Special Paper 336, 115-138.

Davis, J.S., Roeske, S.M., McClelland, W.C., Kay, S.M., 2000. Mafic and ultramafic crustal fragments of the southwestern Precordillera terrane and their bearing on tectonic models of the early Paleozoic in western Argentina. Geology 28 (2), 171-174.

DePaolo, D.J., 1981. Neodymium isotopes in the Colorado Front Range and crust-mantle evolution in the Proterozoic. Nature 291, 193-196.

DePaolo, D.J., Wasserburg, G.J., 1976. Nd isotopic variations and petrogenetic models. Geophysical Research Letters 3, 249-252.

DePaolo, D.J., Linn, A.M., Schubert, G., 1991. The Continental Crustal Age Distribution, Methods of determining mantle separation ages from Sm-Nd isotopic data and application to the Southwestern United States, Journal of Geophysical Research 96, 2071-2088.

Dick, H.J.B., Bullen, T., 1984. Chromian spinel as a petrogenetic indicator in abyssal and alpine-type peridotites and spatially associated lavas. Contributions to Mineralogy and Petrology 86, 54-76.

Dickin, A.P., McNutt, R.H., 1989. Nd model age mapping of the southeast margin of the Archean foreland in the Grenville province of Ontario. Geology 17, 299-302.

Dodson, M.H., Compston, W., Williams, I.S., Wilson, J.F., 1988. A search for ancient zircons in Zimbabwe sediments. Journal of the Geological Society of London 145, 977-983.

Egenhoff, S.O., Lucassen, F., 2003. Chemical and Isotopic Composition of Lower to Upper Ordovician Sedimentary Rocks (Central Andes/South Bolivia): Implications for Their Source. Journal of Geology 111, 487-497.

Eriksson, K.A., Campbell, I.H., Palin, J.M., Allen, C.M., 2003. Predominance of Grenvillian magmatism recorded in detrital zircons from Modern Appalachians rivers. Journal of Geology 111, 707-717.

Evans, B.W., Frost, B.R., 1975. Chrome-spinel in progressive metamorphism – a preliminary analysis. Geochimica et Cosmochimica Acta 39, 959-972.

Fail, R.T., 1997. A geologic history of the North-Central Appalachians, Part 1. Orogenesis from the Mesoproterozoic through the Taconic Orogeny. American Journal of Science 297, 551-619.

Fail, R.T., 1998. A geologic history of the North-Central Appalachians, Part 3. The Alleghany Orogeny. American Journal of Science 298, 131-179.

Fanning, C.M., Pankhurst, R.J., Rapela, C., Baldo, E., Casquet, C., Galindo, C., 2004. K-bentonites in the Argentine Precordillera contemporaneous with rhyolite volcanism in the Famatinian Arc. Journal of the Geological Society of London 161, 747-756.

Fauqué, L., Villar, L.M., 2003. Reinterpretación estratigráfica y petrología de la Formación Chuscho, provincia de La Rioja. Revista de la Asociación Geológica Argentina 58 (2), 218-232.

Fedo, C.M., Nesbitt, H.W., Young, G.M., 1995. Unraveling the effects of potassium metasomatism in sedimentary rocks and paleosols, with implications for paleoweathering conditions and provenance. Geology 23 (10), 921-924.

Fedo, C.M., Young, G.M., Nesbitt, H.W., Hanchar, J.M., 1997. Potassic and sodic metasomatism in the Southern Province of the Canadian Shield: Evidence from the Paleoproterozoic Serpent Formation, Huronian Supergroup, Canada. Precambrian Research 84, 17-36.

Feng, R., Kerrich, R., 1990. Geochemistry of fine-grained clastic sediments in the Archean Abitibi greenstone belt, Canada: Implications for provenance and tectonic setting. Geochimica et Cosmochimica Acta 54, 1061-1081.

Fernández Noia, E.A., Sumay, C.A., Meissl, E.F., 1990. Petrografía de los cuerpos magmáticos del Ordovícico de las Sierras de la Yerba Loca y del Alto de Mayo, San Juan, Argentina. X Congreso Geológico Argentino, Actas 1, 46-51.

Ferracutti, G., Bjerg, E., Mogessie, A., 2004. Cromo espinelos de Las Águilas, provincia de San Luis, como indicadores tectónicos. Séptima Reunión de Mineralogía y Metalogenia (MINMET), Actas, 321-326. Río Cuarto.

Finney, S., 2005. Global Series and Stages for the Ordovician System: a progress report. Geologica Acta 3 (4), 309-316.

Finney, S., 2007. The parauthochthonous Gondwanan origin of the Cuyania (greater Precordillera) terrane of Argentina: a re-evaluation of evidence used to support an allochthonouc Laurentian origin. Geologica Acta 5 (2), 1-33.

Finney, S.C., Gleason, J., Gehrels, G.E., Peralta, S.H., Vervoort, J.D., 2003a. U/Pb geochronology of detrital zircons from Upper Ordovician Las Vacas, La Cantera and Empozada Formations, NW Argentina. In: Albanesi, G.L., Beresi, M.S., Peralta, S.H. (Eds.), Ordovician from the Andes. INSUGEO, Serie Correlación Geológica 17, 191-196.

Finney, S., Gleason, J., Gehrels, G., Peralta, S., 2003b. Post-Ordovician juxtaposition of the Cuyania Terrane and the Famatinian arc. 10° Congreso Geológico Chileno, Actas on CD, 7 pp.. Concepción.

Finney, S., Gleason, J., Gehrels, G., Peralta, S., Aceñolaza, G., 2003c. Early Gondwanan connection for the Argentine Precordillera terrane. Earth and Planetary Sciences Letters 205, 349-359.

Finney, S., Gleason, J., Gehrels, G., Peralta, S., Aceñolaza, G., 2004. Corrigendum to Early Gondwanan connection for the Argentine Precordillera terrane (Earth and Planetary Sciences Letters, v. 205, p. 349-359). Earth and Planetary Sciences Letters 219, 413.

Finney, S., Peralta, S., Gehrels, G., Marsaglia, K., 2005. The early Paleozoic history of the Cuyania (greater Precordillera) terrane of western Argentina: evidence from geochronology of detrital zircons from Middle Cambrian sandstones. Geologica Acta 3 (4), 339-354.

Fortey, R.A., Harper, D.A., Ingham, J.K., Owe, A.W., Rushton, A.W., 1995. A revision of Ordovician Series and Stages from the historical type area. Geological Magazine 132 (1), 1-16.

Frigerio, P.V., Uriz, N.J., Alfaro, M.B., 2005. Un nuevo registro de Graptolithina en la Formación Río Bonete (Ordovícico), Precordillera de Jagué, La Rioja. XVI Congreso Geológico Argentino, Actas en CD, La Plata.

Furque, G., 1963. Descripción geológica de la Hoja 17b, Guandacol, La Rioja – San Juan. Boletín Dirección Nacional de Geología y Minería 92, 1-104. Buenos Aires.

Furque, G., 1965. Geología de la región del Cerro Bolsa (provincia La Rioja). Segundas Jornadas Geológicas Argentinas, Actas 3, 181-215. Buenos Aires.

Furque, G., 1983. Descripción Geológica de la Hoja 19c, Ciénaga de Gualilán. Secretaria de Minería, Boletín 193, 111pp.

Furque, G., Cuerda, A., 1979. Precordillera de La Rioja, San Juan y Mendoza. II Simposio de Geología Regional Argentina, Publicación Especial Academia Nacional de Ciencias, Córdoba.

Furque, P., Caballé, M., 1985. Paleozoico inferior en el Cerro Bayo, Sierra de la Invernada, San Juan. Revista Museo de La Plata (Nueva Serie). Geología X (81), 1-18.

Galindo, C., Casquet, C., Pankhurst, R.J., Rapela, C., Baldo, E., Saavedra, J., 2004. Sr, C and O isotope geochemistry and stratigraphy of Precambrian and Lower Paleozoic carbonate sequences from the Western Sierras Pampeanas of Argentina: tectonic implications. Precambrian Research 131, 55-71.

Gallardo, G., Heredia, S., 1995. Estratigrafía y sedimentología del Miembro Inferior de la Formación Empozada (Ordovícico Medio y Superior), Precordillera Argentina. Boletín de la Academia Nacional de Ciencias de Córdoba, T 60 (3-4), 449-460.

Garzanti, E., Andò, S., Scutellà, M., 2000. Actualistic Ophiolite Provenance: The Cyprus Case. The Journal of Geology 108, 199-218.

Garzanti, E., Vezzoli, G., Andò, S., 2002. Modern sand from Obducted Ophiolite Belts (Sultanate of Oman and United Arab Emirates). The Journal of Geology 110, 371-391.

Gehrels, G.E., 2000, Introduction to detrital zircon studies of Paleozoic and Triassic strata in western Nevada and northern California: Geological Society of America, Special Paper 347, 1-17.

Gerbi, C., Roeske, S.M., Davis, J.S., 2002. Geology and structural history of the southwest Preordillera margin, northern Mendoza province, Argentina. Journal of South American Earth Sciences 14, 821-835.

Gleason, J.D., Finney, S.C., Peralta, S.H., 2001. Neodymium-graptolite stratigraphy of Ordovician shales from the Precordillera Terrane, Argentina: Laurentian or Gondwanan source? Geological Society of America, Annual Meeting, Paper # 19774.

Gleason, J.D., Finney, S.C., Peralta, S.H., Gehrels, G.E., Marsaglia, K.M., 2006. Zircon and whole-rock Nd-Pb isotopic provenance of Middle and Upper Ordovician siliciclastic rocks, Argentine Precordillera. Sedimentology, doi: 10.1111/j.1365-3091.2006.00820.x.

González Bonorino, G., 1991. Evolución comparada de la Precordillera de San Juan en el Paleozoico temprano y del margen atlántico de Norteamérica en el Mesozoico-Cenozoico. Revista de la Asociación Geológica Argentina 46, 10-19.

González Bonorino, G., González Bonorino, F., 1991. Precordillera de Cuyo y Cordillera Frontal en el Paleozoico temprano: terrenos 'bajo sospecha' de ser autóctonos. Revista Geológica de Chile 18 (2), 97-107.

González Díaz, E.F., 1981. Nuevos argumentos a favor del desdoblamiento de la denominada Serie de La Horqueta del Bloque de San Rafael, Provincia de Mendoza. VIII Congreso Geológico Argentino, Actas 3, 241-256.

Gradstein, F.M., Ogg, J.G., Smith, A.G., Bleeker, W., Lourens, L.J., 2004. A new Geologic Time Scale, with special reference to Precambrian and Neogene. Episodes 27, 83-100.

Haller, M.J., Ramos, V.A., 1984. Las ofiolitas famatinianas (Eopaleozoico) de las provincias de San Juan y Mendoza. IX Congreso Geológico Argentino, Actas II, 66-83. S.C. de Bariloche.

Harrington, H.J., 1957. Ordovician Formations of Argentina. In: Harrington, H.J., Leanza, A.F. (Eds.), Ordovician trilobites of Argentina. University of Kansas, Special Publication, 1-59.

Harrington, H.J., Leanza, A.F., 1957. Ordovician trilobites of Argentina. University of Kansas, Department of Geological Sciences, Special Publication 1, 259 pp. Lawrence.

Hartmann, L.A., Santos, J.O.S., 2004. Predominance of high Th/U, magmatic zircon in Brazilian Shield sandstones. Geology 32 (1), 73-76.

Hemming, S.R., McLennan, S.M., 2001. Pb isotope compositions of modern deep sea turbidites. Earth and Planetary Sciences Letters 184, 489-503.

Heredia, S., 1990. Geología de la Cuchilla del Cerro Pelado, Precordillera de Mendoza, Argentina. XI Congreso Geológico Argentino, Actas 2, 101-104. San Juan.

Heredia, S., 1996. El Ordovícico del Arroyo Ponón Trehué, sur de la provincia de Mendoza. XIII Congreso Geológico Argentino y III Congreso de Exploración de Hidrocarburos, Actas I, 601-605.

Heredia, S., 2002. Upper Llanvirn-Lower Caradoc conodont biostratigraphy, southern Mendoza, Argentina. In: Aceñolaza, F.G. (Ed.), Aspect of the Ordovician System in Argentina. ISUGEO, Serie Correlación Geológica 16, 167- 176.

Heredia, S., 2006. Revisión estratigráfica de la Formación Ponón Trehué (Ordovícico), Bloque de San Rafael, Mendoza. INSUGEO, Serie Correlación Geológica 21, 59-74.

Heredia, S., Gallardo, G., 1996. Las megaturbiditas de la Formación Empozada: un modelo interpretativo para el Ordovícico turbidítico de la Precordillera argentina. Revista Geológica de Chile 23 (1), 17-34.

Herrera, Z.A., Benedetto, J.L., 1991. Early Ordovician brachiopod faunas of the Precordillera basin, Western Argentina: Biostratigraphy and Paleobiogeographical affinities. In: McKinnon, D.I., *et al.* (Eds.), Brachiopods through time. Rotterdam, Netherlands, Balkema, 283-301.

Hisada, K., Arai, S., Yamaguchi, T., 1998. Detrital chromian spinels from site 960 in the Côte D'Ivoire – Ghana transform margin. In: Mascle, J., Lohmann, G.P., Moullade, M. (Eds.), Proceedings of the Ocean Drilling Program. Scientific Results 159, 133-139.

Hofmann, A., 1988. Chemical differentiation of the Earth: the relationship between mantle, continental crust and oceanic crust. Earth and Planetary Sciences Letters 90, 297-314.

Hole, M.J., Trewin, N.H., Still, J., 1992. Mobility of the high field strength, rare earth elements and yttrium during late diagenesis. Journal of the Geological Society of London 149, 689-692.

Hoskin, P.W.O., Schaltegger, U., 2003. The composition of zircon and igneous and metamorphic petrogenesis. In: Hanchar, J.M., and Hoskin, P.W.O. (Eds.), Zircon. Reviews in Mineralogy and Geochemistry 53, 27-62.

Huff, W.D., Bergström, S.M., Kolata, D.R., Cingolani, C.A., Davis, D.W., 1995. Middle Ordovician K-bentonites discovered in the Precordillera of Argentina: geochemical and paleogeographic implications. In: Cooper, J., Droser, M.L., Finney, S.C. (Eds.), Ordovician Odyssey. Pacific section SEPM 77, 343-348.

Huff, W.D., Bergström, S.M., Kolata, D.R., Cingolani, C.A., Astini, R.A., 1998. Ordovician K-bentonites in the Argentine Precordillera: relations to Gondwana margin evolution. In: Pankhurst, R.J., Rapela, C.W. (Eds.), The Proto-Andean Margin of Gondwana. Geological Society of London, Special Publications 142, 107-126.

Huff, W.D., Bergström, S.M., Kolata, D.R., Cingolani, C., Krekeler, P., Prokopenko, M., 2003. Ordovician K-bentonites in the Argentine Precordillera and their relation to Laurentian volcanism. In: Albanesi, G.L., Beresi, M.S., Peralta, S.H. (Eds.), Ordovician from the Andes. INSUGEO, Serie Correlación Geológica 17, 197-202.

Hünicken, M.A., Pensa, M.V., 1989. Stratigraphical significance of conodonts in two Middle Ordovician olistholites, Guandacol River, La Rioja province, Argentina. Courier Forsch. - Inst. Senckenberg 117, 51-54.

Irvine, T.N., 1965. Chromian spinel as a petrogenetic indicator; Part 1: Theory. Canadian Journal of Earth Sciences 2, 648-671.

Irvine, T.N., 1967. Chromian spinel as a petrogenetic indicator; Part 2: Petrologic Applications. Canadian Journal of Earth Sciences 4, 71-103.

Kamenetsky, V.S., Crawford, A.J., Meffre, S., 2001. Factors controlling chemistry of magmatic spinel: an empirical study of associated olivine, Cr-spinel and melt inclusions from primitive rocks. Journal of Petrology 42 (4), 655-671.

Kay, S.M., Ramos, V.A., Kay, R., 1984. Elementos mayoritarios y trazas de las vulcanitas ordovícicas en la Precordillera Occidental: Basaltos de rift oceánicos tempranos (?) próximos al margen continental. IX Congreso Geológico Argentino, Actas 2, 48-65.

Kay, S.M., Orrell, S., Abbruzzi, J.M., 1996. Zircon and whole rock Nd-Pb isotopic evidence for a Grenville age and Laurentian origin for the basement of the Precordilleran terrane in Argentina. Journal of Geology 104, 637-648.

Kay, S.M., Boucakis, K.A., Porch, K., Davis, J.S., Roeske, S.M., Ramos, V.A., 2005. E-MORB- like mafic magmatic rocks on the western border of the Cuyania terrane, Argentina. Gondwana 12 Conference, Abstracts, 216.

Keller, M., 1996. Anatomy of the Precordillera (Argentina) during Cambro-Ordovician times: implications for the Laurentia-Gondwana transfer of the Cuyania Terrane. III International Symposium on Andean Geodynamics, 775-778.

Keller, M., 1999. The Argentine Precordillera – sedimentary and plate tectonic history of a Laurentian crustal fragment in South America. Geological Society of America, Special Paper 341, 1-239.

Keller, M., Dickerson, P.W., 1996. The missing continent of Llanoria – Was it the Argentine Precordillera? XIII Congreso Geológico Argentino y III Congreso de Exploración de Hidrocarburos, Actas V, 355-367.

Keller, M., Lehnert, O., Buggisch, W., 1993. The transition from diagenesis to low-grade metamorphism in the argentine Precordillera: an application of the conodont colour alteration index. XII Congreso Geológico Argentino y II Congreso de Exploración de Hidrocarburos, Actas 1, 294-299.

Keller, M., Buggisch, W., Lehnert, O., 1998. The stratigraphical record of the Argentine Precordillera and its plate tectonic background. In: Pankhurst, R.J., Rapela, C.W. (Eds.), The Proto-Andean Margin of Gondwana. Geological Society of London, Special Publication 142, 35-56.

Kerlleñevich, S.C., 1985a. Localidades con Monograptus priodon (Graptolithina) en la Formación La Chilca, Precordillera de San Juan. Primeras Jornadas sobre Geología de la Precordillera, Acta I, 139-144. San Juan.

Kerlleñevich, S.C., 1985b. Graptolitos de la Formación Alcaparrosa, en el flanco occidental de la Sierra de Tontal (Precordillera de San Juan). Primeras Jornadas sobre Geología de la Precordillera, Actas I, 124-127. San Juan.

Kerlleñevich, S.C., Cuerda, A., 1986. Monograptus priodon (Bronn) (Graptolithinia) en la Formación La Chilca, Precordillera de San Juan, Argentina. Ameghiniana 23 (1), 119-126.

Kisch, H.J., 1991. Illite crystallinity: recommendations on sample preparation, X-ray diffraction settings, and interlaboratory samples. Journal of Metamorphic Geology 9, 665-670.

Kolata, D.R., Huff, W.D., Bergström, S.M., Cingolani, C.A., 1994. Ordovician K-bentonite beds discovered in the Precordillera of Argentina. Geological Society of America Abstracts with Programs 26 (7), 503.

Krumm, S., 1994. Winfit 1.0 - A computer program for X-ray diffraction line profile analysis. XIII Conference on Clay Mineralogy and Petrology, Acta Universitatis Carolinae Geologica 38, 253-261.

Krumm, S., Warr, L.N., 1994. VLGM homepage.

Lehnert, O., 1994. A *Cordylodus proavus* fauna from West-Central Argentina (Los Sombreros Fm., Sierra del Tontal, San Juan province). Zentralblatt Geologie und Palaontologie. Teil I, 1993 (1/2), 245-261.

Lehnert, O., Keller, M., 1993. The conodont record of the Argentine Precordillera: problems and possibilities. Zentralblatt Geologie und Palaontologie. T I, H 1/2, 231-244.

Lehnert, O., Miller, J.F., Repetski, J.E., 1997. Paleogeographic significance of Clavohamulus hintzei Miller (Conodonta) and other Ibexian conodonts in an early Paleozoic carbonate platform facies of the Argentine Precordillera. Geological Society of America Bulletin 109, 429-443.

Leveratto, M.A., 1968. Geología de la zona al oeste de Ullúm – Zonda, borde oriental de la Precordillera de San Juan, eruptividad subvolcánica y estructura. Revista de la Asociación Geológica Argentina 23, 129-157.

Loewy, S.L., Connelly, J.N., Dalziel, I.W.D., 2004. An orphaned basement block: The Arequipa-Antofalla Basement of the central Andean margin of South America. Geological Society of America Bulletin 116, 171-187.

López, J.P., Rodriguez Areal, M.M., Sales, A., Kawashita, K., 2006. Sm-Nd data in granitic and mylonitic rocks in the Sierras Pampeanas of Catamarca and La Rioja, Northwestern Argentina. IV South American Symposium on Isotope Geology, Actas, 586-588.

López, V.L., Gregori, D.A., 2004. Provenance and evolution of the Guarguaráz Complex, Cordillera Frontal, Argentina. Gondwana Research 7 (4), 1197-1208.

Loske, W.P., 1992. Sedimentologie, Herkunft und geotektonische Entwicklung palaozoischer Gesteiner der Prakordillere Westargentiniens. Munchner Geologische Hefte 7, 155pp.

Loske, W.P., 1993. La Precordillera del Oeste Argentino: una cuenca de back-arc en el Paleozoico. XII Congreso Geológico Argentino y II Congreso de Exploración de Hidrocarburos, Actas I, 5-13.

Loske, W.P., 1994. The West-Argentine Precordillera: a Palaeozoic back arc basin. Zeitschrift der Deutschen Geologischen Gesellschaft 145, 379-391.

Lucassen, F., Becchio, R., Wilke, H.G., Thirlwall M.F., Viramonte, J., Franz, G., Wemmer, K., 2000. Proterozoic-Paleozoic development of the basement of the Central Andes (18º-26º), a mobile belt of the South American craton. Journal of South American Earth Sciences 13, 697-715.

Lucassen, F., Harmon, R., Franz, G., Romer, R.L., Becchio, R., Siebel, W., 2002. Lead evolution of the Pre-Mesozoic crust in the Central Andes (18-27º): progressive homogenisation of Pb. Chemical Geology 186, 183-197.

Ludwig, K.R., 2001. User's Manual for Isoplot/Ex rev. 2.49, a Geochronological Toolkit for Microsoft Excel. Berkeley Geochronology Centre, Special Publications, 1a.

Manassero, M., Cingolani, C.A., Cuerda, A.J., Abre, P., 1999. Sedimentología, Paleoambiente y Procedencia de la Formación Pavón (Ordovícico) del Bloque de San Rafael, Mendoza. Revista de la Asociación Argentina de Sedimentología 6 (1-2), 75-90.

Manassero, M., Cingolani, C.A., Abre, P., Uriz, N., 2005. Facies sedimentarias de la Formación Río Seco de los Castaños (Silúrico-Devónico) del Bloque de San Rafael, Mendoza. XVI Congreso Geológico Argentino, Actas en CD.

Mange, M.A., Maurer, H.F.W., 1992. Heavy minerals in colour. Chapman and Hall, London, 147 pp.

Martina, F., Astini, R.A., Becker, T.P., Thomas, W.A., 2005. The northern boundary of the Precordillera terrane. Gondwana 12 Conference, Abstracts 243. Mendoza.

McDaniel, D.K., Hemming, S.R., McLennan, S.M., Hanson, G.N., 1994. Petrographic, geochemical, and isotopic constraints on the provenance of the Early Proterozoic Chelmsford Formation, Sudbury Basin, Ontario. Journal of Sedimentary Research 64A, 632-642.

McDonough, M.R., Ramos, V.A., Isachsen, C.E., Bowring, S.A., Vujovich, G.I., 1993. Edades preliminares de circones del basamento de la Sierra de Pie de Palo, Sierras Pampeanas Occidentales de San Juan: sus implicancias para el supercontinente proterozoico de Rodinia. XII Congreso Geológico Argentino y II Congreso de Exploración de Hidrocarburos, Actas III, 340-342.

McLennan, S.M., 1989. Rare earth elements in sedimentary rocks: influence of provenance and sedimentary processes. Mineralogical Society of America Reviews in Mineralogy 21, 169-200.

McLennan, S.M., 1993. Weathering and global denudation. The Journal of Geology 101, 295-303.

McLennan, S.M., Taylor, S.R., 1991. Sedimentary rocks and crustal evolution: tectonic setting and secular trends. The Journal of Geology 99 (1), 1-21.

McLennan, S.M., Nance, W.B., Taylor, S.R., 1980. Rare earth element-thorium correlations in sedimentary rocks, and the composition of the continental crust. Geochimica et Cosmochimica Acta 44, 1833-1839.

McLennan, S.M., McCulloch, M.T., Taylor, S.R., Maynard, J.B., 1989. Effects of sedimentary sorting on Nd-isotopes in deep-sea turbidites. Nature 337, 547-549.

McLennan, S.M., Taylor, S.R., McCulloch, M.T., Maynard, J.B., 1990. Geochemical and Nd-Sr isotopic composition of deep-sea turbidites: Crustal evolution and plate tectonic associations. Geochimica et Cosmochimica Acta 54, 2015-2050.

McLennan, S.M., Hemming, S., McDaniel, D.K., Hanson, G.N., 1993. Geochemical approaches to sedimentation, provenance, and tectonics. In: Johnsson, M.J., Basu, A. (Eds.), Processes controlling the composition of clastic sediments. Geological Society of America, Special Paper 284, 21-40.

McLennan, S.M., Simonetti, A., Goldstein, S.L., 2000. Nd and Pb isotopic evidence for provenance and post-depositional alteration of the Paleoproterozoic Huronian Supergroup, Canada. Precambrian Research 102, 263-278.

McLennan, S.M., Bock, B., Hemming, S.R., Hurowitz, J.A., Lev, S.M., McDaniel, D.K., 2003. The roles of provenance and sedimentary processes in the geochemistry of sedimentary rocks. In: Lentz, D.R. (Ed.): Geochemistry of sediments and sedimentary rocks: evolutionary considerations to minerals deposit-forming environments. Geological Association of Canada, GeoText 4, 7-38.

McLennan, S.M., Taylor, S.R., Hemming, S.R., 2006. Composition, differentiation, and evolution of continental crust: constraints from sedimentary rocks and heat flow. In: Brown, M., Rushmer, T. (Eds.), Evolution and differentiation of the continental crust. Cambridge: 377 pp.

Mendoza, N., Banchig, A., Bordonaro, O., 1997. Petrografía de los clastos de las psefitas ordovícicas de la Sierra del Tontal y su vinculación con la Sierra de Pie de Palo, San Juan. II Jornadas de Geología de la Precordillera, San Juan.

Merodio, J.C., Spalletti, L.A., 1990. Geoquímica de pelitas: su empleo en la definición de ambientes sedimentarios y tectónicos para el Ordovícico de la Precordillera Occidental. Revista Asociación Geológica Argentina 45 (3-4), 336-345.

Meschede, M., 1986. A method of discriminating between different types of mid-ocean ridge basalts and continental tholeiites with the Nb-Zr-Y diagram. Chemical Geology 56, 207-218.

Morton, A.C., 1991. Geochemical studies of detrital heavy minerals and their application to provenance studies. In: Morton, A.C., Todd, S.P., Haughton, P.D.W.

(Eds.), Developments in Sedimentary Provenance Studies. Geological Society of London, Special Publication 57, 31-45.

Morton, A.C., Hallsworth, C.R., 1994. Identifying provenance specific features of detrital heavy mineral assemblages in sandstones. Sedimentary Geology 90, 241–256.

Morton, A.C., Hallsworth, C.R., 1999. Processes controlling the composition of heavy mineral assemblages in sandstones. In: Bahlburg, H., Floyd, P.A. (Eds.), Advanced Techniques in Provenance Analysis of Sedimentary Rocks. Sedimentary Geology 124, 3–29.

Mosher, S., 1998. Tectonic evolution of the southern Laurentian Grenville orogenic belt. Geological Society of America Bulletin 110, 1357-1375.

Mutti, D., González Chiozza, S., Geuna, S., Di Marco, A., 2000. Influencia de la mineralogía y del metamorfismo en las propiedades magnéticas de los depósitos alpinos cromoespinelíferos. El complejo Los Guanacos, Pcia. de Córdoba. Mineralogía y Metalogenia, INREMI, Publicación 6, 343-350.

Naipauer, M., 2007. Análisis de la procedencia sedimentaria del Grupo Caucete (Sierras Pampeanas Occidentales) y su comparación con unidades cámbricas de Precordillera. Tesis doctoral, Universidad Nacional de La Plata, unpublished.

Naipauer, M., McClelland, W.C., Vujovich, G.I., Cingolani, C.A., Ellis, J.R., 2005a. U/Pb and $^{207}Pb/^{206}Pb$ ages on detrital zircons from El Quemado Quartzite (Caucete Group), Sierra de Pie de Palo, San Juan Province. XVI Congreso Geológico Argentino, Actas en CD, La Plata.

Naipauer, M., Cingolani, C.A., Valencio, S., Chemale Jr, F., Vujovich, G.I., 2005b. Estudios isotópicos en carbonatos marinos del terreno Precordillera-Cuyania: ¿plataforma común en el Neoproterozoico-Paleozoico inferior? Latin American Journal of Sedimentology and Basin Analysis 12 (2), 89-108.

Nance, W.B., Taylor, S.R., 1976. Rare earth element patterns and crustal evolution I: Australian post-Archean sedimentary rocks. Geochimica et Cosmochimica Acta 40, 1539- 1551.

Nelson, B.K., DePaolo, D.J., 1988. Application of Sm-Nd and Rb-Sr isotopes systematics to studies of provenance and basin analysis. Journal of Sedimentary Petrology 58, 348-357.

Nesbitt, H.W., 2003. Petrogenesis of siliciclastic sediments and sedimentary rocks. In: Lentz, D.R. (Ed.): Geochemistry of sediments and sedimentary rocks: evolutionary considerations to minerals deposit-forming environments. Geological Association of Canada, GeoText 4, 39-51.

Nesbitt, H.W., Young, G.M., 1982. Early Proterozoic climates and plate motions inferred from major element chemistry of lutites. Nature 199, 715-717.

Nesbitt, H.W., Young, G.M., 1984. Prediction of some weathering trends of plutonic and volcanic rocks based on thermodynamic and kinetic considerations. Geochimica et Cosmichimica Acta 48, 1523-1534.

Nesbitt, H.W., Young, G.M., 1989. Formation and diagenesis of weathering profiles. The Journal of Geology 97, 129-147.

Nesbitt, H.W., Young, G.M., McLennan, S.M., Keays, R.R., 1996. Effects of chemical weathering and sorting on the petrogenesis of siliciclastic sediments, with implications for provenance studies. Journal of Geology 104, 525-542.

Núñez, E., 1979. Descripción Geológica de la Hoja 28d, Estación Soitué, Provincia de Mendoza. Servicio Geológico Nacional 166, 1-67. Buenos Aires.

Oberhänsli, R., Wendt, A.S., Goffé, B., Michard, A., 1999. Detrital chromites in metasediments of the East-Arabian continental margin in the Saih Hatat area: constraints for the palaeogeographic setting of the Hawasina and Semail basins (Oman Mountains). International Journal of Earth Sciences 88, 13-25.

Ortega, G., Brussa, E., Astini, R., 1991. Nuevos hallazgos de graptolitos en la Formación Yerba Loca y su implicancia estratigráfica, Precordillera de San Juan, Argentina. Ameghiniana 28 (1-2), 163-178.

Ortega, G., Brussa, E., Toro, B., 1993. Las zonas de graptolitos de la Formación Gualcamayo (Arenigiano tardío - Llanvirniano temprano) en el norte de la Precordillera (provincias de La Rioja y San Juan), Argentina. Revista Española de Paleontología 8 (2), 207-219.

Ortiz, A., Zambrano, J.J., 1981. La Provincia geológica Precordillera Oriental. VIII Congreso Geológico Argentino, Actas 3, 59-74. San Luis.

Ottone, E.G., Albanesi, G.L., Ortega, G., Holfeltz, G.D., 1999. Palynomorphs, conodonts and associated graptolites from the Ordovician Los Azules Formation, Central Precordillera, Argentina. Micropaleontology 45 (3), 225-250.

Pankhurst, R.J., Rapela, C.W., Saavedra, J., Baldo, E., Dahlquist, J., Pascua, I., Fanning, C.M., 1998. The Famatinian magmatic arc in the central Sierras Pampeanas: An Early to Mid-Ordovician continental arc on the Gondwana margin. In: Pankhurst, R.J., Rapela, C.W. (Eds.), The Proto-Andean margin of Gondwana. Geological Society of London, Special Paper 142, 343-368.

Patchett, P.J., Ruiz, J., 1989. Nd isotopes and the origin of Grenville-age rocks in Texas: Implications for Proterozoic evolution of the United States mid-continent region. Journal of Geology 97, 685-695.

Payolla, B.L., Bettencourt, J.S., Kozuch, M., Leite Jr., W.B., Fetter, A.H., Van Schmus, W.R., 2002. Geological evolution of the basement rocks in the east-central oart of the Rondonia Tin Province, SW Amazon craton, Brazil: U-Pb ans Sm-Nd isotopic constraints. Precambrian Research 119, 141-169.

Peralta, S.H., 1986. La graptofauna ordovícica de la Formación La Cantera, Precordillera Oriental de San Juan. IV Congreso Argentino de Paleontología y Bioestratigrafía, Actas I, 67-71.

Peralta, S.H., 1993. Estratigrafía y consideraciones paleoambientales de los depósitos marino-clásticos eopaleozoicos de la Precordillera Oriental de San Juan. XII Congreso Geológico Argentino y II Congreso de Exploración de Hidrocarburos, Actas I, 128-137.

Peralta, S.H., 2003a. An introduction to the geology of the Precordillera, western Argentina. In: Peralta, S.H., Albanesi, G.L., Ortega, G. (Eds.), Ordovician and Silurian of the Precordillera, San Juan province, Argentina. INSUGEO 10, 7-22.

Peralta, S.H., 2003b. The Cerro La Chilca, Central Precordillera, San Juan province In: Peralta, S.H., Albanesi, G.L., Ortega, G. (Eds.), Ordovician and Silurian of the Precordillera, San Juan province, Argentina. INSUGEO 10, 45-63.

Peralta, S.H., 2005. Formación Los Sombreros: un evento diastrófico extensional del Devónico (Inferior?–Medio?) en la Precordillera Argentina. XVI Congreso Geológico Argentino, Actas on CD. La Plata.

Peralta, S.H., Baldis, B.A., 1990. Glyptograptus persculptus en la Formación Don Braulio (Ashgilliano tardío - Llandoveriano temprano), en la Precordillera Oriental de San Juan, Argentina. V Congreso Argentino de Paleontología y Bioestratigrafía, Serie Correlación Geológica 7, 67-72. Tucumán.

Peralta, S.H., Heredia, S.E., 2005. Depósitos de olistostroma del Devónico (Inferior?–Medio?), Formación Los Sombreros, en la Quebrada de San Isidro, Precordillera de Mendoza, Argentina. XVI Congreso Geológico Argentino, Actas on CD. La Plata.

Peralta, S., Finney, S.C., Gehrels, G., Gleason, J., Aceñolaza, G.F., 2003a. The Gondwanan origin of the Cuyania terrane, Western Argentina, based on Early Paleozoic U-Pb geochronology and chemostratigraphy. IV South American Symposium on Isotope Geology, 382-385.

Peralta, S.H., Finney, S.C., Basilici, G., 2003b. Portezuelo del Tontal Formation (Lower Caradoc), Western Precordillera, San Juan province: its biostratigraphic and paleogeographic significance. In: Albanesi, G.L., Beresi, M.S., Peralta, S.H. (Eds.), Ordovician from the Andes. INSUGEO, Serie Correlación Geológica 17, 119-123.

Pereyra, B., 1989. Estratigrafía de la Formación Yerba Loca de la Sierra de Los Túneles (Ordovícico Superior), Departamento Jáchal, Provincia de San Juan. Correlación Geológica 5, 211-216. Primer Reunión Internacional del Proyecto 270. Chile.

Pettijohn, F.J., Potter, P.E., Siever, R., 1987. Sand and sandstone. Springer Verlag, New York.

Pober, E., Faupl, P., 1988. The chemistry of detrital chromian spinels and its implications for the geodynamic evolution of the Eastern Alps. Geologische Rundschau 77 (3), 641-670.

Poiré, D., Cingolani, C., Morel E., 2002. Características sedimentológicas de la Formación Río Seco de los Castaños en el perfil de Agua del Blanco: Pre-Carbonífero del Bloque de San Rafael, Mendoza. XV Congreso Geológico Argentino, Actas 1, 129-133.

Porcher, C., Fernandes, L.A.D., Vujovich, G., Chernicoff, C.J., 2004. Thermobarometry, Sm/Nd ages and geophysical evidence for the location of the suture zone between Cuyania and the Western Proto-Andean Margin of Gondwana. Gondwana Research, 7(4), 1057-1076.

Pöthe de Baldis, E.D., 1987. Microplancton del Llandoveriano superior – Wenlockiano inferior, asociación de Deunffia y Domasia, de la Formación La Chilca, Aguada de los Azulejitos, San Juan, Argentina. X Congreso Geológico Argentino, Actas III, 89-94. Tucumán.

Pöthe de Baldis, E.D., 2001. Nuevos aportes sobre acritarcas y prasinofíceas de la Formación Don Braulio (Llandoveriano temprano-medio), Precordillera Oriental, San Juan, Argentina. Ameghiniana 38 (4), 429-440.

Proenza, J.A., Ortega-Gutiérrez, F., Camprubí, A., Tritlla, J., Elías-Herrera, M., Reyes-Salas, M., 2004. Paleozoic serpentinite-enclosed chromitites from Tehuitzingo (Acatlán Complex, southern Mexico): a petrological and mineralogical study. Journal of South American Earth Sciences 16, 649-666.

Ramos, V.A., 1988. Late Proterozoic-Early Paleozoic of South America – a collisional history. Episodes 11, 168-174.

Ramos, V.A., 2004. Cuyania, an exotic block to Gondwana: review of a historical success and the present problems. Gondwana Research 7 (4), 1009-1026.

Ramos, V.A., Basei, M., 1997. The basement of Chilenia: An exotic continental terrane to Gondwana during the early Paleozoic. In: Bradshaw, J.D., Weaver, S.D. (Eds.), Terrane Dynamics – 97: International Conference on Terrane Geology, Conference Abstracts, 140-143.

Ramos, V.A., Vujovich, G., 2000. Hoja Geológica 3169-VI, San Juan. Servicio Geológico Minero Argentino, Boletín 243, 1-82.

Ramos, V.A., Jordan, T.E., Allmendiger, R.W., Mpodozis, C., Kay, S., Cortés, J.M., Palma, M., 1986. Paleozoic terranes of the central Argentine-Chilean Andes. Tectonics 5 (6), 855-880.

Ramos, V.A., Vujovich, G.I., Kay, S.M., McDonough, M.R., 1993. La orogénesis de Grenville en las Sierras Pampeanas Occidentales: La Sierra de Pie de Palo y su integración al supercontinente proterozoico. XII Congreso Geológico Argentino y II Congreso de Exploración de Hidrocarburos, Actas III, 343-357.

Ramos, V.A., Vujovich, G.I., Dallmeyer, R.D., 1996. Los klippes y ventanas tectónicas de la estructura preándica de la Sierra de Pie de Palo (San Juan): Edad e implicaciones tectónicas. XIII Congreso Geológico Argentino y III Congreso de Exploración de Hidrocarburos, Actas 5, 377-392. Buenos Aires.

Ramos, V.A., Dallmeyer, R., Vujovich, G., 1998. Time constraints on the Early Paleozoic docking of the Precordillera, central Argentina. In: Pankhurst, R.J., Rapela, C.W. (Eds.), The Proto-Andean Margin of Gondwana. Geological Society of London, Special Publication 142, 143-158.

Ramos, V.A., Escayola, M., Mutti, D., Vujovich, G.I., 2000. Proterozoic – early Paleozoic ophiolites of the Andean basement of southern South America. Geological Society of America, Special Publication 349, 331-349.

Rapalini, A.E., 1996. Evidencias de un evento de remagnetización regional en Precordillera asociado a la Fase San Rafael. XII Congreso Geológico Argentino y II Congreso de Exploración de Hidrocarburos, Actas III, 415-422.

Rapalini, A.E., 2005. La historia acrecional de América del Sur en el Neoproterozoico y Paleozoico: Algunas consideraciones. XVI Congreso Geológico Argentino, Actas en CD, La Plata.

Rapalini, A.E., Astini, R.A., 1998. Paleomagnetic confirmation of the Laurentian origin of the Argentine Precordillera. Earth and Planetary Science Letters 155, 1-14.

Rapalini, A.E., Cingolani, C.A., 2004. First Late Ordovician Paleomagnetic pole for the Cuyania (Precordillera) terrane of western Argentina: a microcontinent or a Laurentian plateau? Gondwana Research 7 (4), 1089-1104.

Rapalini, A.E., Tarling, D.H., 1993. Multiple remagnetizations in the Cambrian – Ordovician carbonate platform of the Argentine Precordillera and their tectonic implications. Tectonophysics 227 (1-4), 49-62.

Rapela, C.W., Toselli, A., Heaman, L., Saavedra, J., 1990. Granite plutonism of the Sierras Pampeanas; an inner Cordilleran Paleozoic arc in the southern Andes. In: Kay, S.M., Rapela, C.W. (Eds.), Plutonism from Antarctica to Alaska. Geological Society of America, Special Papers 241, 77-90.

Rapela, C.W., Coira, B., Toselli, A., Saavedra, J., 1992. El magmatismo del Paleozoico inferior en el sudoeste de Gondwana. In: Gutiérrez-Marco, J.C., Saavedra, J., Rábano, I. (Eds.), Paleozoico inferior de Ibero-América. Publicaciones Universidad de Extremadura, España, 21-68.

Rapela, C., Pankhurst, R.J., Casquet, C., Baldo, E., Saavedra, J., Galindo, C., 1998. Early evolution of the Proto-Andean margin of South America. Geology 26 (8), 707-710.

Rapela, C.W., Pankhurst, R.J., Casquet, C., Fanning, C.M., Baldo, E.G., González-Casado, J.M., Galindo, C., Dahlquist, J., 2007. The Río de la Plata Craton and the assembly of SW Gondwana. Earth Science Reviews 83, 49-82.

Rivers, T., Martingnole, J., Gower, C.F., Davidson, A., 1989. New tectonic division of the Grenville Province, southeast Canadian shield. Tectonics 8, 63-84.

Robinson, D., Bevins, R.E., Rubinstein, N., 2005. Subgreenschist facies metamorphism of metabasites from the Precordillera terrane of western Argentina; constraints on the later stages of accretion onto Gondwana. European Journal of Mineralogy 17, 441-452.

Rogers, J.J.W., Unrug, R., Sultan, M., 1995. Tectonic assembly of Gondwana. Journal of Geodynamics 19, 1-34.

Rubinstein, N., Sellés Martínez, J., Morello, O., 1995. Paragenesis of sub-greenschist to greenschist facies in Alcaparrosa Formation, Argentina. An obducted ophiolitic complex. IX Congreso Latinoamericano de Geología, Actas, 1010-1017. Caracas.

Sack, R.O., Ghiorso, M.S., 1991. Chromian spinels as petrogenetic indicators: Thermodynamics and petrological applications. American Mineralogist 76, 827-847.

Sánchez, T.M., 1990. Bivalvos del Ordovícico Medio – Tardío de la Precordillera de San Juan (Argentina). Ameghiniana 27 (3-4), 251-261.

Sánchez, T.M., Benedetto, J.L., Astini, R.A., 1993. Eventos de recambio faunístico en secuencias depositacionales del Ordovícico tardío - Devónico temprano de la Precordillera de San Juan, Argentina. XII Congreso Geológico Argentino y II Congreso de Exploración de Hidrocarburos, Actas II, 281-288.

Sato, A.M., Tickyj, H., Llambías, E.J., Sato, K., 2000. The Las Matras tonalitic-trondhjemitic pluton, central Argentina: Grenvillian age constraints, geochemical characteristics and regional implications. Journal of South American Earth Sciences 13, 857-610.

Sato, A.M., Tickyj, H., Llambías, E.J., Basei, M.A.S., González, P.D., 2004. Las Matras Block, Central Argentina (37º S-67º W): the southernmost Cuyania terrane and its relationship with the Famatinian Orogeny. Gondwana Research 7 (4), 1077-1087.

Sato, K., Tassinari, C.G., Kawashita, K., Petronilho, L., 1995. O método geocronológico Sm-Nd no IG/USP e suas aplicações. Anales da Academia brasileira do Ciencias 67 (3), 313-336.

Schwartz, J.J., Gromet, L.P., 2004. Provenance of a late Proterozoic – early Cambrian basin, Sierras de Córdoba, Argentina. Precambrian Research 129, 1-21.

Scowen, P.A.H., Roeder, P.L., Heltz, R.T., 1991. Reequilibration of chromite within Kilauea Iki lava lake, Hawaii. Contributions to Mineralogy and Petrology 107, 8-20.

Sircombe, K.N., Stern, R.A., 2002. An investigation of artificial biasing in detrital zircon U-Pb geochronology due to magnetic separation in sample preparation. Geochimica et Cosmochimica Acta 66 (13), 2379-2397.

Spalletti, L.A., Cingolani, C., Varela, R., Cuerda A.J., 1989. Sediment gravity flow deposits of an Ordovician depth sea fan system. Sedimentary Geology 61, 287-301.

Stacey, J.S., Kramers, J.D., 1975. Approximation of terrestrial lead isotope evolution via two-stage model. Earth and Planetary Sciences Letters 26, 207-221.

Sun, S.S., McDonough, W.F., 1989. Chemical and isotopic systematics of oceanic basalts: implications for mantle composition and processes. In: Saunders, A.D., Norry, M.J. (Eds.), Magmatism in the Ocean Basins. Geological Society Special Publication 42, 313-345.

Taylor, S.R., McLennan, S.M., 1985. The Continental Crust. Its Composition and Evolution. Blackwell, London, 312 pp.

Thomas, W.A., 1976. Evolution of the Ouachita-Appalachian continental margin. Journal of Geology 84, 323-342.

Thomas, W.A., 1991. The Appalachian-Ouachita rifted margin of southeastern North America. Geological Society of America Bulletin 103, 415-431.

Thomas, W.A., Astini, R.A., 1996. The Argentine Precordillera: A traveler from the Ouachita embayment of North American Laurentia. Science 273, 752-757.

Thomas, W.A., Astini, R.A., 1999. Simple-shear conjugate rift margins of the Argentine Precordillera and the Ouachita embayment of Laurentia. Geological Society of America Bulletin 111, 1069-1079.

Thomas, W.A., Astini, R.A., 2003. Ordovician accretion of the Argentine Precordillera terrane to Gondwana: a review. Journal of South American Earth Sciences 16, 67-79.

Thomas, W.A., Astini, R.A., Denison, R.E., 2001. Strontium isotopes, age and tectonic setting of Cambrian Salinas along the rift and transform margins of the Argentine Precordillera and southern Laurentia. The Journal of Geology 109, 231-246.

Thomas, W.A., Astini, R.A., Bayona, G., 2002. Ordovician collision of the Argentine Precordillera with Gondwana, independent of Laurentian Taconic Orogeny. Tectonophysics 345, 131-152.

Thomas, W.A., Becker, T.P., Samson, S.D., Hamilton, M.A., 2004. Detrital zircon evidence of a recycled orogenic foreland provenance for Alleghanian clastic-wedge sandstones. Journal of Geology 112, 23-37.

Tickyj, H., Cingolani, C.A., Chemale Jr., F., 2001. Rb-Sr ages from La Horqueta Formation, San Rafael Block (Argentina). III South American Symposium on Isotope Geology.

Tickyj, H., Llambías, E., Melchor, R.N., 2003. Ordovician rocks from La Pampa province. In: Aceñolaza, F.G. (Ed.), Aspects of the Ordovician System in Argentina. INSUGEO, Serie Correlación Geológica 16, 257-266.

Tohver, E., Bettencourt, J.S., Tosdal, R., Mezger, K., Leite, W.B., Payolla, B.L., 2004. Terrane transfer during the Grenville orogeny: tracing the Amazonian ancestry of southern Appalachian basement through Pb and Nd isotopes. Earth and Planetary Sciences Letters 228, 161-176.

Tosdal, R.M., 1996. The Amazon-Laurentian connection as viewed from Middle Proterozoic rocks in the Central Andes, western Peru and northern Chile. Tectonics 15, 827-842.

Tosdal, R.M., Munizaga, F., Williams, W.C., Bettencourt, J.S., 1994. Middle Proterozoic crystalline basement in the Central Andes, Western Bolivia and Northern Chile: A U-Pb and Pb isotopic perspective. VII Congreso Geológico Chileno, Actas 2, 1464-1467.

Totten, M.W., Hanan, M.A., Weaver, B.L., 2000. Beyond whole-rock geochemistry of shales: The importance of assessing mineralogic controls for revealing tectonic discriminants of multiple sediment sources for the Ouachita Mountain flysch deposits. Geological Society of America Bulletin 112 (7), 1012-1022.

Uliarte, E.R., 1977. Geología del área central de la Sierra de Villicúm. Trabajo Final de Licenciatura. Universidad Nacional de San Juan, 76 pp. (unpublished).

Vaccari, N.E., 1994. Las faunas de trilobites de las sucesiones carbonáticas del Cámbrico y Ordovícico temprano de la Precordillera Septentrional Argentina. Tesis doctoral de la Universidad Nacional de Córdoba, Argentina, 271 pp. (unpublished).

Varela, R., 1973. Estudio geotectónico del extremo sudoeste de la Precordillera de Mendoza, República Argentina. Revista de la Asociación Geológica Argentina 28, 241-267.

Varela, R., Dalla Salda, L., 1992. Geocronología Rb-Sr de metamorfitas y granitoides del extremo sur de la Sierra de Pie de Palo, San Juan. Revista de la Asociación Geológica Argentina 47 (3), 271-275.

Varela, R., López de Luchi, M., Cingolani, C., Dalla Salda, L., 1996. Geocronología de gneises y granitoides de la Sierra de Umango, La Rioja. Implicancias tectónicas. XIII Congreso Geológico Argentino y III Congreso de Exploración de Hidrocarburos, Actas 3, 519-527. Buenos Aires.

Varela, R., Valencio, S., Ramos, A., Sato, K., González, P., Panarello, H., Roverano, D., 2001. Isotopic strontium, carbon and oxygen study on Neoproterozoic marbles from Sierra de Umango, Andean foreland, Argentina. III South American Symposium on Isotope Geology, 450-453.

Varela, R., Basei, M.A.S., Sato, A.M., González, P.D., Siga Jr., O., Campos Neto, M.C., Cingolani, C.A., 2003. Grenvillian basement and Famatinian events of the Sierra de Umango (29ºS): A review and new geochronological data. IV South American Symposium on Isotope Geology, 304-306.

Vavra, G., Schmid, R., Gebauer, D., 1999. Internal morphology, habit and U-Th-Pb microanalysis of amphibolite-to-granulite facies zircons: Geochronology of the Ivrea Zone (Southern Alps). Contributions to Mineralogy and Petrology 134, 380-404.

Vermeesch, P., 2004. How many grains are needed for a provenance study? Earth and Planetary Science Letters 224, 441-451.

Vilas, J.F., Valencio, D.A., 1970. Palaeomagnetism and K-Ar age of the Upper Ordovician Alcaparrosa Formation, Argentina. Geophys. J. R. ustr. Soc. 55, 143-154.

Villar, L.M., 2003. Lavas almohadilladas del Cerro Chuscho, provincia de La Rioja, como parte de la ofiolita de la Precordillera Occidental: correlaciones petrológicas en Cuyania y Chilenia. 10º Congreso Geológico Chileno, Actas on CD. Concepción.

Villar, L.M., Escayola, M.P., 1996. Metallogenetic aspects of ophiolites and other types of mafic and ultramafic complexes of Argentina. In: Coyner, A.R., Fahey, P.L. (Eds.), Geology and Ore deposits of the American Cordillera. Geological Society of Nevada Symposium Proceedings III, 1487-1499. Nevada.

Villar, L.M., Segal, S.J., Acevedo, R.D., 2001. Aportes al estudio mineralógico de los espinelos de la ofiolita de Sierra Grande de Córdoba, provincia de Córdoba y del gabro estratificado de Fiambalá, provincia de Catamarca, Argentina. XI Congreso Latinoamericano de Geología y III Congreso Uruguayo, 089 on CD.

Voldman, G.G., Albanesi, G.L., 2005. Paleotermometría del Sistema Ordovícico de la Precordillera Argentina sobre la base del Índice de Alteración del Color de Conodontes. XVI Congreso Geológico Argentino, Actas en CD.

von Gosen, W., 1992. Structural evolution of the Precordillera (Argentina): The Río San Juan section. Journal of Structural Geology 14, 643-667.

von Gosen, W., 1997. Early Paleozoic and Andean structural evolution in the Río Jáchal section of the Argentine Precordillera. Journal of South American Earth Sciences 10 (5-6), 361-388.

von Gosen, W., Buggisch, W., 1992. A west-east transect across the Precordillera Argentina. Zentralblatt Geologie und Palaontologie T I (H 6), 1597-1614.

von Gosen, W., Prozzi, C., 1998. Structural evolution of the Sierra de San Luis (eastern Sierras Pampeanas, Argentina): implications for the Proto-Andean margin of Gondwana. In: Pankhurst, R.J., Rapela, C.W. (Eds.), The Proto-Andean Margin of Gondwana. Geological Society of London Special Publications 142, 235-258.

von Gosen, W., Buggisch, W., Lehnert, O., 1995. Evolution of the Early Paleozoic mélange at the Eastern margin of the Argentine Precordillera. Journal of South American Earth Sciences 8, 405-424.

Vujovich, G.I., 2003. Metasedimentos silicoclásticos proterozoicos en la Sierra de Pie de Palo, San Juan: procedencia y ambiente tectónico. Revista de la Asociación Geológica Argentina 58, 608-622.

Vujovich, G.I., Kay, S.M., 1996. Evidencias geoquímicas del origen y ambiente geológico de las rocas metamórficas de composición máfica e intermedia de las Sierras Pampeanas Occidentales. XIII Congreso Geológico Argentino y III Congreso de Exploración de Hidrocarburos, Actas 4, 17-22. Buenos Aires.

Vujovich, G.I., Kay, S.M., 1998. A Laurentian? Grenville-age oceanic arc/back-arc terrane in the Sierra de Pie de Palo, Western Sierras Pampeanas, Argentina. In: Pankhurst, R.J., Rapela, C.W. (Eds.), The Proto-Andean Margin of Gondwana. Geological Society of London, Special Publications 142, 159-179.

Vujovich, G.I., Fernandes, L.A.D., Porcher, C.C., Fauque, L., 2001. Sierras Pampeanas Noroccidentales, La Rioja, Argentina: su integración regional. XI Congreso Latinoamericano de Geología, Actas on CD.

Vujovich, G.I., van Staal, C. R., Davis, W., 2004. Age constraints on the tectonic evolution and provenance of the Pie de Palo Complex, Cuyania Composite Terrane, and the Famatinian Orogeny in the Sierra de Pie de Palo, San Juan, Argentina. Gondwana Research 7 (4): 1041-1056.

Vujovich, G.I., Porcher, C., Chernicoff, C.J., Fernandes, L.A.D., Pérez, D.J., 2005. Extremo norte del basamento del terreno Cuyania: nuevos aportes multidisciplinarios para su identificación. AGA, Serie D, Publicación Especial n. 8, 15-41.

Wareham, C.D., Pankhurst, R.J., Thomas, R.J., Storey, B.C., Grantham, G.H., Jacobs, J., Eglington, B.M., 1998. Pb, Nd, and Sr isotope mapping of Grenville-age crustal provinces in Rodinia. The Journal of Geology 106, 647-659.

Warr, L.N., 1996. Standardized clay mineral crystallinity data from the very low-grade metamorphic facies rocks of southern New Zealand. European Journal of Mineralogy 8, 115-127.

Warr, L.N., Rice, A.H.N., 1994. Interlaboratory standardization and calibration of clay mineral crystallinity and crystallite size data. Journal of Metamorphic Geology 12, 141-152.

Winchester, J.A., Floyd, P.A., 1977. Geochemical discrimination of different magma series and their differentiation products using immobile elements. Chemical Geology 20, 325-343.

Wood, B.J., Virgo, D., 1989. Upper mantle oxidation state: Ferric iron contents of lherzolite spinels by 57Fe Mössbauer spectroscopy and resultant oxygen fugacities. Geochimica et Cosmochimica Acta 53, 1277-1291.

Wood, D.A., Joron, J.L., Treuil, M., 1979. A reappraisal of the use of trace elements to classify and discriminate between magma series erupted in different tectonic settings. Earth and Planetary Science Letters 45, 326–336.

Zhu, B., Kidd, W.S.F., Rowley, D.B., Currie, B.S., 2004. Chemical compositions and tectonic significance of chrome-rich spinels in the Tianba Flysch, Southern Tibet. Journal of Geology 112, 417-434.

Zimmermann, U., 2005. Provenance studies of very low- to low-grade metasedimentary rocks of the Puncoviscana complex, northwest Argentina. In: Vaughan, A.P.M., Leat, P.T., Pankhurst, R.J. (Eds.), Terrane processes at the margins of Gondwana. Geological Society of London, Special publications 246, 381-416.

Zimmermann, U., Bahlburg, H., 2003. Provenance analysis and tectonic setting of the Ordovician clastic deposits in the southern Puna Basin, NW Argentina. Sedimentology 50, 1079–1104.